UNIVERSITA' DEGLI STUDI DI NAPOLI FEDERICO II

DOTTORATO DI RICERCA IN

INGEGNERIA GEOTECNICA XXII CICLO

COORDINATORE

***Prof. Ing.* CARLO VIGGIANI**

"Analysis of slope failure mechanism in unsaturated pyroclastic soils, based on testing site monitoring"

Ottobre 2009

DOTTORANDA
Ing. MARIANNA PIRONE

RELATORE
Prof. Ing. **GIANFRANCO URCIUOLI**

CORRELATORE
Prof. Ing. **LUCIANO PICARELLI**

RELATORE ESTERNO
Dr. Ing. **LIDJIA ZDRAVKOVIC**

Acknowledgements

First, I would like to thank my supervisor Prof. Eng. Gianfranco Urciuoli for his guidance and encouragement throughout the period of this work.
I would like to express my gratitude to my external supervisor Dr L. Zdravkovic for her help and assistance during the period at Imperial College in London. I think it was difficult for her to understand my "English", so I have to thank her for the patience. I'll never forget how she loves her work and her university activities.
Many thanks are due to all my colleagues in the numerical section at Imperial College for their contribution in numerous ways and particularly to Katerina, specially because she helped me to use the numerical code, and Kostas. I would like to thank my friends at College: Joana, Miguel, Reinhard, Ramtin and Barbara because every time I went out with them I enjoyed very much and I felt as comfortable.

In the following I would like to complete the acknowledgements in Italian because I can express them better.

Vorrei prima di tutto ringraziare il mio relatore: Prof. Gianfranco Urciuoli; in italiano mi riesce meglio esprimere tutta la mia gratitudine verso di lui. Lo ringrazio per aver creduto in me fin dall'inizio, di avermi guidato, e di avermi fornito l'opportunità di avvicinarmi alla ricerca, e quindi di svolgere nell'arco di questi tre anni ciò che mi appassionava maggiormente. "Grazie per avermi trasmesso in questi anni la precisione e la maggiore criticità con cui affrontare qualsiasi tipo di problema".
Grazie al mio correlatore: Prof. Ing. Luciano Picarelli che mi ha sempre incoraggiato e stimolato in tutte le attività svolte nell'ambito di questi tre anni, apprezzando sempre il lavoro svolto.

I miei ringraziamenti vanno a tutto il gruppo di ricerca con cui ho lavorato in questi tre anni e senza il quale non avrei potuto portare a termine questo lavoro, e quindi a: Dott. Ing. Marco Valerio Nicotera e Dott. Ing. Raffaele Papa. Grazie a Marco per tutti i suggerimenti e gli interessanti spunti di riflessione forniti in questi tre anni; collaborando con lui ho imparato molte cose. Grazie a Raffaele, che fin dall'inizio mi ha aiutato a risolvere i problemi riscontrati in questi anni, grazie alla sua pazienza e alla sua continua disponibilità e alla sua

simpatia, grazie alla quale tutti noi dottorandi affrontiamo ogni giornata di lavoro con un sorriso in più.
Grazie anche ai miei colleghi del XXII ciclo di dottorato, nonché miei compagni di avventura, con i quali si é instaurato un bel rapporto di amicizia: Flaviana Moccia, Raffaele Di Laora, Lorenza Evangelista e Diego Lamante.
Ancora la mia gratitudine va: Dr. Ing. Emilio Bilotta specialmente per l'aiuto fornitomi talvolta nell'uso della lingua inglese; ai miei compagni di stanza con i quali si è creato un bel feeling umano e professionale: Anna, dalla personalità vivace e coinvolgente e Carmine, generoso e umano. Ringraziamenti ad Antonella, per i momenti di pausa dall'attività trascorsi insieme e per il sostegno datomi nei momenti più impegnativi. Grazie ancora a tutti i miei amici di dottorato e colleghi: Roberta, Giovanni, Guido e Antonio, Ivan.

Nei ringraziamenti non può mancare la mia famiglia che mi é sempre stata vicina anche quando ero distante infondendomi serenità e tranquillità. L'impegno e la tenacia li devo all'esempio che miei genitori mi hanno sempre dato nella vita. Grazie a mia madre, che ha saputo incoraggiarmi e stimolarmi a far sempre meglio e ha saputo capirmi anche nel silenzio dei momenti più impegnativi. Grazie al mio fratellino, Pasquale, ormai quindicenne ma per me sempre un bambino, che ha saputo allietarmi nei momenti più duri con la sua "verve" e con la sua vivacità intellettuale.

Infine grazie ad una persona molto speciale, Dario, che ha saputo soprattutto negli ultimi mesi, quelli più duri, incoraggiarmi e iniettarmi una dose di maggior autostima. "Grazie per avermi spesso ascoltato e per avermi fatto anche dimenticare tutti i problemi nei momenti condivisi insieme".

Grazie a tutti,

Marianna

Table of contents

Introduction

In the Campania region the pyroclastic soils resting on the limestone massif are often affected by mudflows. These landslides involve more superficial deposits, products of the volcanic eruption of the districts: Campi Flegrei and Somma Vesuvius.
The triggering mechanism in these soils are induced by rainfalls that can produce a significant increase in the degree of saturation and, consequently, significant reductions in suction and shear strength.

In order to analyse the failure mechanism, the experimental research project on mudflows was developed at University of Naples and it is going on from the winter 2005. Based on geological and geomorphologic considerations, the testing site of Monteforte Irpino (AV) was selected to collect experimental data through laboratory testing on undisturbed samples recovered in site and by monitoring climatic conditions, matric suction and water content in the field. The soils recognized in site are constituted by the products of a series of eruptions of Somma Vesuvius, hence they represent well the large area of Campania affected by the mudflows. Mechanical and hydraulic characterization of pyroclastic soils sampled in the test site are available, thanks to a previous PhD thesis (Papa, PhD thesis 2007). The instrumentation installed in site consists of 94 tensiometers, 40 TDR probes, 6 Casagrande piezometers and a weather station.

To analyse the factors predisposing the failure, the "hydraulic regime" in the subsoil and the influence of rainfall on the distribution of pore water pressure have to be investigated. Hence, in this thesis the data collected in situ: suction, water content and climatic conditions are shown. The elaboration of measurements are presented too, in particular the intensity and direction of the water flows in the subsoil. Moreover it was possible to get some conclusion about the water balance in the subsoil and to identify the rule of the pumices interposed between the pyroclastic layers.

The central part of thesis concerns the numerical analyses of the triggering mechanism by using the monitoring data and the results of the test lab already available (Papa, 2007). The numerical code used was ICFEP (Imperial College Finite Element Program). The model was validated simulating the observed conditions over one hydrologic year. Then the slope stability analyses were carried out to understand how the failure mechanism changes varying the rainfall history applied on the upper boundary, the saturated permeability, the critical state angle, the initial conditions. By processing the numerical results, the influence on the failure mechanism of each factor is identified and the critical threshold in terms of daily rain intensity can be developed.

Outline of thesis

The central part of the thesis consists of numerical analyses carried out by using ICFEP. The large number of experimental results obtained by the lab tests on undisturbed samples, in saturated and partially saturated conditions, allowed to characterize completely the soils in the domain analyzed (Papa, 2007). The failure mechanism in terms of type of failure, of depth of sliding surface, total rain (causing the collapse), and hydraulic conditions at failure was investigated by carrying out the slope stability analyses.

The thesis is divided into two sections. The first section consists of three chapters: the first contains the description of the pyroclastic soil in the Campania region, in particular these recognized in the experimental field of Monteforte Irpino; the second one the mechanical behaviour and constitutive model for partially saturated soils; the third one the description of mudflows in the Campania region. The second section contains the central part of thesis and it consists of six chapters which represent the six phases of the research developed during the three years of PhD course. In the following a brief description concerning the chapters of the second sections is presented.

In the *chapter four* a brief description of geological, morphological and stratigraphic features of the test site and the instrumentations installed are presented. The simplified profile of the soils are introduced too (*Papa, PhD Thesis 2007*).

In the *chapter five* suction and volumetric water content measurements are shown. In particular seasonal variations of matric suction and water content in the different layer of pyroclastic cover are retrieved by averaging the measurements of all instruments situated at the same depth. Matric suction measurements from tensiometers disposed along the longitudinal section, B-B, of the instrumented area are employed to obtain the ground water head in the soil cover. Vertical water flows through the top and the intermediate part of the soil profile are estimated. Water mass balance in the pumice layer 3 is calculated and an important additional understanding about the water flow in this layer is also achieved.

In the *chapter six* mechanical and hydraulic properties of the soils recognized in the testing site are elaborated, in order to obtain all the parameters necessary for the calibration of both the mechanical and hydraulic models used in the analyses. The chapter first presents the constitutive model and its calibration, successively the hydraulic model is analysed.

In the *chapter seven* the validation of the modelization of the Monteforte Irpino slope is presented. A section of the slope was discretized into a finite element mesh assuming plane strain conditions. After the simulation of the geological sedimentation of top soils over the limestone, one year of measured rainfall infiltration and evapotranspiration was applied at the ground surface. The predicted suction profiles from numerical analysis were compared with the measured suction profiles on site at the same locations.

The *chapter eight* deals with the s*lope stability analyses* of the monitored slope of Monteforte Irpino. The failure mechanism is analysed by carrying out parametric analyses, investigating the role of the parameters that influence slope stability in unsaturated soils. Different *rain boundary conditions*, *mechanical and hydraulic properties*, and *initial conditions* are studied in order to analyze how these factors influences the triggering starting time and the type of failure, the depth of the sliding surface, the distribution of pore water pressure and the profile of permeability at failure.

In the *chapter nine* the study of potential failure mechanism and the development of the critical threshold are introduced by using results of numerical analyses.
By evaluating results of slope stability analyses, it was possible to determine which mechanical and hydraulic parameters influences heavily the type of failure and how the triggering mechanism changes varying the climate conditions applied on the upper boundary.
Moreover the processing of these results (as suction values at failure, cumulated rainfall generating collapse and the number of days over which it is applied) allowed to develop the critical threshold in terms of daily rain intensity against rainfall duration.

Section I: Partially saturated soils

This section is divided in three chapters.
In the chapter 1 the pyroclastic soils covering the Campania region are described and in particular these recognized in the experimental field of Monteforte Irpino with their hydraulic and mechanical properties are introduced (Papa, PhD thesis,2007; Nicotera et al., 2008).
In the chapter 2 a review of the mechanical behaviour and constitutive model for partially saturated soils is introduced (Papa, 2007; Georgiadis, 2003).
Moreover in the chapter 3 the mudflows affecting the Campania region are described, the typical setting, stratigraphic and morphological conditions where these types of landslides occur are presented too.

Chapter 1

Pyroclastic soils in Campania region

1.1 Synopsis

In this chapter the pyroclastic soils covering the Campania region are introduced. The pyroclastic deposits are divided in volcanic products of: Somma Vesuvius and Campi Flegrei.

The soils recognized in the experimental field of Monteforte Irpino (AV) analysed in this phd thesis are the volcanic products of Somma Vesuvio. The experimental survey available on these soils is very large, in fact it was object of a previous PhD thesis (Papa, 2007). In the following the grain size distribution, the physic, the hydraulic and the mechanical properties of these soils are presented briefly.

1.2 Origin

Campania region is covered by a succession of the pyroclastic soils produced in the past by some volcanic eruptions (Rolandi et al., 1998). Their physic, hydraulic and mechanical properties are strongly related to the distance from the eruption centre and to the deposition mechanism. These deposits can be coarse or fine, cemented or loose, fractured or intact and they present a structure varying along the vertical and horizontal directions. The most famous volcanic districts in Campania region are: the district of Campi Flegrei and that of Somma Vesuvius. These districts are still active within the area called “Zona vulcanica campana”. Moreover their products could be affected by: erosion, slope instability, subsidence of structures and collapse of ancient caves. Among these engineering problems, the most important is the slope instability.

1.2.1 District of Campi Flegrei

The volcanic activity of Campi Flegrei began around 150 k. y. ago; the latest events occurred in 1301 (Ischia) and in 1538 (origin of Monte Nuovo). The depression of Campi Flegrei

presents a structure as a caldera where more than seventy eruptive centre were active (Budetta et al., 1993; Orsi et al., 1996; Rolandi et al., 2003).

This structure is the result of the two episodes of subsidence: the eruption of "Ignimbrite campana" and that of "Tufo Giallo Napoletano".

Some authors divide the volcanism activity in four cycles:

- I Cycle (> 35,000 years from now): explosive activities in the west part of Campi Flegrei. The products of this activity are poorly widespread on the mainland.

- II Cycle (35,000 ÷ 30,000 years from now): the volcanic products are Piperno, Breccia Museo and the Ignimbrite campana (Tufo Grigio Campano). The tufo grigio campano eruption was the most important event. The mechanism consisted of a pyroclastic flow and of a very fine ash too. In some areas (Piana Campana) this soil now has a thicknesses of 50 ÷ 60 m.

- III Cycle (18,000 ÷ 10,000 years ago): there was the origin of the Tufo stratified (Soccavo) and the Tufo Giallo Napoletano. The latter one presents pumices and lithic fragments. After the eruption of the Tufo Giallo Napoletano, there was the formation of the caldera and the hills of Camaldoli and Posillipo and the Rione Terra.

- IV Cycle (10,000 years from now ÷ 1538 after.c.): there was an intense explosive activity. At the beginning there was the formation of Tufo Giallo stratified, in the second phase the pyroclastic loose products (eruption of Monte Nuovo, 1538). The pyroclastic loose products in this cycle are very common throughout the area flegrea and consist mainly of pumice, lapilli, ash (pozzolana).

1.2.2 District of Somma Vesuvio

The volcano consists of the old district of Somma, there the caldera caused the subsidence of the southern sides and the origin of the Vesuvius cone (Rolandi et al., 1998).

Data from survey carried out in area of Trecase suggested an ancient volcanic activity around 400 k.y. Up to 17 k.y. years ago, the volcanic activity consisted of effusive and explosive phases, then it became explosive only (eruption of 1631). From that year to the last eruption (1944) the eruptive events have taken frequently the features of flows (Rolandi et al., 1998). Thus, the pyroclastic deposits are the result of the volcanic explosive activity. In agreement with the type of transport and deposition, they can be classified as: pyroclastic ash, pyroclastic flow and surges.

1.3 The stratigraphic features

In the following a brief summary about some features of pyroclastic soils covering Campania region is introduced. In particular the soils produced from the explosive activity of Somma-Vesuvius are presented.

The soils produced during the explosive activity of Campi Flegrei are either dissolved and lithified. The origin of these pyroclastic soils is related to the type of eruptive activity. The area of Naples, therefore, consists of a variety of pyroclastic deposits which, even if are similar in composition, size grains, age and pre-eruptive environment, appear very different in degree and type of alteration.

The pyroclastic deposits, belonged to the explosive Somma-Vesuvius area, are distributed heterogeneously according to the axes of dispersion (*Fig. 1.1*) of each eruption, reaching a thickness varying between 4 and 7 meters around the mountains of Sarno and 2 meters around the Lattari Mountains (*Fig. 1.2*) (Rolandi et al., 2000; Di Crescenzo and Santo, 2005).
After deposition on the limestone, the pyroclastic soils were subject to instability, generally due to the rain events of high intensity; in fact, along the slopes, the pyroclastic volcanic series are incomplete (De Vita and Celico, 2006).
Thus the most recent volcanic sequence produced by the eruptions of Somma Vesuvius is highly discontinuous on the limestone. This sequence is found, however, fully and continued below “the Campania flat”.

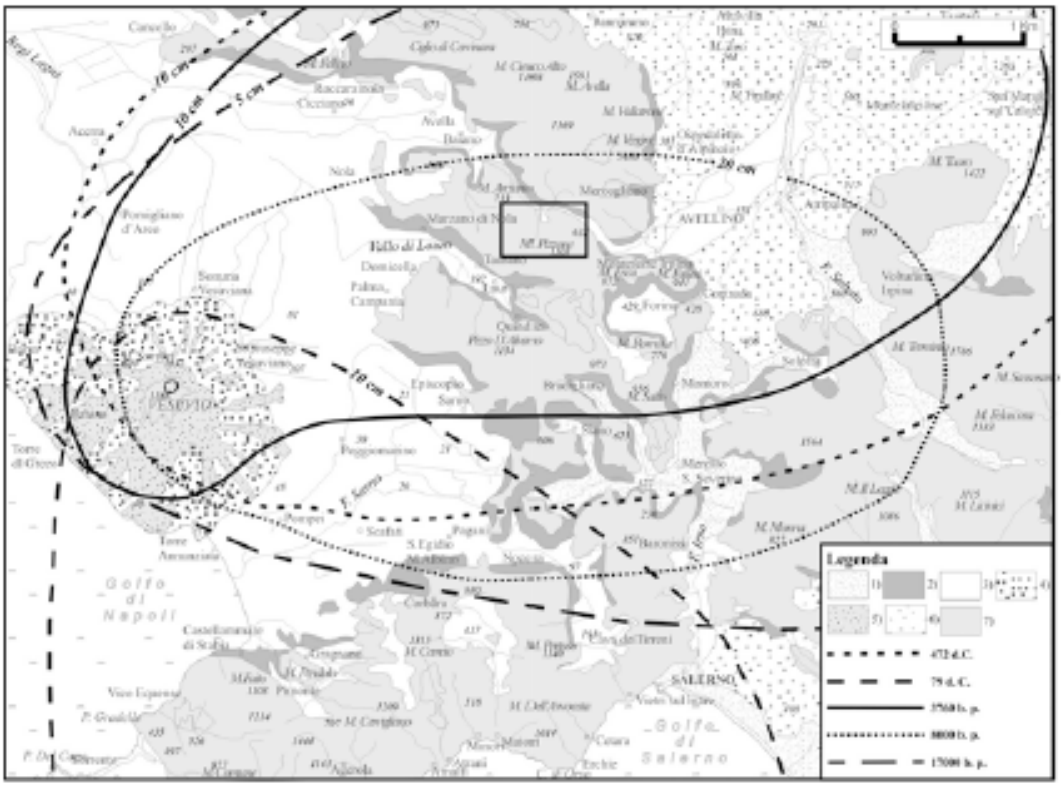

Figure 1.1: Geologic map of the major deposits belonged to Somma - Vesuvius (Di Crescenzo et al., 2007)

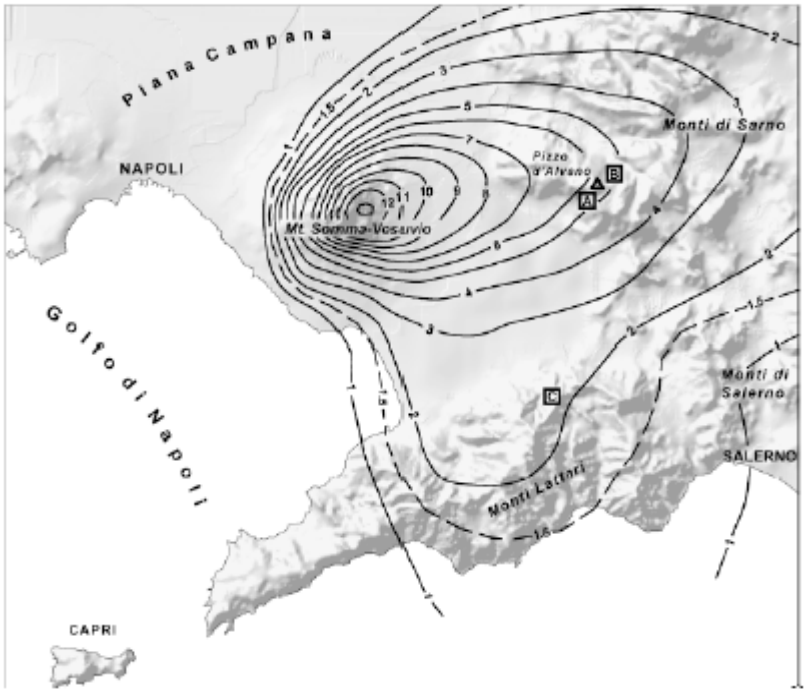

Figure 1.2: Isopache map of the recent pyroclastic complex (Rolandi et al., 2000)

1.4 Pyroclastic soils of Somma Vesuvio

The pyroclastic deposits generated from district of Somma - Vesuvius are presented extensively in literature; they are: Cervinara (Olivares et al., 2002; Damiano, 2004; Lampitiello, 2004) and Pizzo d'Alvano (Bilotta et al., 2005). In the following these recognized in the experimental site of Monteforte Irpino, object of this PhD thesis, are introduced only.

1.4.1 Pyroclastic soils of experimental field of Monteforte Irpino (AV)

A brief summary of the physic, hydraulic and mechanical properties of the pyroclastic soils sampled in the experimental field of Monteforte Irpino (AV) (Papa, 2007) is presented. Essentially the results of the lab tests, object of a previous PhD thesis (Papa, 2007), are shown.

1.4.1.1 Grain size distribution and mean physic properties

At the test site of Monteforte Irpino (AV) the stratigraphic succession can be described as a series of soil layers essentially parallel to the ground surface. Starting from the ground surface the sequence consists of (*fig.1.3*): 1) topsoil; 2) weathered and humified ashy soil; 3) pumices from the Avellino eruption (3.7 ky b.p.); 4) palaeosoil consisting of weathered volcanic ashes; 5) pumices from the Ottaviano eruption (8.0 ky b.p.); 6) palaeosoil consisting of weathered volcanic ashes; 7) volcanic sand; 8) highly weathered fine-grained ashy soil. Grain-size distributions of the eight layers are reported in *Figure 1.4 (Papa, 2007).*

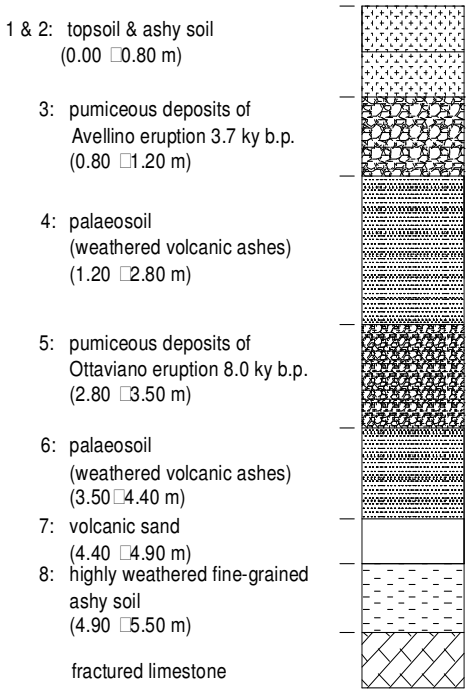

Fig. 1.3: Simplified profile (Nicotera et al.,2008)

The grain-size envelopes of investigated soils exhibit limited scatter, demonstrating the uniformity of the deposits. Shallower layers (1 and 2) have quite similar grain-size distribution: the two envelopes are partially superimposed (light grey area in Figure 1.4a) even if layer 1 is rather finer (dark grey area in Figure 1.4a). Soil 4 (Figure 1.4b) is well-graded, ranging from sand to silt with a small clay fraction. Layers 6 and 8 (Figure 1.4c) are significantly finer than the others. Soils 3, 5 and 7 (Figure 1.4d) should be described as quite uniform coarse-grained materials: soil 7 is a medium silty sand, soil 5 is a coarse sand and soil 3 is a gravel (*Papa et al., 2008*).

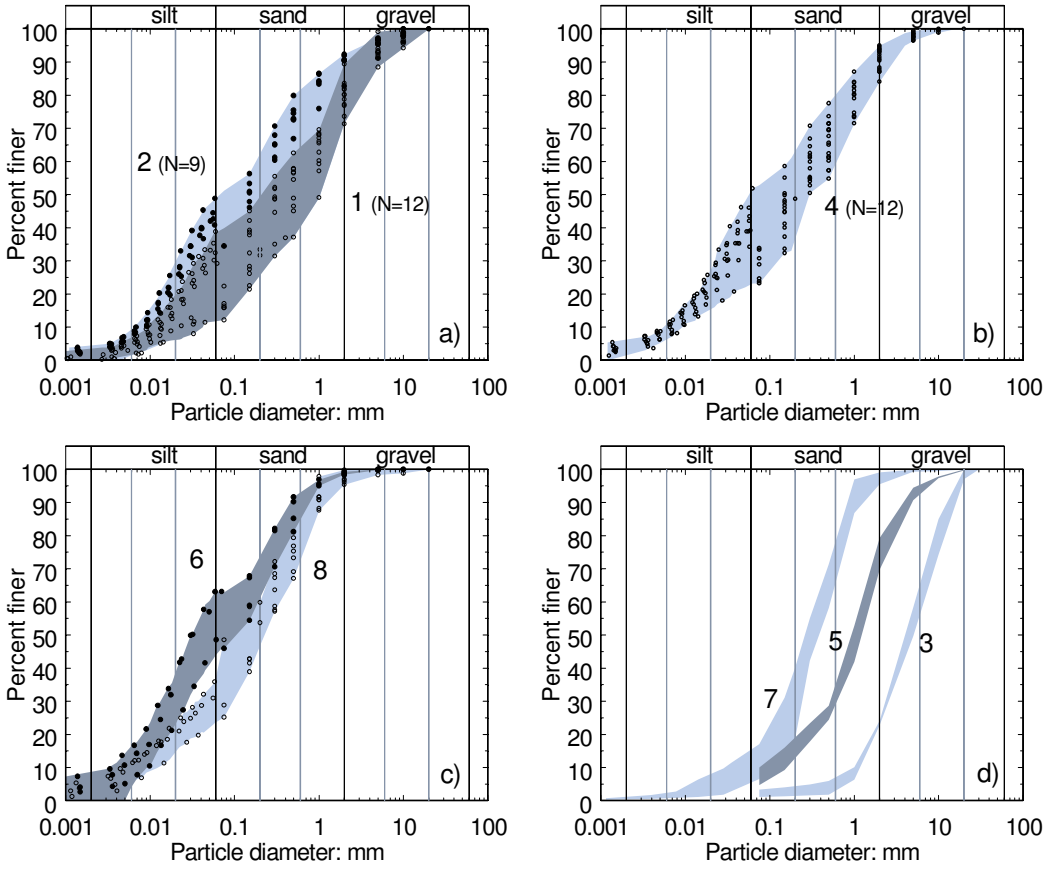

Fig. 1.4: Grain size distributions of soils constituting the cover on the limestone substratum, in the trial field at Monteforte Irpino (Papa, 2007)

Mean values of the main soil physical properties are reported in *Table 1.1*. All the soils are extremely porous. All the layers are partially saturated but the deeper ones have higher values of the saturation degree (see table 1.1). However, the saturation condition varies with a seasonal trend (*Chapter 5*)(*Papa et al., 2008*).

Tab.1.1 Mean physic properties of soils (Papa, 2007)

soil	G_s	γ_d (kN/m^3)	γ (kN/m^3)	n	S_r
1	2.65	8.06	11.91	0.69	0.57
2	2.66	7.77	12.49	0.70	0.69
4	2.57	7.11	12.11	0.71	0.71
6	2.57	7.13	12.51	0.72	0.77
7	2.47	7.71	11.93	0.69	0.64
8	2.49	10.64	15.49	0.58	0.87

1.4.1.2 Hydraulic characterization

The results available of hydraulic tests performed on undisturbed samples recovered in the site are briefly presented below (Papa, 2007).

Constant head tests were used to determine saturated permeability while forced evaporation tests and drying tests in a pressure plate apparatus allowed both water retention curves and permeability functions to be determined. The test procedures adopted were quite innovative and are extensively described by Papa (2007). The water retention curves and the permeability functions of the studied soils are reported in *Figure 1.5 ÷ 1.8*. All these curves were determined along a drying process starting from totally saturated conditions. As regards water retention properties, all the investigated soils behave like coarse-grained materials; they have an air entry value in the range from 6–8 kPa to 12 kPa. Starting from saturated conditions, they become almost dry when the applied matric suction reaches about 100 kPa. However, some differences can be recognised between the shallower and intermediate layers (1 & 2 and 4) and the deeper ones (6 and 8). Careful comparison of the water retention curves reveals that layers 6 and 8 have a substantially higher air entry value than the shallower strata. Furthermore, saturated water permeability (the experimental determinations are conventionally reported in *figures 1.5 ÷ 1.8* as isolated points corresponding to a suction value of 0.1 kPa) clearly decreases with soil layer depth. In particular, the hydraulic conductivity of layer 8 is significantly lower than that of all other soils along the whole investigated suction range.

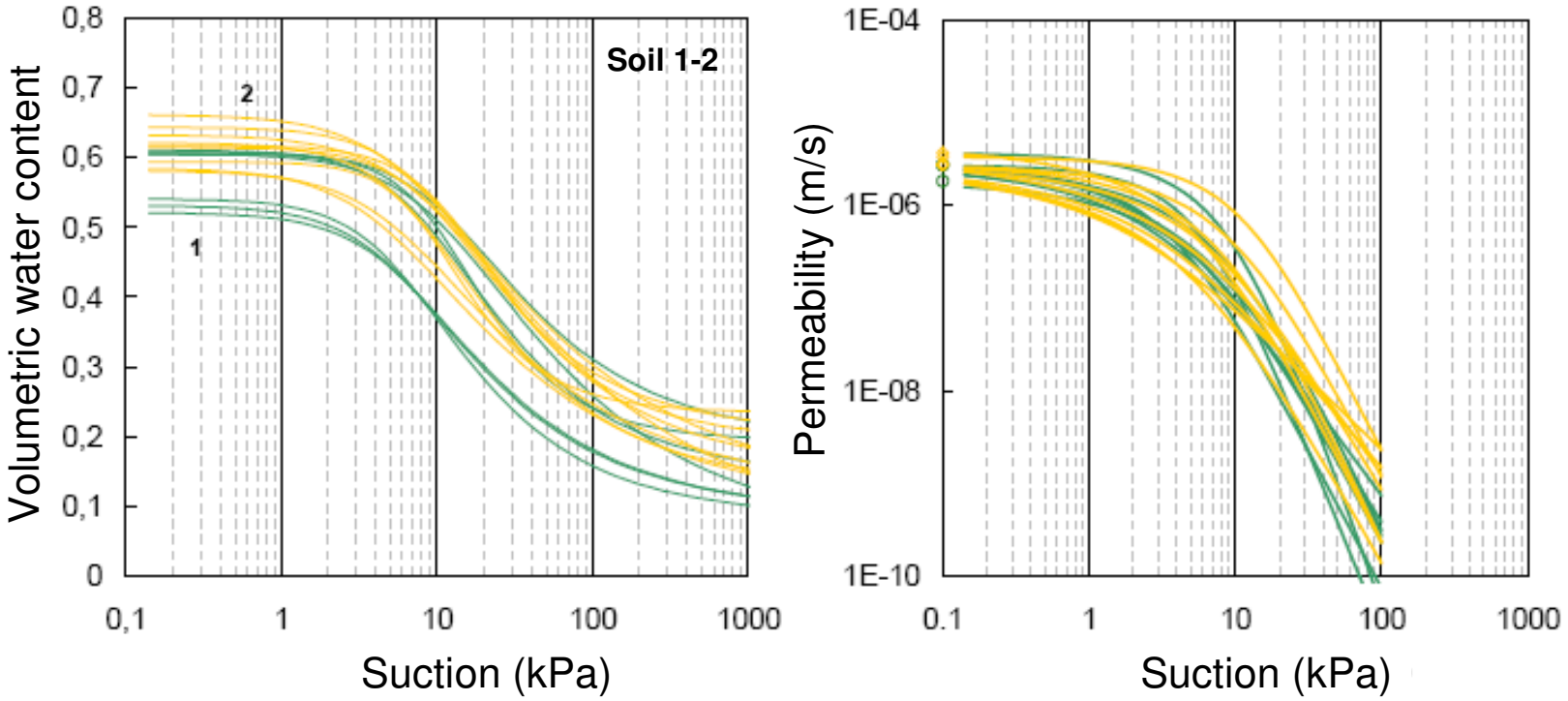

Fig. 1.5: Water retention curves obtaining in drying conditions, soil 1-2 and Permeability curve in drying conditions, soil 1-2 (Papa, 2007)

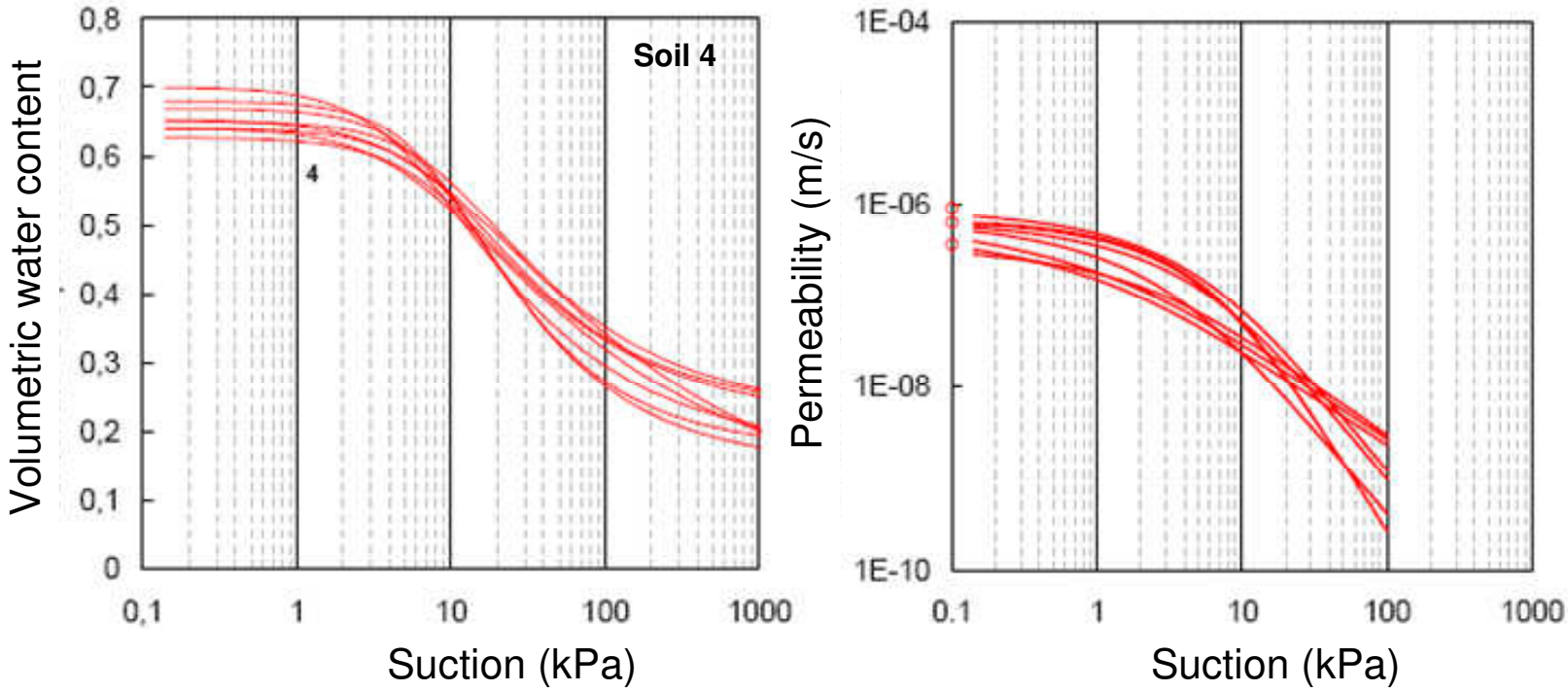

Fig. 1.6: Water retention curves obtaining in drying conditions, soil 4 and Permeability curve in drying conditions, soil 4 (Papa, 2007)

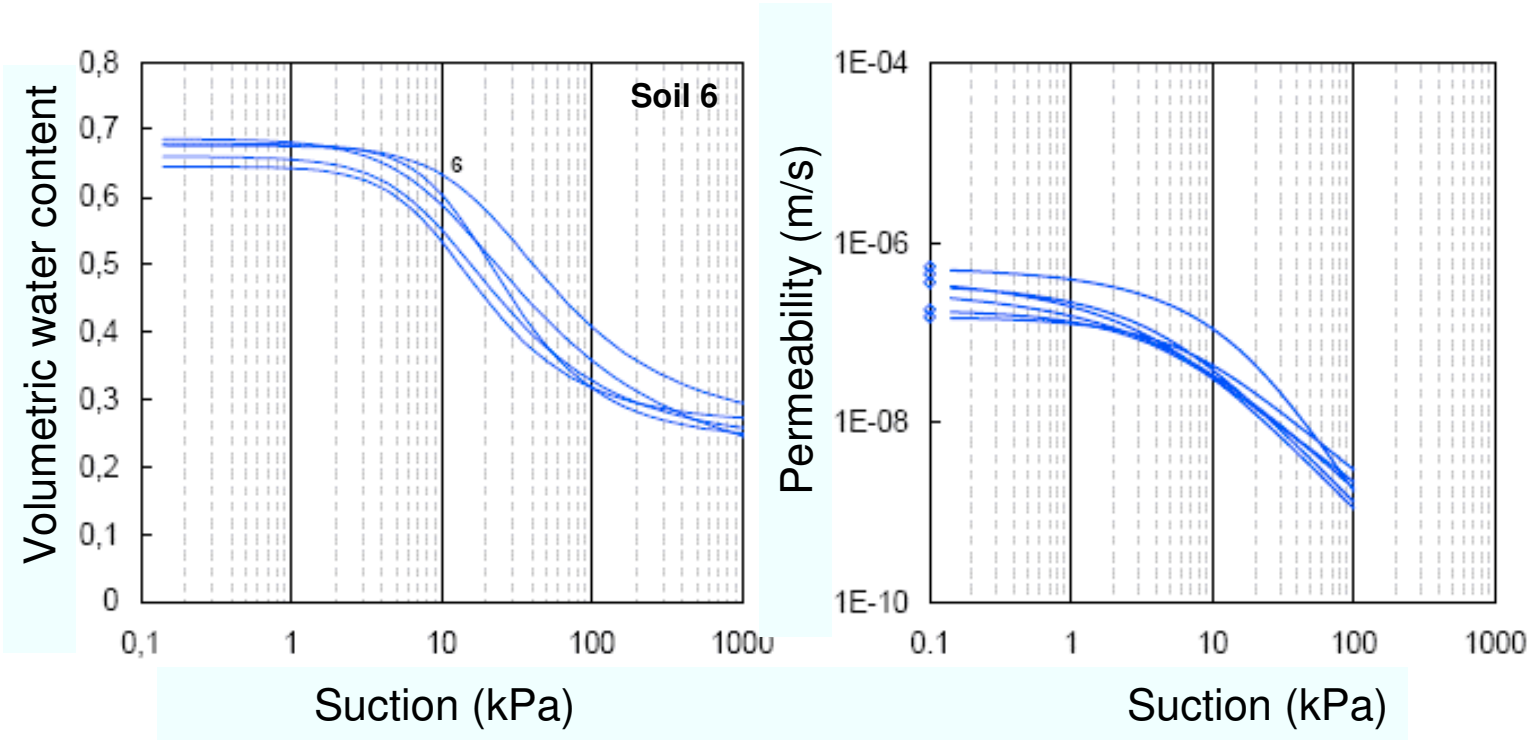

Fig. 1.7: Water retention curves obtaining in drying conditions, soil 6 and Permeability curve in drying conditions, soil 6 (Papa, 2007)

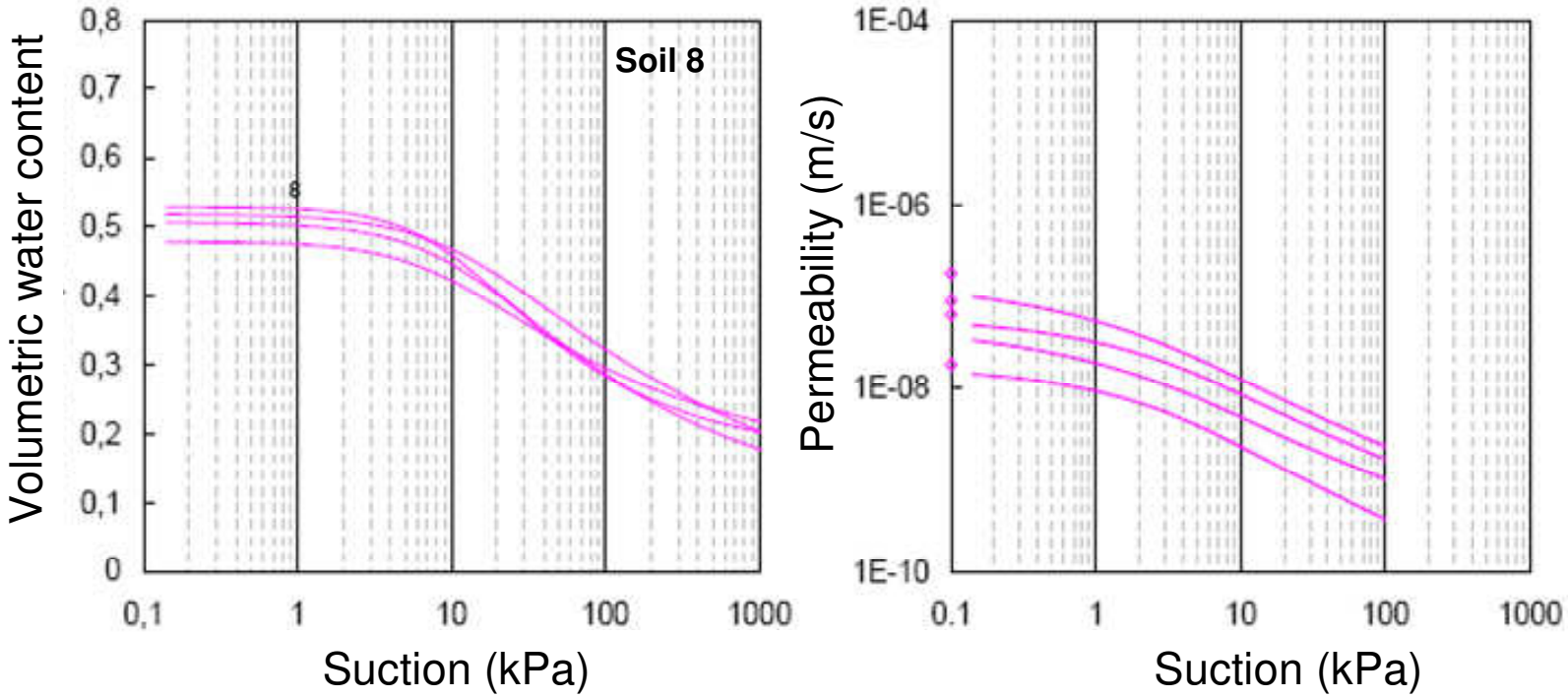

Fig. 1.8: Water retention curves obtaining in drying conditions, soil 8 and Permeability curve in drying conditions, soil 8 (Papa, 2007)

1.4.1.3 Mechanical characterization

The results of 48 stress-path controlled triaxial compression tests performed on undisturbed specimens previously saturated in the triaxial cell are available in the PhD thesis of Papa 2007. These tests were carried out on all the studied soils, apart the soils 3 and 5 (pumices of Avellino and Ottaviano). By contrast, 9 suction-controlled tests on naturally unsaturated undisturbed specimens were executed only on soil 4.

1.4.1.3.1 Mechanical characterization in saturated conditions

Triaxial tests on saturated specimens consisted of the following phases: saturation under minimal effective confining stress (≈2 kPa) by means of back-pressurising and upward flushing with de-aired water; isotropic compression; shearing. The shearing phases were performed either in drained or undrained conditions at constant mean stress (p or p' equal to

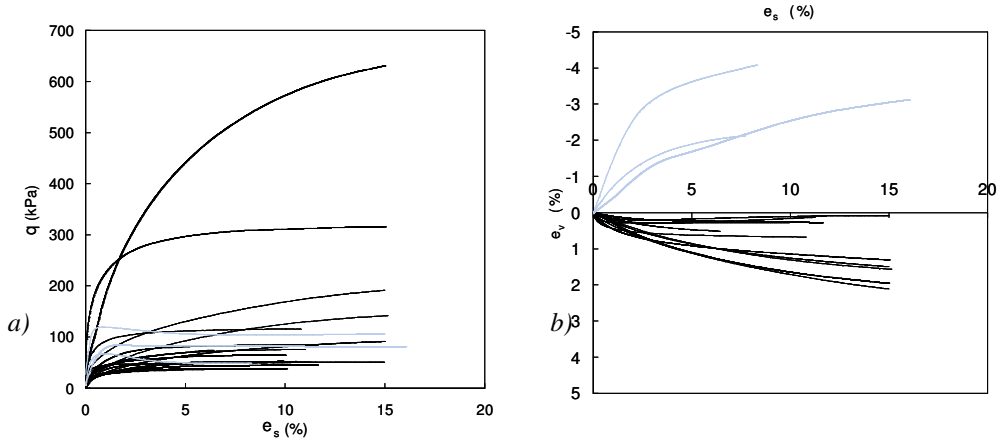

Figure 1.9. Mechanical behaviour of soil 4 in saturated triaxial compression tests (black lines for normally consolidated specimens, gray lines for overconsolidated specimens): a) deviator versus shear strain, b) volumetric strain versus shear strain (Papa, 2007)

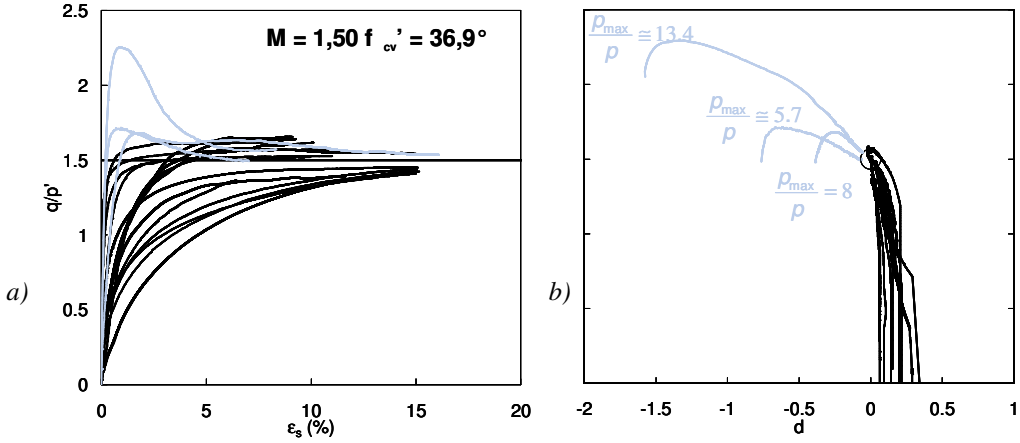

Figure 1.10. Representation of saturated tests on soil 4 in terms of stress obliquity ratio as function of both deviatoric strain and dilatancy (Papa, 2007).

30, 50 and 70 kPa) or at constant confining stress (σ_r or σ_r' equal to 30, 50 and 70 kPa).
The isotropic compressions were completed at a loading rate of 5 kPa/hours. Some tests on soil 4 were performed on specimens artificially overconsolidated by isotropic compression up to $p' = 400$ kPa and subsequent unloading to $p' = 30$, 50 and 70 kPa. The drained shearing phases were carried out in strain-controlled conditions at a strain rate of 0.1 %/hours.

Hence, by evaluating the results of the triaxial tests in saturated conditions, it is possible to asses: the soils 1, 2 and 4 showed a highly contractive and ductile behaviour in all the tests, the soil 6 behaved as brittle and rather dilative in tests executed under a mean effective stress equal to 30 kPa and as ductile and contractive in tests performed at higher stress levels. Finally, soils 7 and 8 behaved brittly in the entire stress range.
Results of triaxial compression tests on soil 4 are reported in *Fig. 1.9 ÷ 1.10* in terms of deviatoric stress q ($= \sigma_a - \sigma_r$) and volumetric strain ε_v as functions of shear strain ε_s [$= 2/3 \cdot (\varepsilon_a - \varepsilon_r)$]. The black lines in the *Fig. 1.9* refer to tests on normally compressed specimens; the grey lines refer to tests on overconsolidated specimens. Results in *Fig.1.9* shows as the strain level reached in the tests on normally consolidated specimens was indeed insufficient to mobilize the critical shear strength due to the highly ductile behaviour showed by the investigated soils. Hence a different procedure was adopted to identify the critical state line in the p', q plane. The results were plotted in terms of stress obliquity ratio η ($= q/p'$) as function of both deviatoric strain ε_s and dilatancy d ($= d\varepsilon_v/d\varepsilon_s$). As a matter of fact in the ε_s, η plane all test should converge asymptotically towards the same horizontal line representative of the critical value M of the stress obliquity ratio as the deviatoric strain increase but the same tests in the plane d, η should tend to an unique point laying on the η axis corresponding to the critical state condition $d = 0$. The described representation of test on soil 4 is reported in *Fig. 1.10.* The value of M is clearly identified in the diagram; in particular it resulted $M = 1.5$.

Some of the experimental results are summarised in *Fig. 1.11a*: for each test deviatoric stress q at "near" critical state is reported as a function of mean effective stress p' [$= 1/3(\sigma_1 + 2\sigma_3) - u_w$]. Experimental points lay in quite a narrow area bounded by the critical strength envelopes of soil 2 and 7; it is worth noting that the critical friction angles range from 36.2° to 40.3°. Furthermore in Fig. 1.11b final conditions of each TXT test are reported in terms of void ratio as function of *logp'*. In the same diagram a tentative identification of critical state line is reported for soil 1, 2, 4 and 6 only.

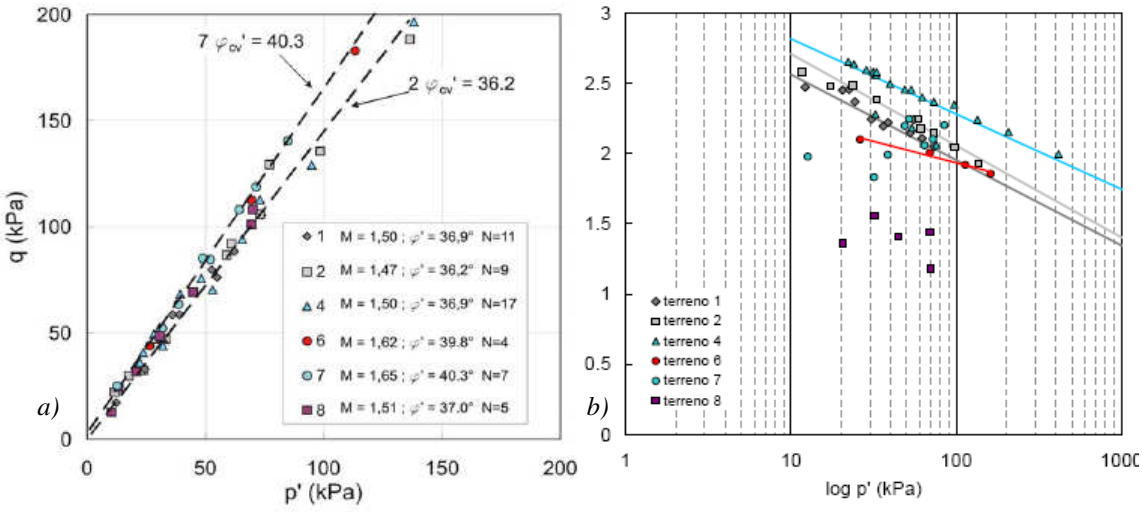

Figure 1.11. Critical state condition of all the investigated soils: a) deviatoric stress versus effective stress; b) void ratio versus logarithm effective stress (Papa, 2007)

1.4.1.3.2 Mechanical characterization in unsaturated conditions

Triaxial tests on natural unsaturated specimens of soil 4 were carried out by means of a stress-path and suction-controlled triaxial apparatus (*Aversa & Nicotera, 2002*).

Each test consisted of the following phases: measurement of the initial suction by means of the axis translation technique; equalisation to an assigned suction value; isotropic compression at constant suction; shearing at constant suction (6 kPa, 12 kPa and 20 kPa) and constant mean net stress (30 kPa, 50 kPa and 70 kPa). Only one test was performed on an artificially overconsolidated specimens (isotropic compressed up to $p_{net} = 650$ kPa and subsequently unloaded to $p_{net} = 50$ kPa).

The results of the suction-controlled triaxial tests are reported in *Fig. 1.12* in terms of deviatoric stress q and volumetric strain ε_v as functions of shear strain ε_s. In *Fig. 1.12* the stress strain curve corresponding to the same mean net stress p_{net} $[= 1/3(\sigma_1+2\sigma_3)-u_a]$ but to different values of the matric suction s $(= u_a-u_w)$ can be compared to each other as well as to three triaxial tests on a saturated specimen carried out at equivalent values of effective mean stress p'. The maximum deviatoric stress reached in each constant suction test is much higher than that recorded in the corresponding test on the saturated specimen. However, a relationship between the deviatoric stress and the value of matric suction is not clearly recognizable, showing that matric suction is not suitable, as an independent stress variable, to describe the shear strength of a partially saturated soil.

The comparison between the volumetric strain recorded in suction-controlled triaxial tests and triaxial tests on saturated specimens is reported in Fig. 1.12b. It is evident that the unsaturated specimens behave as more contractive than the saturated one at a similar stress state.

Nevertheless, it must be observed *(Fig. 1.12b)* that at the end of the tests corresponding to a

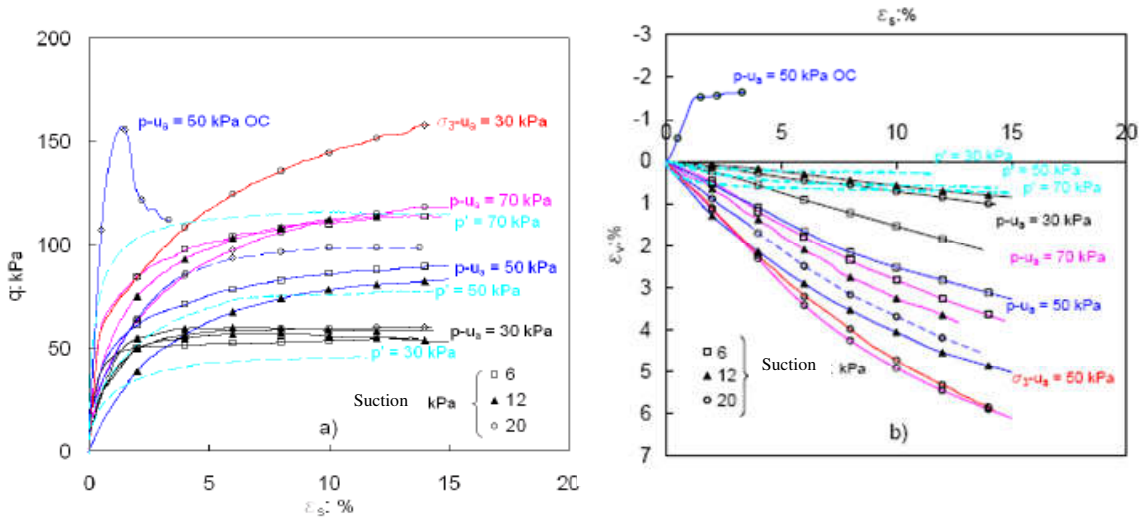

Figure 1.12. Mechanical behaviour of soil 4 in unsaturated triaxial compression tests: a) deviator versus shear strain, b) volumetric strain versus shear strain(Papa, 2007)

shear strain value of about 15% the volumetric strain of the unsaturated specimens was still rising while that of the saturated specimens was almost "stationary". Hence the deviatoric stress recorded at the end of the suction-controlled test may well be slightly smaller than the corresponding critical one.

In *Fig. 1.13a* the final value of the deviatoric stress recorded in each test is reported as a function of mean net stress and compared to the critical state line inferred for the saturated material. The experimental points corresponding to suction-controlled triaxial tests lie well above the saturated critical state line, indicating the matric suction effect on critical shear strength. Nevertheless, the shear strength increment cannot be justified by a linear dependence on matric suction as proposed by a number of authors (e.g. Fredlund & Morgenstern 1977). In *fig. 1.13b* the final value of the void ratio recorded in each test in saturated (black points) and unsaturated conditions (blue points) is reported as a function of mean net stress and compared to the normal compressive line, NCL, inferred for the saturated material and unsaturated conditions at suction of 20 kPa.

On the contrary, a better interpretation can be achieved by representing the data in terms of mean *Bishop stress* (p'):

$$p' = \frac{1}{3}\cdot\left(\sigma_1 + 2\cdot\sigma_3\right) + S_r \cdot s \qquad (1.1)$$

as originally proposed by Jennings (1960) and subsequently adopted by others (Jommi 2000; Gallipoli et al. 2003). This representation is proposed in *Fig. 1.14a*: the experimental data seem to be arranged along a single envelope; moreover, this envelope is well described by the same line adopted for representing the critical state of the saturated soil. In *fig. 1.14b* the final

value of the void ratio recorded in each test in saturated (black points) and unsaturated conditions (blue points) is reported as a function of mean *Bishop stress* ($p^{\prime}$) and compared to the normal compressive line, NCL, inferred for the saturated material and unsaturated conditions at suction of 20 kPa.

This result confirms that the stress state acting in unsaturated soils can be accurately represented only if the adopted stress variables take into account both matric suction and degree of saturation (e.g. Nuth & Laloui 2007).

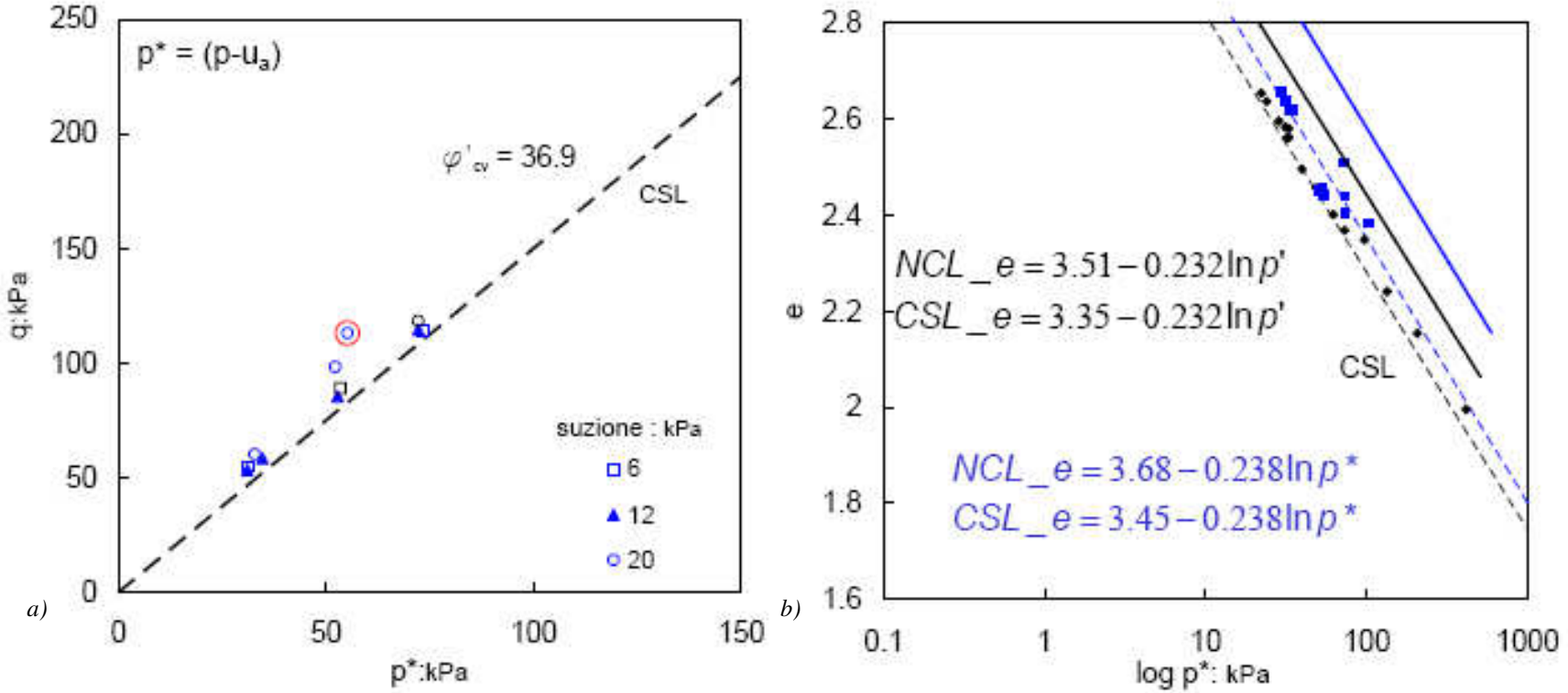

Figure 1.13. Critical shear strength of soil 4 from suction-controlled triaxial tests by net stress interpretation in the plan q, and p a); in the plan e, log p* b); (Papa, 2007)*

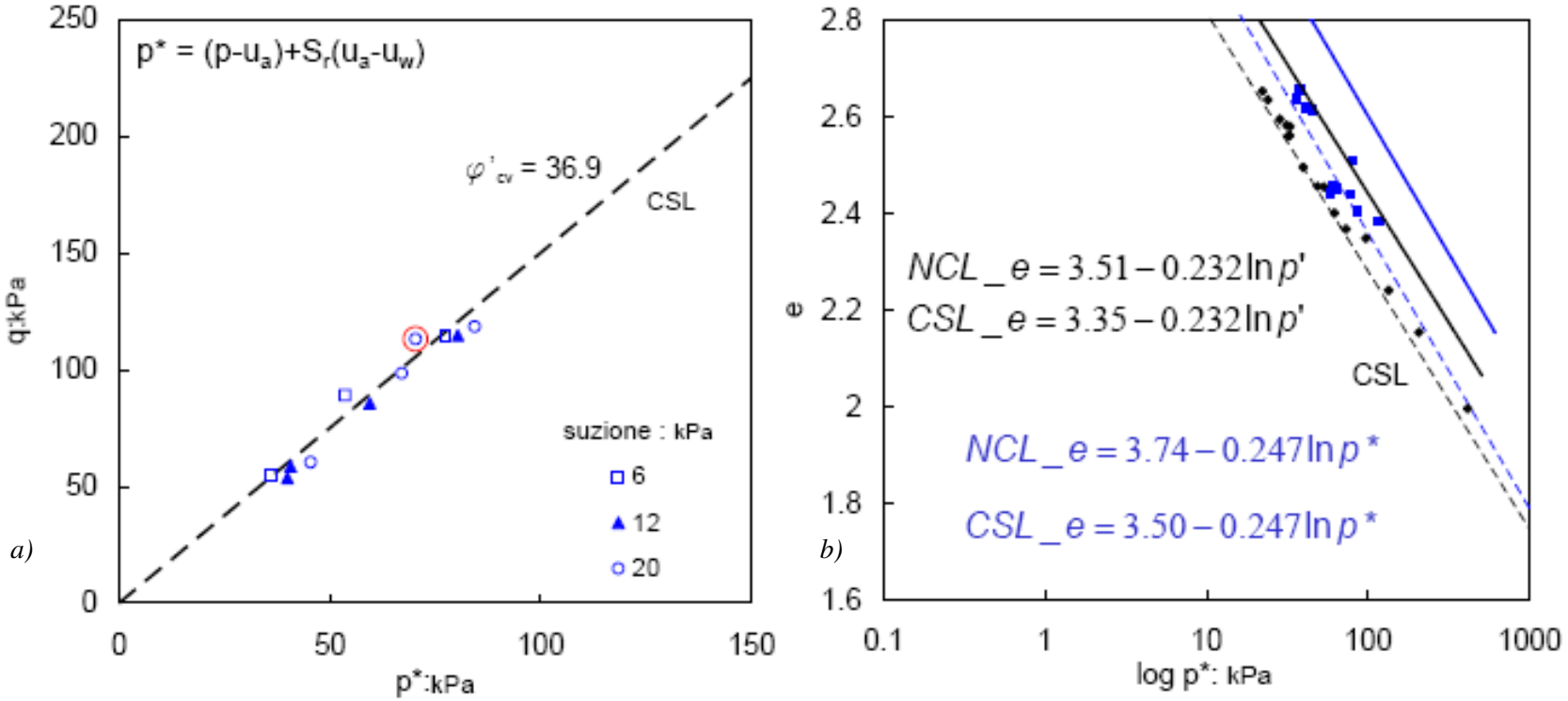

Figure 1.14. Critical shear strength of soil 4 from suction-controlled triaxial tests by Bishop stress interpretation in the plan q, and p a); in the plan e, log p* b); (Papa, 2007)*

Chapter 2

Mechanical Behaviour and Constitutive Models for Partially Saturated Soils

2.1 Synopsis

This chapter is subdivided into two main parts. The first part deals with the basic features of the mechanical behaviour of partially saturated soils. Essentially the stress variables, the volume change behaviour and the shear strength are introduced. In the second part the constitutive modelling of the mechanical behaviour of such soils is reviewed. In particular the Barcellona basic model is presented.

2.2 Mechanical behaviour

2.2.1 Stress state variables

One of the first attempts to express the mechanical behaviour of the unsaturated soils was the relationship proposed by Bishop (1959):

$$\sigma' = \sigma - u_a + \chi(u_a - u_w) \tag{2.1}$$

Where σ is the total tension, u_a the air pressure, u_w the pore water pressure, σ' the effective stress and the parameter χ is a function of the degree of saturation, S_r. In particular the parameter χ is null for S_r = 0 and is equal to one for S_r = 1. This means the expression proposed by Bishop is reduced to that of Terzaghi at fully saturation. The evolution of the parameter χ for intermediate values of degree of saturation, S_r, is then determined experimentally.

Jennings and Burland (1962) objectioned to the validity of the Bishop approach (2.1) because

of the experimental evidence regarding the compressibility of the unsaturated soils. In particular, the expression (2.1) was not able to predict the collapse when the strong decreasing of suction occurs (wetting) at constant mean net stress. However, in addition to the Bishop expression, in the same period there were other expressions based on the same approach (Donald, 1956; Croney, 1958; Aitchison, 1961; Richards, 1966).

Burland (1964 and 1965) concluded that the tension effective stress approach could not be formulated in the case of the partially saturated soils and hence, the mechanical behaviour must be described using two independent stress variables: $\sigma - u_a$ and $(u_a - u_w)$.
Also Aitchison (1967) reached the same conclusions.

In the following years several authors employed the approach of independent stress variables to plot the results of compression tests on partially saturated soils. Fredlund and Morgenstern (1977) concluded that the mechanical behaviour of unsaturated soils could be described by any two of the three variables, $\sigma - u_a$, $\sigma - u_w$, $(u_a - u_w)$. The most common choice is to use the net total stress, $\sigma - u_a$, and the suction, $(u_a - u_w)$, as independent variables. This approach used first by Coleman (1962) is the main basis for the development of the constitutive models.

2.2.1.1 The influence of the hydro-mechanical coupling on the stress variables

The behaviour of the unsaturated soils is influenced by the hydraulic hysteresis due to the water flow in or out going from the specimen. This phenomena is very clear when the retention curve of a soil is expressed in terms of degree of saturation (*Fig. 2.1*). In fact it is well known that before observing a degree saturation smaller than one, significant values of suction (less than the air entry value) must be applied on the boundary of the specimen. Conversely, if the suction applied to a unsaturated soil is reduced to zero, the degree of saturation can remain significantly below unity. Hence, this hydraulic hysteresis influences the effect of suction on the soil skeleton.

A method to take into account this effect would be to consider the degree of saturation as a third independent variable (as implicitly proposed by Toll, 1990) or within a stress variable. According to the second hypothesis, $\sigma - u_w$ and $(1 - Sr)(u_a - u_w)$ could be the two variables to use. Indeed, the figure 2.1 shows that the parameter $(1 - Sr)(u_a - u_w)$ can have different values for both samples B and D which have the same value of σ, (u_w), (u_a) but different degree of saturation. Moreover, this parameter is nil at saturation, without taking into account the suction applied smaller than the air entry value.

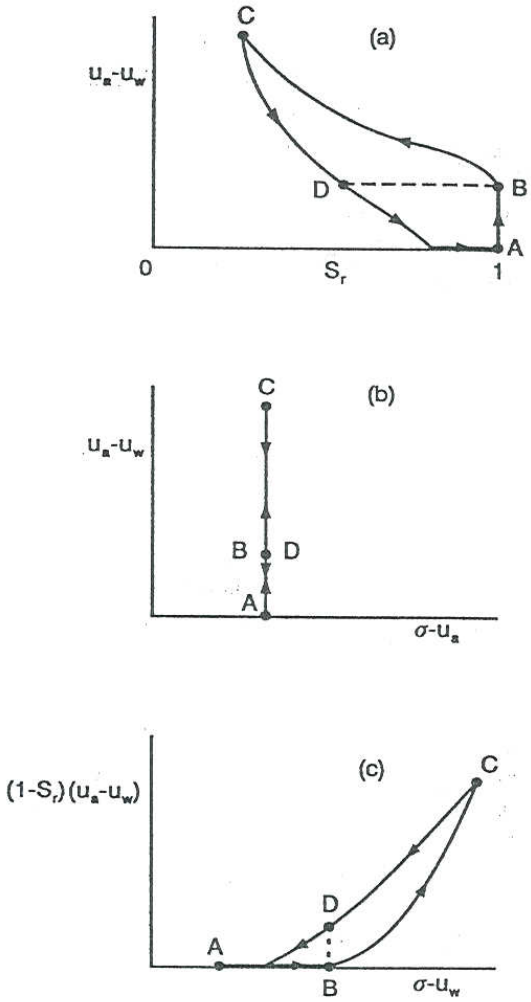

Figure 2.1: Influence of the hydraulic hysteresis in a cycle of wetting-drying at constant mean net stress (Wheeler and Karube, 1996)

Other examples of the degree of saturation as a third variable is provided by work of Karube, Kato, Hamada, and Honda (1995) and Kato, Honda and Karube, Fujiwara (1995).

S.K. Vanapalli et al., (1996), provide in their work a relationship between the retention curves and the shear strength of unsaturated soil considering the effect of suction too. They emphasize that the low values of matric suction (i.e. a high degree of saturation) increase the effective stress and hence contribute to increase the shear strength. This condition persists until when the soil starts to desaturate. Therefore the increase of the shear strength provided by the suction may be connected to the water area dimensionless over the total water area available in the soil. Hence, the water area normalized is defined as:

$$a_w = \frac{A_{dw}}{A_{tw}} \tag{2.2}$$

where A_{tw} is the total area corresponding to the fully saturation, and A_{dw} the area of water corresponded to a given value of the degree of saturation.
Moreover since there is a similarity between the water area normalized, a_w and the volumetric water content normalized, $\Theta = \frac{\theta}{\theta_s}$, the following relationship is proposed:

$$a_w = (\Theta)^k \tag{2.3}$$

Where k is a parameter fitting used to obtain the best match between the values measured and estimated. Ultimately, therefore, the authors proposed this relation as the equivalent effective stress:

$$\sigma'_{eq} = (\sigma - u_a) + \Theta^k (u_a - u_w) \tag{2.4}$$

Oberg and Sallfors (1997), proposed to replace in the Bishop relation (2.1) the parameter χ, with the ratio between the area of the pores occupied by the water and the total area, based on a simple analytic approach assuming a soil composed of ideal spheres. In this way the effective equivalent stress can be defined:

$$\sigma'_{eq} = \left(\sigma - \frac{A_w}{A_{tot}} u_w - \frac{A_a}{A_{tot}} u_a \right) \tag{2.5}$$

Where $\frac{A_w}{A_{tot}}$ (corresponding to χ) is the percentage of pore area filled by water and $\frac{A_{air}}{A_{tot}}$ is that filled by the air. Such relationships can, with reasonable accuracy, be replaced respectively, by Sr and (1-Sr). For an ideal soil, the variation of $\frac{A_w}{A_{tot}}$ with the degree of saturation is shown in *Fig. 2.2*.

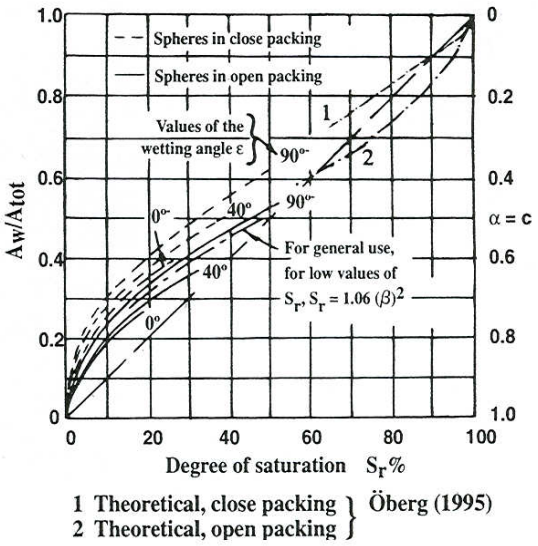

Figure 2.2: Relation between the $\frac{A_w}{A_{tot}}$ *and degree of saturation for the ideal soil*

It is also clear to the authors that the geometry and microstructure of a real soil is much more complex than the model used. In fact, for very fine-grained soils there is the double porosity which consists of two different classes of pores: the intra-aggregate pores (free water), inter-aggregate pores (meniscus). It follows that when the suction increases in a fine-grained soil, the water goes out from the larger pores (intra-aggregate) while the smaller pores (inter-aggregate) are not initially affected. Increasing the suction, the pores larger continue to desaturate and the ratio $\frac{A_w}{A_{tot}}$ continues to decrease. However the water content, and the relative degree of saturation Sr, remain high due to the presence of water between the inter-aggregates. Therefore, the soil has a high degree of saturation for the small value of suction and the function χ is well below the line χ = Sr, as also is highlined by several authors fig. 2.3 (Bishop et al., 1960, Wu et al., 1984). It follows that this approach is valid for Sr high, at least more than 50%, and for clay soils.

Khallili and Khabbaz (1998) have extended the Bishop equation (2.1) to predict the shear strength of unsaturated soil assuming as parameter χ a constant empirical value equal to:

$$\chi = \left\{ \frac{(u_a - u_w)_f}{(u_a - u_w)_b} \right\}^{-0.55} \tag{2.6}$$

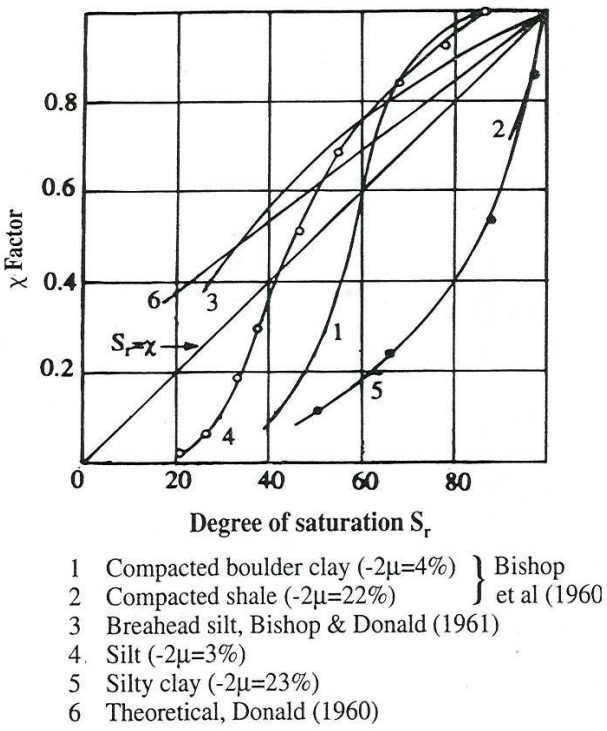

Figure 2.3: Relationship between X and Sr for different soils

Where $(ua - uw)_f$ is the suction in the sample at failure, $(ua-uw)_b$ is the air entry value and the apex η is assumed to be -0.55 based on data available in literature for 13 different soils.

2.2.1.2 Recent developments

Jommi (2000) shows that the constitutive model for unsaturated soils, the choice of stress variables often plays a key role. Therefore she defines in her model a single stress variable called *average soil skeleton stress*, which represents the difference between the total normal stress and the fluid pressure weighed on the degree of saturation Sr:

$$\sigma_{eq}' = \sigma - Sr \cdot u_w - (1 - Sr) \cdot u_a \tag{2.7}$$

$$\sigma_{eq}' = \sigma - u_a + Sr \cdot (u_a - u_w) \tag{2.8}$$

The expressions (2.7) and (2.8) are the same of Oberg and Sallfors (1997), but they are not obtained by replacing χ with Sr. Moreover it is also useful note that the increase of suction can be considered equivalent to an increase of the mean stress. In fact, experimental evidence shows that, starting from saturated conditions, an increase of suction produces an increase of the shear strength and the shear and the volumetric stiffness.

Gallipoli et al. (2003) in their constitutive model accept the average soil skeleton stress proposed by Jommi, but introduce an additional variable, ξ, which takes into account the effect of cementation due to the suction (bonding – debonding effect). The magnitude of the bond effect is given by two contributions:
- number of menisci per unit volume of the solid fraction;
- the intensity of the normal force exerted from a single meniscus between two particles.
Hence the variable ξ is defined as the product of two factors: the degree of air saturation (1-Sr), and a function of suction, f (s):

$$\xi = f(s)\,(1\text{-}Sr) \tag{2.9}$$

The factor (1-Sr) takes into account the number of menisci per unit solid volume. The existence of a unique relationship between the value of (1-Sr) and number of menisci per unit solid volume is an assumption physically reasonable. However, the uniqueness is valid only for deformable solid skeleton and when each value of the degree of saturation corresponds to a particular arrangement of the particles. The function f(s) is instead assumed monotonically varying between 1 and 1.5 for suction values ranging between zero and infinity, respectively, (Fig. 2.4). In particular, this function expresses the ratio between the value of the stabilizing force at a given suction and the value of the stabilizing force at nil suction, assuming the menisci located at the contact between two identical spherical particles.
The presence of the menisci also provides a physical explanation that, at the same value of the average soil skeleton stress, the value of the voids ratio on the NCL in the unsaturated conditions is always greater than the value corresponding on the NCL in the saturated conditions. In according with the experimental observations, the authors in their model states that along the NCL in unsaturated conditions the relationship between the current void ratio

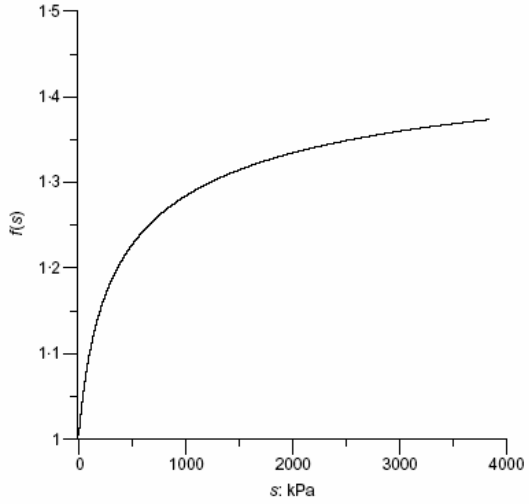

Fig. 2.4: Relationship between the forces inter-particles at a given suction s and at nil suction value, due to the meniscus located between two identical spheres (Gallipoli et al., 2003)

and that in saturated conditions at the same value of average soil skeleton stress is a unique function of the variable ξ, through the relation:

$$\frac{e}{e_s} = 1 - a \cdot \left[1 - \exp(b\xi)\right] \tag{2.10}$$

Where *a* and *b* are two fitting parameters.

Wheeler et al. (2003) proposed the same stress variable of Jommi. This variable represents the contribution respectively of the total normal stress, the air pressure and the pore water pressure. These contributions also produce qualitatively the same variations (tangential and normal) of forces between the contacts, so it is reasonable to assume that they can be combined into a single variable. However, this stress variable is not able to express the stabilizing effect provided by presence of the menisci. So the authors use as the second variable stress: the product of the porosity and suction:

$$s^* = n \cdot (u_a - u_w) \tag{2.11}$$

Toll (1990) and Toll et al. (2003) arrive at a definition of the stress variable very similar to that proposed by Vanapalli et al.(1995).

Following the most recent developments, Tarantino and Tombolato (2005) and Tarantino (2007), on the basis of many tests on compacted clay samples, adfirm that the meniscus exerts a negligible effect on the shear strength. Therefore they suggest a model for the shear strength only in terms of average skeleton stress, but using the degree of saturation of macro-pore, S_{rm}, instead of the total degree of saturation, S_r. In fact, if instead of the grains there are the aggregates of particles (as in the case of compacted clay), the degree of saturation which effectively controls the mechanical behaviour of aggregates is the degree of saturation of macro-pore.

2.2.2 Volume change behaviour

First the behaviour due to changes of suction at constant mean net stress will be considered, followed by the effect of isotropic loading at constant suction and finally the overall behaviour will be presented.

2.2.2.1 Volume change due to changes in suction

The volumetric behaviour of partially saturated soils due to changes in suction at constant mean net stress can be due to drying and wetting:

• Total volume changes due to drying

During the initial stages of drying from zero suction (path A to B in Figure 2.5), the soil remains fully saturated and the total volume change is equal to the pore water volume change, in fact at this stage the increase of suction is equivalent to an increase of isotropic total stress. The desaturation occurs beyond the value of suction, called the air entry value of suction, *sair*, it is largely dependent on the particle size for granular soils and on the pore size for clayey soils.

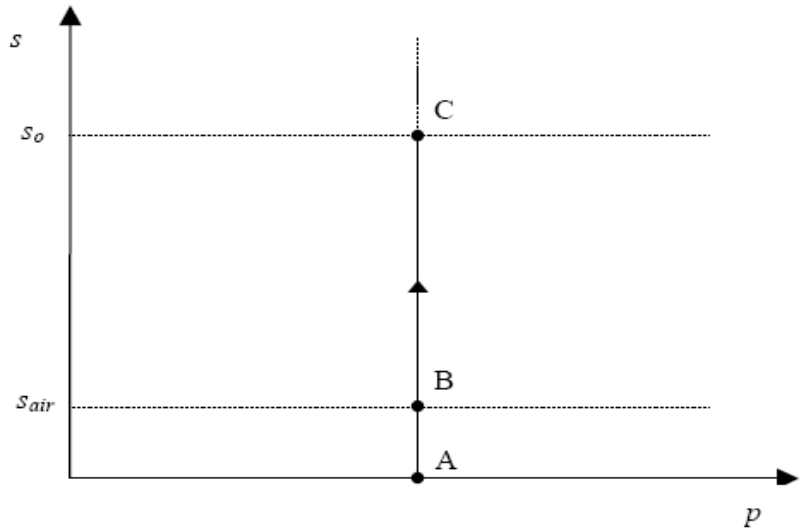

Fig.2.5: Drying path from zero suction

The reduction in total volume after desaturation (point B) is smaller than the pore water volume reduction (Fig.2.6). The total volume changes are expressed in terms of void ratio, e, and the water volume changes in terms of equivalent void ratio, *ew* (= volume of water / volume of solids). Line A to B is equivalent to the fully saturated normal compression line (NCL) and is followed by both the void ratio line (1) and the equivalent void ratio line (2) indicating that the total volume changes are equal to the water volume changes.

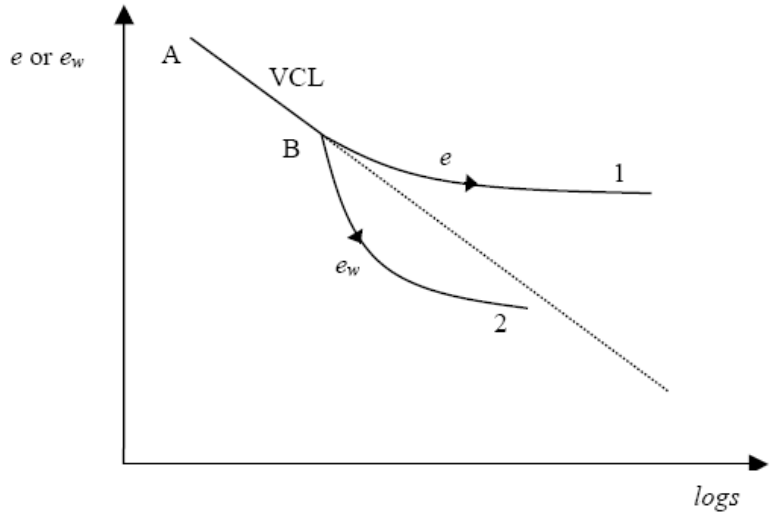

Figure 2.6: Volume changes due to drying (after Toll (1995))

After desaturation (point B) both the void ratio and the equivalent void ratio lines deviate from the NCL. Void ratio decreases slightly after point B while the water volume decreases sharply. Clearly the effects of suction changes are not equivalent to mean net stress changes once the soil has entered the partially saturated state.

It is generally accepted that for low plasticity soils volumetric changes during drying beyond desaturation are small and reversible. At high values of suction however plastic deformations may take place. Alonso et *al*. (1990) proposed that the yield suction (point C in Figure 2.5), s_o, beyond which the soil is elasto-plastic, is independent of the confining stress and equal to the maximum previously attained value of suction. Wheeler & Karube (1996) suggested that yielding due to drying is only possible for partially saturated soils containing saturated clay packets. Chen et *al*. (1999), however, performed drying tests on compacted low plasticity loess which exhibited a distinct yield value of suction. The obtained yield suction was not however equal to the maximum previously attained value suction (as proposed by Alonso et *al*. (1990)). They argued that the value of the yield suction depends not only on the drying-wetting history but also on the initial soil density e_w. For high plasticity expansive soils, the volumetric deformations due to increasing suction (beyond point B in figure 2.5) can by large and irreversible.

• Total volume changes due to wetting

The most important features of partially saturated soil behaviour is the potential of collapse upon wetting. Alonso et *al*. (1987) stated that a partially saturated soil may either expand or collapse upon wetting if the confining stress is sufficiently low (expansion) or high (collapse), and that a soil could first expand and then collapse (initial expansion followed by collapse).

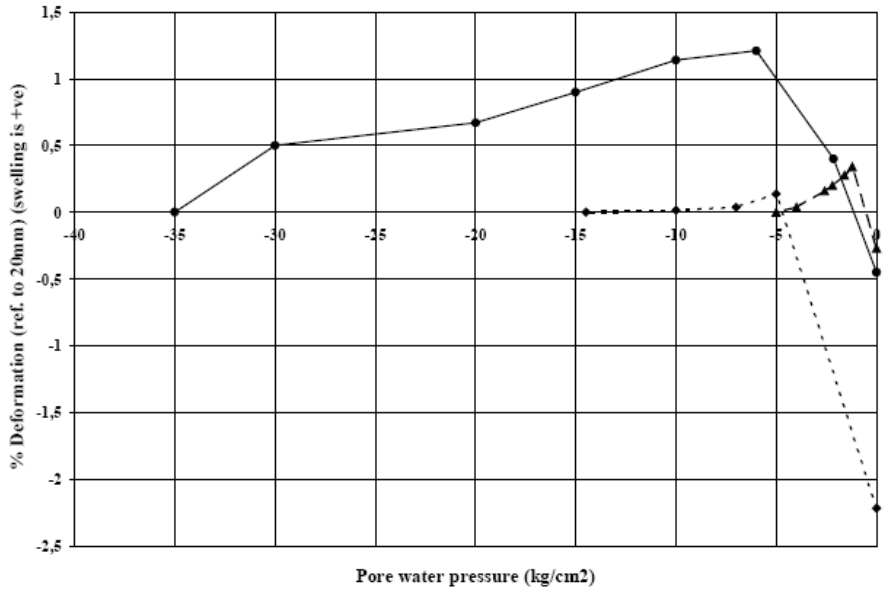

Figure 2.7: Swelling followed by collapse during wetting under constant load for three different initial values of tensile pore water pressure (after Escario &Saez (1973))

This behaviour has been reported amongst others by Escario & Saez (1973), Josa et *al*. (1987) and Burland & Ridley (1996). Figure 2.7 shows the initial swelling followed by collapse during wetting at constant load experienced by three samples of remoulded clay with different initial values of moisture content and tensile pore water pressure (Escario & Saez (1973)). Similar behaviour can be seen in the results of Josa et *al*. (1987)). In general if the stress state is not high enough to cause collapse upon wetting, the swelling experienced by a low plasticity non-expansive soil will be small and reversible. On the other hand high plasticity expansive clays can experience large irreversible volumetric strains.

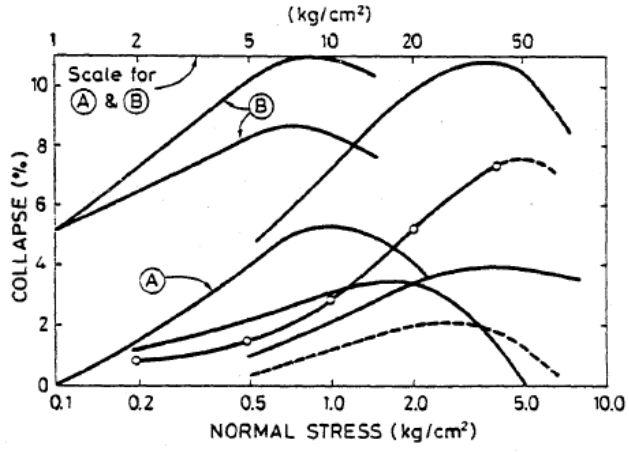

Figure 2.8: Relationship between collapse and normal stress for different soil types (after Yudhbir (1982))

The volumetric deformations experienced by a given soil when the stress state is such that collapse occurs upon wetting depend on the confining stress at which wetting (reduction of suction) takes place. Results presented by Matyas & Radharkrishna (1968), Booth (1975), Yudhbir (1982) and others indicate that for many soils the amount of collapse increases with confining stress at low stress regions, reaches a maximum and then decreases with stress becoming very small at high confining stresses (*Fig.2.8*).

• Water volume changes due to drying-wetting

Total volume changes for fully saturated soils are equal to the water volume changes since for the stress ranges relevant to engineering practice both water and solid phases are nearly incompressible and the volume changes are caused by inflow or outflow of water.
In the case of partially saturated soils the presence of a third phase (air) in the soil means that the water volume changes are no more equivalent to the overall volume change. In order to fully understand the behaviour of partially saturated soils both the overall and the water volume changes due to changes of stress and suction need to be defined. Water volume changes due to drying and wetting are usually investigated for unconfined conditions and are presented in the form of relations between volumetric water content, ϑ, degree of saturation, S_r, or gravimetric moisture content, w, and suction. These relationships are called water retention curves. Volumetric water content, ϑ, is the ratio of the volume of water to the total volume and is related to the other variables through the following relationships:

$$\theta = \frac{S_r e}{1+e} = S_r n$$

$$\theta = w \rho_d / \rho_w \qquad (2.12)$$

where e is the void ratio, n is the porosity, ρ_d is the dry density and ρ_w is the water density..
Three stages can be identified during drying. The capillary saturation or boundary effect stage where the soil remains fully saturated, the desaturation or transition stage and the residual stage. Similar stages can be identified for the wetting phase.
An important feature of the water retention curve is the hysteresis observed between drying and wetting behaviour. Hysteresis means that a soil can be in a very different state for the same value of suction and therefore have different properties depending on the drying-wetting history. Many researchers have proposed empirical mathematical expressions for the soil-water characteristic curve (e.g. Burdine (1953), Gardner (1958), Maulem (1976), van Genuchten (1980), Fredlund & Xing (1984)). Most of these ignore hysteresis and assume that soil moves along the same curve during drying and wetting. In particular the equation proposed by van Genuchten (1980), is given by:

$$\theta = \left[\frac{1}{1+\left(s_{eq}\cdot\psi\right)^{\xi}}\right]^{\omega}\left(\theta_s-\theta_r\right)+\theta_r \tag{2.13}$$

where, ξ, ω and ψ are fitting parameters, and the subscripts *r* and *s* denote residual and saturated conditions, respectively.

2.2.2.2 Volume change due to changes in confining stress

The main effects of suction on the volumetric response of partially saturated soils to changes in the confining stress are the following:

• Suction contributes to an increase in the isotropic yield stress, p_o.

Figure 2.10 shows the stress paths followed by compacted speswhite kaolin samples in the mean net stress (p) – suction (s) stress space as reported by Wheeler &Sivakumar (1995).

The samples were subjected initially to a pore pressure equalization stage from point A to different values of mean net stress and suction (points C0, C1, C2 and C3) and were subsequently consolidated under constant applied suction. The yield points observed during the consolidation stage are plotted on Figure 2.10b. The increase of the yield stress with suction is evident for the samples consolidated from points C1, C2 and C3. Samples consolidated from a fully saturated state (point C0) slightly deviated from the observed trend because yield had already occurred during wetting indicating that the fully saturated yield stress was even smaller.

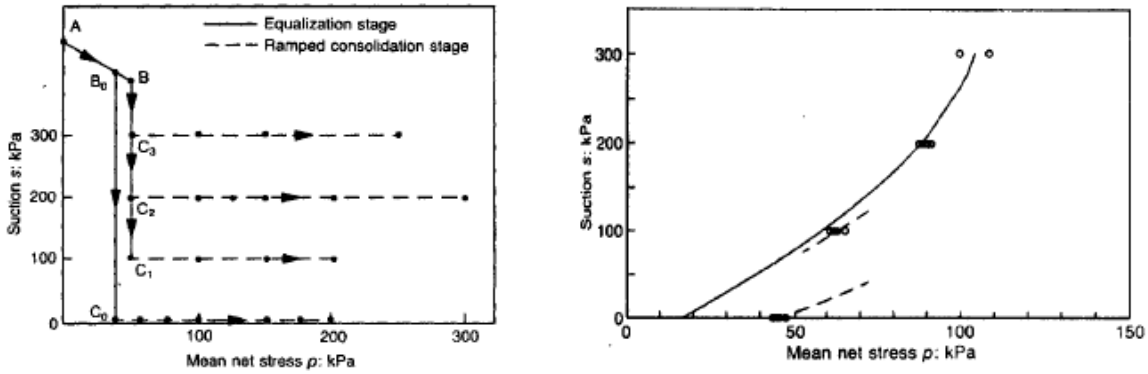

Figure 2.10: a) Stress paths, and b) yield points for compacted kaolin (after Wheeler & Sivakumar (1995))

• Suction influences the compressibility of partially saturated soils.

The pre yield (elastic) compressibility, κ, is commonly assumed for simplification to be independent of suction. However experimental data indicate that it may decreases lightly with suction. Figure 2.12 shows the influence of suction on the elastic compressibility coefficient, κ, and the elasto plastic (post-yield) compressibility coefficient, λ reported by Rampino et *al*. (2000). Parameter, κ, decreases only slightly with suction (approximately 9%). The parameter, λ, however, is largely affected by suction (approximately 38%). Josa (1988) reported a similar variation of λ with suction.

The amount of potential collapse due to wetting initially increases with confining stress, reaches a maximum value and then decreases. The amount of collapse in the e-log p space represents the difference between the partially and fully saturated isotropic compression lines (Figure 2.12).

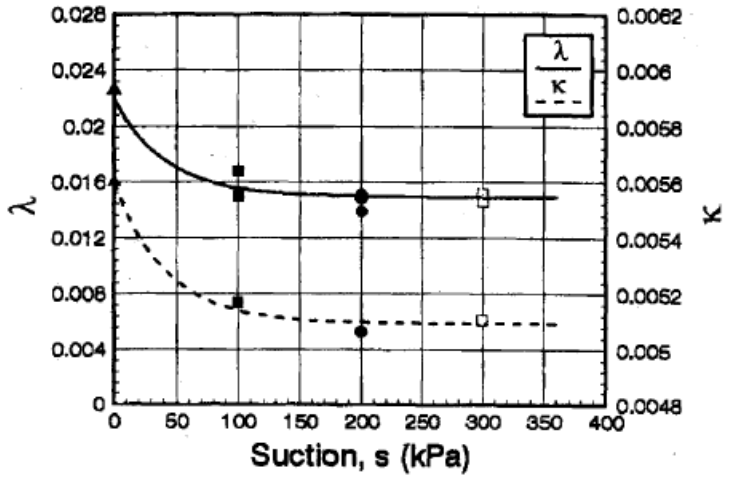

Figure 2.11: Influence of suction on parameters κ and λ (after Rampino et al. (2000))

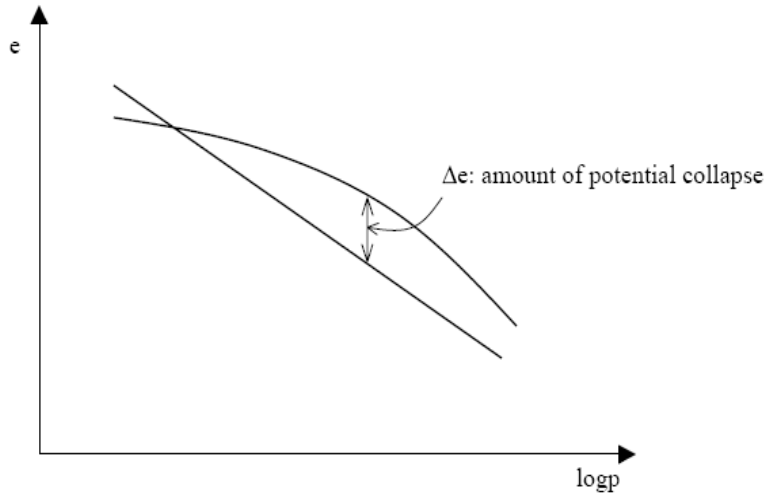

Figure 2.12: Partially and fully saturated isotropic compression lines.

The value of λ and its dependency on suction measured in laboratory experiments probably depends on the range of mean net stress at which the tests were conducted. As noted by Wheeler & Karube (1996) the increase of λ with suction seen in Figure 2.11 presumably implies that the stress range investigated by Wheeler & Sivakumar (1995) was above the value of p corresponding to the maximum collapse for the particular soil.

2.2.2.3 Volume change due to changes in both confining stress and suction

As mentioned in the previous sections the overall volume change behaviour of partially saturated soils is usually described as a function of net stress and suction. Bishop & Blight (1963) schematically related net stress and suction to void ratio, *e*. Subsequently researchers derived analytical expressions for the state surfaces relating void ratio and degree of saturation or water content to net stress and suction.
In the following the expressions proposed by Fredlund (1979) are presented:

$$e = e_o - C_t \log \frac{(\sigma - u_a)_f}{(\sigma - u_a)_o} - C_m \log \frac{(u_a - u_w)_f}{(u_a - u_w)_o}$$

$$w = w_o - D_t \log \frac{(\sigma - u_a)_f}{(\sigma - u_a)_o} - D_m \log \frac{(u_a - u_w)_f}{(u_a - u_w)_o}$$

(2.14)-(2.15)

where the *f* subscript represents the final stress state and *o* represents the initial stress state, C_t is the compressive index with respect to total stress, C_m is the compressive index with respect to suction, *w* is the water content, D_t is the water content index with respect to total stress, and D_m is the water content index with respect to suction. When the degree of saturation approaches 100%, C_t is equal to the conventional compressive index C_c and approximately equal to C_m.

2.2.3 Shear strength

In unsaturated soils the menisci increase the normal stress that acts between the contacts. This produces an increasing of the shear strength which reaches an asymptotic value, function of suction value. Therefore in a un-saturated soil the shear strength is a function of suction. For saturated soils, the model most used is the that of Mohr-Coulomb:

$$\tau = c' + \sigma' \tan\varphi' \tag{2.16}$$

Where c' is the effective cohesion and σ' is the effective stress.
If we refer to a single variable stress, it is immediate to extend the Mohr-Coulomb criterion to unsaturated soils. It is enough to replace the effective stress with one of the possible expressions introduced in the previous paragraphs (Jommi, (2000), Gallipoli et al. (2003); Wheeler et al. (2003)).

To take into account the effect of suction on shear strength, Fredlund et al. (1978) proposed the following extension of the Mohr-Coulomb model for the unsaturated soils:

$$\tau = c' + (\sigma - u_w) \cdot \tan\phi' + (u_a - u_w) \cdot \tan\phi'' \tag{2.17}$$

or:

$$\tau = c' + (\sigma - u_a) \cdot \tan\phi' + (u_a - u_w) \cdot \tan\phi_b \tag{2.18}$$

$$\tan\phi' = \tan\phi^b - \tan\phi'' \tag{2.19}$$

where c 'and φ' are the strength parameters in saturated conditions; φ'' is the friction angle representing the shear strength increase produced by an increase of suction when $(\sigma - u_w)$ is kept constant; ϕ^b is the friction angle representing the shear strength increase produced by an increase of suction when $(\sigma - u_a)$ is held constant.

Fredlund et al. (1987) and Gan et al. (1988) have also shown that the parameter ϕ^b varies with the suction: at saturated conditions and at nil suction it is equal to φ' until the suction applied reaches the air entry value. Beyond this value ϕ^b decreases until it reaches a constant value (fig. 2.13).

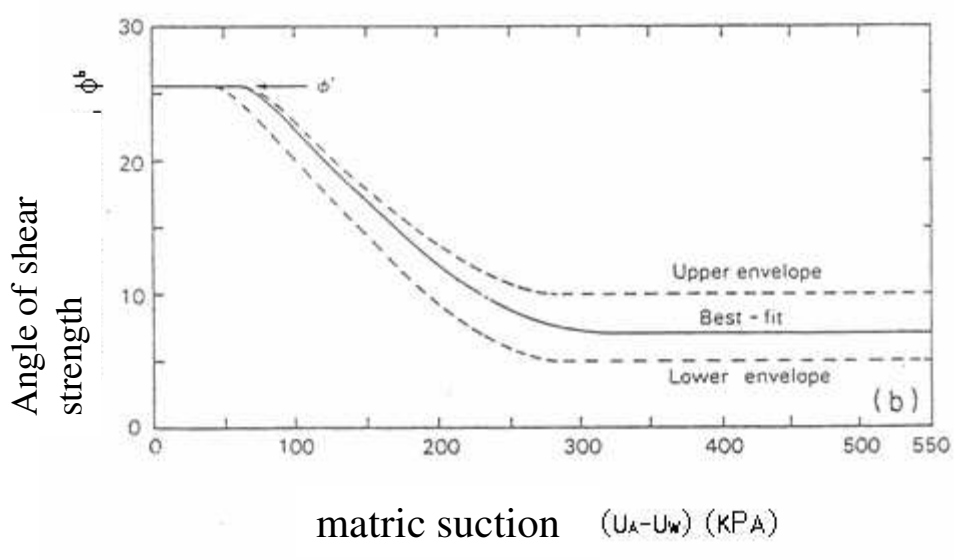

Fig 2.13: Influence of suction on the friction angle (Gan et al., 1988)

At saturation and at low values of suction (less than the air entry value) the water fills almost all the pores and a variation of suction has the same effect as a variation of the pore water pressure in a saturated soil. Therefore $\varphi b = \varphi'$. When the suction increases, the water goes out gradually from the pores and there are the menisci at the contact points between the particles only, the shear strength continues to grow but not indefinitely, in fact it reaches an asymptotic value. Consequently if the suction goes to infinity, $\tan \varphi_b$ becomes nil. Based on these considerations Wheeler (1997) suggests the following expression for the shear strength of unsaturated soil:

$$\tau = c' + (\sigma - u_a) \cdot \tan \phi' + f(u_a - u_w) \tag{2.20}$$

where f is a nonlinear function of suction.

Lamborn (1986) proposed the following equation:

$$\tau = c' + (\sigma - u_a) \cdot \tan \phi' + (u_a - u_w) \cdot \theta_w \cdot (\tan \phi') \tag{2.21}$$

Where ϑ_w is the volumetric water content, non linear function of suction.

Vanapalli et al. (1995) expressed the contribution of suction to the shear strength in terms of $\frac{A_w}{A_{tot}}$:

$$\tau_{us} = (u_a - u_w) \cdot (a_w \cdot \tan \phi') \tag{2.22}$$

From which:

$$\tau_{us} = (u_a - u_w) \cdot (\Theta^k \cdot \tan \phi') \tag{2.23}$$

It follows that the increase of the shear strength due to suction, dτ, can be obtained by differentiating respect to the suction the previous expression. In particular we have:

$$d\tau_{us} = d(u_a - u_w)[(\Theta^k \cdot (\tan \phi'))] + (u_a - u_w) \cdot [d(\Theta^k) \cdot (\tan \phi')] \tag{2.24}$$

comparing the (2.24) with the relation proposed by Fredlund (1978):

$$\tan \phi^b = \frac{d\tau}{d(u_a - u_w)} = \left[(\Theta^k) + (u_a - u_w) \cdot \frac{d(\Theta^k)}{d(u_a - u_w)} \right] \cdot (\tan \phi') \tag{2.25}$$

Up to the air entry value the value of Θ is equal to one and there are not variation of $\frac{A_w}{A_{tot}}$.

Ultimately we have that the shear strength in unsaturated conditions is:

$$\tau = c' + (\sigma - u_a) \cdot \tan \phi' + [(\Theta^k) \cdot \tan \phi'](u_a - u_w) \tag{2.26}$$

The first part of the equation (2.26), $c' + (\sigma - u_a) \cdot \tan \phi'$, is the shear strength in saturated conditions, when the air pressure is equal to the pore water pressure. The second part of the equation (2.26), $[(\Theta^k) \cdot \tan \phi'](u_a - u_w)$, is the contribution of suction to shear strength .

Oberg and Sallfors (1997) proposed an equation to predict the shear strength in unsaturated conditions in the absence of clay. The equation proposed is the following:

$$\tau = c' + (\sigma - u_a) \cdot \tan \phi' + [Sr \cdot \tan \phi'](u_a - u_w) \tag{2.27}$$

where the parameter χ proposed by Bishop was replaced by the degree of saturation, S_r.

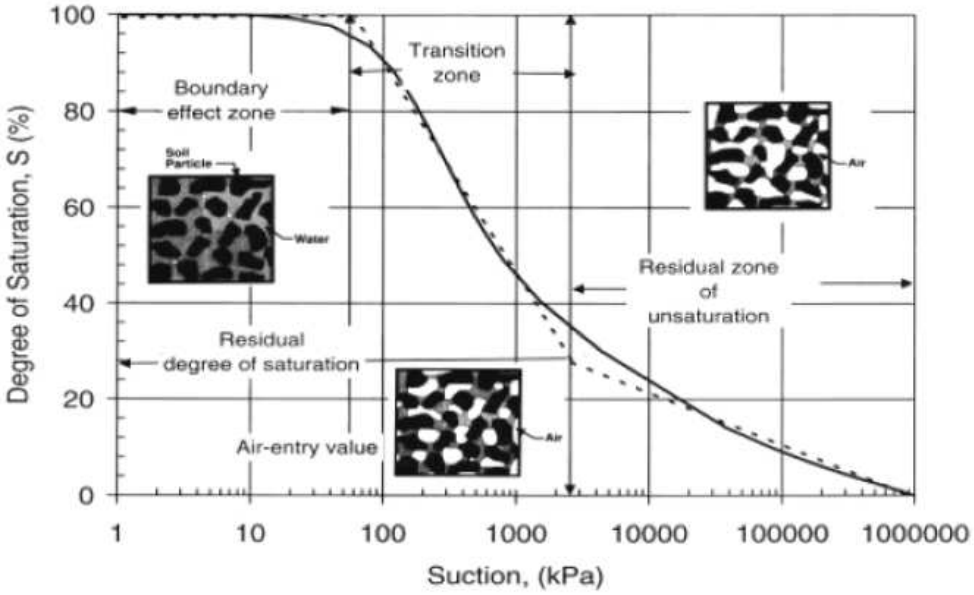

Figure 2.14: Retention curve at the transition zone (Vanapalli et al., 1996)

Moreover it is called as the transition zone the suction range between the air entry value and the value corresponding to the degree of saturation residue (Vanapalli et al.1996a). The characteristic curve in that area is linear in semi-logarithmic scale (Fig. 2.14).
Bao et al. (1998) proposed another equation to predict the shear strength in the transition zone taking into account the linear variation of the retention curve in that zone. In particular:

$$\tau = c' + (\sigma - u_a)\cdot \tan\phi' + \left[\tan\phi'\right](u_a - u_w)\left[\xi - \zeta \log(u_a - u_w)\right] \tag{2.28}$$

where:

$$\xi = \frac{\log(u_a - u_w)}{\log(u_a - u_w)_r - \log(u_a - u_w)_b}$$
$$\zeta = \frac{1}{\log(u_a - u_w)_r - \log(u_a - u_w)_b} \tag{2.29}$$

$(u_a - u_w)_r$ = suction at the residual value of the water content,
$(u_a - u_w)_b$ = suction at the air entry value

The parameter ξ represents the intercept on the horizontal axis and the parameter ζ the slope of the curve in the transition zone. The authors also suggest to use as an expression of the retention curve, the following expression:

$$\frac{(\theta_w - \theta_s)}{(\theta_s - \theta_r)} = \xi - \zeta \cdot \log(u_a - u_w) \tag{2.30}$$

Tarantino and Tombolato (2005) and Tarantino (2007), achieve that the contribution of suction to the shear strength, $\Delta\tau$, may be expressed in the following form:

$$\Delta\tau = \tau - (\sigma - u_a) \cdot \tan\phi' \tag{2.31}$$

where τ is the shear strength of the soil in unsaturated conditions, $(\sigma - u_a)$ is the net normal stress and $\varphi'$is the critical state angle in saturated conditions. For s < s_a (s_a = air entry value), the soil remains saturated and the shear strength is controlled by the sum of the effective stress and suction. It follows that the $\Delta\tau$ grows linearly with the suction , with a coefficient of proportionality equal to tanφ' (*Fig. 2.15*).

For s> s_a the soil desaturates and the increment of shear strength, $\Delta\tau$,has an increment less than linear up to assume a constant value. For the compressive soils, the air entry value is not constant but depends on the void ratio (Romero and Vaunat, 2000; Karube and Kawai, 2001).

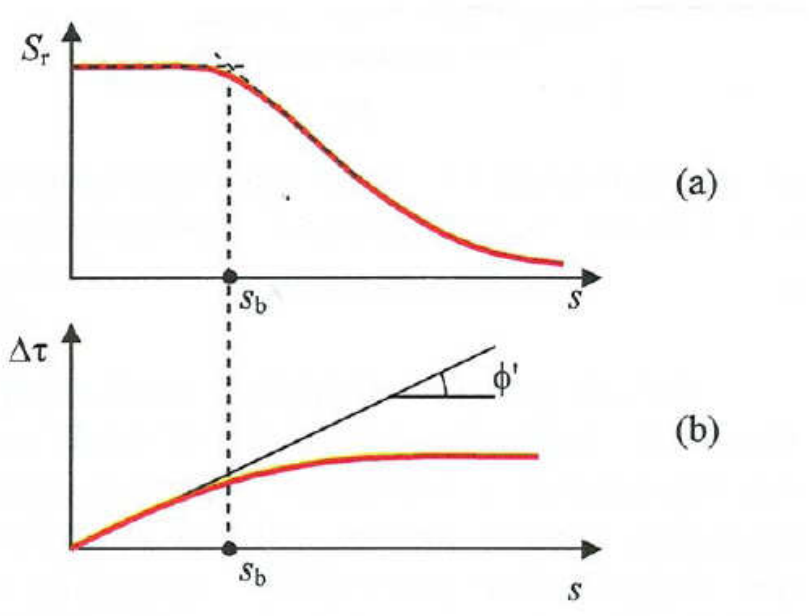

Figure 2.15 - Relationship between retention curve and shear strength (Tarantino, 2006)

2.3 Constitutive Models

One of the first elasto plastic constitutive models for partially saturated soils was the Barcelona Basic Model (Alonso *et al*. (1990)), based on the theoretical framework proposed by Alonso *et al*. (1987). This model was an extension of the Modified Cam-Clay model for fully saturated soils to partially saturated states through the introduction of the concept of the Loading-Collapse yield surface. The concept allows the reproduction of many important features of partially saturated soil behaviour, such as collapse upon wetting, and it is the basis upon which most other elasto plastic models. There are two main categories of elasto plastic models; expansive and non expansive models. Expansive soil (high plasticity clays) modelling is not discussed in the following. Some of the existing models for expansive soils are the models by Gens &Alonso (1992), Alonso et *al*. (1994) and Alonso et *al*. (2000). Non-expansive models for low plasticity soils can in turn be separated into two categories; total stress models, which use net mean stress and suction (or some form of equivalent suction) as stress variables, and 'effective stress' models, which use some definition of effective stress and suction or equivalent suction as stress variables. Three of the best known total stress models are presented in this section: the Barcelona Basic model by Alonso et *al*. (1990), the Josa et *al*. (1992) model and the Wheeler & Sivakumar (1995) model. Most elasto plastic constitutive models are based on critical state models for fully saturated soils. For this reason a brief description of the basic elements of critical state models will first be given.

2.3.1 Critical state models

Critical State soil mechanics theory was developed in the 1950's through the work by Drucker et *al*. (1957), Roscoe et *al*. (1958) and Calladine (1963). The first critical state models were the Cam Clay model (Roscoe & Schofield (1963) and Schofield & Wroth (1968)) and the modified Cam Clay model (Roscoe &Burland (1968)). A large number of constitutive models have been developed since within the Critical State framework. Most of these models are elasto plastic and require the following elements to be defined:

a) A yield function: $F(\{\sigma'\},\{k\}) = 0$, where $\{\sigma'\}$ is the stress state and $\{k\}$ are state parameters. The yield function represents the surface, which separates purely elastic from elasto plastic behaviour. The projection of these two yield surfaces is shown in Fig. 2.16 and 2.17 .

b) A plastic potential function $P(\{\sigma'\},\{m\}) = 0$, where $\{m\}$ are state parameters. This function determines the relative magnitudes of the plastic strains at each point of the yield surface and also the position of the critical state line in the specific volume, v, mean effective stress, p', and deviatoric stress, J, space (fig.2.18). The critical state line is the line on the yield surface, along which the following condition is satisfied: $\frac{\partial P(\{\sigma'\},\{m\})}{\partial p_i'} = 0$, giving zero volumetric strains and infinite shear strains. The Cam Clay

and modified Cam Clay models assume a plastic potential function identical to the yield function.

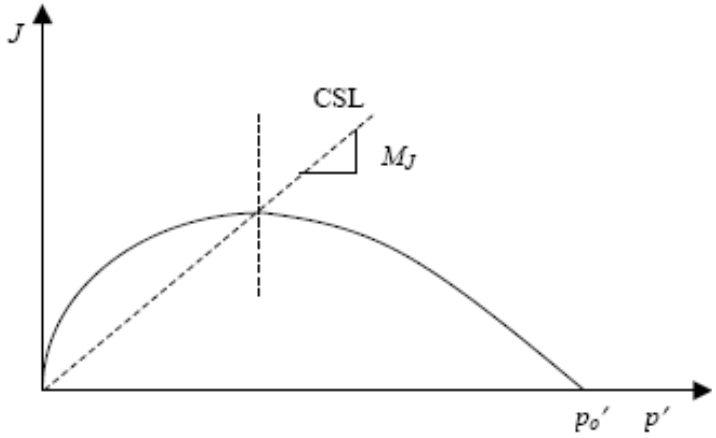

Fig. 2.16 : Projection of yield surface onto J – p' plane for Cam Clay

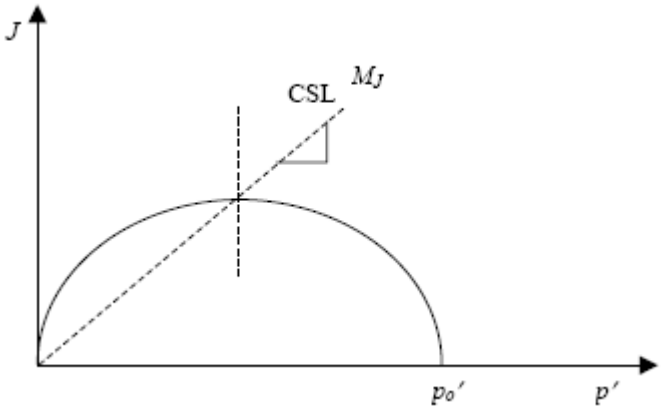

Fig. 2.17.: Projection of yield surface onto J – p' plane for modified Cam Clay

The six components of incremental plastic strain, $d\varepsilon_i^p$, are determined from the plastic potential function through a flow rule, which can be expressed as follows:

$$d\varepsilon_i^p = \Lambda \frac{\partial P(\{\sigma'\},\{m\})}{\partial \sigma_i'}$$

where Λ is a scalar multiplier which depends on the hardening/softening rule discussed below.

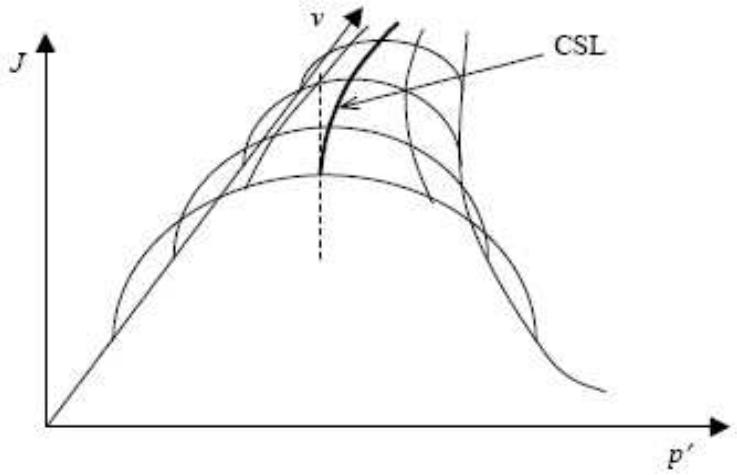

Figure 2.18: State boundary surface for modified Cam Clay

c) A hardening/softening rule, which determines the magnitude of the plastic strains.
d) Definition of the elastic behaviour within the yield surface. The volumetric elastic strains are given from the shape of the swelling lines.

2.3.2 Barcelona Basic Model

The Barcelona Basic model (Alonso et *al*. (1990)) is intended for partially saturated soils which are slightly or moderately expansive, such as partially saturated sands, silts, clayey sands, sandy clays and clays of low plasticity. The model is formulated in the (q, p, s) stress space, where q is the deviator stress, p is the net mean total stress, and s is the suction.

2.3.2.1 Formulation of model for isotropic stress states

The proposed variation of the specific volume, $v = 1 + e$, with the net mean total stress, p, and suction, s, along virgin and unloading-reloading stress paths is shown in Figures 2.18a, b. The virgin compression line (at constant s) is given by:

$$v = N(s) - \lambda(s) \ln \frac{p}{p_c} \tag{2.32}$$

where pc is a reference stress state for which $v = N(s)$. The unloading-reloading paths (at constant s) are assumed to be elastic:

$$dv = -\kappa \frac{dp}{p} \tag{2.33}$$

where κ is assumed to be independent of s.

Figure 2.18a shows the response to isotropic loading of a saturated sample (s =0) and a partially saturated sample. The saturated sample yields at a stress po (point 3), while the partially saturated sample yields at the higher stress po (point 1). If both points, 1 and 3, belong on the same yield curve in the (p, s) space (Figure 2.18b), the relationship between p_o and p_o* can be obtained by relating the specific volumes at points 1 and 3 through a virtual path which involves an initial unloading, at constant s, from point 1 to point 2, and a subsequent reduction in suction, at constant p, from point 2 to point 3:

$$v_3 = v_1 + \Delta v_p + \Delta v_s \tag{2.34}$$

The suction unloading (wetting) from 2 to 3 occurs in the elastic domain, so:

$$\Delta v_s = \kappa_s \ln \frac{s + p_{atm}}{p_{atm}} \tag{2.35}$$

where p_{atm} is the atmospheric pressure, and κ_s is the compressibility coefficient for suction changes within the elastic domain. p_{atm} is included in the above equation in order to avoid the

calculation of infinite strains as suction tends to zero.

The unloading from 1 to 2 also occurs in the elastic domain, so:

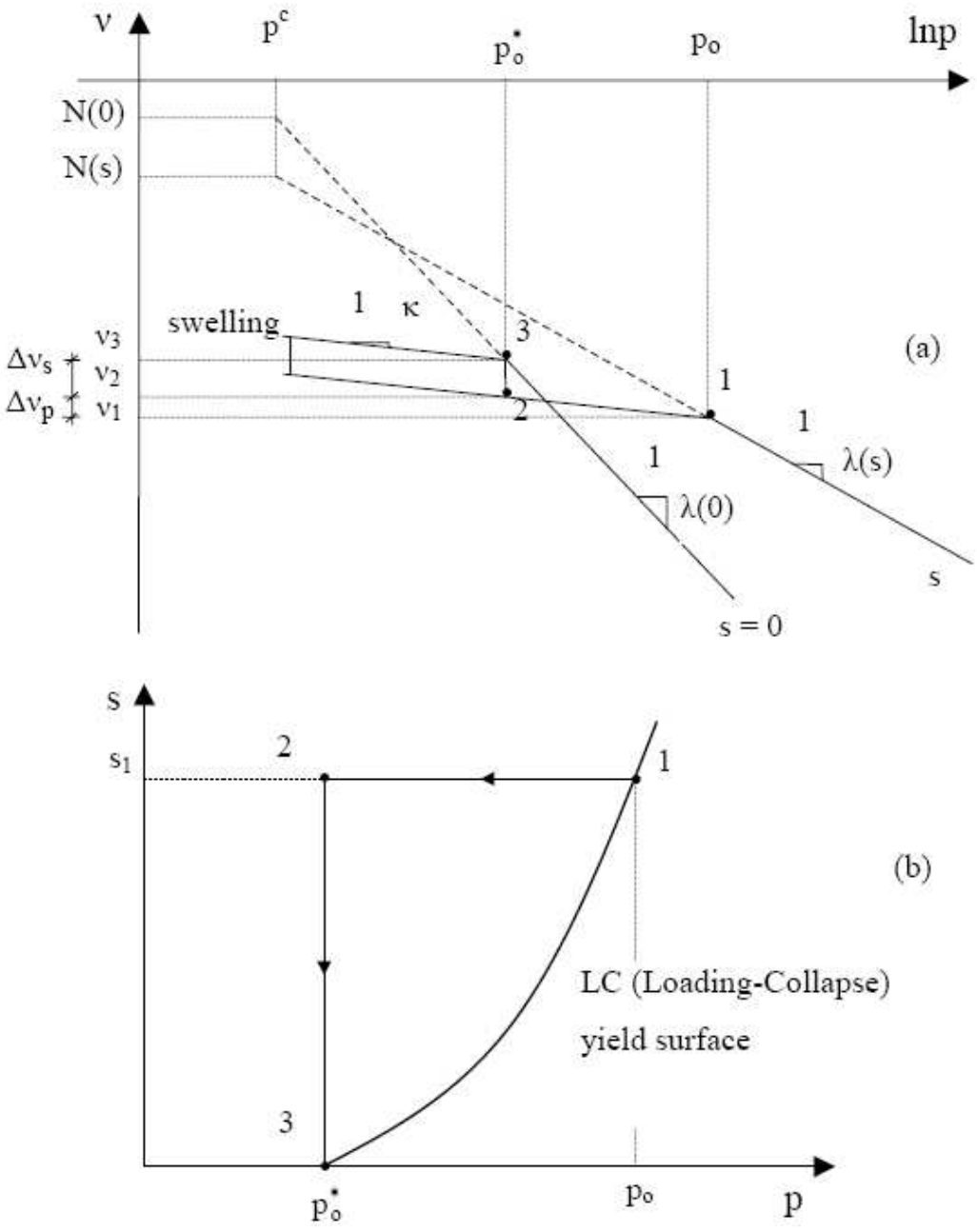

Fig. 2.18: a) assumed isotropic compression lines, and b) LC yield surface (after Alonso et al. (1990))

$$dv_p = -\kappa \ln \frac{p_o}{p_0^*} \tag{2.36}$$

The above equations are combined giving:

$$N(s) - \lambda(s) \ln \frac{p_o}{p^c} + \kappa \ln \frac{p_0}{p_0^*} + \kappa_s \ln \frac{s + p_{atm}}{p_{atm}} = N(0) - \lambda(0) \ln \frac{p_0^*}{p^c} \tag{2.37}$$

The above equation can be simplified if the assumption is made that p_c is the mean net stress at which a sample may reach the saturated virgin compression line, starting from a partially saturated virgin compression line, through a path involving only (elastic) swelling. In that case $po^* = pc = po$ and the LC yield curve becomes a straight line so that changes in suction do not result in plastic deformations:

$$\Delta v\left(p^c\right)\Big|_s^0 = N(0) - N(s) = \kappa_s \ln \frac{s + p_{atm}}{p_{atm}} \tag{2.38}$$

Equation 2.37 is now simplified to:

$$\left(\frac{p_0}{p^c}\right) = \left(\frac{p_0^*}{p^c}\right)^{(\lambda(0)-\kappa)/(\lambda(s)-\kappa)} \tag{2.39}$$

The soil stiffness $\lambda(s)$ can be obtained from the following empirical equation:

$$\lambda(s) = \lambda(0)\left[(1-r)e^{-\beta s} + r\right] \tag{2.40}$$

where r is a constant related to the maximum stiffness of the soil (for an infinite suction), $r = \lambda(s \to \infty)/\lambda(0)$, and β is a parameter which controls the rate of increase of soil stiffness with suction. An increase in suction may also induce irrecoverable strains. Another yield condition is introduced to take account of this fact (Figure2.19b):

$$s = so = constant \tag{2.41}$$

where s_o is the maximum previously attained value of suction.

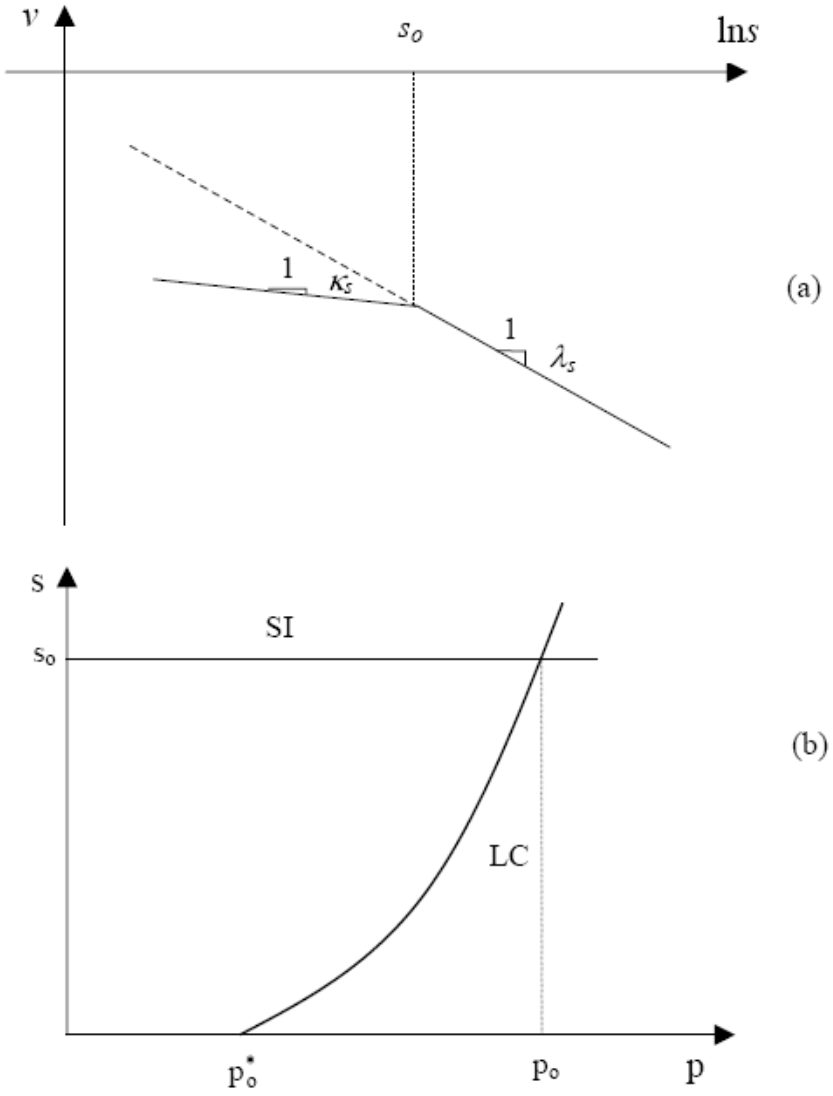

Fig. 2.19.: Definition of the Suction Increase (SI) yield surface (after Alonso et al. (1990))

The elastic, plastic and total volumetric deformations caused by an increase in p or s can be obtained from the following equations:

• Increase of mean total stress, p:

Elastic:
$$d\varepsilon_{vp}^{e} = -\frac{dv}{v} = \frac{\kappa}{v}\frac{dp}{d} \tag{2.42}$$

Total: $$d\varepsilon_{vp}^{e} = -\frac{dv}{v} = \frac{\kappa}{v}\frac{dp}{d} \tag{2.43}$$

Along the isotropic compression line $dp/p = dp_o/p_o$ and the plastic strains are given by,

Plastic: $$d\varepsilon_{vp}^{p} = \frac{\lambda(s)-\kappa}{v}\frac{dp_0}{p_o} = \frac{\lambda(0)-\kappa}{v}\frac{dp_0^*}{p_0^*} \tag{2.44}$$

• Increase of suction, s:

Elastic: $$d\varepsilon_{vs}^{e} = \frac{\kappa_s}{v}\frac{ds}{(s+p_{atm})} \tag{2.45}$$

Total: $$d\varepsilon_{vs} = \frac{\lambda_s}{v}\frac{ds_0}{(s_0+p_{atm})} \tag{2.46}$$

When the SI yield surface is active throughout the entire suction increment, $ds/(s+patm) = ds_o/(s_o+p_{atm})$ and the plastic strains are given by,

Plastic: $$d\varepsilon_{vs}^{p} = \frac{\lambda_s-\kappa_s}{v}\frac{ds_0}{s_0+p_{atm}} \tag{2.47}$$

Both sets of plastic deformations have similar effects. The two yield curves are coupled and their position is controlled by the total plastic volumetric deformation:

$$d\varepsilon_{v}^{p} = d\varepsilon_{vs}^{p} + d\varepsilon_{vp}^{p} \tag{2.48}$$

The hardening laws for the two yield curves are the following:

LC yield surface: $$\frac{dp_0^*}{p_o^*} = \frac{v}{\lambda(0)-\kappa}d\varepsilon_v^p \tag{2.49}$$

SI yield surface: $$\frac{ds_o}{s_o+p_{atm}} = \frac{v}{\lambda_s-\kappa_s}d\varepsilon_v^p \tag{2.50}$$

2.3.2.2 Formulation of model for triaxial stress states

A version of the modified Cam-clay model is adopted in this model to include the effect of shear stresses. The yield surfaces in the (q, p) stress space for a constant suction s and for s = 0 are shown in Figure 2.20a. The yield surfaces are given by the following equation:

$$q^2 - M^2(p + p_s)(p_0 - p) = 0 \tag{2.51}$$

where $ps = k \cdot s$. k is a constant which controls the expansion of the yield surface in the tensile stress region (increase of the apparent cohesion with suction).

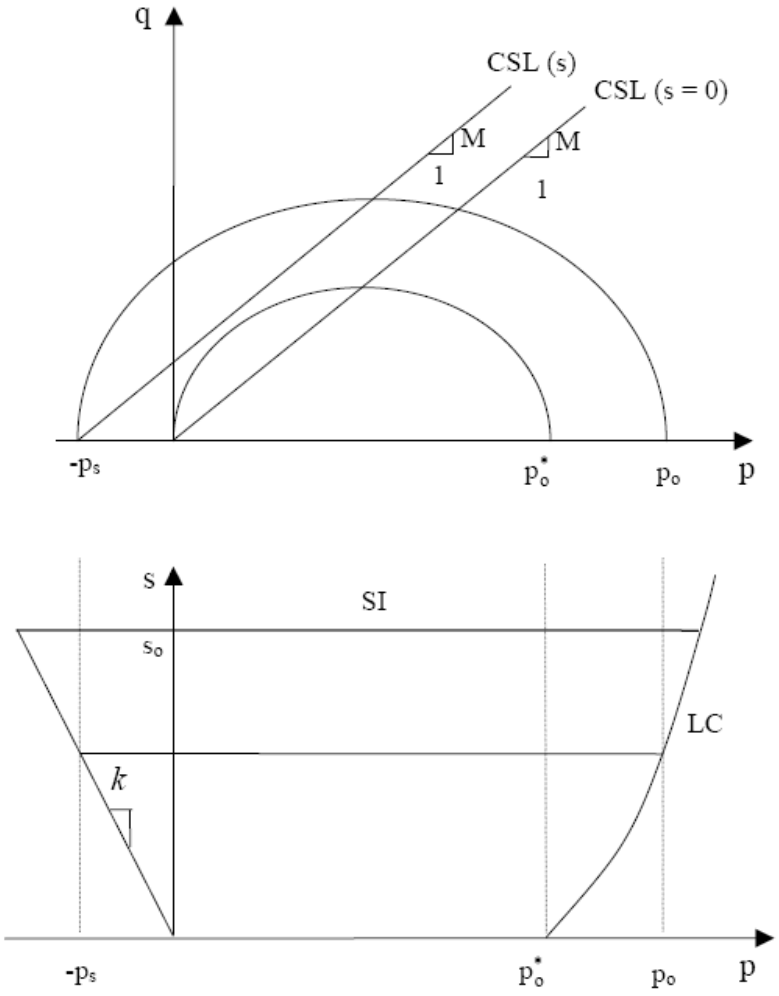

Fig. 2.20: Yield surfaces of the Barcelona Basic model (after Alonso et al. (1990))

A non-associated flow rule is suggested on the constant *s* planes. To avoid overestimation of *Ko* values (Gens & Potts, 1982a) the expression for the associated flow rule is modified by introducing a parameter α (Ohmaki, 1982) resulting in the following equation:

$$\frac{d\varepsilon_s^p}{d\varepsilon_{vp}^p} = \frac{2q\alpha}{M^2(2p + p_s - p_0)} \tag{2.52}$$

α, is a constant which can be derived by requiring that the direction of the plastic strain increment for zero lateral deformation,

$$d\varepsilon_s^p = \frac{2}{3} d\varepsilon_{vp}, \qquad d\varepsilon_{vp} = d\varepsilon_{vp}^p + d\varepsilon_{vp}^e \quad \text{and} \quad \frac{d\varepsilon_{vp}^p}{d\varepsilon_{vp}^e} = \frac{\lambda(s) - \kappa}{\kappa}$$

$$\Rightarrow \frac{d\varepsilon_s^p}{d\varepsilon_{vp}^p} = \frac{2}{3} \frac{1}{1 - \frac{\kappa}{\lambda(s)}} \tag{2.53}$$

is found for stress states satisfying *Ko* conditions:

$$\frac{q}{p} + p_s = 3\frac{1 - K_o}{1 + 2K_o} \tag{2.54}$$

The elastic strains induced by changes in *q* are given by the following equation:

$$d\varepsilon_s^e = \frac{2}{3}\left(d\varepsilon_1^e - d\varepsilon_3^e\right) = \frac{1}{3G} dq \tag{2.55}$$

2.3.3 Josa et *al*. (1992) model

Josa et *al*. (1992) proposed a modified version of the Barcelona Basic model (Alonso et *al*. (1990)). The main modification is related to the prediction of potential collapse. The Barcelona Basic model assumes linear isotropic compression lines for partially saturated conditions constantly diverging from the fully saturated isotropic compression line. This implies that the amount of potential collapse due to wetting increases indefinitely with confining stress. However, for most partially saturated soils the amount of potential collapse initially increases with confining stress reaches a maximum value and then decreases tending to zero at very high stresses. The modified model addresses this issue. The formulation is similar to the Barcelona Basic model and will not be presented here in full.

2.3.3.1 Modifications to the Barcelona Basic model

The model proposed by Josa et *al*. (1992) allows the prediction of maximum collapse at some value of confining stress through the introduction of a modified expression for the Loading Collapse yield surface in the mean net stress (p) –suction (s) space:

$$p_0 = \left(p_0^* - p^c\right) + p^c\left[(1-m)e^{as} + m\right] \tag{2.56}$$

where $\alpha\,\alpha$ is a parameter that controls the shape of the yield surface and m is related to the difference between p_o for high suction values ($p_o{}^{\infty}$) and $p_o{}^*$, and is always higher than 1. Figure 2.21 shows the resulting yield surfaces for different values of po^*. m is a function of po^* and is required to satisfy the following conditions:

- when $po^* = pc$, $m = 1$
- for large values of po^*, $m = 1$
- m presents a peak ($po^* = \zeta x$, $m = \zeta y$)

The following equation is given for m:

$$m = 1 + \frac{\zeta_y - 1}{\zeta_x - p^c}\left(p_0^* - p^c\right)e^{\frac{\zeta_x = p_o^*}{\zeta_x = p^c}} \tag{2.57}$$

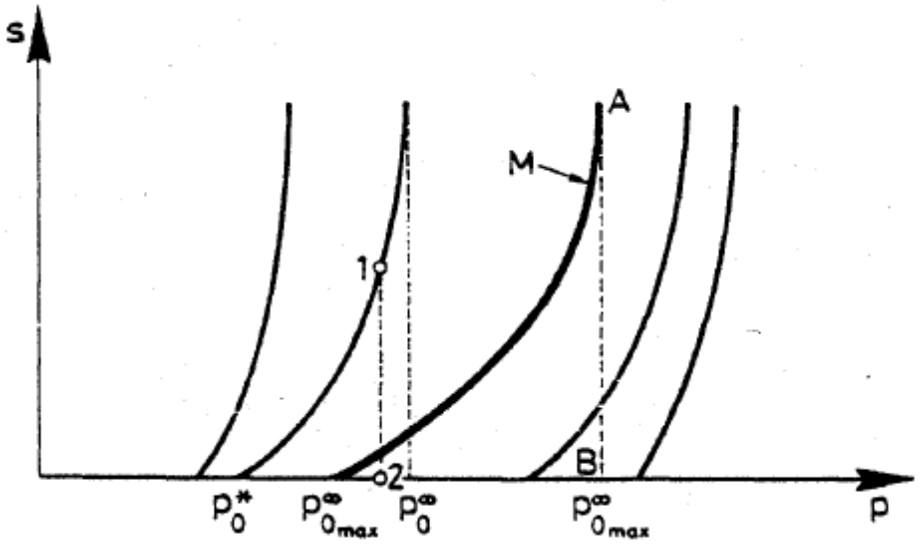

Fig. 2.21: Loading-Collapse yield surfaces in the (p – s) space for different values of po(after Josa et al. (1992))

Figure 2.22 shows the variation of *m* with p_o^*. Josa et *al*. (1992) suggest that the parameters ζx and ζy can be replaced by the value of p_o^* corresponding to maximum collapse and the maximum plastic volumetric strain, $\varepsilon_{v\max p}$, respectively. They also note that the range of validity of this expression is limited by the condition that adjacent yield surfaces should not

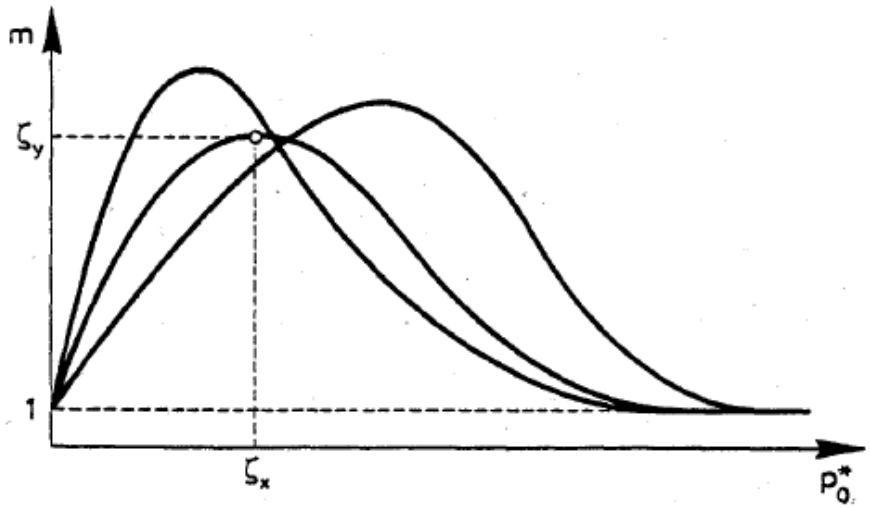

Fig.2.22: Shape of m for generic values of ζ z and ζ y (after Josa et al. (1992))

intersect. No specific limits are provided however in their paper.

A second modification to the Barcelona Basic model regards the hardening laws. Equations 2.49 and 2.;50 of the original model are replaced by:

LC yield curve:
$$\frac{dp_o^*}{p_0^*} = \frac{d\varepsilon_v^p}{\lambda(0) - \kappa} \tag{2.58}$$

SI yield curve:
$$\frac{ds_o}{s_o + p_{at}} = \frac{d\varepsilon_v^p}{\lambda_s - \kappa_s} \tag{2.59}$$

giving hyperbolic relationships between void ratio and mean net stress for saturated conditions and between void ratio and suction

Similarly hyperbolic relationships are defined for elastic paths:

$$d\varepsilon_v^e = \kappa \frac{dp}{p} + \kappa_s \frac{ds}{s + p_{atm}} \tag{2.60}$$

2.3.4 Wheeler & Sivakumar Model

Wheeler & Sivakumar (1995) used the data from a series of controlled suction triaxial tests on samples of compacted speswhite kaolin, in the development of an elasto plastic critical state framework for partially saturated soil. The framework is formulated in the (q, p, s) stress space.

2.3.4.1 Formulation of model for isotropic stress states

Figure 2.23 shows the stress paths in the (p , s) space, followed by four samples during the equalisation stage (wetting). The behaviour of the samples during this stage was found to be consistent with the existence of the LC yield surface (as defined by Alonso et *al*. (1990)).
The behaviour of the samples during the consolidation stage (isotropic at constant suction) also indicated the existence of this curve. When the yield stress at a particular value of suction, s, was exceeded, the soil state fell on a unique isotropic normal compression line defined by a linear relationship:

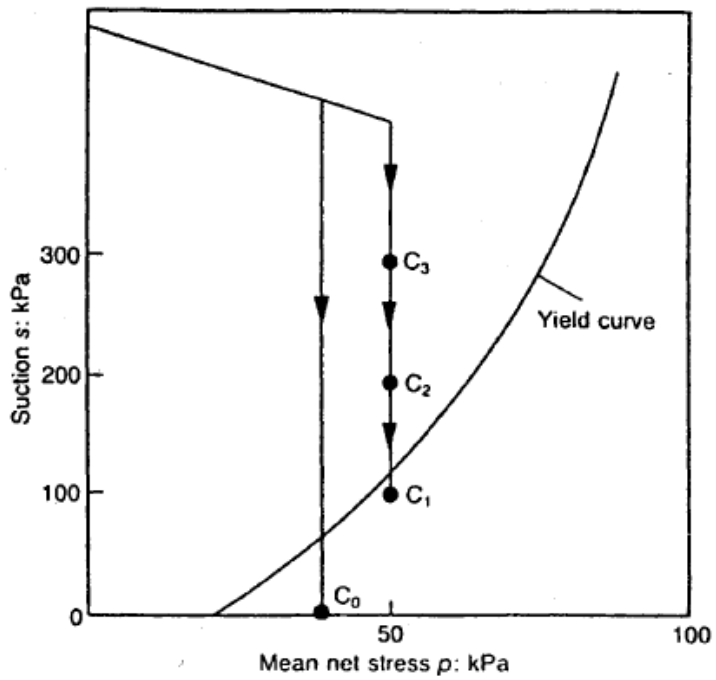

Fig.2.23: Loading-Collapse yield surface inferred from equalisation stage results (after Wheeler & Sivakumar (1995))

$$v = N_a(s) - \lambda(s)\ln\frac{p}{p_{atm}} \tag{2.61}$$

where p_{atm} is the atmospheric pressure and $N\alpha(s)$ is the specific volume at $p = p_{atm}$.
The test data showed that $N\alpha(s)$ is larger for larger values of suction. $\lambda(s)$ showed relatively little variation for suctions between 100 and 300kPa but a significant drop when $s = 0$. This result is in contrast with the predictions of the Barcelona Basic model, which assumes a reduction of both $\lambda(s)$ and $N\alpha(s)$ with increasing suction.
The shape of the LC yield curve is defined in this model in the same way as in the Barcelona Basic model:

$$(\lambda(0)-\kappa)\ln\frac{p_o(0)}{p_{atm}} + N_a(0) - N_a(0) + \kappa_s \ln\frac{s + p_{atm}}{p_{atm}} = (\lambda(s)-\kappa)\ln\frac{p_0}{p_{atm}} \tag{2.61}$$

where $po(0)$ is the isotropic yield stress for full saturation, $Na(0)$ is the intercept for full saturation, and κ and κs are the elastic stiffness parameters for changes in net mean effective stress and suction, respectively.
The assumption made in the Barcelona Basic model that a limiting situation exists at which the LC yield curve becomes a straight vertical line at some reference value of po, the characteristic pressure pc, is not adopted in this model, so the above expression is not simplified. Furthermore no assumption is made regarding the variation of $\lambda(s)$ with suction and the form of the elastic behaviour inside the yield curve. Instead it is assumed that empirical equations are given for $\lambda(s)$, $N(s)$ and the form of elastic behaviour in the elastic region. Wheeler & Sivakumar (1995) argued that this approach has the advantage, over the Barcelona Basic model, that it is easier and more direct to measure values of $N(s)$ at a few different values of suction than it is to measure pc. Moreover the basis of the simplification introduced in the Barcelona Basic model, has never been validated experimentally.
The experimental results confirmed the assumption, first made by Alonso et al. (1990), that the phenomenon of collapse on wetting is essentially the same process as the plastic compression that occurs on isotropic loading beyond the yield point. This assumption was therefore included in the developed model.

2.3.4.2 Formulation of model for triaxial stress states

The existence of a critical state was confirmed by the test results. The critical state lines are given by:

$$q = M(s)p + \mu(s) \tag{2.62}$$

where $M(s)$, $\mu(s)$, $\Gamma(s)$ and $\psi(s)$ are functions of suction. The experimental results showed that the assumption made by Alonso et *al*. (1990) that $M(s)$ is constant might be realistic. In

contrast the value of $\mu(s)$, which is equivalent to ks, varied with suction in a non-linear fashion.

For a given value of suction fig.2.24a represents the projection of the critical state line on the $v - lnp$ plane. Alonso et *al*. (1990) did not explicitly provide a similar equation; the formulation of the model, however, implied a particular relationship, which did not fit well the experimental results reported by Wheeler & Sivakumar (1995).

The proposed form for the state boundary relationship is shown in Figure 2.24, and defined as follows:

$$
\begin{aligned}
q^2 &= M_*^2 (p_0 - p)(p + p_0 - 2p_x) \\
M_* &= \frac{M(s)p_* + \mu(s)}{p_0 - p_x} \\
\frac{p_0}{p} &= \exp\left[\frac{N(s) - \lambda(s)\ln\left(p/p_{atm}\right) - v}{\lambda(s) - \kappa}\right] \\
\frac{p_x}{p} &= \exp\left[\frac{\Gamma(s) - \psi(s)\ln\left(p/p_{atm}\right) - v}{\psi(s) - \kappa}\right]
\end{aligned}
\tag{2.63}
$$

An associated flow rule is assumed for the determination of the plastic strain increments, while the value of the elastic shear modulus G is assumed to be constant.

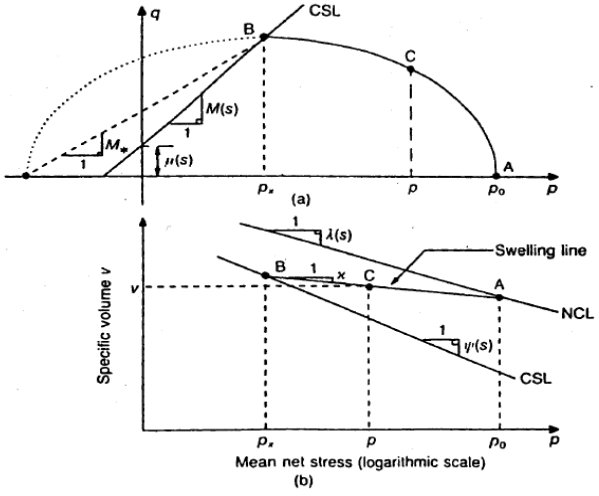

Fig. 2.24: a) Yield surface, and b) normal compression and critical state lines (after Wheeler & Sivakumar (1995))

Chapter 3

Mudflows in Campania region

3.1 Synopsis

In this chapter the mudflows affecting Campania region are described. The triggering factors, function of the deposition and of the stratigraphic and morphological conditions, are introduced. In particular the rule of the environmental conditions and the effects of rain on the slope stability in unsaturated pyroclastic soils are highlighted. Further the catastrophic events that affected the town of Sarno in the 98's are describes briefly.

3.2 Typical setting, stratigraphic and morphological conditions

In the last ten years a series of catastrophic mudflows, involving pyroclastic unsaturated soils, has caused severe damage and a number of fatalities in Campania region (Italy).
Mudflows affect the pyroclastic cover resting on the limestone massif in the region. Rainwater infiltration is the likely mechanism that leads or predisposes to slope failures by reducing matric suction in unsaturated soils and, hence, reducing the shear strength.
There are other hypotheses on failure mechanisms for cases in which the subsoil water regime can play a major role due to local stratigraphic and hydro-geologic conditions.
The pyroclastic cover is constituted by ash and volcanic pumice, and a cineritic layer is often present at the bottom. These soils take origin from the volcanic eruption several thousand years ago; they are characterized by a grain size distribution and a thickness depending on the characteristics of the eruptions and on the distance of deposition from the eruption centre (*Chapter 1*).

At the top of slope the pyroclastic succession usually has a thickness of few meters; however, the absence of some layers could be due to the local ancient landslides.

At the bottom the slope is covered by an accumulation zone of the materials re-deposited (as

result of erosion and transport), the thicknesses are significant, they reach several meters. These covers consist of a cineritic matrix mixed with pumice or with the detritus of ancient landslides.

The pyroclastic layers are not affected by groundwater, and they result partially saturated. The low degree of saturation often determines the very high suction, function of the particle size and of the environmental conditions.

De Riso et al. (1999) found that the profiles of the slopes covered by the pyroclastic layers are very steep at the top and more sweet at the bottom. The critical inclination is usually between 35 ° and 40 °.

3.3 Environmental conditions

The stability in these soils is a function of the environmental conditions, because it is related to the values of suction, continuously variable with the rainfall. In fact the collapse is due to the reduction of suction or to the compressive pore water pressure within one of the layers.

If the slope is modelled as an infinite slope and the suction is nil on any plane parallel to the ground surface, the critical inclination is equal to the critical state angle. Therefore, being the critical state angle between 35° and 39° in the pyroclastic layers in question, when the suction is nil (without generation of the compressive pore water pressure), all part of slope characterized by an inclination greater than 35° - 39° would achieve the failure within the pyroclastic layers. In fact, the critical inclinations, based on data collected by De Riso et al., (1999), are between 35° and 40° (*Fig. 3.1*).

De Riso et al. report also landslides occurred along the slopes with inclination greater than 39° and less than 35°. In the first case, this implies that the failure would occur again at values of suction higher than zero. In the second case, in slopes with inclination less than 35°, the collapse could be justified by the formation of saturated areas where the pore water pressure is compressive.

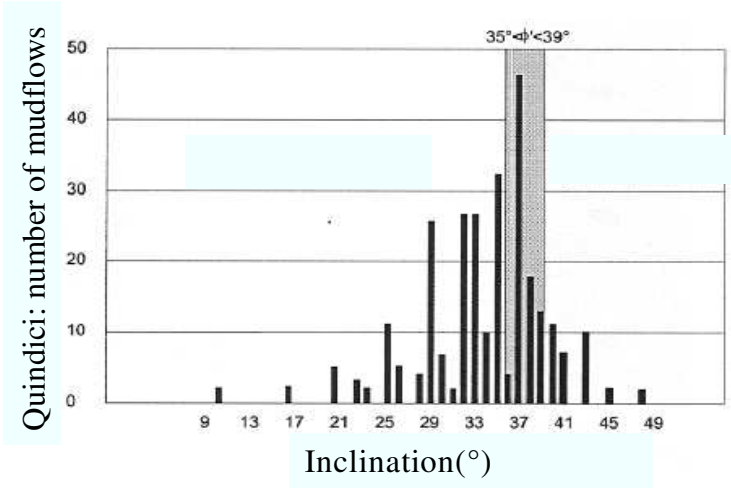

Figure 3.1: Critical inclination along the natural slopes in Quindici (modified from De Riso et al., 1999)

3.4 Failure mechanism and evolution post-failure

The type of landslides involving the pyroclastic soils could be: mudflows, sliding and fall if the soil has a small cohesion (De Riso et al., 1999). Because the mudflows cause the most serious damages, in the following the factors predisposing to this type of landslides are summarized briefly.

Already in the 60 -70's, several authors assumed that the mudflows were the result of a collapse mechanism and liquefaction.

By using the results of the lab tests in undrained conditions, Olivares and Picarelli (2001) validated this assumption for the pyroclastic soils of Campania region only if these soils are saturated and susceptible to the static liquefaction. Moreover the lab tests performed at the University of Naples (Nicotera, 1998) and of Salerno (Sorbino and Wood, 2002) and the model tests in small scale performed at the University of Naples Federico II (Zingariello, 2006) and Aversa (Damiano, 2003) provide evidence on the liquefaction of these soils. However, in the absence of one or more of the conditions necessary for the liquefaction (saturation, the compressive pore water pressure in undrained conditions), the failure mechanism and its evolution might also be different from that of the mudflows.

Olivares and Picarelli (2002) provided a simplified pattern where the influence of the different conditions on the evolution of failure (post-failure) are shown.

This pattern (Olivares and Picarelli, 2002) is applied mainly to the infinite slope and, in particular, it is assumed that the failure is not progressive.

For the not steep slopes the collapse is probably due to the increase of the ground water level. In fact the infiltration of rain causes the recharge of groundwater and so the increase of pore water pressure. If the soils are susceptible to liquefaction, the failure is immediate and it is characterized by the compressive pore water pressure. However, a mudflow occurs if the permeability is low enough to allow the compressive pore water pressure are present during the generation and development of the landslide. For soils characterized by the high permeability (pumice), a mudflow could be possible but, the equilibrium rapidly is reached due to the rapid dissipation of the increment of pore water pressure (Hutchinson, 1986).

When the slope is steep, the presence of groundwater is unreasonable and the soils are in the partially saturated conditions (very common in Campania). The failure is caused by the decrease of suction and the mechanism depends on the geometry of the slope and on the critical state angle. Therefore, in correspondence of the critical values of rain intensity and of the duration, the slope can reach the collapse, depending on the initial conditions (suction) and on the permeability of various layers.

Fig. 3.2 Zones around Sarno where the triggering mechanism started

3.5 Geological features of Sarno

The instability of the pyroclastic cover resting on the Mountains of Avella, Sarno and Lattari, is one of the problems most analysed in the recent years by the scientific community, specially after the tragic events of 4 and 5 May 1998. The studies were mainly directed to the analyses of the factors predisposing to the failure. It is known that the collapse is due to the rainfall and even the small volume can be very dangerous because it is enriched of new materials going on the bottom part of the slope (Cruden and Varnes, 1996). In fact the soil volume involved by the mudflow increases rapidly, and it can be defined "debris avalanche" in the intermediate phase; moreover it is possible that the liquefaction of pyroclastic soils incorporated in the landslide volume occurs.

There are numerous scientific papers about the mudflows (geomorphology, geotechnical, hydrogeological, ideological, etc.). However, among the main results identified, there are: the influence of the artificial cuts on the collapse (Celico and Gain, 1998); the local stratigraphic features (Terribile et al., 2000), the rule of the rains intensity on the failure mechanism (Chirico et al., 2000, De Vita, 2000).

3.5.1 The events of May 1998

After the heavy rainfall measured between 4 and 5 May 1998, the area surrounding Pizzo D'Alvano was affected by several hundreds of landslides located at different heights. Because of particular geomorphologic features, some mudflows affected the town of Sarno, Quindici, Siano and Bracigliano, causing more than 150 victims and damages. The deposit of the Sarno mountains consists of a sequence of pumice and ash usually confined by paleosoil. The rain infiltration in the pyroclastic soils and the hydraulic regime play a major rule in triggering mechanism. Indeed, the data rainfall measured at the station of Ponte Camerelle in April was 175 mm cumulated on 15 days of rain, 88mm measured between 16 and 19 April. A total of 102 mm between 1 and 5 May was measured, 95.6 mm of rain between 4 and 5 May, just when the collapse occurred.

Figure 3.3: The area of Sarno affected by the mudflow of 4-5th May '98

Section II: Analysis of slope failure mechanism based on testing site monitoring

This section consists of six chapters and it deals with the central part of PhD thesis.
The chapters 4 and 5 concern the experimental field of Monteforte Irpino(AV); in particular in the chapter 4 a brief description of testing site is introduced, in the chapter 5 the in situ monitoring, the data collected and analyses, are presented. In the chapter 6, 7, 8 the results of numerical analyses carried out by using the code ICFEP (Imperial College Finite element program) (Potts&Zdravkovic, 1999) are shown. In particular the mechanical and hydraulic models used in the analyses and their calibration are presented in the chapter 6, the validation model and the slope stability analyses respectively in the chapter 7 and 8.
Moreover in the chapter 9 the results of slope stability analyses are used to develop a failure forecasting.

Chapter 4

Testing Site

4.1 Synopsis

In order to analyse the triggering mechanism affecting the pyroclastic cover resting on the limestone massif in Campania region, a Testing Site at Monteforte Irpino (AV) was chosen and instrumented. Based on geological and morphological considerations, the test site was selected to collect experimental data from laboratory tests on undisturbed samples (*Papa, phd Thesis 2007*) and to monitor climatic conditions (affecting infiltration), matric suction and water content in the subsoil. In the following a brief description of geological, morphological and stratigraphic features of the site and the instrumentation installed are reported.

4.2 Description of the testing Site

The testing site is situated on the west side of a limestone mountain called *Monte Faggeto,* about 40 km northwest of the volcano *Somma-Vesuvius* (*Fig.4.1*). Five recent flowslides and a number of ancient accumulation zones were recognized, demonstrating the area's high landslide susceptibility (*Figs. 4.2-4.3*). The limestone massif has a pyroclastic unsaturated soil cover several meters thick constituted by the products of a series of eruptions of the *Somma-Vesuvius*.

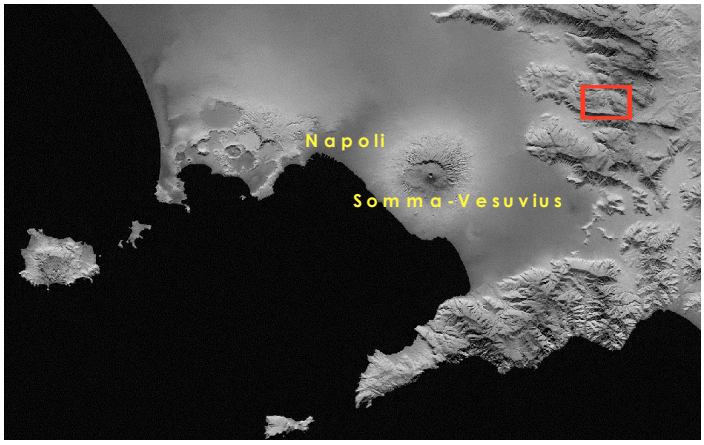

Fig.4.1: Position of Testing Site

The whole investigated area has the same exposure towards the eruption and is aligned along the principal axis of dispersion of the some of the main plinian eruptions of Vesuvius (*Di Crescenzo et al. 2007*). These geological features are quite similar

to those of other sites in Campania in which some huge mudflows occurred in the recent past (e.g. *Pizzo D'Alvano*, *Monti di Avella* and *Monte Partenio*). Furthermore, the vegetation at the site consisting of chestnut woods and shrubland is representative of the mountainous area of the Campania region (*Fig.4.4*).

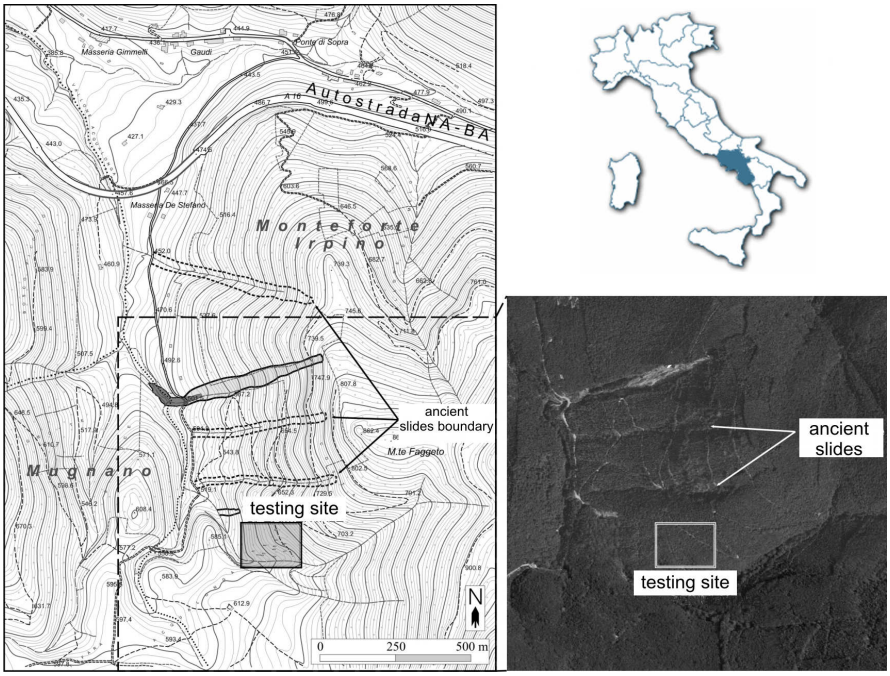

Fig.4.2: Testing site map and ancient accumulation zones (Papa, 2007)

Fig 4.3: Zones close to the area selected for the testing site

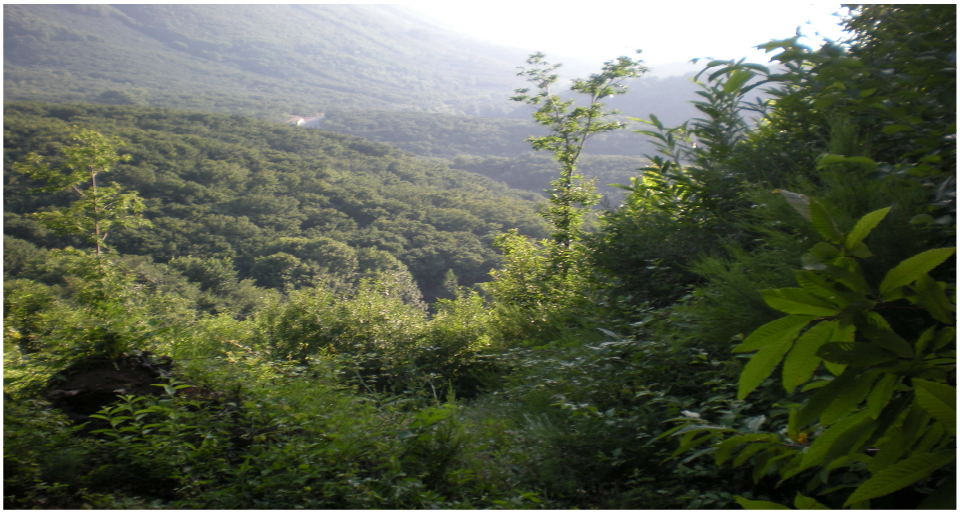

Fig.4.4: Typical vegetation in site

4.2.1 Morphological and geological features

From a *morphological* point of view the test site is quite regular. The slope is characterized by an average slope angle of 25°–30°, but this angle is locally higher, reaching 35°– 40°.

In situ experimentation focused on an area of about 14,500 m^2 where the chestnut trees were previously coppiced.

The *geological* features of this area were investigated by means of *5* boreholes (maximum depth 6.00 m) and *15* deep exploration trenches. This investigation allowed to a high resolution model of the subsurface.

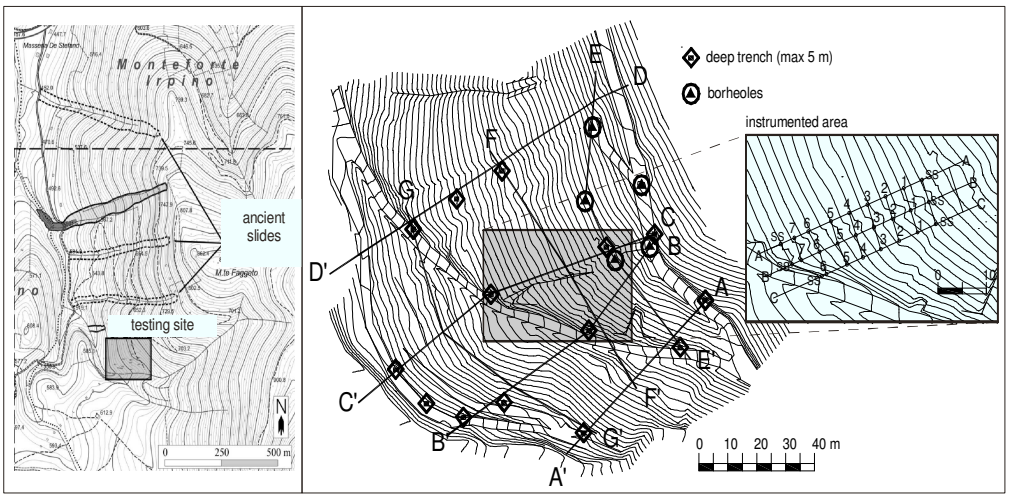

Fig. 4.5: Map of the deep trenches and boreholes carried out (Nicotera et al, 2008)

The positions of boreholes and trenches and the traces of the inferred geological sections are presented in *Figure 4.5.* Using the data collected, it was possible to evaluate the total thickness of the soil cover quite accurately. In spite of the regularity of the slope morphology the buried surface of limestone has quite an uneven pattern. In particular, a hidden depression deeper than 10 m was identified in the bedrock.

4.2.2 Stratigraphic features

The stratigraphic succession can be described as a series of soil layers essentially parallel to the ground surface. Starting from the ground surface the sequence consists of: topsoil (humified ashes including roots and organic matter); a weathered and humified ashy soil; three pumices layers of various colours and grain size from the Avellino eruption (3.7 ky b.p.); a palaeosoil consisting of weathered volcanic ashes; a layer of yellowish pyroclastic sand resting on some pumiceous strata from the Ottaviano eruption (8.0 ky b.p.); a palaeosoil consisting of weathered volcanic ashes; a volcanic sand from the Agnano eruption (10.5 ky b.p.); two strata of highly weathered fine-grained brownish ashy soils. The section C-C' (marked in *figure 4.5*) is reported in *Fig. 4.6*.

Based on the experimental investigation of the geotechnical properties of the pyroclastic cover (*Papa et al. 2008*), a simplified profile was derived (*Fig.4.7*); starting from the ground surface: layer 1) topsoil; layer 2) weathered and humified ashy soil; layer 3) pumices from the Avellino eruption (3.7 ky b.p.); layer 4) palaeosoil consisting of weathered volcanic ashes; layer 5) pumices from the Ottaviano eruption (8.0 ky b.p.); layer 6) palaeosoil consisting of weathered volcanic ashes; layer 7) volcanic sand; layer 8) highly weathered fine-grained ashy soil.

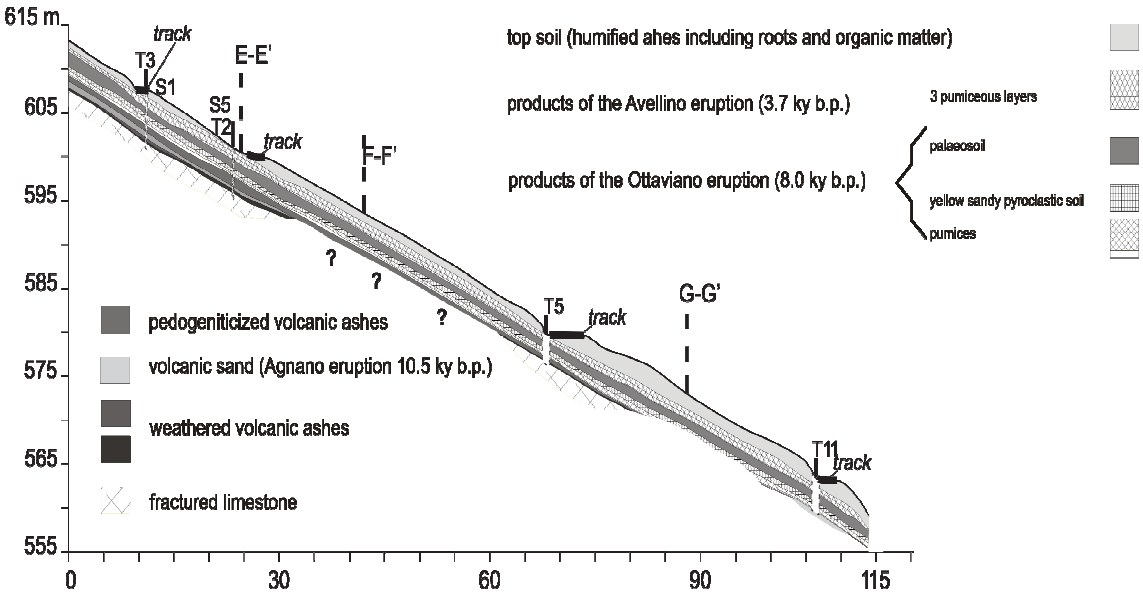

Fig. 4.6: Section C-C' (Di Crescenzo D. et al.,2007)

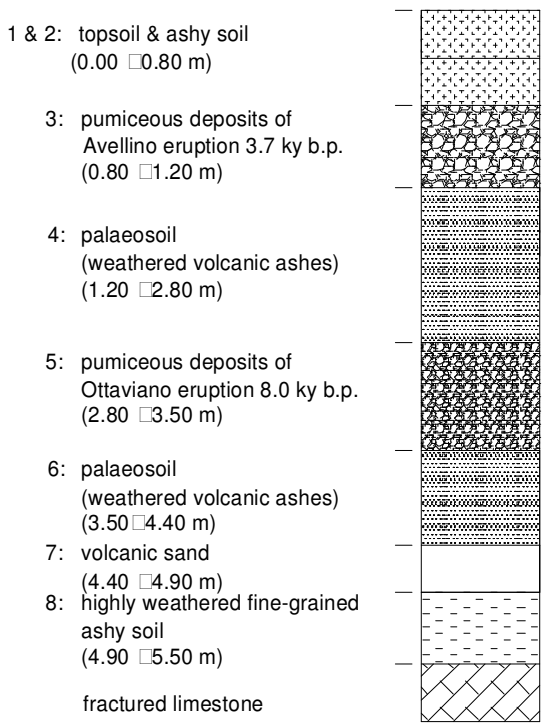

Fig. 4.7: Simplified profile (Nicotera et al.,2008)

The continuity of the strata and their thickness were carefully considered in order to investigate the interaction of the pyroclastic cover with both the atmosphere and the limestone bedrock in the numerical analysis.

As regards soil layer continuity, it is worth noting that accurate inspection of stratigraphical data showed that while the layers from the Ottaviano eruption are found throughout the investigated area, those from the Avellino eruption and the underlying palaeosoil are absent in areas with slope angles higher than 35°. These observations suggest that in those areas with a slope angle exceeding 35°, these layers were scoured as a consequence of some kind of instability phenomenon. Hence it is argued that slides may well have occurred along surfaces affecting the palaeosoil interbedded between eruptive products from Avellino and Ottaviano.

4.3 Instrumentation installed

The field instrumentation was designed to measure *matric suction* and *water content* in the pyroclastic cover and the *climatic conditions (rain intensity, air temperature, air humidity, net radiation, wind speed and direction)* as well. An area of about 230 m^2 was chosen on the slope in question. In this area 26 instrumented vertical sections were executed. These vertical sections were distributed at the vertex of a fairly rectangular grid formed by 14 square meshes 4 m × 4 m (*Figs. 4.8-4.9*).

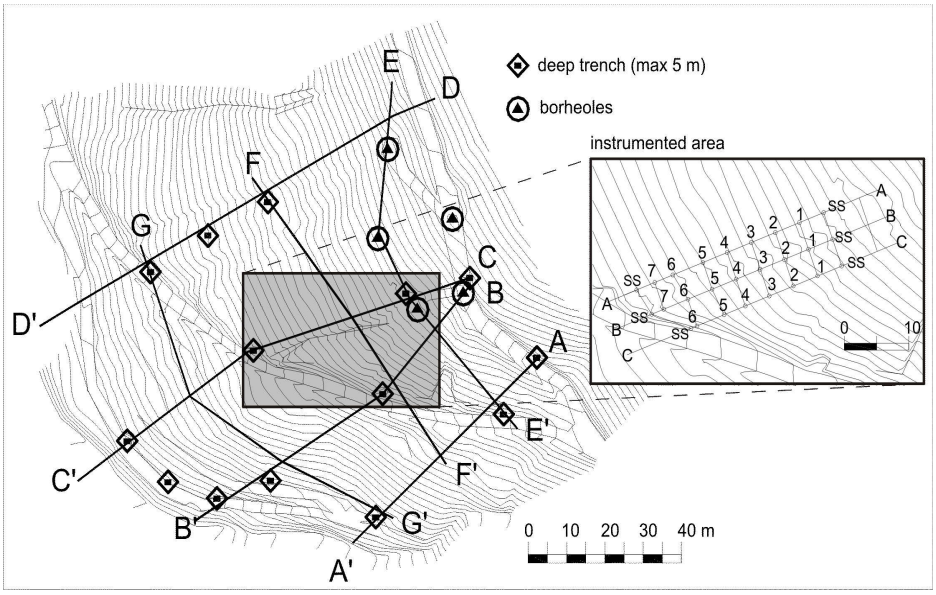

Fig. 4.8: Instrumented area (Nicotera et al.,2008)

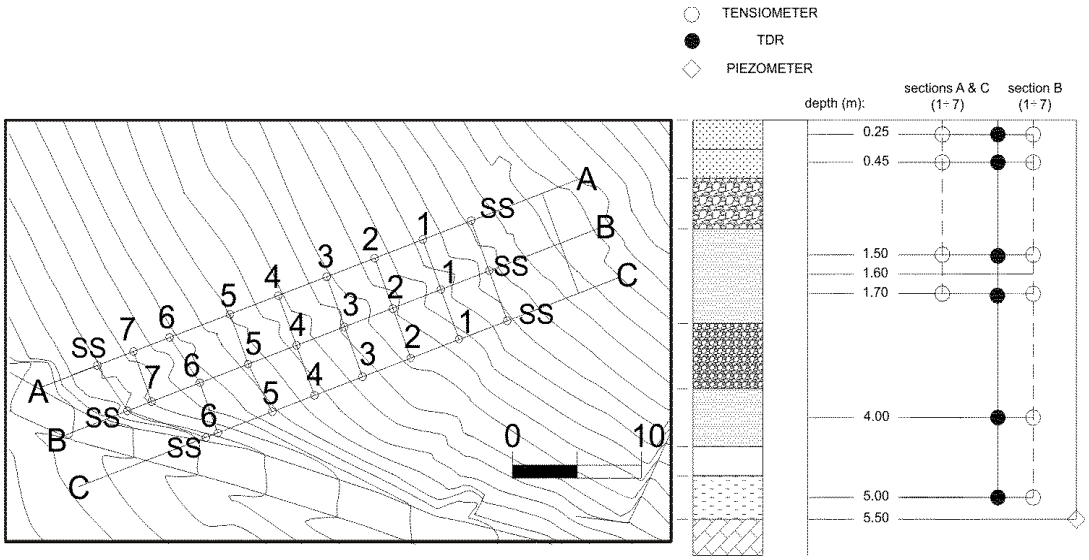

Fig. 4.9: Instrumentation plan distribution (Nicotera et al.,2008)

4.3.1 Measurements of suction and volumetric water content in the subsoil

On 8th November 2006 four *tensiometers* were arranged along each vertical section: one in the soil 1, one in the soil 2, two in the soil 4 (see *Fig.4.9*). Then, on 18th July 2008, installation of two more tensiometers in the deeper soil layers, soil 6 and soil 8 (*Fig.4.9*) along the verticals of the central section B-B (see *Figs.4.8-4.10*), was carried out.
The following type of tensiometers has been installed in site:
- tensiometers "jet-fill" produced by Soilmoisture with vacuometer**;**
- tensiometers produced by SDEC France with pressure transducer "SMS 2500 S".

The measurements of pressure are obtained by using a *vacuum gauge* for Soilmoisture tensiometers and an electric transducer for SDEC France tensiometers, and they are collected twice a month. The maximum suction value which can be measured is 70 kPa, because the higher values causes cavitations' phenomena (*Caso, 2009*).

Furthermore, in each of the boreholes along section B-B, a *Casagrande piezometers* at the bottom of the pyroclastic cover was set up to measure any positive pore water pressure at the upper limestone surface (*Fig 4.9*).

In order to measure the volumetric water content, *TDR probes* were installed along the verticals of the section B-B, in all the soils apart the coarse grained soils, at the same depth of tensiometers (*Fig 4.9*). The probes installed are long 15 cm and are vertically positioned; the reading are collected twice a month, together suction measurements, by using a TDR pocket portable produced and assembled ad hoc.

Probes were calibrated previously in the lab on the samples of the soil 1, 2 and 4, then the in situ measurements started on 30th April 2008.

The presence in the pyroclastic cover of two thick layers of coarse-grained soils (layers 3 and 5) significantly conditioned the instrumentation design. Both tensiometers and TDR probes were ineffective for measuring matric suction and water content inside these pumiceous strata. Furthermore, the hydraulic properties (water retention curve and permeability function) of these coarse grained soils differ greatly from those of the other soil layers.
Hence summarizing, the sensor probes were arranged in order to investigate the pore water pressure field: in the top part of the soil profile (superficial layers 1 and 2), in the intermediate part (intermediate layer 4) and in the bottom part only (deep layers 6,7 and 8).
In the table 4.1 all the instruments installed in each vertical section of the experimental field are reported.

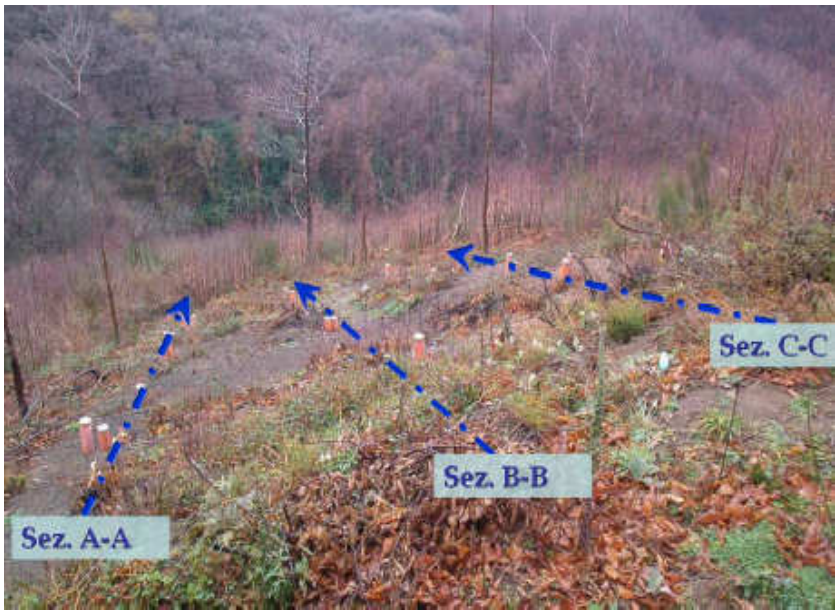

Fig.4.10: Plan of instrumented area (Caso, 2009)

Fig. 4.11: The PVC pipe coating of tensiometers installed (Caso, 2009)

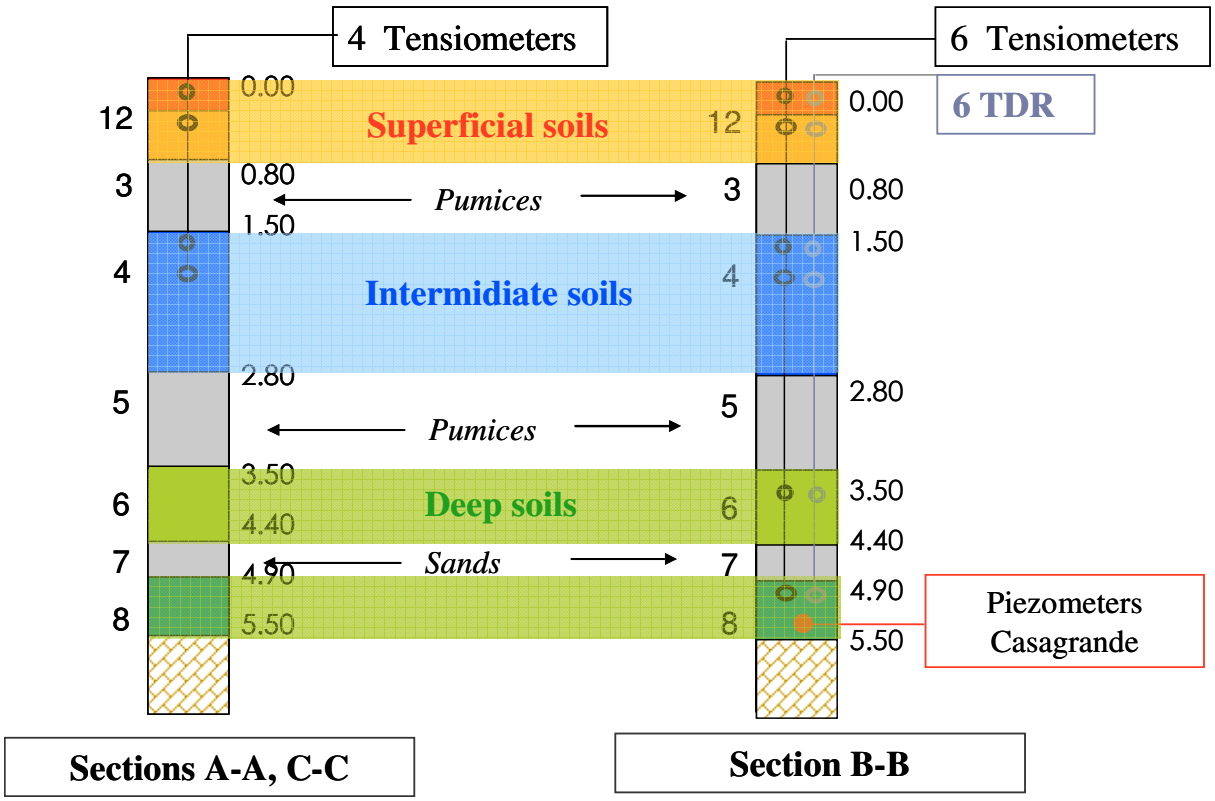

Fig. 4.12: Simplified stratigraphic profile and the strumentations installed

tab.4.1: Instrumentation installed

	tensiometer						TDR probes						
vertex N.	soil 1 (m)	soil 2 (m)	soil 4 (m)	soil 4 (m)	soil 6 (m)	soil 8 (m)	soil 1 (m)	soil 2 (m)	soil 4 (m)	soil 4 (m)	soil 6 (m)	soil 8 (m)	PIEZOMETER (m)
1 A	0.25	0.45	1.75	1.8	/	/	/	/	/	/	/	/	/
1 B	0.25	0.45	2.1	2.15	3.35	3.5	0.20	0.40	2.05	2.10	3.30	3.45	3.65
1 C	0.25	0.45	1.6	1.7	/	/	/	/	/	/	/	/	/
2 A	0.25	0.45	2.05	2.25	/	/	/	/	/	/	/	/	/
2 B	0.25	0.45	1.45	1.6	3.35	3.65	0.20	0.40	1.40	1.55	3.30	3.60	3.8
2 C	0.25	0.45	1.8	/	/	/	/	/	/	/	/	/	/
3 A	0.25	0.45	2.2	2.3	/	/	/	/	/	/	/	/	/
3 B	0.25	0.45	2.2	2.3	3.5	3.65	0.20	0.40	2.15	2.25	3.40	3.60	3.8
3 C	0.25	0.45	2	2.2	/	/	/	/	/	/	/	/	/
4 A	0.25	0.45	1.55	1.75	/	/	/	/	/	/	/	/	/
4 B	0.25	0.45	1.4	1.55	3.5	3.9	0.20	0.40	1.35	1.50	3.45	3.85	4
4 C	0.25	0.45	1.8	1.95	/	/	/	/	/	/	/	/	/
5 A	0.25	0.45	1.3	1.6	/	/	/	/	/	/	/	/	/
5 B	0.25	0.45	1.35	1.55	3.1	3.6	0.20	0.40	1.30	1.50	3.05	3.50	3.65
5 C	0.25	0.45	1.95	2.05	/	/	/	/	/	/	/	/	/
6 A	0.2	0.4	1.4	1.45	/	/	/	/	/	/	/	/	/
6 B	0.25	0.45	1.4	1.5	3.2	3.7	0.20	0.40	1.35	1.45	3.10	3.90	4.1
6 C	0.25	0.45	1.3	1.35	/	/	/	/	/	/	/	/	/
7 A	0.25	0.45	1.3	1.55	/	/	/	/	/	/	/	/	/
7 B	0.25	0.45	1.35	1.45	/	/	0.20	0.40	1.30	1.40	/	/	/

4.3.2 Monitoring of the climate conditions

Finally, a weather station was installed to monitor the climate conditions affecting the pore water pressure field in the soil cover (i.e. rainfall, solar net radiation, air temperature, air pressure, air humidity, wind speed and direction) on 26th June 2009 (*Figs.4.13-4.15).*

a) 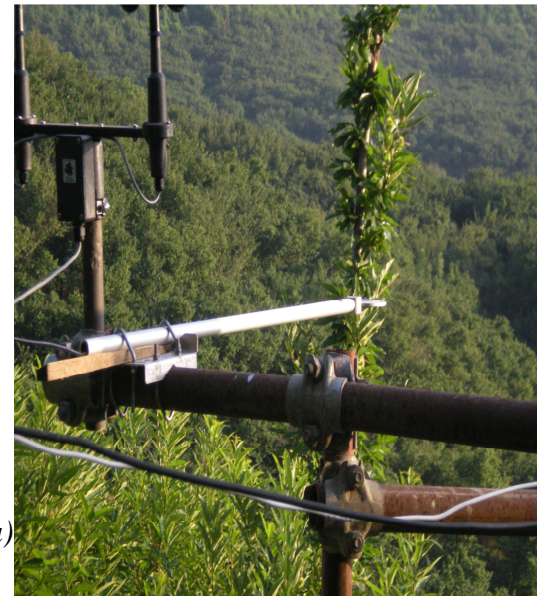 *b)* 

Fig.4.13: Net Radiometer a); Solar Panel to power the Datalogger b)

a)  *b)* 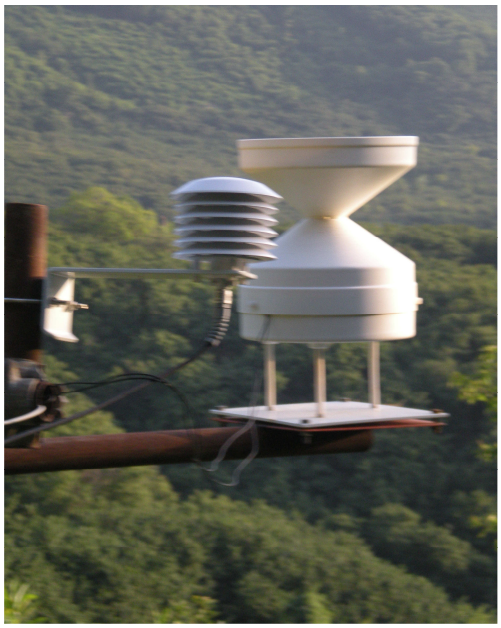

Fig.4.14: Anemometer a); Rain gauge and termoigrometer b)

All sensors of the meteorological station are connected to Campbell Scientific datalogger which registers the rain intensity every ten minutes and the other data every four hours.
From 8th November 2006 the daily rain intensity is collected by the Monteforte rain gauge too.

Fig. 4.15: The meteorological station installed in site

Chapter 5

In situ monitoring: collected data and analyses

5.1 Synopsis

In this chapter suction and water content resulting from about four years of monitoring are presented and analysed. Suction and volumetric water content measurements are shown. In particular seasonal variations of matric suction and water content in the different layer of pyroclastic cover are retrieved by averaging the measurements of all instruments situated at the same depth.
Matric suction measurements from tensiometers disposed along the longitudinal section B-B and the transversal section (D-D) of the instrumented area are employed to obtain the ground water head field in the cover. Vertical water flows through the top, the intermediate of the soil profile are estimated too.
Water mass balance in the pumice of Avellino, layer 3, is performed and some important additional understanding about the water flow in this layer is also achieved.
All the measurements collected are necessary to carry on the hydraulic analyses (*Chapter 7*) and hence, to validate the model used.

5.2 Measurements collected in site

Suction[1], volumetric water content and climate conditions[2] measurements are shown.
In the table 5.1 the measurements collected, the type and the number of instruments used, the period observed and the frequency of the measurements are specified.

[1] The suction measurements collected from 8th November 2006 to 8th November 2007 are used to validate the results of "the hydraulic analyses" over hydrologic year (*Chapter 7*).
[2] The climate conditions measured from 8th November 2006 to 8th November 2007 are used to calculate the upper boundary conditions in the "hydraulic analyses" over hydrologic year (*Chapter 7*).

Tab. 5.1 Measurements description

measure	instruments	number	observation period	frequency of measure
matric suction	portable tensiometers	1	13-10-05 / 2-06-06	ten days
	permanent tensiometers	94	from 8-11-06	ten days
water content	tdr probe	40	from 30-04-08	ten days
rainfall	Monteforte raingauge	1	from 1-10-05	one day
	Avella raingauge	1	1-10-2005/ 1-12-07	one day
	site raingauge	1	from 26-06-09	ten minutes
air temperature	portable termo-igrometer	1	13-10-2005/ 1-03-08	four hours
	termo-igrometer sensor	1	from 26-06-09	ten days
air relative humidity	portable termo-igrometer	1	13-10-2005/ 1-03-08	four hours
	termo-igrometer sensor	1	from 26-06-09	ten days
net radiation	net radiometer sensor	1	from 26-06-09	four hours
wind speed & direction	anemometer sensor	1	from 26-06-09	four hours

5.2.1 Suction measurements

The suction monitoring started on 13th October 2005, and the measurements were collected by the *quick draw tensiometers* in many points of the testing site at the depth of 0.30 cm (soil 1) and 0.60 cm (soil 2) from the ground surface (*see Fig. 5.2, QD1, QD2*).
The measurements collected by the Jet fill and SDEC France tensiometers (*Chapter 4*) in all the sections instrumented (*Chapter 4)* started from the 8th November 2006. The measurements refer to the depth of 0.25 cm in the soil 1 (*Fig 5.2* TL1), of 0.45cm in the soil 2 (*Fig 5.2* TL2), of 1.30 ÷ 2.20 m in the soil 4 (*Fig 5.2* TL4sup), of 1.35 ÷ 2.30m in the soil 4 (*Fig 5.2* TL4inf). The measurements in the deeper soils started from the 18th July 2008; those refer to the depth of 3.10 ÷ 3.50m in the soil 6 (*Fig 5.2* TL6), of 3.50 ÷ 3.90 m in the soil 8 (*Fig. 5.2* TL8).

Each year of monitoring was subdivided in four parts for each part of profile: wet, intermediate drying, drying and intermediate wetting. Each time interval was identified by observing the time derivative of suction measurements:

- wet period: range of time where the time derivative is more or less nil because the suction almost constant;
- intermediate dry period: range of time where the time derivative start to increase;
- dry period: range of time where the time derivative increases very steeply, in fact the suction reaches in few days the values around 60-70 kPa;
- intermediate wet: range of time where the time derivative decreases because the first rainfalls occur.

In table 5.2 the time intervals identified for top, intermediate and bottom part of profile are reported. In table 5.3 the mean, minimum and maximum suction value collected in each layer over time interval previous identified are reported. In table 5.4 the mean, minimum and maximum suction value collected in top, intermediate, deep part[3] of vertical profile over time interval previous identified are reported.

In the *figure 5.2b* the suction measurements collected over about four years (October 2005- September 2009) are plotted. In *figures 5.2a* daily rainfall measured by Monteforte rain gauge (502 m s.l.)(the black one) and by the meteorological station installed on site (603 m s.l.)(the pink one) are plotted too, in order to analyse the influence of rainfall on the suction values.

In the *superficial soils* (see *fig. 5.3,* TL1, TL2) the suction measurements seem to be affected by a single rainy event, however the seasonal variations play a major rule.
Suction value is between 5 ÷ 10 kPa during the wet season (winter and spring)(see tab. 5.4), it reaches 60 kPa in the soil 2 and exceeds 70 kPa in the soil 1[4] in the dry period(see tab. 5.3);

[3] The mean, minimum and maximum values in top, intermediate and bottom part are obtained by averaging the mean, minimum and maximum values calculated in the layers 1 and 2 for the top part, in the layers 4superior and 4 inferior for the intermediate part, in the layers 6 and 8 for the deep part.
[4] The suction value higher than 70kPa is not measurable because of desaturation tensiometers.

so the amplitude of the seasonal oscillation is around 60 kPa. Suction values starts to decrease in Autumn due to the rainfall: in September in soil 1 and in October in soil 2 (see tab. 5.2).

In the *intermediate soils (figure 5.2*, TL4sup, TL4inf) the suction variation is always seasonal like in the superficial soils but the measurements are not influenced by a single rainy day. The maximum suction value is between 40-50 kPa in the summer, the minimum one is between 5 – 10 kPa in the winter like in the superficial soils (see tables 5.3, 5.4). The amplitude of the seasonal oscillations decreases with the distance from the ground surface, in fact in these soils it is around 30 kPa. Suction usually starts to decrease in the half of November and the decreasing is as faster as drier the previous summer is (see table 5.2). For example the summer of 2007 was drier than that of 2008, so the suction reached the typical wet value, 5-10 kPa, after four months (March 2008) in the year 2008, and after only one months (January2009) in the year 2009.

In the *deep soils (fig.5.3*, TL6, TL8) the suction variation is still seasonal and it isn't influence by the single rain event. The amplitude of the seasonal oscillations is very small, it is 10 kPa only, the maximum value is 15 kPa in the summer and the minimum one is 3 kPa in the winter (see tables 5.3, 5.4). In these soils suction starts to decrease at the end of November (see table 5.2).

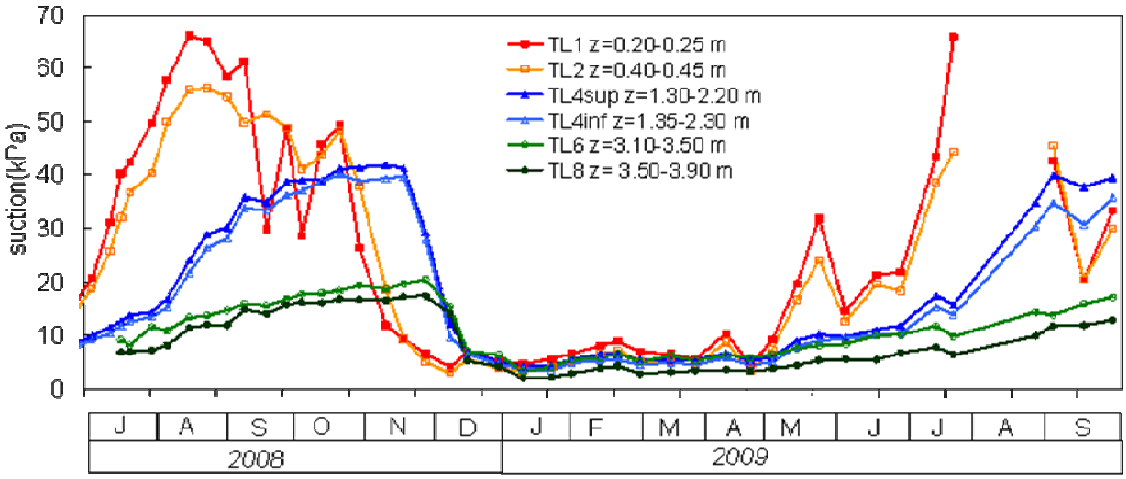

Fig.5.1: Mean values of matric suction for each layer against the time, July 2008-September 2009

Hence the suction variation is everywhere seasonal, and only the superficial soils are influenced by the single rain event. The amplitude of the seasonal oscillations decreases with the depth, in the deeper soils is only 10 kPa, while in the superficial soils is 60 kPa at least.

Tab.5.2: The time intervals identified for each year of monitoring

		top		intermediate		bottom	
	seasons	start	end	start	end	start	end
2005	intermediate - wetting	20/10	19/11	-	-	-	-
	wet	19/11	31/12	-	-	-	-
2006	wet	1/1	24/3	-	-	-	-
	intermediate - drying	24/3	12/5	-	-	-	-
	dry	12/5	-	-	-	-	-
	intermediate - wetting	-	25/11	-	25/11	-	-
	wet	25/11	31/12	25/11	31/12		
2007	wet	1/1	14/3	1/1	14/3	-	-
	intermediate - drying	14/3	8/5	14/3	22/7	-	-
	dry	8/5	23/9	22/7	18/11	-	-
	intermediate - wetting	23/9	18/11	18/11	28/3	-	-
	wet	18/11	31/12				
2008	wet	1/1	8/3	28/3	20/6	-	-
	intermediate - drying	8/3	20/5	20/6	8/8	-	-
	dry	8/6	26/8	8/8	23/11	-	3/12
	intermediate - wetting	26/8	14/12	23/11	22/12	3/12	16/1
	wet	14/12	31/12	22/12	31/12	16/1	31/12
2009	wet	31/12	29/4	31/12	29/4	31/12	20/5
	intermediate - drying	29/4	6/7	29/4	30/7	20/5	30/7
	dry	6/7	-	30/7	-	30/7	-
	intermediate - wetting	-	-	-	-	-	-

tab.5.3: Minimum, maximum and mean suction values for each soil calculated over time intervals identified

	tensiometer level:	1			2			4 superior			4 inferior			6			8		
circa	seasons	min	max	mean	min	max	mean	min	max	mean	min	max	mean	min	max	mean	min	max	mean
2005	wet																		
	intermediate - drying																		
	dry																		
	intermediate - wetting	10.8	19.15	14.24	9.45	19.4	14.43												
2006	wet	5.4	7.26	6	4.85	8.65	6.37												
	intermediate - drying	13.8	21.25	16.37	13	17.5	15.33												
	dry	-	-	-	-	-	-												
	intermediate - wetting	-	-	-	-	-	-												
2007	wet	4	10	7	3.41	8.31	5.65	6.25	10.89	8.16	5.2	9.84	7.07						
	intermediate - drying	4.75	11.7	9	3.58	10.14	7.71	5.4	8.5	6.94	4.23	7.6	5.9						
	dry	23.95	64.9	43.37	20.63	59.22	43.66	10.64	40	24	10	40.07	22.83						
	intermediate - wetting	9.41	40.92	28.01	11.04	57.64	39.26	41.83	48	45.6	41.74	49	45						
2008	wet	4.48	16.48	9.25	3.35	15.48	8.12	6	47	24	5.05	49	23						
	intermediate - drying	6.43	13.56	10.08	5.06	13.09	8.72	6	9	7.5	6	8.22	6.87						
	dry	5.24	66.15	36.69	3.43	56.27	31	10	17	14	9.18	15.26	12.12						
	intermediate - wetting	4.07	61.09	31.04	2.96	54.62	34.29	24	42	37	21.8	40.17	34.48	3.34	20.46	10.53	2.03	17.44	8.59
2009	wet	4.5	10.39	6.68	3.26	8.8	5.21	4.27	30	7.8	3.5	28	6.86	4.08	7.57	5.89	2.15	4.48	3.44
	intermediate - drying	9.25	31.82	19.74	7.41	24.17	16.46	6	17.5	11.4	5.08	15.33	10.16	8.17	11.8	9.73	5.3	7.83	6.23
	dry	-	-	-	-	-	-	-	-	-	-	-	-	-	-	-	-	-	-
	intermediate - wetting	-	-	-	-	-	-	-	-	-	-	-	-	-	-	-	-	-	-

tab.5.4: Minimum, maximum and mean suction values for the top, intermediate, deep part of soil profile calculated over time intervals identified

	part of soil profile:	top			intermediate			bottom		
circa	seasons	min	max	mean	min	max	mean	min	max	mean
2005	wet									
	intermediate - drying									
	dry									
	intermediate - wetting	10	19.2	14.3						
2006	wet	5	7.8	7						
	intermediate - drying	13.4	19	16						
	dry	-	-	-						
	intermediate - wetting	-	-	-						
2007	wet	3.8	9	6.5	5.7	10.3	7			
	intermediate - drying	4	11	8.1	4.7	8	6.4			
	dry	22.5	62.5	43.5	10	40	23			
	intermediate - wetting	10	49.5	34	41	48.5	45.3			
2008	wet	3.9	16	8.7	5.5	48	23.5			
	intermediate - drying	5.7	13.2	9.2	6	8.7	7			
	dry	4.24	61	34	10	16	13			
	intermediate - wetting	3.5	58	33	23	41	36	2.7	19	9.5
2009	wet	3.7	9.4	7.3	4	29	7	3.15	6	4.5
	intermediate - drying	8.41	28.5	18.3	5.5	11	13.5	6.7	9	7.9
	dry	-	-	-	-	-	-	-	-	-
	intermediate - wetting	-	-	-	-	-	-	-	-	-

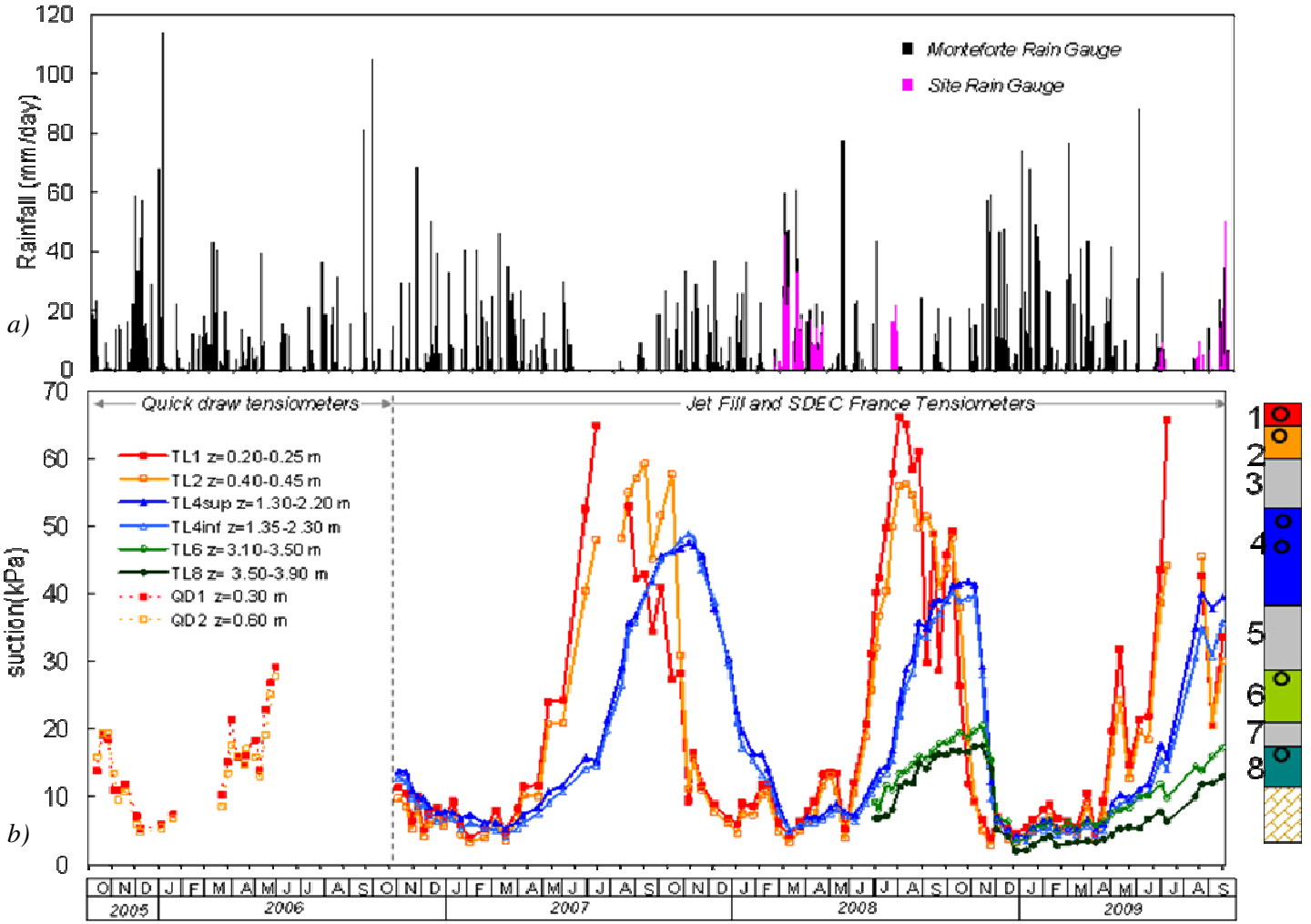

Fig.5.2: a) Daily rainfall, b) Mean values of matric suction in testing site

a)

b)

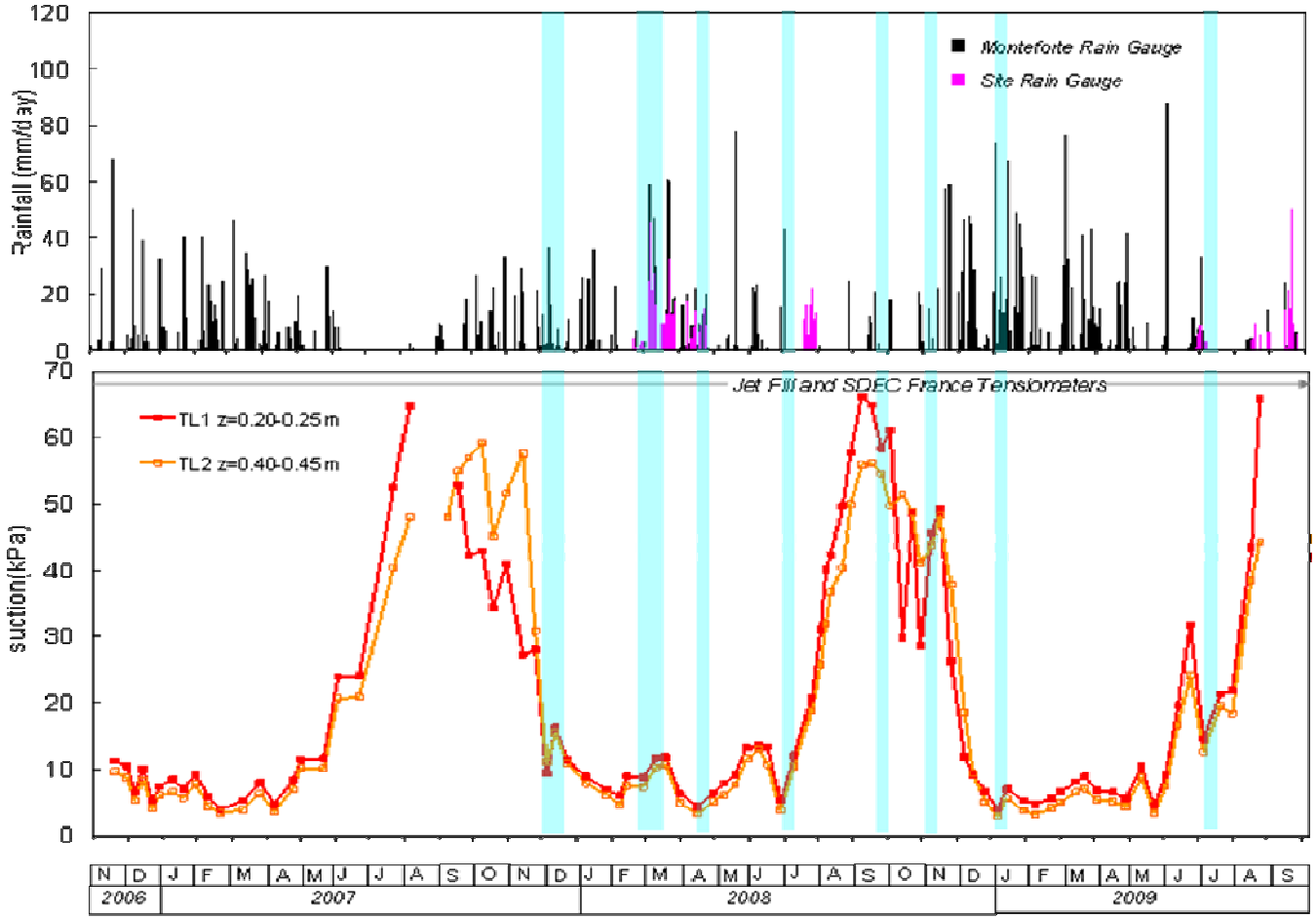

Fig.5.3: a) Daily Rain intensity, b) Mean values of matric suction in test site

5.2.2 Water content measurements

The water content monitoring started on 30th April 2008, and the measurements are collected by using the mini TDR portable. The measurements concern the verticals of the longitudinal section B-B (*Chapter 4*) and they refer to the depth of 0.25 cm in the soil 1 (*Fig 5.4* TDR1), of 0.45 cm in the soil 2 (*Fig 5.4* TDR2), of 1.30 - 2.20 m in the soil 4 (*Fig 5.4* TDR4sup), of 1.35 - 2.30 m in the soil 4 (*Fig 5.4* TDR4inf).

In the *figure 5.4b* the suction and volumetric water content measurements averaged over the verticals of the longitudinal section B-B' in the soil 1, 2, 4 against the time are plotted.

In table 5.5 the mean, minimum and maximum water content value collected in each layer over time interval previous identified are reported (table 5.2). In table 5.6 the mean, minimum and maximum water content values collected in top, intermediate, deep part[5] of vertical profile over time interval previous identified are reported.

In the *superficial soils* (*fig. 5.4b,* TDR1, TDR2) the water content measurements are influenced by single rainy days but the seasonal trend takes a major rule as with suction measurements collected at the same depth. Water content value is between 0.35 – 0.40 during the wet season (winter and spring)(see table 5.6), it reaches 0.35 in the soil 2 and exceeds 0.45 in the soil 1(see table 5.5). The most low values are reached during August and September and are close to 0.15 (table 5.5).

In the *intermediate soils (fig. 5.4b*, TDR4sup, TDR4inf) the water content variation is always seasonal like in the superficial soils but the measurements does not influenced by a single rainy day just as with suction measurements collected at the same depth. In these soils the maximum value is 0.50 in the winter (December-April); the minimum one is 0.38 in the autumn (October - November), this is because the soils more deeper are influenced later by the seasonal changes (see tables 5.5, 5.6).

In the *deep soils* water content measurements have not been processed yet because the TDR probes in these soils were not calibrated in the lab.

Hence, by observing the *figure 5.4* a good agreement results between the suction and volumetric water content measurements, both are characterized by the seasonal variations and show an amplitude of the seasonal oscillation function of the distance from ground surface.

[5] The mean, minimum and maximum values in top, intermediate and bottom part are obtained by averaging the mean, minimum and maximum values calculated in the layers 1 and 2 for the top part, in the layers 4superior and 4inferior for the intermediate part, in the layers 6 and 8 for the deep part.

5.2.2.1 Water content and suction measurements on the retention curve plane

Water content and suction measurements are collected at the same depth, so it was possible to represent them in the plan of the retention curve in order to analyse the hysteresis of these soils.

In the *figure 5.5 a, b* the water content and suction measurements collected in the verticals instrumented along the section B-B'(*Chapter 4*) and the experimental retention curves obtained in drying paths on the undisturbed samples in the lab (*Papa, 2007*) are plotted for the superficial soils (1-2) and intermediate soils (4)(*Nicotera et al., 2008*).
The suction and water content measurements collected in site from 30th April 2008 are always below the dry retention curves but fall in the hysteresis domain (*Nicotera et al., 2008*)(*fig.5.5a, b*). Moreover when suction reaches 50-60 kPa, the paths of measurements approach to the experimental drying curves and the hysteresis phenomena vanishes. In the *figures 5.6a, b - 5.12a, b* the suction and water content measurements collected in each vertical section in the soil 1, 2 and 4 are plotted too.

The volumetric water content in the superficial soils 1-2 decreases during the summer and in the same time the suction approaches to the constant value; this is because the suction measurements higher than 70kPa can not collected by the tensiometers installed in situ *(fig.5.13b)*. The figure *5.13a* shows the suction measurements collected from April 2008 to September 2009 compared with the suction value corrected during the summer only (from July to October). The corrected values are read on the drying experimental curve in correspondence of water content measured in the dry months; they reaches 200 kPa, and so are more than double of the values measured. Of course if the suction values corrected are used, the experimental paths in dry period approach to the experimental drying curve (*fig.5.13c*) (*Nicotera et al., 2008*).

	tensiometer level:	1			2			4 superior			4 inferior		
circa	seasons	min	max	mean	min	max	mean	min	max	mean	min	max	mean
2008	wet	-	-	-	-	-	-	-	-	-	-	-	-
	intermediate-drying	0.31	0.35	0.32	0.35	0.39	0.36	0.45	0.47	0.46	0.47	0.48	0.475
	dry	0.22	0.37	0.27	0.25	0.41	0.3	0.41	0.44	0.42	0.43	0.45	0.44
	intermediate-wetting	0.14	0.38	0.29	0.16	0.43	0.26	0.35	0.38	0.37	0.36	0.39	0.38
2009	wet	0.33	0.39	0.36	0.38	0.43	0.41	0.4	0.48	0.45	0.41	0.51	0.47
	intermediate-drying	0.25	0.34	0.29	0.3	0.38	0.34	0.46	0.49	0.48	0.48	0.52	0.5
	dry	-	-	-	-	-	-	-	-	-	-	-	-
	intermediate-wetting	-	-	-	-	-	-	-	-	-	-	-	-

tab.5.5: Minimum, maximum and mean water content values for each soil over time intervals identifyed

	part of soil profile:	top		intermediate			
circa	seasons	min	max	mean	min	max	mean
2008	wet	-	-	-	-	-	-
	intermediate - drying	0.33	0.37	0.34	0.4	0.47	0.465
	dry	0.235	0.335	0.28	0.42	0.445	0.43
	intermediate - wetting	0.15	0.405	0.275	0.355	0.385	0.375
2009	wet	0.355	0.41	0.385	0.405	0.5	0.46
	intermediate - drying	0.275	0.36	0.33	0.417	0.505	0.49
	dry	-	-	-	-	-	-
	intermediate - wetting	-	-	-	-	-	-

tab.5.6: Minimum, maximum and mean water content values for each part of soil profile over time intervals identified

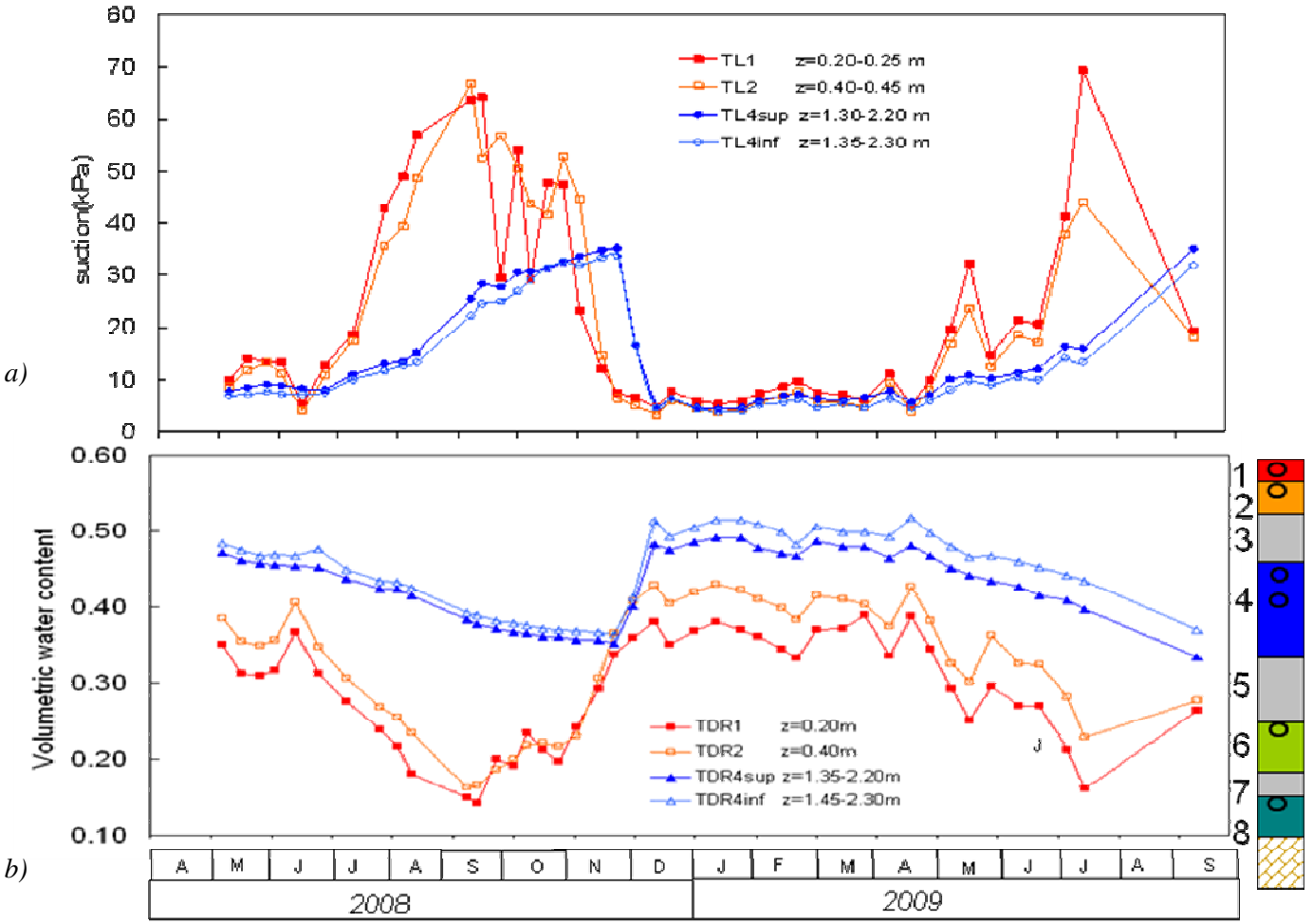

Fig.5.4: Mean values of suction b) Mean values of volumetric water content measurements against the time, April 2008-September 2009

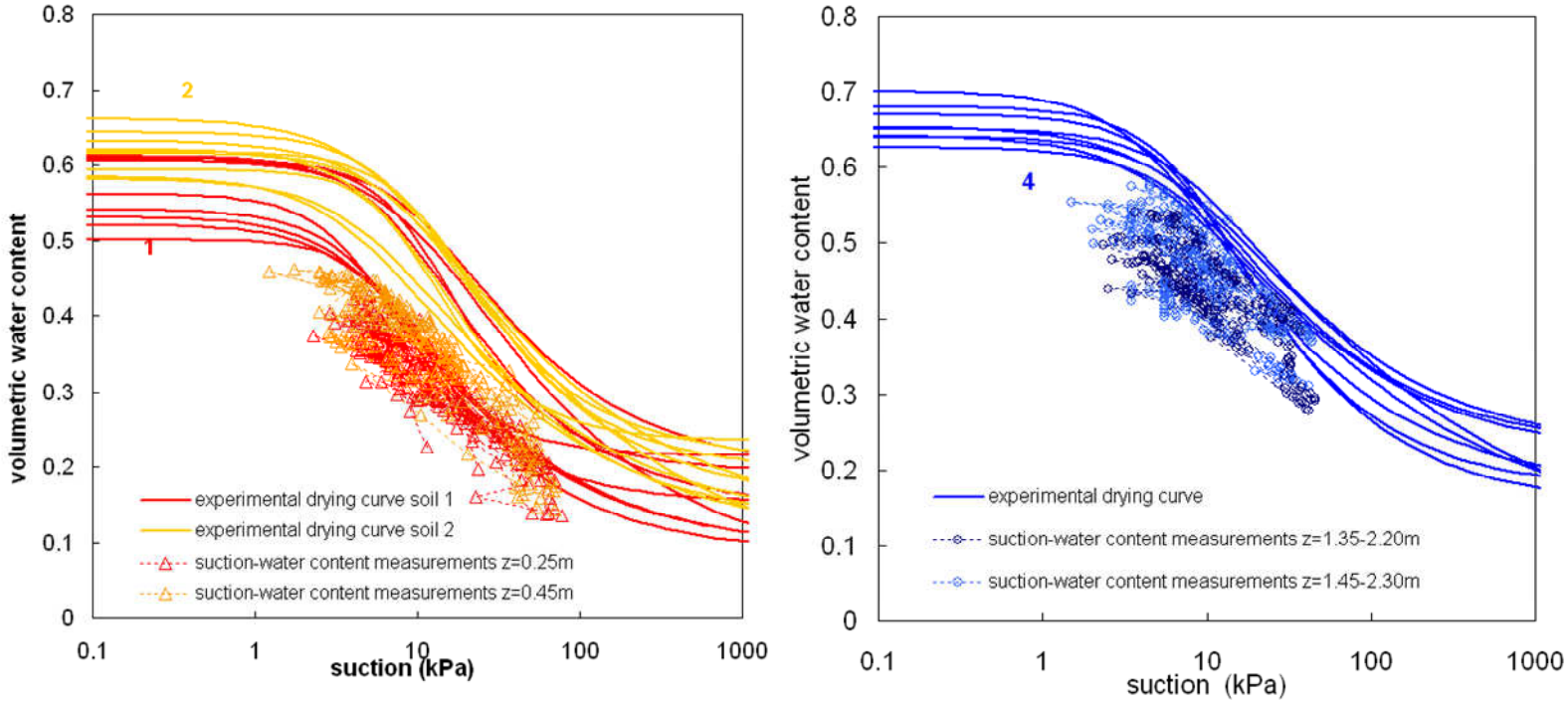

Fig.5.5: Suction and water content measured in the verticals along the section B-B'(Nicotera et al., 2008),and experimental retention curves (Papa,2007) in the soils 1-2 a); in the soil 4 b)

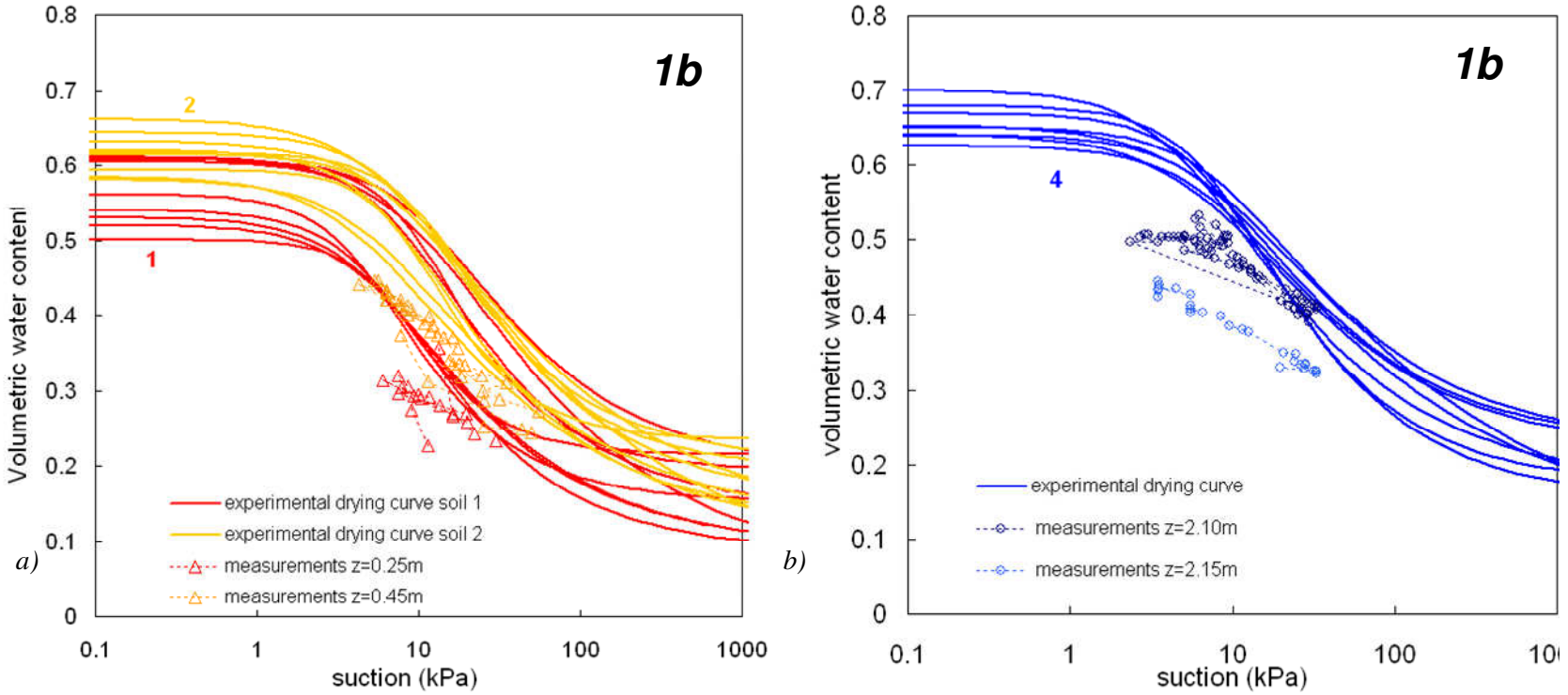

Fig.5.6: Suction and water content measured in the vertical 1b of the section B-B' and experimental retention curves (Papa,2007) in the soils 1-2 a); in the soil 4 b)

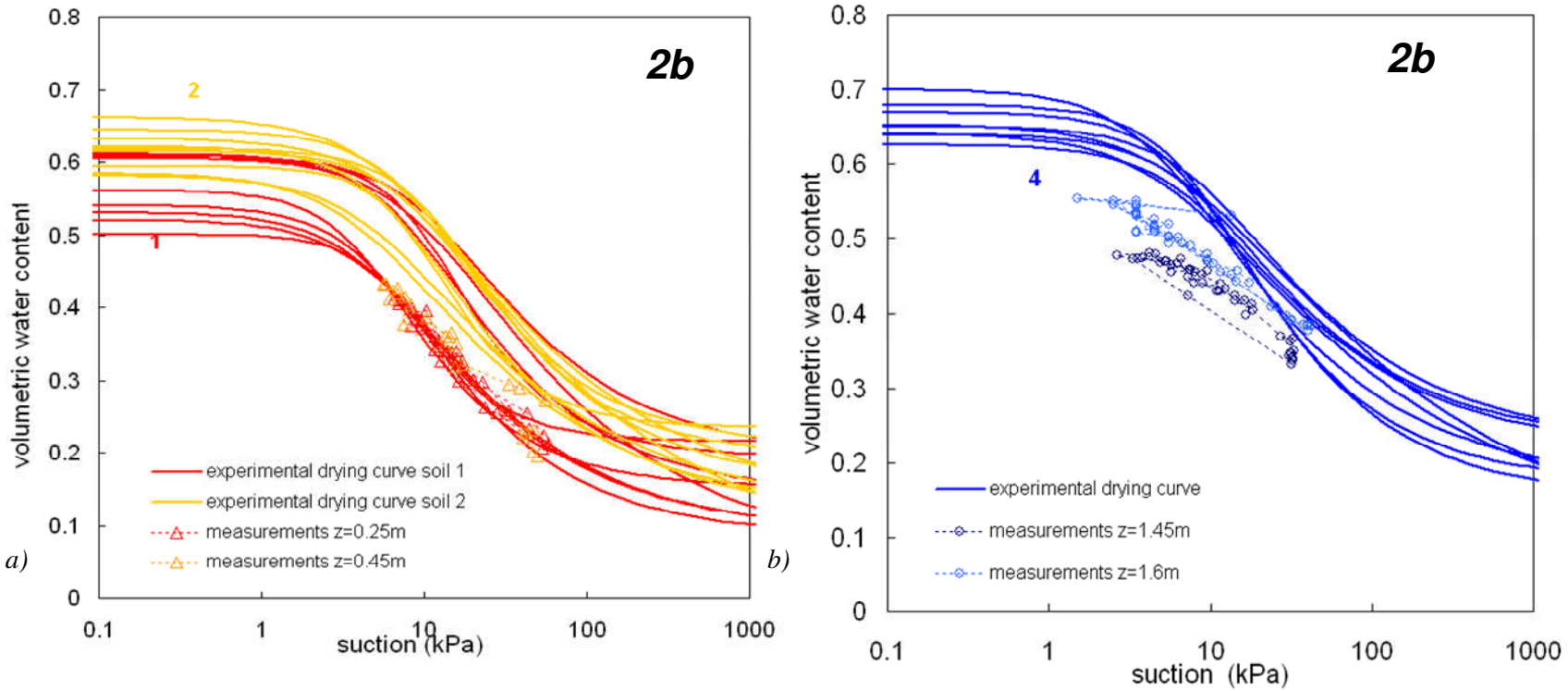

Fig.5.7: Suction and water content measured in the vertical 2b of the section B-B' and experimental retention curves (Papa,2007) in the soils 1-2 a); in the soil 4 b)

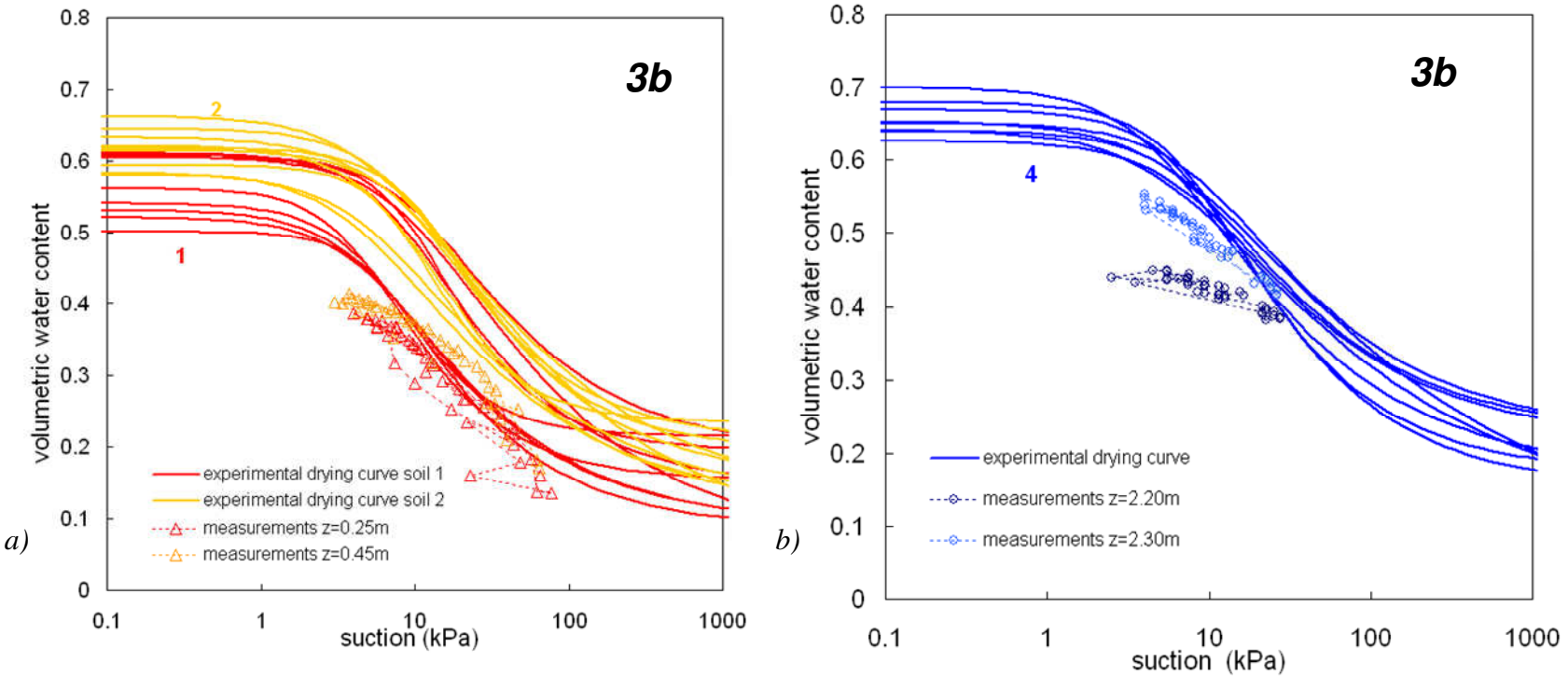

Fig.5.8: Suction and water content measured in the vertical 3b of the section B-B' and experimental retention curves (Papa,2007) in the soils 1-2 a); in the soil 4 b)

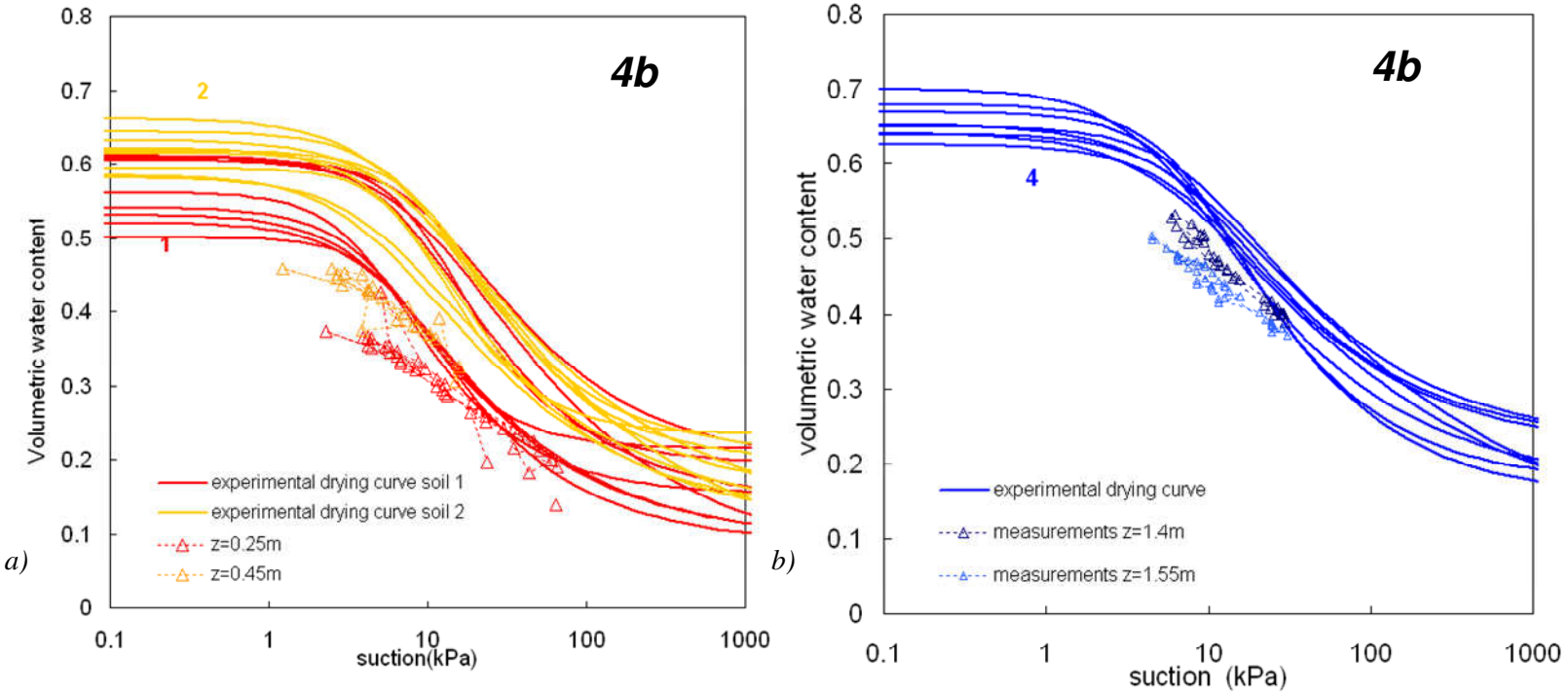

Fig.5.9: Suction and water content measurements in the vertical 4b of the section B-B' and experimental retention curves (Papa,2007) in the soils 1-2 a); in the soil 4 b)

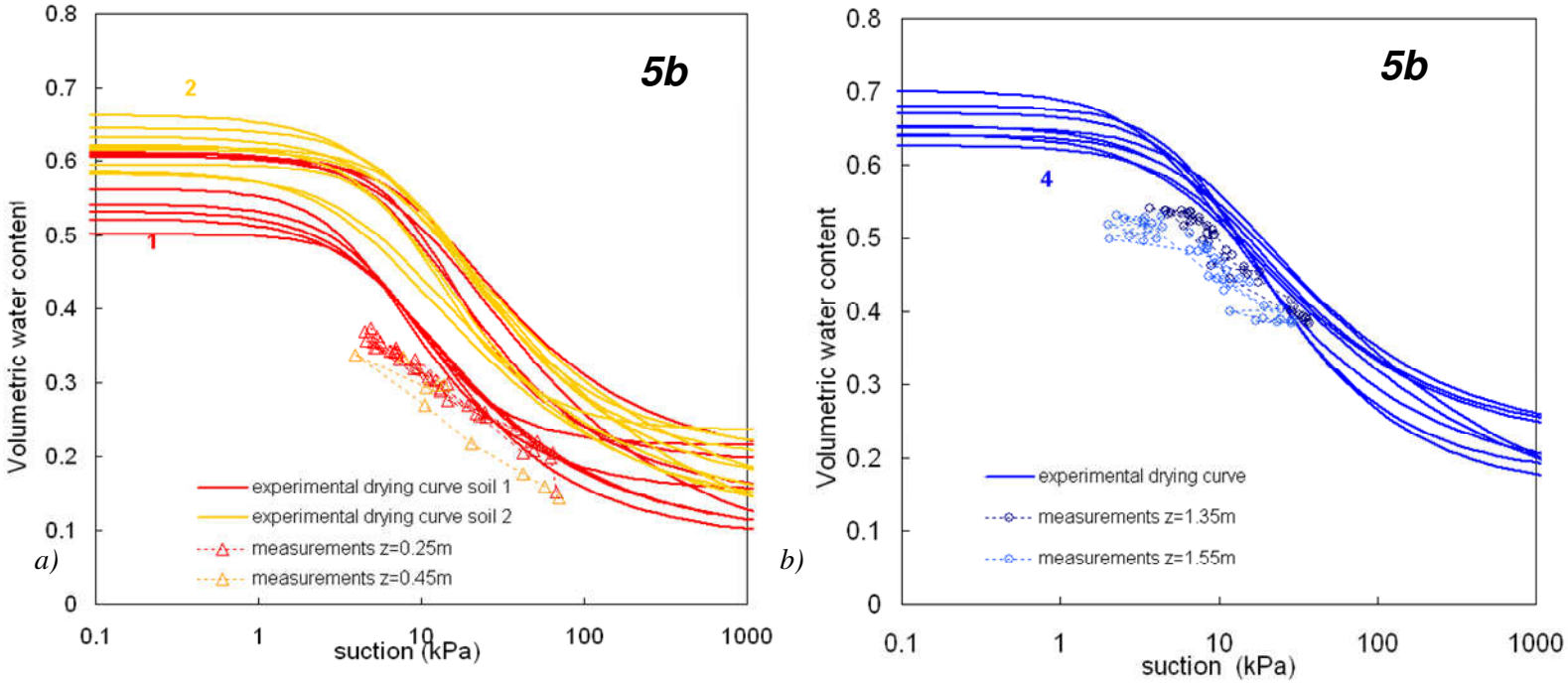

Fig.5.10: Suction and water content measured in the vertical 5b of the section B-B' and experimental retention curves (Papa,2007) in the soils 1-2 a); in the soil 4 b)

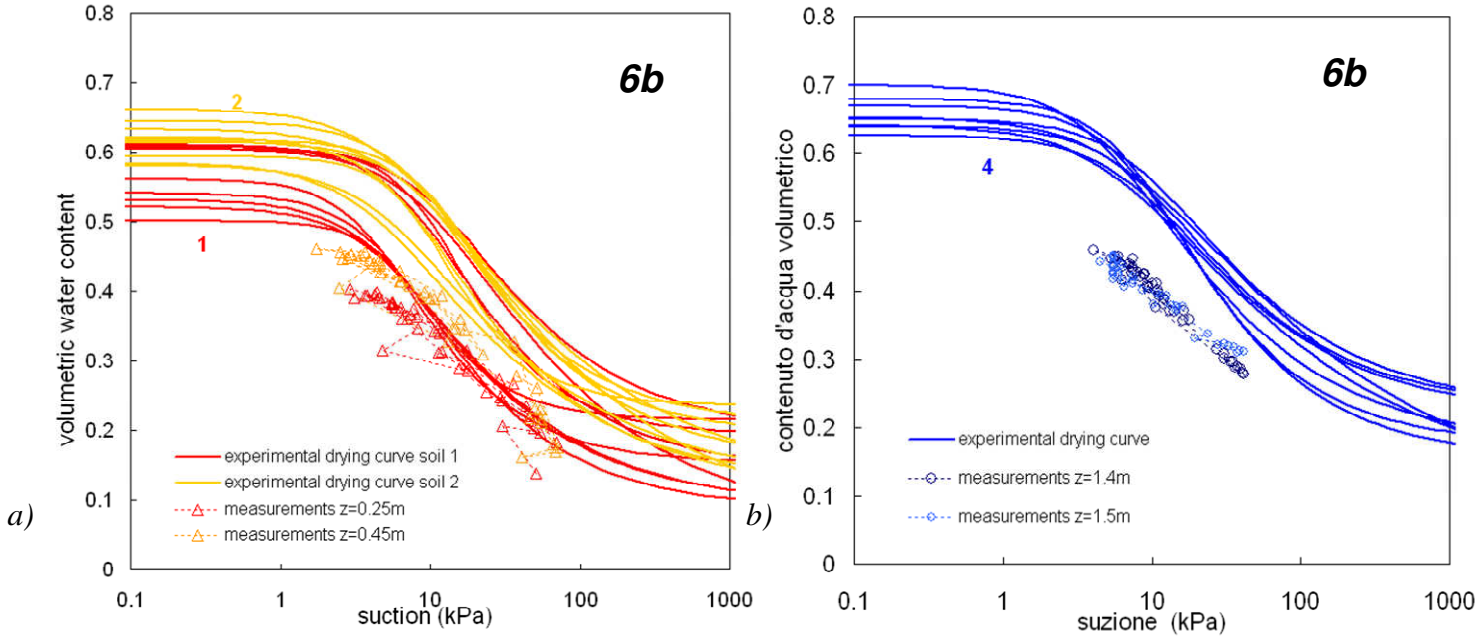

Fig.5.11: Suction and water content measured in the vertical 6b of the section B-B' and experimental retention curves (Papa,2007) in the soils 1-2 a); in the soil 4 b)

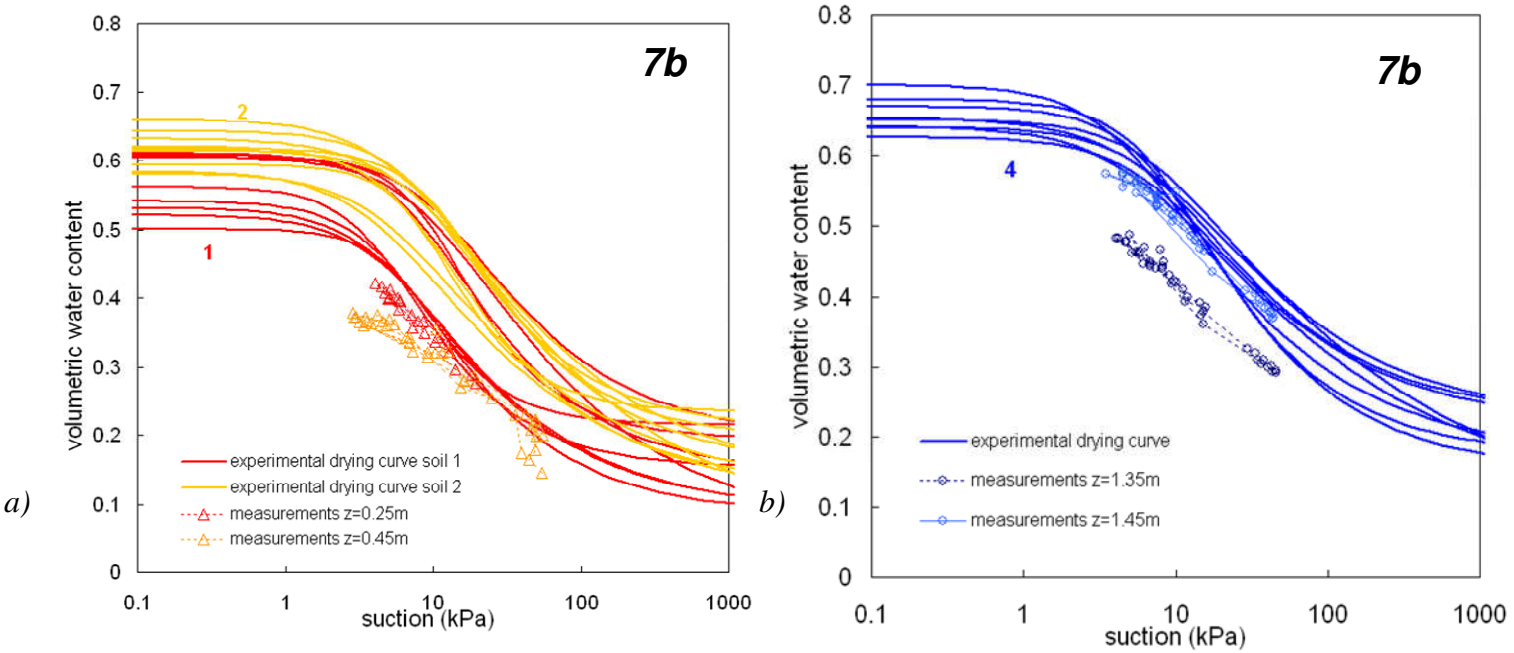

Fig.5.12: Suction and water content measured in the vertical 7b of the section B-B' and experimental retention curves (Papa,2007) in the soils 1-2 a); in the soil 4 b)

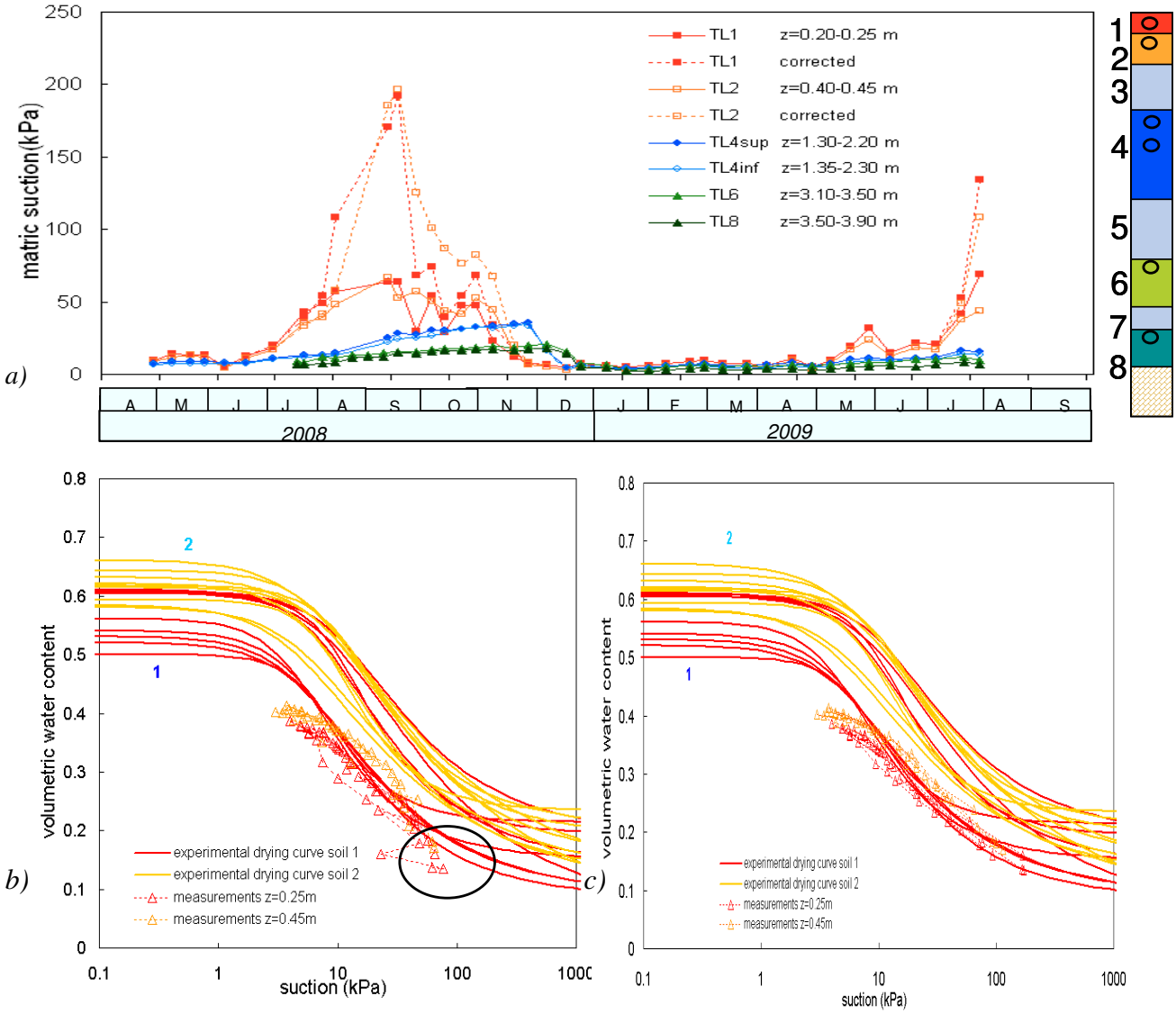

Fig.5.13: Suction measured and suction corrected in the dry period averaged over the verticals along the section B-B' against the time (Papa et al., 2009) a); suction and water content measurements collected in the superficial soils along the vertical 3b along the section B-B' and the experimental retention curves (Papa,2007) b); suction corrected and water content measurements of the superficial soils in the vertical 3b along the section B-B 'and the experimental retention curves (Papa,2007) c)

5.2.3 Climatic conditions measurements

5.2.3.1 Rainfall

The daily rain collected by Monteforte Rain gauge (502m s.l.), close to the test site, is available from 1st October 2005; the intensity collected by Avella Rain gauge is available from 1st October 2005 to 30th November 2007 too (*Fig.5.14*).

A first weather station was installed in the test site (605 m s.l.) on 21st February 2008; because of its failure, a second one was installed on 26th June 2009[6]. Therefore, the daily rain intensity on the test site is available from 21st February 2008 to 31st August 2008 and from 26th June 2009 (*Fig. 5.14*).

Both rain gauge installed on site collect the rainfall every ten minutes in order to know how rain is distributed over one day (*Figs. 5.15a,b*). In the *figure 5.15a,b* Rainfall collected on 16th and 20th September every ten minutes over all the day is plotted.

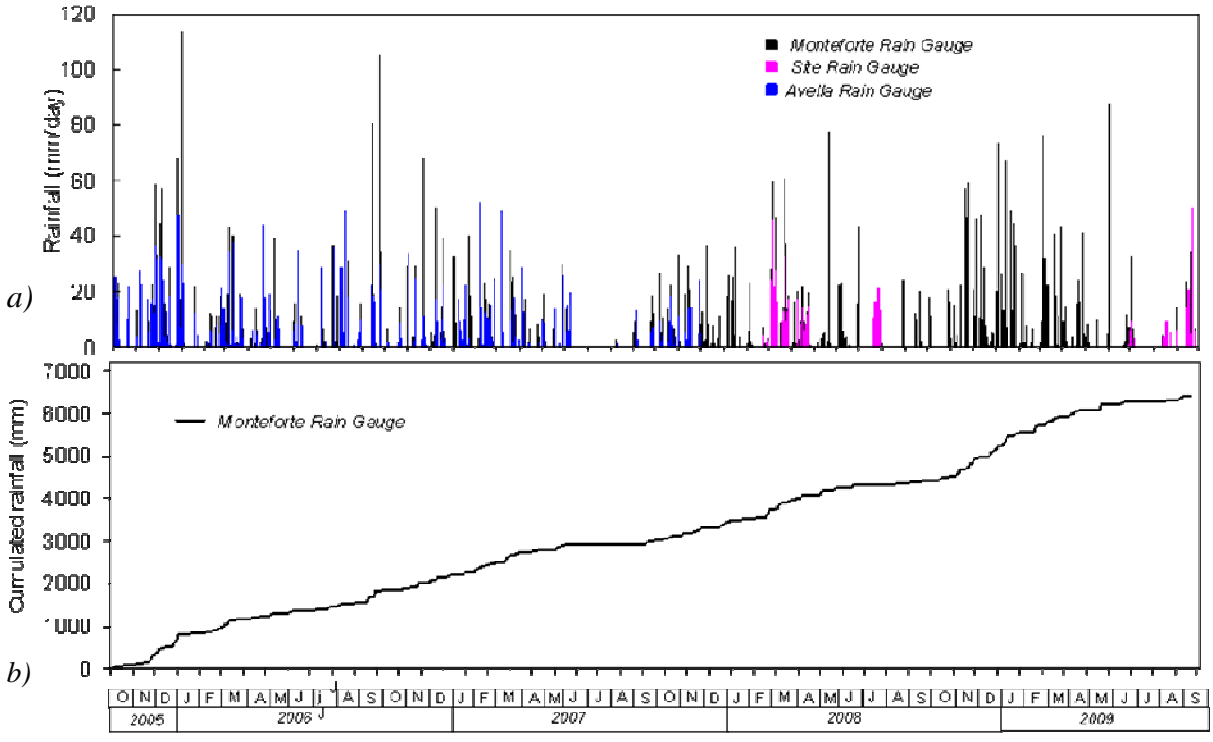

Fig. 5.14: Daily rainfall collected by the Monteforte, Avella rain gauge and by the meteorological station installed on the site a); Cumulated rainfall measured by Monteforte Rain gauge b)

[6] The first meteorological station was installed on 21st February 2008 and it worked for five months; then was replaced by the second one on 26th June 2009. Both collect the rainfall cumulated over ten minutes.

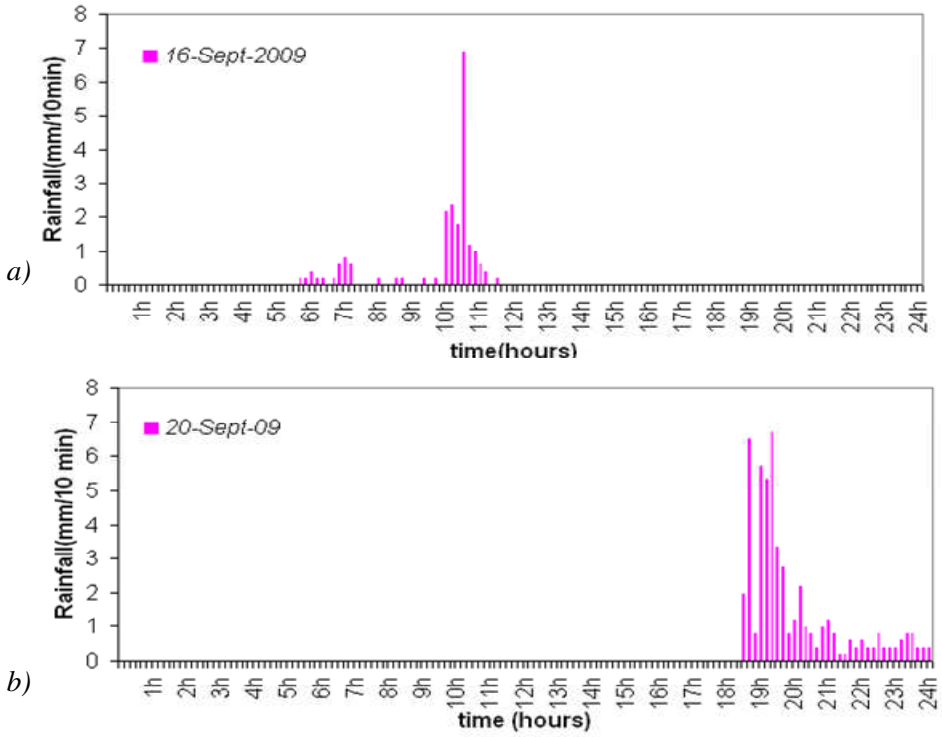

Fig.5.15: Rainfall collected every ten minutes over one day, 16th September 2009 a); 20th September 2009 b)

5.2.3.2 Net Radiation

Net radiation measurements are collected from 26th June 2009 by the net radiometer installed in site and connected to Campbell scientific data logger.

The measurements are sampled every four hours in order to view the daily oscillations (*figs.5.16a, 5.22*). The values measured at 4.00 a.m. are always close to the minimum value 50 W/m^2, and the direction of the heat flow results out-going from the subsoil (negative flow)(*fig.2.22*). Those measured at 4.00 p.m. are between 200 – 550 W/m^2 and are function of the temperature (*see fig.5.21*), the direction of the heat flow is in-going in the subsoil (positive flow)(*fig.5.22*).

In the figure *2.16b* the daily values are plotted, the heat flows is in-going in the subsoil and so they are positive. In fact the absolute values of the net radiation in the night (the heat flows out going from the subsoil), is lower than these in the morning at least in the summer months.

.

a)

b)

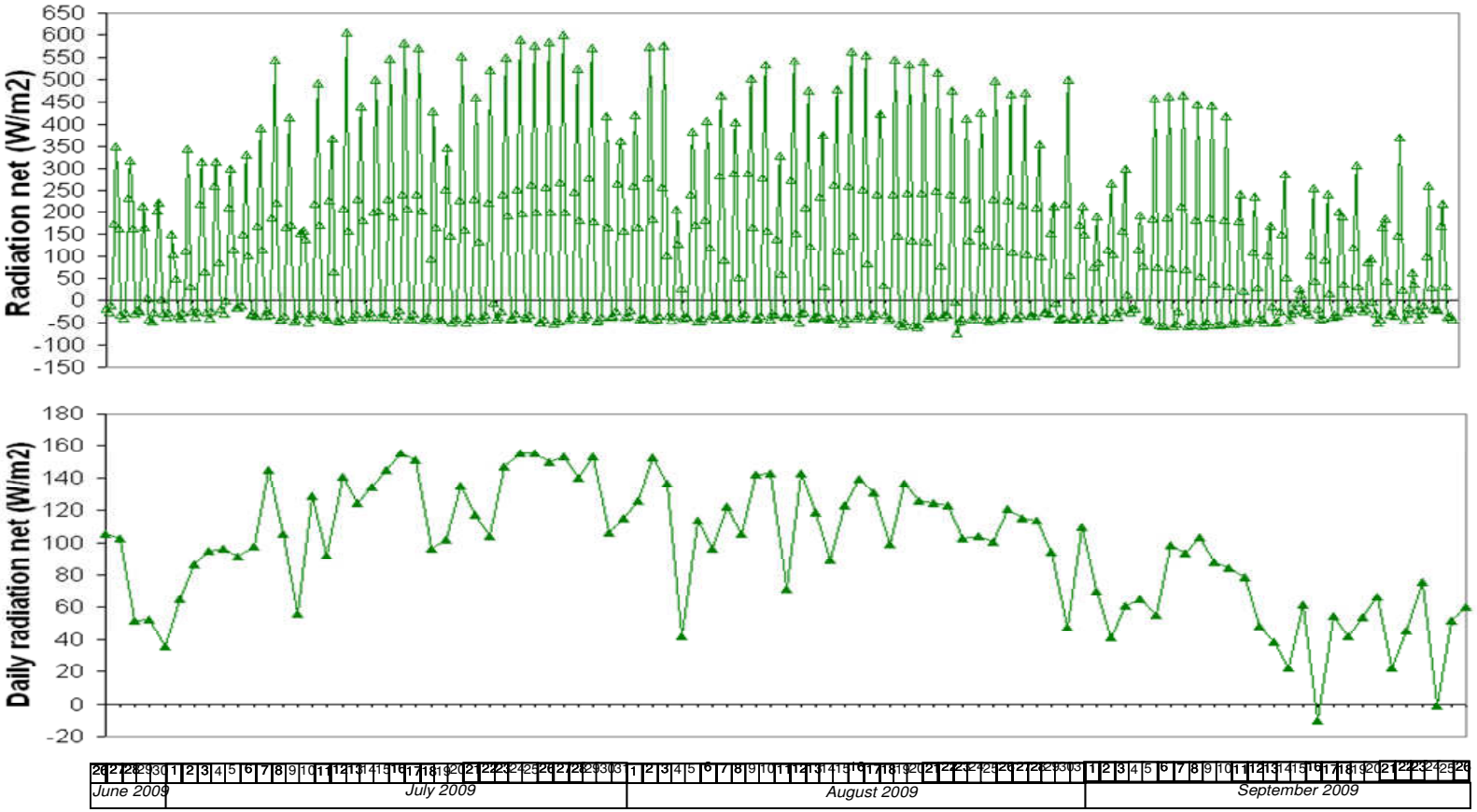

Fig.5.16: Radiation net measured in site every four hours from 26th June 2009 to 26th September2009 a);daily radiation net b)

5.2.3.3 Air Temperature - Air Humidity measurements

Air temperature and air humidity were measured from 8th November 2006 to 1st March 2008 by using a termoigrometer portable in the same days when suction measurements were collected (*Fig.5.17a, b*).[7]

Then the values sampled every four hours were collected from 21st February 2008 to 31st August 2008 by the first meteorological station installed in site and now are collected by the last one installed on 26th June 2009. The daily mean values are plotted in the *figure 5.18b, 5.19b*.

By observing the figure 5.*17a* in winter the main temperature is around 10 °C and in summer it's around 25 - 30°C, the variations seems to be seasonal (see *fig. 5.21*). The air humidity seems not to follow properly a seasonal trend, in fact it is influenced heavily by the rainfall (see *figs. 5.17b, 5.21*).

In the *figures 5.18a,b, 5.19a,b* the temperature and humidity measurements either sampled every four hours and the daily values measured from 26th June 2009 to 26th September 2009 are plotted (see *fig. 5.21*). By observing fig. *5.22b* air temperature reaches the daily highest value at 4.00 p.m. and the lowest one at 4.00 a.m.

It is interesting to point out that the daily range of air temperature is seasonally too, in fact in the summer it reaches 10°C, while in the spring, 5 - 7° C (*fig.5.22*).

5.2.3.4 Wind speed measurements

Wind speed measurements are collected every four hours and are plotted in *figure 5.20a* from 26th June 2009 to 26th September 2009. The minimum value of 0.2 m/s is imposed in the program used by the data logger to collect the data.

In the figure 5.*20b* the daily values measured are plotted. The wind speed values allow to calculate the evapotranspiration flow.

[7] Air temperature and air humidity measured by the termoigrometer portable *in the figure 5.17* are the average over the two measurements collected in site at morning and at noon.

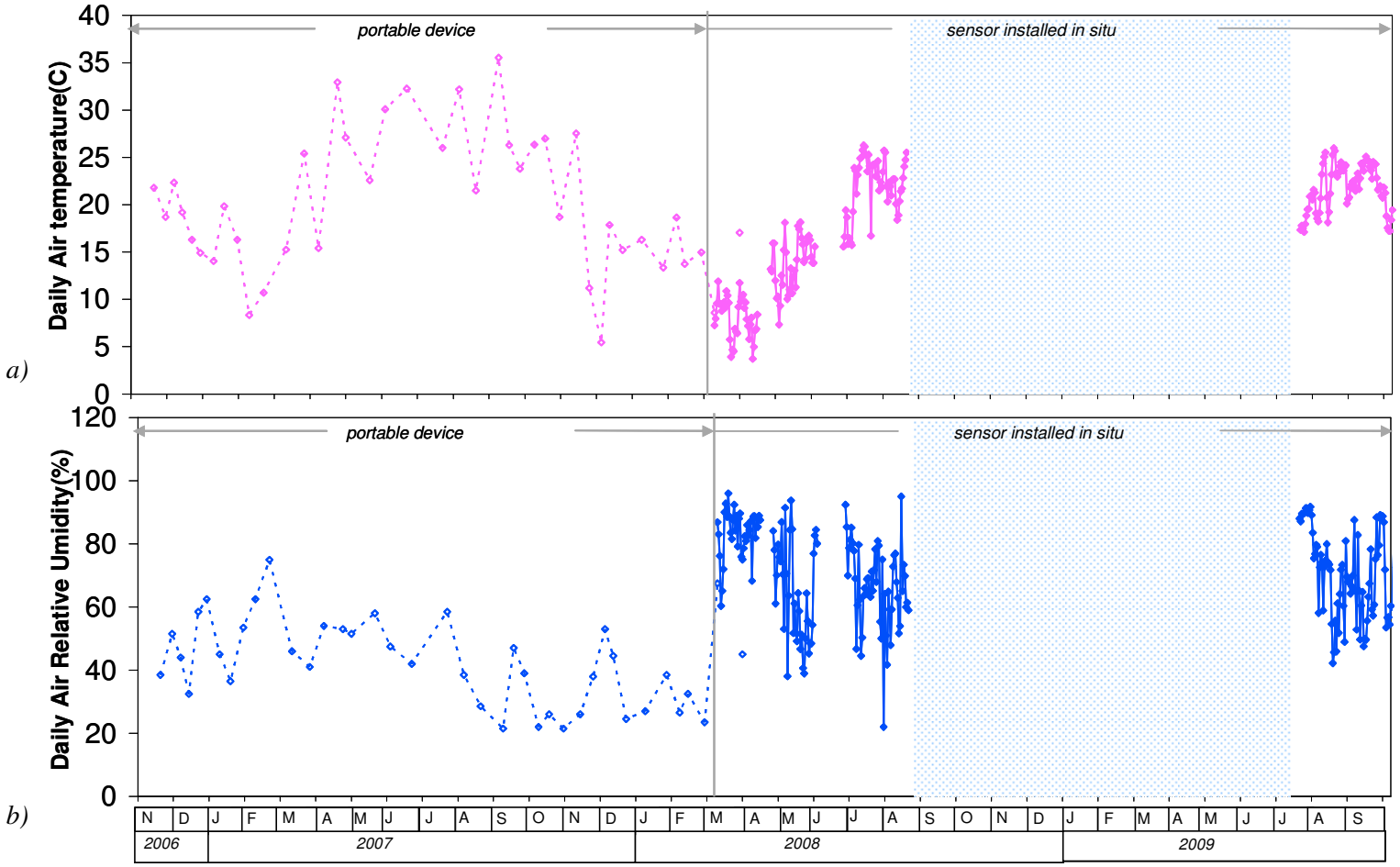

Fig.5.17: Air temperature measured in site every ten days from 8 November 2006 to 8March 2008, every four hours from 8 March 2008 to 26th September a); air Relative Humidity measured in site from 8th November 2006 to 26th September b)

a)

b)

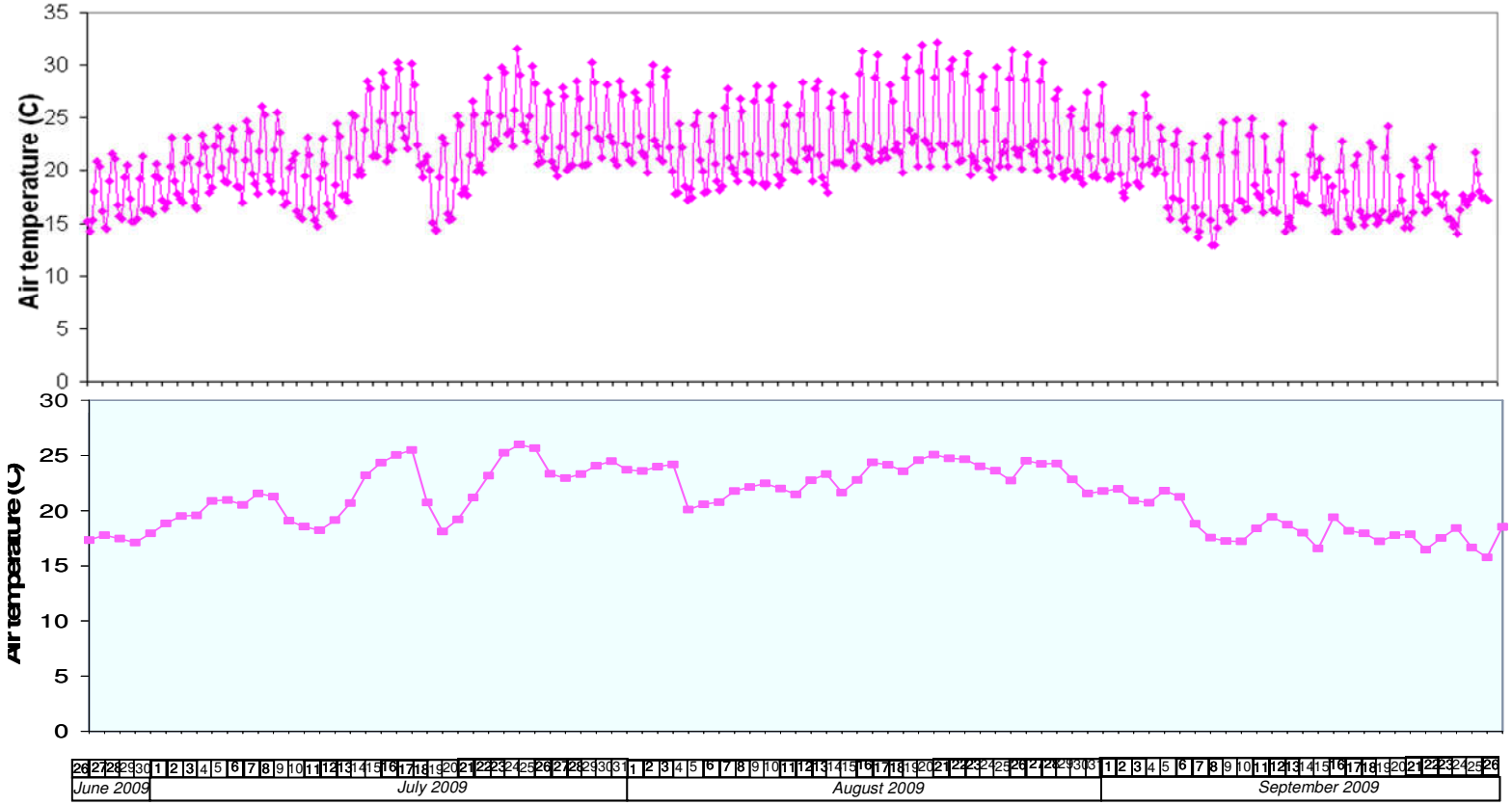

Fig.5.18: Air Temperature measured in site from 26th June 2009 to 26th September2009 a); daily air temperature b)

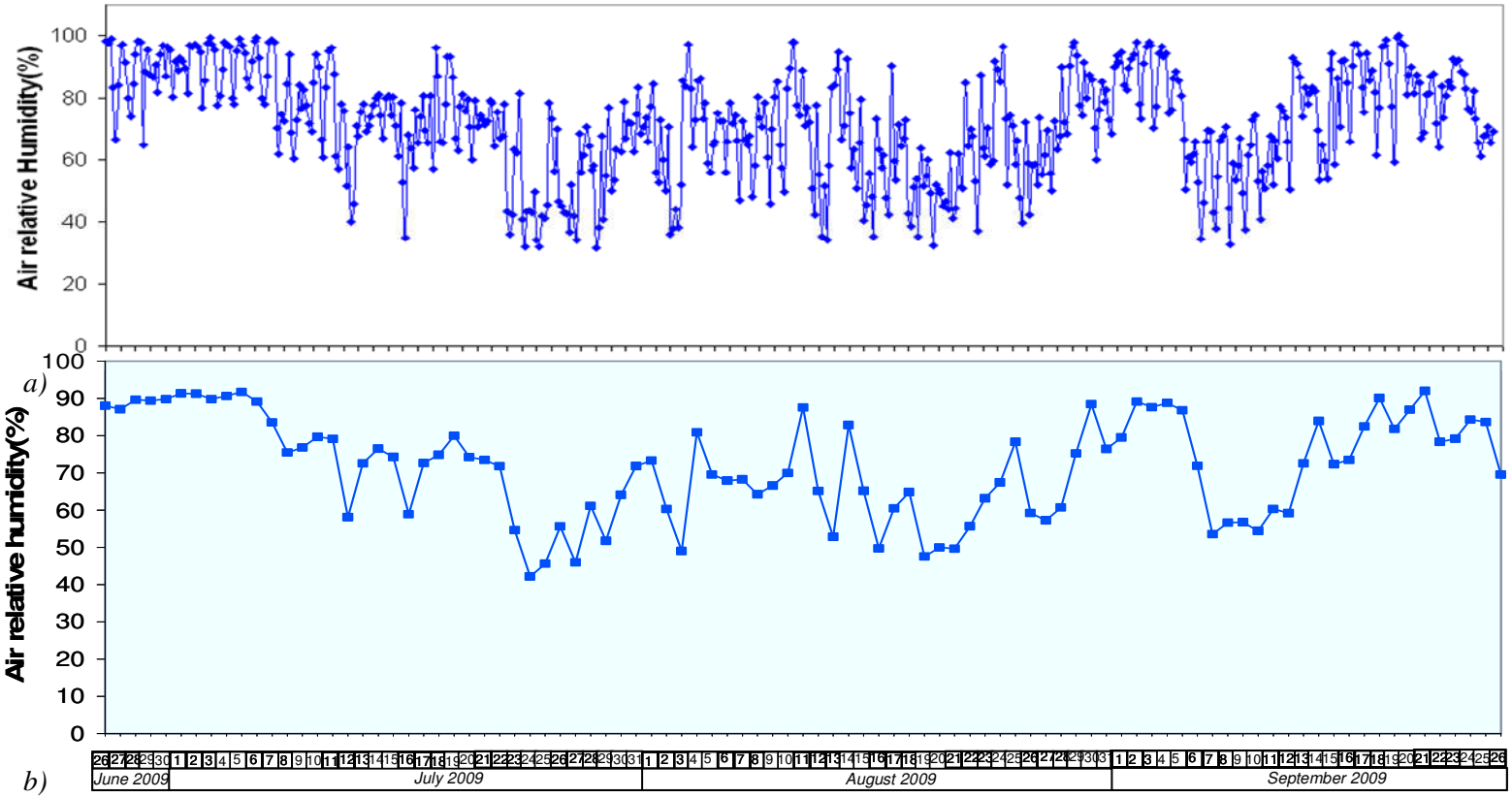

Fig.5.19: Air humidity measured in site from 26th June 2009 to 26th September2009 a); daily air humidity b)

a)

b)

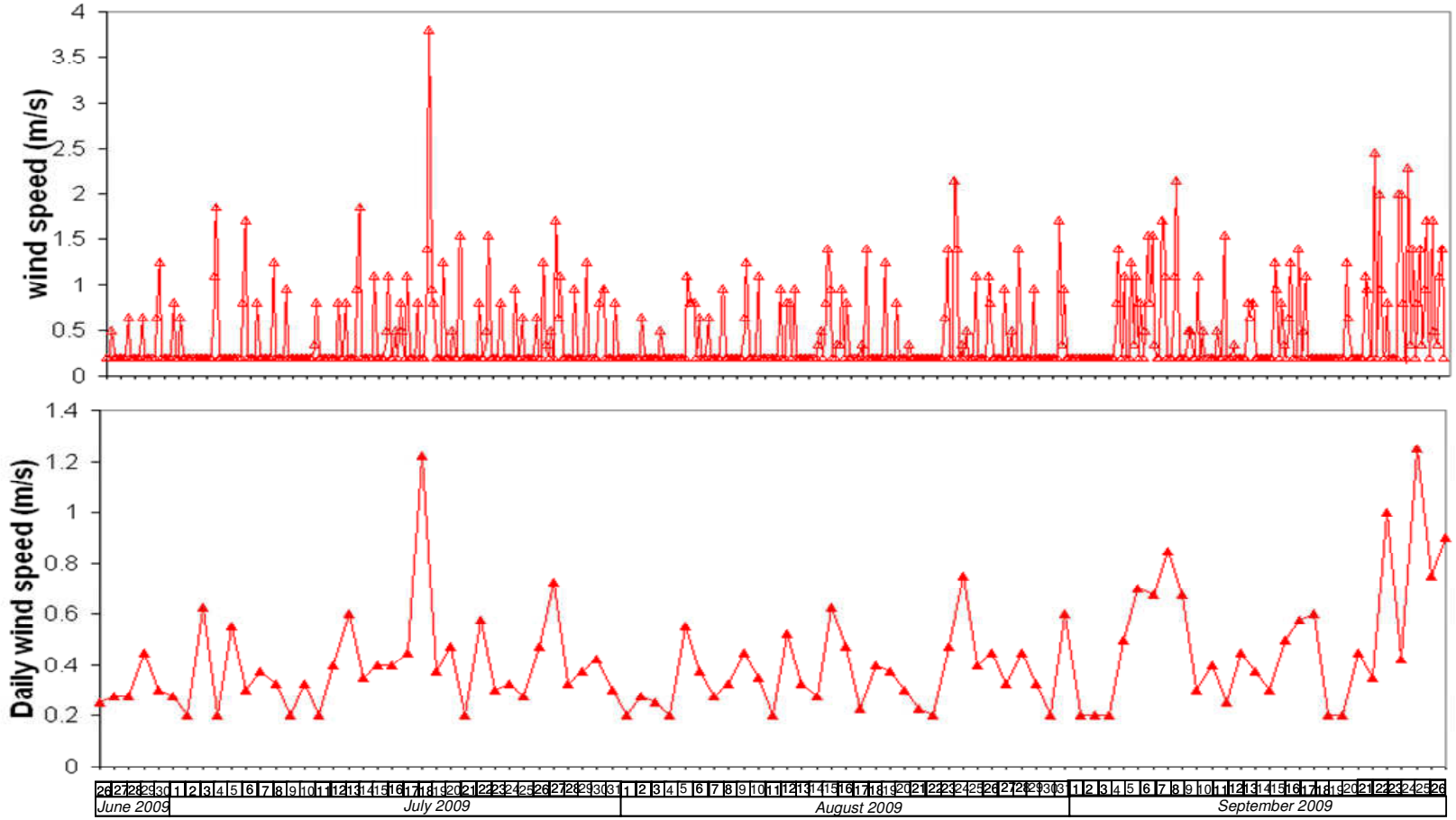

Fig.5.20: Wind speed measured in site from 26th June 2009 to 26th September2009 a); daily wind speed b)

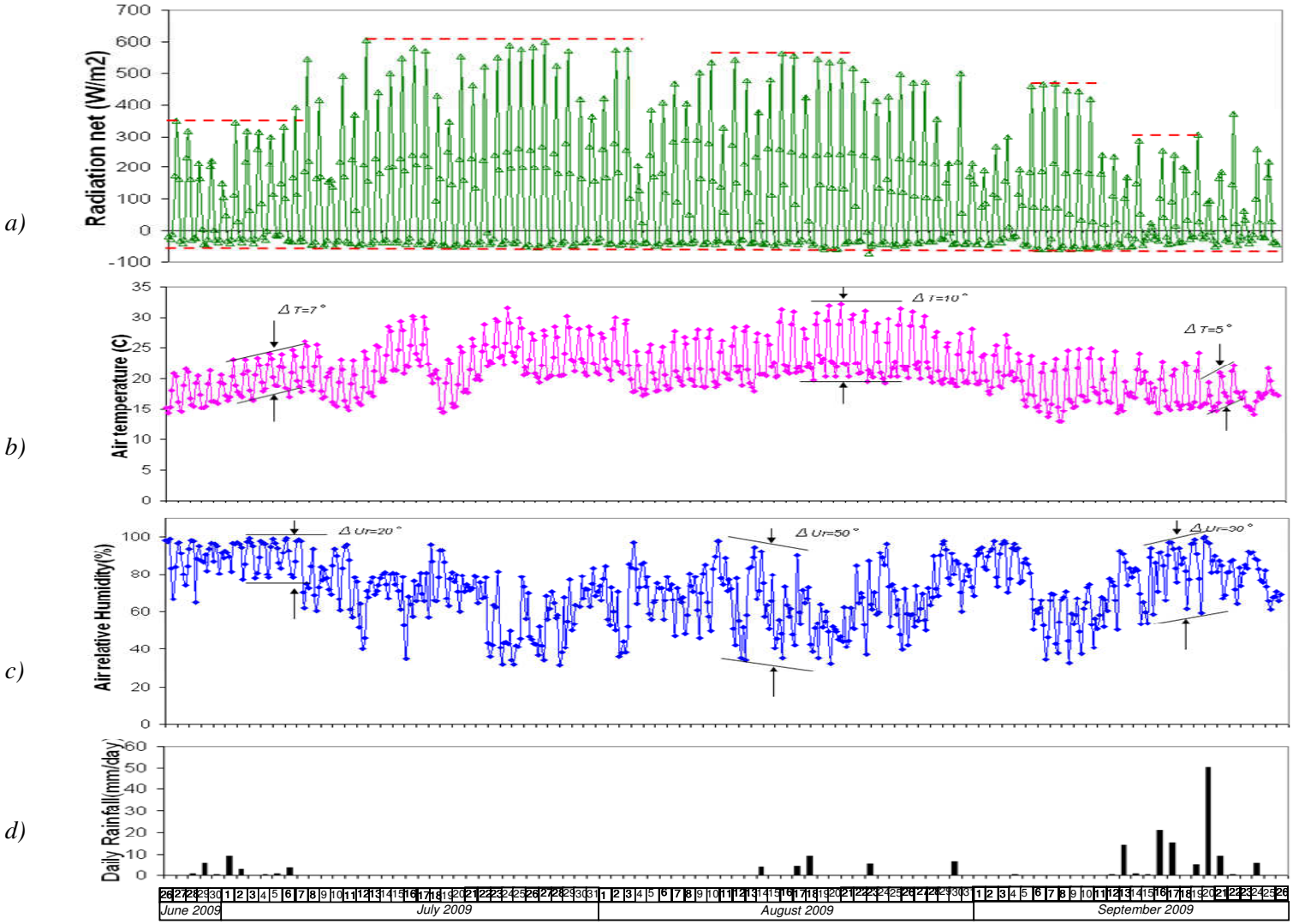

Fig.5.21: Radiation net a), air temperature and air humidity b), c), Daily rainfall d) measured in site from 26th June 2009 to 26th September2009

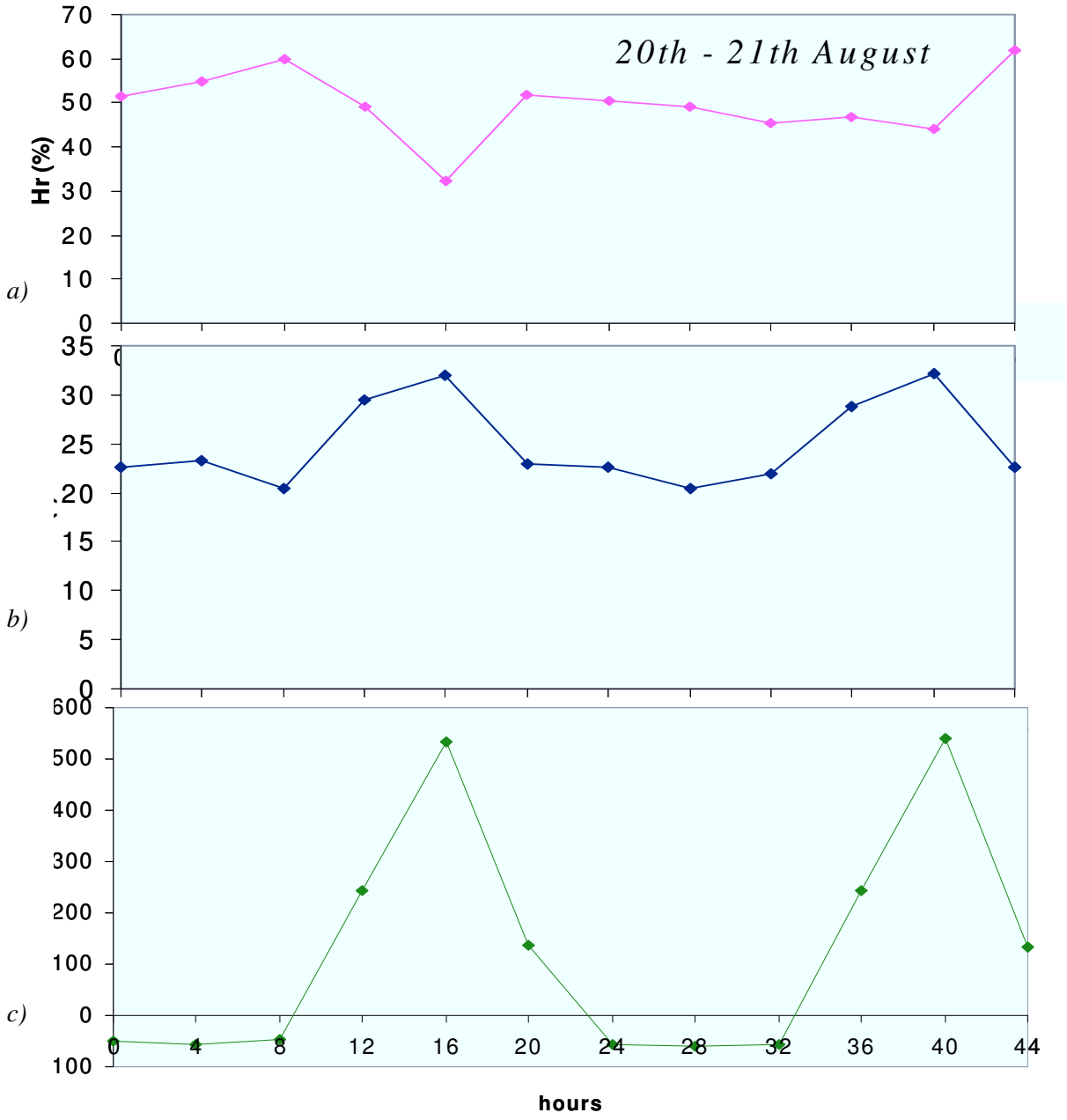

fig. 5.22: Relative Humidity a), Air temperature b) , Radiatio net c), measured over two days, 20th-21th August.

5.3 Data analysis

In this section a spatial analysis in terms of piezometric head and suction measurements is presented. By using a technique of interpolation, the isopiezic lines and directions of the water flow vectors in the subsoil are obtained by using the suction measurements available. The longitudinal section B-B', the transversal section D-D', and the alignment stratigraphic of the site (see fig. 5.23) are investigated essentially in order to understand the flow phenomena in the pyroclastic cover.
Then the water flows intensity are calculated by using the suction measurements and the water content. Some conclusions are achieved about the water flow in the pumices of Avellino (soil 3).

5.3.1 Piezometric heads and direction of the water flow vectors

The spatial analysis of the suction measurements provides some information about the flow phenomena within the slope. The suction and the piezometric head values can be determined in other points where there are no measurements, by using the kriging interpolation[8]. Knowing the piezometric heads values it is possible to draw the isopiezic lines and the direction of the water flow vectors in the subsoil.
The sections analyzed in the following paragraphs are plotted in *Figure 5.23*:

- the longitudinal section B-B;
- the cross section D-D;
- the section of stratigraphic alignment 4inf

5.3.1.1 Monitoring of the longitudinal section B-B

By evaluating the piezometric heads along a longitudinal section, the variation of the longitudinal (x) and vertical (y) components of the flow during the seasons can be identified. The longitudinal section B-B' is considered, there suction measurements in the deeper soils (soil 6-8) are available too. The stratigraphic sequence was derived from a careful geological survey performed during the installation of instrumentation (*Fig. 5.23*). In the *figure 5.23* the position of both tensiometers and TDR probes and the pumice layers of Avellino and Ottaviano are shown.

[8] Kriging is a regression method that allows to interpolate a magnitude in the space, minimizing the mean square error. Assuming that the piezometric head varies over the space with the continuity, the unknown values in one point is calculated with a weighted average of the known values.

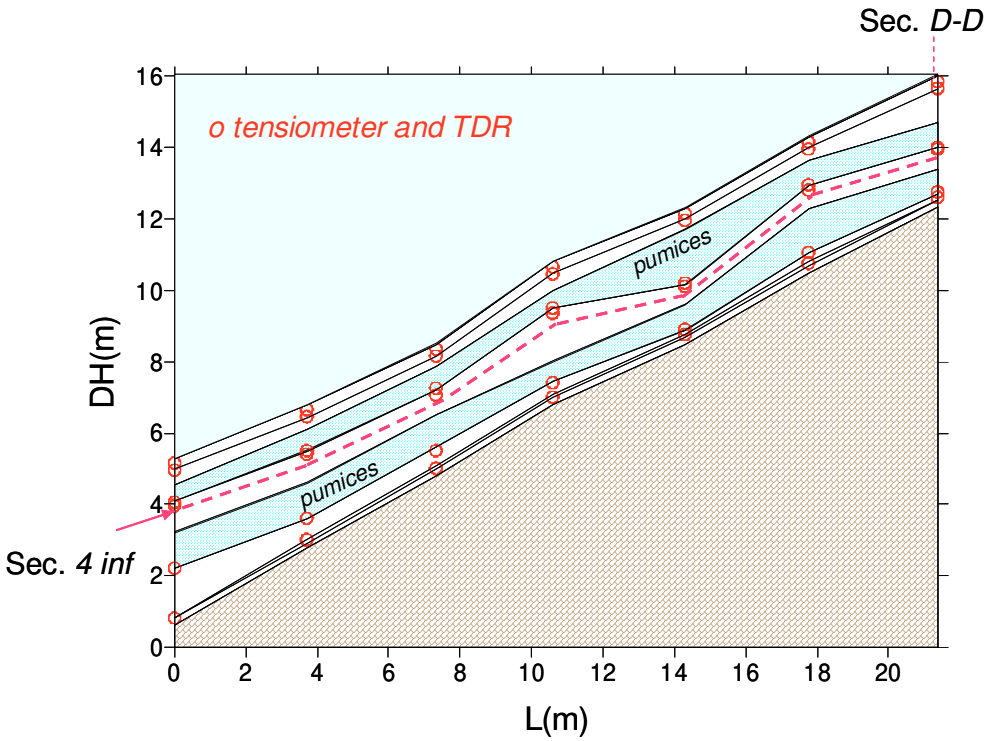

Fig.5.23: The longitudinal section B-B', the cross section D-D, the section of stratigraphic alignment 4inf

The isopiezic lines and the water flow vectors within the longitudinal section B-B at different days over one year are plotted (*fig. 5.24–5.28*). The seasonal cycle from summer 2008 to summer 2009 is analysed. Moreover in the pumice (soils 3, 5, 7) no information is extrapolated because there are not the suction measurements in those soils.

The piezometric lines move from upstream to downstream with the approach of winter, indicating an increase of the piezometric head in time at the same depth. When Spring starting, the piezometric head decreases and the isopiezic lines come back to the summer conditions.

The isopiezic lines rotate too: they are almost normal to the slope during the period of low rainfall (flow parallel to the slope) and tend to the sub-horizontal configuration when the rainfall increases (vertical flow to the slope and directed downward).

The direction of hydraulic gradients shows two main components of the ground water flow: a component parallel to the slope; a component normal to the slope. The first one is to be considered constant and related to the geometry and the morphology of the slope, the second one is variable and is a function of the water infiltrating into the subsoil. When rainfall occurs and the intensity of infiltration is very high, the superficial gradients increases and they array with those intermediate and deep. As during the wet season whole the water circulation is vertical, the infiltration process is mono-dimensional.

In the summer an upward water flow connected to evaporation phenomena in the superficial soils is observed.

.

a)

b)

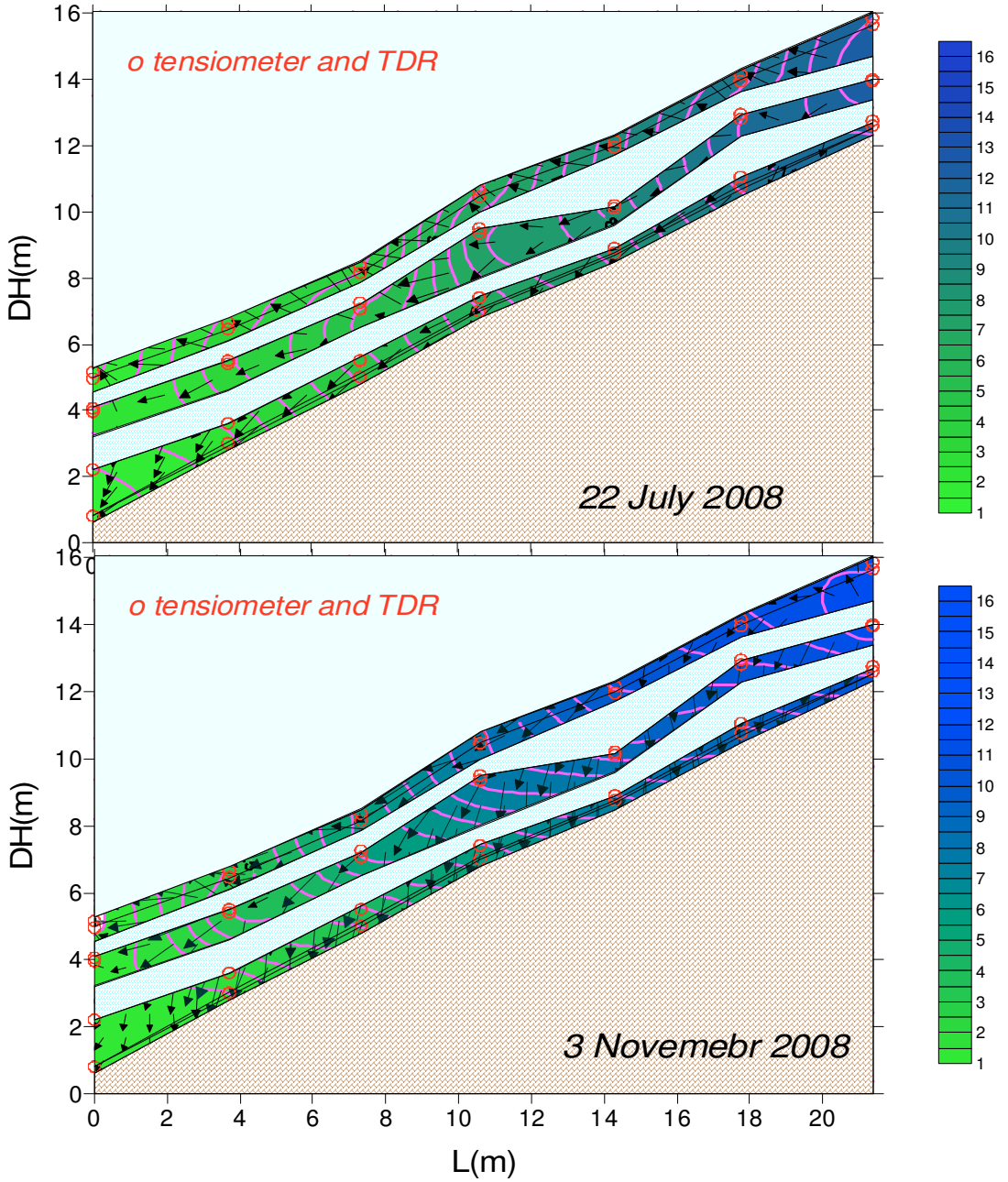

Fig.5.24: The isopiezic lines and water flow vectors along longitudinal section B-B' at 22nd July 2008 a), at 3rd November 2009 b)

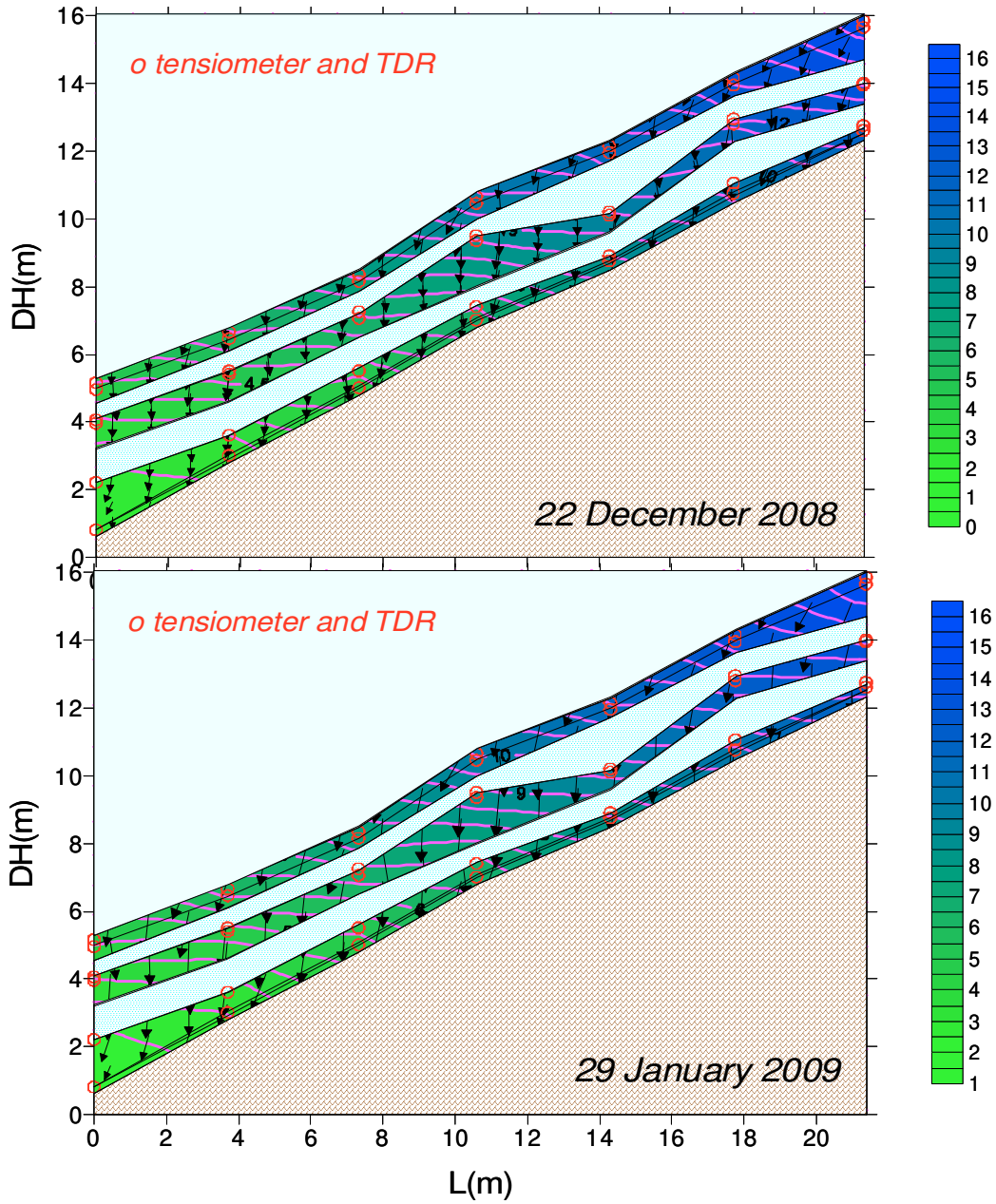

Fig.5.25: The isopiezic lines and water flow vectors along longitudinal section B-B' at 22nd December 2008 a), at 29th January 2009 b)

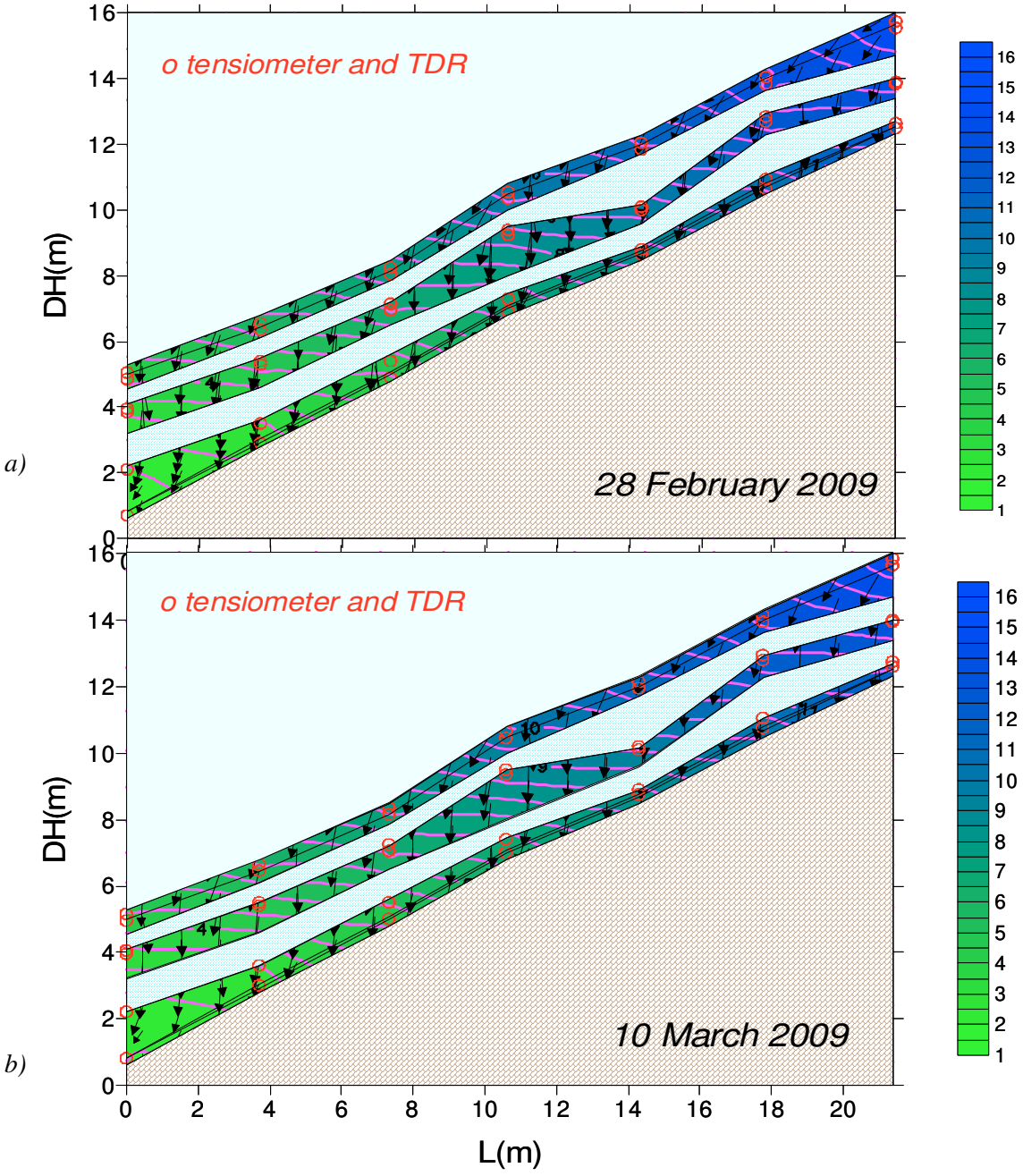

Fig.5.26: The isopiezic lines and water flow vectors along longitudinal section B-B' at 28th February 2009 a), at 10th March 2009 b)

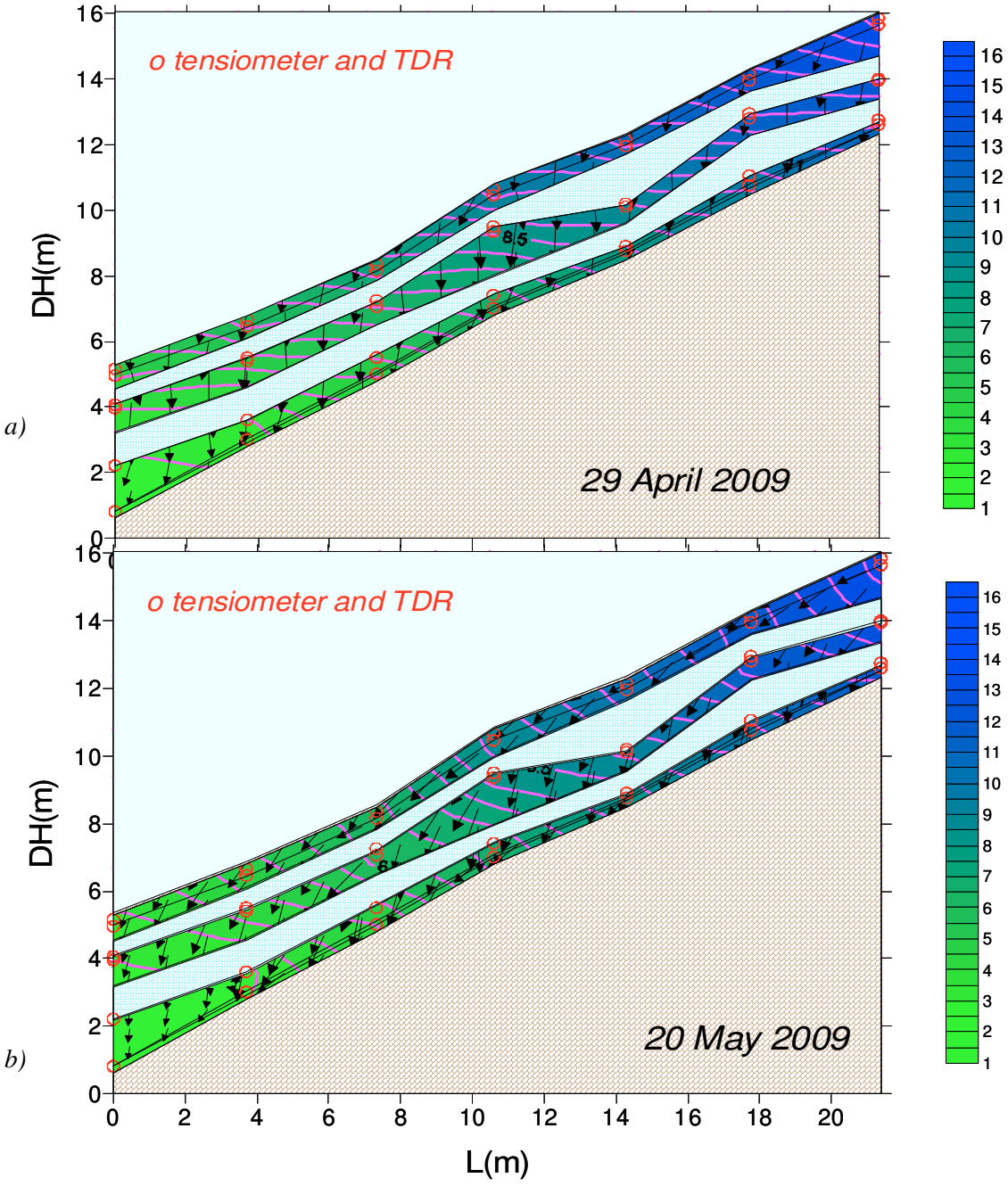

Fig.5.27: The isopiezic lines and water flow vectors along longitudinal section B-B' at 29th April 2009 a), at 20th May 2009 b)

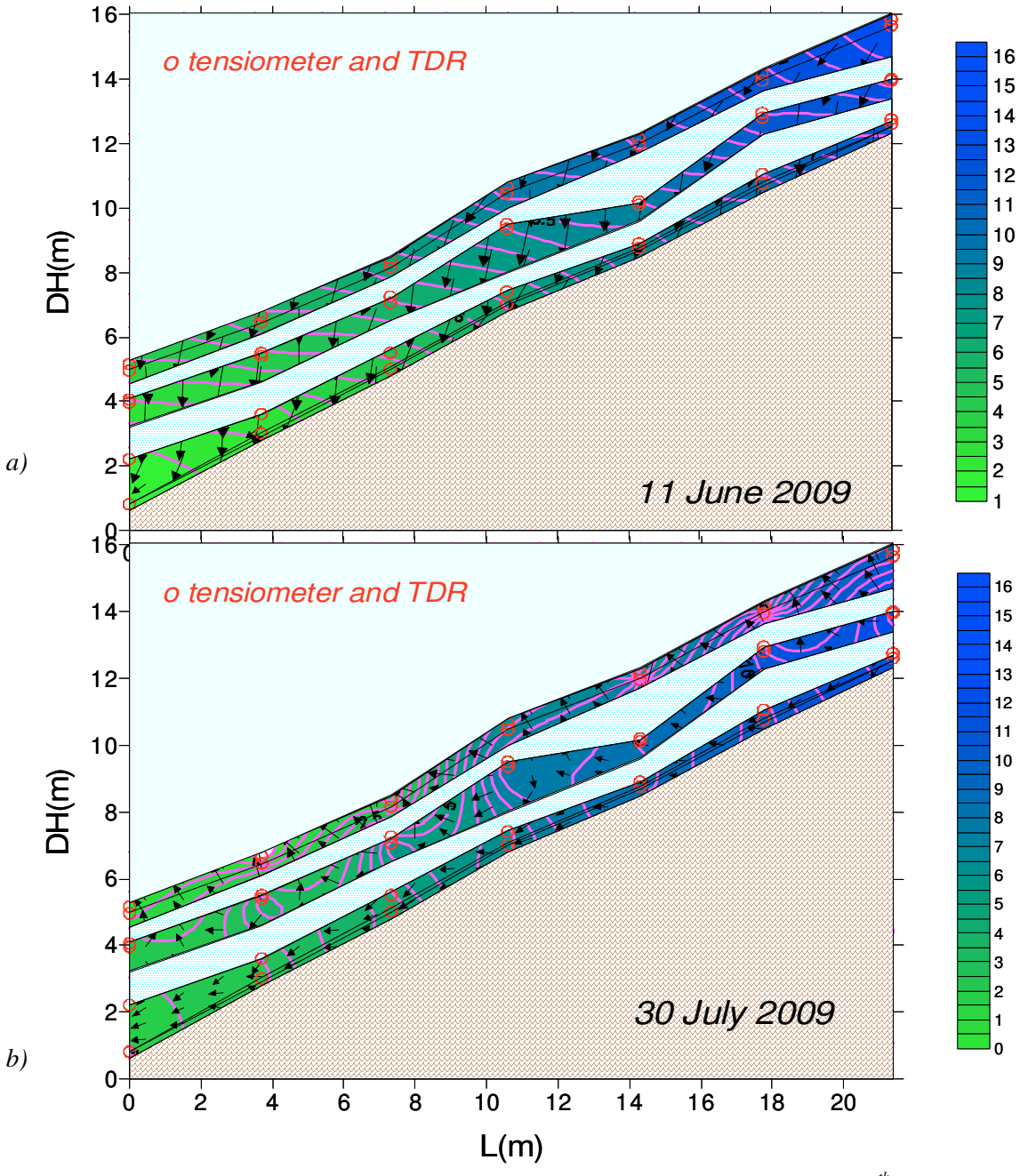

Fig.5.28: The isopiezic lines and water flow vectors along longitudinal section B-B' at 11th June 2009 a), at 30th July 2009 b)

In order to investigate variations of the hydraulic conditions over the time, the mean gradients and the mean directions are determined for each layer as a function of the suction measurements collected (Fig. *5.29*). In the *figure 5.29a, b* the mean gradient and the angle between the direction of the mean gradient and the vertical over the time are reported; the mean inclination of the slope, 27° (63° from the vertical) and the normal values to it (153 °) in the diagram are also indicated.

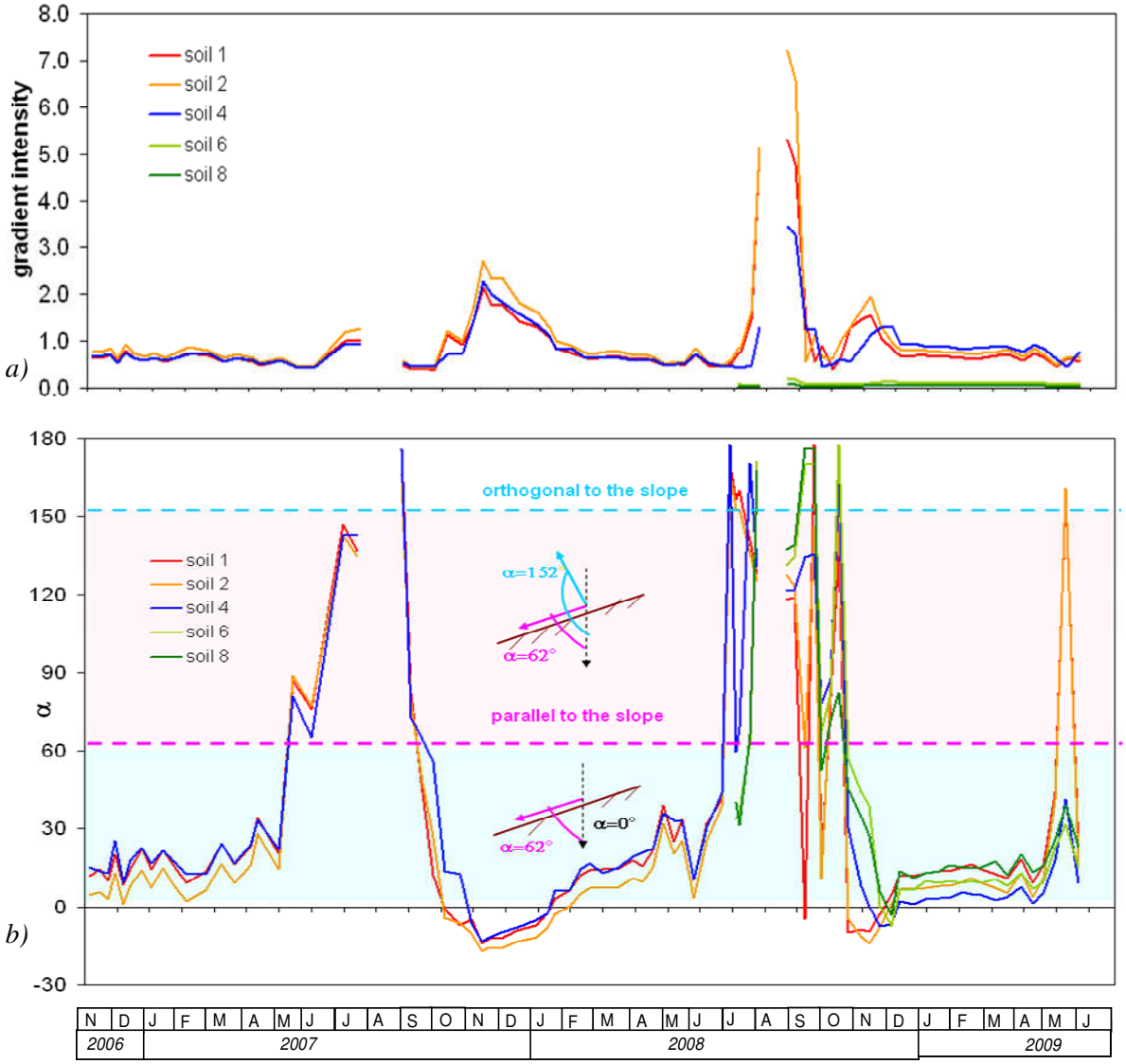

Fig. 5.29: The mean gradients a), the angle between the direction of the mean gradient and the vertical b) over the time from November2006 to July 2009

By observing *figures 5.29a,b*, it is clear the trend of the mean gradient and its rotation towards the vertical direction during the winter (November and December 2007, November and December 2008) within all the layers. This is because there is a high contribution of rainfall in winter.

In summer 2008, a peak of main gradient can be seen, in fact suction value (corresponding to the volumetric water content measurements[9]), changes heavily with the depth causing the development of the very high hydraulic gradients. Therefore in dry periods the angle described by the superficial gradients is around 150 °(evaporation flow normal to the slope), while in the intermediate and deep layer the mean gradients are parallel to the slope. The evaporation phenomena in the intermediate and deep layers occur when the directions of the superficial flows reverse downward (September, October and November 2008).

The mean gradient and the mean direction are displayed together also by using a graph in polar coordinates (angle and module) where dotted line shows the average inclination of the slope (*Fig. 5.30*). By evaluating *figure 5.30* the higher gradients occur in the superficial soils (soil 2) in the dry period and their direction is normal to the slope. In any way even if the gradients are very high in summer, the evaporation flows are very small, that is due to a very low permeability. It may be also seen that the mean gradient in the deep layers are an order of magnitude lower respect to these in the superficial and intermediate soils (*Figs.5.30 d, e*).

In the following graphs (*Figs.5.31-5.36*) the values of suction along the longitudinal section B-B are plotted. The same days of the plots about the piezometric heads are selected, from to the summer 2008 to the summer 2009. The diagrams show, as expected, that the suction values decrease with the depth. This distribution of suction become uniform in winter when high rainfalls occur.

[9] Suction values in the dry period are read on the drying retention curves (Papa, 2007) in correspondence of the volumetric water content measurements. In fact in that period the measurements are not reliable because of the tensiometers desaturation.

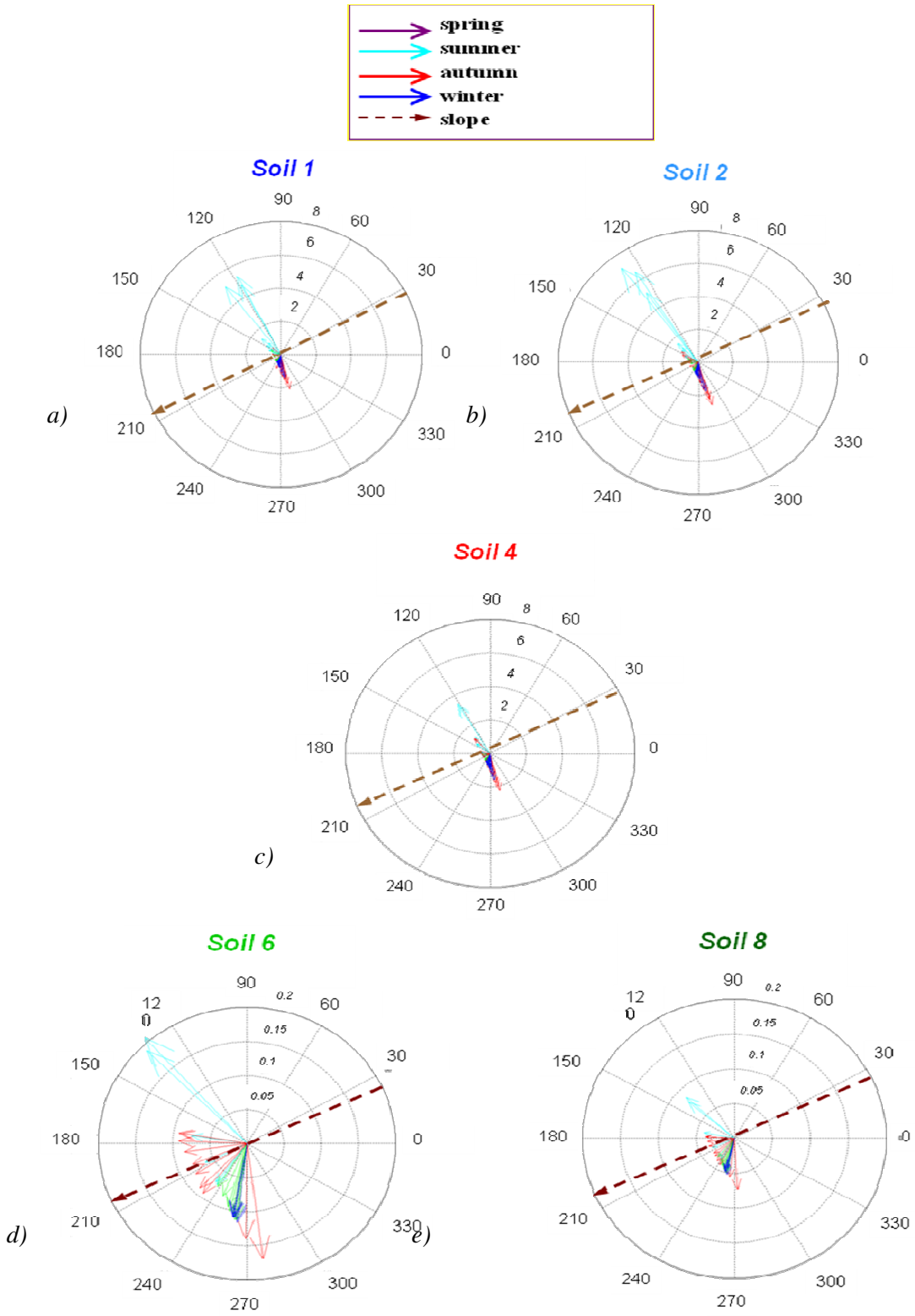

Fig. 5.30: The mean gradient and the mean direction represented by the polar coordinates for soil 1 a), for soil 2 b), for soil 4 c), for soil 6 d), for soil 8 e)

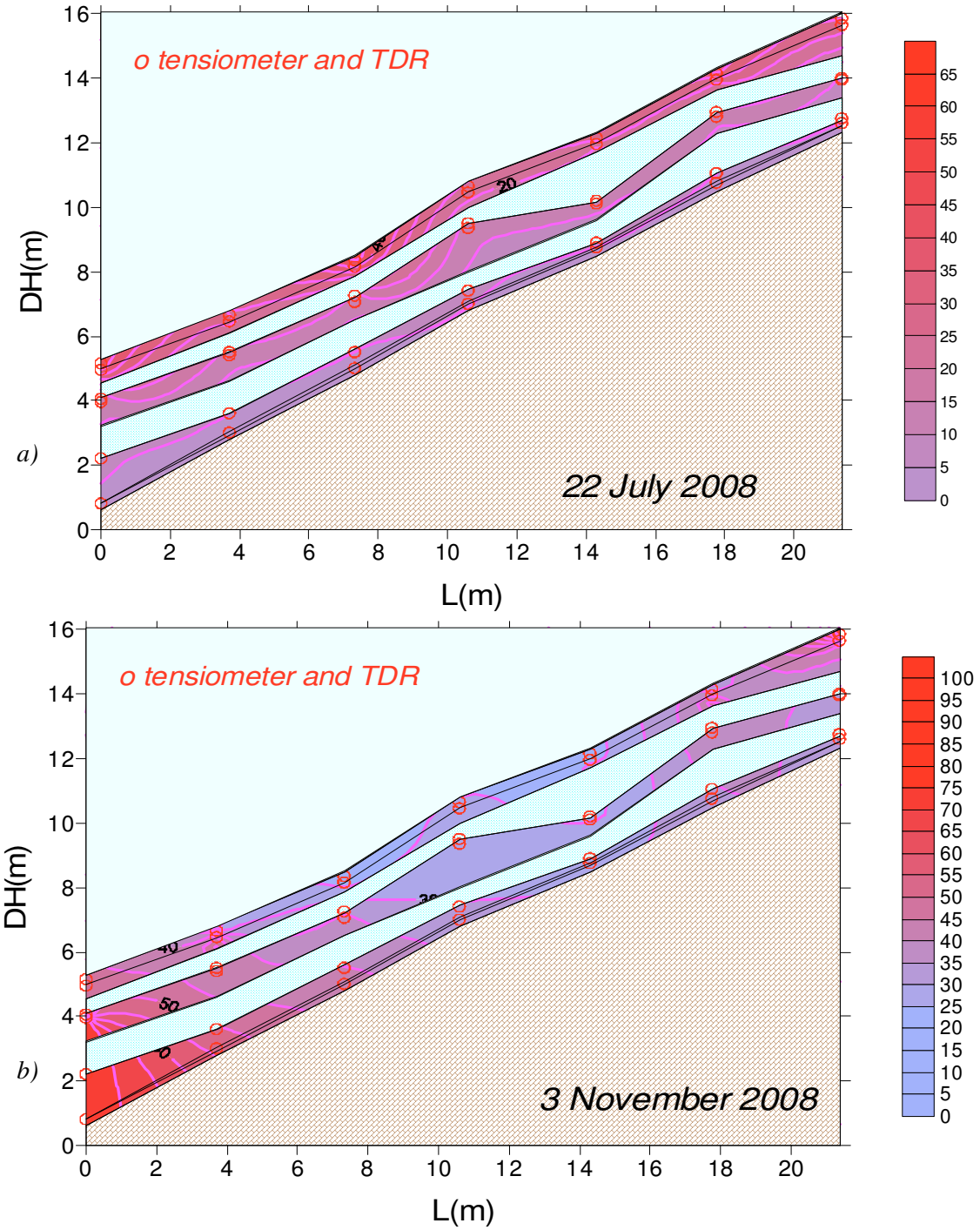

Fig.5.31: The suction values along longitudinal section B-B' at 22nd July 2008 a), at 3rd November 2008 b)

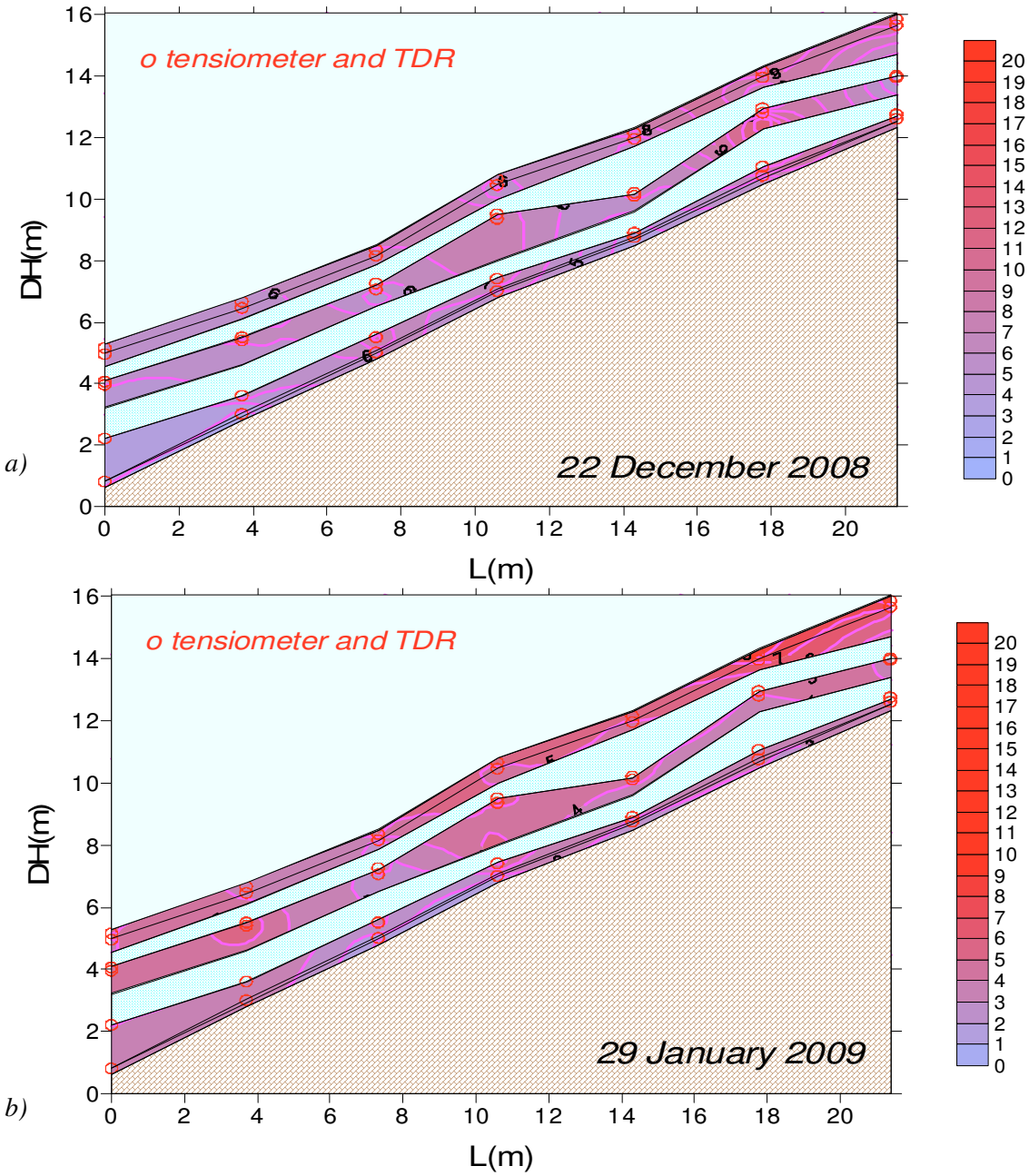

a)

b)

Fig.5.32: The suction values along longitudinal section B-B' at 22nd December 2008 a), at 29th January 2009 b)

a)

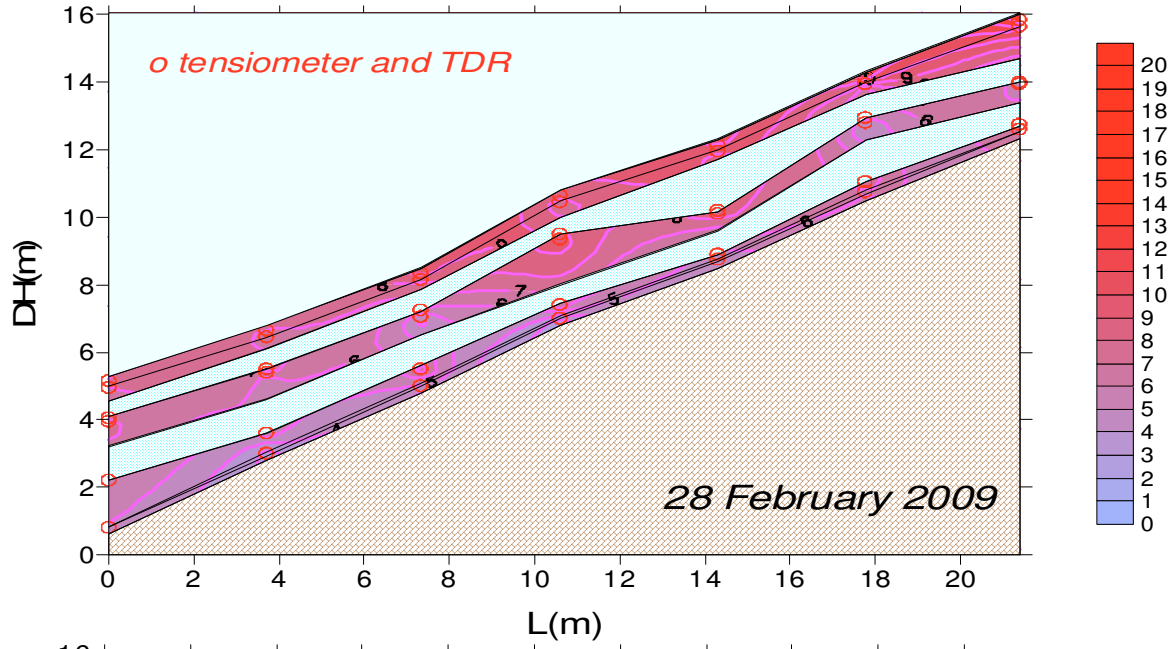

b)

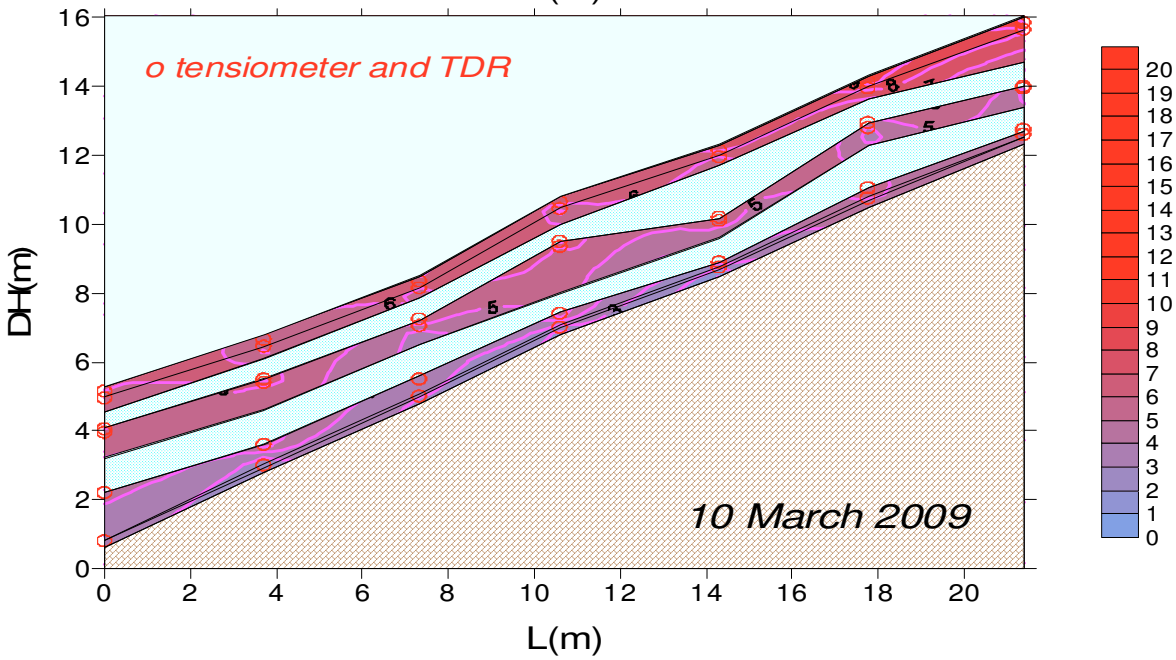

Fig.5.33: The suctionvalues along longitudinal section B-B' at 28th February 2009 a), at 10th March 2009 b)

a)

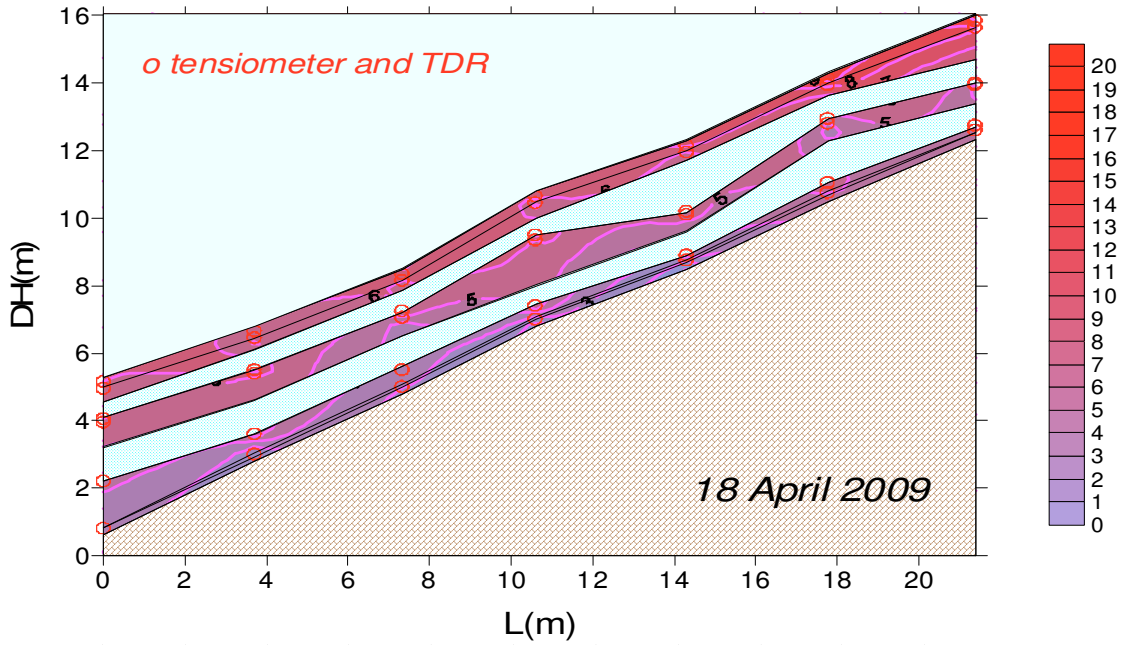

b)

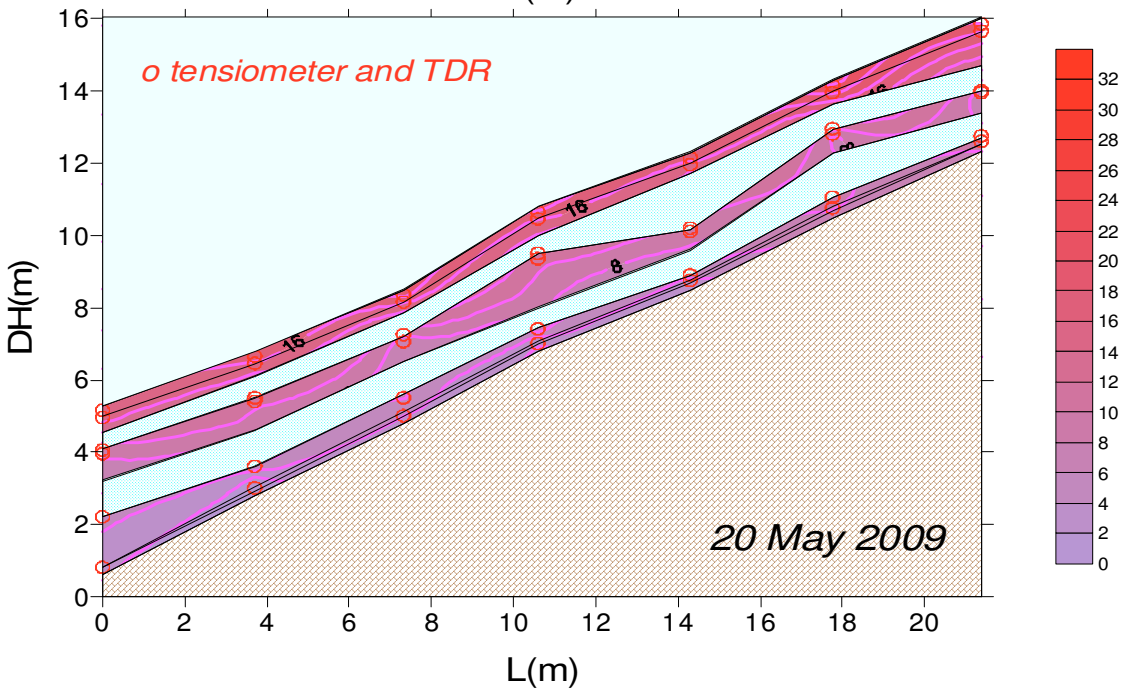

Fig.5.34: The suctionvalues along longitudinal section B-B' at 29th April 2009 a), at 20th May 2009 b)

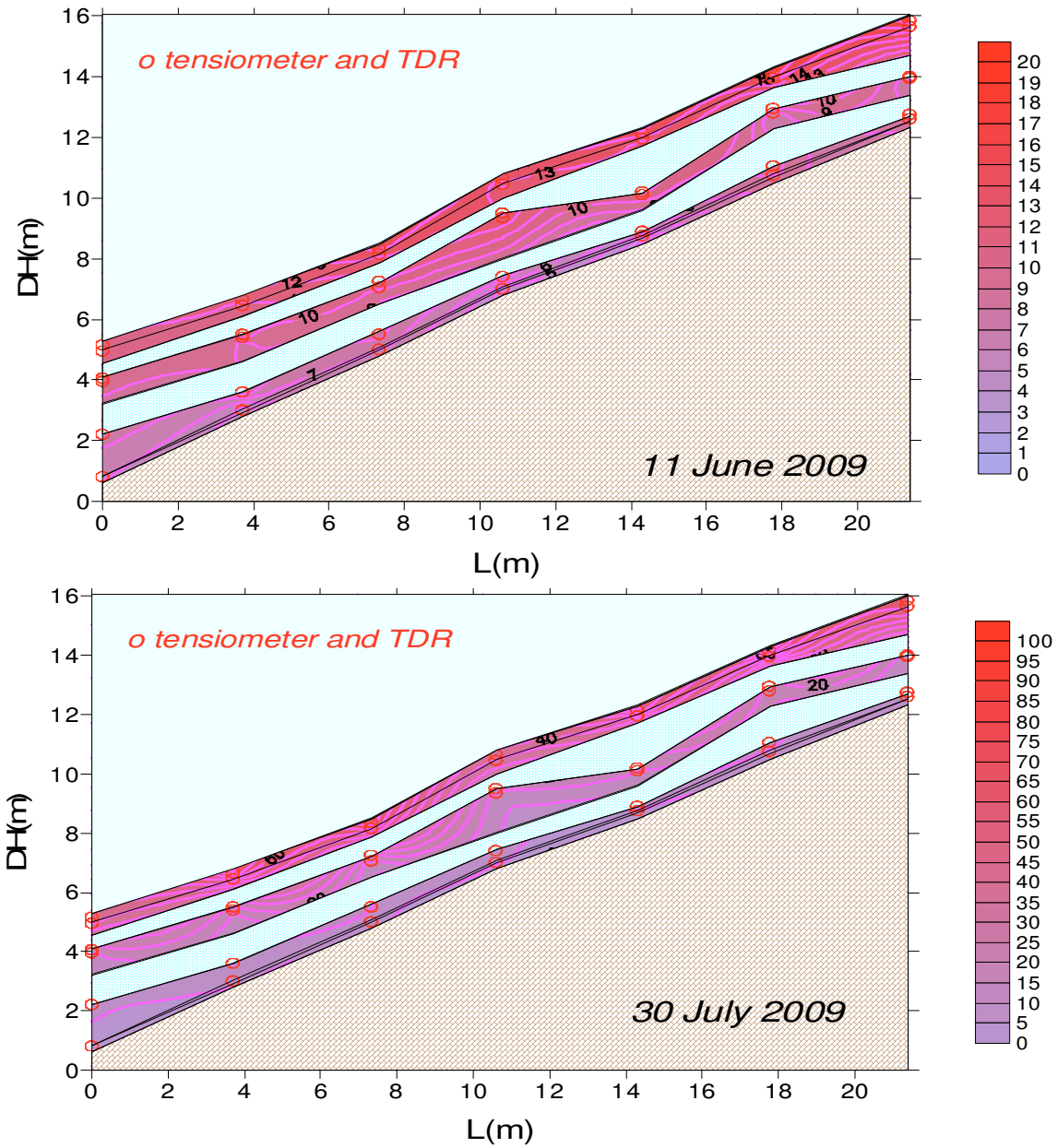

Fig.5.35: The suctionvalues along longitudinal section B-B' at 11th June 2009 a), at 30th July 2009 b)

5.3.1.2 Monitoring of the cross sections D-D

By analysing the piezometric heads along a cross section the flow directions can be identified in the plan z, y. The cross sections D-D (*Fig. 5.23*) is considered (*Fig. 5.36-5.37*). The water flow vectors are mostly vertical and directed downward.

In the following graphs (Fig. *5.38-5.39*) the spatial distribution of suction along the same section is examined. Again the diagrams show a suction distribution decreasing with depth, moreover the evaporation phenomena on the surface in the summer enhances the difference in the suction values between the superficial layers.

5.3.1.3 Monitoring of the section of stratigraphic alignment 4inf

By analysing the hydraulic head along a section of stratigraphic alignment, the preferential flow directions can be identified in the plan x, z. The section of stratigraphic alignment corresponding to the deeper tensiometers installed in the intermediate layer (*Fig. 5.23*), at a depth between 1.35 m and 2.30 m is considered.

The diagrams (*Figs. 5.40, 5.41*) shows that the isopiezic lines move from the mountain to valley. In correspondence of the verticals 6A, 6C and 7A there is the preferential water circulation towards the sides of the field due to the evaporation front.

In the rest part of the section, however, the gradients are nearly constant and arranged in the direction of inclination of the slope. The same phenomena can be clearly represented by the distribution of suction along the same section (Fig.*5.41*). In the autumn the advancing of the evaporation front towards the downstream of the field amplifies the spatial in non homogeneous of the measurements. In the other periods the observed suction values are more uniform.

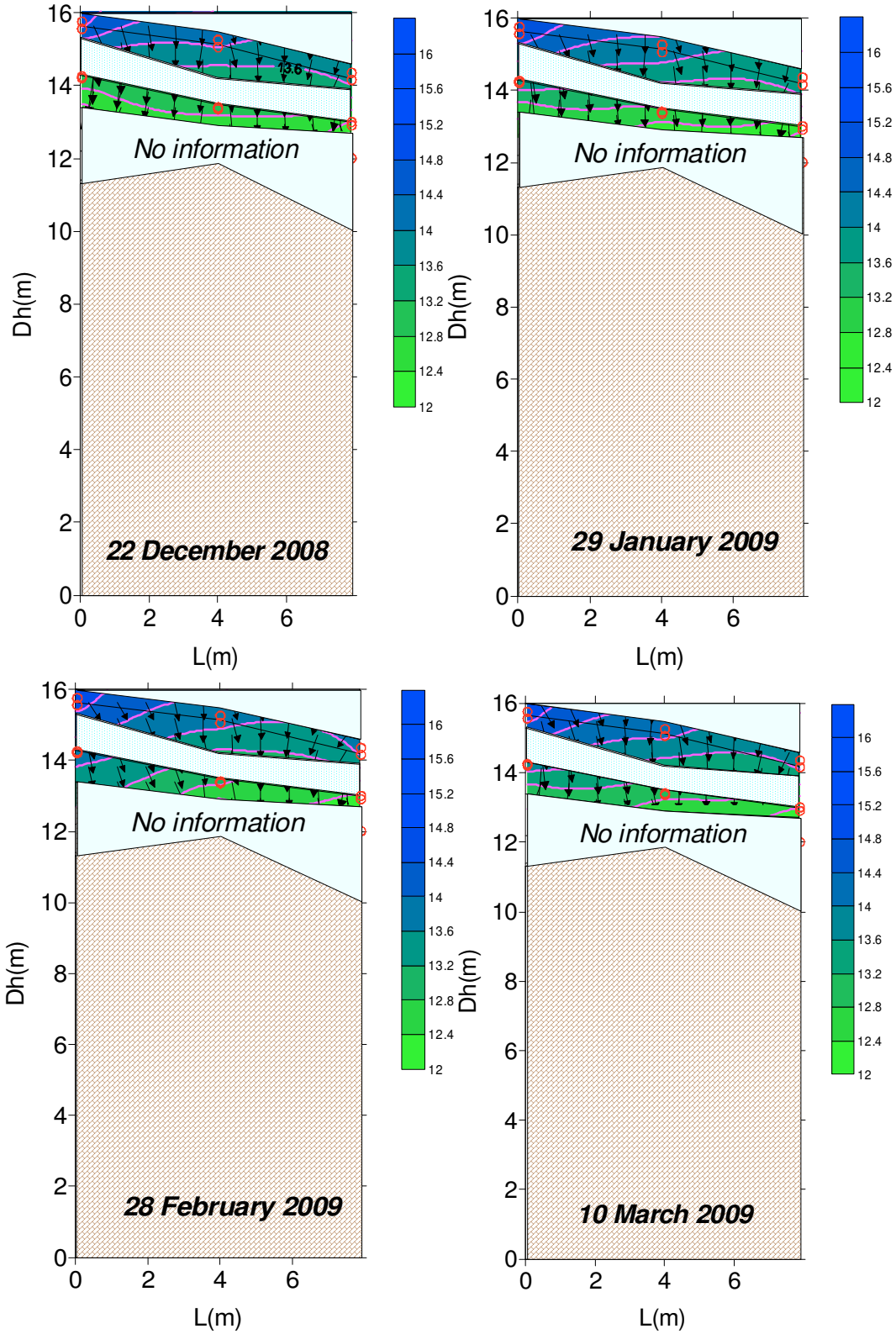

Fig.5.36: The isopiezic lines and water flow vectors along the cross section D-D'

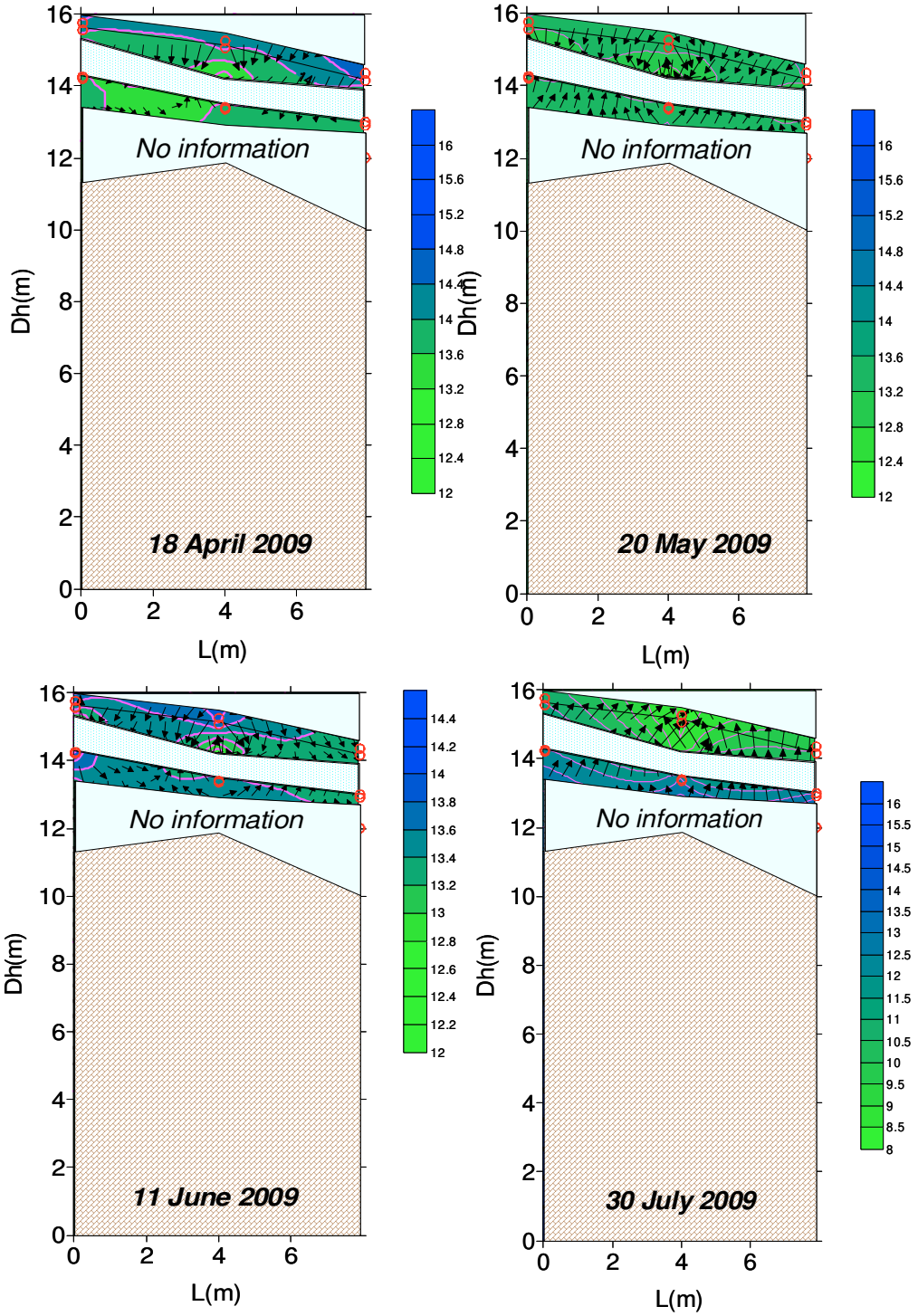

Fig.5.37: The isopiezic lines and water flow vectors along the cross section D-D'

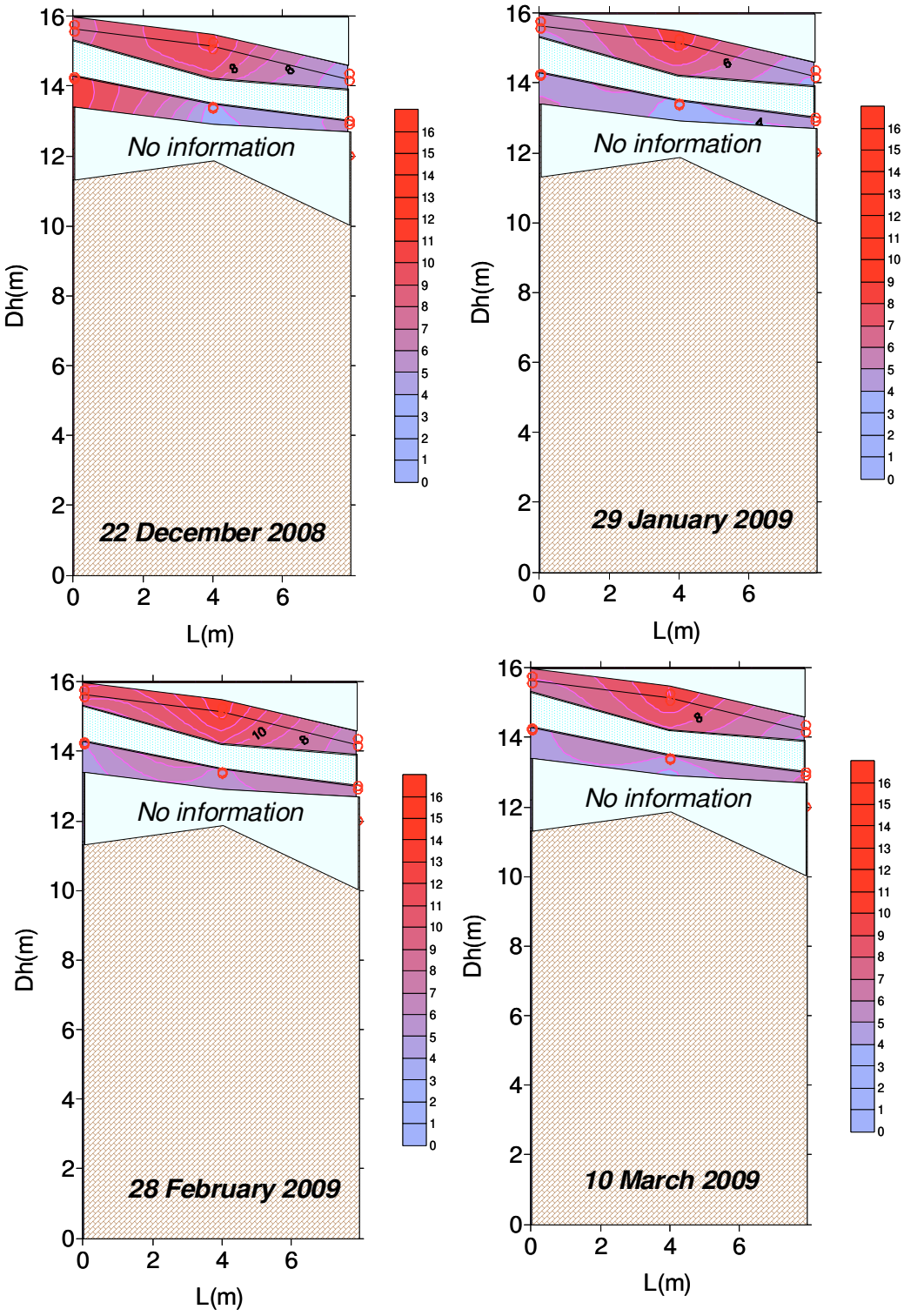

Fig.5.38: The suction values along the cross section D-D'

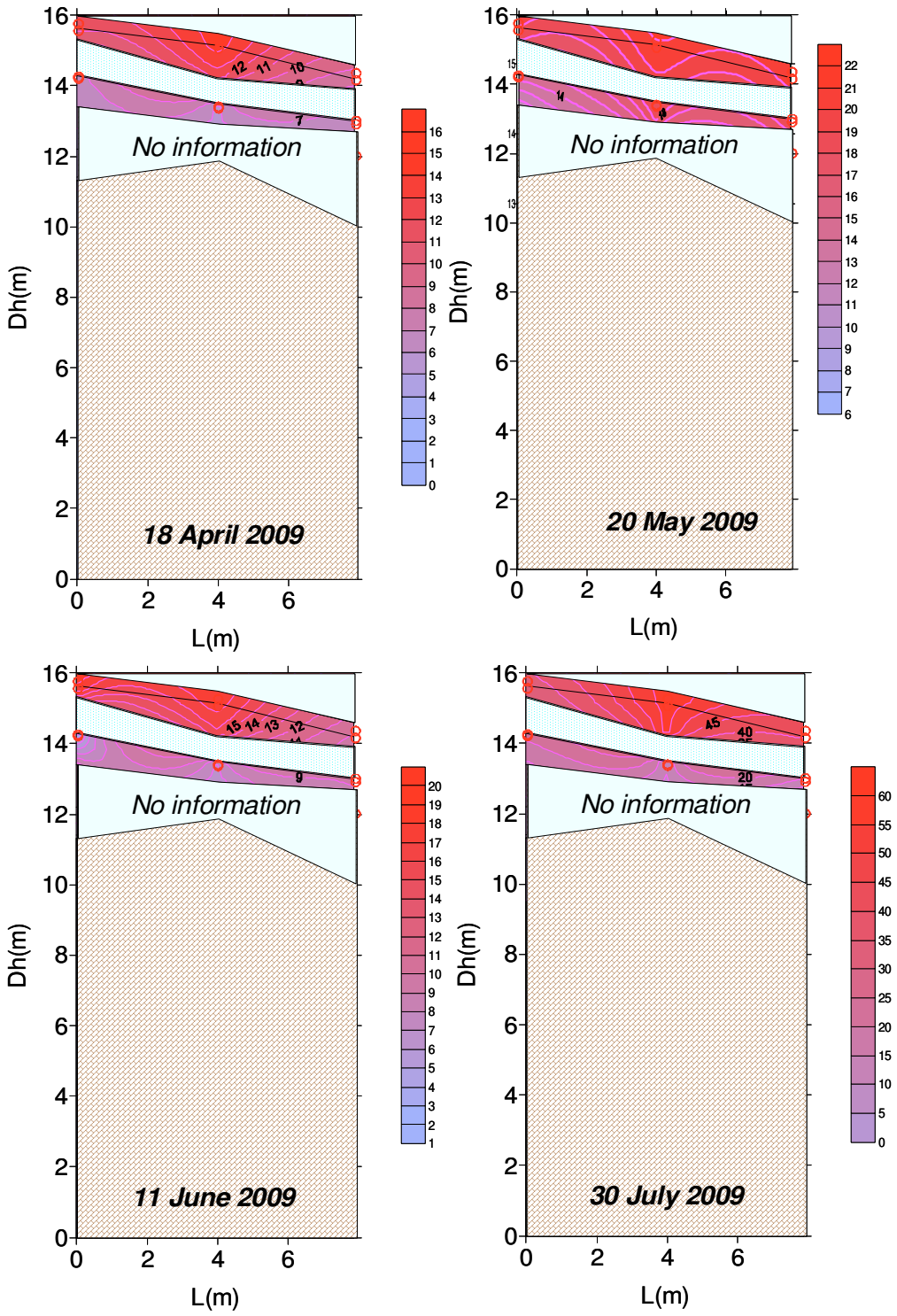

Fig.5.39: The suction values along the cross section D-D'

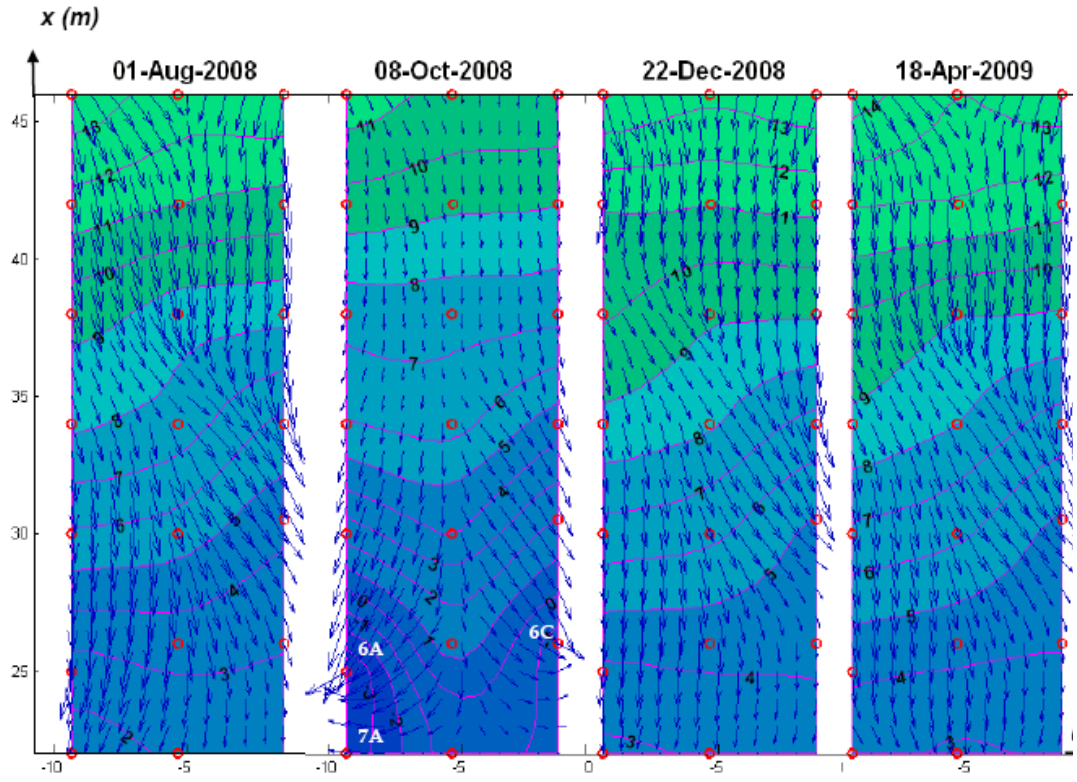

Fig.5.40: The isopiezic lines and water flow vectors along the section of stratigraphic alignment 4inf

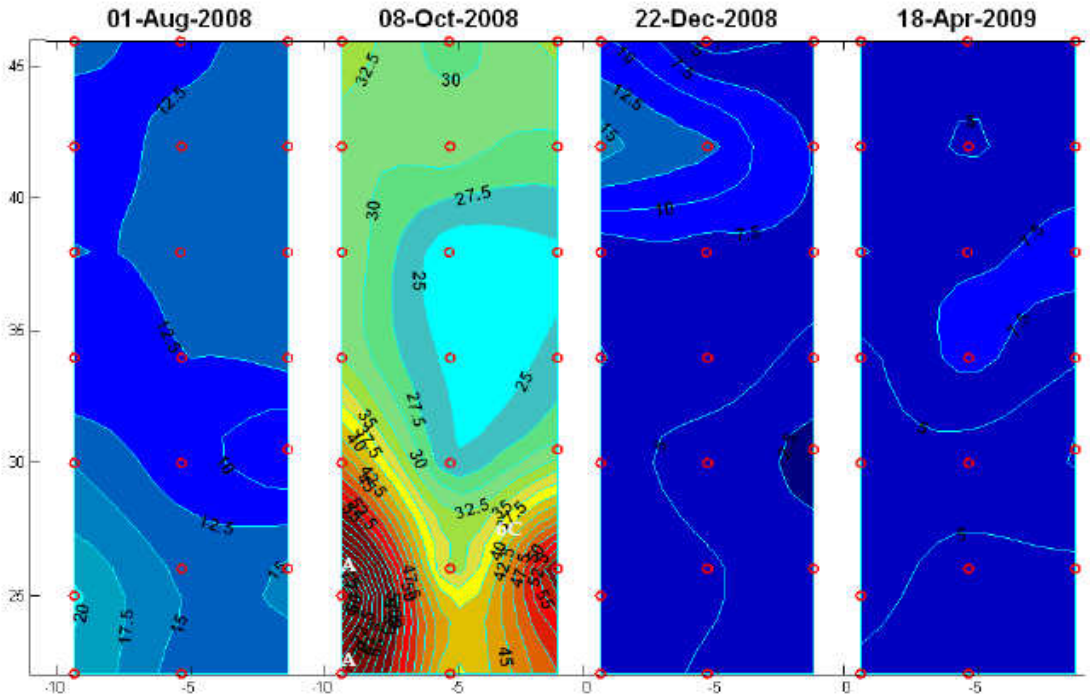

Fig.5.41: The suction values along the section of stratigraphic alignment 4inf

5.3.2 Analysis of the vertical water flows

The total flow of water filtrating vertically into the upper and the intermediate part of the soil cover were estimated on the basis of both monitoring and lab data:

$$q_y = -K_y \cdot \frac{dh}{dy} \tag{5.1}$$

where K_y, is the partially-saturated vertical permeability, $\frac{dh}{dy}$ is the gradient calculated in vertical direction. Concurrent readings of the tensiometers installed along the same vertical section were used to estimate the hydraulic gradients in each vertex of the instrumented grid at two different depths (i.e. between tensiometers TL1 and TL2 and between tensiometers TL3 and TL4). The partially saturated permeability is obtained in two different ways:

1) Parameters of the Mualem-van Genuchten model for water retention and hydraulic conductivity were derived from lab tests on undisturbed samples recovered in each soil layer (Papa, 2007). These parameter were determined along drying tests; however accordingly to Topp and Miller (1966) the relationship between volumetric water content and water permeability was assumed to be non hysteretic. Therefore a first estimate of the hydraulic conductivity corresponding to each of the gradients was derived by generating the main-wetting retention curve from the main experimental drying curve (Papa, 2007) by simply doubling the value of the parameter α, as suggested in the literature (*Kool and Parker, 1987, Nielsen and Luckner, 1992*). Hence the value of the permeability was obtained from the value of the volumetric water content corresponding to the measured matric suction value along the estimated main wetting curve;

2) The partially-saturated permeability is obtained by the non-hysteretic relation of Mualem - van Genuchten, directly as function of water content measurements:

$$k(S_e) = k_{sat} S_e^{\lambda} [1 - (1 - S_e^{n/(n-1)})^{1-1/n}]^2 \tag{5.2}$$

where S_e:

$$S_e = \frac{\theta - \theta_r}{\theta_s - \theta_r} = \frac{1}{[1 + (\alpha \overline{s})^n]^{1-1/n}} \tag{5.3}$$

The parameter S_e, represents the relative degree of saturation, estimated as function of the volumetric water content measurements, and hence it is calculated only for the verticals along the longitudinal section B-B where the measurements are available. The parameters ϑ_s, ϑ_r are obtained from the experimental evidence in the lab (Papa, 2007).

Finally, the flows in each vertical were calculated by applying Darcy's law and these estimated in correspondence of first permeability were integrated over the whole instrumented area and these estimated in correspondence of second permeability were integrated over the central longitudinal section of site, B-B.

5.3.1.1 Vertical water flows averaged over whole the test site

The vertical water flow over each layer examined, is calculated by solving a volume integral by using the trapezoidal method.

In the *fig. 5.42a,b* the daily rainfalls and the vertical water flows averaged over whole the field are plotted. The flow directed downward is assumed positive. So, the vertical water flows in the superficial layers are positive (infiltration flow) during all the year apart the summer, and their intensity is correlated to the rainfall. In dry period the flows are negative (evaporation flow) and reach values around few mm/day .

In the *fig. 5.42c* the vertical water flows and the rain intensity cumulated on the same interval of observation are plotted. In wet periods the evolution of the flows through the superficial soil follows the rain trend, but a most part of rainfall does not infiltrate because of the run-off phenomena and intercepted by the vegetation. It is clear that just 50% of the cumulated rainfall infiltrates in the surface layers, and only 25% of the infiltration reaches the intermediate layer.

In this way only a very rough estimation of unsaturated permeability and so, the flows through the layers is obtained. This is because there are the uncertainties about the way to calculate the partially saturated permeability, in addition the errors related to the extrapolation of the flows calculated along the single vertical to the whole field. Moreover, in the dry period measurements are not available along all the verticals of the site due to the desaturation of the tensiometers and, where available, are not always reliable. Ultimately the flows calculated in summer could be significantly underestimated.

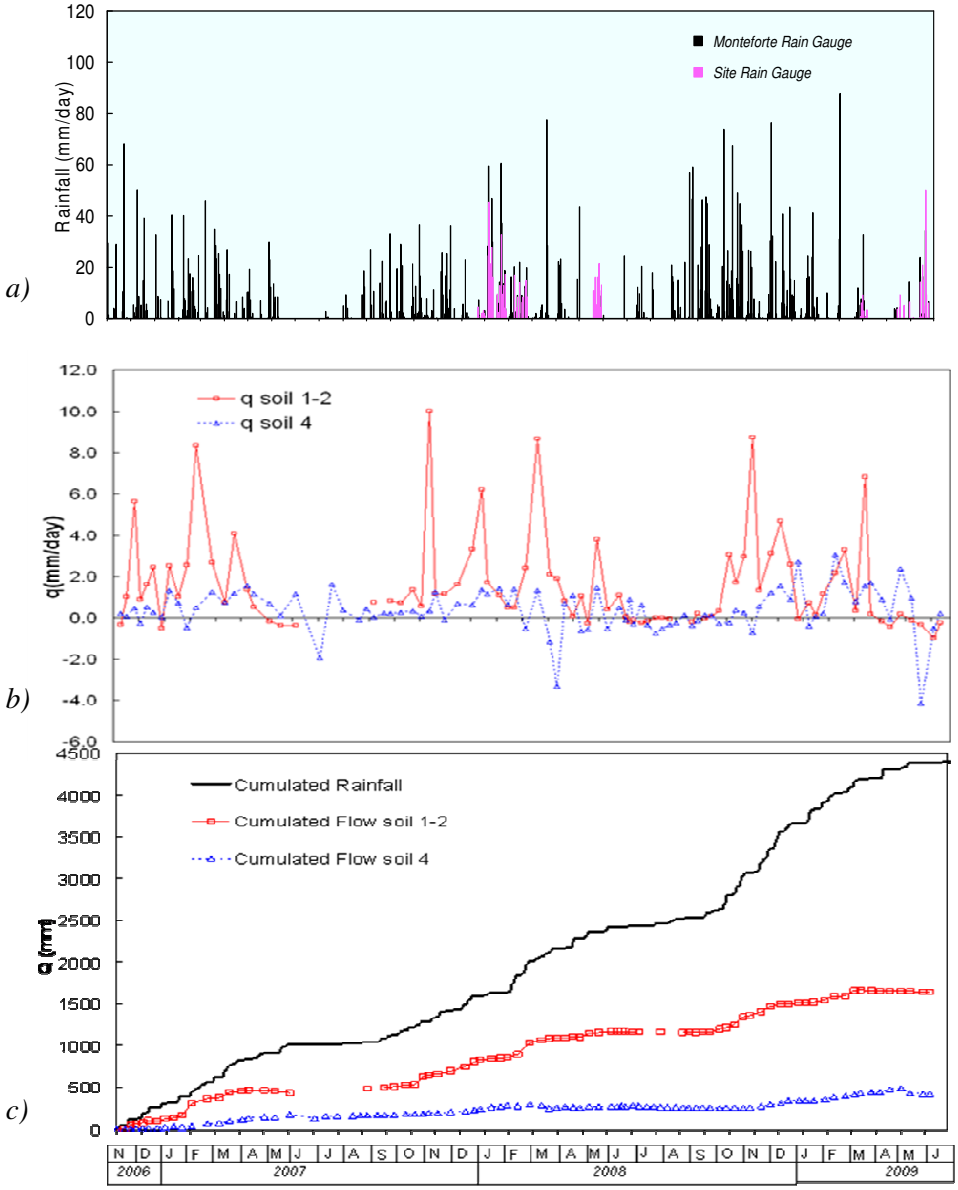

Fig.5.42: The daily rainfall a), daily vertical water flows b) and the Cumulated Rainfall and cumulated flows c) against the time in the superficial soils and in the intermediate soils

5.3.1.2 Vertical water flows average over the longitudinal section B-B

The calculation of the vertical water flows is then repeated by using the non-hysteretic relation for the permeability directly as function of volumetric water content measured performed in site, available in the verticals along the section B-B from 30 April 2008.

The water flows q2 thus obtained (continuous line in Fig. *5.43b*), are compared with daily rainfall and the flows q1 estimated as function of the suction measurements as explained above (dotted line in Fig. *5.43b*). It may be seen that the peaks of the infiltration and of the evaporation of q2 are smaller than these of q1. In fact the permeability obtained as function of the volumetric water content measured in site are smaller than these obtained using the permeability curve in drying condition with the double values of α. Moreover the partially saturated permeability calculated as function of water content measurement take in account of the actual paths described by suction - water content measurements in each soil. In Fig. *5.43c* the vertical water flow, q2, and the rainfall cumulated over the same period are represented.

Hence, the vertical water flows q2 in the superficial layers are positive (infiltration flow) during all the year apart the summer when they reach values around 1 mm/day, and their intensity is strongly correlated to the rainfall. The vertical water flows q2, in the intermediate layers are negative (evaporation flow) from the spring to the autumn and they assume absolute value around 0.5 ÷ 1.0 mm/day.

By evaluating the total flows (*fig.5.43c*), the most part of rainfall does not infiltrate into the superficial soils because of the run-off phenomena and intercepted by the vegetation. The water flow cumulated over one year through the superficial soil is not nil but the inward flows (due to infiltration) exceed the outward flows (due to evaporation). Just about 15% of the cumulated vertical flow in the superficial layers reaches the intermediate part of the soil cover. In the intermediate layers the cumulated flow over one year is almost nil, hence the inward flows (produced by infiltration) balances the outward ones (generated by evaporation phenomena at the soil surface).

An estimate of the total water content inside each soil layer was obtained by means of the TDR measurements. In figure 5.44 a, c the total vertical flows in the superficial and intermediate layers are compared with the variation of the water volume calculated. The shape of the water volume curves in the superficial and the intermediate soils are similar. The water balance over one year for both layers seem to be in equilibrium. On the contrary, while the total flow in the soils 4 is nil, the total inward flow through the superficial soils in the wet period is not balanced by the outward flow in the dry period. It results that a large total flow infiltrates through the pumiceous layer 3.

In order to analyse the hydraulic behaviour of the pumiceous layer, interposed between the

superficial and intermediate layers, the difference between the normal components to the slope of the total vertical flows, q2, in the superficial and the intermediate layers was calculated and the values are reported in Fig. 5.44b. This difference is equal to the sum of two terms: the total water flow which develops throughout the pumices in the direction of the layer (i.e. parallel to the slope); the variation of water volume contained inside layer 3. It is worth noticing that the aforementioned sum grows up during the observation period (see Fig. 5.44b) while water balance in layer it is likely to be in equilibrium as previously observed for layers 1,2 and 4. Therefore it can be concluded that the major part of water leaves this soil as a flow parallel to the slope.
By observing the figure 5.45: in spring and in autumn the sum increase at the pumice layers (April and May 2008, March, April and May 2009) in fact the vertical water flow arrives either from the superficial layers and from the intermediate layers; in summer, it decreases because of the evaporative flow from the surface and the infiltration flow into the intermediate layer. In winter (January, February and March 2009), the sum does not increase because almost all the vertical flows from the surface infiltrate in the intermediate layers completely through this pumiceous layer.

5.3.1.3 The total water flows average over the longitudinal section B-B

The mean value of the modulus and the main direction of the water flow vectors inside each layer were determined (Fig. 5.46a, b). The groundwater head field along the central longitudinal alignment of the instrumented area was estimated by a spatially interpolation of the available matric suction measurements; hence the groundwater head gradients were derived from the estimated field. The value of the partially saturated permeability in each point of the analysed section was derived by estimating the water content along a scanning curve contained in the water retention hysteresis domain. The modulus of the groundwater flow vectors in each points of the grid were finally calculated by applying Darcy's law. The mean values of modulus were calculated by integrating the water flows over each the layers (1, 2 and 4) (Fig. 5.46a). In the figure 5.46b the angle between the vertical direction and the mean direction of the groundwater flow vectors is plotted as function of time, t. The water flow is very small during the summer in all the layers even if the gradients are very high because of the lower hydraulic conductivity in the dry period. In the rest part of the year, the water flow modulus is five time higher than in the summer in the superficial soils, four time in the intermediate soils.

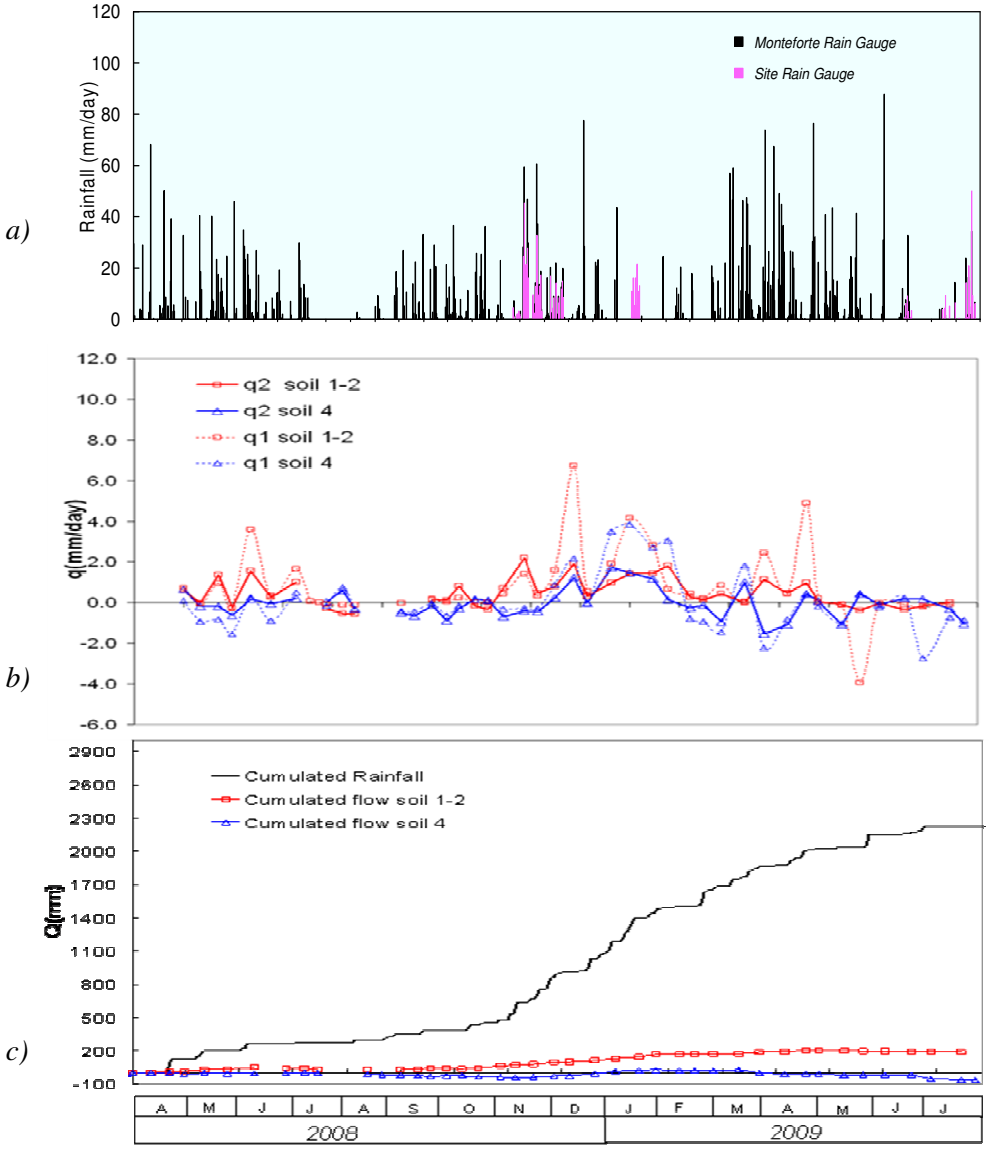

Fig.5.43: Rainfall a), the vertical water flows q1 and q2 b) and Rainfall and the vertical flows q2 cumulated over the time (April 2008 to June 2009) c) in the superficial soils and in the intermediate soils

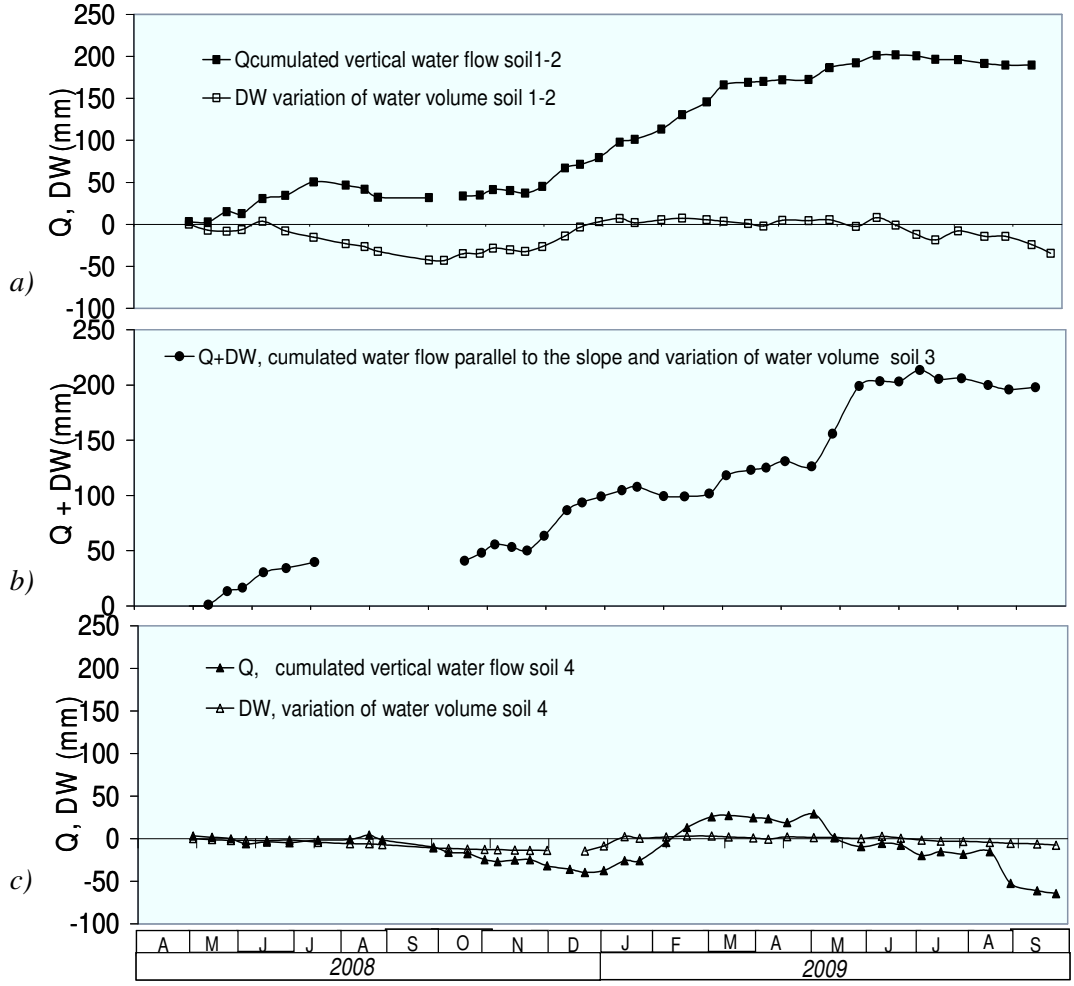

Fig.5.44: Total vertical water flows, q2, and the variation of water volume against the time (April 2008 to June 2009) in the superficial soils a) and in the intermediate soils c); sum of the total water flows parallel to the slope and variation of water volume in the pumice of Avellino (soil 3)b)

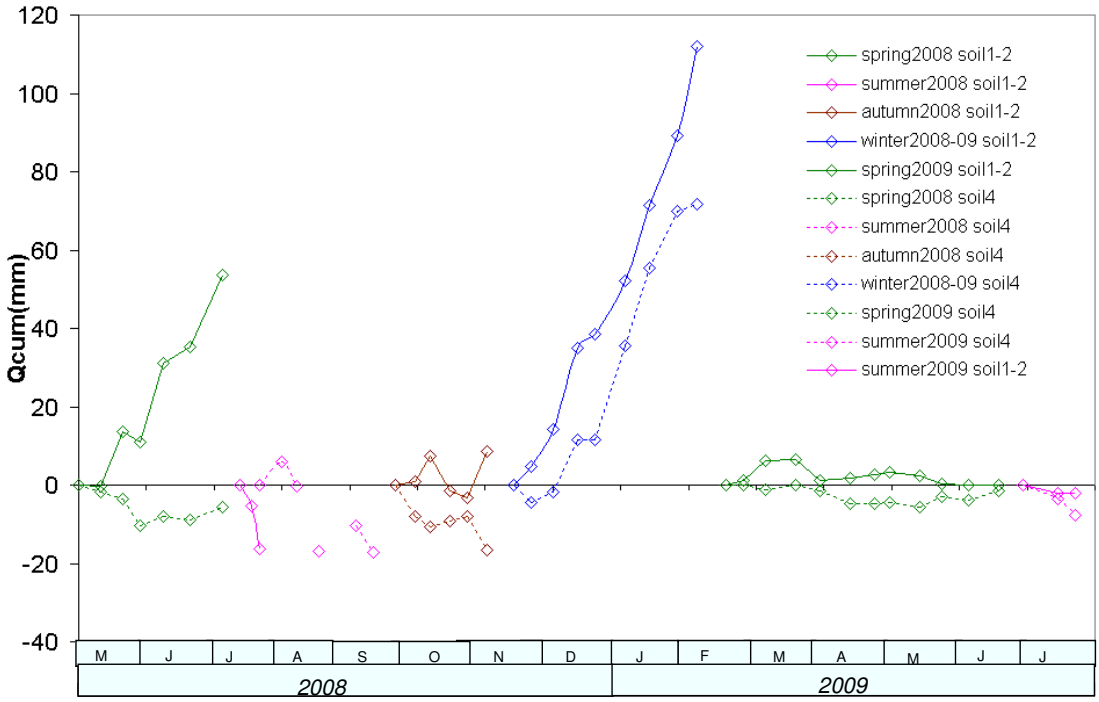

Fig.5.45: Total vertical water flows, q2, over each single season against the time (April 2008 to June 2009) in the superficial soils and in the intermidiate soils

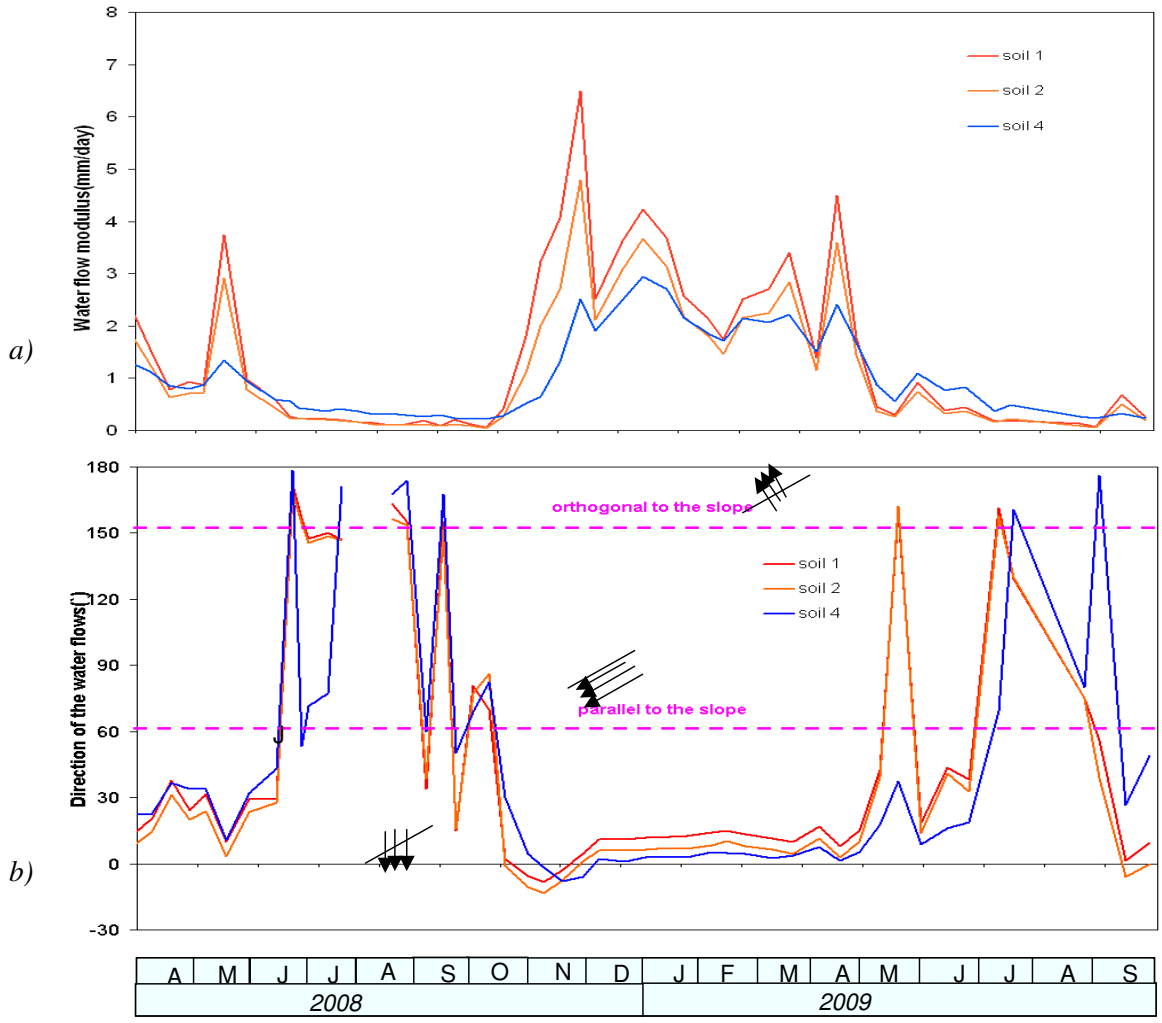

Fig. 5.46:Mean water flow modulus a), the angle between the direction of the mean gradient and the vertical b) against the time from April 2008 to September 2009

5.4 Discussion

The suction and water content measurements collected in situ and their analysis show some features about the hydraulic regime in the subsoil. The monitoring results clearly show the seasonal variation in matric suction and volumetric water content. The matric suction and volumetric water content on the top part of the cover seems to be affected by singular rainfall events but the corresponding variations are relatively small if compared to the seasonal ones; conversely, they in the intermediate part and in the deeper part of the cover follows a trend unaffected by individual rainfall events. The suction distribution in the subsoil depends essentially on the distance from soil surface, where the variation of climatic conditions occurs. In fact by observing the measurements, the amplitude of the seasonal oscillations in the superficial layers is larger than in the intermediate and the deeper soils. Moreover the maximum suction is reached in August in superficial soils, in November in the intermediate and in December in the deeper soils (at contact with limestone). This is because the permeability in the dry periods is very low specially in the deeper soils so the water flow moves very slowly from the layer to an other one deeper. In the wet period the permeability increases and the flows move faster from the surface toward the intermediate and deeper layers and no delay in the suction trend is observed.
In the pumice layer the total water is divided into two terms: a flow parallel to slope and a contribute to the variation of the water content.

These observations highline the complexity of the problem, because the hydraulic proprieties of these soils change, apart over the space, over the time too. Hence, in the interaction between subsoil - atmosphere it is essential to estimate the right partially saturated permeability of all the soils.

Chapter 6

Mechanical and hydraulic models and their calibration

6.1 Synopsis

In this chapter the mechanical and hydraulic properties of the soils of the Testing Site are elaborated, in order to obtain all the parameters necessary for the calibration of both the mechanical and hydraulic models used in the subsequent analyses. The results of some triaxial compression tests, performed in saturated and unsaturated conditions (*Papa, PhD thesis 2007*) on undisturbed samples taken from the Site, have been used for the determination of the mechanical parameters of the model. The experimental retention curve and permeability curve (*Papa, PhD thesis 2007*), obtained by pressure plate tests and evaporation tests, have been used to calculate the hydraulic parameters. The structure of the chapter is such that it first presents the constitutive model and then its calibration, followed by the presentation of the hydraulic model and its calibration.

6.2 Constitutive model for mechanical behaviour

The constitutive model used in this thesis to represent the mechanical behaviour of unsaturated soils is based on the Barcelona Basic Model (BBM, Alonso et al. 1990). The model was developed by Georgiadis (2003), Georgiadis et al. (2005), and implemented into the Imperial College Finite Element Program (ICFEP; Potts & Zdravkovic, 1999).
ICFEP was used for all analyses presented in this thesis.

The model can simulate both fully and partially saturated soil behaviour. For the former case, the model is formulated in terms of effective stresses. When a particular value of suction is exceeded, called the air entry value of suction s_{air}, the soil becomes partially saturated and a different set of stress variables is required. The model therefore adopts two independent stress

variables; a convenient choice is: the ***net total stress***, $\sigma - u_a$, as difference between the total stress and pore air pressure; and the ***suction equivalent***, as value of suction $s = u_a - u_w$, in excess of the air entry value: $s_{eq} = s - s_{air}$. The model is generalised in four stress variables:

- J , the generalised deviatoric stress:

$$J = 1/\sqrt{2}\left[(\sigma_x - p)^2 + (\sigma_y - p)^2 + (\sigma_z - p)^2 + 2\tau^2_{xy} + 2\tau^2_{xz} + 2\tau^2_{yz}\right]^{\frac{1}{2}} \tag{6.1}$$

- p , the mean stress:

$$p = (\sigma_x + \sigma_y + \sigma_z)/3 \tag{6.2}$$

- ϑ, the Lode's angle:

$$\theta = -\frac{1}{3}\sin^{-1}\left[\frac{3\sqrt{3}}{2}\frac{\det \boldsymbol{s}}{J^3}\right] \tag{6.3}$$

where det***s*** is the determinant of the deviator stress matrix:

$$\det \mathbf{s} = \begin{vmatrix} \sigma_x - p & \tau_{xy} & \tau_{xz} \\ \tau_{yx} & \sigma_y - p & \tau_{yz} \\ \tau_{zx} & \tau_{zy} & \sigma_z - p \end{vmatrix} \tag{6.4}$$

- s_{eq} , the equivalent suction.

For fully saturated conditions: $\sigma_x, \sigma_y, \sigma_z$ are effective stress.
For partially saturated conditions: $\sigma_x, \sigma_y, \sigma_z$ are net total stress.

6.2.1 Yield and plastic potential surfaces

6.2.1.1 Primary yield surface

The yield and plastic potential surfaces are the Lagioia et al. (1996) expressions for saturated conditions, extended to include also the unsaturated conditions.

The expression for the yield, F_1, and plastic potential, G_1, surfaces for fully saturated conditions is given in Equation (6.5):

$$\left.\begin{matrix} F_1 \\ G_1 \end{matrix}\right\} = \frac{p'}{p'_c} - \frac{\left(1+\frac{\eta}{K_2}\right)^{\frac{K_2}{\beta}}}{\left(1+\frac{\eta}{K_1}\right)^{\frac{K_1}{\beta}}} = 0 \tag{6.5}$$

where the constants K_1, K_2, β are given by

$$K_1 = \frac{\mu(1-\alpha)}{2(1-\mu)}\left(1+\sqrt{1-\frac{4\alpha(1-\mu)}{\mu(1-\alpha)^2}}\right)$$
$$K_2 = \frac{\mu(1-\alpha)}{2(1-\mu)}\left(1-\sqrt{1-\frac{4\alpha(1-\mu)}{\mu(1-\alpha)^2}}\right) \tag{6.6}$$

$$\beta = (1-\mu)(K_1 - K_2)$$

α, μ are the input parameters which control the shape of the surface,

p'_c is the isotropic effective yield stress,

η is the generalised normalised ratio,

$$\eta = \sqrt{\frac{J_{2\eta}}{J_{2\eta i}}} \tag{6.7}$$

$J_{2\eta}$ is the square of the stress ratio,

$$J_{2\eta} = \left(\frac{J}{p'}\right)^2 \tag{6.8}$$

$J_{2\eta i}$ is the failure value of $J_{2\eta}$, obtained by solving the Matsuoka-Nakai cubic equation:

$$\frac{2}{\sqrt{27}} \cdot C \cdot \sin(3\vartheta) \cdot J_{2\eta i}^{3/2} + (C-3) \cdot J_{2\eta i} - (C-9) = 0 \tag{6.9}$$

in which

$$C = \frac{9 - M^2}{\frac{2M^3}{27} - \frac{M^2}{3} + 1} \tag{6.10}$$

Where M is the gradient of the critical state line in the conventional q-p space, corresponding to triaxial compression and ϑ is the Lode's angle.

When the plastic potential surface is calculated from the above equations, the parameters α, μ and M are denoted as α_g, μ_g and M_g. Similarly, when the yield surface is calculated the parameters α, μ and M are denoted as α_f, μ_f and M_f. For triaxial compression $J_{2\eta i} = M^2/3$. For the conditions of associated flow, the above parameters for the yield and plastic potential surfaces are the same.

The Lagioia et al. (1996) expression (6.5) is obtained by integrating:

$$\frac{dp'}{p'} = -\frac{d\left(\sqrt{J_{2\eta}}\right)}{d + \sqrt{J_{2\eta}}} \tag{6.11}$$

where d is the dilatancy ($= d\varepsilon_v^p / dE_d^p$). The variation of dilatancy with the stress ratio is selected such that, according to *Figure 6.1:*

$$\begin{cases} \sqrt{J_{2\eta}} \to 0 & \Rightarrow d \to \infty \\ \sqrt{J_{2\eta}} = \sqrt{J_{2\eta g}} & \Rightarrow d \to 0 \end{cases}$$

and:

$$d = \mu\left(\sqrt{J_{2ng}} - \sqrt{J_{2n}}\right)\cdot\left(\frac{\alpha\sqrt{J_{2ng}}}{\sqrt{J_{2n}}} + 1\right) \tag{6.12}$$

The major advantage of the expression for the yield and plastic potential surfaces is that, by changing the parameters α and μ it is possible to reproduce different shapes of the surfaces.

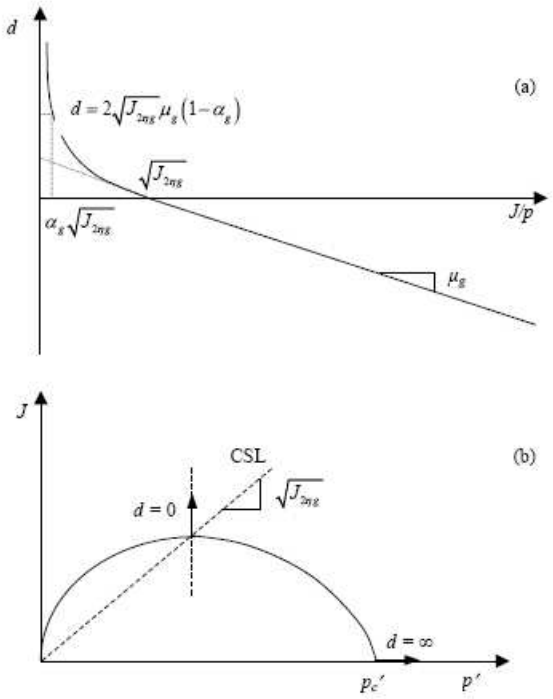

Fig.6.1 a) Dilatancy-Stress ratio relation; b) Plastic Potential Surface

For the unsaturated conditions, Equation (6.5) is written in the following form:

$$\left.\begin{matrix} F_1 \\ G_1 \end{matrix}\right\} = \frac{p + f(s_{eq})}{p_0 + f\left(s_{eq}\right)} - \frac{\left(1 + \dfrac{\eta}{K_2}\right)^{\frac{K_2}{\beta}}}{\left(1 + \dfrac{\eta}{K_1}\right)^{\frac{K_1}{\beta}}} = 0 \tag{6.13}$$

where p_0 is the isotropic total yield stress at the current value of suction, and $f(s_{eq})$ is a measure of the increase of apparent cohesion due to suction (see Figure 6.2), $J_{ci} = M_{Ji} f(s_{eq})$.

The expression for the square of stress ratio $J_{2\eta}$ is now:

$$J_{2\eta} = \left(\frac{J}{p + f(s_{eq})} \right)^2 \tag{6.14}$$

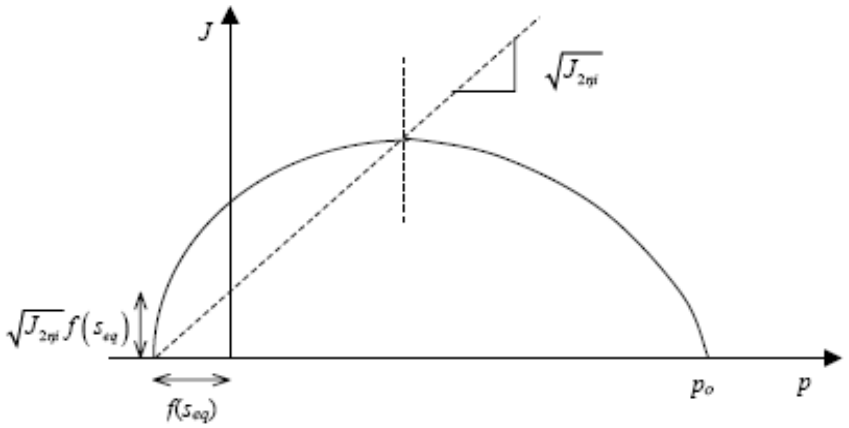

Fig.6.2 Yield function and Plastic Potential surface for partially saturated conditions

The increase of apparent cohesion due to suction, $f(s_{eq})$, can be taken into account in two ways:

Option 1: $f(s_{eq}) = k s_{eq} + s_{air}$, where k is a constant, giving a linear increase of apparent cohesion with equivalent suction (as formulated in BBM);

Option 2: $f(s_{eq}) = S_r s_{eq} + s_{air}$, where S_r is the degree of saturation, giving a non-linear increment of apparent cohesion with equivalent suction according to the shape of the retention curve. This option is more realistic as the apparent cohesion increases with suction up to superior limit beyond which it does not grow more. Moreover by using the option 2 the hydraulic-mechanical coupled model is considered.
When s_{air} = 0, Bishop's effective stress approach is given with the parameter χ set equal to S_r.

The parameters α, μ and M, do not change from saturated to unsaturated conditions. The parameters M_g, M_f are equal to $\sqrt{3J_{2ng}}, \sqrt{3J_{2nf}}$, in triaxial compression. In particular, M_g is related to the critical state angle, ϕ_{cs}:

$$M_g = \frac{6\sin\phi_{cs}}{3-\sin\phi_{cs}} \tag{6.15}$$

The parameters α_g, μ_g determine the variation of dilatancy, *d*, with stress ratio (*Fig.6.1*), the parameters α_f, μ_f are determined by fitting the experimental curve.

6.2.1.2 Secondary yield surface

This model contains the second yield surface, known as the suction increase yield surface, as introduced in the Barcelona Basic model:

$$F_2 = G_2 = \frac{s_{eq}}{s_o} - 1 = 0 \tag{6.16}$$

where s_0 (yield suction) is a limit value of suction beyond which the plastic volumetric strains occur. The existence of such a yield surface is supported by limited experimental data.

6.2.2 Isotropic compression line

The *isotropic compression line* for fully saturated conditions is given by:

$$v = v_1 - \lambda(0)\ln p_c' \tag{6.17}$$

Where v and v_1 are respectively the specific volume at current state and at the p'= 1kPa, and $\lambda(0)$ is the fully saturated compressibility coefficient.

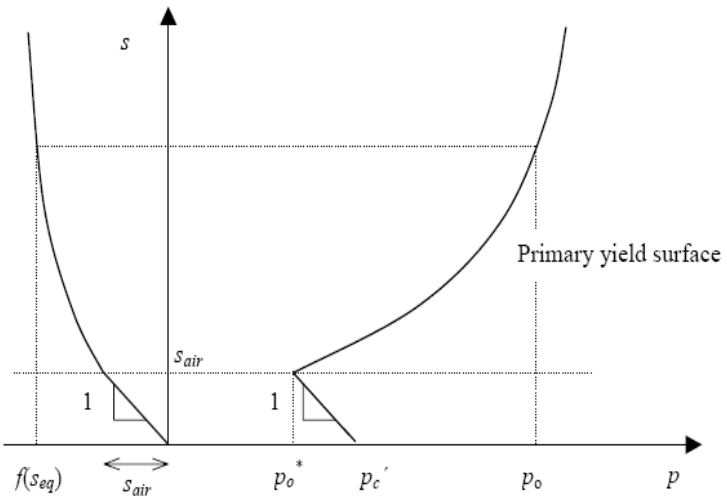

Fig.6.3 Primary yield surface in isotropic stress space

The isotropic yield stress, $p_c^{'}$, is the hardening/softening parameter, which controls the size of the yield surface. For partially saturated conditions the hardening/softening parameter is a net stress defined as the equivalent fully saturated isotropic yield stress at the transition from fully saturated isotropic yield stress to partially saturated conditions (s= s_{air}):

$$p_0^* = p_c^{'} - s_{air} \tag{6.18}$$

The shape of the yield surface in the isotropic stress space p-s is defined by the relationship between the partially saturated yield stress, p_0, and the equivalent fully saturated yield stress, p_0^*. This relationship depends on the assumed shape of the isotropic compression line (*Fig.6.3*).

With respect *the compressibility behaviour in partially saturated conditions* there are tree options implemented in the model:

1) The Normal Compression Line in unsaturated condition is constantly diverging from the fully saturated isotropic compression line (*fig.6.4*).
2) The Normal Compression Line in unsaturated condition is constantly diverging from the fully saturated isotropic compression line up to a particular value of mean net stress, p_m , beyond which the slope of the NCL in partially saturated condition is equal to the saturated Normal Compression Line (*fig.6.5*).
3) The Normal Compression Line in unsaturated condition is represented by a non-linear expression which for low stresses state diverges from the fully saturated isotropic compression line up to a particular value of mean net stress, p_m, and then for the high stress state the NCL in partially saturated condition arrive to touch the saturated Normal Compression Line.

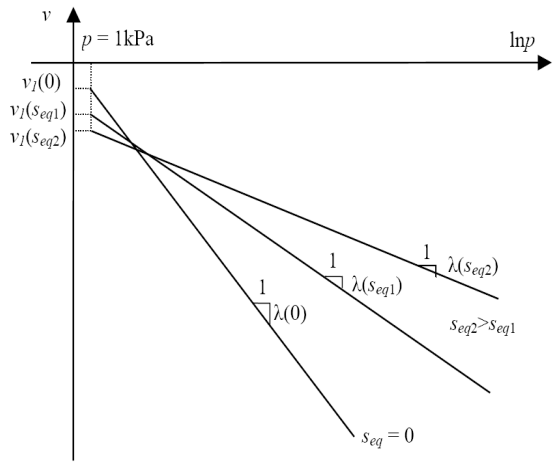

Fig.6.4 Isotropic compression line-Option 1

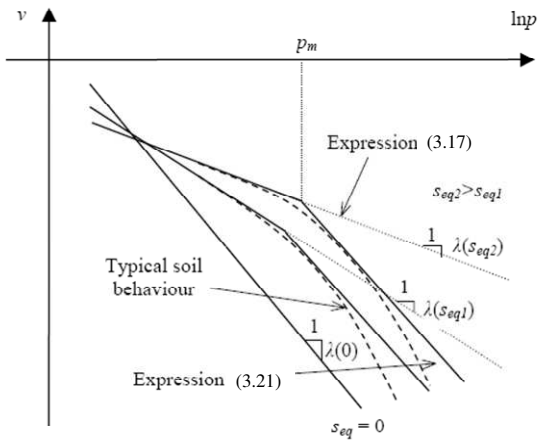

Fig.6.5 Isotropic compression line-Option 2

In particular in the option 2 the NCL in a partially saturated conditions up to the value p_m, is described from the following expression:

$$v = v_1(s_{eq}) - \lambda(s_{eq}) \ln p_0 \tag{6.19}$$

Where $\lambda(s_{eq})$ is the partially saturated compressibility coefficient, given by the empirical expression (Alonso et al. 1990):

$$\lambda(s_{eq}) = \lambda(0)\left[(1-r)e^{-\beta s_{eq}} + r\right] \tag{6.20}$$

Where β and r are the model parameters which are known by isotropic compression tests at different value of suction. Parameter r is related to the maximum value of the initial compressibility coefficient, while parameter β controls its rate of increase with equivalent suction.

Up to the value p_m the partially saturated NCL (6.19) implies that the amount of potential collapse due to wetting (vertical distance between the fully and partially saturated lines in the v-ln p plane) increases linearly with the increasing of the logarithm of the confining stress, p.

The isotropic compression line for stresses beyond, p_m, is given by:

$$v = v_1 + \Delta v_{\max} - \lambda(0) \ln p_0 \tag{6.21}$$

Where $\Delta v_{\max}$ is the maximum potential collapse due to wetting at the mean stress value of p_m. The amount of the potential collapse is constant beyond p_m (*fig.6.5*).

These assumptions for the NCL (option 2) lead to the following expression relating the isotropic yield stress, p_0, to the equivalent fully saturated yield stress, p_0^*:

$$p_0 = p_0^* (\alpha_c)^{(\lambda(o)-\lambda(s_{eq}))/(\lambda(s_{eq})-\kappa)} \tag{6.22}$$

Where, $\alpha_c = p_0^* / p_c$ is a model parameter.

Moreover two parameters are required in order to determinate the elastic volumetric strain due to the change in suction and the plastic volumetric strains due to activation of the secondary yield surface: the compressibility coefficient due to changes in suction, λ_s, and the elastic compressibility coefficient due to changes in suction, κ_s.

6.2.3 Hardening/Softening rules

The magnitude of the plastic volumetric strains when either of the two yield surfaces is activated is related to the change of the hardening softening parameters, *po** and *so*, through the following equations for both models:

Primary yield surface:

$$\frac{dp_o^*}{p_0^*} = \frac{v}{\lambda(0)-\kappa} d\varepsilon_v^p \tag{6.23}$$

Secondary yield surface:

$$\frac{ds_0}{p_{atm}+s_0} = \frac{v}{\lambda_s - \kappa_s} d\varepsilon_v^p \tag{6.24}$$

Equations 6.23 and 6.24 imply that the two yield surfaces are coupled.

6.2.4 Elastic behaviour

The volumetric elastic changes due to changes in suction or in mean net stress are given from elastic loading/unloading and wetting/drying lines:

$$d\varepsilon_{vp}^{e} = -\frac{\kappa}{vp} dp$$
$$d\varepsilon_{vs}^{e} = -\frac{\kappa_s}{v(s_{eq} + p_{atm})} ds_{eq} \tag{6.25}$$

In order to avoid to calculate the infinite strains for p = 0, a minimum bulk modulus ($K = \frac{vp}{\kappa}$), *Kmin* = 100 kPa is adopted. Incremental strains, related to changes in the deviatoric stress invariant, *J*, are given by:

$$dE_d^e = \frac{dJ}{\sqrt{3}G} \tag{6.26}$$

Where G is the elastic shear modulus, given by the following equation:

$$G = \frac{3(1-2\mu)}{2(1+\mu)} K \tag{6.27}$$

The program allows to assume the value of G or the value of μ such that the other parameter is determined by the equation (6.27) being it a function of the stress level (*K*).

6.3 Calibration of the Mechanical model

In the following the calibration of the mechanical model is introduced by using the results of some lab tests (*Papa, 2007*).

6.3.1 Yield and plastic potential surface

6.3.1.1 Primary yield surface

The option 2 for the expression of $f(s_{eq})$ agrees with the results of the triaxial tests at controlled suction, performed on the samples of soil 4 (Papa, 2007). The diagram of Figure 6.6 shows the relationship between the deviatoric stress q and the effective mean stress $p' = (p - u_a) + f(s_{eq})$ at failure, for tests performed at controlled suctions of 6, 12, and 20 kPa. All the points coincide with the critical state line (CSL), thus justifying the use of option 2 for the apparent cohesion.

In the analyses the hypothesis of the *associated flow* is adopted and its validity is also checked, as it will be explained in the following (*fig.6.9*); so from now on the subscripts, g and f, will be neglected.

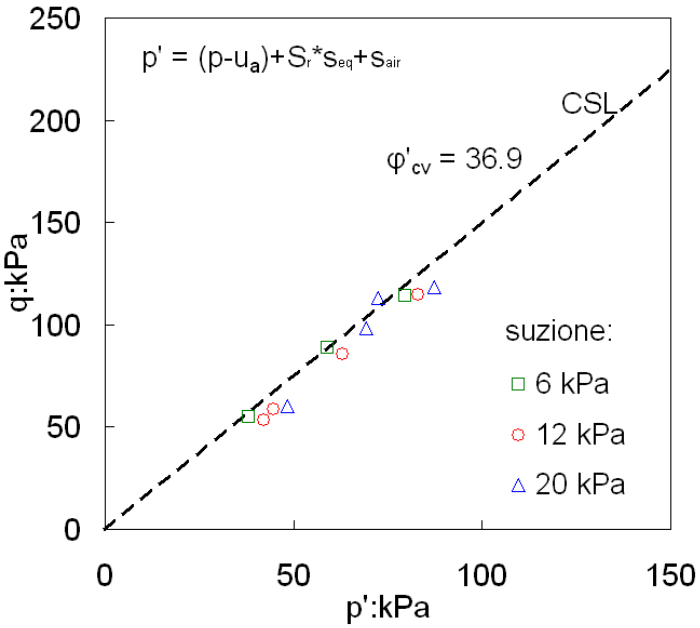

Fig.6.6 Representation according to the used model
of values of deviatoric stress, q, and p' at failure for the soil 4 at different values of suction
(experimental data from Papa, 2007)

The parameters M is obtained from the results of the triaxial tests on completely saturated

samples (*Papa, PhD thesis 2007*). The experimental curves in *figure 6.8* refer to all the soil layers apart the pumice ones (soils 3 and 5) for which it is not possible to take undisturbated samples. These experimental results are presented in the plane $\frac{q}{p'} vs \varepsilon_s$, where $\varepsilon_s = \frac{2}{3}(\varepsilon_a - \varepsilon_r)$, ε_a is the total axial strain and ε_r is the total radial strain. The resulting φ_{cr} and M parameters are summarized in table 6.1.

With respect to pumices, the angle of shearing resistance is obtained by using the testing of Pellegrino et al., 1967 (*fig.6.7*). The experimental value of unit dry weight, γ_d, obtained for the pumices of Avellino and Ottaviano (soil 3 and 5) is between 4-5 kN/m^3 (Papa, 2007). By using the diagram of *figure 6.7* in a range of mean total stress, p, from 0 to 100kPa, and of unit dry weight between 4-5 kN/m^3, the reasonable values of φ varies between 40°and 50°. The value $\varphi = 46°$ is adopted in the analyses for soil 3 and $\varphi = 42°$ for soil 5.

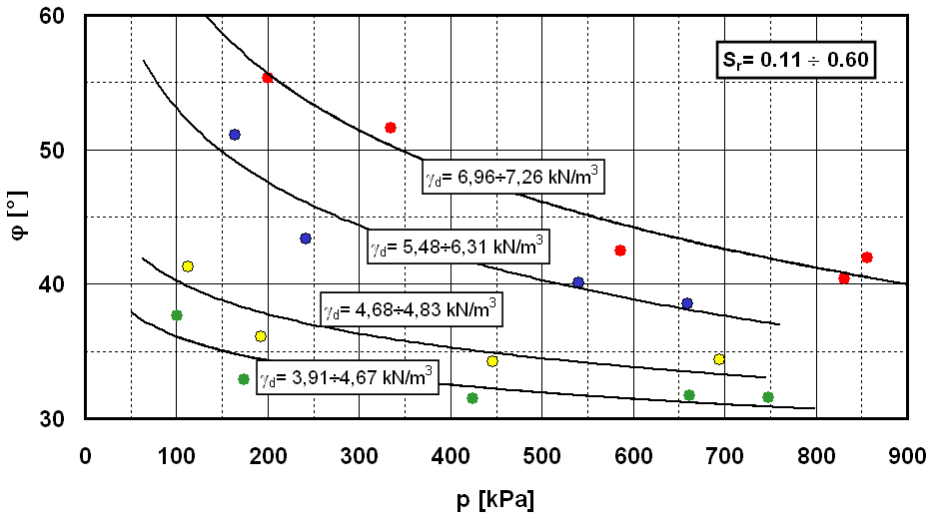

Fig.6.7 Pumices of Campania Region, peak shear strength for different values of unit dry weight (personal communication from Nicotera, experimental data from Pellegrino, 1967)

The parameters, α, μ are obtained by matching the experimental dilatation-stress ratio relation with the numerical expression (6.11) implemented in the model (*Fig.3.9*). The experimental curves refer to the triaxial tests on saturated samples. The higher values of these parameters make the elastic field bigger. The μ value controls the slope of the curve in the region of negative dilatancy values, while the α value controls the value of dilatation for zero stress ratio. In order to validate the hypothesis of the associated flow, the experimental stress paths of triaxial tests on saturated samples and the yield surface expression corresponded to the α, μ values previously obtained, are represented together in the

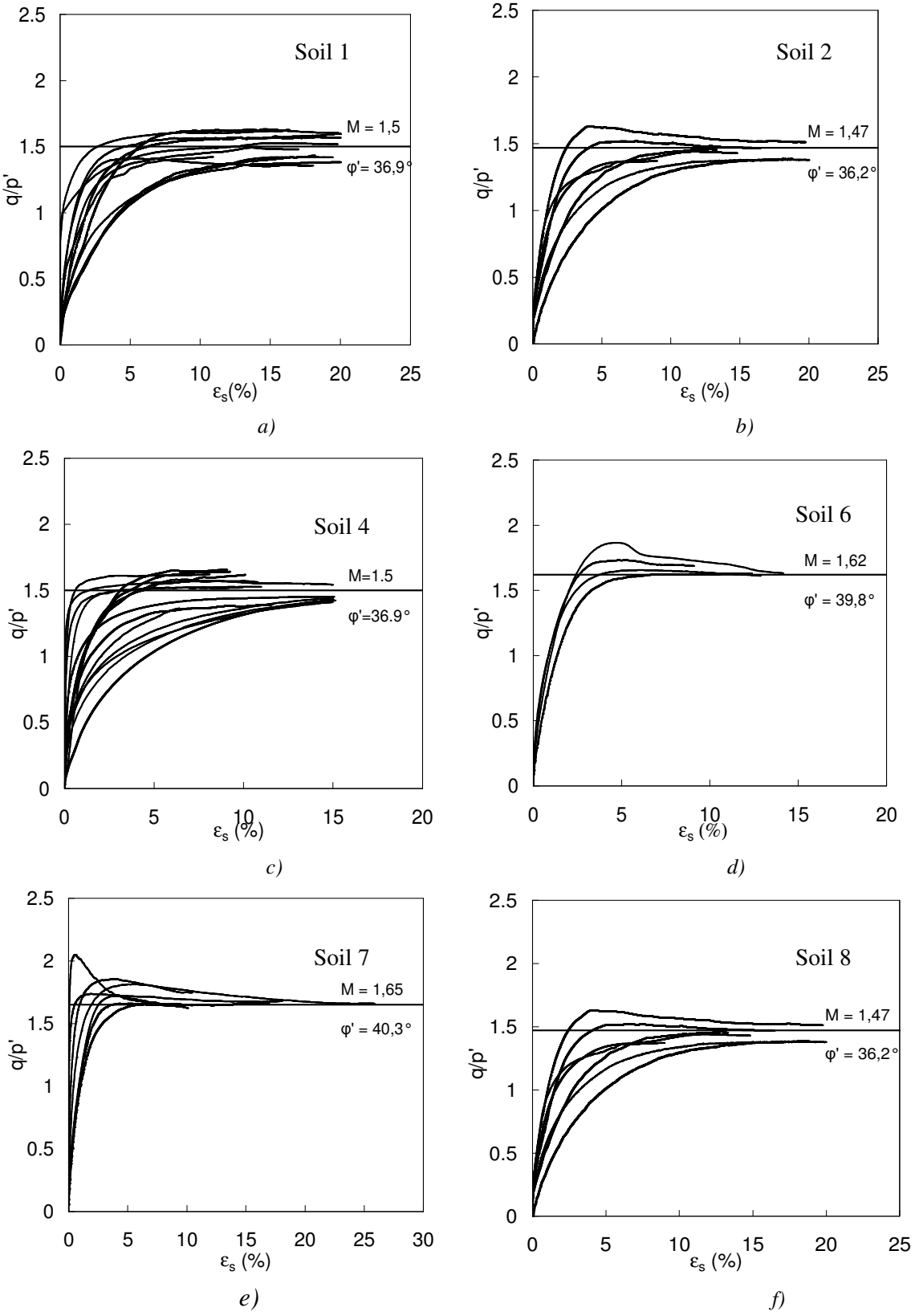

Fig.6.8 Results of the triaxial tests on saturated samples (Papa, 2007) soil1 a); soil 2 b); soil 4 c); soil 6 d); soil 7 e); soil 8 f)

dimensionless plane $(\frac{J}{p_e^{'}} vs \frac{p^{'}}{p_e^{'}})$ (*Fig. 6.9*). The mean effective equivalent stress, $p_e^{'}$, is the mean effective stress read by NCL in saturated conditions for every value of void ratio during the stress path of the triaxial tests and is obtained by the following expression (Hvorslev, 1937):

$$p_e^{'} = \exp\left(\frac{N-e}{\lambda}\right) \tag{6.28}$$

where e is void ratio, N is the void ratio value at mean effective stress of 1kPa and λ is the slope of NCL. The value of N and λ are obtained from isotropic compression test (Papa, 2007).

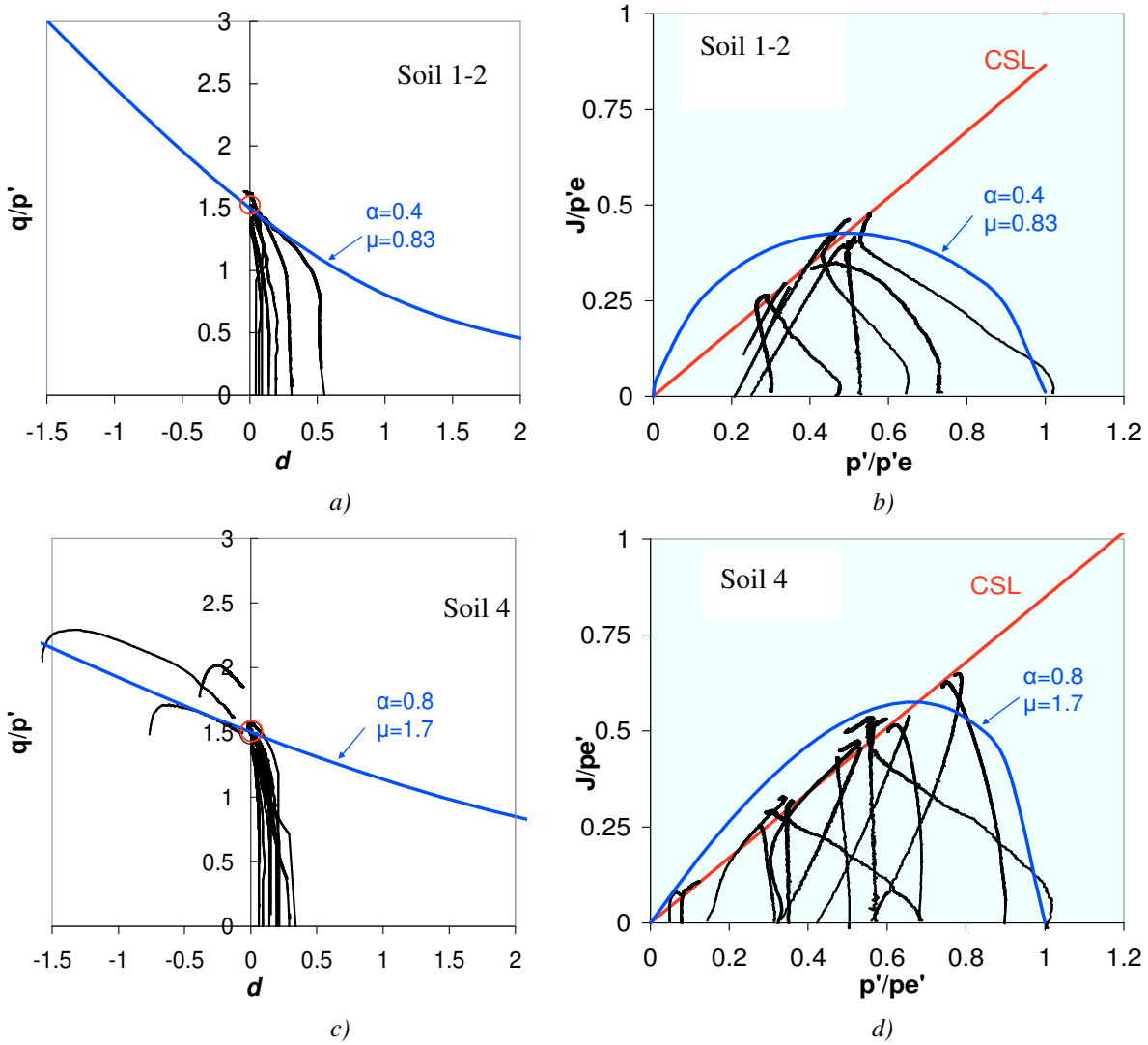

Fig.6.9: Matching of the experimental dilatation-stress ratio relation and analytic expression implemented in the model for soil 1-2 a); soil 4 c); matching of the experimental stress paths and yield surface expression on dimensionless plane for soil 1-2 b); soil 4 d) (experimental data from Papa 2007)

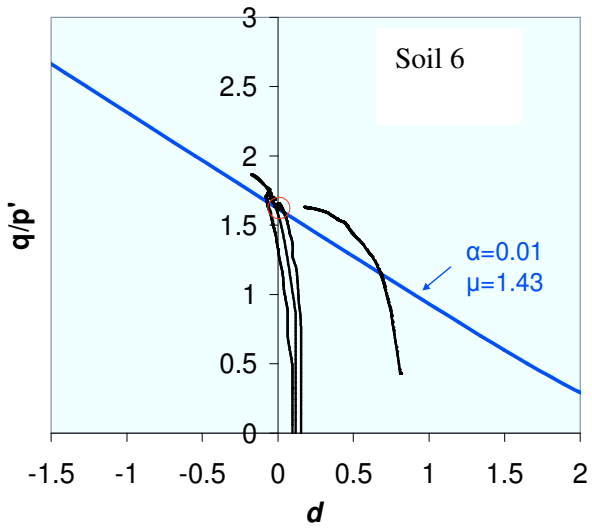

a)

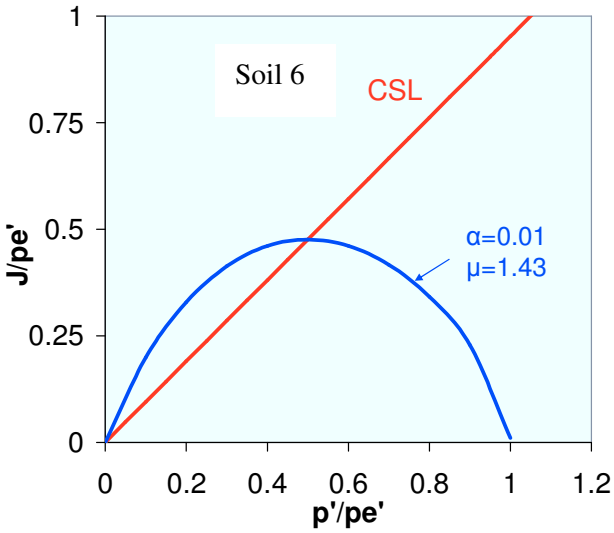

b)

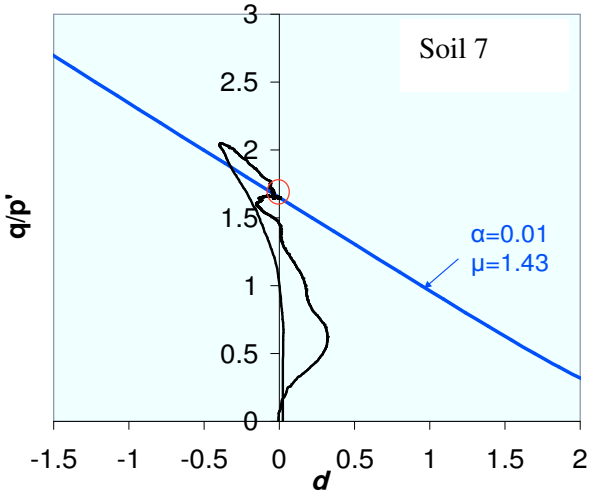

c)

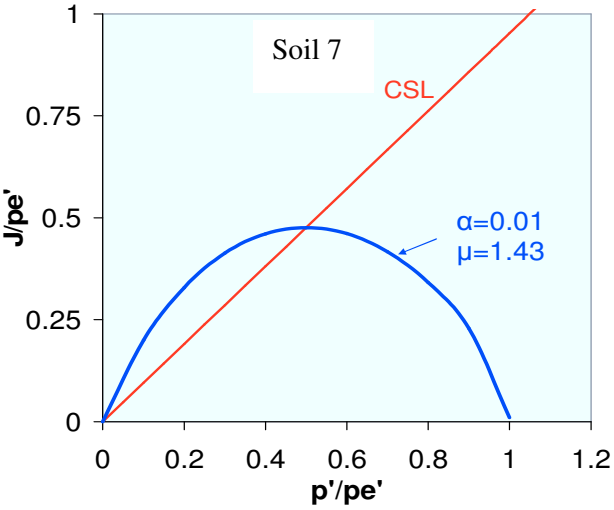

d)

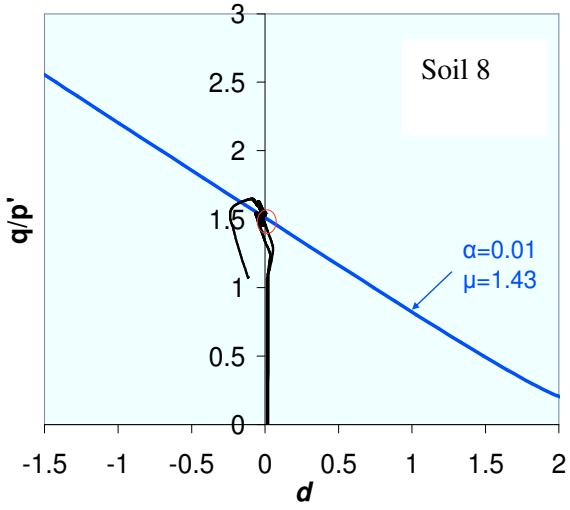

e)

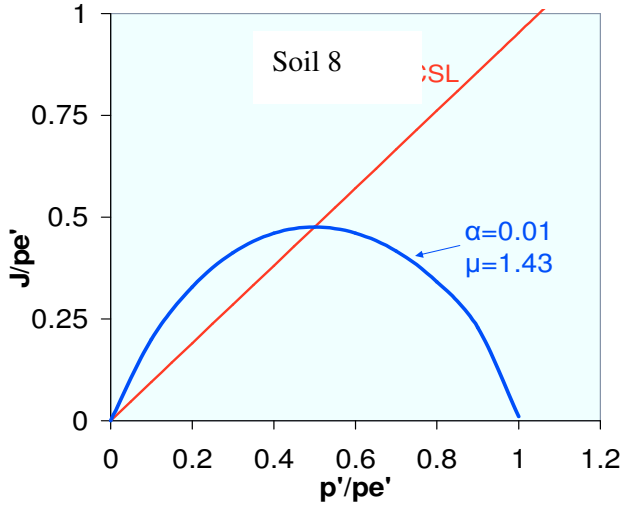

f)

Fig.6.10: Matching of the experimental dilatation-stress ratio relation and analytic expression implemented in the model for soil 6 a); soil 7 c); soil 8 e); yield surface expression on dimensionless plane for soil 6 b); soil 7 d) ;soil 8 f) (experimental data from Papa 2007)

For soils 6 and 7 there is no data regarding NCL, for soil 8 the number of stress paths is not enough to obtain the yield surface envelope (*Fig.6.10*). Therefore for the soils 6, 7, and 8, the yield surface is only drawn in correspondence of values of α, μ obtained matching the experimental dilatation and stress ratio and the model.
At least for soils 1, 2 and 4, for which it is possible to match the yield surface with experimental stress paths, the hypothesis of associated flow seems to be reasonable.
However the shape-parameters α, μ do not influence the mechanism of failure as it will proved in the Chapter 8 containing slope stability analyses.
The table with the parameter values for all the soils introduced until now are reported in the table:

Tab.6.1: Failure parameters of all the soils

	φ_{cs}	M	α	μ
Soil 1	36.9°	1.50	0.4	0.83
Soil 2	36.2°	1.47	0.4	0.83
Soil 3	46°	1.81	0.8	1.7
Soil 4	36.9°	1.50	0.8	1.7
Soil 5	42°	1.70	0.01	1.43
Soil 6	39.8°	1.62	0.01	1.43
Soil 7	40.3°	1.65	0.01	1.43
Soil 8	37°	1.51	0.01	1.43

6.3.1.2 Secondary yield surface

There are no lab tests to obtain the yield suction s_0; therefore the high value of 1000 kPa is assumed.

6.3.2 Isotropic compression parameters and hardening/softening parameters

The compressibility parameters in saturated conditions are obtained by the experimental results of the isotropic compression tests (Papa, 2007) (*Fig.6.11*). In the *figure 6.11* the NCL and the points corresponded to the void ratio and mean effective stress at failure are reported; for soil 7-8 there is no possibility to envelope the CSL by experimental points, for soil 6 and 7 there are no normal compression tests available.

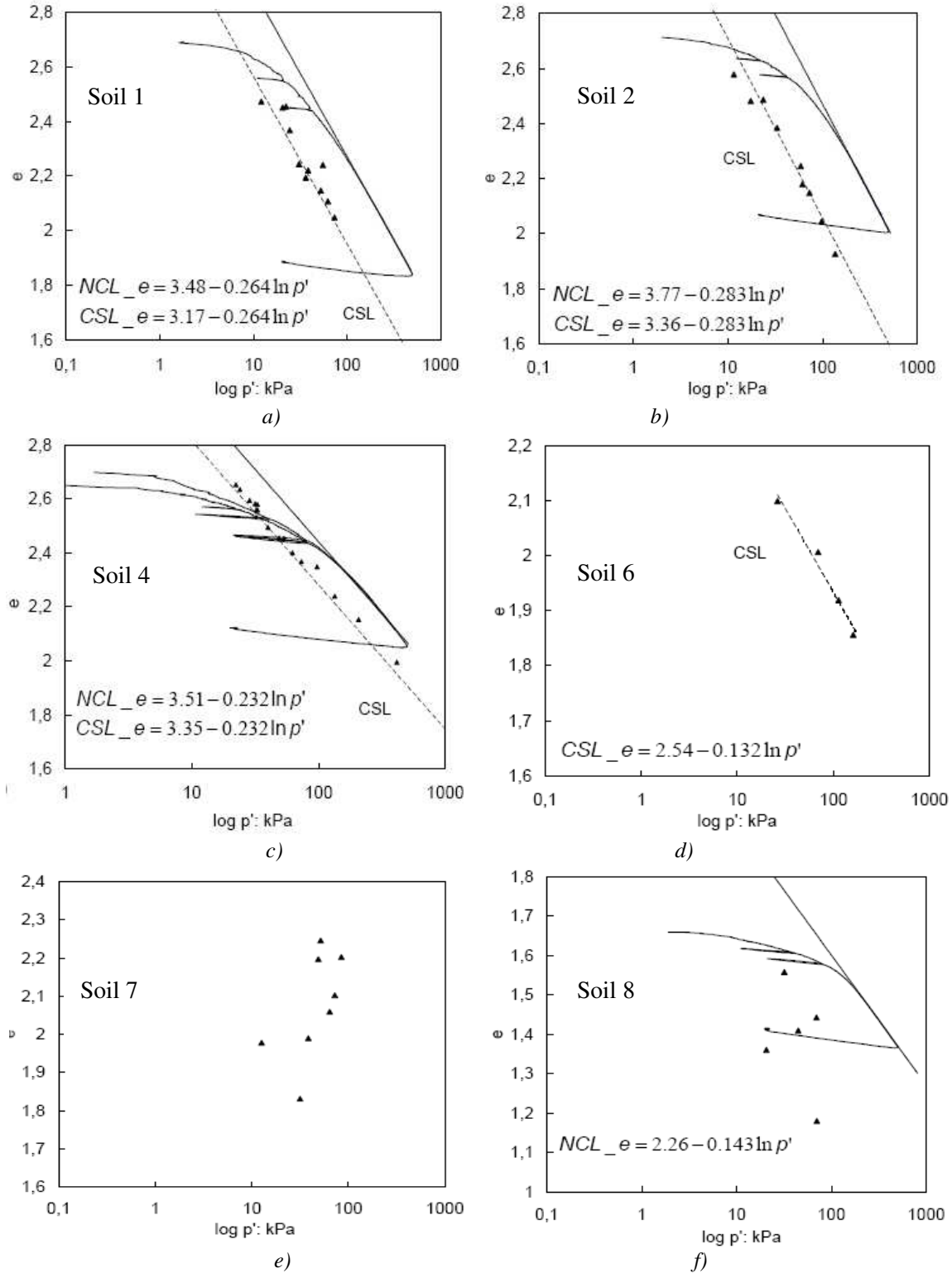

Fig.6.11 Normal Compression Line obtained from normal compression tests (Papa, 2007) and enveloping of Critical state line by the void ratio and mean effective stress values at failure for soil 1 a); soil 2 b); soil 4 c); soil 6 d); soil 7 e); soil 8 f)

According to the evidence of the results of isotropic compression test at controlled suction, the option 2 for partially saturated NCL is taken. Therefore the Normal Compression Line in unsaturated condition is constantly diverging from the fully saturated isotropic compression line up to a particular value of mean net stress, p_m, beyond which the slope of the NCL in partially saturated condition is equal to the saturated Normal Compression Line (*fig.6.5*).

It is available only an isotropic compression test at controlled suction (s=20 kPa) on sample of soil 4 (Papa, 2007), so on the plan ($\lambda(s_{eq})$ vs s_{eq}) two points are reported, one related to the test at saturated conditions and other one at s = 20kPa of suction just on the soil 4. Unfortunately the value β and r that define $\lambda(s_{eq})$ (see equation *6.20*) are obtained only by

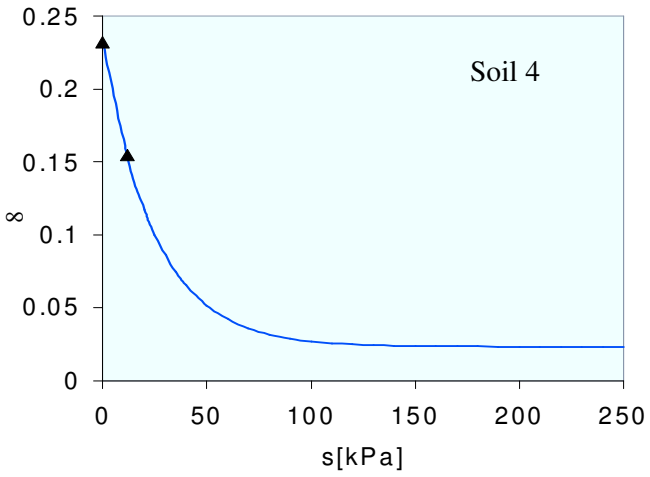

Fig.6.12 Empirical expression of Alonso et al.,1990 and experimental points ($\lambda(s_{eq})$, s_{eq}) by isotropic compression test

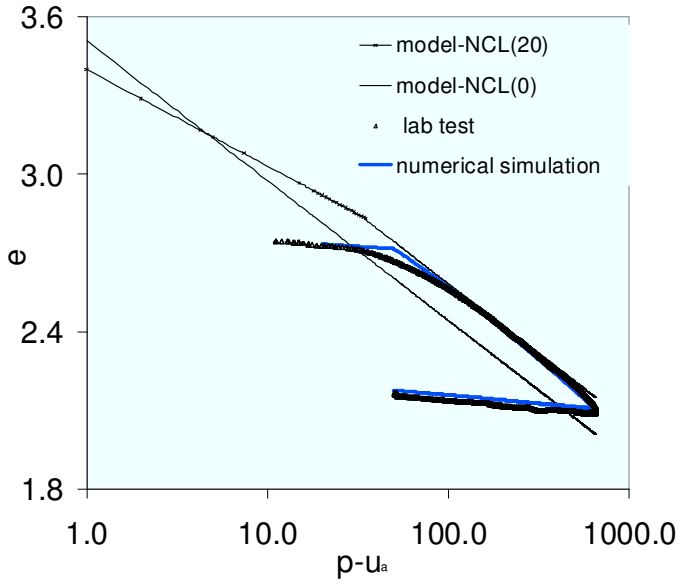

Fig.6.13 Numerical simulation of isotropic compression test at suction of 20 kPa and experimental curve (experimental data from Papa 2007)

two experimental points (*Fig.6.12*) and are assumed valid for all the soils.
The value of α_c parameter is obtained simulating numerically the isotropic compression test at controlled suction by using ICFEP and matching it with the experimental curve (*Fig.6.13*). As this type of testing lab is unique and it has been carried out only for the soil 4, α_c is calculated only for this soil and is assumed valid for the other soils.

About κ_s and λ_s, there are no lab test available to obtain these two parameters, therefore their values are assumed equal to 0.005 for κ_s and 0.08 for λ_s according to the literature. It is not important to know the exact λ_s value because the soil is never subjected to the suction beyond s_0, 1000 kPa.

In the following the table with the parameter values about the compressibility behaviour for all the soils introduced until now is reported:

Tab.6.2: Compressibility parameters of all the soils

	$\lambda(0)$	κ	$v_1(0)$	r	β	α_c
Soil 1	0.284	0.03	4.48	0.1	0.036	3.87
Soil 2	0.283	0.03	4.77	0.1	0.036	3.87
Soil 3	0.130	0.03	4.68	0.1	0.036	3.87
Soil 4	0.264	0.03	4.51	0.1	0.036	3.87
Soil 5	0.130	0.02	3.40	0.1	0.036	3.87
Soil 6	0.132	0.02	3.86	0.1	0.036	3.87
Soil 7	0.130	0.02	3.40	0.1	0.036	3.87
Soil 8	0.130	0.02	3.40	0.1	0.036	3.87

6.3.3 Elastic behaviour

In the following analyses the value of $\mu = 0.3$ is assumed for all the soils, the shear modulus G is obtained from the equation 6.27 as a function of stress level.

6.4 Hydraulic model

6.4.1 Soil water retention curve

The Retention curve implemented in ICFEP is Van Genuchten expression (1980)(*Fig.6.14*). This curve is non-linear and non-hysteretic.
The expression of Van Genuchten curve is the following:

$$S = \left[\frac{1}{1 + \left[(s - s_{des})\alpha \right]^n} \right]^m (1 - S_0) + S_o \tag{6.29}$$

Where s_{des} is the suction at the beginning of de-saturation, S_0 is the Degree of saturation residual, α, n, m are the model parameters.

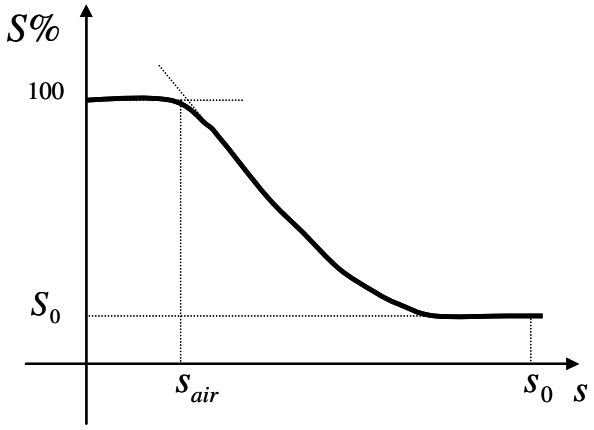

Fig 6.14 Retention Curve: Van Genuchten model

6.4.2 Soil permeability model

About the permeability curve, the de-saturation model is adopted.

Hence the permeability curve is given by the following expression:

$$\log k = \log k_{sat} - \frac{s - s_1}{s_2 - s_1} \log \frac{k_{sat}}{k_{\min}} \tag{6.30}$$

Where s_1 is the pore pressures at which permeability begins to change, s_2 is the pore pressure at which the permeability completes its changes *(fig.6.15).*

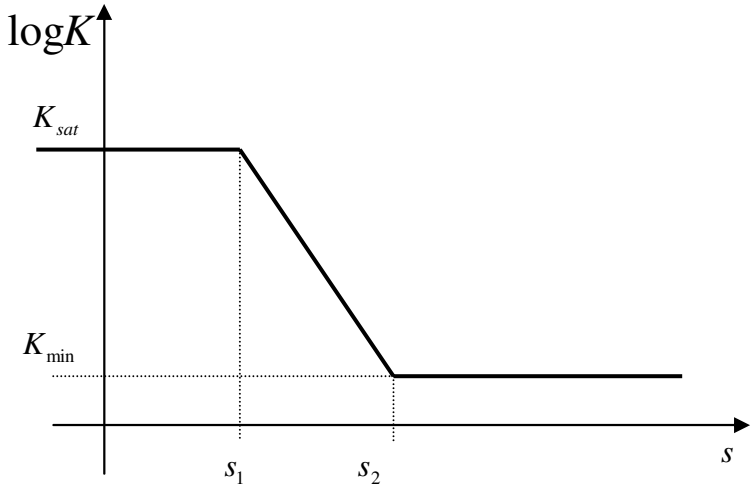

Fig.6.15 Permeability curve model

6.5 Calibration of the Hydraulic model

6.5.1 Soil water retention curve

In the analyses the parameters of soil water retention curve are changed according to the wet period or the dry period simulated in order to use respectively the wetting curve and the drying curve. In fact according to the experimental results the hysteresis of these soil is not negligible (*Chapter 5*). The parameters in dry condition are obtained matching the experimental retention curves of each soil (Papa, 2007) and the Van Genuchten model curve used in the analyses (*Fig.6.16, 6.17*). The parameters in wetting condition have been determined by drawing the wet retention curve as the lowest limit of the experimental data (measurements of suction and water content) that identify the scanning path (*Fig.6.16*). They are obtained only for soil 1-2 and 4, in fact there are not measurements of water soil content for the other soils. However the hysteresis phenomena can be negligible for deeper soils. All parameters resulting are summarized in the table 6.2.

6.5.2 Soil Permeability

The permeability curve parameters in dry conditions are obtained by matching the permeability curves model (6.29) and the experimental dry retention curve created by the inverse analysis (Hydrus 1-D, Papa,2007). About the curve in wet conditions, the parameters are searched by using a back analysis. In fact it was imposed that the numerical profile of suction, resulted by numerical analyses simulating one hydrologic year on the testing site, matches the measurements collected along the instrumented vertical 3B (Chapter 7). The wet parameters are searched only for the superficial and intermediate soils (1-2, 4) as it has been done for the retention curve (*fig.6.16-6.17*). All the parameters obtained are summarized in the table 6.2.

Tab.6.2: Hydraulic parameters of all soils

	s_{air} [kPa]	**a**	**n**	**m**	S_0	s_0 [kPa]	k_{sat}/k_{min}	k_{sat} [m/s]	p_1 [kPa]	p_2 [kPa]
1-dry	7.02	0.12	1.45	0.31	0.15	1000	10000	$1*10^{-6}$	-30	85
1-wet	1	0.1	1.66	0.4	0.15	1000	37500	$3*10^{-6}$	-5	25
2-dry	7.02	0.12	1.45	0.31	0.15	1000	10000	$2*10^{-6}$	0.4	55
2-wet	1	0.1	1.66	0.4	0.15	1000	37500	$3*10^{-6}$	-5	25
3-dry	10	0.024	1.85	0.46	0.014	1000	1000	$3.50*10^{-7}$	10	130
4-dry	8.19	0.115	1.35	0.259	0.15	1000	275	$5.50*10^{-6}$	-6	35
4-wet	1	0.08	1.66	0.4	0.23	1000	500	$2*10^{-6}$	-10	18
5-dry	12.28	0.05	1.64	0.39	0.35	1000	133.33	$2*10^{-7}$	0.2	60
6-dry	12.28	0.05	1.64	0.39	0.35	1000	133.33	$2*10^{-7}$	0.2	60
7-dry	12.28	0.05	1.45	0.31	0.28	1000	14.28	$1*10^{-8}$	0.2	50
8-dry	12.28	0.05	1.45	0.31	0.28	1000	14.28	$1*10^{-8}$	0.2	50

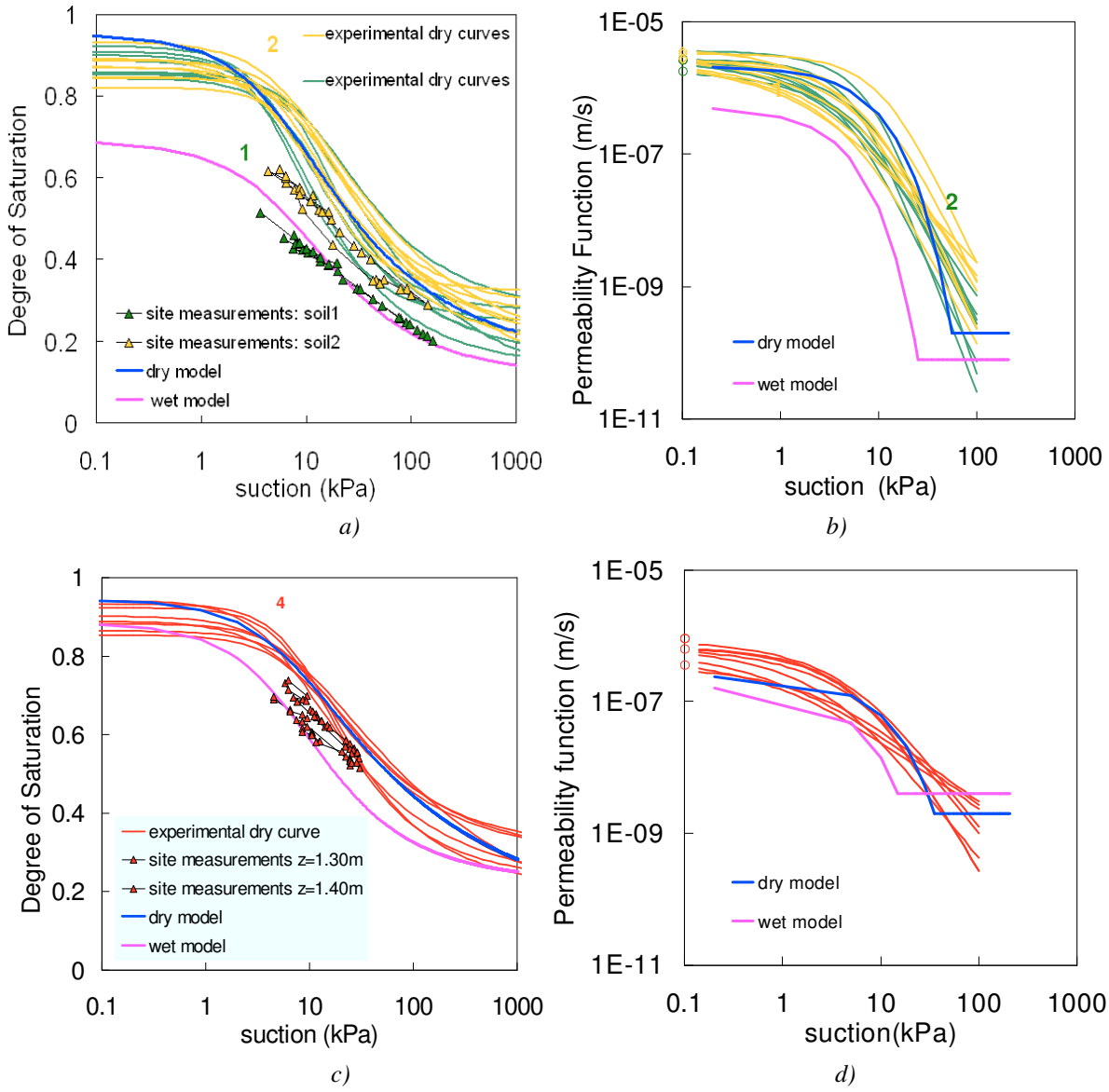

Fig.6.16 Matching of the wet-dry retention curve model with the experimental curves of soil 1-2 a), soil4 c); matching of the wet dry permeability curve model with the experimental curves of soil 1-2 b), soil4 d)

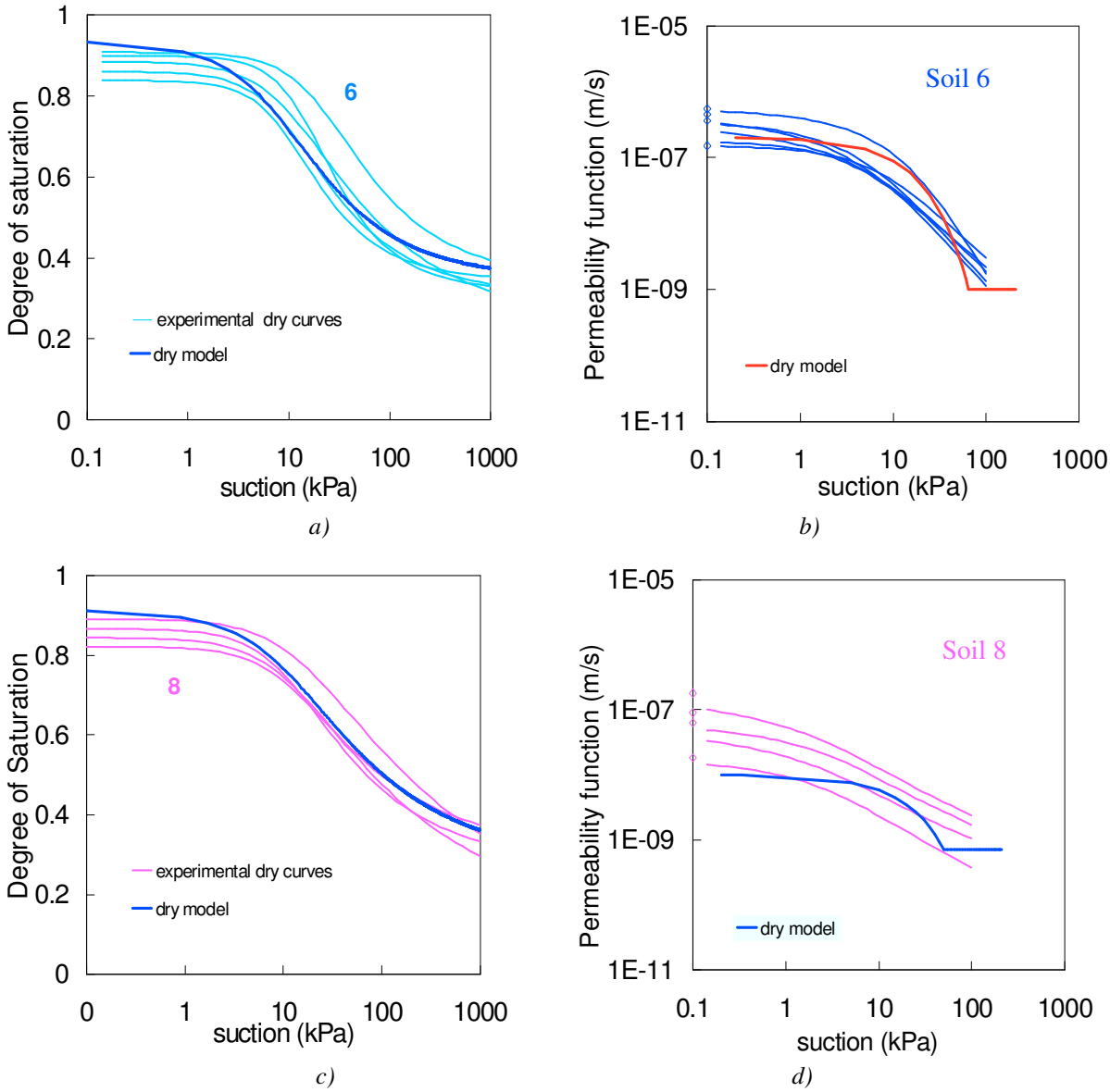

Fig.6.17 Matching of the retention curve model with the experimental dry curves of soil 6 a), soil 8 c); matching of the dry permeability curve model with the experimental curves of soil 6 b), soil8 d)

About the retention and permeability curve of soil 3 (pumices of the Avellino eruption), the experimental curve of pumices belonged to the same eruption but sampled in another site is used (Nicotera et al., 2003)(*Fig. 6.18*). It is characterized by the double porosity but only the second porosity is modelled, assuming the hypothesis that the emptying close to the saturation happens so fast that it can be negligible.

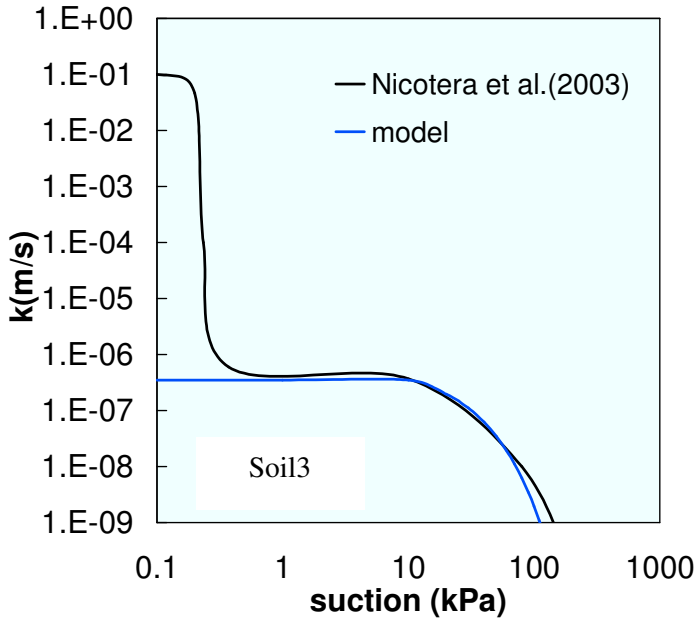

Fig 6.18 Matching of the permeability curve model with the experimental curves for the pumices (soil3)

Chapter 7

Validation of the numerical model

7.1 Synopsis

This chapter presents the validation of the numerical model adopted for the analysis of the Monteforte Irpino slope. A section down the slope was discretised into a finite element mesh assuming plane strain conditions. After the geological sedimentation of top soils over the limestone, one year of measured rainfall infiltration and evapotranspiration was applied on the slope surface. The predicted suction profiles from numerical analysis were compared with the measured suction profiles on site at the same locations. These showed excellent agreement, thus giving confidence in the developed numerical model and calibration to interpret of mechanical and hydraulic behaviour presented in the previous chapter.
All the analyses were coupled, in a sense that both the mechanical deformation and hydraulic flow are calculated simultaneously in the same analysis. The analyses were performed with the Imperial College Finite Element Program (ICFEP, Potts & Zdravkovic 1999).

7.2 Geometry of the slope

The triggering mechanism of fast debris flows is numerically studied in the hypothesis of plane-strain conditions, so analyses are carried out using a two dimensional mesh, which reproduced a section of the monitored slope.
The section reproduced by the mesh is the C-C'one (*fig.7.1*). There are eight different soils that cover the limestone (*fig.7.2*) and each of them is considered like a layer. The eight layers are:
-layer *1-2* top pyroclastic soil (mean thickness 0.8 m)
-layer *3* pumiceous deposit of Avellino eruption 3.7 kyb.p (mean thickness 0.40 m),
-layer *4* paleosoil (weathered volcanic ashes, mean thickness 1.60 m)
-layer *5* pumiceous deposit of Ottaviano eruption 8.0 kyb.p (mean thickness 0.70 m),

-layer *6* paleosoil (weathered volcanic ashes, mean thickness 0.90 m)
-layer *7* volcanic sand (mean thickness 0.50m),
-layer *8* highly weathered fine-grained ashy soil (mean thickness 0.60 m),

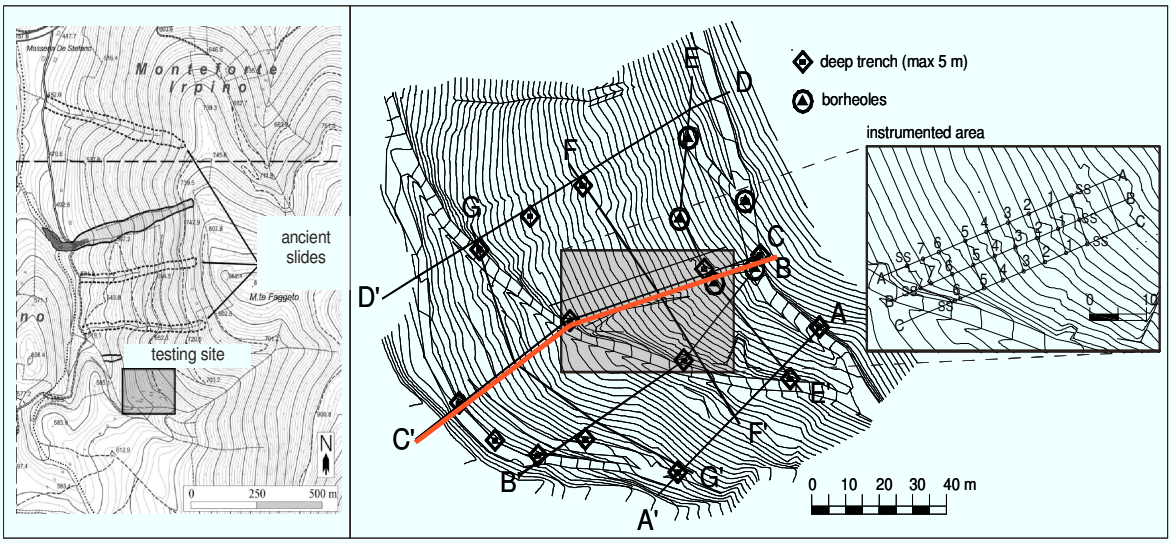

Fig.7.1 Map's site (Papa,2007)

The layer 9 is the limestone on which the pyroclastic soils rest.
The soils 7-8 (volcanic sand and cineritic soil) have not continuity.
The mean thickness of the pyroclastic soil resting on the massif is 5 m, the local slope changes between 25 and 30°. The height of the domain reproduced is 56 meters and the length is 114 meters (*fig.7.2*).

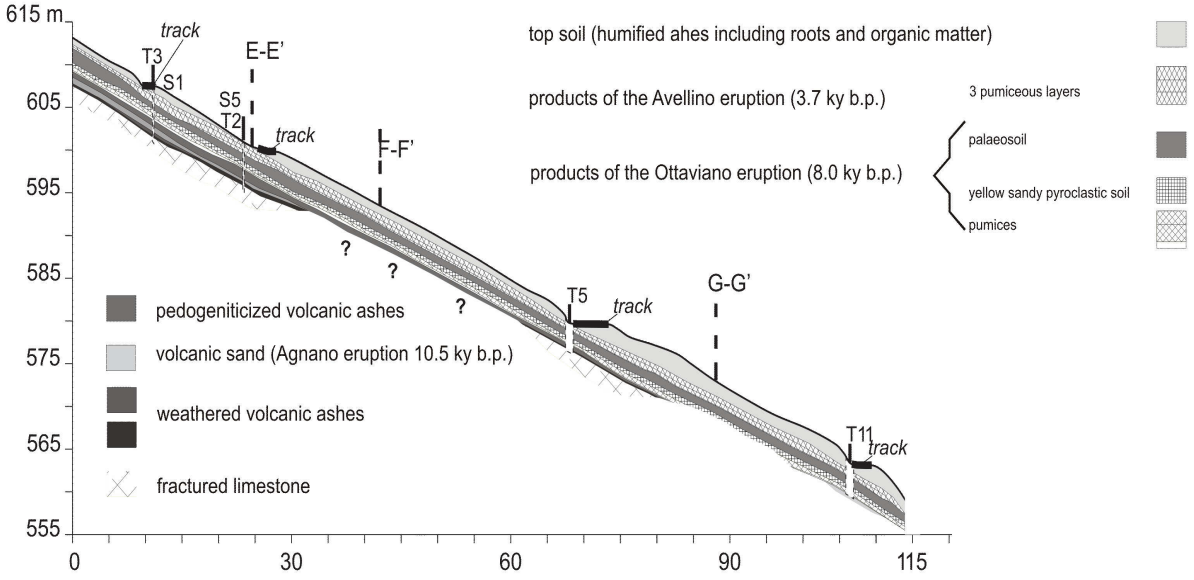

Fig.7.2 Longitudinal section C-C' reproduced by the mesh 2-D (Di Crescenzo et al.,2007)

7.3 Finite element mesh

The FE mesh consists of *1714* elements and *5318* nodes (*fig.7.3 and 7.4*). Nine set of mechanical and hydraulic properties are assigned to each layer, to reproduce the real stratigraphy.

Elements of the pyroclastic layers were treated as consolidating, thus having a pore pressure degree of freedom at each node, in addition to the displacement degrees at freedom. Limestone was treated as a linear elastic material. The finite element mesh is presented in figure 7.4. For numerical accuracy, there are two elements per thickness of each layer.

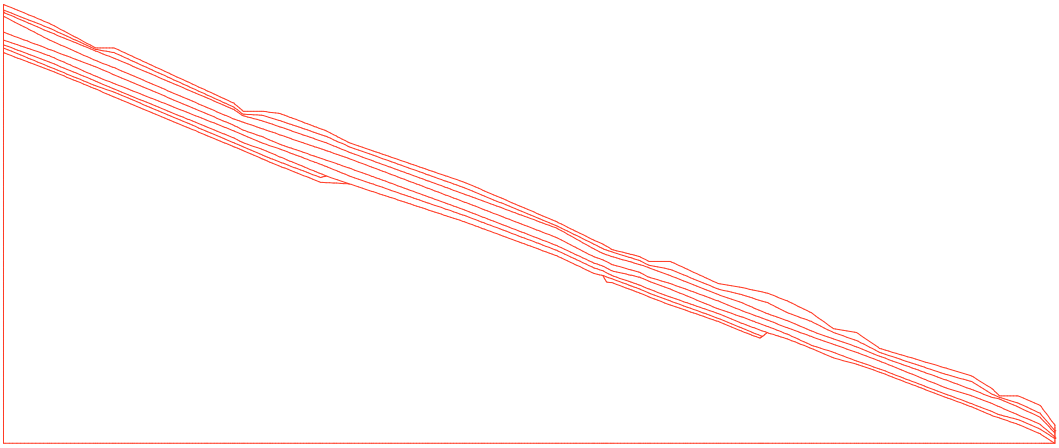

Fig 7.3 Material zones

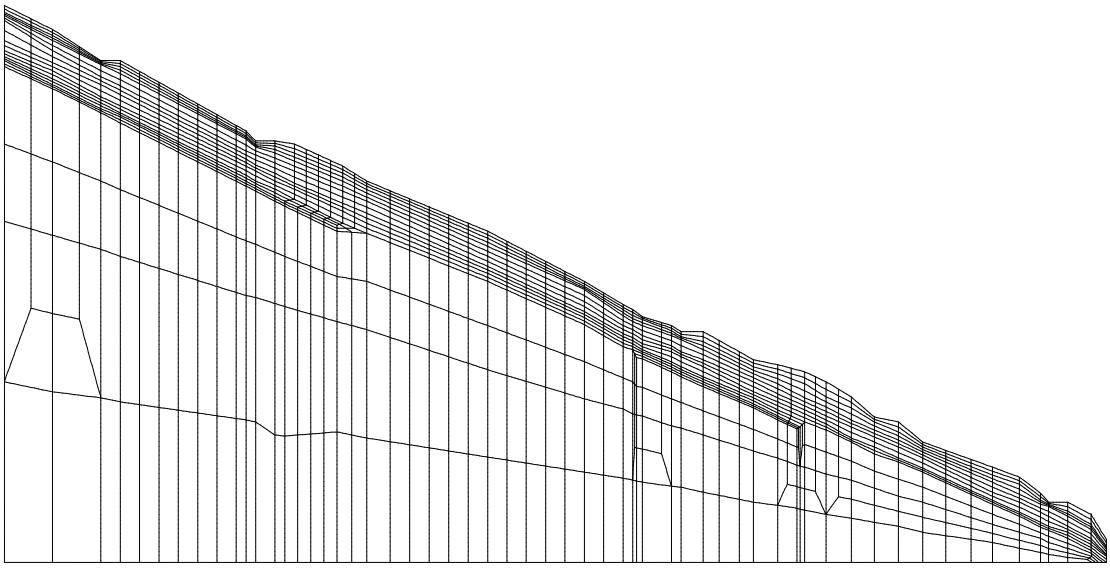

Fig. 7.4 Mesh 2-D

7.4 Initial stress in the slope

To obtain the *initial stress state* in the slope, the deposition of each pyroclastic soil layer on the limestone is simulated in drained conditions, so the mesh is constructed by constructing layers one by one.

Therefore the procedure consists of applying the layers one by one, having assigned to the limestone the values of pore pressures and the stress state at the initial conditions. The pore pressures, $u_{w,}$ in the limestone are uniform everywhere and are assigned to zero for all the following analyses. While the stress state is:

$$\sigma_v = \gamma_{\lim estone} * y(x)$$
$$\sigma_x = \sigma_y$$
$$\tau_{xy} = 0$$

where $\gamma_{\lim estone}$ is the unit weight, 19 KN/m$^{3.}$. The depth $y(x)$ is a function of the length x, in order to consider the real topography of limestone surface.

The superficial part of the mesh (the pyroclastic soil layers, 1 to 8) is deactivated in the initial phase of the analyses, then each layer is constructed into two years. Before the deposition, the layer is characterized by elastic behaviour; when it is activated, by the elasto-plastic behaviour (the constitutive law specified in the analyses). Prior to construction, the accumulated stress and pore pressures in the layers to be constructed are zero. Displacements, strain within these layers are reset to zero immediately after construction; the hardening parameters are also reset at this stage, being them dependent on the stresses and material proprieties. Pore pressures are assigned in each layer after its construction equal to the measurements of suction collected on site on 8th November 2006 along the borehole 3B (corresponded to the vertical section of the mesh at x=50m). So the hydrologic year can be

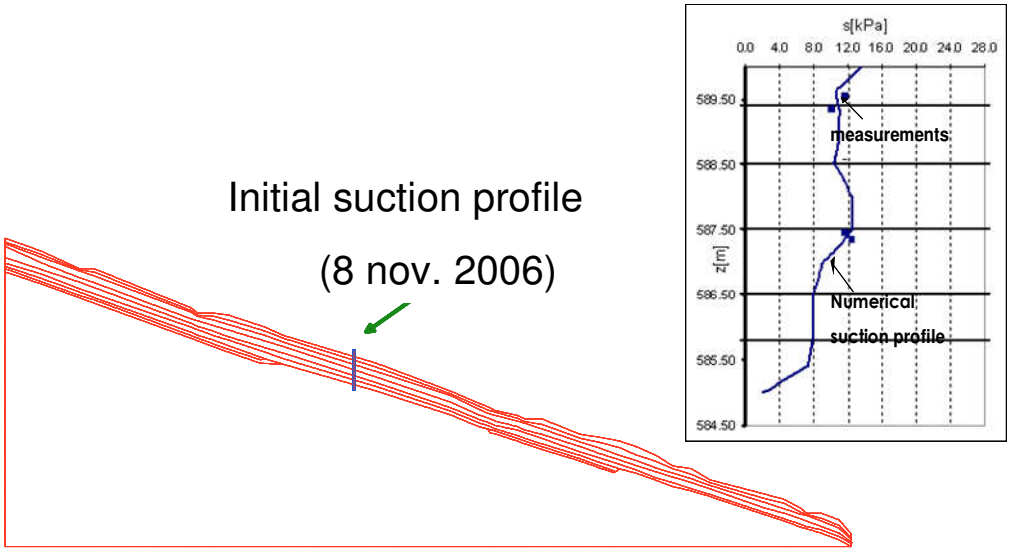

Fig.7.5 Initial suction profile assumed along all the slope

reproduced starting from 9th November 2006 (*fig.7.5*).
It is not a big error to assume the same suction measured along one vertical acting in all the slope, because these values are very close to the mean suction in the whole field. Moreover the influence of initial condition on the results vanishes into two weeks as it is possible to verify by doing two analyses with two different initial conditions and the same rainfall history applied on the upper boundary.

7.5 Boundary conditions

In order to simulate one hydrological year and to calculate hydraulic conditions in the subsoil, the meteorological conditions registered on site from 9th November 2006 to 9th November 2007 have been applied to ground surface of the mesh. Being the model hydro-mechanical coupled, both conditions on *displacements and pore pressures or flow* have to be applied on all the boundaries (*fig.7.6*).

7.5.1 Kinematic boundary conditions

The *kinematic boundary conditions* applied are (*fig.7.6a*):

- displacements impeded vertically and horizontally at the bottom of limestone,
- displacements impeded horizontally along the right and left sides.

The vertical and horizontal displacements at the limestone bottom and the horizontal ones at the vertical edges of the analysed domain are assigned equal to zero during the construction of the layers.

7.5.2 Hydraulic boundary conditions

Only the limestone is excluded from the consolidation, so the lower boundary conditions in terms of pore pressure or flow are applied at the contact between the soil 8 and the limestone.
The *Hydraulic boundary conditions* applied are (*fig.7.6b*):

- The normal flow prescribed to zero on both vertical sides.
- The suction value equal to zero at bottom (contact between the limestone and soil 8); this choice agrees with the experimental evidence, in fact the piezometers installed on site at the contact with the limestone are empty over whole the year.
- The climatic conditions registered on site from 9th November 2006 to 9th November 2007 applied on the top (ground surface)

Hereinafter it is explained how the rain and the evapotranspiration are accounted for the model.

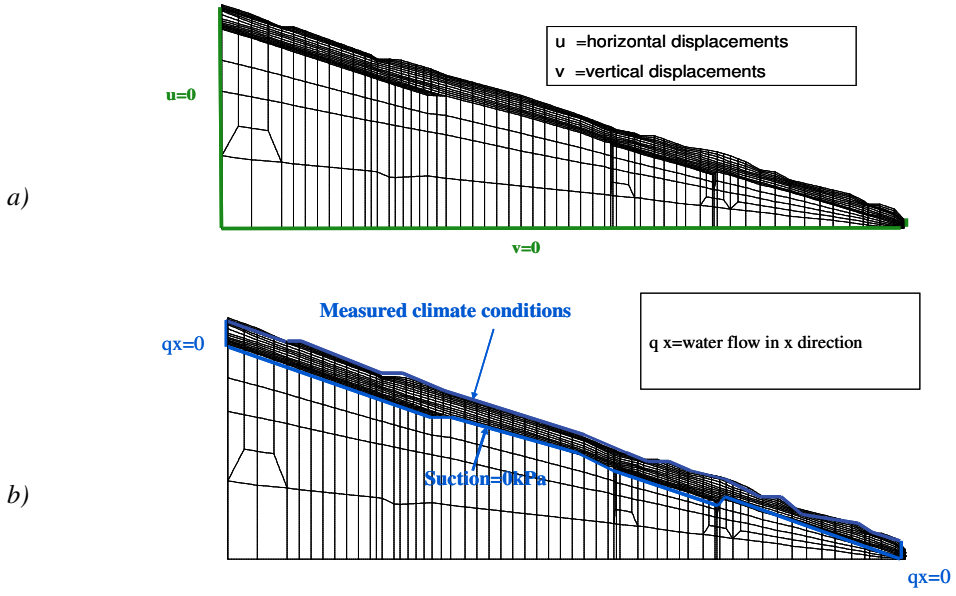

Fig.7.6 Cinematic Boundary Conditions a), Hydraulic Boundary Conditions b)

7.5.2.1 Infiltration

The rainfall is usually divided into *infiltration* and *runoff*, but in the following analyses the second part is negligible due to the not very high intensity of the rainfalls considered. So it is assumed all the rainfall infiltrates into the soil, then by elaboration of the results, the suction on the ground surface is at maximum equal to zero and never compressive. This is compatible with the hypothesis that the runoff is negligible.

Moreover the total vertical flow over one year through the superficial soils 1-2 calculated by the in situ measurements of suction and water content (Chapter 5), is close to the value of the recharge, R, calculated in these analyses (defined as the difference between cumulated rainfall over one year and evapotranspiration cumulated over one year), and they are around 200 mm (see fig.7.7b).

The daily rainfall are registered by the rain gauge in Monteforte, in a zone very close to the testing site; measurements analysed cover just the hydrological year investigated (from 9th November 2006 to 9th November 2007)(*Fig.7.7*).

In the analyses the rainfall is applied uniformly on the whole ground surface and it is represented as vertical flow ingoing into the soils. The hypothesis that daily rain is distributed uniformly over the day is undertaken.

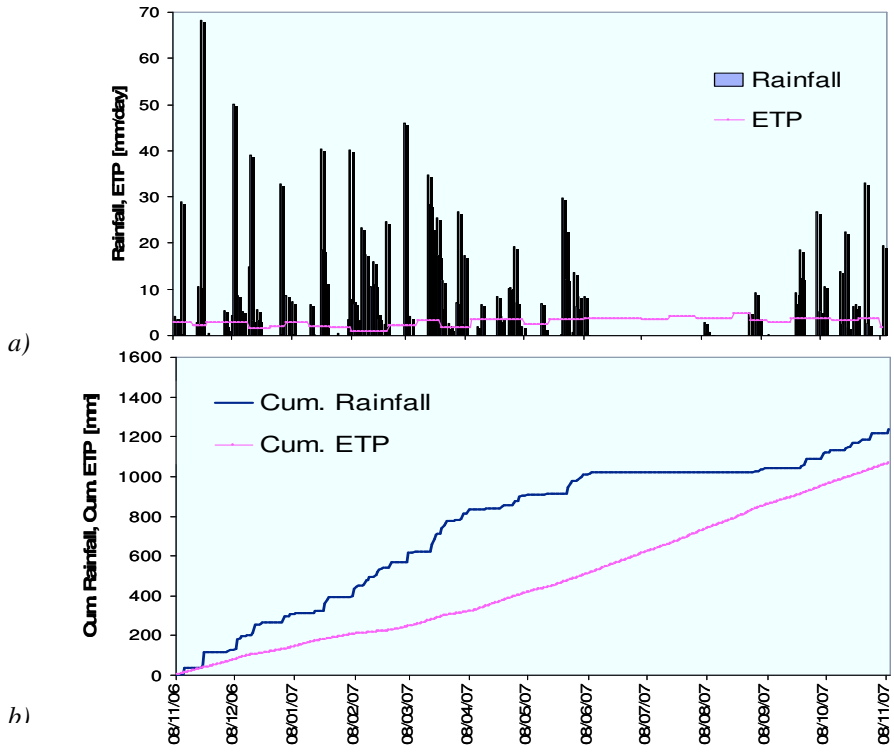

Fig.7.7: a) Daily rain and Daily Evapotranspiration b) Cumulated Rain and Evapotranspiration,

7.5.2.2 Evapotranspiration

On the ground surface it is possible to account for evapotranspiration too. In fact the software models the evaporation like a flow outgoing from the top soil and the transpiration like a sink along the depth until the roots extend.

The evapotranspiration flow (ETP) is applied uniformly on the whole top boundary and it is distributed constantly over each day. ETP applied in the analysis is the result of *the Penmann Equation (Penmann, H.L.,1948)*, by using the measurements of air temperature, air relative humidity and wind speed measured in site; the climatic measurements are available twice a month, so a ETP flows constant over two weeks is calculated and then applied in the analyses (*fig. 7.7*). The Evapotranspiration is then divided into Potential Transpiration and Potential Evaporation by taking in account the Leaf Area Index (LAI). The Leaf Area Index (LAI), a dimensionless quantity, is the leaf area (upper side only) projected to the soil below it. On dependence of different type of vegetation, the LAI varies between 1 and 2,7 *(Fao, Irrigation and Drainage Paper No 56).*

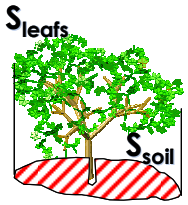

$$LAI = \frac{S_{leafs}}{S_{soil}} \qquad (7.1)$$

Fig.7.8: LAI as a ratio between the leaf area and its projection to the soil below

The *Penmann equation* to calculate ETP flow, is:

$$ETP = \frac{\frac{\Delta R_n}{L_V \rho_w} + \gamma * 0.165 * (p_{vs} - p_v)(0.8 + u_2/100)}{\Delta + \gamma} \quad \text{[mm/day]} \qquad (7.2)$$

where:

-Lv is the latent heat of vaporization [2.45 MJ/kg]

- ρ_w is the water density [1000kg/m^3]

- u_2 is the wind speed at 2 m above ground surface [Km/day]

- p_v is the vapour pressure in the air (= Air Relative Humidity multiplied by Saturation vapour pressure) [mbar]

- p_{vs} is the saturation vapour pressure at the Air Temperature [mbar]

$$p_{vs} = 0.611 * \exp(\frac{17.27 * T°}{T° + 237.3}) \tag{7.3}$$

- Δ is the slope of the Saturation-vapour pressure Curve:

$$\Delta = 4098 * \exp(\frac{17.27 * T°}{T° + 237.3}) / (T + 237.3)^2 \tag{7.4}$$

where T° is the Air Temperature [°C]

- γ_{ps} is the psychrometric constant [kPa/°C]

$$\gamma = 0.665 \cdot 10^{-3} p_{atm} \tag{7.5}$$

where p_{atm} is the Atmospheric pressure [kPa]

- Rn is the Net Radiation $\left[MJ / m^2 d\right]$

So in order to be able to calculate ETP from the (7.2), the measurements of air temperature & air humidity and wind speed are necessary at least.

7.5.2.2.1 Air temperature and air relative humidity measurements

The air temperature and the air relative humidity are measured in site (*fig.7.9*) with a portable termo-igrometer in the same days when the suction measurements are taken; the data are collected every two weeks over the hydrological year investigated.

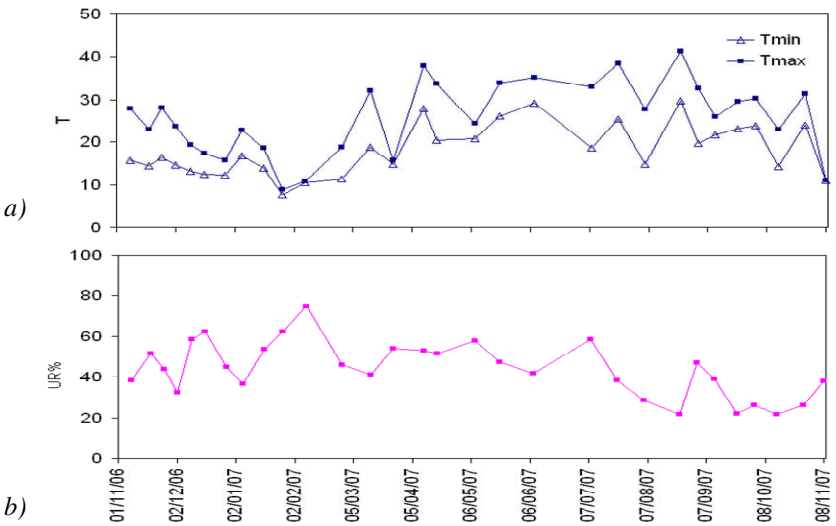

Fig.7.9: Measurements of air temperature a) and air relative humidity b)

7.5.2.2.2 Calculation of net radiation

The *Net Radiation* is the difference between incoming and outgoing radiation of both short and long wavelengths (*fig.7.10*); it is normally positive during the daytime and negative during the nighttimes. The total daily value is almost always positive over a period of 24h, except in extreme conditions at high latitudes.
In making estimates of Evapotranspiration flow, all terms of the energy balance should be considered:

$$R_n = G + H + L_e \tag{7.6}$$

Where G is the soil heat flow, H is the air heat flow, Le is the latent heat of vaporization. Because of G and H are small compared to Rn, they are ignored *(FAO, Irrigation and Drainage Paper n°56).*

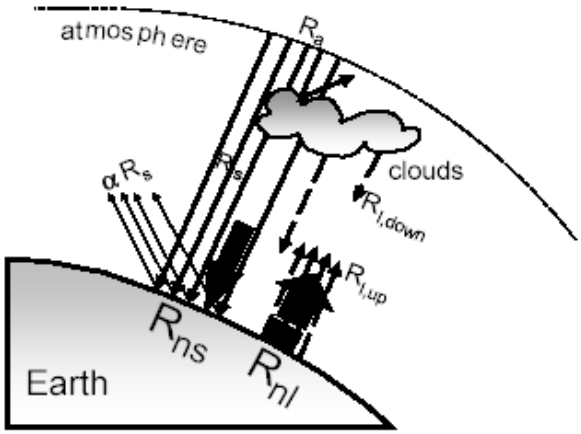

Fig.7.10: Various components of radiation

The *net radiation* is obtained indirectly as function of air temperature following the indications in the Fao manual. This is because in the period (8^{th} November 2006 ÷ 8^{th} November 2007) simulated by the analyses the net radiometer was not installed yet. The values are calculated by using the air maximum temperature and the air minimum temperature collected in the site.
The net radiation is:

$$Rn = Rns - Rnl \tag{7.7}$$

where:

Rns is the shortwave net radiation:

$$Rns = (1-\alpha)Rs \tag{7.8}$$

α is the reflection coefficient, for vegetated area it is equal to 0.23 (FAO, Irrigation and Drainage Paper n°56)

Rs is the Shortwave Radiation, it is calculated by the *Hargreaves' radiation formula*, adjusted and validated at several weather stations in a variety of climate conditions; this one is adapted for the interior regions:

$$Rs = 0.16\sqrt{T\max_{air} - T\min_{air}} * Ra[MJ / m^2 day] \tag{7.9}$$

Ra is the Extraterrestrial radiation (Fao, Irrigation and Drainage Paper n°56):

$$Ra = \frac{26*60}{\pi} Gsc * dr[\cos\omega s \sin\delta \sin\varphi + \sin\omega s \cos\delta \cos\varphi][MJ / m^2 day] \tag{7.10}$$

Gsc is the solar constant $Gsc = 0.0820\,[MJ / m^2 day]$,

dr is the inverse relative distance Earth/Sun:

$$dr = 1 + 0.33\cos(\frac{2*\pi}{365} J) \tag{7.11}$$

where J is the number of the day in the year between 1 and 365 (1 January) or 366 (31 December),

δ is the solar declination:

$$\delta = 0.409\sin(\frac{2\pi}{365} J - 1.39)[rad] \tag{7.12}$$

φ is the latitude:

$$\varphi = \frac{\pi}{180}(latitude)°[rad] \tag{7.13}$$

ω_s is the sunset hour angle:

$$\omega = \arccos[-\tan\varphi \tan\delta][rad] \tag{7.14}$$

Rnl is the Net Long wave Radiation, it is expressed by the Stefan/Boltzmann law:

$$Rnl = \sigma[(T\max,_k^{\,2} + T\min,_k^{\,2})/2](0.34 - 0.14\sqrt{p_v})(1.35\frac{Rs}{Rso} - 0.35) \quad (7.15)$$

where:

σ is the Stefan/Boltzmann constant:

$$\sigma = 4.903 * 10^{-9}[MJ / K^4 m^2 day] \quad (7.16)$$

Rso is the calculated clear/sky radiation:

$$Rso = (0.75 + 2.10^{-5} z)Ra[MJm^{-2}day^{-1}] \quad (7.17)$$

where:

z [m] is the station elevation above sea level.

7.5.2.2.3 Actual evaporation and actual transpiration

The Evapotranspiration flow is divided into *potential transpiration* and *potential transpiration* by using the following equations (*VADOSE W, Krahn, 2004*):

$$PE = ETP * \{1 - (-0{,}21 + 0{,}7\sqrt{LAI})\} \quad (7.18)$$

$$PT = ETP * (-0{,}21 + 0{,}7\sqrt{LAI}) \quad (7.19)$$

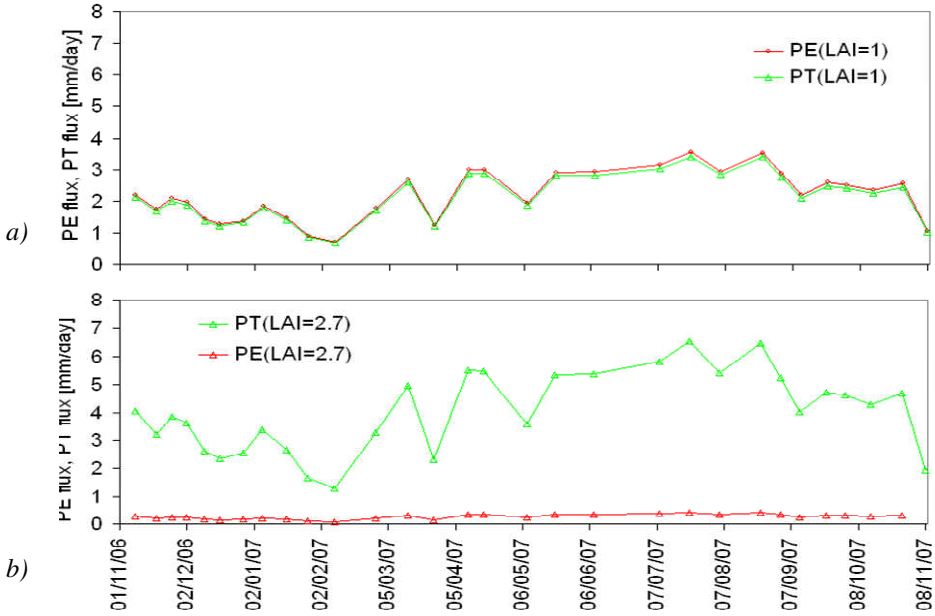

Fig.7.11: PE and PT flows calculated for LAI=1 a), for LAI=2.7 b)

In order to take into account the different distribution of the vegetation on the slope, two values of PE and PT are calculated, one with LAI = 2,7 (the maximum) and an other with LAI = 1 (the minimum). The PE and PT for LAI = 2,7 is applied on the top, the PE and PT for LAI =1 is applied on the bottom, then the program can apply the PE and PT variable linearly between the calculated values on the intermediate part of the slope (*fig.7. 11*).

The decrease of the water available in the subsoil, specially in the summer period, leads to a smaller evaporation flow. In order to consider the real water availability on the ground surface, the *potential evaporation* is multiplied for the decay function (*fig.7.12*) and the resulting flow is called *actual evaporation*:

$$AE = \alpha(s) * PE[mm / day] \tag{7.20}$$

where $\alpha(s)$ is the Decay Function.

The decay function depends on suction and it is equal to 1 for s > s_{air} (s_1) and then decreases linearly to zero in correspondence of the residual suction value s_{res} (s_2). Therefore in the summer the *potential evaporation* reaches the peak value because of the warm temperature but it is decreased by the decay function that accounts for the high values of suction, taking into account the poor availability of water in the subsoil.

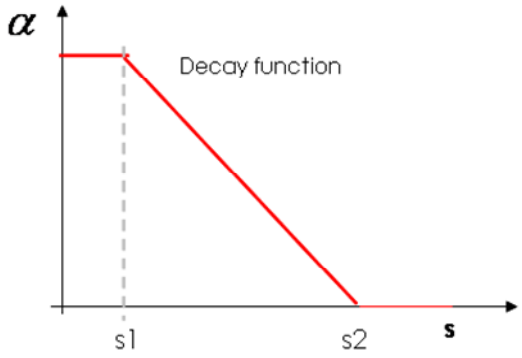

Fig.7.12: The decay function: it transforms the potential evaporation in the actual evaporation

The software allows to apply the transpiration flow, into the soil along the thickness of the cover occupied by the roots, r_{max} (*fig. 7.13*); in these analyses r_{max} =1 m is assumed. In this way it is possible to account for the action of the trees, that transfers humidity from the subsoil to atmosphere.

The transpiration flow is distributed linearly in the soil, the maximum value being at the ground surface and the minimum is at 1 m of depth, r_{max}, as a consequence of the distribution of the roots in the subsoil.

From the integration of the flow q (7.21) along the depth, r_{max}, we obtain the *actual transpiration,* AT:

$$q = 2PT * \alpha_T(s) * (1 - \frac{r}{r_{max}}) / r_{max} \qquad (7.21)$$

where $\alpha(s)_T$ (*fig.3.14*) is a function of suction which accounts for the availability of water. It transforms potential transpiration in actual transpiration. The suction value, s_{1t}, is the air entry value; the suction value, s_{2t} , is the tensile pressure when the plant start to die, here s_{2t} = 20 kPa is assumed; the suction value, s_{3t} , is the residual suction value.

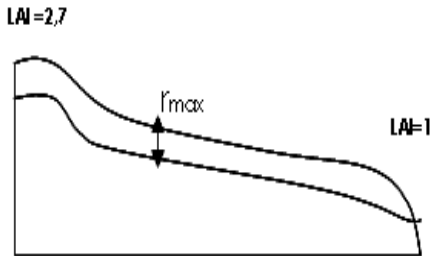

Fig.7.13: The root depth

The tables with PE and PT values applied at the ground surface, during the whole hydrologic year, are attached at the appendix II.

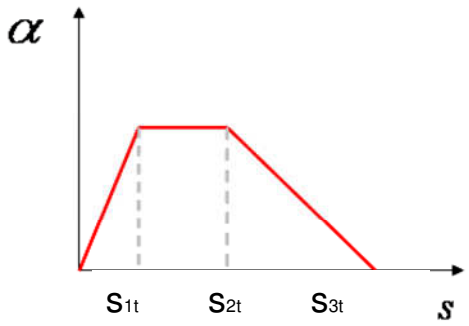

Fig.7.14: The decay function: it transforms the potential transpiration to the actual transpiration

7.6 Simulation of one hydrological year

The analyses simulating one hydrological year, from 9th November 2006 to 9th November 2007, is aimed to interpret the regime of water flow in the subsoil.
The climate conditions, in terms of infiltration and evapotranspiration, registered on site are applied on the ground surface. The numerical suction profile obtained along one vertical section of the mesh is compared with the experimental measurements collected in the field along the same vertical section (borehole 3B) in order to validate the hydraulic model adopted.

7.6.1 Plots of the results: suction profile

Results in terms of suction profile and input of analyses (*figs. from 7.15 to 7.25*) are reported. The points represent measurements collected on site from the tensiometers installed in the borehole 3B; these instruments are installed in the soil 1, at the depth of 0.25m, in the soil 2 at the depth 0.45 m and in the soil 4 at the depth of 2.20 m and 2.40 m (*tab.7.1*). The continuous curves represent the suction profile resulted from the analyses and are referred to the same day of the measurements available. Close to each suction profile, the stratigraphic column of the vertical section 3B is reported. Under the results the daily rain (mm/day) is reported too, in order to show the relation between suction and rainfall.

Tab.7.1: The depth of installation of tensiometers

Vertical 3B	*Depth (m)*
Soil 1	0.25
Soil 2	0.45
Soil 4	2.20
Soil 4	2.40

7.6.1.1 Results of analyses over the *winter*: *9th November 2006 -27th February 2007*

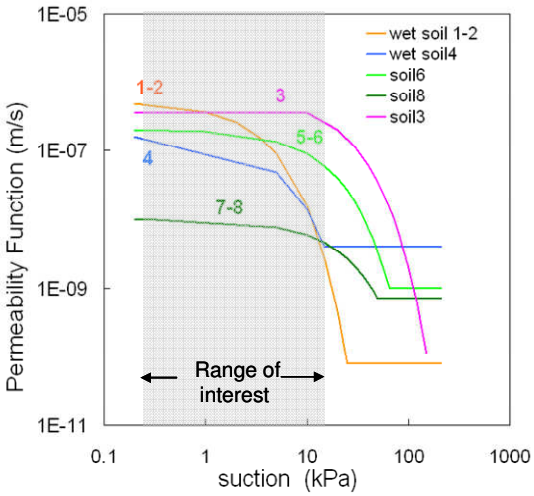

Fig.7.15:Permeability curves used in the analyses for winter, spring and autumn period

During the winter season the retention curves and the permeability curves of the soils 1, 2 and 4 are those obtained for the wetting conditions (fig. 7.15).

The suction profile of 8th November is the initial conditions (Fig.7.*16a*). It is possible to observe that both the numerical profile and the measurements in the soil 1-2 decrease in the period from 18th November to 25th November because of three rainy days (*Fig. 7.16b,c*). In fact in this period the rainiest day of the year occurs, 22nd November with 68 mm of rain. Between 25th November and 2nd December there is no rainfall, hence both the predicted and measured suction profile in the soil 1-2 increase, while suction in the soil 4 remains constant (*fig.7.16 b-c*).

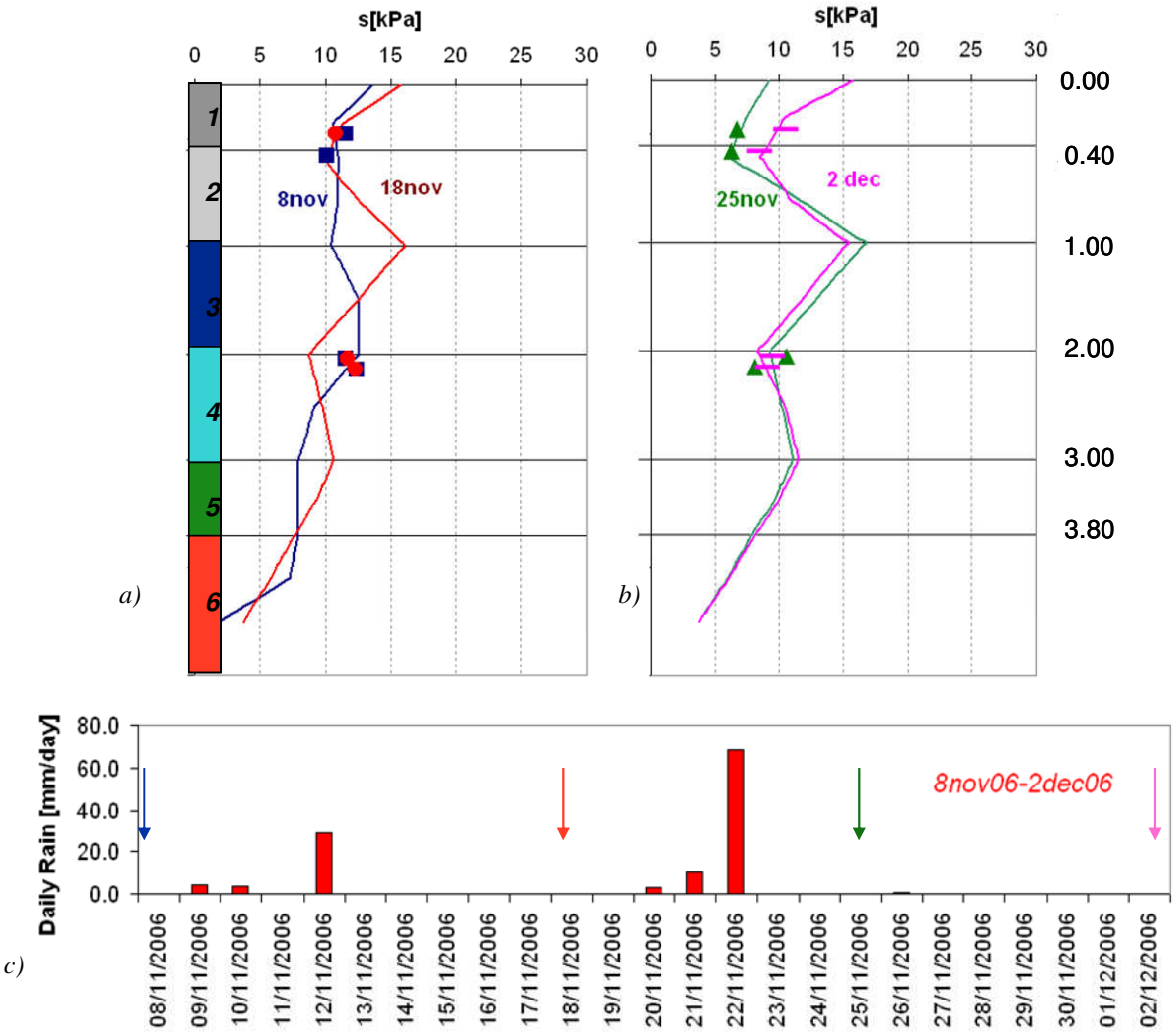

Fig.4.16: a), b) Comparison between numerical profile and measurements at different dates ; c) Daily rain registered in site

In December the predicted and measured profile return back only in the superficial soils because of some rainy days (*fig.7.17 a-b*). In fact only on the 9th December 60 mm fall. There is absence of rain from the 7th and 17th January, so the measurements and the numerical profile go forward in the superficial soils. As rainfall is registered on the 23rd-24th-25th January the profile and the measurements return back to low suctions (*fig.7.18c*).
In February suction reaches 2-3 kPa on the surface and the 8-10 kPa in the soil 4, the numerical profile follows this trend.
Finally by using the wet permeability and wet retention curves in winter time, the comparison between the measurements and the numerical suction profile is good.

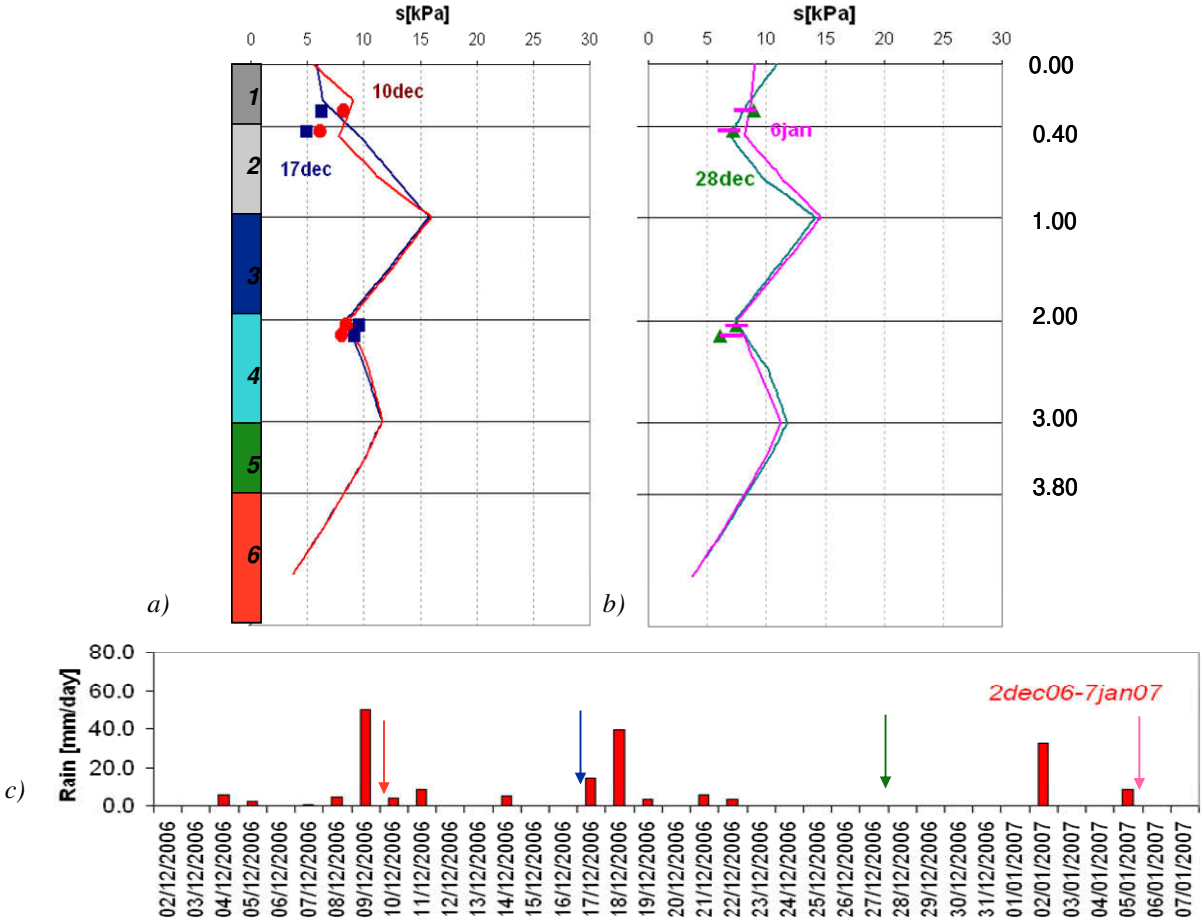

Fig.7.17: a), b) Comparison between numerical profile and measurements at different dates ; c) Daily rain registered in site

In this period suction measurements in the soil 1-2 follow climatic conditions, while in the soil 4, they remain reasonably constant at around 10 kPa, the numerical suction profile show the same behaviour. Regarding the suction at the bottom of the cover, when the analyses were conducted there were no measurements in the deepest strata; however numerical results suggest an increase in pore pressure up to the value s=0 assigned at the contact with the

limestone.

The change in suction gradient with depth at the contact between the soil 2 and 3 is probably due to the different permeability between the layers. Unfortunately it is no easy to measure suction in the pumices so the real value of pore pressure in these soils is not available.

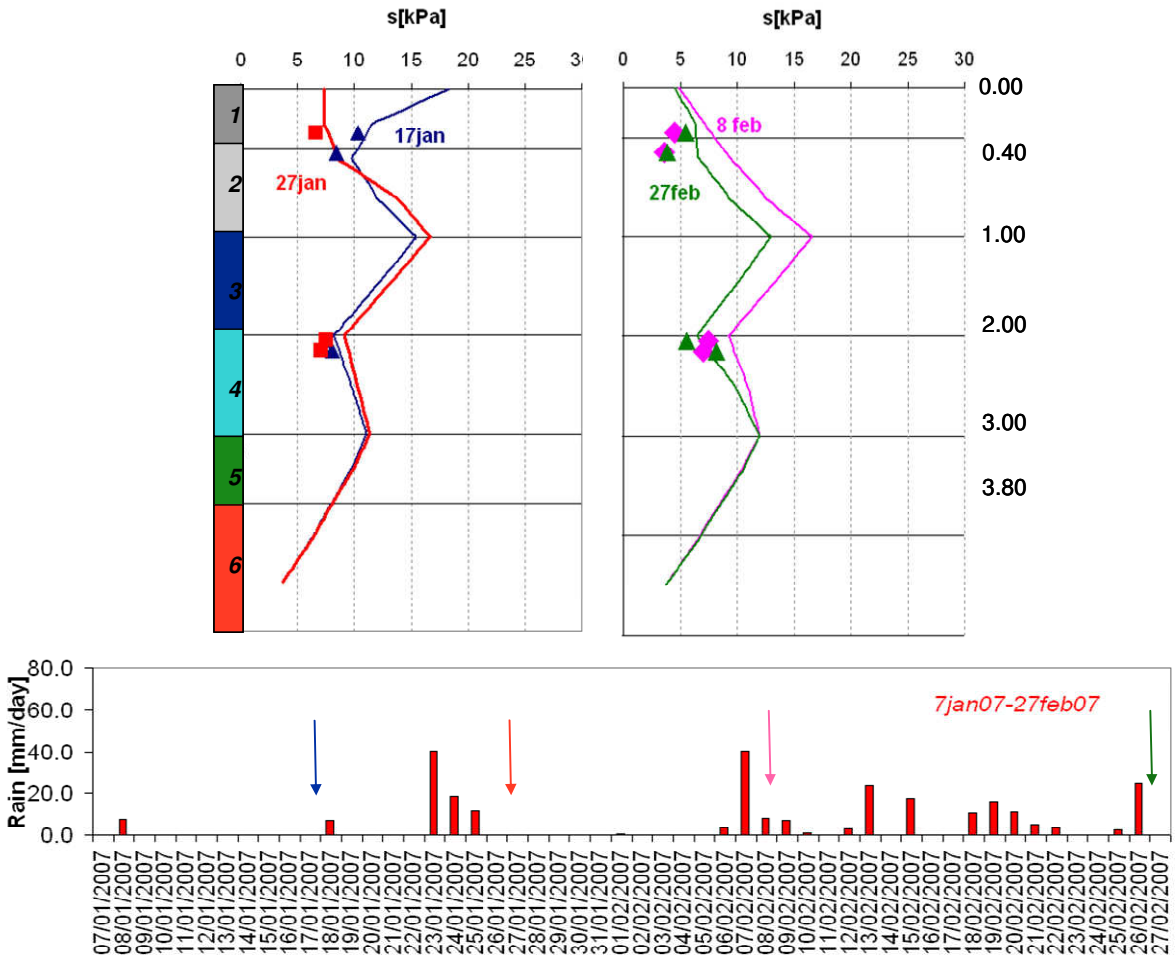

Fig.7.18: a), b) Comparison between numerical profile and measurements at different dates; c) Daily rain registered in site

7.6.1.2 Results of analyses in *Spring*: *1 March 2007 – 31 May 2007*

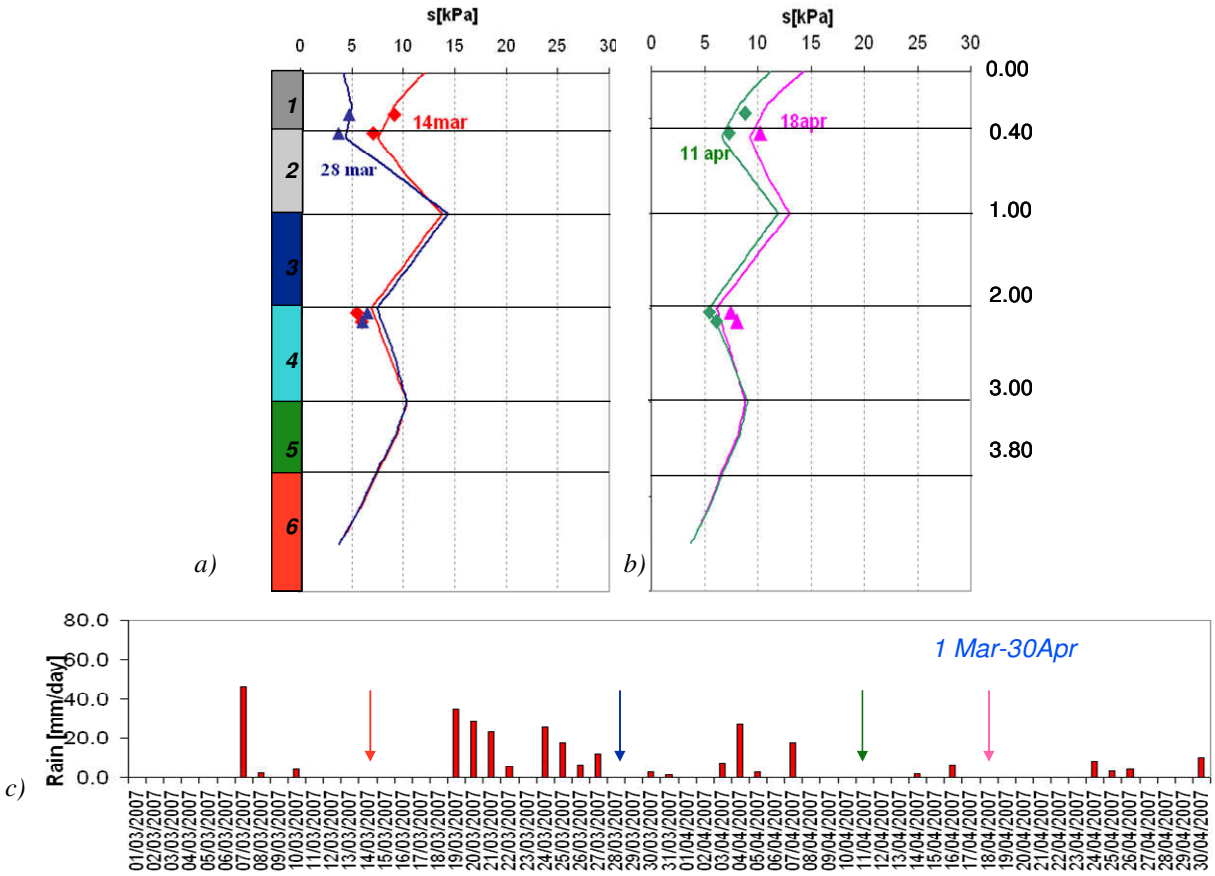

Fig.7.19: a), b) Comparison between numerical profile and measurements at different dates; c) Daily rain registered in site

In further simulation of spring climatic conditions, the same retention curves and permeability curves, that correspond to wetting conditions, were assigned to soil layers in the slope (*fig.7.15*). Suction measurements does not change in the soil 4 during the months of March and April, even if rain is significant (*fig.7.19a*). In the soil 1-2 from the 14th March suction decreases because of intense and persistent rain until the end of March, then in the month of April suction increases and reaches 10-15 kPa (*fig.7.19 b*). From the end of April to 8th May measurements and prediction of the suction profile does not change. Regarding to the suction at the bottom and the pumices (soil 3) the same previous consideration are taken.

When the dry period starts if wet retention curves and wet permeability curves are used in the soil 1-2 and 4, the suction profile does not match more the measurements. In the figure 7.20a the numerical suction profile of 21st May obtained by the wet characterization, is reported. The comparison between measurements and numerical results in the superficial soils is not good. In the figure 7.20b) the numerical profile obtained by the dry characterization is reported, improving the comparison with measured data.

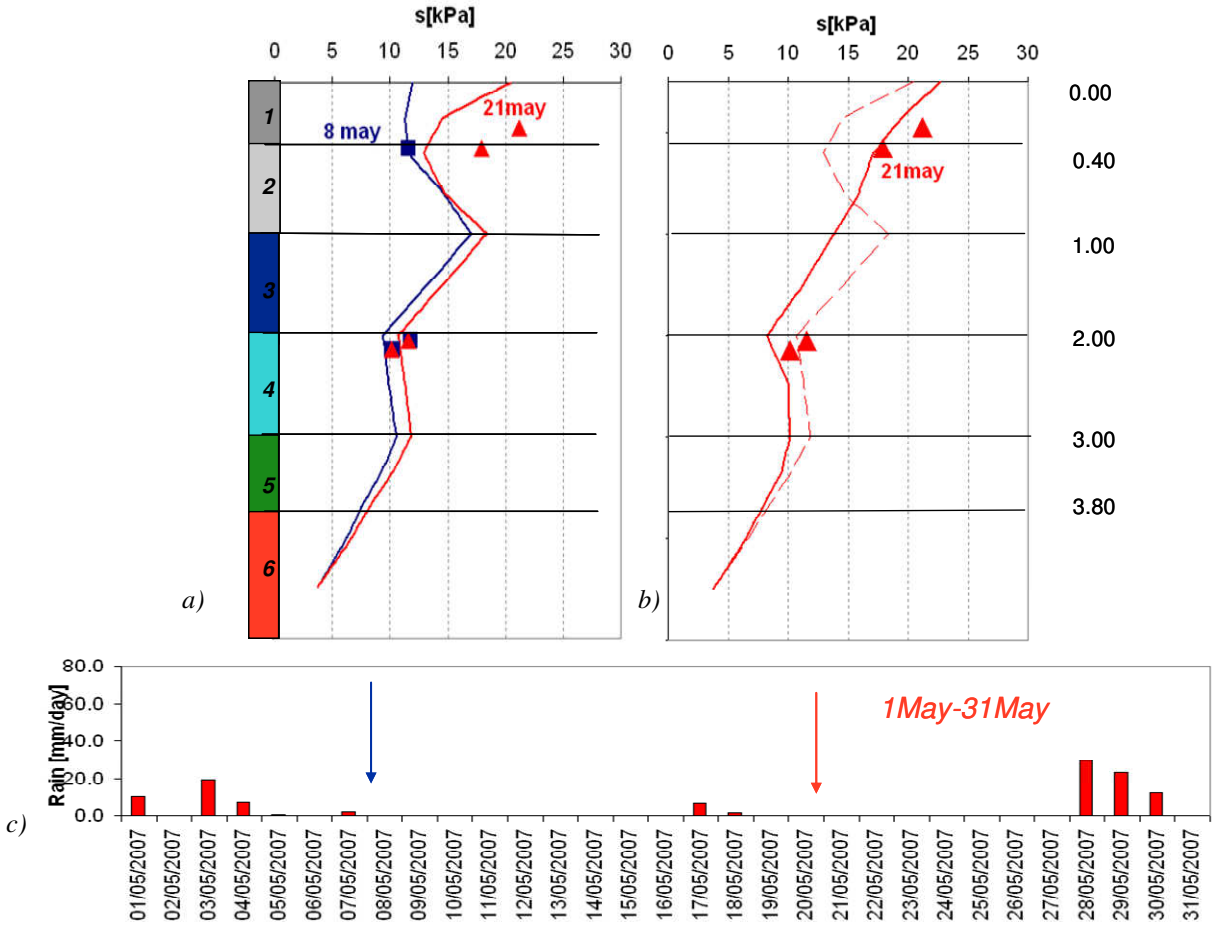

Fig.7.20: a), b) Comparison between numerical profile and measurements at different dates; c) Daily rain registered in site

Hereafter the dry retention curves and the dry permeability curves will be used for the superficial soils 1-2 and the soil 4.

7.6.1.3 Results of analyses in *Summer*: *1 June 2007 – 31 August 2007*

During the Summer season the drying part of retention curves and permeability curves for the soils 1-2 and 4 are used (*fig.7.21*). There is no rain for tree months, June, July and August (*fig.7.24 c*) so the suction is expected to be very high at least on the surface. Unfortunately the desaturation of the tensiometers does not allow measurements. In order to have an estimate of the order of magnitude of the suction in the superficial soils, the suction value is read on the experimental drying curve of soil 1-2 in correspondence of minimum volumetric water content measured in site, even if these measurements refer to a following period: 30th April 2008 -25th October 2008 (*fig.7.22*).

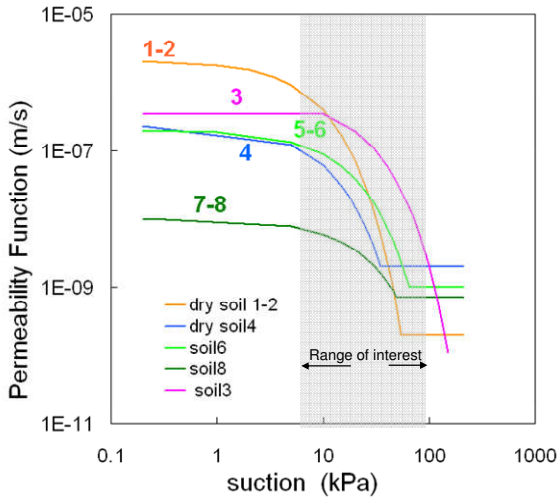

Fig.7.21: Permeability curves used in the analyses f or the summer period

In the soils 1-2 the average water content, of all measures, reaches the minimum value of 0.18 - 0.22 in summer and being the mean porosity around 0.69-0.71 the corresponded degree of

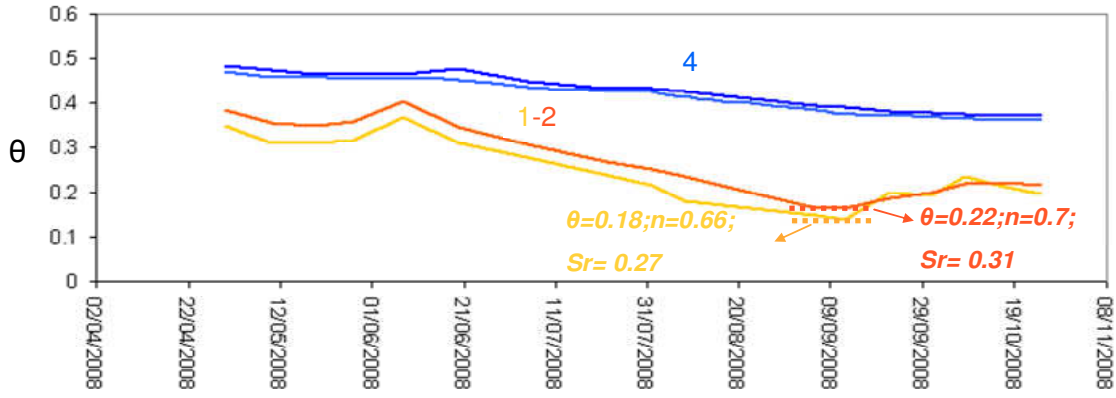

Fig.7.22:Avarage volumetric water content of all measurements in site

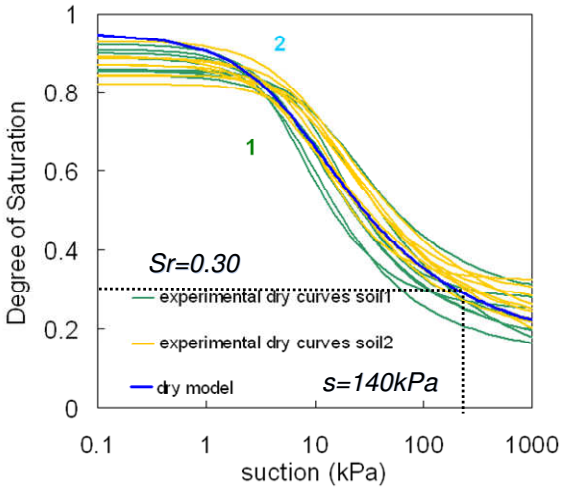

Fig.7.23: Experimental drying retention curve and the curve used in the analyses (Papa, 2007), estimation of the suction acting in site as a function of the water content

saturation is 0.27-0.31. The suction obtained from the drying curve in correspondence of degree of saturation is close to 150 kPa (*fig.7.23*). The numerical profile of suction reaches 140-150kPa on the surface and a big gradient of 100 kPa/m is established just on the first meter of soil where the transpiration flow is prevalent. The match between the measurements and the numerical profile continues to be good in the soil 4.

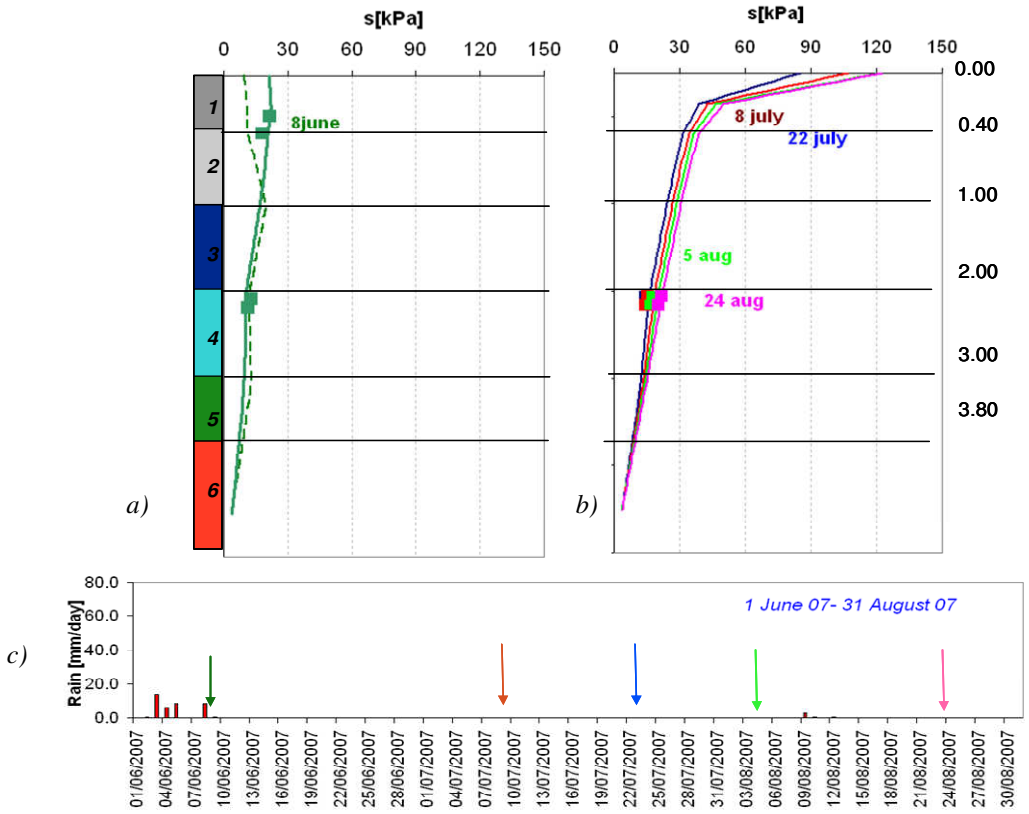

Fig.7.24: a), b) Comparison between numerical profile and measurements at different dates; c) Daily rain registered in site

7.6.1.4 Results of analyses in *autumn* period: *1 September 2007 – 31 October 2007*

In Autumn the dry characterization is used until middle of October (*fig.7.21*), then the wet characterization is used again (*fig.7.15*). In September the suction on the surface is still quite high because of absence of rain, then in October rain starts again and the measurements and predictions of suction decrease at least on the surface. In the soil 4 suction continues to increase in Autumn because the deeper soils follow with delay the climatic conditions. The numerical suction profile agrees with the measurements in autumn.

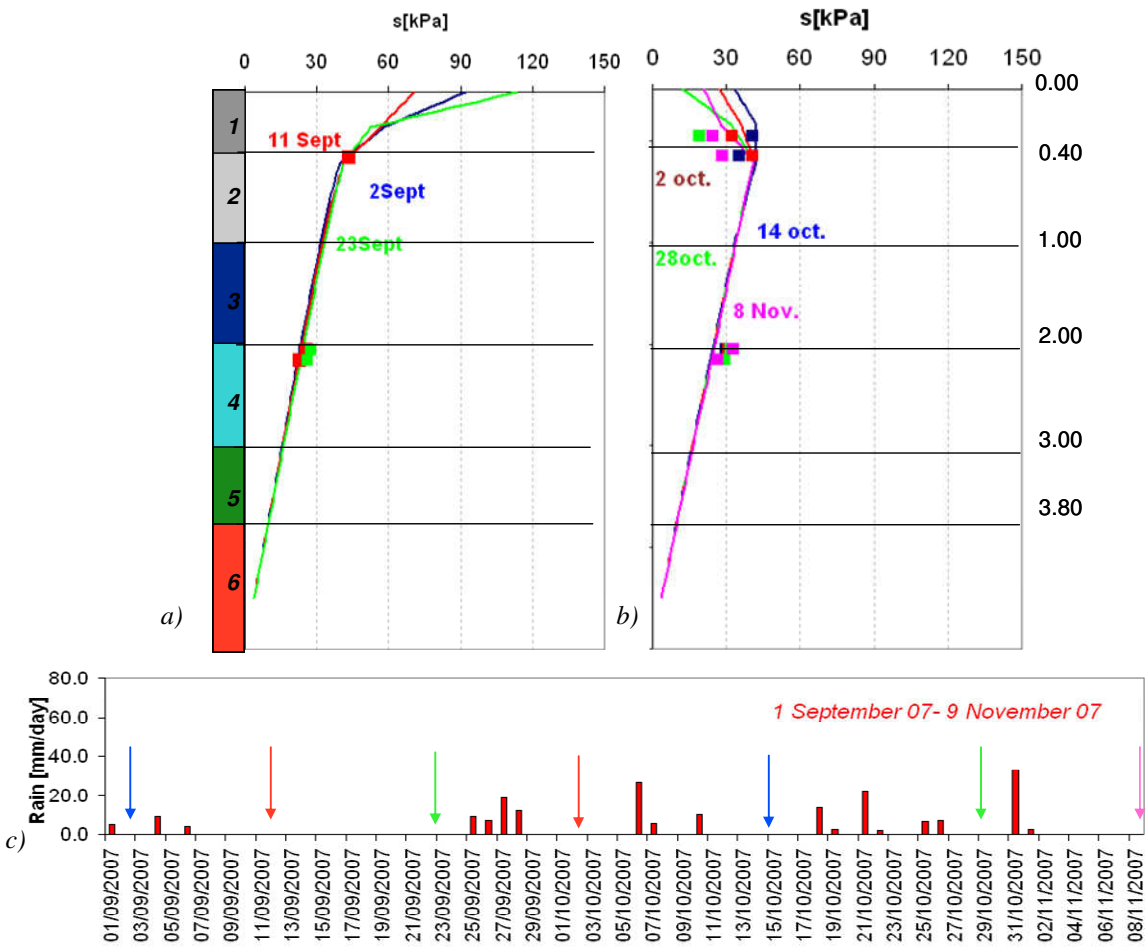

Fig.7.25: a), b) Comparison between numerical profile and measurements at different dates; c) Daily rain registered in site

7.7 Results

7.7.1 Suction ~Time

In *figure 7.26* the suction-time diagrams are plotted for the soil 1, 2, 4. The numerical results refer to the same vertical section of the borehole 3b and to the depth where the measurements are available, at depth of 0.25 m in the soil1 (*fig.7.26a*), of 0.45 m in the soil 2 (*fig.7.26b*), of 2.20 m and 2.30 m in the soil 4 (*fig.7.26c-d*).
In general for all the soils, there is an excellent agreement between numerical predictions and measurements. So at least the hydraulic characterization of the superficial soils (soil 1-2) and intermediate soils (soil 4) seems to be correct. About the deeper soils (5-6-7-8), suction measurements are not available over the hydrological year simulated by these analyses and the comparison with numerical results is not possible.
In particular in the soils 1-2, measurements in the dry period (July-August) are absent because of the desaturation of tensiometers, so there is no way to verify the hydraulic characterization in the drying period and to evaluate if the calculated evapotranspiration flows are right. In the soil 4, the match is good throughout the year examined.

In *figure 7.27* the suction-time diagram for the soils 1 to 6 and the pluviogram in the period considered by the analyses is reported. According to the suction measurements diagram (Chapter 5), the suction in the superficial soils 1-2 are influenced by single rainy event. It is clear that suction decreases in correspondence of the rainy days (for example 22nd November 2006, 9th December 2006, 23rd January2007, 7th and 19th March 2007, 4th April 2007, 28th May 2007, 31st October 2007 and 14th November 2007). The main value of suction in the soil 1-2 at 25 cm and 45 cm from the surface is around 10 kPa during the wet season, the highest values are 70-80 kPa during the dry period. In the deeper soils, 4 and 6, the seasonal suction variations play a major rule and the amplitude of the variations is smaller then that in the superficial soils. The mean value of suction in the soil 4 at 2.20 m and 2.30 m from the surface is around 10 kPa during the wet season, the highest is 30-40kPa during the dry period. About the soil 6, the mean value of suction is 10-15 kPa over the year. Previous considerations agree with the experimental evidence too (Chapter 5).

In *the figure 7.29a, b* the same plot of *figure 7.27a* is reported with the suction values averaged over the vertical sections 1, 2, 3, 4, 5, shown in *fig. 7.28*, in order to analyse the influence of the geometry and of the stratigraphy on the suction results (*fig. 7.28*). In the superficial soils there early is no distinction between average suction and that along section 3 only *(fig.7.29a)* during the wet season; so the suction in the soil 1 and 2 assumes the same value over all the mesh even if the stratigraphy changes. In fact also observing the figure 7.30 a, b where the suction along the single verticals 2, 3, 4, 5 are represented, the curves overlap perfectly in the wet period. In the dry period, the evapotranspiration phenomena play a major

rule and the upper boundary along the domain analyzed is modelled in different ways. In fact on the top the transpiration flow is prevalent respect than at the bottom. Hence it is reasonable to expect different suction distribution in the superficial soils on the surface along the domain in the dry period.

In the intermediate soil the suction values averaged over the vertical sections 1, 2, 3, 4, 5 are smaller than these of the vertical 3 over whole the year. Probably this is because the mean suction values in the soil 4 start to suffer the influence of the different stratigraphy of the verticals considered. In fact the soil 6-7-8 are not present in correspondence of all the verticals considered. In the figure 7.30c, d it is clear the influence of stratigraphy on the results: where the soils 7, 8 are present (sections 2, 4) the pore pressure becomes even compressive in the winter while where the soils 6-8 are missing (sections 5), the curves overlaps with the curve relative to the section 3.

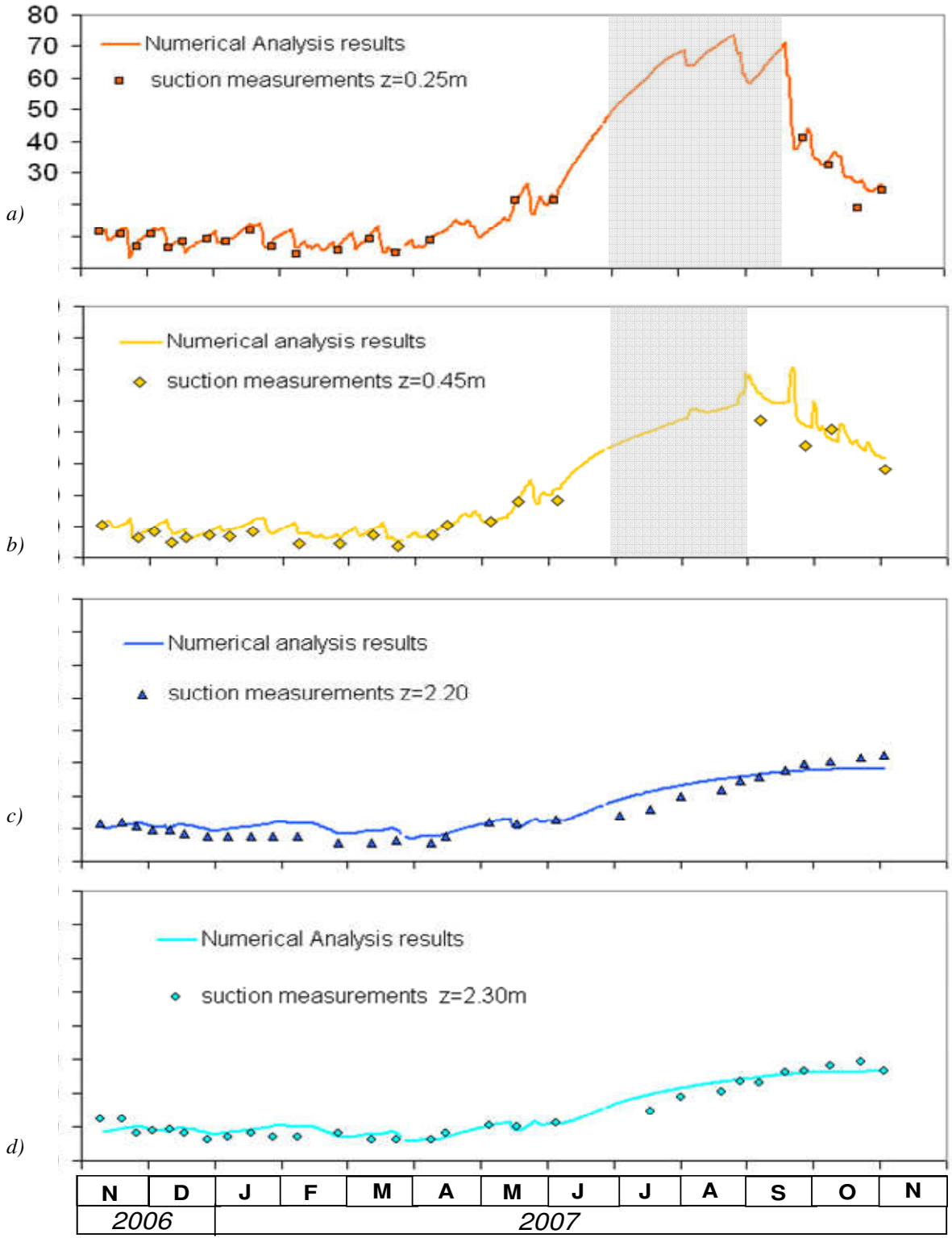

Fig.7.26: Comparison between measurements along the vertical section 3B and numerical results along the same vertical section at the depth of 0.25 m a), 0.45 m b), 2.20 m c), 2.30 m d)

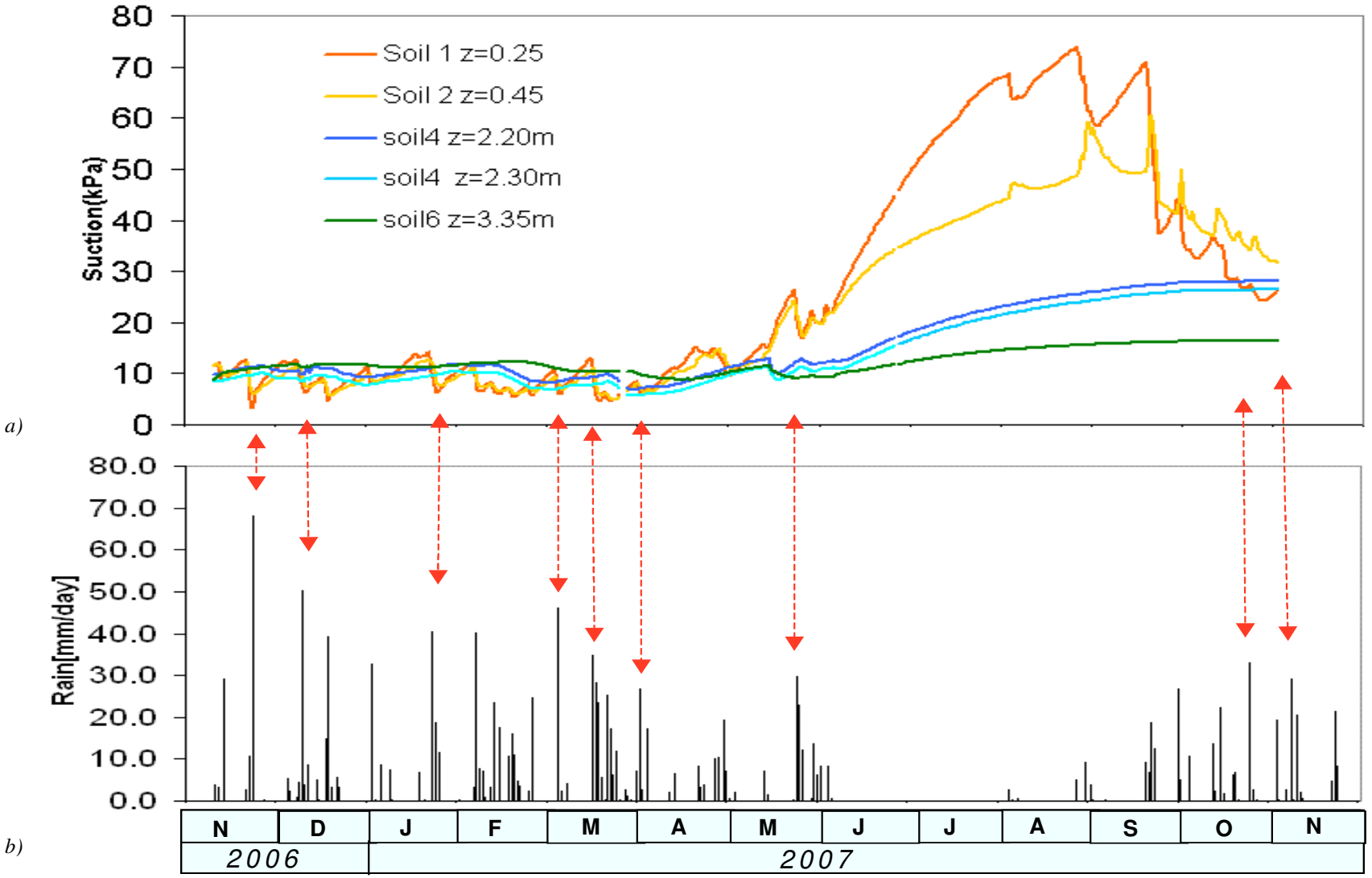

Fig.7.27: a) Calculated suction over the year (November 2006- November 2007), b) daily rain registered in site

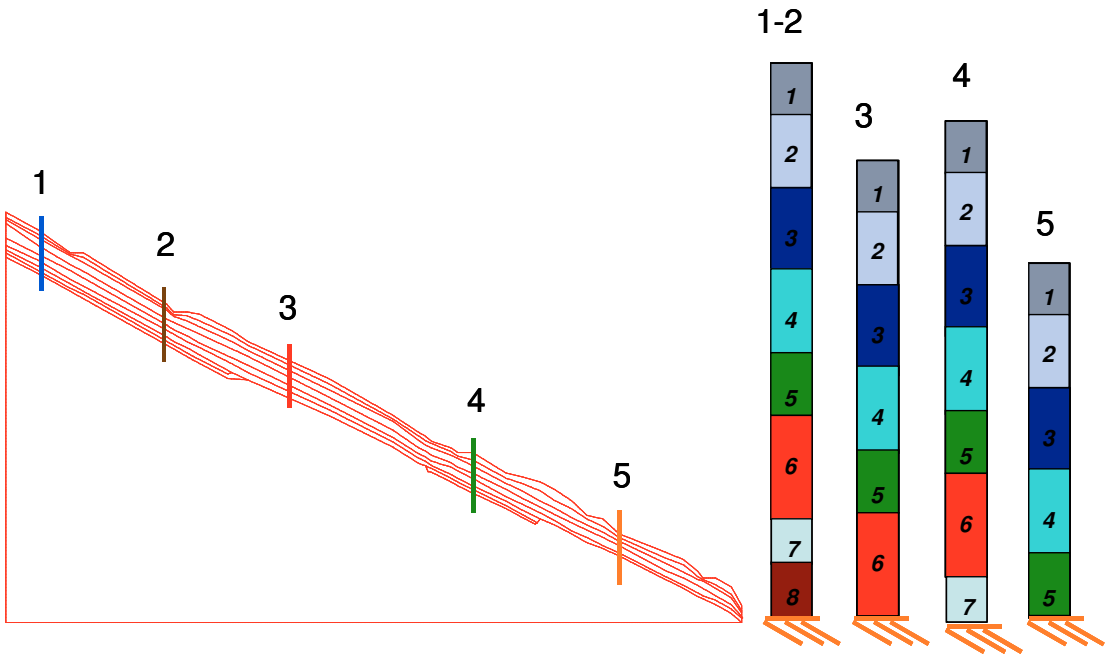

Fig.7.28: Verticals considered to calculate the average values of suctions over whole the mesh

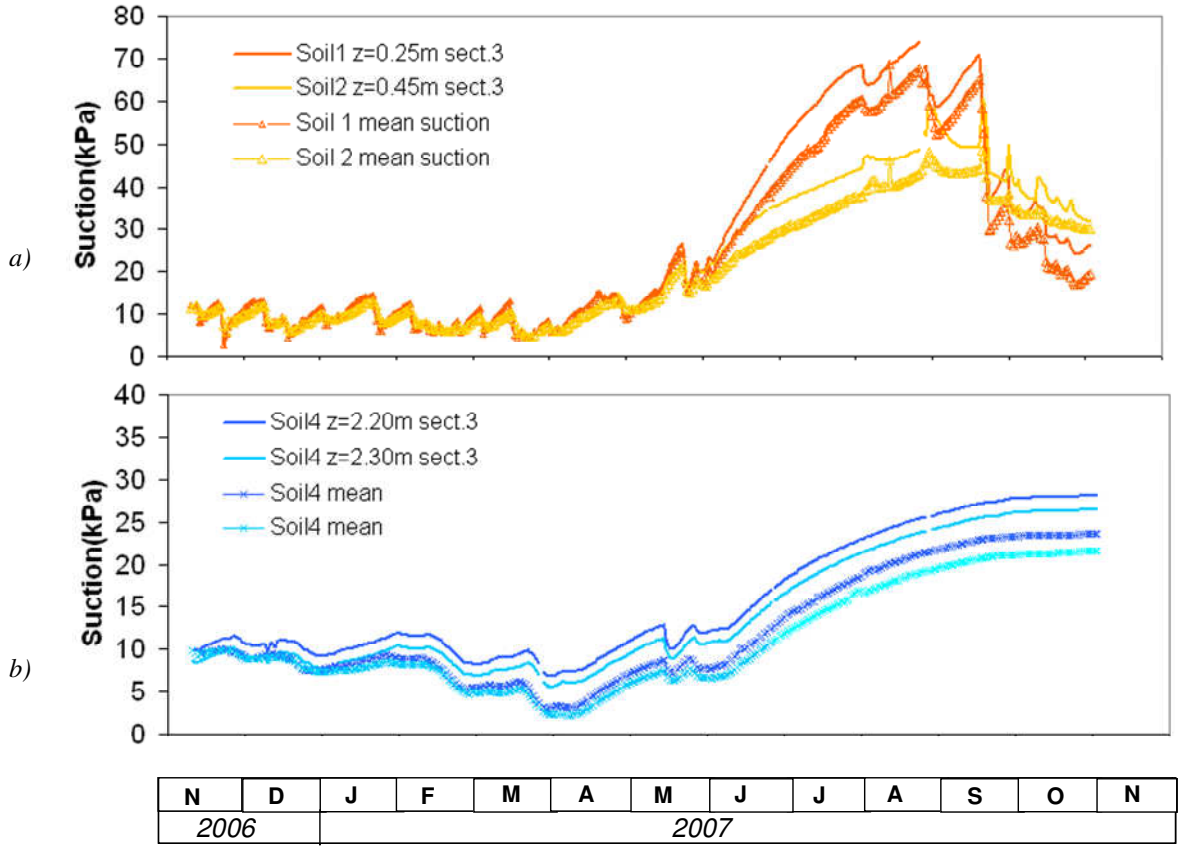

Fig.7.29: Comparison between suction values calculated in the vertical 3 and the values averaged over the 1,2, 4,5 vertical sections in the soil 1-2 a), in the soil 4 b)

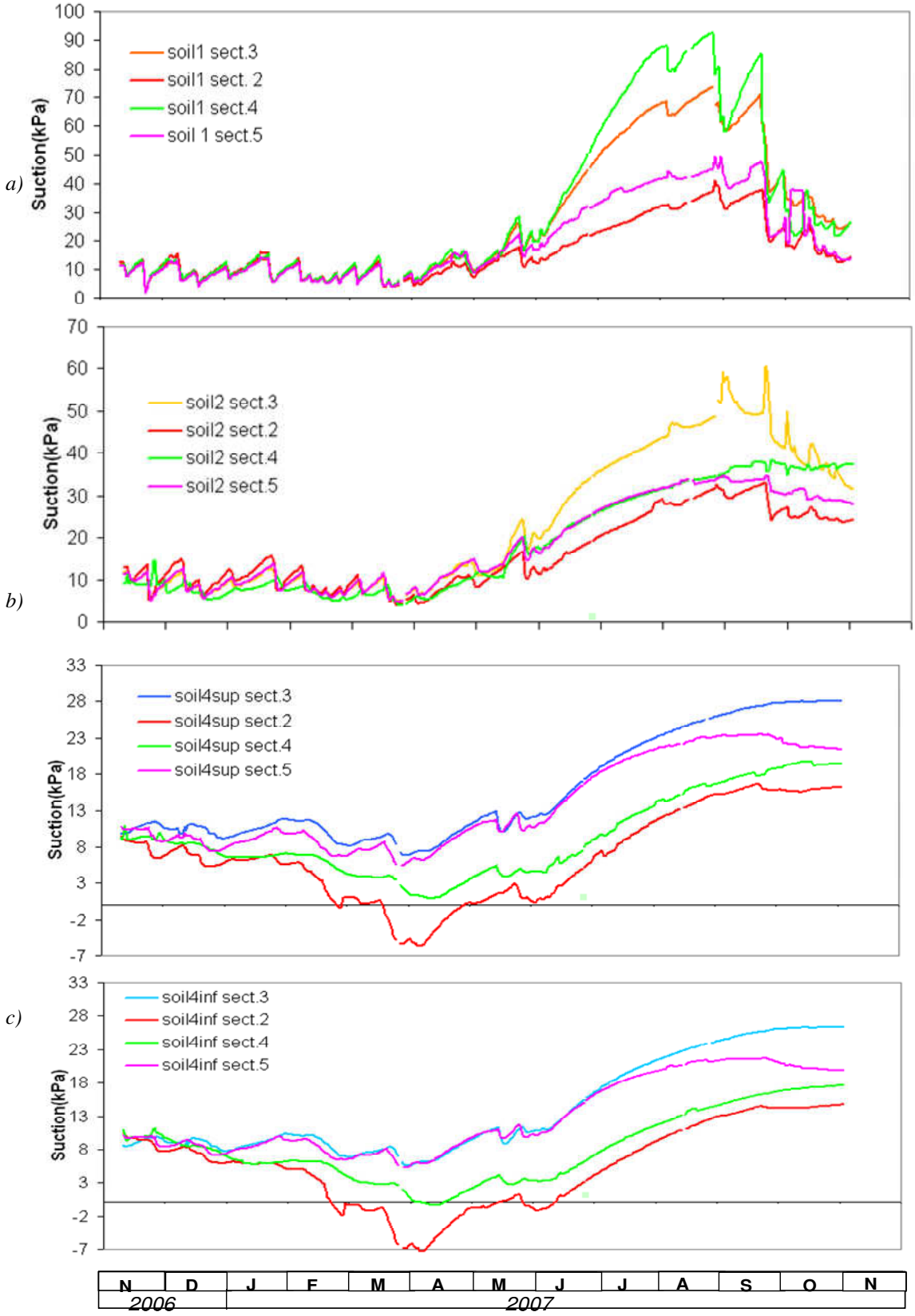

Fig.7.30: Calculated suction vs. time along vertical sections 2,3,4,5 in soils 1 a), soil 2 b), soil 4sup c), soil 4 inf d)

Concluding Remarks

To obtain a good match between measurements and numerical results it's important to use a *right hydraulic characterization* of the soils involved. In particular it could be argued:

- During the **wet period** (November-May) *a right hydraulic characterization in wetting conditions* is necessary in order to model the real water regime in subsoil; the superficial and intermediate soils (1-2 and 4) are characterized by the hysteresis.
  The suction in soils 1-2 and 4 seems to be not influenced by the hydraulic characterization of the deeper soil and by the boundary conditions at bottom, in fact a good match with measurements is guaranteed by only their right characterization.
  The most important flow is the rainfall, it heavily influences the hydraulic response of the soils. The evapotranspiration flow takes a marginal rule.
  The major part of numerical problems are concentrated in the wet period, as the rain has obviously not a constant intensity and it is necessary to change the number of increments for each day as a function of rain intensity.

- During the **dry period** (June-September) *a right evapotranspiration flow* takes a major rule to obtain a good match between the measurements and the numerical suction profile. In this period there is not a important flow in-going but only a more or less *constant and continuous* flow out-going from the subsoil. A correct estimate of the ETP influences the response of the superficial and intermediate soils in terms of suction more than an accurate hydraulic characterization.
  The transpiration dominates the hydraulic behaviour of these soils, because it is a flow distributed in the domain while the evaporation flow is concentrated on the surface and determines a high gradient of suction in the first 10 cm of the soil.
  The value of suction in this dry period and the small value of water content in the soils causes a higher shear strength than in the wet period, so it is enough to investigate the winter and the spring conditions to analyse the slope stability.
  Any way a good model of the summer too allows to generate a right hydraulic response in the autumn and to understand the behaviour of the soils over the whole year investigated.

The tables showing the boundary conditions applied to simulate the hydrological year, 8th November 2006-8th November 2007, are attached in the Appendix II. The tables contain:

- the number of the time increments in which one day is divided,
- the progressive increments corresponded to each day,
- the daily rain registered by the Monteforte Irpino Rain gauge,
- the daily evaporation and transpiration flows calculated by the Penmann equation either for LAI=1 and LAI=2.7,
- the hydraulic characterization used (wetting or drying).

Chapter 8

Slope stability analyses

8.1 Synopsis

This chapter deals with the *Slope Stability Analyses* of the monitored slope of Monteforte Irpino. The failure mechanism is investigated by carrying out parametric analyses, by means of the FEM code ICFEP, investigating the role of the parameters that influence slope stability in unsaturated soils. Different *rain boundary conditions*, *mechanical and hydraulic properties*, and *initial conditions* are studied in order to analyze how these influences the triggering starting time and the type of failure, the depth of the sliding surface, the distribution of pore water pressure and the profile of permeability at failure.

Results suggest that the variation of the rain intensity applied at the top boundary and the hydraulic characterization of the pumices (soil 3), play a major role respect to the other phenomena leading to a very broad range of triggering mechanisms.

8.2 Limit Equilibrium analysis of an infinite slope

The *initial condition* used for these analyses has been chosen as the one acting in the period characterized by the smaller suction and in theory by the smaller safety factor. In order to have an idea about the period more critical for slope stability, calculations on the evolution of the safety factor versus the time are performed under very simple hypothesis. The Testing site is modelled like infinite slope, using the Bishop's effective stress approach to define the stress variables in unsaturated soils.

The inclination of the infinite slope is 28° and the thickness assigned to each layer is the mean value too (fig. 8.1). The safety factor is calculated at the mean depth of the tensiometers installed (fig. 8.1) by using the following relation:

$$Fs = \frac{\tau_{\lim}}{\tau_{es}} = \frac{c' + [(\sigma - u_a) + S_r (u_a - u_w)] \tan \varphi_{crit}'}{\tau_{es}} \qquad (8.1)$$

where:

- τ_{es}, σ are respectively shear and normal total stresses on the sliding surface calculated in the hypothesis of infinite slope:

$$\sigma = \gamma \cdot z \cdot \cos^2 \alpha$$
$$\tau = \gamma \cdot z \cdot \cos \alpha \cdot \sin \alpha \qquad (8.2)$$

α is the slope,

$\gamma = \gamma_d (1 + w)$ γ_d is the dry unit weight, w is water content obtained by the soil retention Curve (Papa, 2007) for each suction measured,

z is the depth at which the tensiometers cell is installed (*fig.8.1*),

- $(u_a - u_w)$ is the suction measured in site,

- S_r is the degree of saturation obtained by the soil retention curve (Papa, 2007) for each suction measured,

- φ_{res}, c are the critical shear angle and the cohesion of the soils, obtained by elaboration of the triaxial compressive tests on saturated samples (Papa,2007) (*Fig.8.2*),

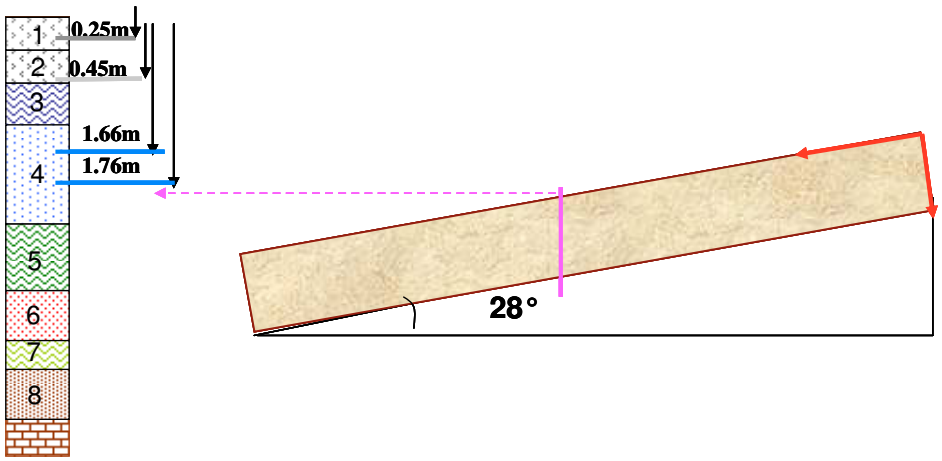

Fig.8.1: The analysed slope: a) stratigraphy of the soil cover, b) geometry of the slope

In the figure 8.3 the factor of safety calculated over the hydrologic year (9th November 2006 - 9th November 2007) is plotted. The trend of FS against the time has the equal shape of the diagram of suction measurements *(fig.8.3a)*; according to this representation, the winter–spring seasons from January to May are characterized by smaller values of FS[10]. Therefore it is reasonable to investigate the failure starting from the conditions established in these seasons. So the initial conditions chosen are those acting on 31st January 2006 and on the 10th May 2007 calculated by the numerical analyses carried out to validate the model (*Chapter 4*).

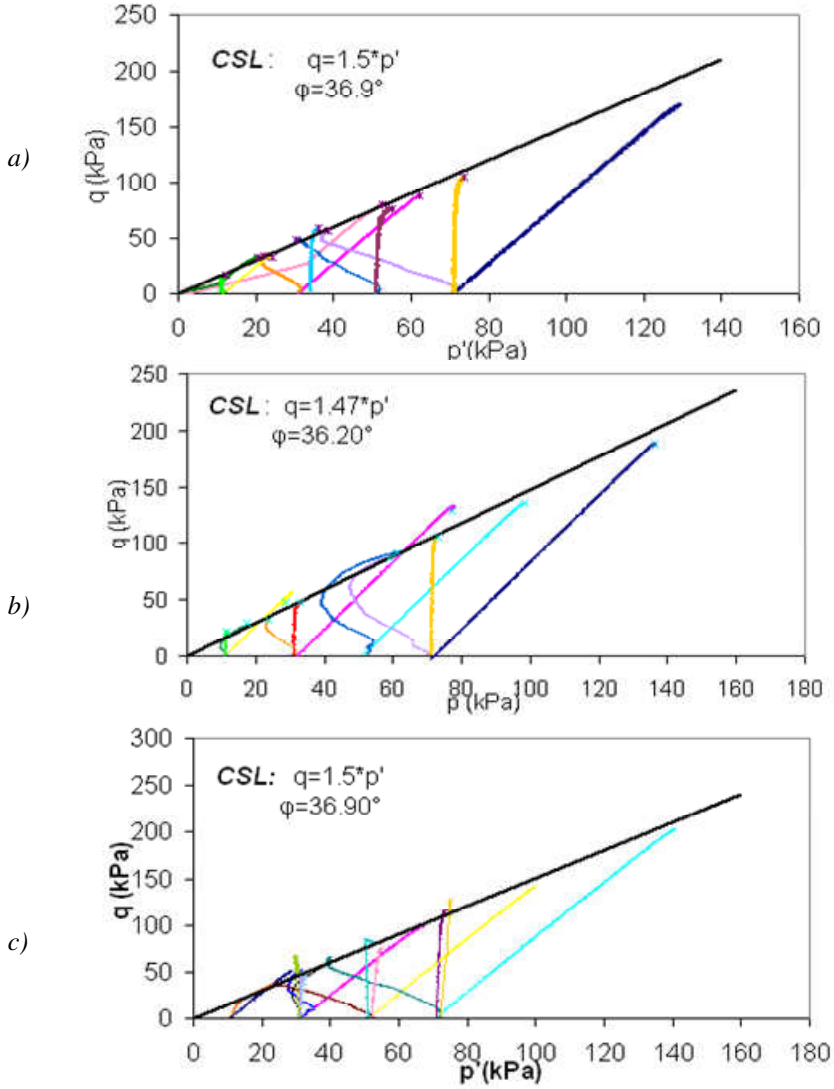

Fig.8.2: Stress paths and critical failure envelopes obtained by triaxial compressive tests on saturated samples (Papa, 2007) of soil1 a), soil 2 b), soil 4 c)

[10]Stability analysis on infinite slope allows only to investigate the influence of suction, hence of water content, on the safety coefficient without undertaking the rule of stratigraphic irregularity; so it is a strong simplification. According to the diagram

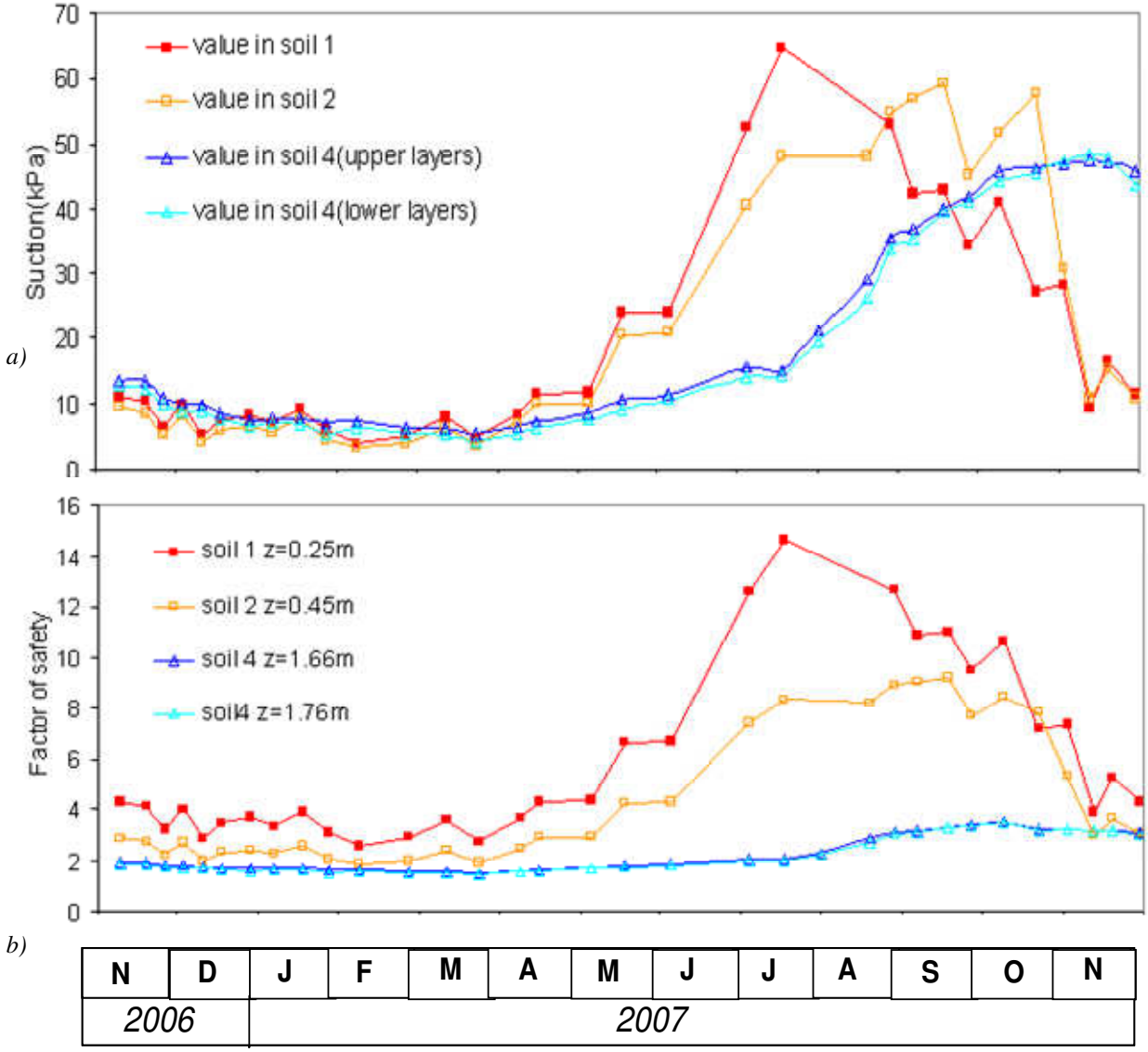

Fig.8.3: Trend of the Factor of Safety during the hydrologic year investigated in the Chapter 2

Moreover, by observing fig. 8.3b, the potential sliding surface always should lie in the intermediate layer (soil 4). While, in the following, the results of parametric analyses suggest that the depth of sliding surface is strongly related to the pluviogram applied on the upper boundary.

---

of the figure 8.3b, the most low values of safety coefficient are close to 2 during winter-spring seasons, so the slope is stable during whole the year investigated.

8.3 Numerical parametric analyses

The *parametric analyses* carried out are divided in four groups; each one takes into account the influence of a different parameter:

(a) rain intensity,
(b) mechanical characterization,
(c) hydraulic characterization,
(d) initial conditions.

Regarding the *Upper Boundary Conditions*, in each analysis the evapotranspiration flow (ETP) is neglected, this is reasonable because the rain intensity in the wet season is very large respect the ETP flows.

The initial conditions chosen are those acting on 31st January 2006 for the analyses (a), (b), (c), and on the 10th May 2007 for the analyses (d).

The following *elaborations of results* will be reported for each analysis:

- Displacements at the ground surface against the time in order to identify the time of the starting of triggering mechanism[11],
- The vectors of total displacements over whole the mesh, to identify the mechanism of failure[12],
- The profile of deep displacements at failure along some vertical sections of the mesh (*fig.8.4*) to investigate the depth of the sliding surface and the soils involved in the landslide,
- The profile of suction[13] and of permeability for different days up to failure, along the same vertical sections of the mesh used to represent deep displacements (*fig.8.4*), in order to follow the hydraulic behaviour of slope during the triggering mechanism.

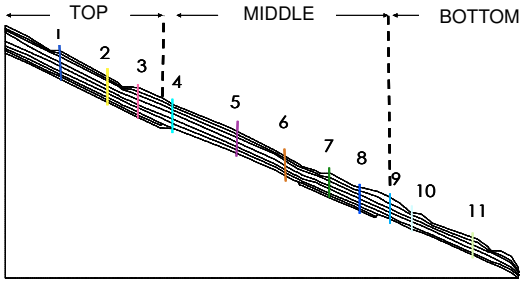

Fig.8.4: Vertical sections chosen to sample results of the analyses

[11] All the analyses are stopped when the collapse conditions establish and the convergence is not more respected.
[12] The mechanism of failure will be called local if the landslide involves some zones of slope only, while it will be called general if the landslide involves whole the slope.

8.3.1 Analyses on the influence of the rain intensity

Five analyses which differ in intensity and distribution of the daily rain applied at ground surface, are performed. All these calculations start by the conditions established on the 31st January 2007, obtained by the validation model analyses (*Chapter 7*).
In the following tables daily rain intensity applied at ground surface is reported.

Tab.8.1: Boundary Conditions applied at the ground Surface, history of rainfall

Time (day)	*1*	*2*	*3*	*4*	*5*	*6*	*7*	*8*	*9*	*10*	*11*	*Total Rain(mm)*
Analysis **R** *Intensity Rain(mm)*	70	70	70	70	70							350
Analysis **R1** *Intensity Rain(mm)*	35	35	35	35	35	35	35	35	35	35		350
Analysis **R2** *Intensity Rain(mm)*	50	50	50	50	50	50	50					350
Analysis **R3** *Intensity Rain(mm)*	35	35	35	35	35	35	-	-	-	70	70	350
Analysis **R4** *Intensity Rain(mm)*	35	35	35	35	35	35	70	70				350

All the analyses were stopped when the collapse conditions in the slope were reached; the total rain applied is always equal to 350 mm (*table 8.1*), while its daily distribution varied.
In analyses R, R1, R2, a continuous and constant rain intensity is applied, while in the R3, R4 ones a discontinuous and variable rain intensity is considered, with a more complex rain history.

8.3.1.1 Results of the analysis R

In the analysis R, a flow of *70mm/day* is applied until the failure occurs; *350 mm of rain* distributed on *five days* are necessary to cause the instability (*tab.8.1*).
In the *figure 8.5* superficial displacements of some vertical sections (*fig.8.4*) calculated during

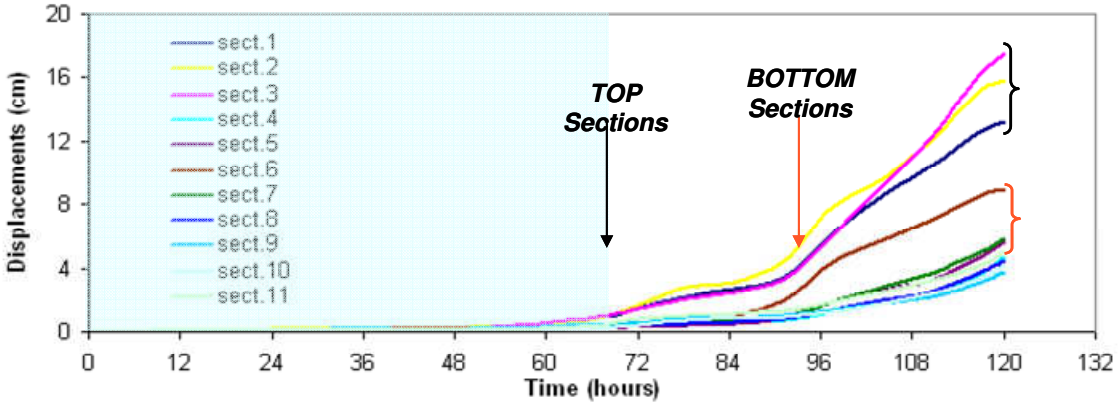

Fig.8.5: Superficial displacements calculated in some vertical sections during the five rainy days

the five rainy days are plotted. This diagram shows that the failure starts *first at the top of the slope* (section 1, 2, 3) after three days of rain and then it occurs at the middle and at the bottom, after four days. After five rainy days the failure involves whole the slope and so it assumes the characteristics of a general failure.

In order to investigate the depth of the sliding surface, the profile of displacements at failure along some vertical sections (*fig.8.6*) and the vectors of displacement on whole the mesh are plotted (*fig.8.7*).

As the figure 8.6 shows, the sliding surface is at *1.00-1.50m* from the ground surface and it lies in the soil 2. Where the top soil becomes thinner, because of the excavation of mountain roads or the stratigraphic irregularity, the depth of sliding surface reaches the soil 3 (section 2, 3) too.

So the triggering mechanism could be defined as *general* because it involves whole the slope and *superficial* because it reaches the contact between the soil 2 and 3 (*fig.8.7*).

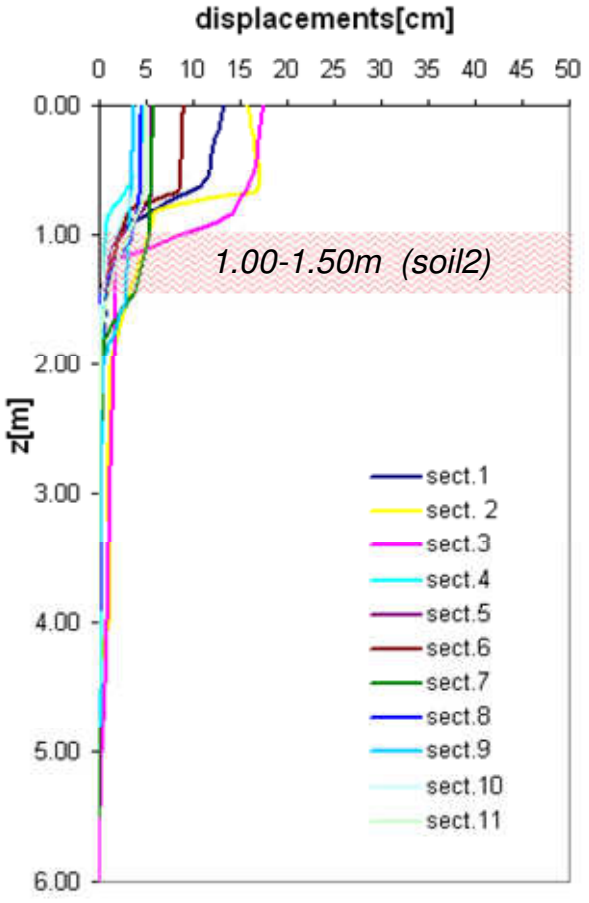

Fig.8.6: Profiles of displacement in some vertical sections at the fifth day of the Rainfall history

The main cause of the instability is the rain, in fact it generates the value of pore water pressure and water content such that lead the slope to the failure. Therefore it is interesting to analyse what happens during the failure in terms of hydraulic variables. In the figures 8.8, 8.9 the profiles of pore water pressures and permeability along three vertical sections represented respectively the top (section 2), the middle (section 6) and the bottom (section 10) of the slope, during five days of rain are plotted. In the figure 8.8a, the initial pore water pressure profile (31st January 2006) is compressive (negative) at the bottom, but in the figure 8.8 b,c it is always tensile. This phenomena is due to the complex stratigraphy which influences the results (*Chapter 7*). In fact along the vertical 2, the soils 7 and 8 are present (*fig.8.8a*) and are characterized by permeability lower than that of soils above.

At *the top vertical section* (*fig.8.8a*) pore water pressure becomes compressive in the soil 1-2-3 at the third day. After five days the failure involves all the slope and the pore water pressure at the top section is compressive in

the intermediate soils too. At *the middle and at the bottom vertical sections* (*fig.8.8b, c*) pore water pressure becomes compressive in the soils involved by the failure when the triggering mechanism starts. Moreover in the middle and bottom section the most compressive value of pore water pressure occurs just at the depth of the sliding surface (*fig.8.8b, c*).
About the permeability profile (*fig.8.9a, b, c*), after five days the soils 1-2-3 above the sliding surface are characterized by the saturated conditions and hence by the value of the saturated permeability. The rainfall always results smaller than Ksat, so the hypothesis used for which all the water fallen infiltrates is right, agreeing with the consideration that Ksat is the minimum value of infiltration (Blight, Rankine Lecture, 1997).
On the base of the previous results some conclusions could be formulated: in the soils involved by the failure the pore water pressure increases to become compressive. The peak of 12 kPa is reached at the contact between the soil 2 and 3 where the sliding surface lies; at failure these soils are characterized by Ksat.

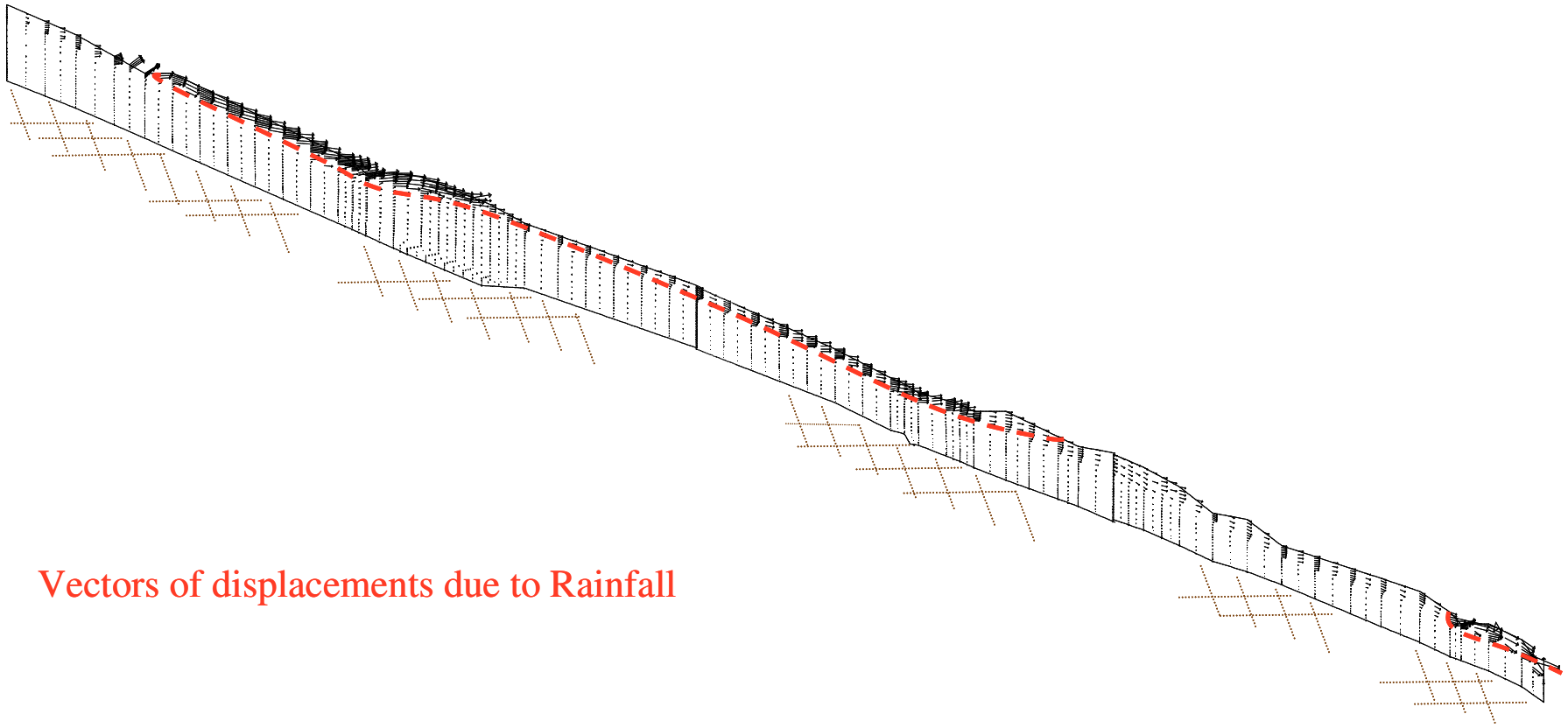

Fig.8.7: Vectors of displacement at failure (at the fifth day of the rainfall history)

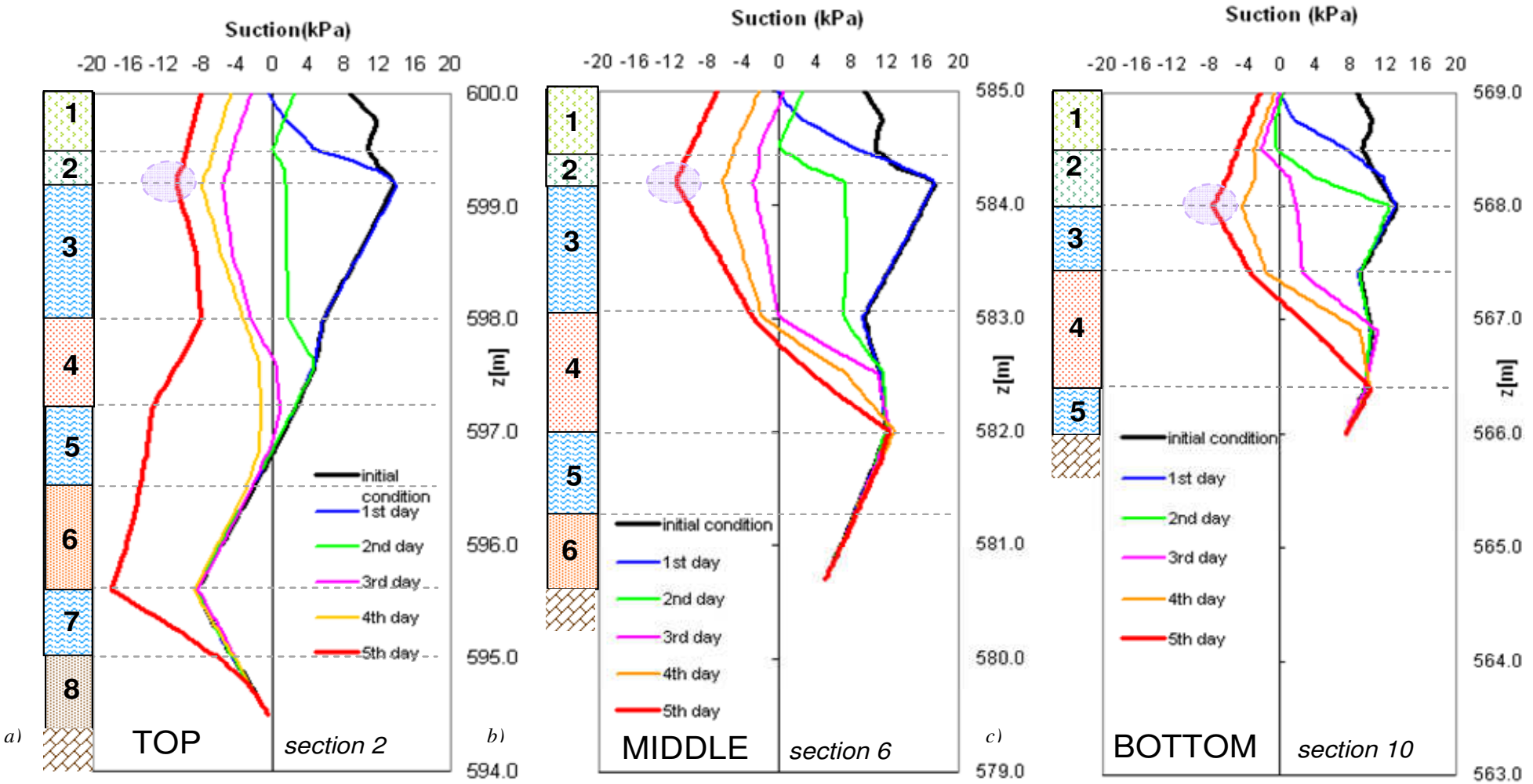

Fig.8.8: Profiles of pore water pressure during the five days of the rainfall history along the section 2 (top slope) a), section 6 (middle slope) b), section 10 (bottom slope) c)

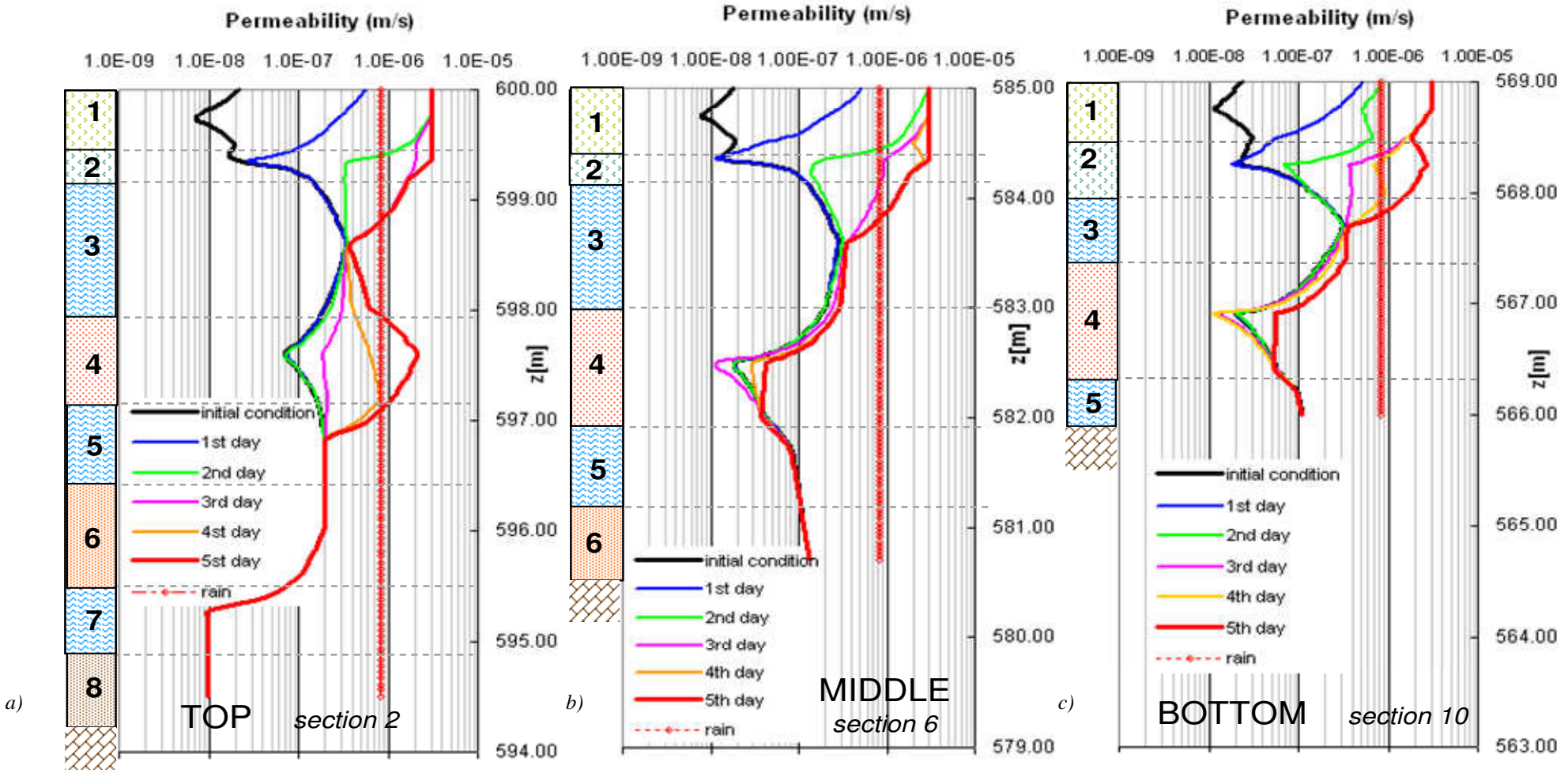

Fig.8.9: Profiles of permeability during the five days of the rainfall history along the section 2 (top slope) a), section 6 (middle slope) b), section 10 (bottom slope) c)

8.3.1.2 Results of the analysis R1

In the analysis R1 the intensity of rain applied at ground surface is 35 mm/day for ten days, amounting again to a total of 350 mm. The total rain necessary for the failure is always 350 mm. Because of a smaller rain intensity applied over a longer period, the failure occurs only

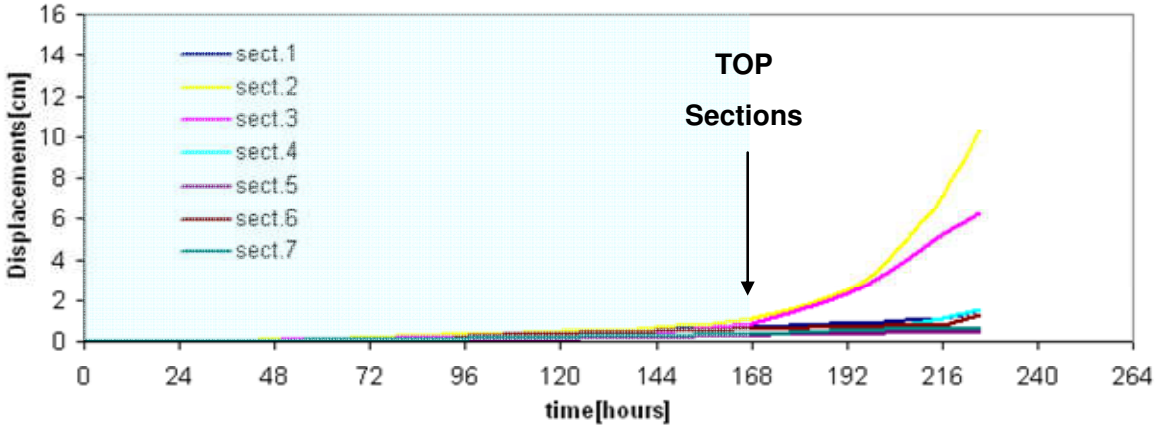

Fig.8.10: Superficial displacements calculated in some vertical sections during ten rainy days

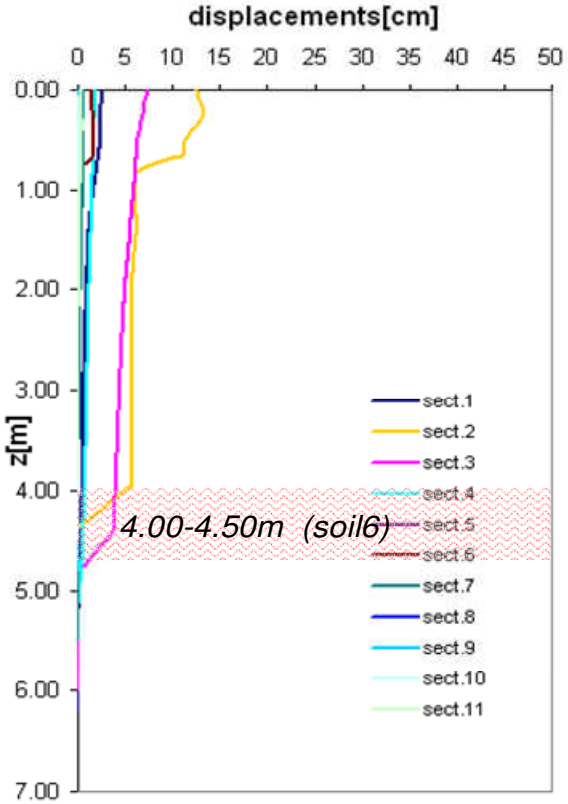

Fig.8.11: Profiles of displacements in some vertical sections at the tenth day of the rainfall history

at the top of the slope after one week (*fig.8.10*). Moreover the depth of the sliding surface is 4.00- 4.50 m, it lies in the soil 6 (*fig.8.11*). Therefore the failure seems *local* because it involves only the top of the slope and it is *deep*, reaching the soil 6 (*fig.8.12*). The zones involved by the collapse (the top slope) are characterized by the presence of soils 7-8 at the bottom, less permeable than the soil above. There the pore pressure profile results compressive already from the initial condition (31st January 2006).

The pore water pressure profile at the top section (2) becomes compressive in all the soils layers when the failure starts (*fig.8.13a*). In the other sections (*fig.8.13b, c*) the failure does not occur, in fact the compressive pore water pressure does not arise there. Permeability reaches the saturated value only at the depth of the sliding surface, in the soil 6 (*fig. 8.14*).

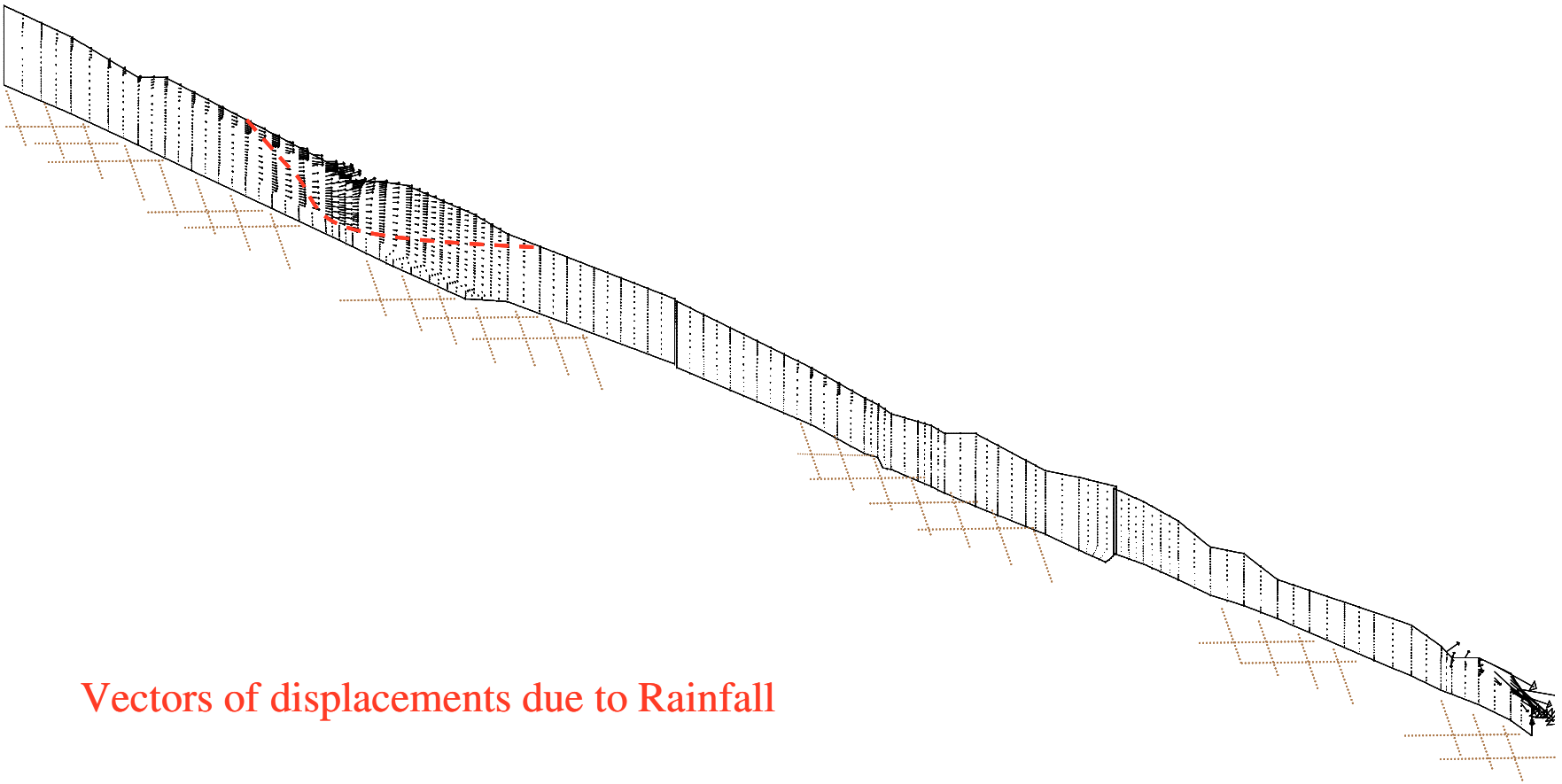

Fig.8.12: Vectors of displacement at failure (at the tenth day of rainfall history)

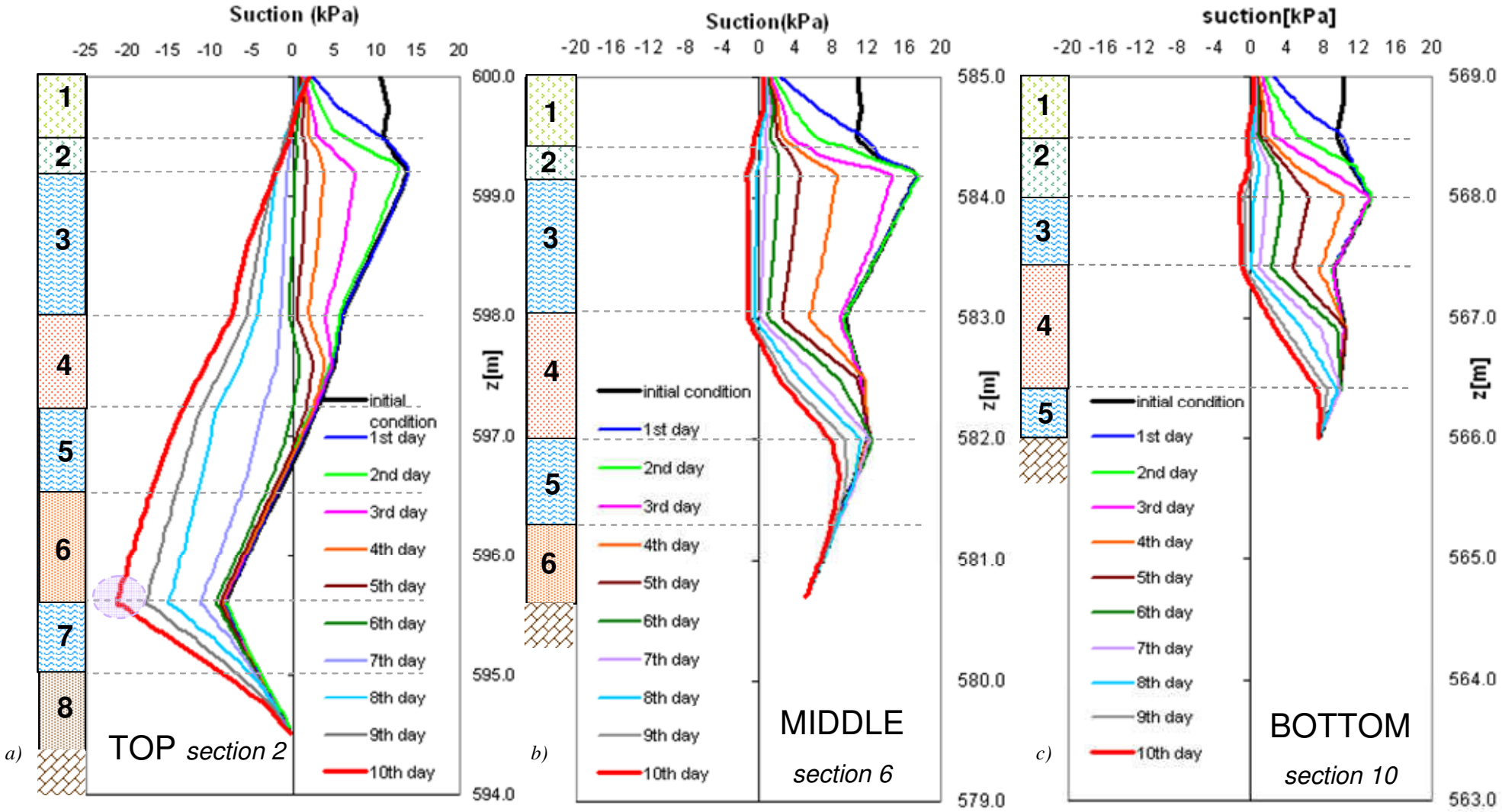

Fig.8.13: Profiles of pore water pressure during the ten days of the rainfall history along the section 2 (top slope) a), section 6 (middle slope) b), section 10 (bottom slope) c)

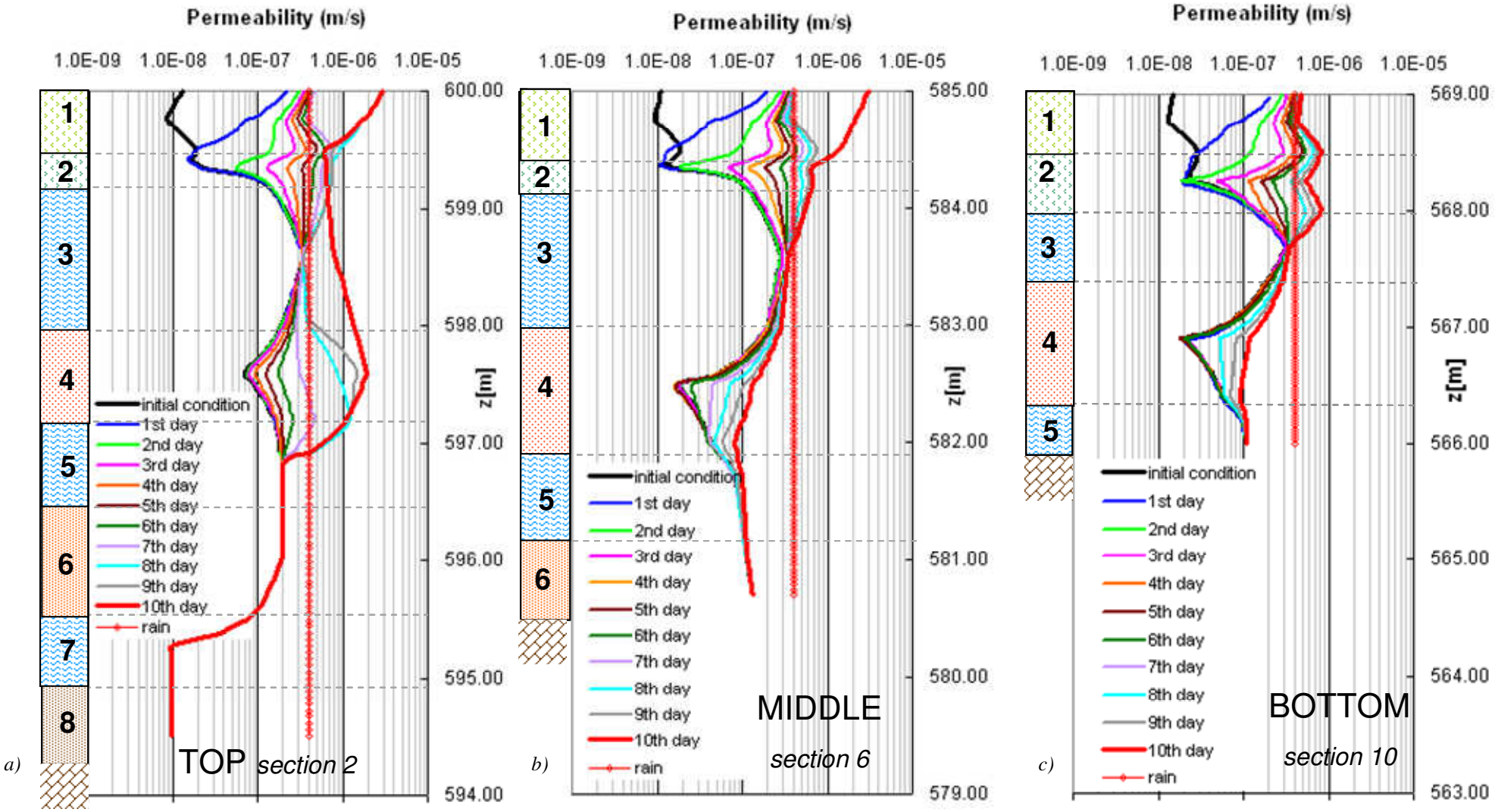

Fig.8.14: Profiles of permeability during ten days of the rainfall history along the section 2 (top slope) a), section 6 (middle slope) b), section 10 (bottom slope) c)

It is clear that the mechanism changes completely varying the daily distribution of the fixed 350 mm of rainfalls; in the analysis R it results *general* and *superficial*, in the analysis R1 *local* and *deep.*

8.3.1.3 Results of the analysis R2

In this analysis 50 mm of rain are applied at the ground surface for seven days, amounting to 350 mm in total. The triggering mechanism starts after five days only at the top and at the middle of slope (at the same time). So the failure is again *local* (*fig.8.15*).

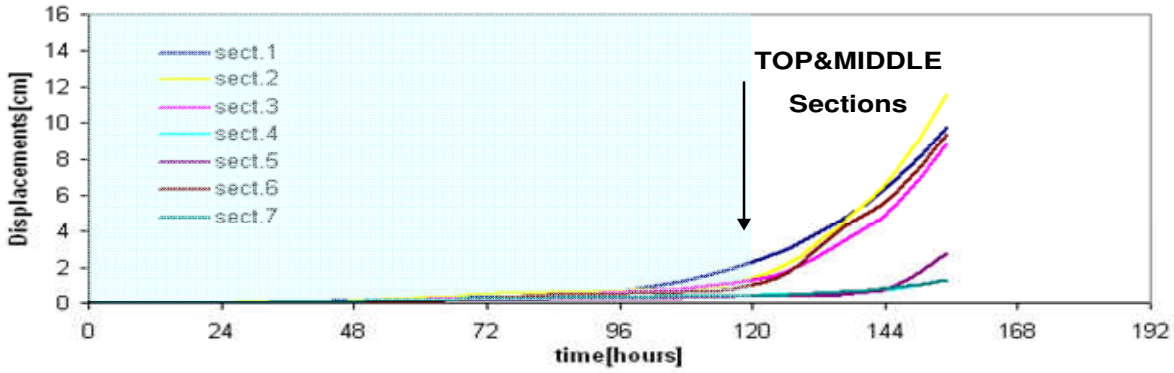

Fig.8.15: Superficial displacements calculated in some vertical sections during the seven rainy days

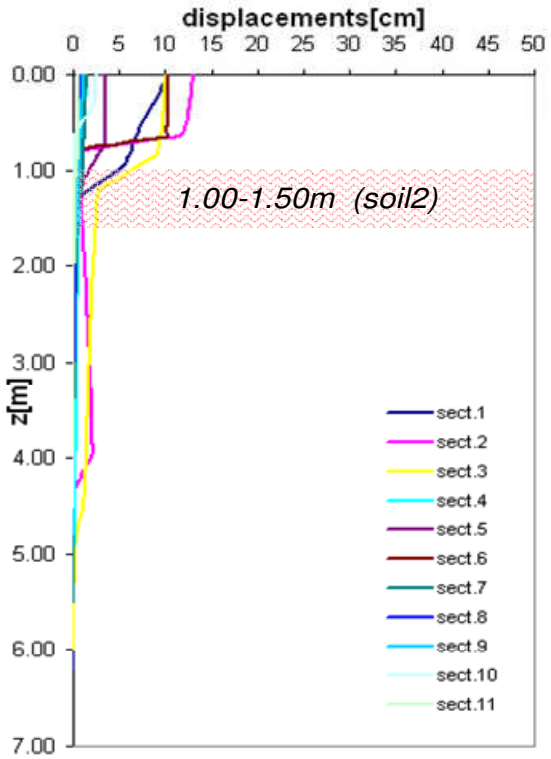

Fig.8.16: Profiles of displacement in some vertical sections at the seventh day of the rainfall history

The depth of the sliding surface is 1.00-1.50 m only, the soil 1-2 are involved in the landslide (*fig.8.16*). The failure mechanism is intermediate between that resulted in the analysis R1 and in the analysis R, it' s local like in the former but superficial like in the latter (*fig.8.17*).

After five days the pore water pressure profiles become compressive in the soils 1-2-3 at the sections involved by the failure (at the top and at the middle). The saturated permeability is reached (*fig.8.18-8.19*) in the superficial soils after five rainy days only along the sections where the failure occurs.

So the *local* failure could verify because of the rain smaller than 50 mm/day and the *superficial* sliding surface could be generated because of rain higher than that intensity; but these considerations can be undertaken assuming constant the total rain applied (350 mm) in all the analyses.

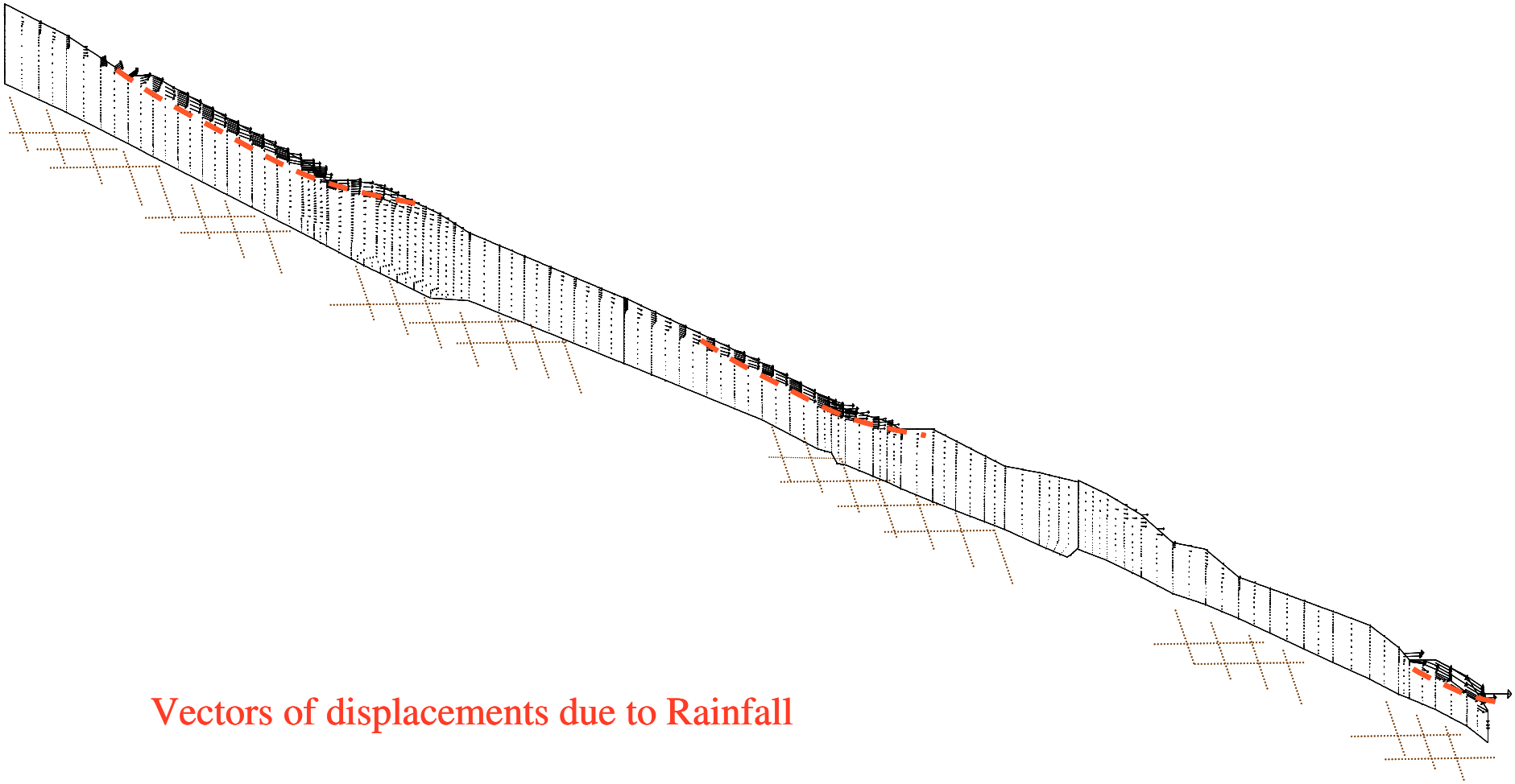

Fig.8.17: Vectors of displacements at failure (at the seventh day of the Rainfall history)

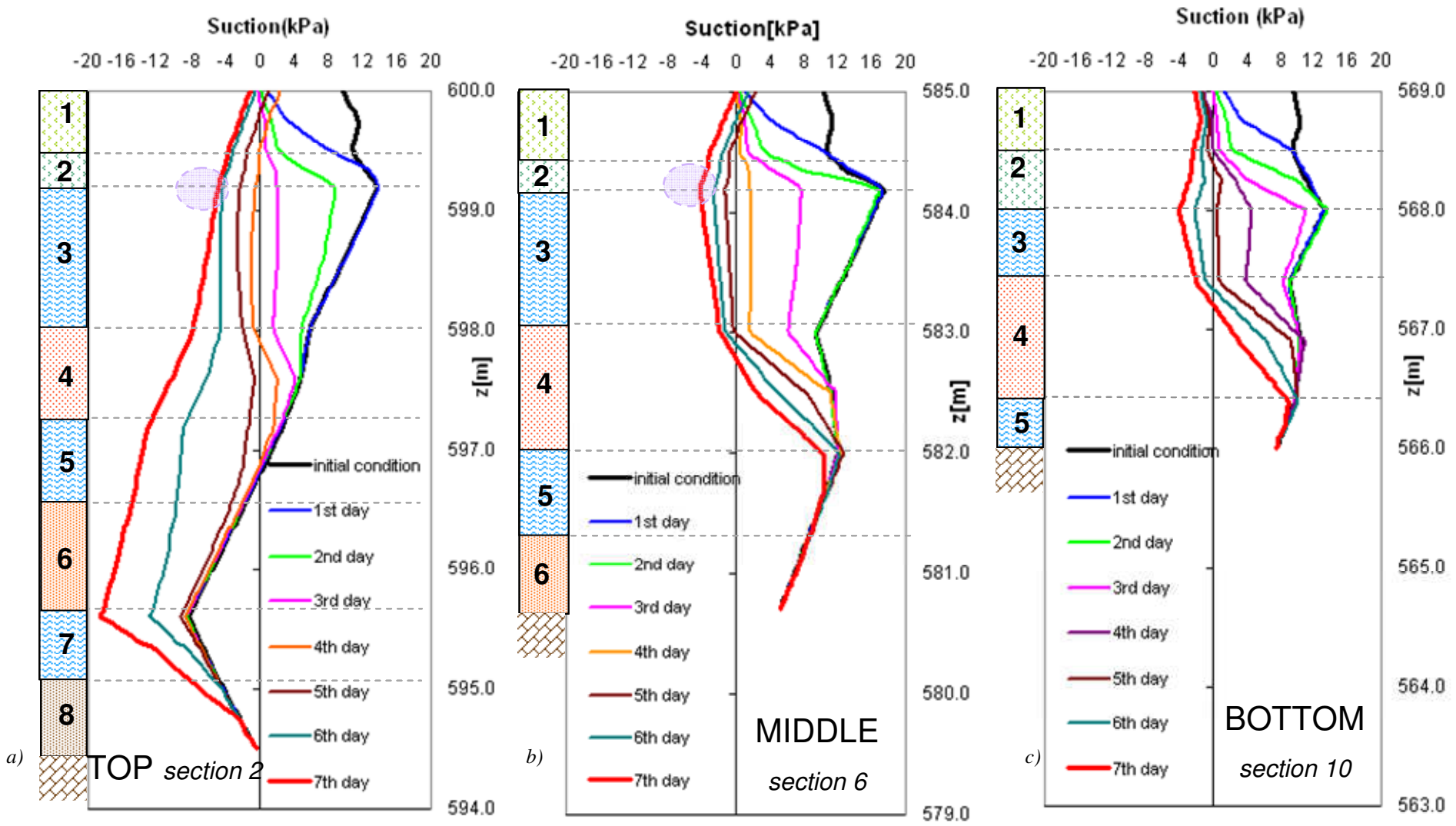

Fig.8.18: Profiles of pore water pressure during the seven days of the rainfall history along the section 2 (top slope) a), section 6 (middle slope) b), section 10 (bottom slope) c)

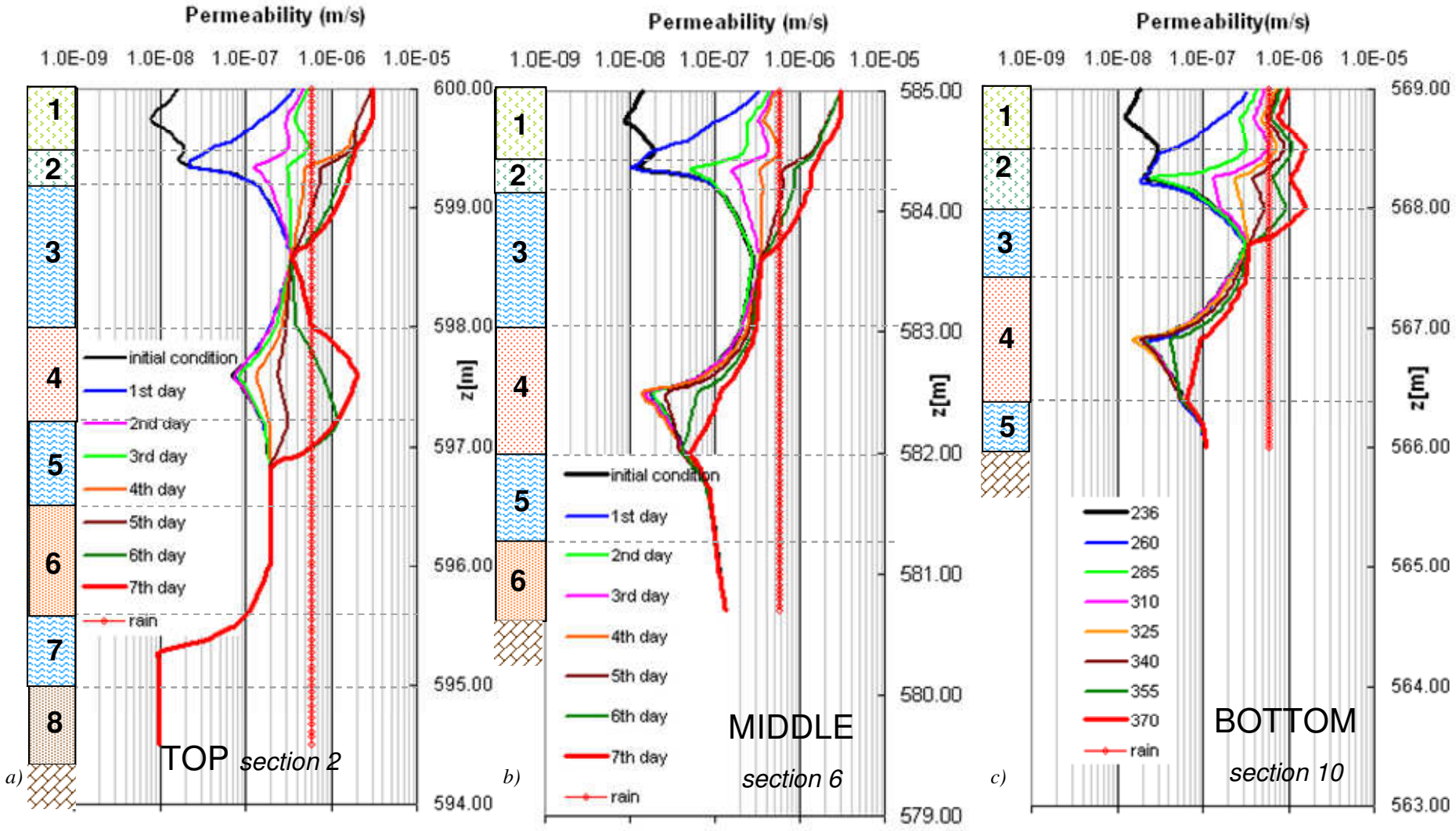

Fig.8.19: Profiles of permeability during the seven days of the rainfall history along the section 2 (top slope) a), section 6 (middle slope) b), section 10 (bottom slope) c)

8.3.1.4 Results of analysis R3

In this analysis two different rain intensities, separated by three days with no rain, are applied at the ground surface. The total rain, causing the failure, is 350 mm as in the previous analyses. A rain consisting in 35mm/day is applied for 6 days, then 70mm/day are applied for 2 days after three dry days. The triggering mechanism starts at the top of the slope after nine days, six rainy and three dry. The failure seems to be *local* (*figs.8.20, 8.22*). So the higher rain

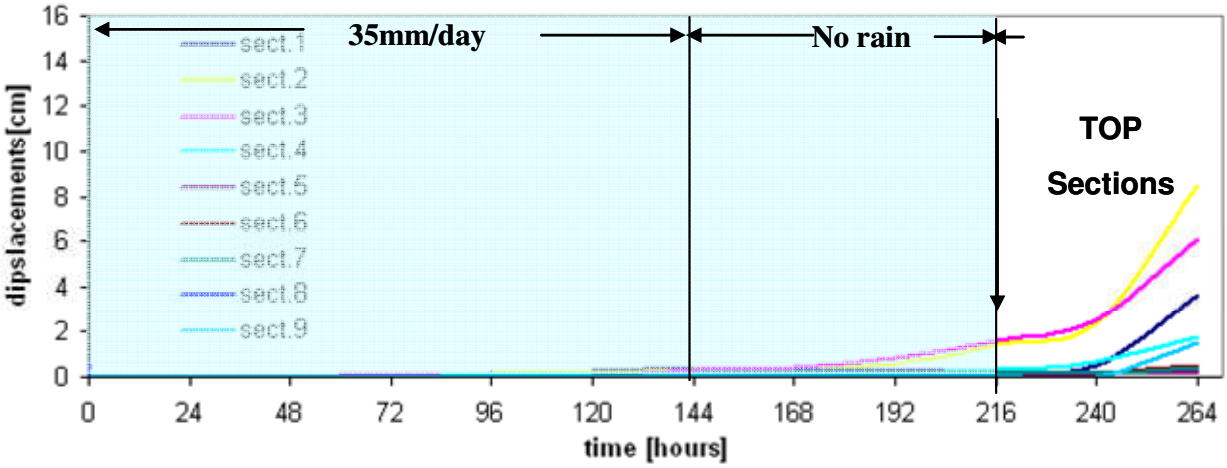

Fig.8.20: Superficial displacements calculated in some vertical sections during eleven rainy days

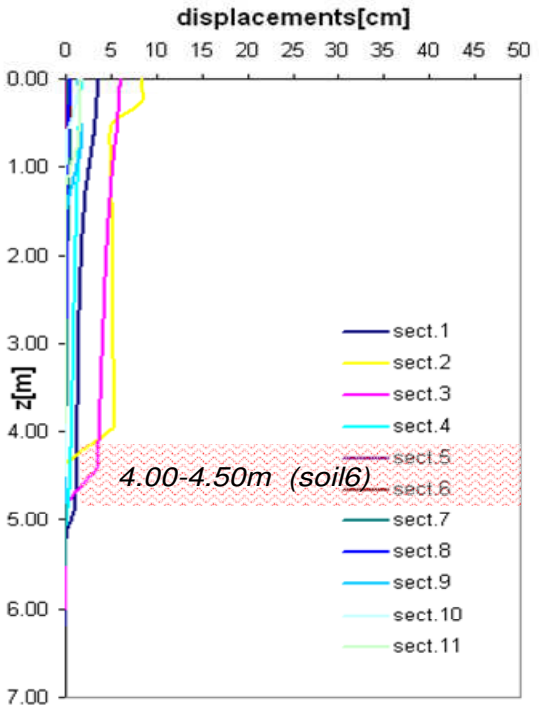

Fig.8.21: Profiles of displacement of some vertical sections at the eleventh day of rainfall history

intensity (70mm/day) causes the failure.

The depth of the sliding surface is very deep, it lies in the soil 6 at 4.00 - 4.50 m as in the analysis R1. So the failure is *local* and *deep* (*fig.8.21*).

Tree days with no rain allows the previous rainfall (35mm for six days) to infiltrate in the subsoil and to arrive in the deeper soil (soil 6). When 70mm/day starts to fall, the failure occurs, so this intensity is responsible for the landslide triggering.

The predominant mechanism of failure is equal to that verifying in the analysis R1, where 35mm of rain are applied for ten days. About the suction and permeability profile the same consideration done in the analysis R1 could be undertaken (figs.8.23-8.24).

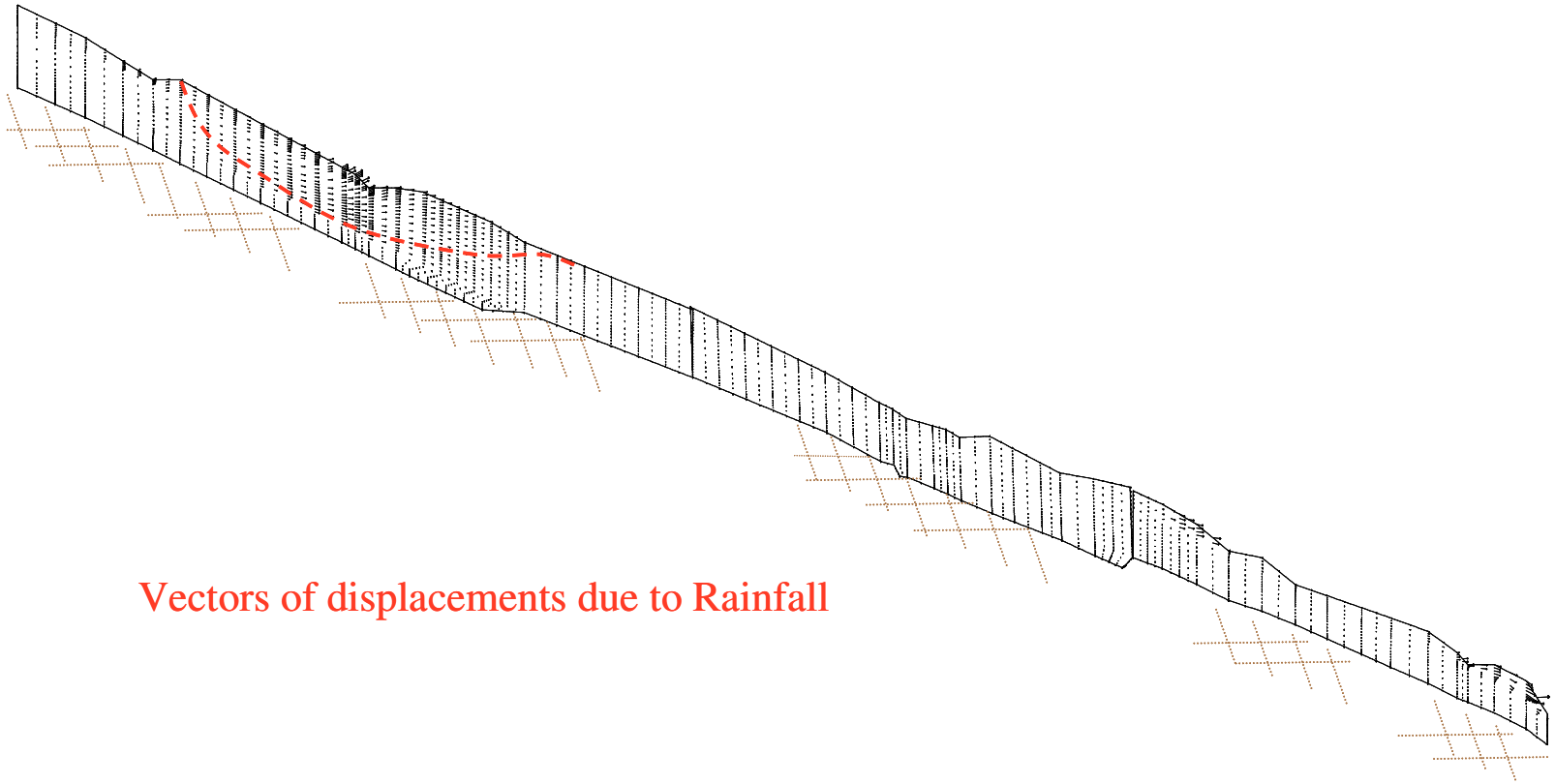

Fig.8.22: Vectors of displacements at failure (at the eleventh day of the rainfall history

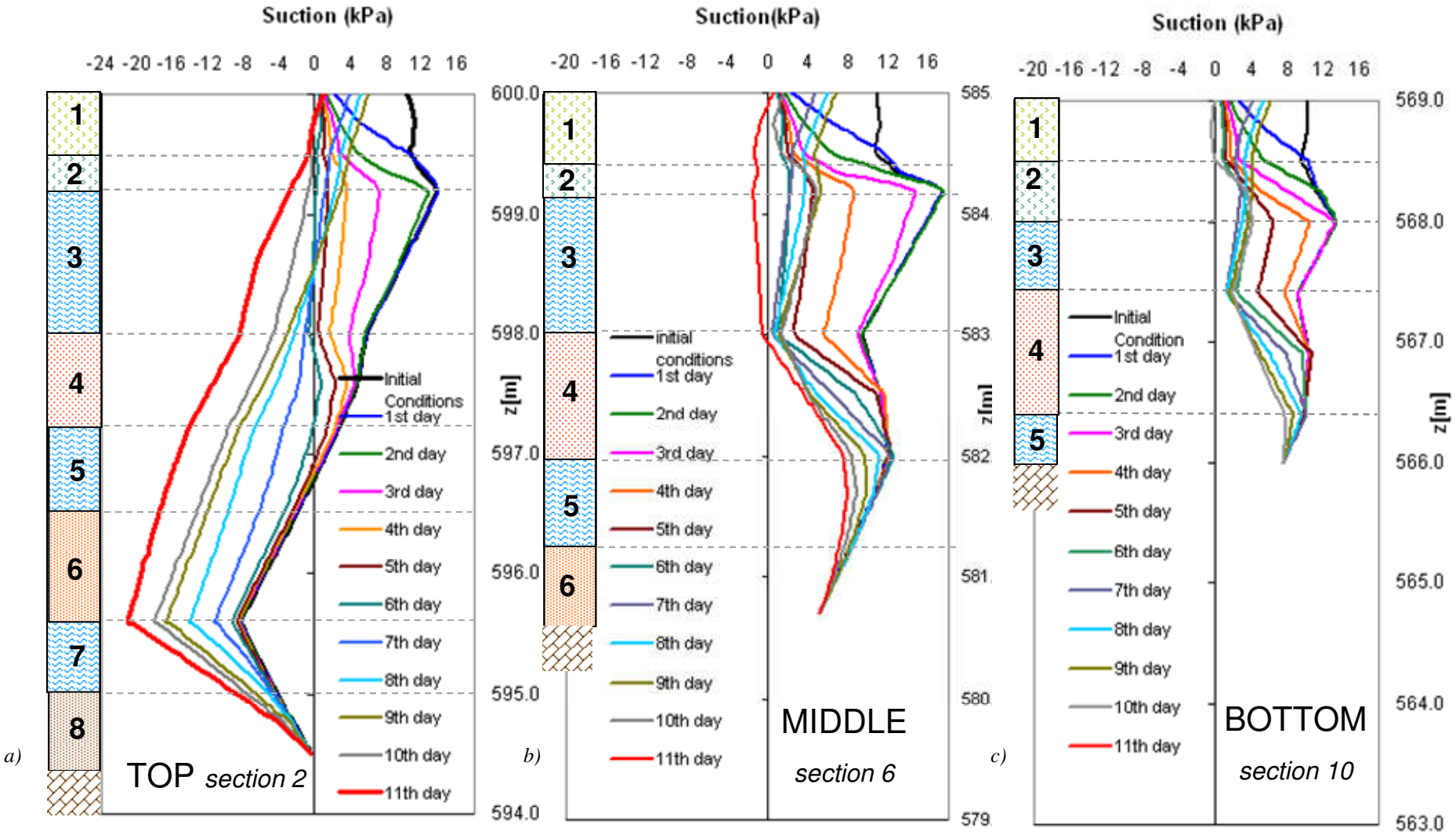

Fig.8.23: Profiles of pore water pressure during the eleven days of the rainfall history along the section 2 (top slope) a), section 6 (middle slope) b), section 10 (bottom slope) c)

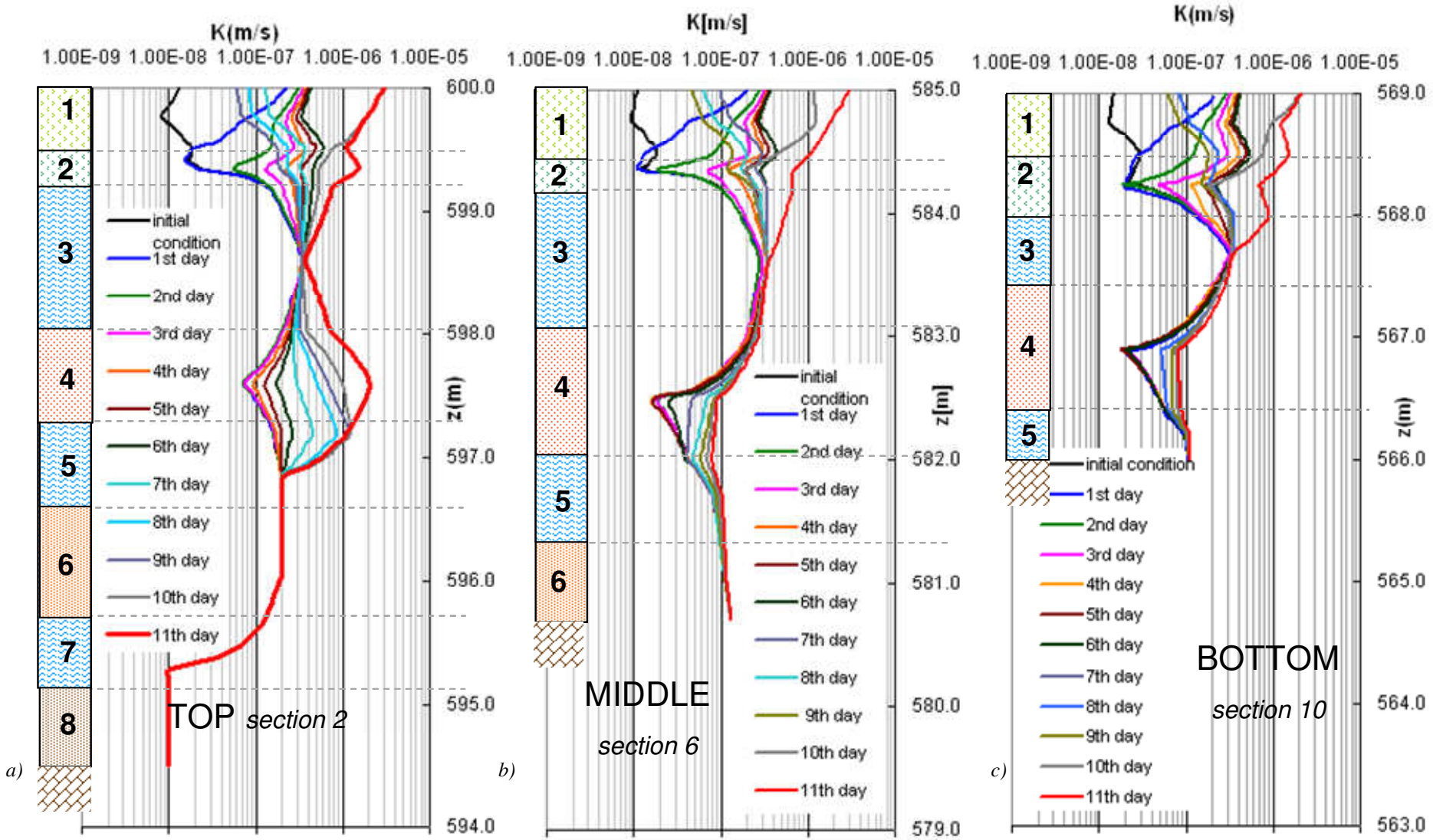

Fig.8.24: Profiles of permeability during the eleven days of the rainfall history along the section 2 (top slope) a), section 6 (middle slope) b), section 10 (bottom slope) c)

8.3.1.5 Results of the analysis R4

In this analysis two different rain intensities are applied. The total rain causing the failure is 350 mm as in the previous analyses, 35mm/day are applied for 6 days, 70mm/day are applied for subsequent 2 days. There is no dry period between the two rain periods.

Triggering mechanism starts at the top of the slope at the seventh day (after six days characterized rainfall of 35mm/day). The failure involves the middle and the bottom too at the eighth day. So the failure seems to be *general* (*figs.8.25-8.27*).

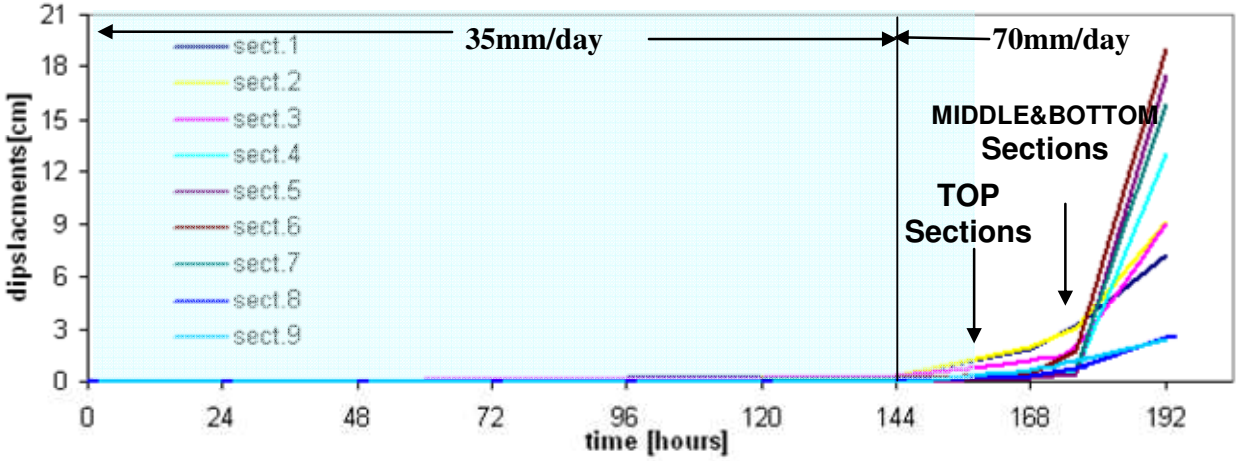

Fig.8.25: Superficial displacements calculated in some vertical sections during eight rainy days

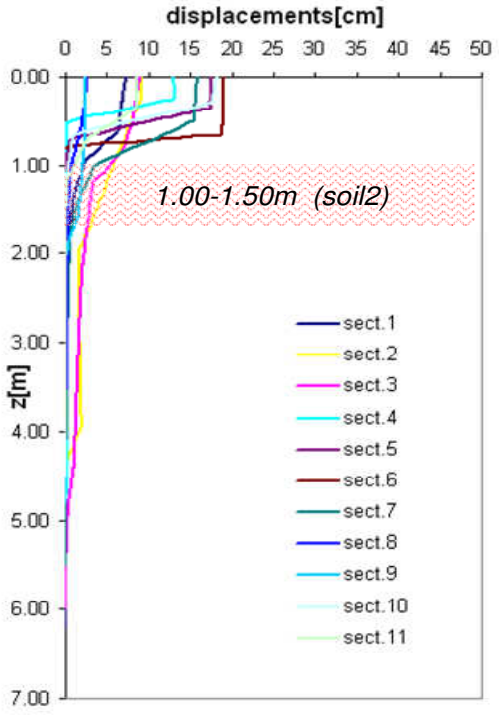

Fig.8.26: Profiles of displacement of some vertical sections at the eighth day of the rainfall history

Specially at the middle and at the bottom of the slope the failure happens suddenly as the displacements increase quickly (*fig.8.25*). It is the higher rain intensity, 70mm/day, that causes the failure. The sliding surface is very superficial, it lies in the soil 2 at the depth of 1.00-1.50 m, so the failure could be defined superficial too (*fig.8.26*). The last two rainy days (70mm/day) play a predominant role in the failure mechanism, that become similar to that occurring in the analysis R. These two days with 70mm/day of rainfall speed up the occurrence of the global failure compared to analysis R1. About the suction and permeability profiles the same consideration done in the analysis R could be undertaken.

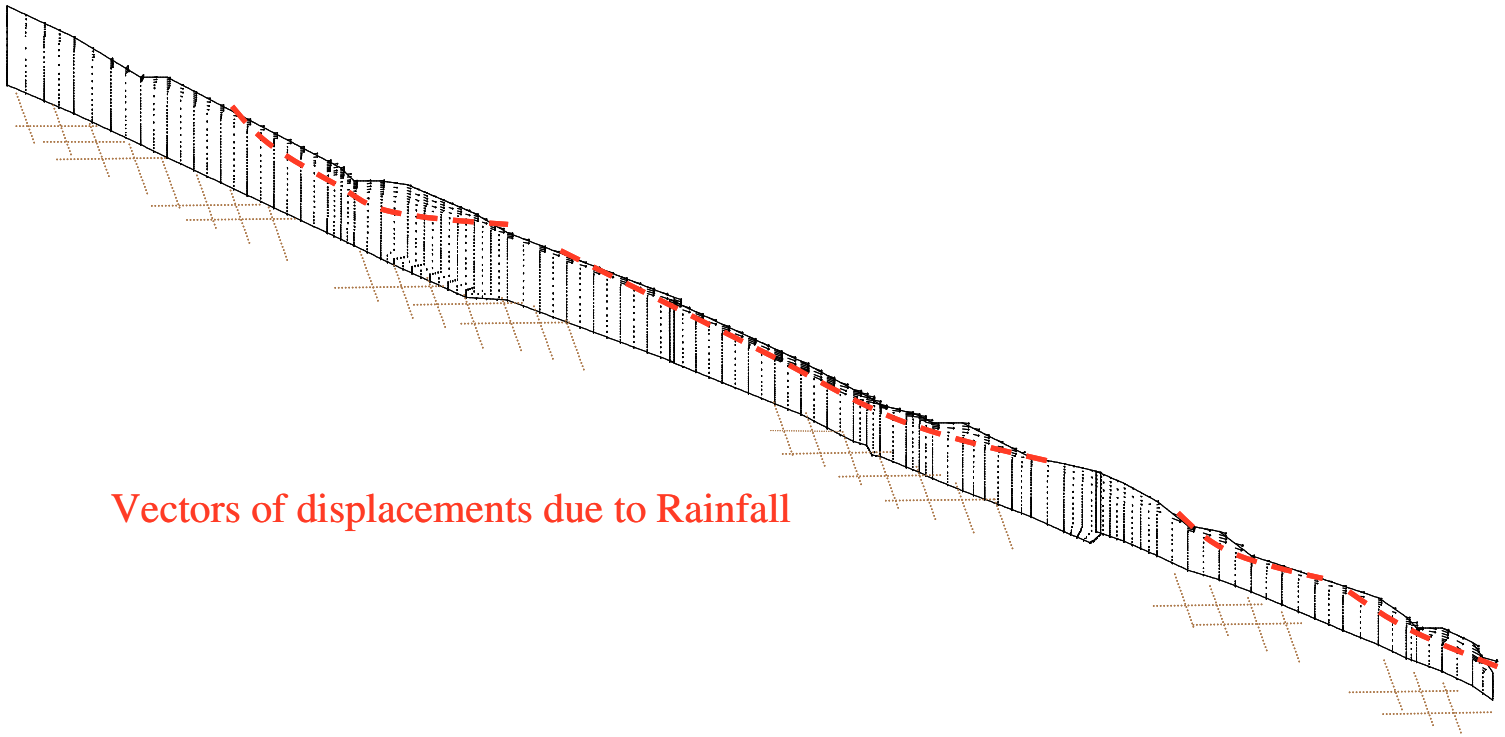

Fig.8.27: Vectors of displacements at failure (at the eighth day of the Rainfall history)

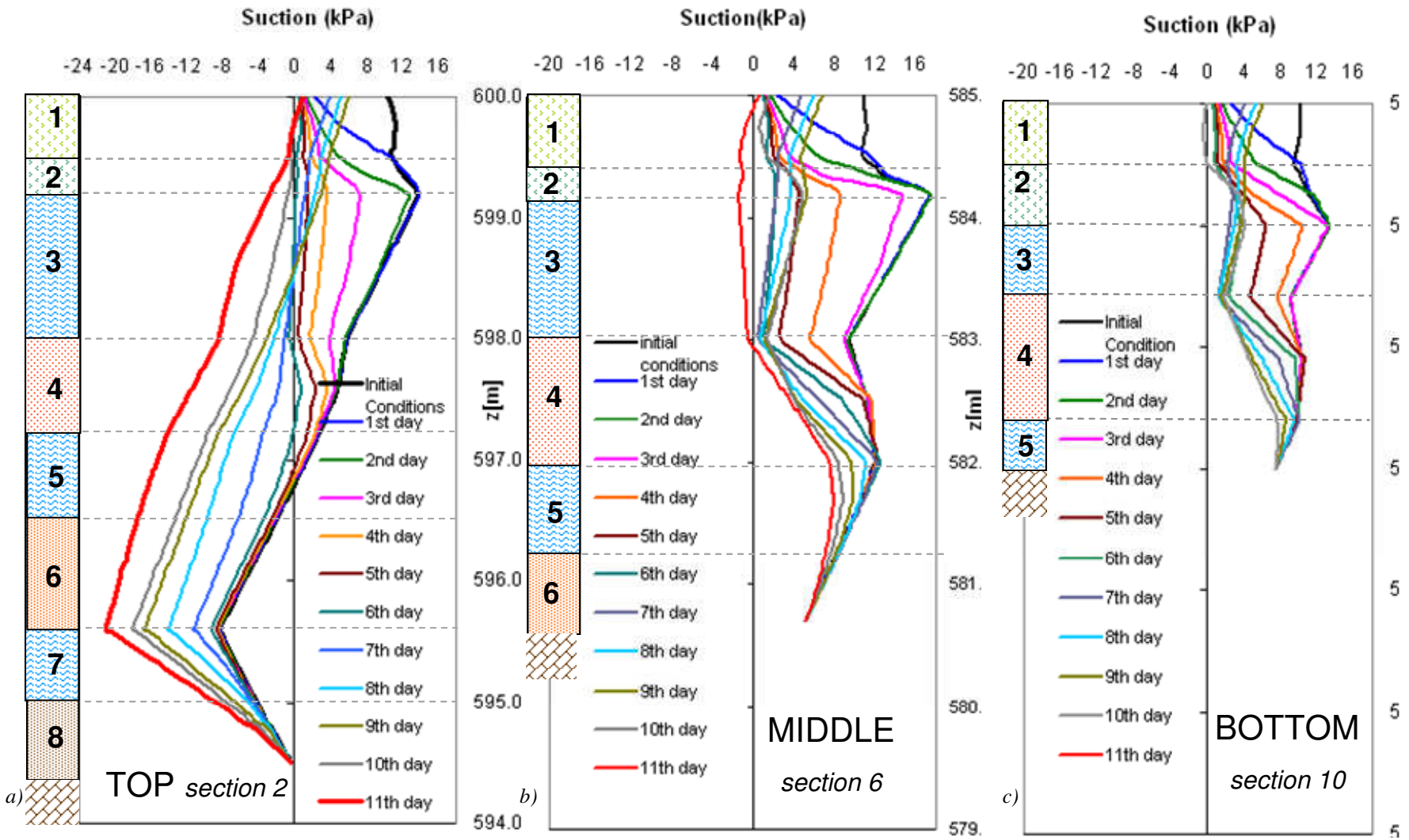

Fig.8.28: Profiles of pore water pressure during the eight days of the rainfall history along the section 2 (top slope) a), section 6 (middle slope) b), section 10 (bottom slope) c)

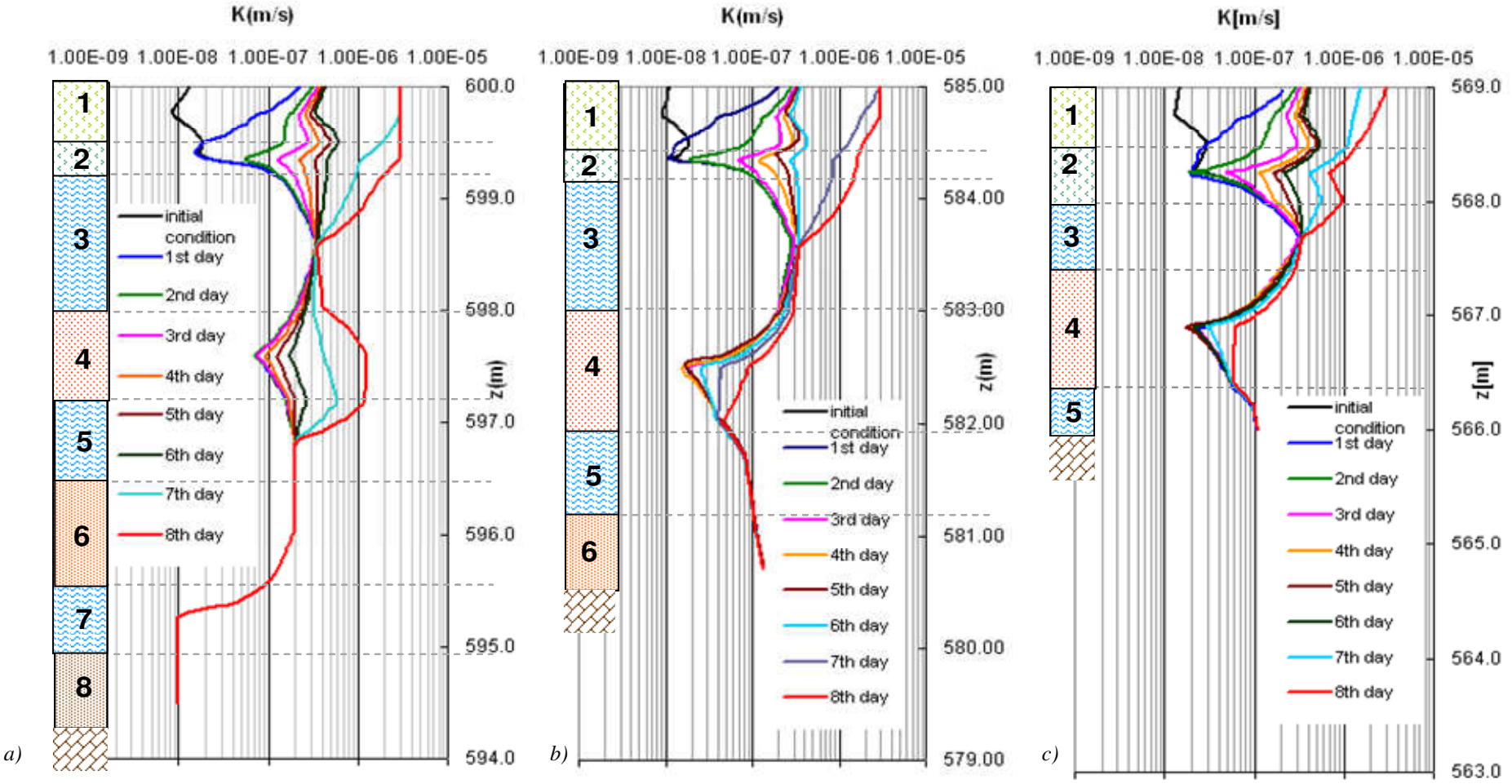

Fig.8.29: Profiles of permeability during the eight days of the Rainfall history along the section 2 (top slope) a), section 6 (middle slope) b), section 10 (bottom slope) c)

8.3.2 Investigation on the influence of the mean rain on slope stability

In this analysis the average rain on the hydrologic year investigated in the *Chapter 7* is applied (15mm/day). The *15 mm/day of rain intensity* for sixteen days are applied as top boundary condition: the total Rain is 240 mm. After six days, the superficial displacements in each section observed assume a constant value, 1 cm about; therefore the *steady condition* is reached (*fig.5.30*). The addition of the second rainy week does not influence the slope stability. By observing the profile of horizontal displacements on the sixteenth day (*fig.8.31*),

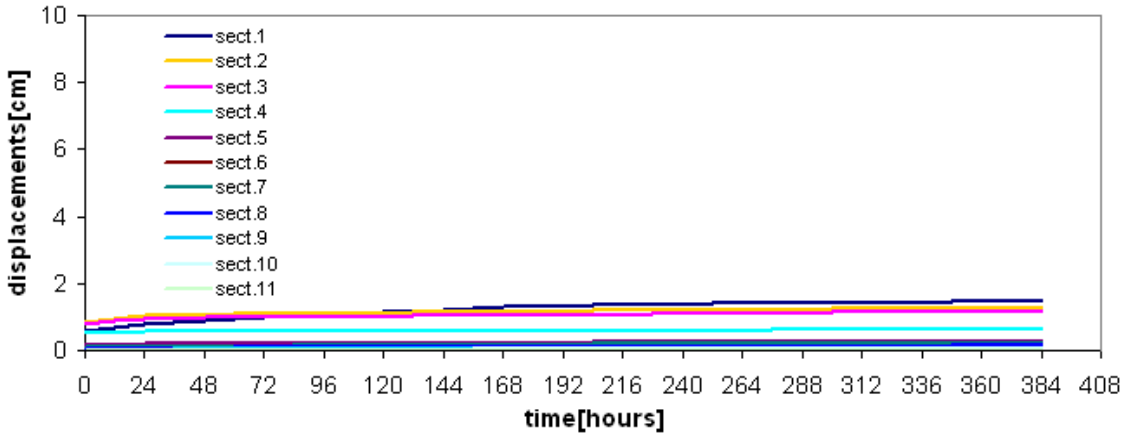

Fig.8.30: Superficial displacements calculated in some vertical sections during sixteen rainy days

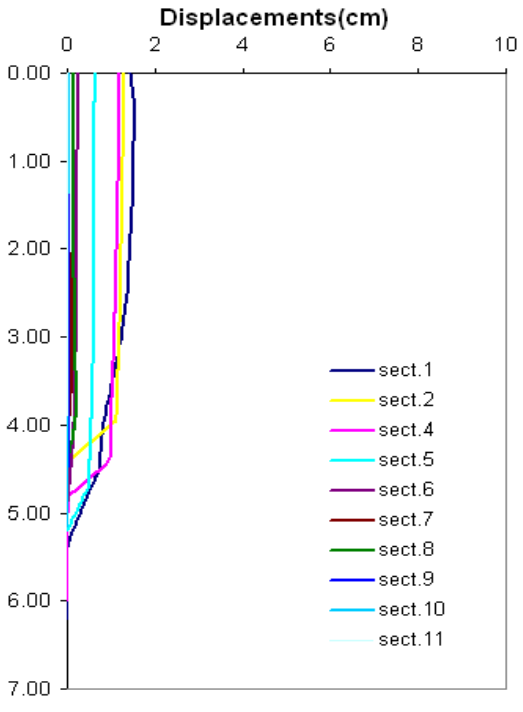

Fig.8.31: Profiles of displacement of some vertical sections at the sixteenth day of the Rainfall history

a small values of 1-2 cm up to the soil 6 characterize the profile. The perturbation caused by the low and durable rain, 15mm/day, arrives in the deeper soil but in any way it does not cause the failure. The pore water pressure profile along the vertical section n°3 (fig.8.4) after six days does not change more (*fig.8.32a*). The same thing occurs in the permeability profile (*fig.8.32b*). If the suction (that regulates failure) keeps on constant, there is a reasonable explanation of the steady condition establishing. The results of this analysis suggest that the mean rain should not cause the failure on a slope characterized by the given stratigraphy and geometry as these analysed, even if the Rain is applied for very long time (two weeks). It is necessary to apply an intensity rain higher than the main value relative to the hydrological year in order to investigate the triggering mechanism.

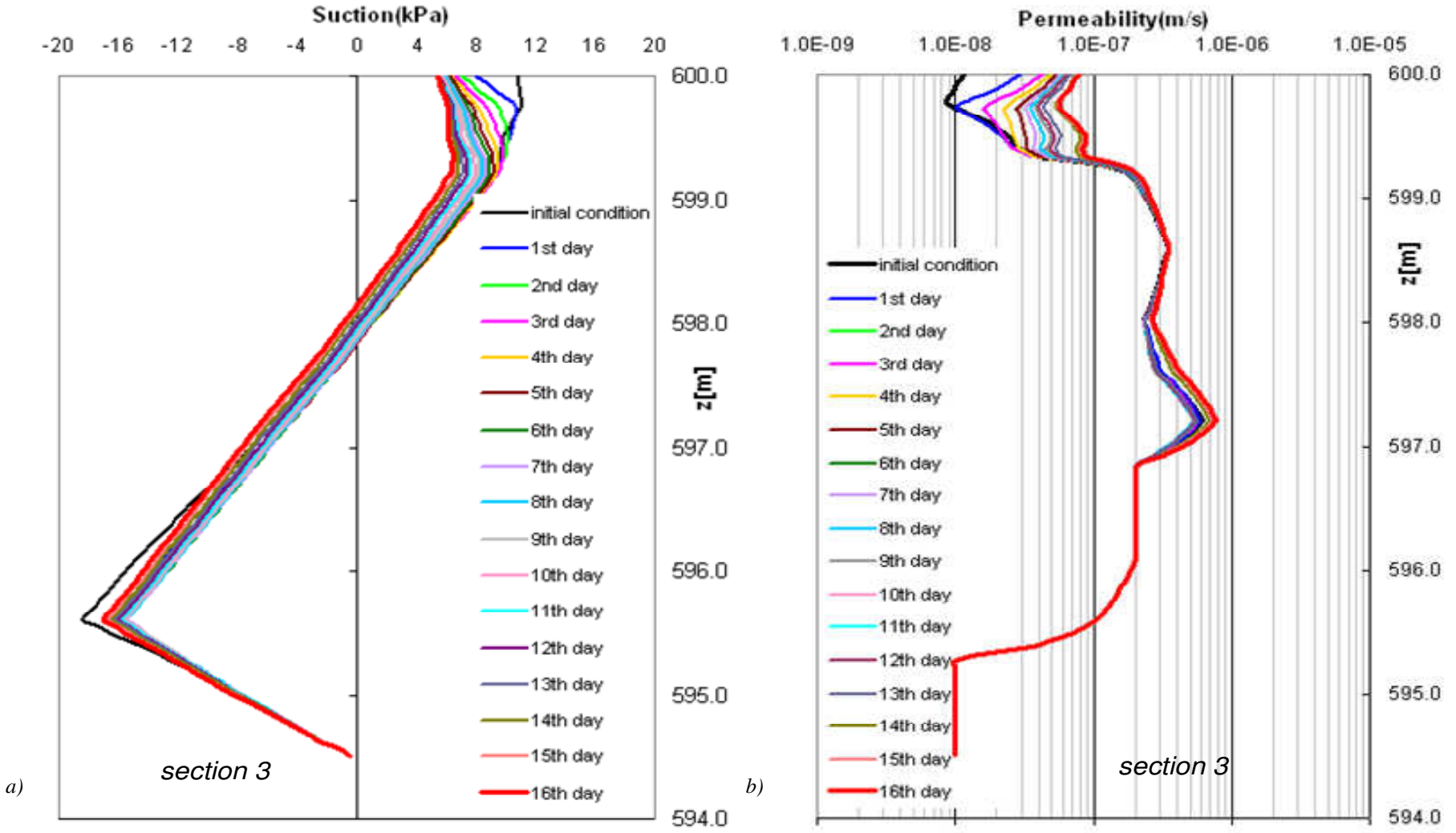

Fig.8.32: Profiles of pore water pressures during sixteen days of the rainfall history along the section 2 (top slope) a), profiles of permeability during the sixteen days of the rainfall history along the section 2 (top slope) b)

Discussion

Some conclusions may be drawn by the results shown previously:

The mean rain during the hydrological year, 15mm/day, does not cause the failure but it allows the steady conditions establishing in terms of suction and displacements. The intensity of daily rain smaller than 15 mm/day does not allow to investigate the triggering mechanism but values higher than the average are necessary to be undertaken. These results refer to the particular geometry and stratigraphy of the slope analysed.

The total rain enough to generate the failure in all the analyses is about 350 mm while the daily distribution of the total rain strongly influences the triggering mechanism. Probably the total water leading to the landslide is a function of the volumetric water content in the initial conditions. The starting of the failure occurs after a cumulated rain of 210-250mm.

The daily rain intensity influences the type of failure and the depth of the sliding surface. The investigation of the various daily rain intensities was useful to find a range of different triggering mechanisms. Rains smaller than 35 mm/day cause the formation of deep sliding surfaces because the rain water has the time to infiltrate in the subsoil and to reach the deeper soils. In order to view the influence of the rain intensity on the depth of the sliding surface, profiles of displacement in the section 2 at failure, for all the analyses, are plotted (*fig.8.33*).

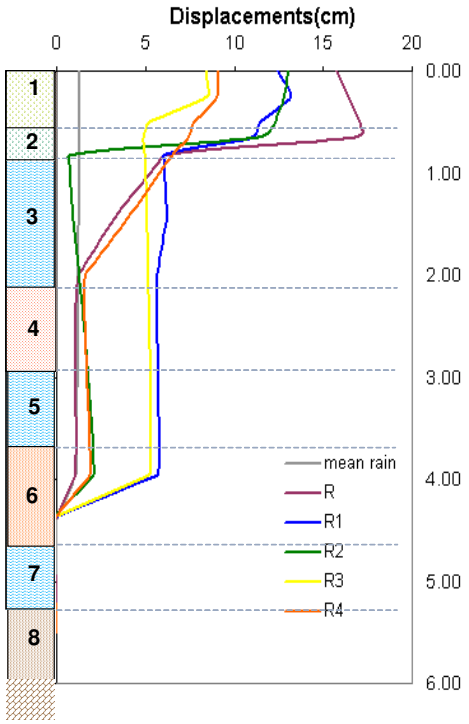

Fig.8.33 Profiles of displacement at failure along the section 2

Rain higher than 70mm/day leads to the *general* failure involving whole the slope. The intermediate values between 35 mm/day and 70 mm/day, as 50 mm/day in the analysis R2, may cause a type of failure intermediate between the two ones limit previously introduced and so it is *superficia*l and

local.

If two different rain intensities are applied constituting an unique rainfall history composed by them (mix boundary conditions, R3, R4), the prevailing failure mechanism is what would have taken place if there were only intense rain (analysis R). Instead if the two intensities of rain were spaced out from dry days, the predominant mechanism would have taken place under less intense rain (R1).

In the following a table summarizing results of all the analyses in terms of: type of failure, sliding surface, total rain applied, cumulated rain which causes the starting of failure and pore pressure at failure on the sliding surface is reported (*tab.8.2*).

Tab.8.2 Mechanism of failure obtained by the analyses R, R1, R2, R3, R4

	Failure	*Type of failure*	*Sliding surface*	*Cumulated Rain applied in the rainfall history (mm)*	*Cumulated rainfall causing triggering failure (mm)*	*Pore pressure at failure along sliding surface (kPa)*
Analysis **Mean Rain** *(15 mm/day)*	-	-	-	*240*	-	-
Analysis **R** *(70 mm/day)*	Yes	General	Superficial (soil 2)	350	210	8-10
Analysis **R1** *(35 mm/day)*	Yes	Local	Deep (soil 6)	350	280	15-20
Analysis **R2** *(50 mm/day)*	Yes	Local	Superficial (soil 2)	350	250	8-20
Analysis **R3** *(35 mm/day, ---,70 mm/day)*	Yes	Local	Deep (soil 6)	350	210	15-20
Analysis **R4** *(35 mm/day,70 mm/day)*	Yes	General	Superficial (soil 2)	350	210	10-15

8.3.3 Analyses on the influence of the mechanical characterization

Results of analyses concerning the influence of *mechanical parameters* on the failure mechanism are reported. The initial conditions and the boundary conditions at the ground surface are the same of the analysis R; only the failure parameters, α, μ and φ' in the constitutive model (*Chapter 6*) are changed. In the following tables (*tab.8.3*) the mechanical characterization for all the soils used in these analyses, are summarized.

Tab.8.3: Mechanical Parameters adopted in the analyses

Mechanical Characterization		Analysis R	Analysis M1	Analysis M2
Soil1	α	***0.4***	***0.4***	***0.8***
	μ	***0.83***	***0.83***	***1.7***
	$M(\varphi')$	***1.47***	***1.47***	***1.47***
Soil2	α	***0.4***	***0.4***	***0.8***
	μ	***0.83***	***0.83***	***1.7***
	$M(\varphi')$	***1.5***	***1.5***	***1.5***
Soil3	α	***0.7***	***0.7***	***0.7***
	μ	***0.8***	***0.8***	***0.8***
	$M(\varphi')$	***1.8***	***1.5***	***1.8***
Soil4	α	*0.7*	*0.7*	*0.7*
	μ	*0.8*	*0.8*	*0.8*
	$M(\varphi')$	*1.5*	*1.5*	*1.5*
Soil5	α	*0.8*	*0.8*	*0.8*
	μ	*1.7*	*1.7*	*1.7*
	$M(\varphi')$	*1.7*	*1.7*	*1.7*
Soil6	α	*0.8*	*0.8*	*0.8*
	μ	*1.7*	*1.7*	*1.7*
	$M(\varphi')$	*1.62*	*1.62*	*1.62*
Soil7	α	*0.01*	*0.01*	*0.01*
	μ	*1.43*	*1.43*	*1.43*
	$M(\varphi')$	*1.65*	*1.65*	*1.65*
Soil8	α	*0.01*	*0.01*	*0.01*
	μ	*1.43*	*1.43*	*1.43*
	$M(\varphi')$	*1.61*	*1.61*	*1.61*

In the analysis M1, the pumices of Avellino (soil 3) are characterized by a value of φ' smaller than in the analysis R, so they are considered weaker (the angle of shearing resistance assumed is lower: 37°). This value, 37°, represents only an lower limit in order to investigate how the failure mechanism changes, making the pumices weaker but the typical values for these soil are well higher than 37° (*Pellegrino et al.,1967*).

In the analysis M2, only the shape parameters α, μ in the superficial soils (*soil 1-2*) are changed. They are assume higher than in the analysis R, so the elastic field becomes larger.

The purpose of these two analyses is to investigate how the type of failure and the depth of the sliding surface varies, as a function of the failure parameters, also to the aim of finding a range of different mechanism failure, as it has done in the previous analyses about the influence of rain intensity.

8.3.3.1 Results of the Analysis M1

In this analysis the failure starts after tree days of rain (70 mm/day) and involves the top of the slope, the failure reaches the middle and the bottom after four rainy days (*fig. 8.34*). The failure could be defined *general* like in the Analysis R. The depth of the sliding surface is between 1.50 - 2.00 m and it lies in the soil 3 or at contact between the soil 2 and 3 (*fig. 8.35*).

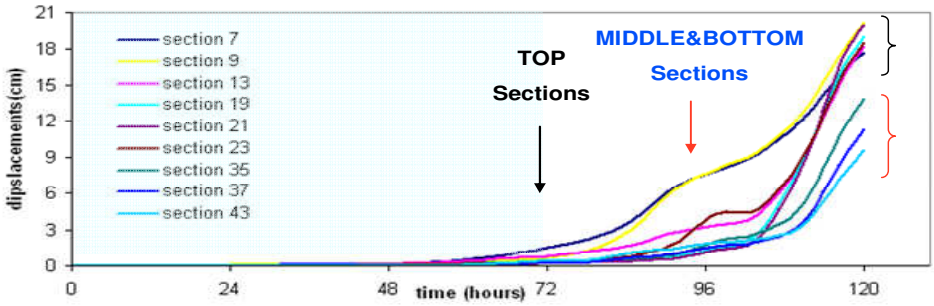

Fig.8.34: Superficial displacements calculated in some vertical sections during five rainy days

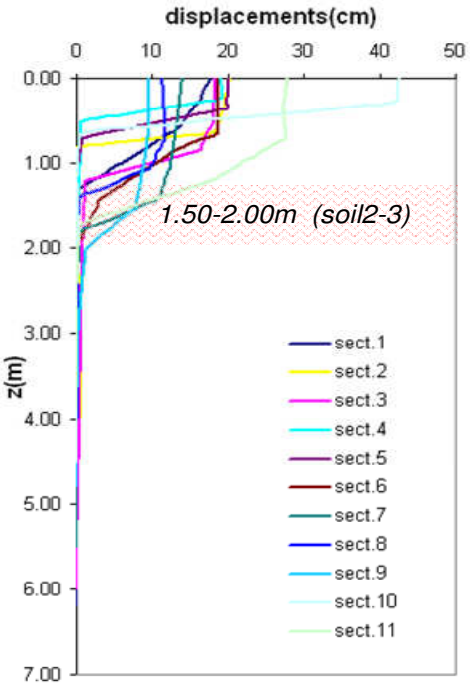

Fig.8.35: Profiles of displacement of some vertical sections at the fifth day of the rainfall

The type of failure does not change respect the analysis R, only the depth of the sliding surface increases and it reaches the soil 3 (Pumices of Avellino), this agrees with the angle of shearing resistance smaller than that used in the analysis R. So the failure involves the soil 3 too. The profile of pore water pressure becomes compressive after tree days at the top section (*fig.8.37a*) and after four days at the middle and bottom sections (*fig.8.37b,c*). At failure the compressive pore water pressure is between 4 and 12 kPa is at the depth of the sliding surface (*fig.8.37 a, b, c*). The value of Permeability at failure is that of the saturated soil in the superficial layers and in the soil 3 (pumices of Avellino). Saturated permeability is higher than the intensity rain, so the hypothesis that whole the rain infiltrates is reasonable (*fig.8.38a, b, c*). Changing the mechanical parameters, the mechanism of failure does not change, but the sliding surface becomes deeper.

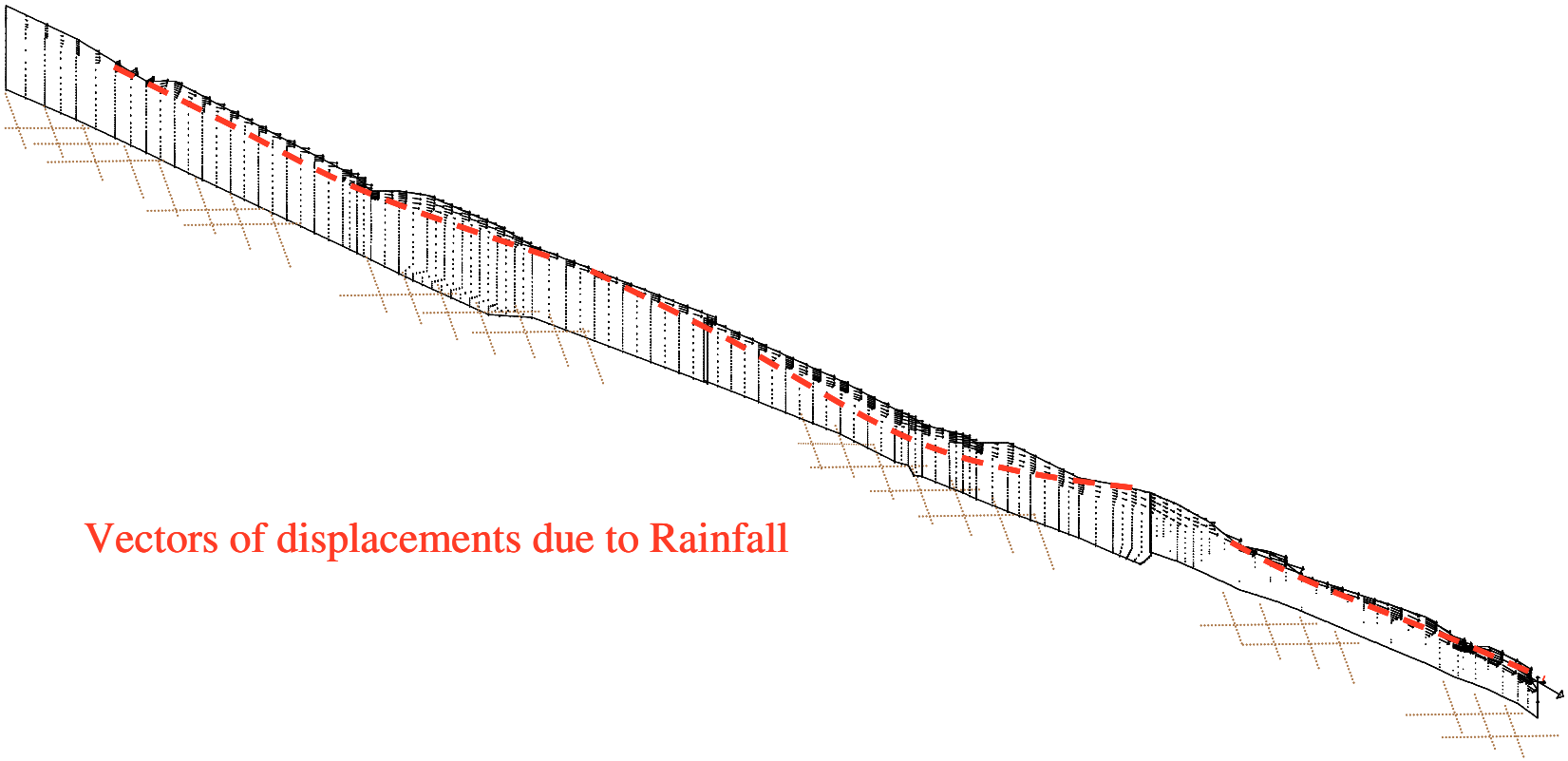

Fig.8.36: Vectors of displacements at failure (at the fifth day of the rainfall history)

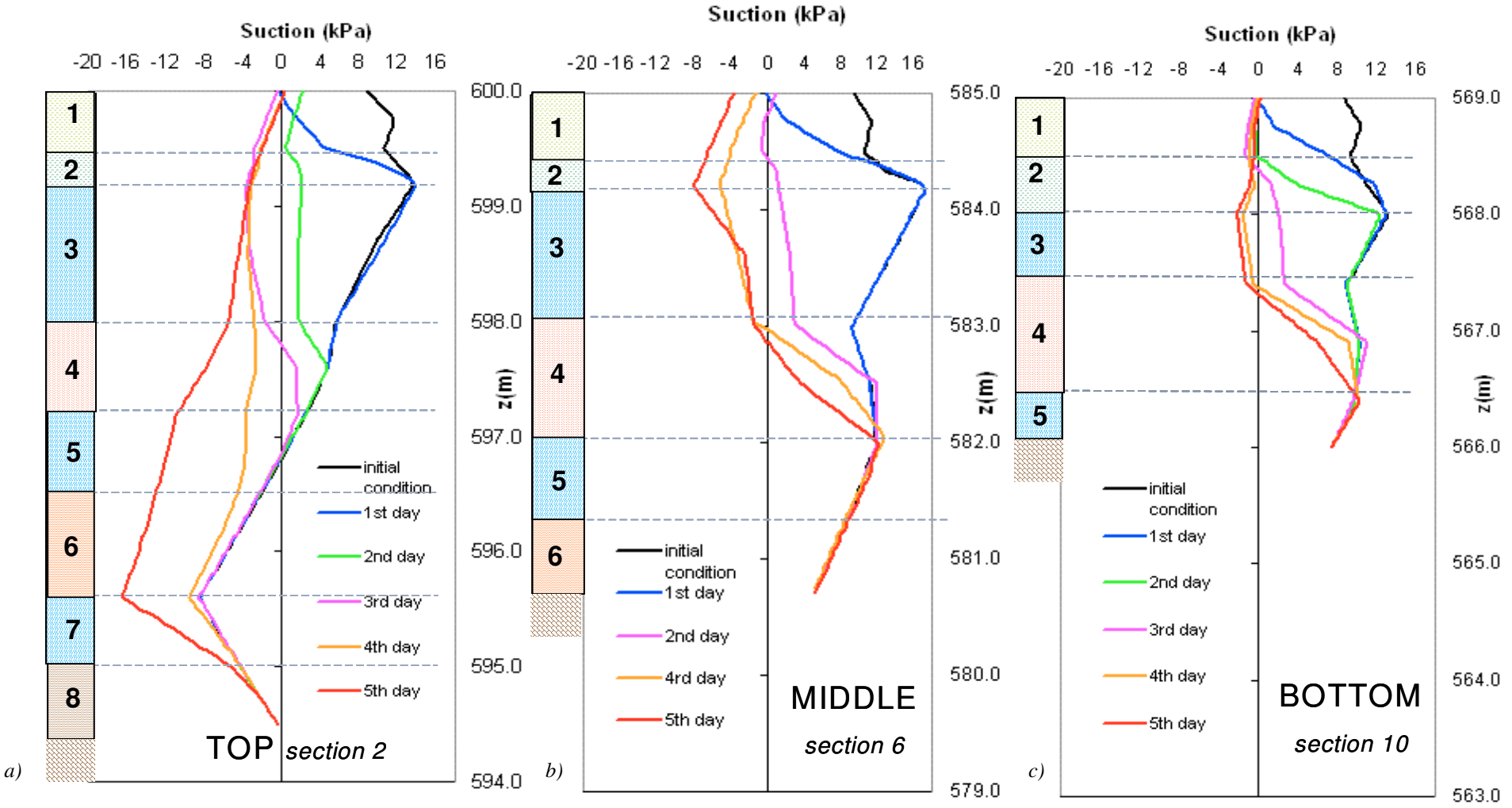

Fig.8.37: Profiles of pore pressure during the five days of the rainfall history along the section 2 (top slope) a), section 6 (middle slope) b), section 10 (bottom slope) c)

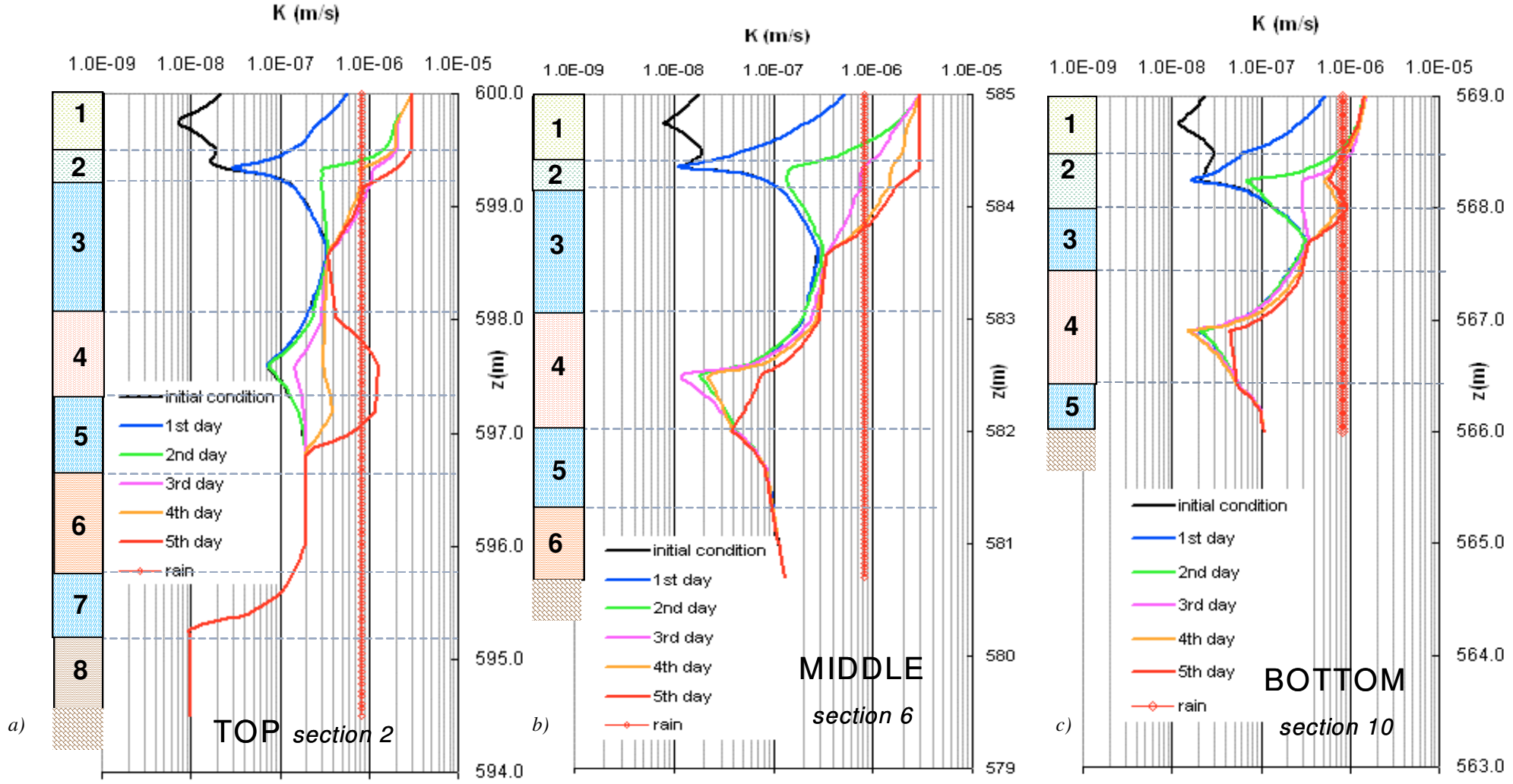

Fig.8.38: Profiles of permeability during the five days of the rainfall history along the section 2 (top slope) a), section 6 (middle slope) b), section 10 (bottom slope) c)

8.3.3.2 Results of the analysis M2

In this analysis the failure starts after four days of rain (70 mm/day) and involves the top of the slope; the instability reaches the middle and the bottom after five rainy days (*fig. 8.39*). The failure could be defined *general* like in the analyses R and M1.

The depth of the sliding surface is between 1.00 and 1.50 m; it lies in the soil 2 or at contact between the soils 2 and 3 (*fig. 8.40*).

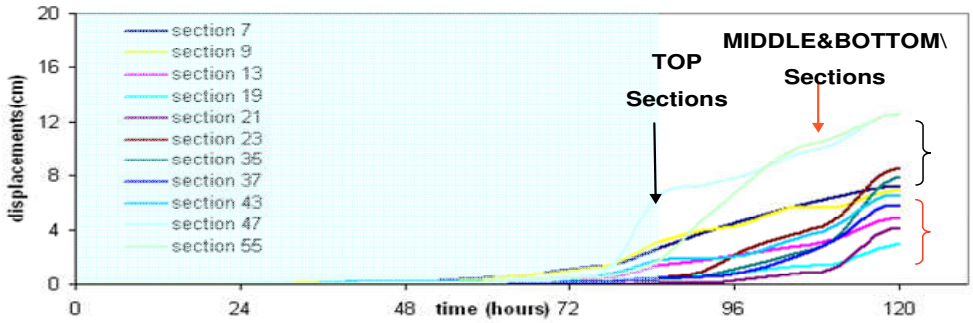

Fig. 8.39: Superficial displacements calculated in some vertical sections during five rainy days

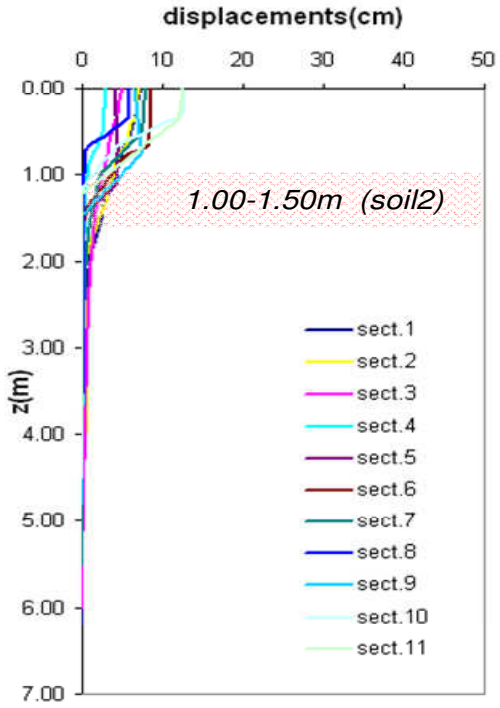

Fig. 8.40: Profiles of displacement of some vertical sections at the fifth day of the rainfall history

The type of failure and the depth of the sliding surface do not change respect to the analysis R, this means that the shape parameters α, μ don't influence heavily the failure mechanism, but they play a role on the starting time of the failure. In fact the higher values of α, μ make the elastic field larger and so they delay the plasticization yielding of the superficial soils, just where the failure happens. The profile of pore water pressure becomes compressive after tree days in the top section (*fig.8.42 a*) and after four days in the middle and bottom sections (*fig.8.42 b, c*). At failure, the compressive pore water pressure is between 4 and 12 kPa on the sliding surface (*fig.8.42a, b, c*). Permeability at failure is the saturated one in the superficial soils (*fig.8.43a).*

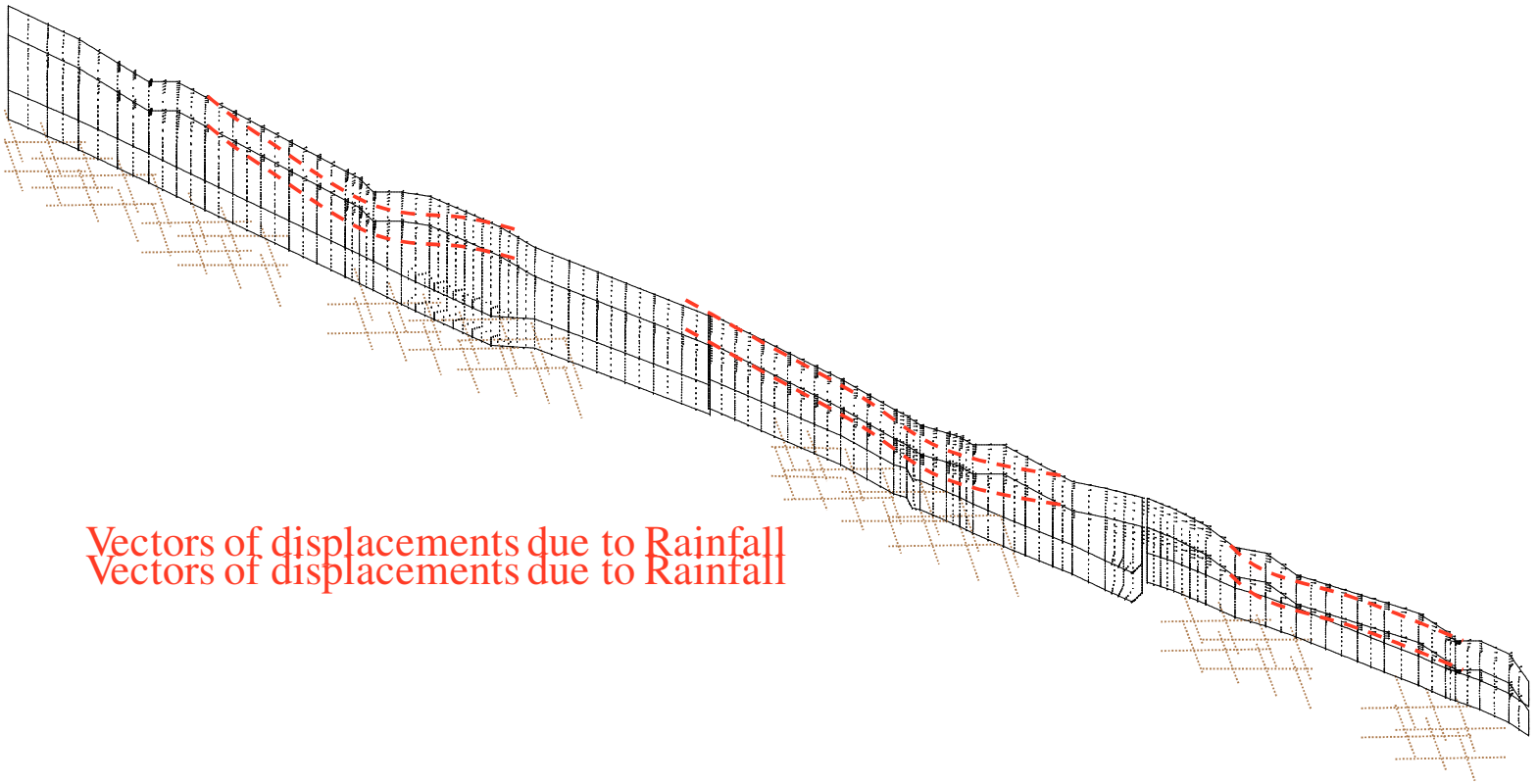

Vectors of displacements due to Rainfall

Fig.8.41: Vectors of displacements at failure (at the fifth day of the rainfall history)

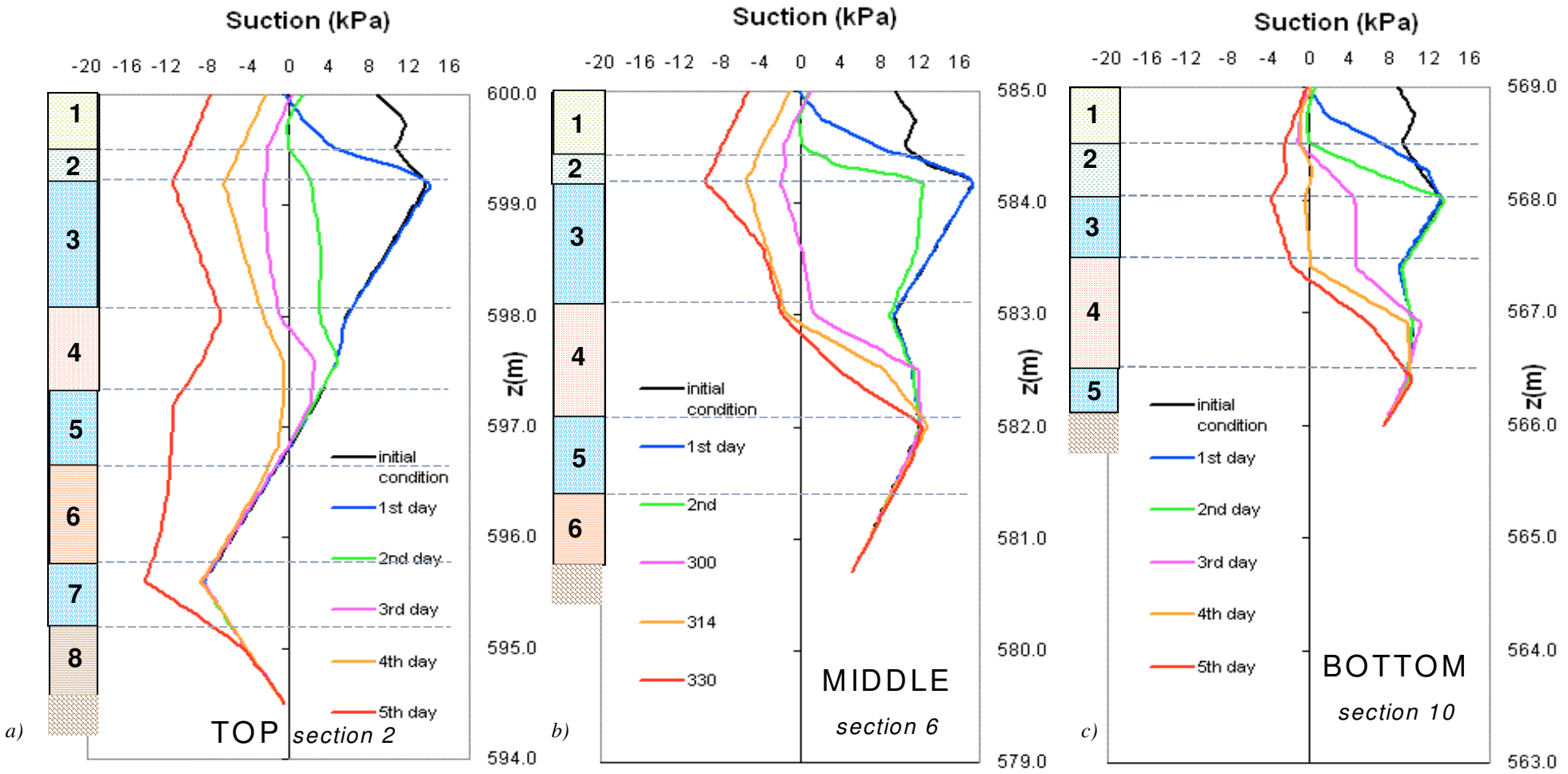

Fig.8.42: Profiles of pore pressure during the five days of the rainfall history along the section 2 (top slope) a), section 6 (middle slope) b), section 10 (bottom slope) c)

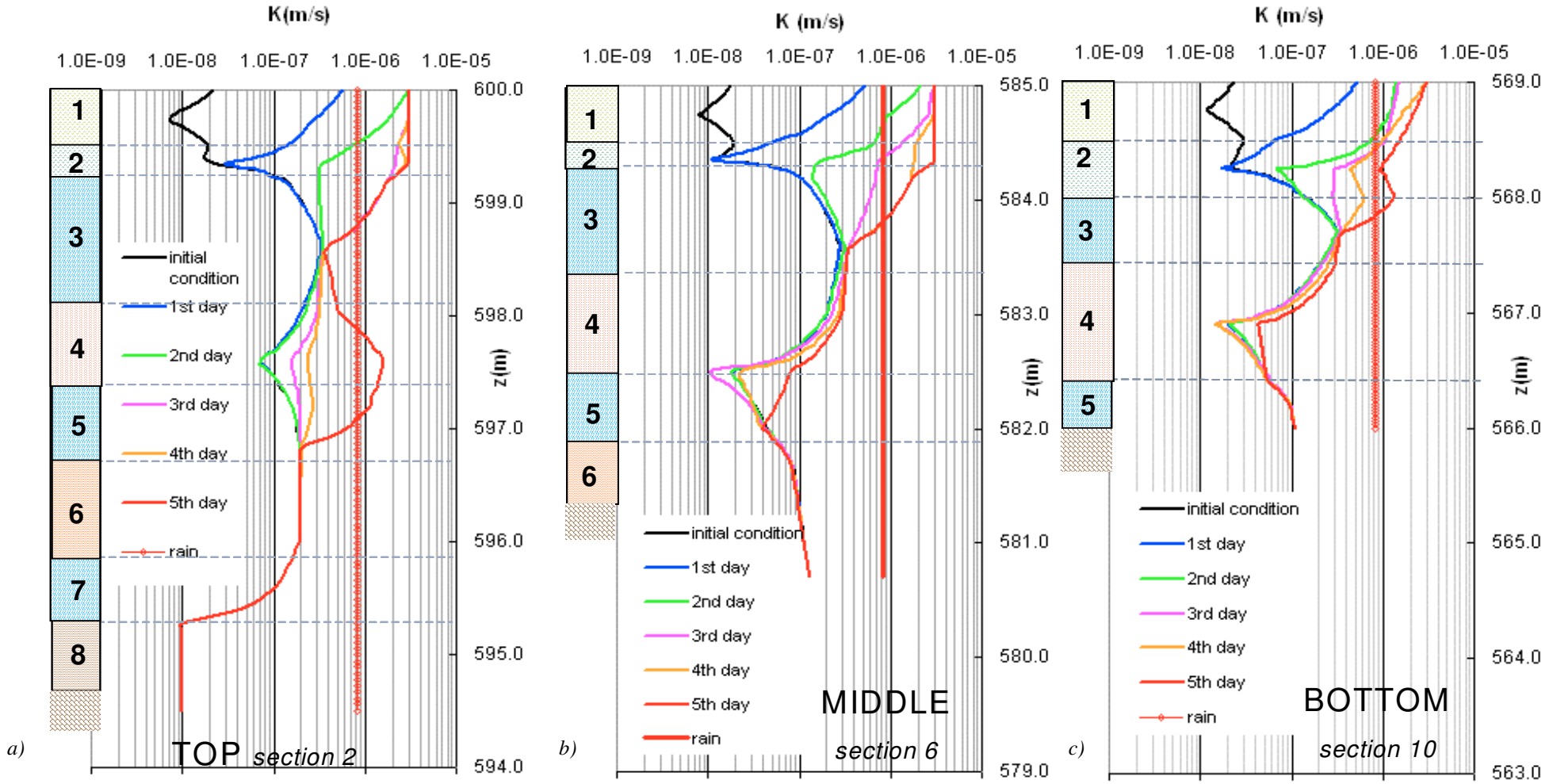

Fig.8.43: Profiles of permeability during the five days of the rainfall history along the section 2 (top slope) a), section 6 (middle slope) b), section 10 (bottom slope)

8.3.4 Analysis on the influence of the hydraulic characterization

In this analysis, the influence of hydraulic characterization is investigated. As there are no experimental data concerning the hydraulic behaviour of the soil 3 (Pumices of Avellino), it may be interesting to change the permeability curve and to analyse how the failure mechanism changes.

The analysis, called H1, is characterized by the same initial condition and by the same boundary conditions at the ground surface of the analysis R but by a different permeability curve for the soil 3. Essentially saturated permeability changes from the value $3.50*10^{-7}$m/s (analysis R) to the value $3.00*10^{-5}$m/s; in the *figure 8.44* the curve used in the model is reported.

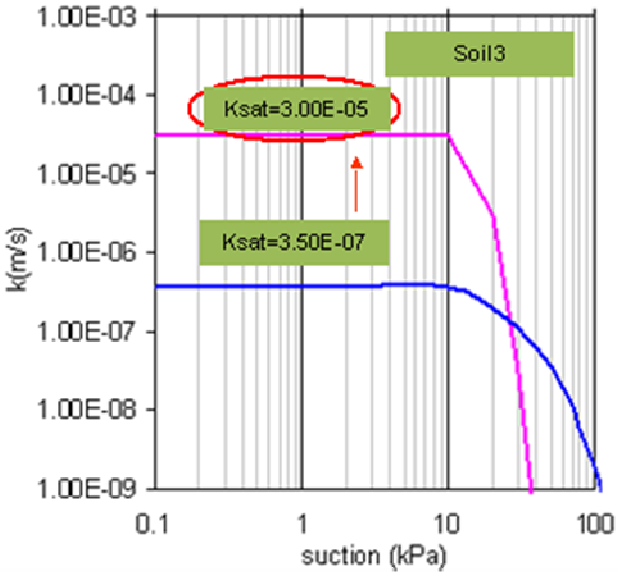

Fig.8.44: Permeability Curve used in the analysis H1

The range of suction in this analysis is between 1 kPa and 15 kPa and so the permeability corresponding to these values is the saturated one. The saturated permeability is increased of two orders of magnitude respect to that one used in the analysis R.

In this case in order to investigate the failure, it is necessary to apply six days with 70 mm/day of rainfall (the total rain is 420 mm). The failure starts after four days of rain (70 mm/day) and it affects the bottom of the slope. The instability reaches the top and the middle of the slope after five rainy days. The failure, as in the analysis R, is extended but more rain has to fall to generate instability (*fig.8.45*).

The depth of the sliding surface is between 1.50 and 2.50 from the ground surface; it lies at the contact between the soil 3 and the soil 4 (*fig.8.46*).

The pore water pressure is compressive at failure and the peak of pore pressure (10 kPa-20 kPa) establishes at the contact between the soil 3 and the soil 4 where the sliding surface lies (*fig.8.47*). Being the soil 3 more permeable than in the analysis R, water infiltrates easily

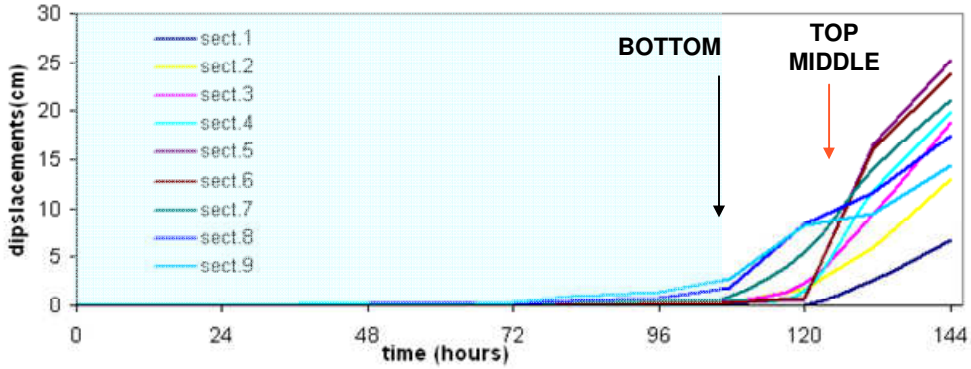

Fig.8.45: Superficial displacements calculated in some vertical sections during six rainy days

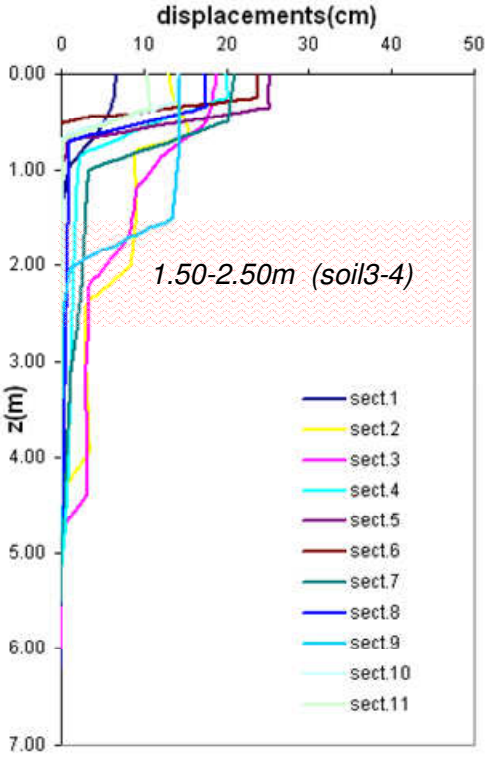

Fig.8.46 : Profiles of displacement of some vertical sections at the sixth day of the Rainfall history

from superficial soils to the soil 4 and the pore pressure becomes compressive at contact between the soil 3 and 4, generating the failure.

At the failure the permeability is the saturated one inside soil 3, along all the vertical sections investigated. The saturated permeability of soil 3 is higher than that of the superficial soils (1-2) and the intermediate soil (4) respectively sited above and below the layer 3 (*fig.8.49*).

Making the soil 3 more permeable, the type of failure remains *general* as in the analysis R but the depth of the sliding surface increases and it reaches the soil 4. This is reasonable because the soil 3 allows that more water cross itself and arrives in the soil 4 where pore pressure increases and then the sliding surface establishes. So the right hydraulic characterization for the pumices of Avellino (soil 3) plays a key role to analyse the real mechanism of failure.

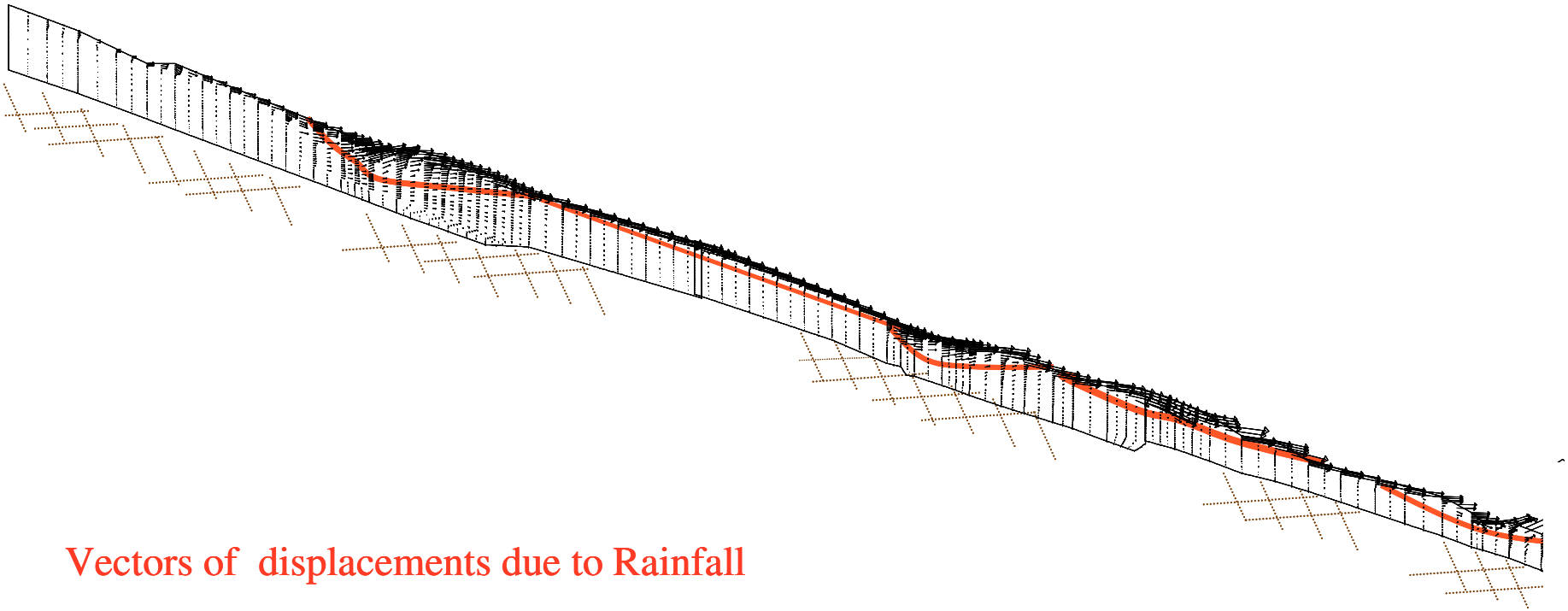

Fig.8.47: Vectors of displacements at failure (at the sixth day of the rainfall history)

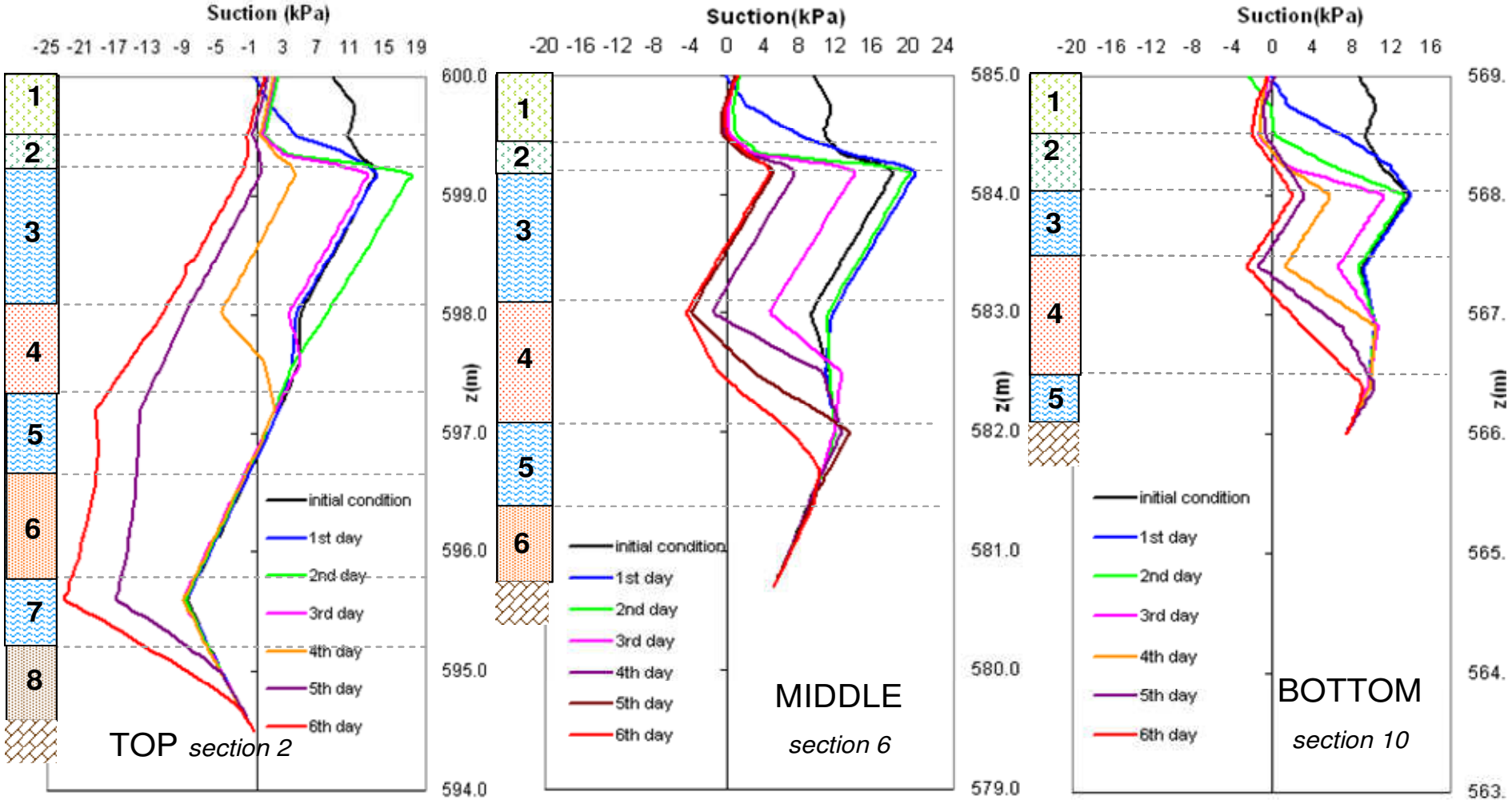

Fig.8.48: Profiles of pore pressure during the six days of the rainfall history along the section 2 (top slope) a), section 6 (middle slope) b), section 10 (bottom slope) c)

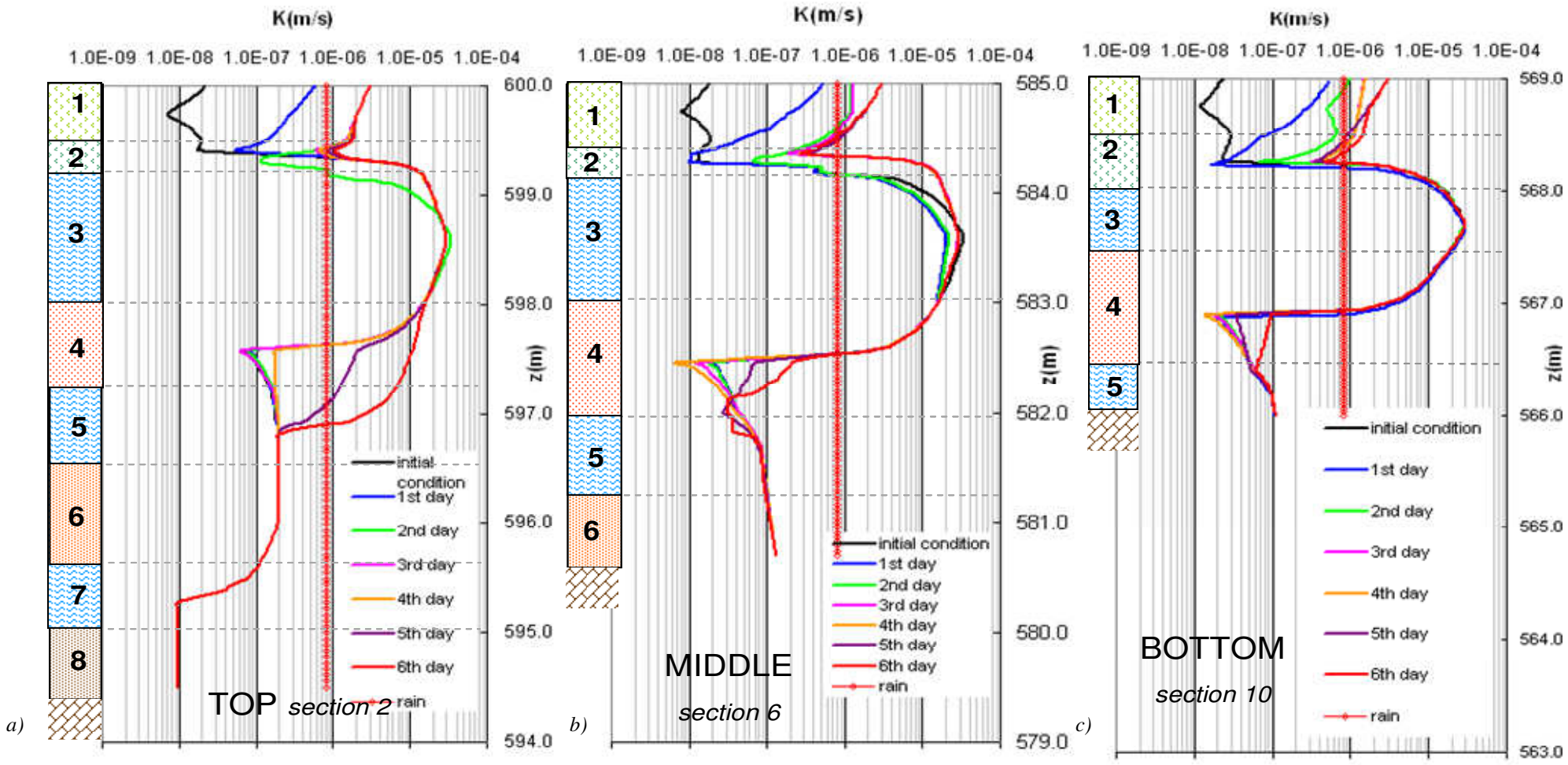

Fig.8.49: Profiles of permeability during the six days of the rainfall history along the section 2 (top slope) a), section 6 (middle slope) b), section 10 (bottom slope) c)

Discussion

If the saturated permeability of soil 3 is increased in the analysis H1 respect to the first hypothesis R, the depth of sliding surface increases and it lies at the contact between the soil 3 and 4, according to the experimental evidence (*fig.8.50*). In fact, in some zones close to the testing site, the superficial soils (1-2) and the pumices of Avellino (soil 3) miss. This observation proves that the failure occurred at the base of soil 3.

Being the soil 3 more permeable in the analysis H1 than in the analysis R, more water reaches the soil 4 and the pore pressure in this soil becomes compressive.

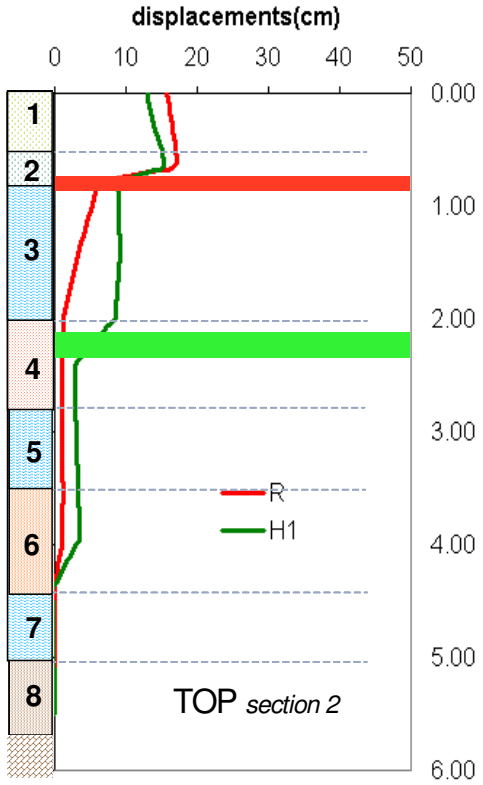

Fig.8.50: Comparison between the profiles of displacements at failure, along section 2, in the analysis R and H1

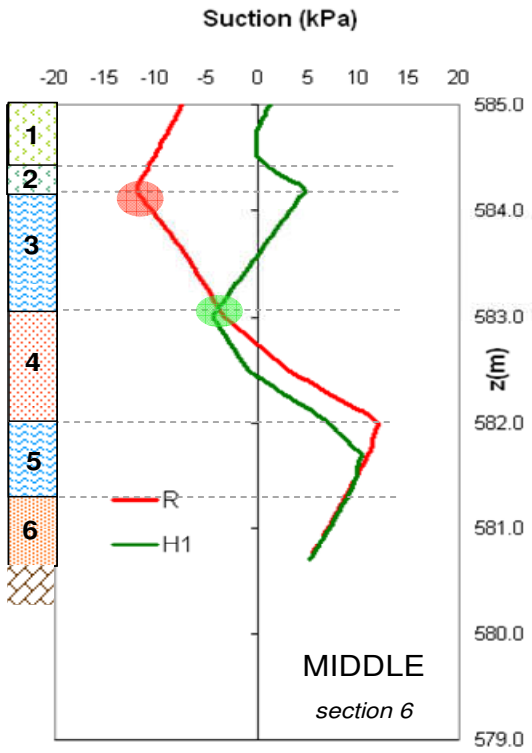

Fig. 8.51: Comparison between the profiles of suction at failure along section 6 in the analysis R and H1

Observing the profile of suction along the vertical 6 of the domain analysed (*fig.8.51*), it is clear that the peak of suction is located where the sliding surface lies, at the contact between the soil 2 and 3 in the analysis R, at the contact between the soil 3 and 4 in the analysis H1. It takes the value of 5 kPa in the first case and of 10 kPa in the last one.

8. 3. 5 Investigation on the influence of the initial conditions on slope stability

In this analysis, called I, the influence of initial condition on the results of slope stability analyses is investigated. These conditions at the ground surface and the mechanical and hydraulic characterization in the soils are those used in the Analysis R. The initial condition refers to the conditions established on 10th May 2007 in the analysis over the hydrological year. In any way the data chosen like initial conditions belong always to the wet season in order to investigate the period more dangerous for the slope stability. The difference in terms of suction between initial conditions used in the Analysis R (31st January 2007) and I (10th May 2007) is not very large, in fact, according to the experimental data(Chapter 5), suction varies between 5 and 20 kPa in the superficial soils (soil 1-2), between 10 and 15 kPa in the intermediate soils (soils 4) during the winter-spring season (*fig.8.52*).

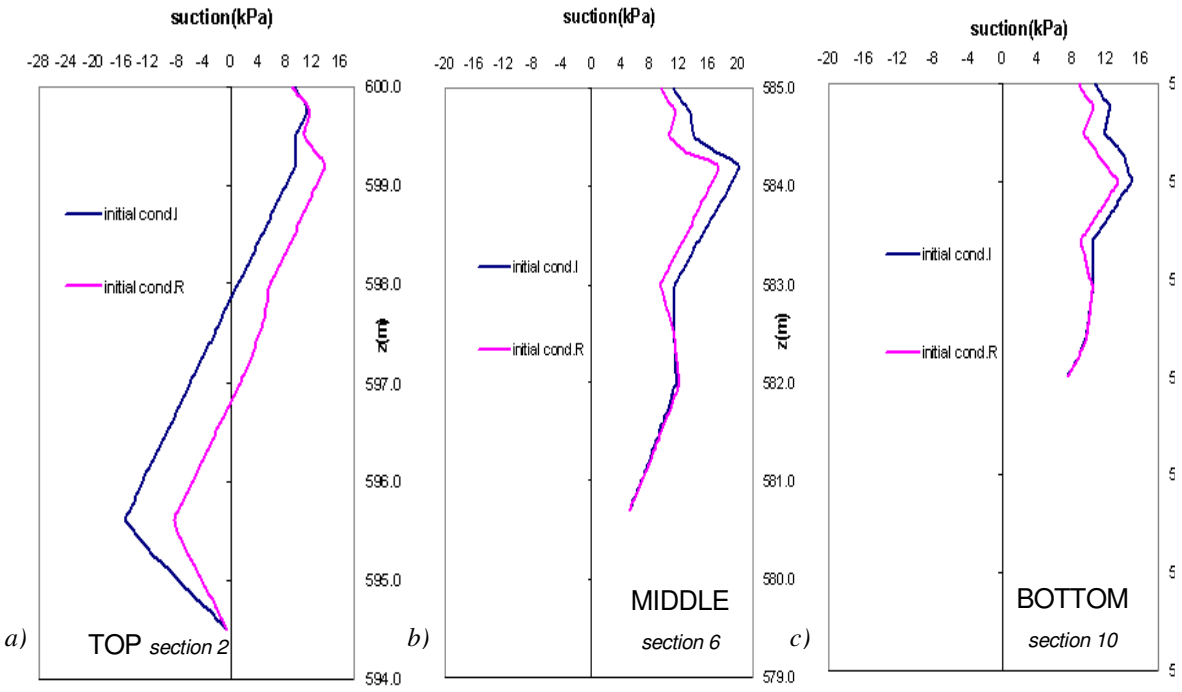

Fig.8.52: Comparison between initial condition in the analysis R and I in the section 2 a), in the section 6 b), in the section 10 c)

The failure starts after tree days and involves the top slope, it reaches the rest of the slope after four days. The type of failure results *general* and it is equal to that of the analysis R (*figs.8.53-8.55*).

The depth of the sliding surface is between 1.00 and 1.50 m; it lies in the soil 2 and 3, so the failure could be defined superficial as in the analysis R (*fig.8.54*).

The pore water pressure becomes compressive when the failure starts (the third, fourth day), just at the depth of the sliding surface. The pore pressure at failure is around 4-20 kPa; the highest value occurs in the the top of the slope, the smallest one in the bottom and the middle (*fig.5.56*).
Moreover the permeability at failure reaches the saturated value in the superficial soils (*fig.8.57*).

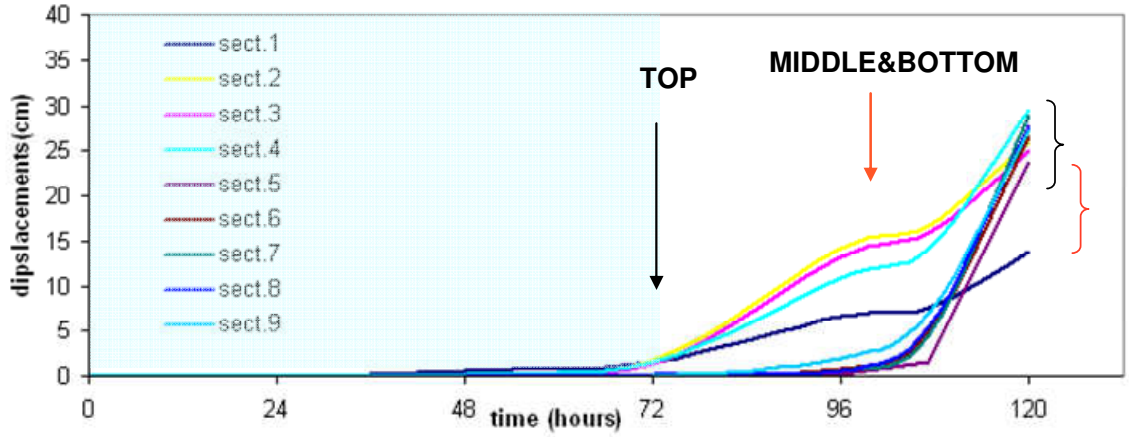

Fig.8.53: Superficial displacements calculated in some vertical sections during five rainy days

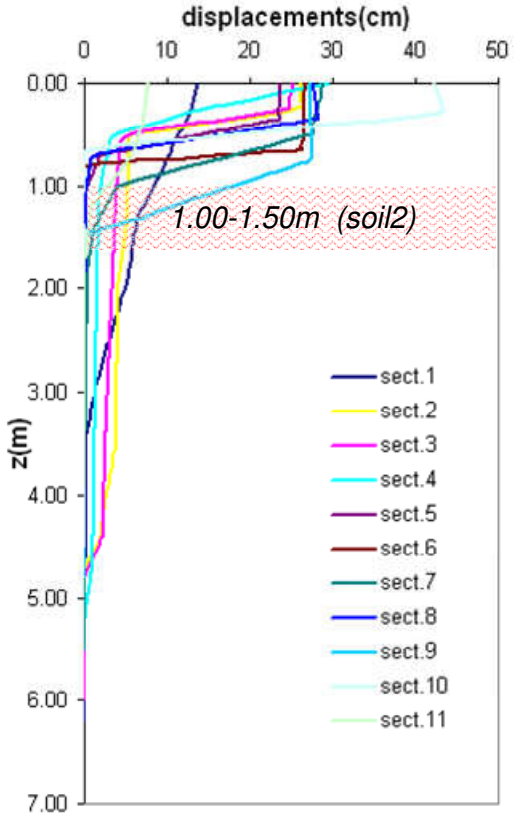

Fig.8.54: Profiles of displacement of some vertical sections at the fifth day of the rainfall history

The initial conditions are obviously very important to determinate the failure mechanism, because they establish, first of all, the hydraulic conditions in the slope. The water content present in subsoil before the landslide, influences the quantity of water enough to generate the failure. In this case, during the wet period (winter and spring), the water content oscillates slightly around a constant average value, so inserting as initial condition a day in the spring or in the winter gives the same results.

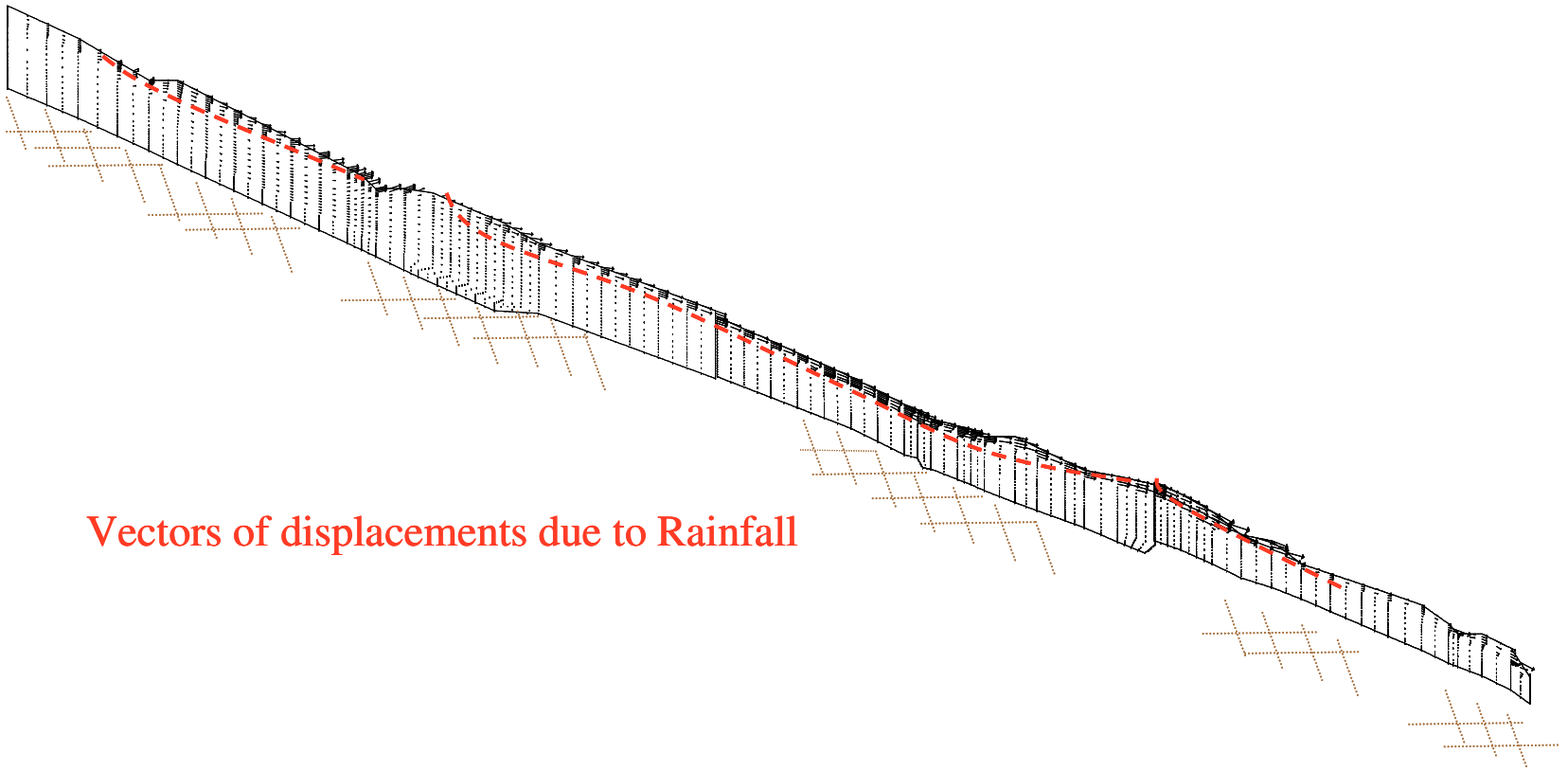

Fig.8.55: Vectors of displacements at failure (at the fifth day of the rainfall history)

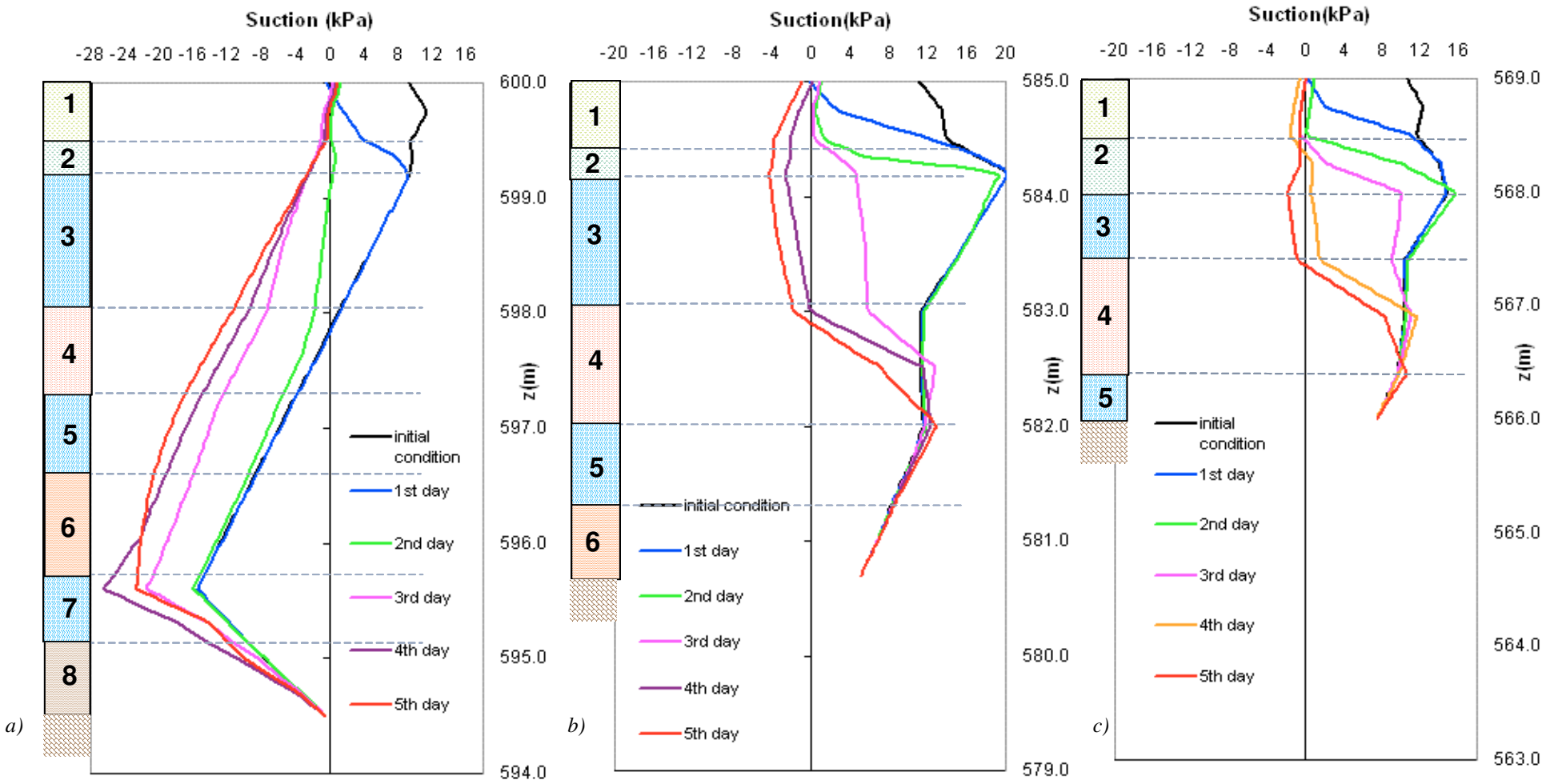

Fig.8.56: Profiles of pore water pressure during the five days of the rainfall history along the section 2 (top slope) a), section 6 (middle slope) b), section 10 (bottom slope) c

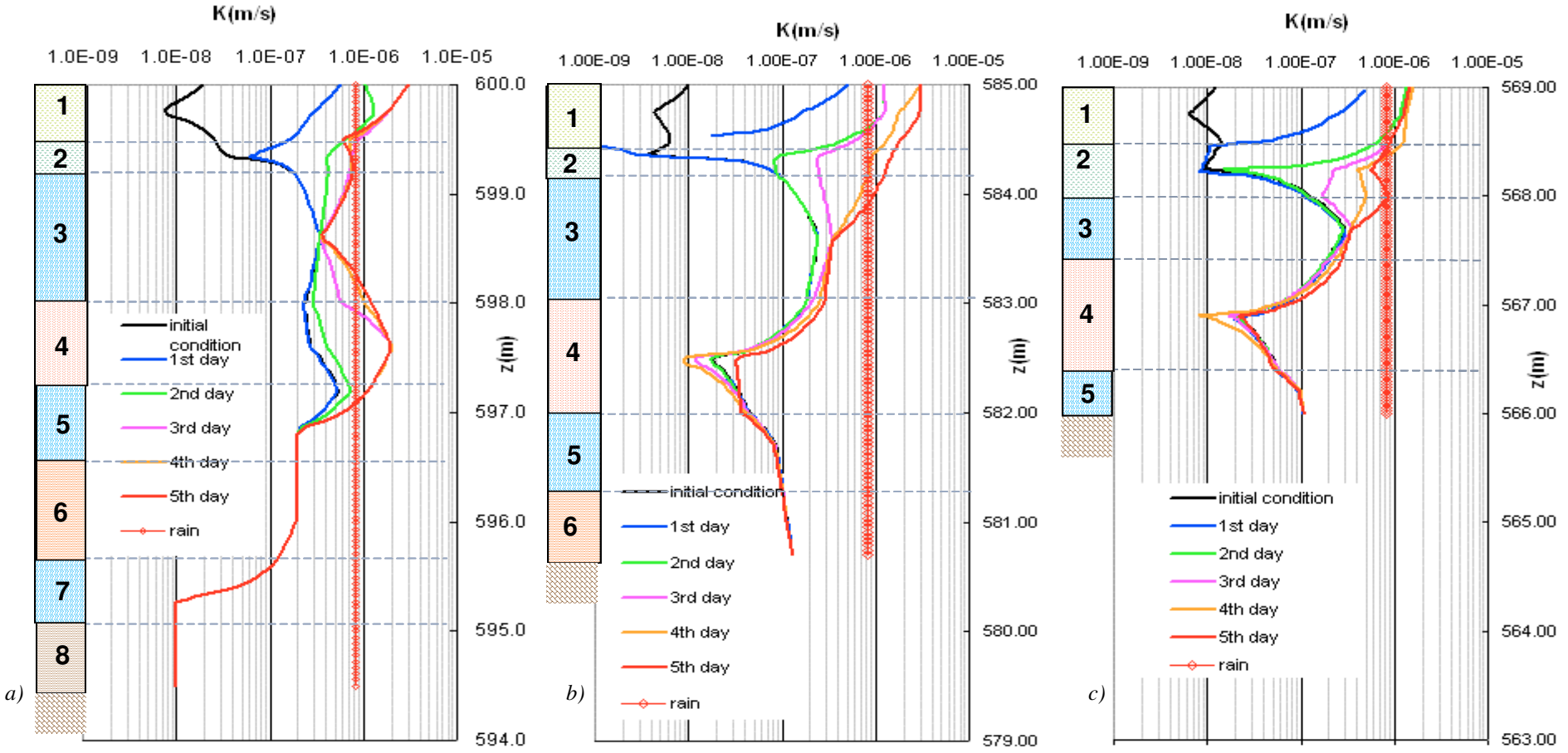

Fig.8.57: Profiles of permeability during the five days of the Rainfall history along the section 2 (top slope) a), section 6 (middle slope) b), section 10 (bottom slope) c)

Concluding Remarks

The parametric analyses shown in the previous sections are carried out to investigate the influence of intensity of rain, mechanical and hydraulic characterization and initial conditions in terms of suction on the failure mechanism. The numerical results obtained suggest that the major role is occupied by the rain intensity, cumulated rainfall and the hydraulic characterization. The following conclusions could be drawn:

The *total quantity of rain* enough to generate instability depends on the water content in the subsoil, because it represents a factor predisposing the slope to the failure. In the domain analyzed, the wet period is characterized by constant mean water content. Either the winter and the spring are the seasons from which to begin the study of the slope stability, in the sense that it is indifferent the day from which the analysis could starts during the wet seasons. A quantity between 200 and 250 mm of rain is necessary to generate the triggering mechanism in the domain analyzed, regardless its daily distribution.

The *rain intensity* plays a key rule in the failure mechanism, in fact it determines the type of failure and the depth of the sliding surface. Assigned the domain with the specific geometry and topography, as that analyzed, the rain intensity less than or equal to the yearly average couldn't cause the failure (because the stationary conditions establish). The slope can find the hydraulic equilibrium under mean rain applied at the ground surface.

Rain smaller than 35mm/day causes a deep sliding surface, because a rain of these intensities can infiltrates in the deeper soils before affecting the slope stability. Moreover the depth of the sliding surface goes down where the excavation or other irregularity are present on the slope; so the topography influences the soils involved by the failure too. Rain intensity higher than 70 mm/day causes the general failure involving the whole slope, in fact the most intensive rains affect all the slope and the superficial soils, having no time to reach the deeper soils.

The *mechanical characterization* influences the depth of the sliding surface only. In particular more soil 3 (pumices of Avellino) is weak, more the sliding surface becomes deep. The type of failure (general or local) and the values of pore water pressure which cause the instability seem not to be influenced by the angle of friction resistance.

The *hydraulic characterization* heavily influences the failure mechanism, in fact a right characterization is necessary to identify a correct failure mechanism. The depth

of the sliding surface and the pore pressure which cause the instability change completely varying the permeability curve of the soils.

In order to use the results of the numerical analysis, like a warning system (*Chapter 9*), first of all it is important to have a *right experimental hydraulic characterization* of all the soils involved: the retention curves and the permeability curves, either in wet and in dry conditions. After reproducing the domain to be analyzed (with all the its details an excavation, road etc…) and adopting the right hydraulic and mechanical characterization for all the soils, it is possible to start from any day belonged to wet period (winter or spring) and then to investigate the stability of slope subjected to different pluviograms.

Chapter 9

Results of slope stability analyses and failure forecasting

9.1 Synopsis

In this chapter the study of potential failure mechanisms and the definition of the critical thresholds, in terms of rainfall inducing landslides, are presented by using results of the numerical analyses.

By evaluating data from slope stability analyses (*Chapter 8*), it was possible to determine which mechanical and hydraulic parameters heavily influence the type of failure and how the triggering mechanism changes, varying the climate conditions at the upper boundary. The use of these observations in practical field is reasonable if it is referred to situations that are similar to the case studied, as regards the stratigraphy and the mechanical and hydraulic properties of the soils as that reproduced in the analyses. This occurs in a large part of the Campania Region.

Moreover the processing of these results (as suction values at failure, cumulated rainfall generating collapse and number of days over which it is applied) allowed to develop the critical threshold in terms of daily rain intensity.

9.2 Analyses of failure mechanism

It's know from experience and historical data that debris flows are induced by heavy rainfalls (*Cascini et al., 2005*). Therefore rain represents the more common triggering factor, but many other ingredients interact and influence the failure mechanism (*Nicotera et al. 2008*), as: hydraulic characteristics of soils (represented by means of water retention curve and permeability curve), morphological irregularity of slope (cut, excavation, etc..), stratigraphy (presence of pumices interposed between cineritic strata), initial water content in the soil, hydro-geological conditions.

Because of interaction of all the phenomena mentioned, a unique relation between the return periods, T[1], of rainfall causing failure and that one of the landslide, probably does not exist. The former is calculated by statistical data, the latter is obtained by historical documents (*Cascini et al., 2002*).

Critical thresholds, in terms of intensity and duration of rainfall, were developed in order to predict landslides and to generate an alarm system. These curves were defined by computing historical series of rainfall measured; so they are valid at regional scale only (*Calcaterra et al., 2000; Guadagno et al., 1991*)(*Fig. 9.1*). This approach to the prevision is based on the statistical interpretation of rainfall, but it does not take into account other factors as stratigraphy, initial water content in the subsoil and as the hydraulic properties of soils.

It's clear that thresholds obtained in this way have a limited validity, hence they could be useful to develop alternative procedures in order to consider the rule of many factors interacting with the triggering mechanism. Numerical analyses may be a tool to investigate the failure mechanism, to understand the influence of each factor and to check the effectiveness of existing thresholds.

However, before considering reasonable results of *slope stability analyses*, the model used has to be validated, so the hydraulic analyses should be made in order to reproduce the observed conditions in site, in terms of suction and water content measurements.

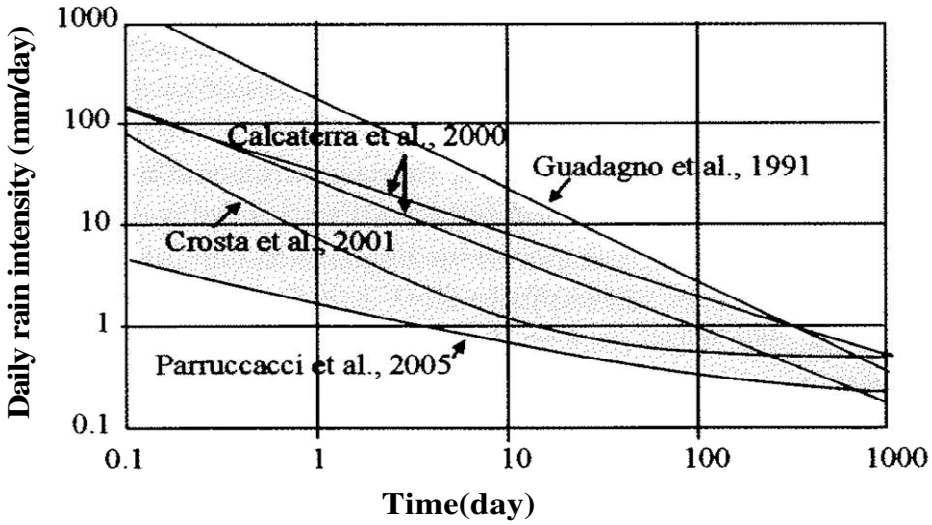

9.1: Critical threshold calculated in Campania Region

[1] The return time of a natural event characterized by a particular intensity is defined as the reverse of occurrence probability P over one year: $\frac{1}{P}$; the not occurrence probability over one year is (1-P), over N years is $(1\text{-}P)^N$.

Therefore the occurrence probability over N years is: $H(N) = 1-(1-P)^N = 1-(1-\frac{1}{T})^N$.

9.2.1 Hydraulic analyses: simulations of observed conditions

The analysis of "hydraulic regime" in subsoil is not very easy, the hydraulic properties change heavily with the depth and with time, as a consequence of climate conditions. In fact in Campania Region pyroclastic soils are usually spaced by the pumices layers (Avellino eruption, Ottaviano eruption and Agnano eruption); the former soils are characterized by a saturated permeability two order of magnitude higher than the latter ones (*Papa, PhD thesis 2007*). Moreover the hydraulic behavior of superficial soils is hysteretic (*Nicotera et al., 2008*), so suction and water content are independent variables, depending on meteorological conditions.

In order to investigate the distribution of pore water pressure in subsoil, and to calculate the water balance at soil surface, it is important to collect measurements of *suction* and *water content* in the subsoil, *climatic conditions* (rain, air temperature, air humidity) at the surface (*Chapter2*). These measurements, together with a correct hydraulic characterization of soils allow to carry out analyses reproducing the conditions measured over one year, in order to validate the model and to use it as a tool for forecasting.

By using a finite element program, i.e. ICFEP, the real stratigraphy can be reproduced and the mechanical-hydraulic coupled model for partially-saturated soils can be used to characterize the domain. Applying as upper boundary, the climate conditions measured in site during one year, pore water pressure distribution in subsoil is calculated and the measurements collected at the same depth in site are compared with them, in order to validate the model (*Chapter 4*). If the agreement is good, as for the superficial and the intermediate soils of the testing site analyzed in this PhD thesis, it is reasonable to investigate the failure mechanism, starting from wetter conditions reproduced by the analyses of one hydrologic year.

9.2.2 Mechanical - Hydraulic coupled analyses: prevision of failure mechanism

After reproducing the "observed conditions" to validate the model, the failure mechanism can be studied. At this aim a FEM code may be a good tool to study the triggering mechanism, because it allow to provide the evolution of strains as a function of the critical rainfall inside the domain analyzed and the sliding surface is automatically localized.

Carrying out parametric analyses it was possible to study in this thesis the influence on triggering mechanisms of: 1) hydraulic and mechanical characterization of soils, 2) the initial condition, and 3) the rain intensity.

By elaborating results of slope stability analyses, relations between the daily rain intensity generating failure, number of rainy days and initial volumetric water content, could be developed.

9.3 Results of slope stability analyses

The influence on failure mechanism of all the parameters investigated in slope stability analyses (*Chapter 5*) is summarized briefly in the following.

The *mechanical characterization*, specially in terms of critical state angle, φ'_{cr}, seems to influence the depth of sliding surface only.

The *hydraulic characterization* plays an important rule as it influences the quantity of cumulated rainfall causing the failure and the depth of sliding surface. In fact the variations of suction due to rainfall depend on the *retention curve* and *permeability curve* adopted. The pumice layers are interposed between the pyroclastic layers and so they influence the water flow balance in the soils and the distribution of pore water pressure. Unfortunately these soils are difficult to characterize because are not sampled easy, but in order to generate a right prevision of triggering mechanism, it is necessary to know the hydraulic properties of all the soils involved.

The *initial conditions*, essentially the initial distribution of water content in the soils, influences the total quantity of rainfall causing the failure. It is possible to establish the relation between the cumulated rainfall distributed on successive days and the initial value of water content.

After assigning the hydraulic and mechanical characterization to the domain, the rule of *rain intensity* has to be investigated. From results of analyses carried on, daily rain intensity determines the type of failure and the depth of sliding surface, so the wide range of collapse mechanism may be investigated applying different rainfall history on the upper boundary.

Apart the type of failure mechanism and the depth of sliding surface, it is worth to know how much *cumulated rainfall* is able to cause the failure, which rule the daily rain intensity plays and which suction value could be a pointer of collapse.

The total quantity of rain causing failure is influenced heavily by the initial water content, but its daily intensity value has not to be lower than the intensity average over year, 15 mm/day. In winter, water content in the subsoil is very high as the soils are close to saturation, the total rain quantity necessary to the failure is smaller than in other seasons. The pore water pressure at failure on the sliding surface are always compressive almost 5 kPa.

In the table 6.1, the influence of all parameters analysed on the failure mechanism are pointed out.

Tab. 9.1: Influence of the parameter analyzed on the failure mechanism

	Type of failure	**Depth of sliding surface**	**Suction value at failure**	**Critical Cumulated Rainfall**
Hydraulic Characterization	X	X	X	X
Mechanical characterization	-	X	-	-
Initial Condition	-	-	X	X
Rain intensity	X	X	X	X

9.3 Elaboration of critical threshold

In order to evaluate the *suction values* at failure, the evolution at the depth of the sliding surface of pore water pressure over the rainfall history applied in the slope stability analyses (*Chapter 8*) are plotted (*Fig.9.2*).

In the *figure 6.2* the pore water pressures are the values averaged over the points reaching the failure in the same time along the sliding surface. Therefore, the curves plotted refer to different depths because the sliding surface for each analysis lies in different soils; in analyses R, R_4, R_2, M_1, I, the depth is between 1.00 - 1.50 m (superficial soils, 1-2), in the analyses R_1, R_3 it is 4.00 - 5.00 m, in the analysis H_1 it is 2.00 - 2.50 m. The initial suction values of the analyses R, R_4, R_2, M_1, are 14-16 kPa, at depth of 1.50 m from ground surface; those of the analyses I, H_1 are smaller because they refer respectively to different initial conditions and to deeper sliding surface. The initial suction values of analyses R_1, R_3 are already negative (compressive pore water pressure), 4 kPa, and they refer to 4.00 m from ground surface where the sliding surface occurs.

The pore water pressure values at failure are between 3 kPa - 4 kPa for the analyses where the initial values are tensile and between 10 kPa - 12 kPa for analyses where the initial values are compressive.

The collapse occurs when soils become saturated, but the pore water pressure values at failure change in function of the depth of sliding surface which is a function of the daily rain intensity. As the hydraulic characterization for the deeper soil was not validated (*Chapter 7*), the exact position of sliding surface when the failure involves the deep soils is not reliable.

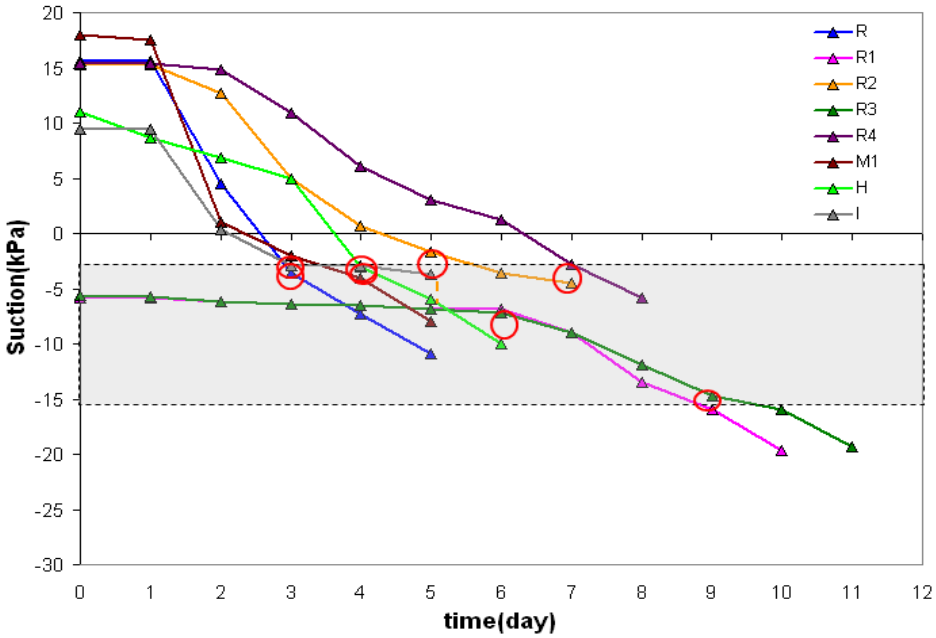

Fig.9.2: Suction over the duration of rainfall history applied in slope stability analyses

In the *figure 6.3* the total quantity of rainfall causing the failure against the initial suction value is plotted for each slope stability analysis.

The total quantity is calculated as the cumulated rainfall which has still to fall in order to cause the failure and the suction value are these calculated on the sliding surface. The curves of analyses R, R_4, R_2, I refer to the depth of sliding surface of 1.00 - 1.50 m (soil2) while the curves of analyses R_1, R_3 to the depth of 4.00 m (soil6). Evaluating the curves of analyses R, R_4, R_2, 210 ÷ 240 mm of Rain should fall to cause failure in the superficial soils at the initial suction value of 16 ÷ 15 kPa and 100 - 80 mm at the initial suction value of 4÷6 kPa; when the pore water pressure are compressive it is enough the total rainfall smaller than 40 mm to cause the failure. Observing the curves of analyses R_1, R_3, for any cumulated rainfall causing failure, the pore water pressure is always compressive, this is because the initial value in the soil 6 is already compressive . Any total quantity of Rain between 240 ÷ 40 mm should fall in order to cause failure in the soil 6 at initial suction value between -8 ÷ -12 kPa, but it's important to point out that the daily rain intensity must be smaller than 35 mm/day in order to reach the soils deeper.

Therefore the relation between the total rain causing the failure and initial suction value at the sliding surface can be obtained and it is a function just of depth of sliding surface and so the daily rain intensity. In fact if , i.e., it is smaller than 35 mm/day, the variation of pore water pressure in the deeper soils due to rainfall applied occurs and the failure probably involves a larger volume of soils, otherwise the pore water pressure change only in the superficial soils and the sliding surface lies at few meters from ground surface.

Even the daily rain intensity smaller than the value averaged over one year, 15mm/day, it would not cause failure for any cumulated rainfall.

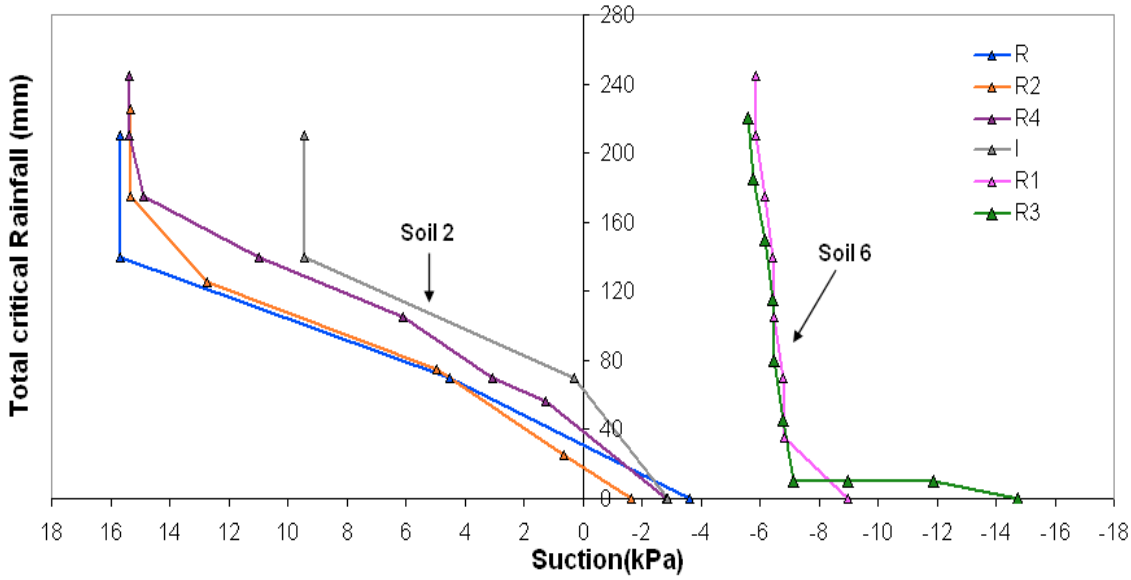

Fig.9.3: Total Rainfall causing failure against the initial suction values

In *figure 6.4* the points representing the mean daily rain intensity, I, and the number of days over which it should be distributed to cause the failure, d, are plotted; the red points refer to analyses R, R_4, R_2 where the sliding surface lies in the superficial soils (soil1-2), the blue and orange ones to analyses R_1, R_3 where the sliding surface lies in the deep soils (soil 4).
For analyses R, R_4, R_2 the points were calculated at four particular initial suction value on the sliding surface during the rainfall history: 15 kPa, 11 kPa, 4.5 kPa and 0 kPa (close to the saturation). By evaluating these points in the plane, I-d, these at the same initial suction value are interpolated by a exponential relation, $y = ax^b$, where a is a value bigger than one and b is a value negative and smaller than one; so four curves, ones for each initial suction value, can be drawn. These curves are very different, in fact keeping constant the daily rain intensity, it has to be applied over less days to cause the failure as more the initial suction value decreases, for example, 70 mm must fall for three days when the initial suction is 15 kPa, for half day when the initial suction is zero. Moreover the daily rain intensity establishing the steady conditions seems to change with the initial suction value, i.e., it is 15mm/day for 15kPa of initial suction value.
This is reasonable if the sliding surface lies in the soil 2 at 1.00-1.50 m from ground surface; as regards the sliding surface at 4.00 m, only two analyses are available, so two points for each initial suction value can be calculated, but they not would be enough to gain a curve.
In any way the critical threshold in terms of daily rain intensity is a function of initial suction value and of the depth of sliding surface, so, of the hydraulic and mechanical soil properties.

In the figures *6.5 - 6.7*, the threshold curves, I-d, concerning respectively the initial suction of 15 kPa, 11 kPa and 4.5 kPa and concerning the superficial failure only, are compared with the mean rain intensity curves calculated as a function of the daily rain intensity measured in testing site. Starting just from the day when the suction measurements were 15 kPa, 11 kPa and 4.5 kPa, the mean daily rain intensity is calculated as the daily rain measured in site cumulated over day by day and divided by the number of days over which it is being integrated.
The mean daily rain calculated starting from 25th November 2007 at initial suction value of 15 kPa (*fig.6.5*), is always below the daily rain intensity of 15mm/day which would not cause the failure according to the numerical results. The mean daily rain calculated starting from 8th November 2006, 6th December 2007, 21st February 2007 and 23rd November 2008 at initial suction value of 11kPa (*fig.6.6*), are always below the threshold curves at 11 kPa; in particular the curve of the 23rd November would cut the threshold curves if there was third rainy day.
The mean daily rain calculated starting from 10th December 2006, 8th February 2007, 25th February 2007, 26th March 2007 and 3rd December 2008 at initial suction value of 4.5kPa (*fig.6.7*), are always below the threshold curves at 4.5 kPa; the curve of the 3rd December would cut the threshold curves if there were other rainy days.

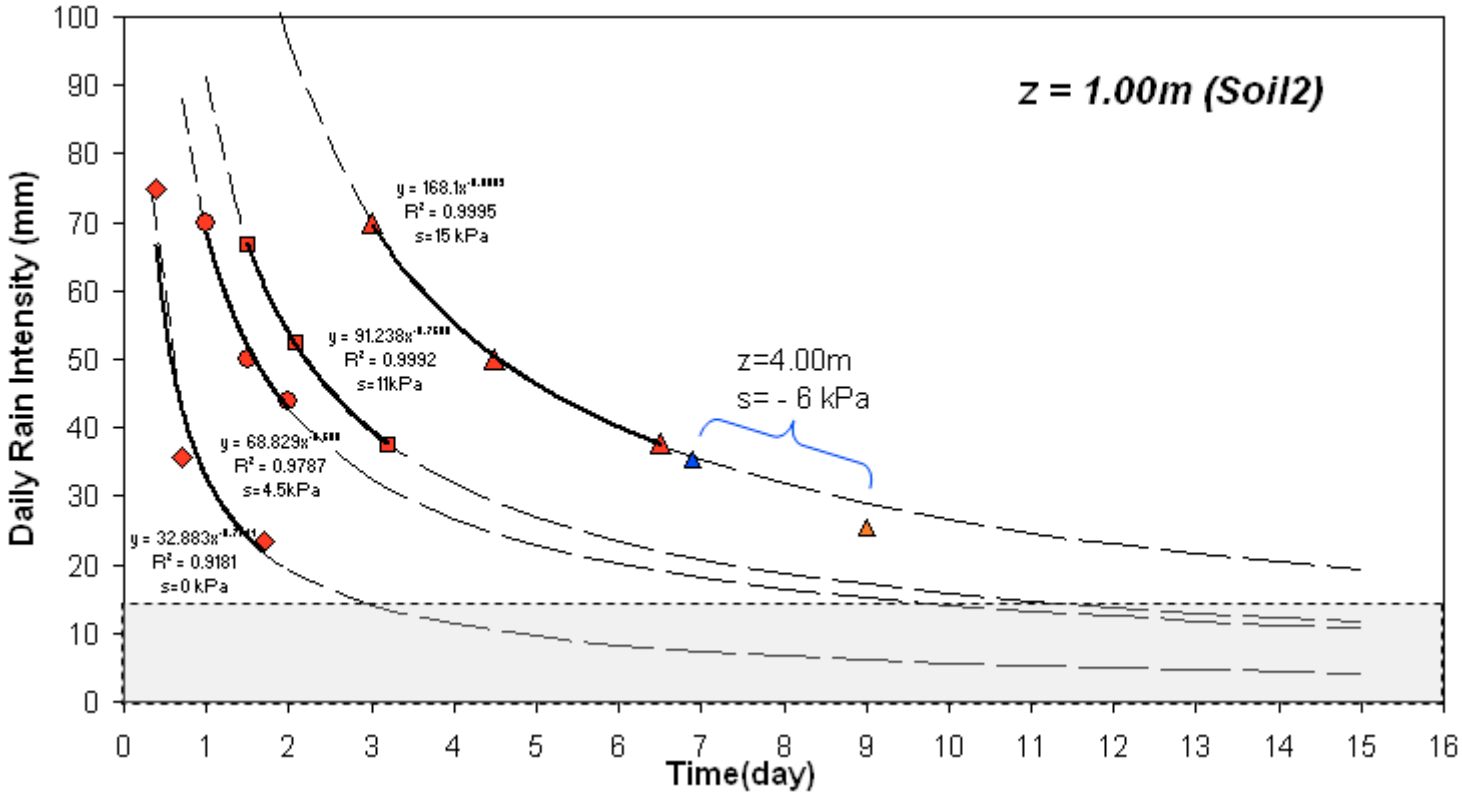

Fig.9.4: Daily Rain intensity against number of days over which it is applied in order to cause the failure at different initial suction values

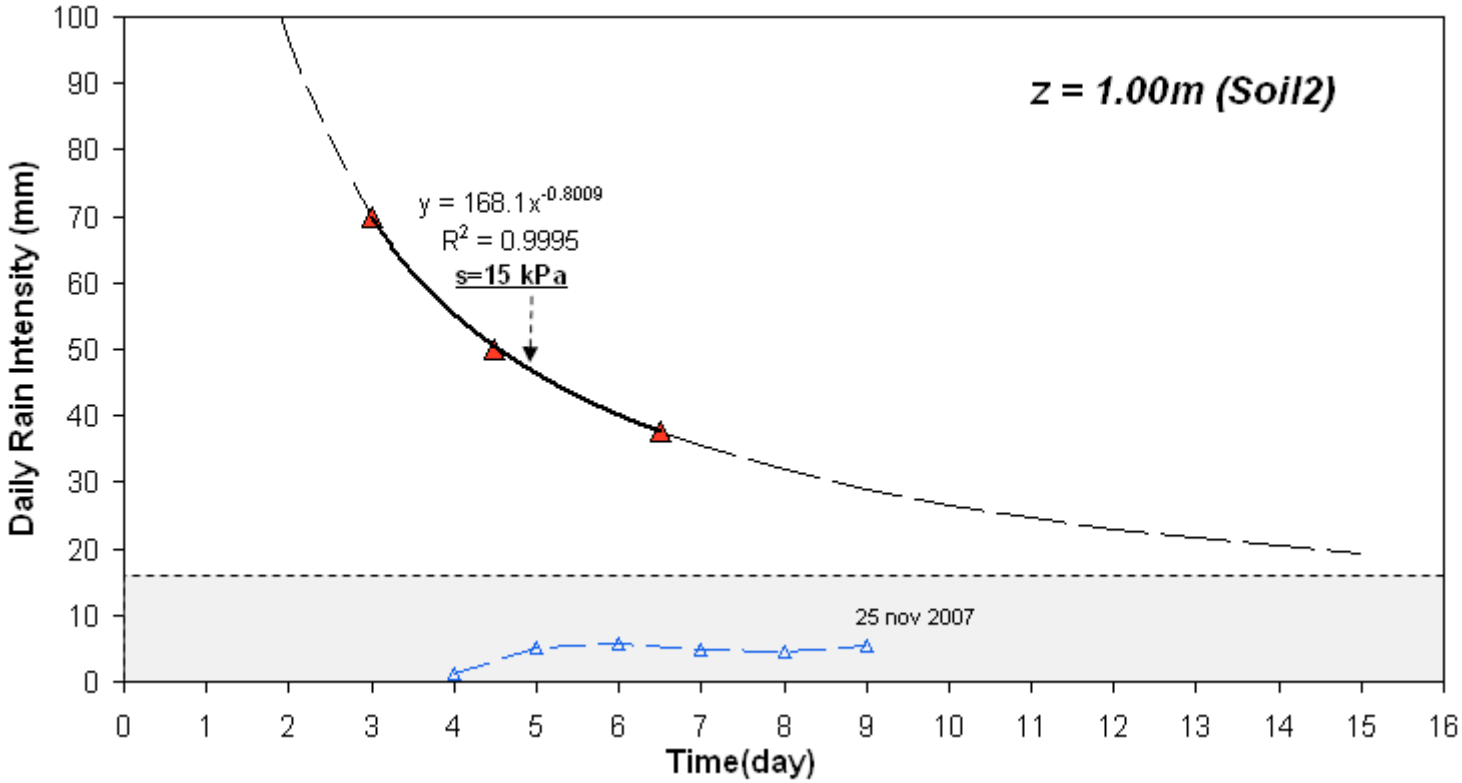

Fig.9.5:Daily Rain intensity causing failure at suction of 15kPa compared with the mean daily rain intensity measured in site

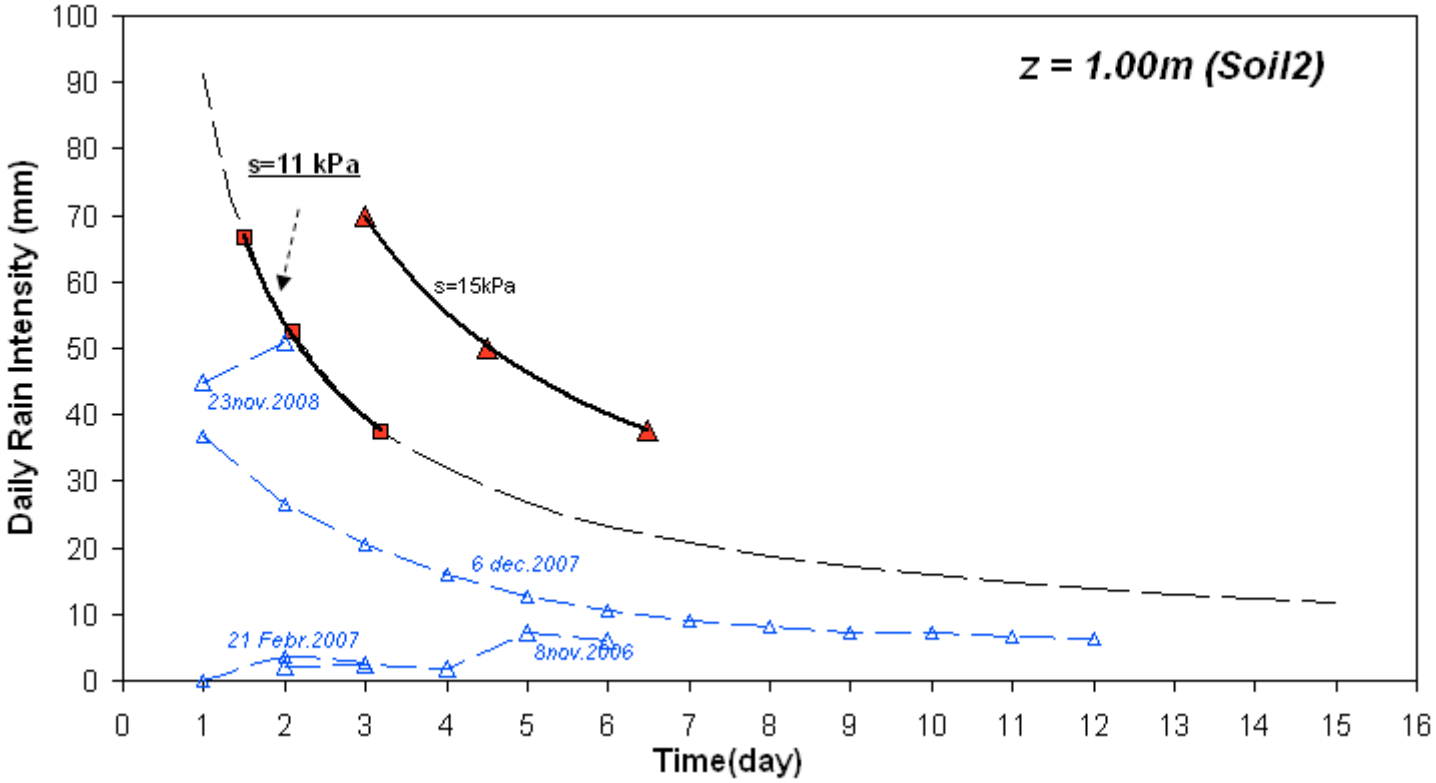

Fig.9.6: Daily Rain intensity causing failure at suction of 11 kPa compared with the mean daily rain intensity measured in site

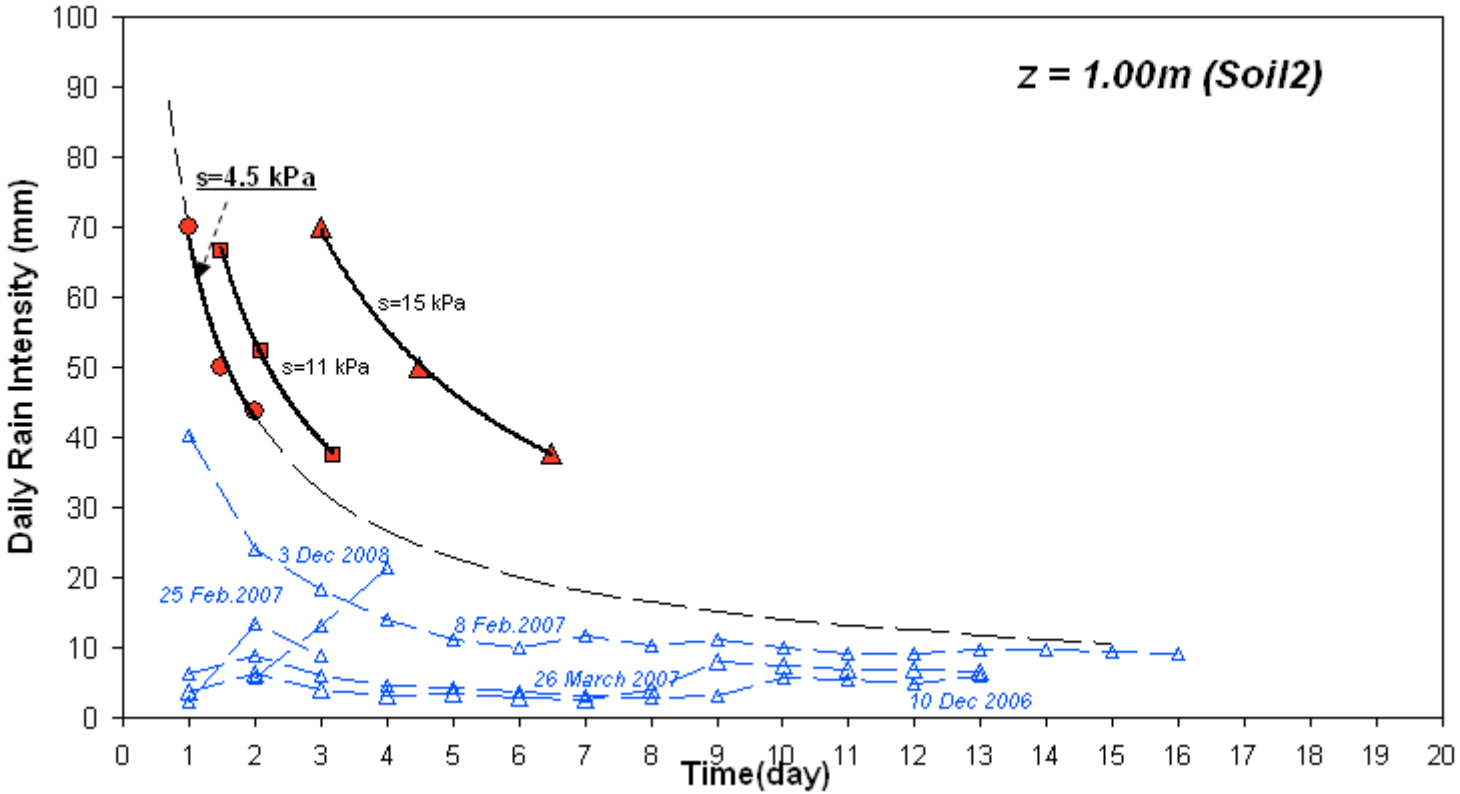

Fig.9.7: Daily Rain intensity causing failure at suction of 4.5 kPa compared with the mean daily rain intensity measured in site

Conclusions

The triggering mechanism of mudflows in partially saturated pyroclastic soils are induced by rainfalls that produce significant increase in the degree of saturation and, consequently, significant reductions in suction and shear strength. The knowledge of pore water pressure distribution and water balance in subsoil against time allows to identify the hydraulic behaviour and the more critical period for slope stability.

Hence, some conclusions concerning the hydraulic regime in the subsoil could be carried out by the elaboration of the monitoring data.

They clearly show seasonal fluctuations of matric suction and volumetric water content in situ, that in the top part of the cover seems to be sensible to singular rainfall events, nevertheless the corresponding variations are relatively small if compared to the seasonal trend. Conversely, in the intermediate part and in the deeper part of the cover, they follows a trend unaffected by individual rainfall events. Furthermore, it must be observed that the seasonal cycle in the intermediate and deep part of the cover is quite delayed and their seasonal range, specially in the soils 6 and 8, is smaller than that in the superficial layers, resulting a function of the distance from the ground surface. The minimum value of suction, so the maximum value of water content, occurs in the winter in all the layers. Moreover the in situ conditions in terms of suction and water content, obtained by measurements collected in site in the superficial and intermediate soils, is always located below the drying retention curves and fall in the hysteresis domain. Hence for these soils, suction and water content represent two independent variables.

As regards the water flow in the superficial and intermediate soils, in winter the direction of the vectors is vertical in all the layers because of high infiltration at ground level, while in spring the directions rotate up to be parallel to the slope. In dry periods the mean direction described by the superficial gradients is around 150° (evaporation flow perpendicular to the slope), while in the intermediate and deep layers it is parallel to the slope. Moreover the water flow intensity is very small during the summer in all the layers even if the gradients are very high. In the other periods of the year, the water flow intensity is larger than in the summer both in the superficial and in the intermediate soils.

The most part of rainfall does not infiltrate into the superficial soils, but it is captured by the vegetation and lost for the run-off phenomena. The cumulated water flow over one year through the superficial soil is not nil but the inward flows (due to infiltration) exceed the downward flows (due to evaporation). Just about 15% of the cumulated vertical flow in the superficial layers reaches the intermediate part of the soil cover. In these layers the cumulated flow over one year is almost nil, hence the inward flow (produced by infiltration) balances the outword ones (generated by evaporation phenomena at the soil surface).

The shape of the water volume curves in the superficial and the intermediate soils are similar. The water balance over one year for both layers seem to be in equilibrium. On the contrary, while the cumulated flows in the soils 4 is nil, the cumulated inward flow through the

superficial soils in the wet period is not balanced by the outward flow in the dry period. It results that a large cumulated flow infiltrates through the pumiceous layer 3.
In the pumice layer the total water is divided into two terms: a flow parallel to slope and a contribute to the variation of the water content.

The potential triggering mechanism can be investigated by carrying out the numerical parametric analyses, being related to very critic rainfall histories, never registered in site. Hence, some conclusions could be carried out about the failure mechanism by the results of slope stability analyses. It's important to point out that the results of analysis could be accepted because the parameters of the model used were obtained by experimental tests and, moreover the model was previously validated by carrying out hydraulic analyses reproducing pore water pressure regime observed in situ. Numerical results of slope stability analyses suggest that the major role is occupied by the rain intensity, cumulated rainfall and the hydraulic characterization. The following conclusions could be pointed out.
The *total quantity of rain* enough to generate instability, depends on the water content in the subsoil, because it represents a factor predisposing to the failure. A quantity between 200 - 250 mm of rain, is necessary to generate triggering mechanism in the domain analyzed.
Rain intensity plays a key rule in the failure mechanism, in fact it determines the type of failure and the depth of the sliding surface. Assigned the specific geometry and topography, as that analyzed, a rain intensity lower than or equal to the yearly average couldn't cause the failure (under this conditions the steady regime establishes). Rain smaller than 35mm/day causes a deep sliding surface, because these intensities can infiltrate in the deeper soils before affecting slope stability. Moreover the depth of the sliding surface goes down where the excavation or other irregularity are present on the slope; so the topography influences the soils involved by the failure too. Rain intensity higher than 70mm/day causes a general failure involving whole the slope, in fact the most intensive rains affect large area, but they involve the superficial soils only, having no time to reach deeper zones.
The *mechanical characterization* influences the depth of the sliding surface only. The type of failure (general or local), and values of pore water pressure which cause instability seem not to be influenced by the angle of shearing resistance. The *hydraulic characterization adopted gives a very different results in terms of* failure mechanism: a right characterization is necessary to identify a correct solutions. The depth of the sliding surface and the pore pressure distribution which cause instability change completely, varying permeability curves of soils.

References

ALONSO E.E., GENS A., JOSA A. (1990) *"A constitutive model for partially saturated soils"*. Geotechnique, Vol.40, No.3 , 405-430

BELFIORE G., URCIUOLI G. (2005) *"Azione delle radici nell'interazione idrica fra sottosuolo ed atmosfera "*. IARG 2005, Ancona, 29 giugno-1 luglio 2005

BILOTTA E., CASCINI L., FORESTA V., SORBINO G., 2005. *'Geotechnical characterisation of pyroclastic soils involved in huge flow slides'*. Geotechnical and geological engineering, Springer eds, 23: 365-402.

BLIGHT G.E. *"Interaction between the atmosphere and the Earth"*. Geotechnique, Vol.47, No.4, 715-767.

BLIGHT G.E. (2002) "The Vadose zone soil-balance and traspiration rates of vegetation". Géotechnique, Vol. 53, No.1, 55-64

BUDETTA P., CALCATERRA D., CORNIELLO A., DE RISO R., DUCCI D., SANTO A., 1993. *'Appunti di geologia dell'Appennino meridionale'*. Istituto di Geologia Applicata Università di Napoli. Pubblicazione n. 332.

CALCATERRA D., DE RISO R., EVANGELISTA A., NICOTERA M.V., SANTO A., SCOTTO DI SANTOLO A., 2003. '*Slope instabilities in the pyroclastic deposits of the Phlegraean district and the carbonate Apennine (Campania, Italy)*'. International Workshop on Occurence and Mechanisms of Flows in Natural Slopes and Earthfills Iw-Flows 2003, Sorrento, 14-16 Maggio 2003.

CAMPBELL SCIENTIFIC, "CR800 Series Measurement and Control System"

CHEN Q., ZHANG L.M. (2006*)"Three-dimensional analysis of water infiltration into the Gouhou rockfill dam using saturated-unsaturated seepage theory"* Canadian Geotechnical journal, vol. 43, 449-461

CASCINI L., CUOMO S., 2004 "Analisi degli effetti indotti dai moti di filtrazione in terreni piroclastici: un caso di studio", IARG 2004, Trento 7-9 luglio 2004

CUI.Y.J., LU Y.F.., DELAGE P., RIFFARD M. (2005) *"Field Simulation of in situ water content and temperature changes due to ground –atmospheric interaction"*. Géotechnique, Vol. 55, No.7, 557-567

CUOMO S., CASCINI L., SORBINO G., 2006."*Colate rapide in terreni piroclastici: Analsi di un tipico meccanismo di innesco*".IARG, 2006, Pisa, 26-28 Giugno 2006.

DAMIANO E., 2004. *'Meccanismi di innesco di colate di fango in terreni Piroclastici'*. Tesi

di Dottorato, Seconda Università di Napoli

De RISO R., BUDETTA P., CALCATERRA D., SANTO A., 1999. *'Le colate rapide in terreni piroclastici del territorio campano. Atti della conferenza Previsione e Prevenzione di Movimenti Franosi Rapidi'*, Trento, pp. 133-150

DI CRESCENZO G., ROTELLA M., SANTO A., 2007. '*Il contributo della geologia per lo studio dei meccanismi di innesco di colate rapide di fango al campo sperimentale di Monteforte Irpino (AV)*'. Piattaforme Evolute di Telecomunicazioni e di Information Technology per l'Offerta di Servizi al settore Ambiente Petit-Osa. Aracne edizione.

EKBLAD J.,ISACSSON U., (2007) *"Time-domain reflectometry measurements and soil-water characteristic curves of coarses granular materials used in road pavimentes"* Canadian Geotechnical journal, Vol. 44, 858-872

EVANGELISTA A., NICOTERA M. V., PAPA R., URCIUOLI G. (2007) "*Esperienze su una piroclastite parzialmente satura della Campania"*. IARG 2007, Salerno, 4-6 luglio 2007

EVANGELISTA A., NICOTERA M.V., PAPA R., URCIUOLI G., (2008) *"Field investigation on triggering mechanism of fast landsides in unsaturated pyroclastic soils",* International conference of usaturated soil, 909-915.

EVANGELISTA A., NICOTERA M. V., PAPA R., URCIUOLI G. (2007) *"Un campo sperimentale per lo studio dell'innesco delle colate di fango. Misure di suzione"*. IARG 2007, Salerno, 4-6 luglio 2007

EVANGELISTA A., NICOTERA M.V., SCOTTO DI SANTOLO A., 2002. '*Caratteristiche geotecniche dei terreni piroclastici della città di Napoli'*. XXI Convegno Nazionale di Geotecnica, L'Aquila, 45-52. Patron, Bologna.

EVANGELISTA A., SCOTTO DI SANTOLO A., 2001. *'Mechanical behaviour of unsaturated pyroclastic soil'*. In M. Kuhne, H.H. Einstein, E. Krauter, H. Klapperic, R. Pottler (eds). Landslides: Causes, Impacts an Countermeasures, proc. Intern.conf., Davos: 35-44.

EVANGELISTA A., NICOTERA M.V., SCOTTO DI SANTOLO A. (2005) *" Valutazione del ruolo degli strati pomicei nell'innesco dei fenomeni di colate di fango",* La mitigazione del rischio da colate di fango, Convegno Nazionale, Napoli 2 e 3 maggio 2005

FREDLUND D.G., XING A., FREDLUND M.D., BARBOUR S.L., 1996. *"The relationship of the unsaturated soil shear strength to the soil water characteristic curve"*. Can. Geotech. J. 33, 440-448.

FREDLUND D.G.,(1999) "*The 1999 R.M.Hardy Lecture: The implementation of unsaturated soil mechanics into geotechical engineering",* Canadian Geotechnical Journal, N°37, 953-986

FREDLUND D.G, RAHARDJO G. (1994)*"Soil mechanics for Unsaturated Soils"* A.Wiley Interscience publication. John Wiley & Sons

FREDLUND D.G. 2006. "*Unsaturated soil Mechanics in engineering practice*". Journal of geotechnical and geo environmental engineering, vol 132, N. 3, 286-321.

JOMMI C., 2000. *"Remarks on the constitutive modelling of unsaturated Soils"*. In Experimental evidence and theoretical approaches in unsaturated soils (eds. A. Tarantino and C. Mancuso), pp. 139-153. Rotterdam: A.A.Balkema.

GALLIPOLI D., GENS A., SHARMA R., VAUNAT J.(2003) *"An elasto-plastic model for unsaturated soil incorporating the effects of suction and degree of saturation on mechanical behaviour"* Geotechnique, Vol.53, No.1, 123-135

GALLIPOLI D., WHEELER S.J., KARSTUNEN M**.** *"Modelling the variation of degree of saturation in a deformable unsaturated soil"* Geotechnique, Vol.53, No.1, 105-112.

GEORGIADIS K.,(2003). *"Development implementation and applicaton of partially saturated soil models in finite Element Analysis*", Phd Thesis, Imperial College of London

GDE BUDI INDRAWAN I, RAHARDJO H., LEONG E. "*Drying and wetting charateristics of a two-layer soil column"* Canadian Geotechnical journal, Vol. 44, 20-32

INDRAWAN B.G.I., RAHARDJO H., LEONG E.C., 2007 "*Drying and wetting characteristics of a two-layer soil column*" Canadian Geotechnical journal, Vol. 44, 20-32

LAGIOIA R., PUZRIN A.M., POTTS D.M**.** (1996). " A new versatile expression for yield and plastic potentina surface ", Computers and geotecnics, Vol.19, No.3, pp 171-191

LU N., ASCE.F. (2008*)."Is matric suction a Stress Variable?"* Journal of Geotechnical and geonviromental engineering, ASCE

NICOTERA M.V.(1998) "*Effetti del grado di saturazione sul comportamento meccanico di un una pozzolana del napoletano"* Tesi di dottorato X ciclo, Dipartimento di Ingegneria Geotecnica, Febbraio 1998

NICOTERA M.V., PAPA R., 2007. *"Comportamento idraulico e meccanico della serie piroclastica di Monteforte Irpino (AV)"*. Piattaforme Evolute di Telecomunicazioni e di Information Technology per l'Offerta di Servizi al settore Ambiente Petit-Osa. Aracne edizione.

MUNOZ-CARPENA R.REGALDO C.M., RITTER A.,ALVREZ-BENEDI J., SOCORRO A. R.,(2005) *"TDR estimation of electircal conductivity and saline solute concentaration in a volcanic soil"*. Geoderma,124, 399-413

KARTHINKEYAN M.,TAN T.S., PHONN K.K.,(2001) *"Numerical oscillation in seepage*

analysis of unsaturated soils" Note Canadian Geotechnical journal, Vol. 38, 639-651

KELLENERS, T. J., R.W.O. SOPPE, J.E. AYARS, J. SIMUNEK, and T.H. SKAGGS. 2005. "*Inverse analysis of upward water flow in a groundwater table lysimeter*". Soil Sci. Soc. Am. J. 4:558-572

KIM T.H., STURE S., (2008) *"Capillary-induced tensile strenght in unsaturated sands", Note.* Canadian Geotechnical journal, Vol. 45, 726-737

KOES J.G.,VAN DAM J.C. *Reference Manual Swap 3.0.3*

KRAHN J. *Vadose zone modelling with vadose/W. An engineering methodology*. Vadose Manual, May 2004

OBERG A., SALFORS G., 1997. ,*"Determination of shear strength parameters of unsaturated silts and sands based on the water retention curve",* geotechnical Testing Journal, GTJODJ,20(1): 40-48.

OLIVARES L., PICARELLI L., ANDREOZZI L., AVORIO B., DAMIANO E., LAMPITIELLO S., 2002. *"Scenari di pericolosità di frana in terreni sciolti di natura Piroclastica".* XXI Convegno Nazionale di Geotecnica, L'Aquila, 173-181. Patron, Bologna.

PAPA R., (2007). "Indagine sperimentale sulla coltre piroclastica di un versante della campania",Tesi di dottorato, Università degli studi di Napoli "Federico II"

PICARELLI L., EVENGELISTA A., ROLANDI G., PAONE A., NICOTERA M.V., OLIVARES L., SCOTTO DI SANTOLO A., LAMPITIELLO S., ROLANDI M., 2007. *"Mechanical properties of pyroclastic soils in Campania Region".* Characterisation and Engineering Properties of Natural Soils. Tan, Phiin, Hight e Leroueil eds.

POTTS D.M., ZDRAVKOVIC L. (2001) "*Finite Element analysis in geothechnical engineering, Theory"* , Ed. Thomas Telford

POTTS D.M., ZDRAVKOVIC L. (2001) *"Finite Element analysis in geothechnical engineering, Application"* , Ed. Thomas Telford

RAHARDJIO H., LEE T.T., LEONG E.C., REZAUR R.B.,(2005)"*Response of a residual soil slope to a rainfall"* Canadian Geotechnical journal, Vol. 42, 340-351

RAHARDJIO H., LEE T.T., LEONG E.C., REZAUR R.B. (2008*)"Effect of antecednt rainfall on pore-water distribution charateristic in a residual soil slopes under tropical rainfall" (*2008), Hydrological processes 22, 506-526

RAHARDJIO H.,ONG T.H., LEE T.T., LEONG E.C., REZAUR R.B. (2007*)"Factors Controlling Instability of Homogeneous SoilSlopes under Rainfall"* Journal of Geotechnical and geonviromental engineering, ASCE

RASSAM D.W., WILLIAMS D.J. (1999) *"A relationship describing the shear strenght of unasaturated soils"* Canadian Geotechnical Journal, N°36, 363-368

REGALDO C.M, (2004) *"A phisical interpretation of logarithmic TDR calibration equations of volcanic soils and their solid fraction permittivity based on Lichtenecker's mixing formulae* " Geoderma,123, 41-50

REGALDO C.M., MUNOZ-CARPENA, SOCORRO A. R., MORENO H.J.M. (2003) *"Time Domain reflectometry models as a tool to understood the dieletric response of volcanic soils*". Geoderma,117, 313-330

ROMANO N., PALLADINO M. (2002)*"Prediction of soil water retention using soil physical data and terrain attributes"*. Journal of Hydrology, N°265 , 56-75

ROMANO N., and A. SANTINI. 1999. *"Determining soil hydraulic functions from evaporation experiments by a parameter estimation approach: Experimental verifications and numerical studies"*. Water resour. Res. 35:3343-3359

ROMERO E., VAUNAT J., 2000. *"Retention curves in deformable clays. In Experimental evidence and theoretical approaches in unsaturated soils"* (eds. A. Tarantino and C. Mancuso), pp. 91-106. Rotterdam: A.A. Balkema. Rosi M., Sbrana A., 1987. The Phlegrean fields. CNR, quaderni di La ricerca scientifica.

SAITO H.,SIMUNEK J.,MOHANTY P.,(2006) "*Numerical analysis of coupled Water, vapour and Heat Transport in the Vadose zone"* Vadose zone Journal, 5,784-800

SCHAARP, M.G., and M.Th. VAN GENUCTHEN. 2006. "*A modified Mualem-van Genuchten formulation for improved description of the hydraulic conductivity near saturation"*. Soil Sci. Soc. Am. J. 5:27-34. 216

SCHAARP, M.G., and F.J. LEIJ. 2000. "*Improved prediction of unsaturated hydraulic conductivity with the Mualem-van Genuchten model*". Soil Sci. Soc. Am. J. 64:843-851

SCHNEIDER J.M., FRATTA D., 2009. *"Time/domain reflectometry-parametric study for the evaluation of physical properties in soils",* Canadian Geotechnical journal, Vol. 46, 753-767.

SCOTTO DI SANTOLO A. (2002) *"Le colate rapide*", Ed. Hevelius

SIMUNEK, J., N.J. JARVIS, M.Th. VAN GENUCTHEN, and A. GARDENAS. 2003. *"Review and comparison of models for describing non-equilibrium and preferential flow and trasport in the vadose zone"*. J. Hydrol. (Amsterdam) 272(1-4):14-35

SIMUNEK, J., SEJENA, M., VAN GENUCTHEN, M. Th. 1998. *"The HYDRUS-1D software package for simulating the one-dimensional movement of water, heat, and multiple solutes in variably saturated media"*. Version 2.0 IGWMCTPS-70, International ground

water modeling center, Colorado school of mines, golden, Colorado, p.202

SIMUNEK J., VAN GENUCHTEN TH.,SEJINA M.,(2005) *,"The hydrus-1D software Packege for simulating One-dimensional movement of water,Heat, and Multiple Solute in Variably-Saturated Media"* Version 3.0, Manual of Hydrus-1D

SMETHURST J.A., CLARKE D., POWRIE W.(2006) *"Seasonal changes in pore water pressure in a grass-covered cut slope in London Clay"* Géotechnique, Vol. 56, No 8, 523-537

SMITH P.G.C. (2003). *"Numerical analysis of infiltration into partially saturated soil slopes",* Phd Thesis, Imperial College of London

SWANSON D.A., BARBOUR S.L., WILSON G.W., O'KANE M.T.K. (2003) "*Soil-atmosphere modelling of an engineered soil cover for acid generatig mine waste in a humid alpine climate*". Canadian Geotechnical journal, Vol. 40, 276-292

TARANTINO A., 2007. *"A possible critical state framework for unsaturated compacted soils"*. Geotechnique 57, N. 4, 385-389. Tarantino A., Tombolato S., 2005. Coupling of hydraulic and mechanical behaviour in unsaturated compacted clay. Geotechnique 55, N. 4, 307-317.

TARANTINO A., TOMBOLATO S.,(2005), "*Coupling of hydraulic and mechanical behaviour in unsaturated compacted clay",*Géotechnique, Vol. 55, N°.4, 307-317

TOLL D.G., 1990. "*A framework for unsaturated soil behaviour*". Geotechnique 40, N. 1, 31-44.

TOLL D.G., ONG B.H., 2003. "*Critical-state parameters for an unsaturated residual sandy clay"*. Geotechnique 53, N. 1, 93-103.

TRINH MINH THU**,** RAHARDJO H., LEONG E. (2007) *"Elastoplastic model for unsaturated soil with incorporation of the soil-water characteristic curve"* Canadian Geotechnical Journal, N°44 , 67-77

VAN GENUCHTEN M. T., (1980). "A closed-form equation for predicting the hydraulic conductivity of unsaturated soils" , *Soil Sci. Soc. Am. J.,* 892-898.

VANAPALLI S.K., FREDLUND D.E., PUFHAL D.E. e CLINTOF A.W., 1996. *"Model for the prediction of shear strength with respect to soil suction"*. Can. Geotech. J. 33, 379-392.

VANAPALLI S.K., FRADLUND D.G., 2000. *"Comparison of different procedures to predict unsaturated soil shear strength"*. Proc. GeoDenver Conf., ASCE Reston, Va., 195-209.

VANAPALLI S.K., FREDLUND D.G., PUFHAL D.E., 1999. *"The influence of soil structure and stres history on the soil-water characteristics of a compacted till"*. Geotechnique 49, N. 2, 143-159.

VAN GENUCTHEN, M.Th. 1980. *A closed form equation for predicting the hydraulic conductivity of unsaturated soils"*. Soil Sci. Soc. Am. J. 44:892-898

VAUNAT J., ROMERO E., JOMMI C., (2000) *"An elastoplastic hydromechanical model for unsaturated soils"* In Experimental evidence and theoretical approaches in unsaturated soils (eds. A. Tarantino and C. Mancuso), 121-138. Rotterdam: A.A. Balkema.

VAUNAT J., ROMERO E., JOMMI C., 2000. *"An elastoplastic hydromechanical model for unsaturated soils"*. In Experimental evidence and theoretical approaches in unsaturated soils (eds. A. Tarantino and C. Mancuso), pp. 121-138. Rotterdam: A.A. Balkema.

VOGEL,T., M.TH. VAN GENUCTHEN, and M. CISLEROVA.2000. "*Effect of the shape of the soil hydraulic functions near saturation on variably-saturated floe predictions"*. Adv. Water resour. 24(2): 133-144
VIGGIANI C., (2003) *"Fondazioni"*, Ed.Hevelius

ZHAN T., NG C.W.W.NG., FREDLUND D.G.(2007)"*Field study of rainfall infiltartion into a grrassed unsaturated expensive soil slope"* Canadian Geotechnical journal, Vol. 44, 392-408

ZHANG L.L., ZHANG L.M., TANG W.H., *"Rainfall-induced slope failure considering variability of soil properties" Thecnical note,*(2005). Geotechnique, Vol.55, N°.2, 183-188

WEEK B., WILSON G.. (2006) *"Prediction of evaporation from soil slopes"* Canadian Geotechnical journal, Vol. 43, 815-829

WHEELER S.J., GALLIPOLI D., KARSTUNEN M.(2002). *"Comments on use of the Barcelona Basic Model for unsaturated soils"* International Journal for numerical and analytical methods in geomechanics, Vol.26, 1561-1571

WHEELER S.J., SHARMA R.S., BUISSON S.R.(2003) *"Coupling of hydraulic and stress strain behaviour in unsaturated soils"* Geotechnique, Vol.53, N°.1, 41-54

WHEELER S.J., SIVAKUMAR V. *"An elasto-plastic critical state framework for unsaturated soil"*.Geotechnique, Vol. 45, N°.1, 35-53

WHEELER S.J., KARUBE D. (1996) *"Constitutive modelling*", Unsaturated soil/ Soil non saturès, Alonso&Delage(eds)

WILSON WARD W., FREDLUD D.G., BARBOUR (1994) *" Coupled soil-atmosphere modeling for soil evaporation"* Canadian Geotechnical Journal, Vol. 31, 151-161

Appendix I

Constitutive model

In the following a brief summary about the constitutive model for partially saturated soils implemented in the ICFEP code (Potts & Zdravkovic, 1999; K. Georgiadis, 2003) is presented. In particular the equations of the model and the symbols of the parameters are introduced. The parameters are divided in:

- yield surface parameters;
- plastic potential parameters;
- hardening and softening parameters;
- elastic parameters;
- initial hardening parameters.

Yield surface:

Primary yield surface:

$$F_1 = \frac{p + f(s_{eq})}{p_0 + f(s_{eq})} - \frac{\left(1 + \frac{\eta}{K_{2f}}\right)^{\frac{K_{f_2}}{\beta_f}}}{\left(1 + \frac{\eta}{K_{1f}}\right)^{\frac{K_{f_2}}{\beta_f}}} = 0$$

where: $p_0 = p_0^*(\alpha_c)^{(\lambda(o)-\lambda(s_{eq}))/(\lambda(s_{eq})-\kappa)}$; $\lambda(s_{eq}) = \lambda(0)\left[(1-r)e^{-\beta s_{eq}} + r\right]$;

$$s_{eq} = s - s_{air}(ifs > s_{air}) or s_{eq} = 0(ifs \le s_{air})\,;$$

$$\eta = \sqrt{\frac{J_{2\eta}}{J_{2\eta f}}}\,; \quad J_{2\eta} = \left(\frac{J}{p + f(s_{eq})}\right)^2;$$

$$K_{f_1} = \frac{\mu_f(1-\alpha_f)}{2(1-\mu_f)}\left(1 + \sqrt{1 - \frac{4\alpha_f(1-\mu_f)}{\mu_f(1-\alpha_f)^2}}\right)$$

$$K_{f_2} = \frac{\mu_f(1-\alpha_f)}{2(1-\mu_f)}\left(1 - \sqrt{1 - \frac{4\alpha_f(1-\mu_f)}{\mu_f(1-\alpha_f)^2}}\right);$$

$$\beta_f = (1-\mu_f)(K_{f_1} - K_{f_2})$$

J_{2nf} is the failure value of J_{2n} and is the solution of the following cubic equation:

$$\frac{2}{\sqrt{27}} \cdot C_f \cdot \sin(3\vartheta) \cdot J_{2f}^{3/2} + (C_f - 3) \cdot J_{2\eta f} - (C_f - 9) = 0$$

where:
$$C_f = \frac{9 - M_f^{\,2}}{\frac{2M_f^{\,3}}{27} - \frac{M_f^{\,2}}{3} + 1}$$

Secondary yield surface:
$$F_2 = G_2 = \frac{s_{eq}}{s_o} - 1 = 0\,;$$

Plastic potential:

$$G = \frac{p + f(s_{eq})}{p_0 + f(s_{eq})} - \frac{\left(1 + \frac{\eta}{K_2}\right)^{\frac{K_2}{\beta}}}{\left(1 + \frac{\eta}{K_1}\right)^{\frac{K_1}{\beta}}} = 0$$

where:
$$\eta = \sqrt{\frac{J_{2\eta}}{J_{2\eta g}}}\,; \quad J_{2\eta} = \left(\frac{J}{p + f(s_{eq})}\right)^2\,;$$

$$K_{g_1} = \frac{\mu_g(1-\alpha_g)}{2(1-\mu_g)}\left(1 + \sqrt{1 - \frac{4\alpha_g(1-\mu_g)}{\mu_g(1-\alpha_g)^2}}\right)$$

$$K_{g_2} = \frac{\mu_g(1-\alpha_g)}{2(1-\mu_g)}\left(1 - \sqrt{1 - \frac{4\alpha_g(1-\mu_g)}{\mu_g(1-\alpha_g)^2}}\right)$$

$$\beta_g = (1-\mu_g)(K_{g_1} - K_{g_2})$$

J_{2ng} is the failure value of J_{2n} and is the solution of the following cubic equation:

$$\frac{2}{\sqrt{27}} \cdot C_g \cdot \sin(3\vartheta) \cdot J_{2\eta g}^{3/2} + (C_g - 3) \cdot J_{2\eta g} - (C_g - 9) = 0$$

where:

$$C_g = \frac{9 - M_g^{\,2}}{\frac{2M_g^{\,3}}{27} - \frac{M_g^{\,2}}{3} + 1}$$

Plastic potential and Yield surface parmeters:

Parameter	Description	Conditions
k	Cohesion	If k >0 $\rightarrow f(s_{eq}) = ks_{eq} + s_{air}$ If k<0, k=S_r $\rightarrow f(s_{eq}) = S_r s_{eq} + s_{air}$
s_{air}	Air entry suction value	≥ 0
α_g	Plastic potential parameter	>0 and $\neq 1$ also if μ_g <1
μ_g	Plastic potential parameter	>0 and $\neq 1$ $\mu_g > 4\alpha_g / \left[(1-\alpha_g)^2 + 4\alpha_g\right]$
M_g	Slope of the critical state line in the q-p stress space for triaxial compression	>0 and <3
α_f	Yield surface parameter	>0 and $\neq 1$ also if μ_f <1
μ_f	Yield surface parameter	>0 and $\neq 1$ $\mu_f > 4\alpha_f / \left[(1-\alpha_f)^2 + 4\alpha_f\right]$
M_f	Yield surface parameter	>0 and <3
s_0	Initial hardening parameter for secondary yield surface	$\geq s_{air}$

Isotropic compressive line and Loading collapse (LC)

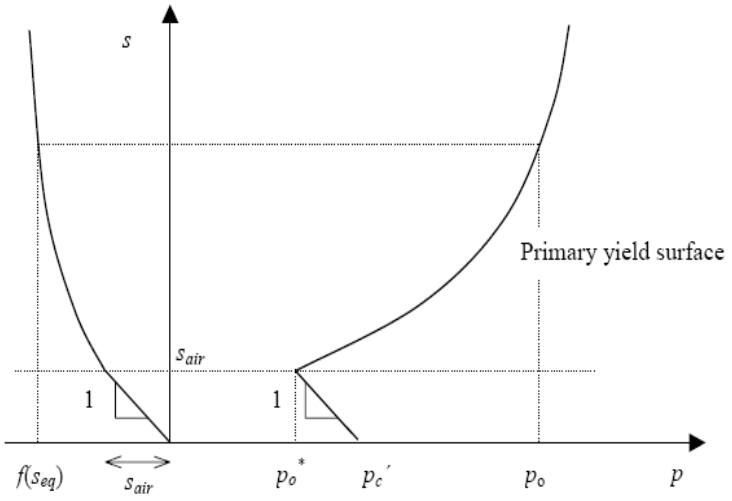

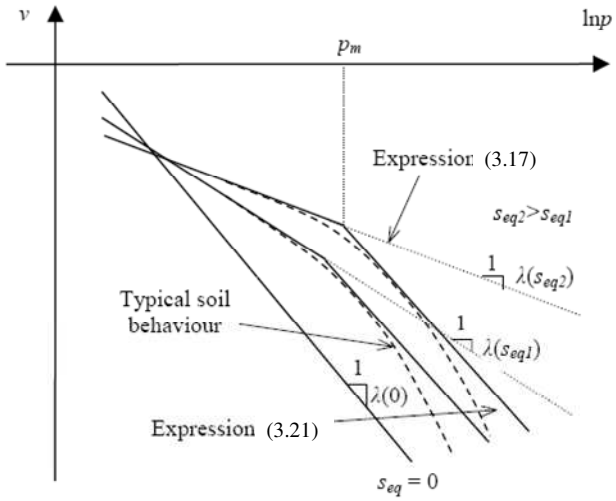

Option 2

If $p<p_m$ $$v = v_1(s_{eq}) - \lambda(s_{eq}) \ln p_0$$

If $p>p_m$ $$v = v_1 + \Delta v_{max} - \lambda(0) \ln p_0$$

Where: $\lambda(s_{eq}) = \lambda(0)\left[(1-r)e^{-\beta s_{eq}} + r\right]$; $p_0 = p_0^*(\alpha_c)^{(\lambda(o)-\lambda(s_{eq}))/(\lambda(s_{eq})-\kappa)}$;

$\alpha_c = p_0^* / p_c$

Hardening and softening parameters:

Parameter	Description	Conditions
α_c	Characteristic stress ratio	< 0 α_c option 2
$\lambda(0)$	Compress. coef. for saturated conditions	$\geq \kappa \geq 0$
κ	Compress. coef. along elastic path	> 0
κ_s	Soil stiffness parameter	> 0
r	Maximum soil stiffness parameters	> 0
β	Soil stiffness increase parameter	> 0
κ_s	Elastic compr. coef. for changes in suction	≥ 0
λ_s	compr. coef. for changes in suction	$> \kappa_s$
v_1	Specific volume at unit pressure (fully saturated)	> 0

Elastic strain

$$d\varepsilon_{vp}^{e} = -\frac{\kappa}{vp} dp$$

$$d\varepsilon_{vs}^{e} = -\frac{\kappa_s}{v(s_{eq} + p_{atm})} ds_{eq}$$

$$dE_d^e = \frac{dJ}{\sqrt{3}G}$$

where:

$$G = \frac{3(1-2\mu)}{2(1+\mu)} K$$

Elastic parameters:

Parameter	Description	Conditions
Kmin	Minimum elastic bulk modulus	> 0
G or G/p_0 or μ	Shear modulus or Poisson's ratio	G (>0)or G/p_0(≥ 0)or μ (<0.5)

Initial Hardening Parameters:

Parameter	Description	Conditions
SSRS	Stress state ratio switch	$\geq 0, \leq 3$
SSR	Stress state ratio	> 0

The SSR value is used to determine the value of the hardening parameter p^*_0 (equivalent fully saturated yield stress). This can be done directly (if SSRS=0.0 or 1.00), or by firstly calculating the current yield stress p_0 from which p^*_0 is then calculated through the Loading Collapse expression (if SSRS=2.0 or 3.0):

If SSRS=0.0 $p_0^* = SSR.|p|$

Where p^*_0 is the equivalent fully saturated yield stress and p the mean total stress.

If SSRS=1.0

If SSR=1. 0 the initial stress state lies on the equivalent fully saturated yield surface and the value of p^*_0, associated with this surface is calculated.

If SSR>1.0 the initial stress state (σ'_x, σ'_y, τ_{xy}, σ'_z) is used to calculate $\sin\varphi'$ and the net vertical stress σ_y and then the vertical stress corresponding to a stress state on the equivalent fully saturated yield surface, σ^*_y: $\sigma_y^* = SSR.|\sigma_y|$

If SSRS=2.0 $p_0 = SSR.|p|$

Where p_0 is the current yield stress and not the equivalent fully saturated yield stress, p^*_0. p is the mean total stress.

If SSRS=3.0

If SSR=1.0 the material is assumed to be normally consolidated and the value of p_0, associated with the yield surface that corresponds to the initial state of stress is calculated.

If SSR>1.0 the initial stress state (σ'_x, σ'_y, τ_{xy}, σ'_z) is used to calculate $\sin\varphi'$ and the net vertical stress σ_y and then the vertical stress corresponding to a stress state on the current partially saturated yield surface, σ_{y0}: $\sigma_{y0} = SSR.|\sigma_y|$.

Appendix II

Validation of the numerical model

In the following the tables about the boundary conditions and the hydraulic characterization applied in the analyses carried out to validate the model shown in the Chapter 7, are reported. In particular the tables contain:

- the number of the time increments in which one day is divided;
- the progressive increments corresponding to each day;
- the daily rain registered by the Monteforte Irpino rrain gauge;
- the daily evaporation and transpiration flows calculated by the Penman equation either for LAI=1 and LAI=2.7;
- the hydraulic characterization used (wetting or drying) for the soils 1, 2 and 4.

date	n° increments	increments	rain [mm/day]	Evap.LAI=1 [mm/day]	Evap.LAI=2.7 [mm/day]	Trasp.LAI=1 [mm/day]	Trasp.LAI=2.7 [mm/day]	Retention curve	Permeability function
9/11/06	3	17-19	**4**	1.47	0.17	1.41	2.71	1-2-4 wetting	1-2-4 wetting
10/11/06	3	20-22	**3.4**	1.47	0.17	1.41	2.71	1-2-4 wetting	1-2-4 wetting
11/11/06	3	23-25	0	1.47	0.17	1.41	2.71	1-2-4 wetting	1-2-4 wetting
12/11/06	3	26-28	**29**	1.47	0.17	1.41	2.71	1-2-4 wetting	1-2-4 wetting
13/11/06	3	29-31	**0.2**	1.47	0.17	1.41	2.71	1-2-4 wetting	1-2-4 wetting
14/11/06	1	32	0	1.47	0.17	1.41	2.71	1-2-4 wetting	1-2-4 wetting
15/11/06	1	33	0	1.47	0.17	1.41	2.71	1-2-4 wetting	1-2-4 wetting
16/11/06	1	34	0	1.47	0.17	1.41	2.71	1-2-4 wetting	1-2-4 wetting
17/11/06	1	35	0	1.47	0.17	1.41	2.71	1-2-4 wetting	1-2-4 wetting
18/11/06	1	36	0	1.13	0.13	1.09	2.08	1-2-4 wetting	1-2-4 wetting
19/11/06	1	37	0	1.13	0.13	1.09	2.08	1-2-4 wetting	1-2-4 wetting
20/11/06	1	38	**2.8**	1.13	0.13	1.09	2.08	1-2-4 wetting	1-2-4 wetting
21/11/06	1	39	**10.6**	1.13	0.13	1.09	2.08	1-2-4 wetting	1-2-4 wetting
22/11/06	3	40-42	**68.2**	1.13	0.13	1.09	2.08	1-2-4 wetting	1-2-4 wetting
23/11/06	4	43-46	0	1.13	0.13	1.09	2.08	1-2-4 wetting	1-2-4 wetting
24/11/06	4	47-50	0	1.13	0.13	1.09	2.08	1-2-4 wetting	1-2-4 wetting
25/11/06	4	51-54	0	1.38	0.16	1.33	2.54	1-2-4 wetting	1-2-4 wetting
26/11/06	4	55-58	**0.4**	1.38	0.16	1.33	2.54	1-2-4 wetting	1-2-4 wetting
27/11/06	4	59-62	0	1.38	0.16	1.33	2.54	1-2-4 wetting	1-2-4 wetting
28/11/06	2	63-64	0	1.38	0.16	1.33	2.54	1-2-4 wetting	1-2-4 wetting
29/11/06	4	65-68	0	1.38	0.16	1.33	2.54	1-2-4 wetting	1-2-4 wetting
30/11/06	2	69-70	0	1.38	0.16	1.33	2.54	1-2-4 wetting	1-2-4 wetting
1/12/06	2	71-72	0	1.38	0.16	1.33	2.54	1-2-4 wetting	1-2-4 wetting
2/12/06	2	73-74	0	1.39	0.16	1.34	2.56	1-2-4 wetting	1-2-4 wetting
3/12/06	2	75-76	0	1.39	0.16	1.34	2.56	1-2-4 wetting	1-2-4 wetting
4/12/06	2	77-78	**5.4**	1.39	0.16	1.34	2.56	1-2-4 wetting	1-2-4 wetting
5/12/06	2	79-80	**2.4**	1.39	0.16	1.34	2.56	1-2-4 wetting	1-2-4 wetting
6/12/06	2	81-82	0	1.39	0.16	1.34	2.56	1-2-4 wetting	1-2-4 wetting
7/12/06	2	83-84	**0.8**	1.39	0.16	1.34	2.56	1-2-4 wetting	1-2-4 wetting

date	n° increments	increments	rain [mm/day]	Evap.LAI=1 [mm/day]	Evap.LAI=2.7 [mm/day]	Trasp.LAI=1 [mm/day]	Trasp.LAI=2.7 [mm/day]	Retention curve	Permeability function
8/12/06	3	85-87	**4.4**	1.39	0.16	1.34	2.56	1-2-4 wetting	1-2-4 wetting
9/12/06	3	88-90	**50.2**	1.39	0.16	1.34	2.56	1-2-4 wetting	1-2-4 wetting
10/12/06	1	91	**3.8**	0.92	0.11	0.88	1.70	1-2-4 wetting	1-2-4 wetting
11/12/06	1	92	**8.6**	0.92	0.11	0.88	1.70	1-2-4 wetting	1-2-4 wetting
12/12/06	1	93	0	0.92	0.11	0.88	1.70	1-2-4 wetting	1-2-4 wetting
13/12/06	1	94	0	0.92	0.11	0.88	1.70	1-2-4 wetting	1-2-4 wetting
14/12/06	1	95	**5.2**	0.92	0.11	0.88	1.70	1-2-4 wetting	1-2-4 wetting
15/12/06	1	96	**0.2**	0.92	0.11	0.88	1.70	1-2-4 wetting	1-2-4 wetting
16/12/06	1	97	0	0.92	0.11	0.88	1.70	1-2-4 wetting	1-2-4 wetting
17/12/06	1	98	**14.8**	0.81	0.10	0.78	1.50	1-2-4 wetting	1-2-4 wetting
18/12/06	4	99-102	**39.2**	0.81	0.10	0.78	1.50	1-2-4 wetting	1-2-4 wetting
19/12/06	4	103-106	**3.2**	0.81	0.10	0.78	1.50	1-2-4 wetting	1-2-4 wetting
20/12/06	4	107-110	0	0.81	0.10	0.78	1.50	1-2-4 wetting	1-2-4 wetting
21/12/06	4	111-114	**5.6**	0.81	0.10	0.78	1.50	1-2-4 wetting	1-2-4 wetting
22/12/06	3	115-117	**3.2**	0.81	0.10	0.78	1.50	1-2-4 wetting	1-2-4 wetting
23/12/06	5	118-122	0	0.81	0.10	0.78	1.50	1-2-4 wetting	1-2-4 wetting
24/12/06	5	123-127	0	0.81	0.10	0.78	1.50	1-2-4 wetting	1-2-4 wetting
25/12/06	2	128-129	0	0.81	0.10	0.78	1.50	1-2-4 wetting	1-2-4 wetting
26/12/06	2	130-131	0	0.81	0.10	0.78	1.50	1-2-4 wetting	1-2-4 wetting
27/12/06	5	132-136	0	0.81	0.10	0.78	1.50	1-2-4 wetting	1-2-4 wetting
28/12/06	3	137-139	0	0.98	0.12	0.94	1.81	1-2-4 wetting	1-2-4 wetting
29/12/06	3	140-142	0	0.98	0.12	0.94	1.81	1-2-4 wetting	1-2-4 wetting
30/12/06	3	143-145	0	0.98	0.12	0.94	1.81	1-2-4 wetting	1-2-4 wetting
31/12/06	3	146-148	0	0.98	0.12	0.94	1.81	1-2-4 wetting	1-2-4 wetting
1/1/07	3	149-151	0	0.98	0.12	0.94	1.81	1-2-4 wetting	1-2-4 wetting
2/1/07	4	152-155	**32.8**	0.98	0.12	0.94	1.81	1-2-4 wetting	1-2-4 wetting
3/1/07	1	156	**0.2**	0.98	0.12	0.94	1.81	1-2-4 wetting	1-2-4 wetting
4/1/07	1	157	0	0.98	0.12	0.94	1.81	1-2-4 wetting	1-2-4 wetting
5/1/07	1	158	**8.6**	0.98	0.12	0.94	1.81	1-2-4 wetting	1-2-4 wetting
6/1/07	1	159	0	1.31	0.15	1.26	2.42	1-2-4 wetting	1-2-4 wetting
7/1/07	1	160	0	1.31	0.15	1.26	2.42	1-2-4 wetting	1-2-4 wetting

date	n° increments	increments	rain [mm/day]	Evap.LAI=1 [mm/day]	Evap.LAI=2.7 [mm/day]	Trasp.LAI=1 [mm/day]	Trasp.LAI=2.7 [mm/day]	Retention curve	Permeability function
08/01/07	2	161-162	**7.4**	1.31	0.15	1.26	2.42	1-2-4 wetting	1-2-4 wetting
09/01/07	2	163-164	**0.2**	1.31	0.15	1.26	2.42	1-2-4 wetting	1-2-4 wetting
10/01/07	2	165-166	0	1.31	0.15	1.26	2.42	1-2-4 wetting	1-2-4 wetting
11/01/07	2	167-168	0	1.31	0.15	1.26	2.42	1-2-4 wetting	1-2-4 wetting
12/01/07	2	169-170	0	1.31	0.15	1.26	2.42	1-2-4 wetting	1-2-4 wetting
13/01/07	2	171-172	0	1.31	0.15	1.26	2.42	1-2-4 wetting	1-2-4 wetting
14/01/07	5	173-177	0	1.31	0.15	1.26	2.42	1-2-4 wetting	1-2-4 wetting
15/01/07	5	178-182	0	1.31	0.15	1.26	2.42	1-2-4 wetting	1-2-4 wetting
16/01/07	5	183-187	0	1.31	0.15	1.26	2.42	1-2-4 wetting	1-2-4 wetting
17/01/07	5	188-192	0	0.97	0.11	0.93	1.79	1-2-4 wetting	1-2-4 wetting
18/01/07	5	193-197	**6.8**	0.97	0.11	0.93	1.79	1-2-4 wetting	1-2-4 wetting
19/01/07	5	198-202	0	0.97	0.11	0.93	1.79	1-2-4 wetting	1-2-4 wetting
20/01/07	5	203-207	**0.2**	0.97	0.11	0.93	1.79	1-2-4 wetting	1-2-4 wetting
21/01/07	5	208-212	0	0.97	0.11	0.93	1.79	1-2-4 wetting	1-2-4 wetting
22/01/07	5	213-217	0	0.97	0.11	0.93	1.79	1-2-4 wetting	1-2-4 wetting
23/01/07	2	218-219	**40.4**	0.97	0.11	0.93	1.79	1-2-4 wetting	1-2-4 wetting
24/01/07	2	220-221	**18.6**	0.97	0.11	0.93	1.79	1-2-4 wetting	1-2-4 wetting
25/01/07	2	222-223	**11.6**	0.97	0.11	0.93	1.79	1-2-4 wetting	1-2-4 wetting
26/01/07	2	224-225	0	0.97	0.11	0.93	1.79	1-2-4 wetting	1-2-4 wetting
27/01/07	2	226-227	0	0.60	0.07	0.58	1.11	1-2-4 wetting	1-2-4 wetting
28/01/07	2	228-229	0	0.60	0.07	0.58	1.11	1-2-4 wetting	1-2-4 wetting
29/01/07	2	230-231	0	0.60	0.07	0.58	1.11	1-2-4 wetting	1-2-4 wetting
30/01/07	2	232-233	0	0.60	0.07	0.58	1.11	1-2-4 wetting	1-2-4 wetting
31/01/07	2	234-235	0	0.60	0.07	0.58	1.11	1-2-4 wetting	1-2-4 wetting
01/02/07	2	236-237	**0.4**	0.60	0.07	0.58	1.11	1-2-4 wetting	1-2-4 wetting
02/02/07	2	238-239	0	0.60	0.07	0.58	1.11	1-2-4 wetting	1-2-4 wetting
03/02/07	2	240-241	0	0.60	0.07	0.58	1.11	1-2-4 wetting	1-2-4 wetting
04/02/07	2	242-243	0	0.60	0.07	0.58	1.11	1-2-4 wetting	1-2-4 wetting
05/02/07	2	244-245	0	0.60	0.07	0.58	1.11	1-2-4 wetting	1-2-4 wetting
06/02/07	2	246-247	**3.4**	0.60	0.07	0.58	1.11	1-2-4 wetting	1-2-4 wetting
07/02/07	2	248-249	**40.2**	0.60	0.07	0.58	1.11	1-2-4 wetting	1-2-4 wetting

date	n° increments	increments	rain [mm/day]	Evap.LAI=1 [mm/day]	Evap.LAI=2.7 [mm/day]	Trasp.LAI=1 [mm/day]	Trasp.LAI=2.7 [mm/day]	Retention curve	Permeability function
08/02/08	2	250-251	**7.8**	0.46	0.05	0.44	0.85	1-2-4 wetting	1-2-4 wetting
09/02/07	2	252-253	**7.0**	0.46	0.05	0.44	0.85	1-2-4 wetting	1-2-4 wetting
10/02/07	2	254-255	**1.0**	0.46	0.05	0.44	0.85	1-2-4 wetting	1-2-4 wetting
11/02/07	2	256-257	0.0	0.46	0.05	0.44	0.85	1-2-4 wetting	1-2-4 wetting
12/02/07	2	258-259	**3.2**	0.46	0.05	0.44	0.85	1-2-4 wetting	1-2-4 wetting
13/02/07	2	260-261	**23.4**	0.46	0.05	0.44	0.85	1-2-4 wetting	1-2-4 wetting
14/02/07	2	262-263	0.0	0.46	0.05	0.44	0.85	1-2-4 wetting	1-2-4 wetting
15/02/07	2	264-265	**17.4**	0.46	0.05	0.44	0.85	1-2-4 wetting	1-2-4 wetting
16/02/07	2	266-267	0.0	0.46	0.05	0.44	0.85	1-2-4 wetting	1-2-4 wetting
17/02/07	2	268-269	0.0	0.46	0.05	0.44	0.85	1-2-4 wetting	1-2-4 wetting
18/02/07	2	270-271	**10.6**	0.46	0.05	0.44	0.85	1-2-4 wetting	1-2-4 wetting
19/02/07	2	272-273	**16.0**	0.46	0.05	0.44	0.85	1-2-4 wetting	1-2-4 wetting
20/02/07	2	274-275	**11.0**	0.46	0.05	0.44	0.85	1-2-4 wetting	1-2-4 wetting
21/02/07	2	276-277	**4.8**	0.46	0.05	0.44	0.85	1-2-4 wetting	1-2-4 wetting
22/02/07	2	278-279	**3.6**	0.46	0.05	0.44	0.85	1-2-4 wetting	1-2-4 wetting
23/02/07	2	280-281	0.0	0.46	0.05	0.44	0.85	1-2-4 wetting	1-2-4 wetting
24/02/07	2	282-283	0.0	0.46	0.05	0.44	0.85	1-2-4 wetting	1-2-4 wetting
25/02/07	5	284-288	**2.4**	0.46	0.05	0.44	0.85	1-2-4 wetting	1-2-4 wetting
26/02/07	5	289-293	**24.6**	0.46	0.05	0.44	0.85	1-2-4 wetting	1-2-4 wetting
27/02/07	5	294-298	0.0	1.15	0.13	1.10	2.12	1-2-4 wetting	1-2-4 wetting
28/02/07	5	299-303	0.0	1.15	0.13	1.10	2.12	1-2-4 wetting	1-2-4 wetting
01/03/07	5	304-308	0.0	1.15	0.13	1.10	2.12	1-2-4 wetting	1-2-4 wetting
02/03/07	5	309-313	0.0	1.15	0.13	1.10	2.12	1-2-4 wetting	1-2-4 wetting
03/03/07	5	314-318	0.0	1.15	0.13	1.10	2.12	1-2-4 wetting	1-2-4 wetting
04/03/07	5	319-323	0.0	1.15	0.13	1.10	2.12	1-2-4 wetting	1-2-4 wetting
05/03/07	5	324-328	0.0	1.15	0.13	1.10	2.12	1-2-4 wetting	1-2-4 wetting
06/03/07	5	329-333	0.0	1.15	0.13	1.10	2.12	1-2-4 wetting	1-2-4 wetting
07/03/07	5	334-338	**46.0**	1.15	0.13	1.10	2.12	1-2-4 wetting	1-2-4 wetting

date	n° increments	increments	rain [mm/day]	Evap.LAI=1 [mm/day]	Evap.LAI=2.7 [mm/day]	Trasp.LAI=1 [mm/day]	Trasp.LAI=2.7 [mm/day]	Retention curve	Permeability function
08/03/07	3	339-341	**2.4**	1.15	0.13	1.10	2.12	1-2-4 wetting	1-2-4 wetting
09/03/07	3	342-344	0.0	1.15	0.13	1.10	2.12	1-2-4 wetting	1-2-4 wetting
10/03/07	3	345-347	**4.2**	1.15	0.13	1.10	2.12	1-2-4 wetting	1-2-4 wetting
11/03/07	3	348-350	0.0	1.15	0.13	1.10	2.12	1-2-4 wetting	1-2-4 wetting
12/03/07	3	351-353	0.0	1.15	0.13	1.10	2.12	1-2-4 wetting	1-2-4 wetting
13/03/07	3	354-356	0.0	1.15	0.13	1.10	2.12	1-2-4 wetting	1-2-4 wetting
14/03/07	3	357-359	0.0	1.69	0.20	1.63	3.12	1-2-4 wetting	1-2-4 wetting
15/03/07	3	360-362	0.0	1.69	0.20	1.63	3.12	1-2-4 wetting	1-2-4 wetting
16/03/07	3	363-365	0.0	1.69	0.20	1.63	3.12	1-2-4 wetting	1-2-4 wetting
17/03/07	3	366-368	0.0	1.69	0.20	1.63	3.12	1-2-4 wetting	1-2-4 wetting
18/03/07	3	369-371	0.0	1.69	0.20	1.63	3.12	1-2-4 wetting	1-2-4 wetting
19/03/07	3	372-374	**34.8**	1.69	0.20	1.63	3.12	1-2-4 wetting	1-2-4 wetting
20/03/07	3	375-377	**28.4**	1.69	0.20	1.63	3.12	1-2-4 wetting	1-2-4 wetting
21/03/07	3	378-380	**23.4**	1.69	0.20	1.63	3.12	1-2-4 wetting	1-2-4 wetting
22/03/07	3	381-383	**5.6**	1.69	0.20	1.63	3.12	1-2-4 wetting	1-2-4 wetting
23/03/07	3	384-386	**0.2**	1.69	0.20	1.63	3.12	1-2-4 wetting	1-2-4 wetting
24/03/07	3	387-389	**25.4**	1.69	0.20	1.63	3.12	1-2-4 wetting	1-2-4 wetting
25/03/07	3	390-392	**17.2**	1.69	0.20	1.63	3.12	1-2-4 wetting	1-2-4 wetting
26/03/07	3	393-395	**6.2**	1.69	0.20	1.63	3.12	1-2-4 wetting	1-2-4 wetting
27/03/07	3	396-398	**11.8**	1.69	0.20	1.63	3.12	1-2-4 wetting	1-2-4 wetting
28/03/07	5	399-403	**0.2**	0.87	0.10	0.84	1.61	1-2-4 wetting	1-2-4 wetting
29/03/07	5	404-408	0.0	0.87	0.10	0.84	1.61	1-2-4 wetting	1-2-4 wetting
30/03/07	5	409-412	**2.6**	0.87	0.10	0.84	1.61	1-2-4 wetting	1-2-4 wetting
31/03/07	5	413-417	**1.2**	0.87	0.10	0.84	1.61	1-2-4 wetting	1-2-4 wetting
01/04/07	5	418-422	**0.2**	0.87	0.10	0.84	1.61	1-2-4 wetting	1-2-4 wetting
02/04/07	5	423-427	0.0	0.87	0.10	0.84	1.61	1-2-4 wetting	1-2-4 wetting
03/04/07	5	428-432	**7.2**	0.87	0.10	0.84	1.61	1-2-4 wetting	1-2-4 wetting
04/04/07	5	433-437	**26.8**	0.87	0.10	0.84	1.61	1-2-4 wetting	1-2-4 wetting
05/04/07	5	438-442	**2.8**	0.87	0.10	0.84	1.61	1-2-4 wetting	1-2-4 wetting
06/04/07	5	443-447	0.0	0.87	0.10	0.84	1.61	1-2-4 wetting	1-2-4 wetting
07/04/07	5	448-452	**17.2**	0.87	0.10	0.84	1.61	1-2-4 wetting	1-2-4 wetting

date	n° increments	increments	rain [mm/day]	Evap.LAI=1 [mm/day]	Evap.LAI=2.7 [mm/day]	Trasp.LAI=1 [mm/day]	Trasp.LAI=2.7 [mm/day]	Retention curve	Permeability function
8/4/07	5	453-457	**2.4**	0.87	0.10	0.84	1.61	1-2-4 wetting	1-2-4 wetting
9/4/07	5	458-462	0.0	0.87	0.10	0.84	1.61	1-2-4 wetting	1-2-4 wetting
10/4/07	5	463-467	**4.2**	0.87	0.10	0.84	1.61	1-2-4 wetting	1-2-4 wetting
11/4/07	5	468-472	0.0	1.76	0.21	1.69	3.25	1-2-4 wetting	1-2-4 wetting
12/4/07	5	473-477	0.0	1.76	0.21	1.69	3.25	1-2-4 wetting	1-2-4 wetting
13/4/07	5	478-482	0.0	1.76	0.21	1.69	3.25	1-2-4 wetting	1-2-4 wetting
14/4/07	5	483-487	0.0	1.76	0.21	1.69	3.25	1-2-4 wetting	1-2-4 wetting
15/4/07	5	488-492	0.0	1.76	0.21	1.69	3.25	1-2-4 wetting	1-2-4 wetting
16/4/07	5	493-497	0.0	1.76	0.21	1.69	3.25	1-2-4 wetting	1-2-4 wetting
17/4/07	5	498-502	0.0	1.76	0.21	1.69	3.25	1-2-4 wetting	1-2-4 wetting
18/4/07	3	503-507	0.0	1.72	0.20	1.66	3.18	1-2-4 wetting	1-2-4 wetting
19/4/07	3	508-512	**34.8**	1.72	0.20	1.66	3.18	1-2-4 wetting	1-2-4 wetting
20/4/07	3	513-517	**28.4**	1.72	0.20	1.66	3.18	1-2-4 wetting	1-2-4 wetting
21/4/07	3	519-523	**23.4**	1.72	0.20	1.66	3.18	1-2-4 wetting	1-2-4 wetting
22/4/07	3	524-528	**5.6**	1.72	0.20	1.66	3.18	1-2-4 wetting	1-2-4 wetting
23/4/07	3	529-533	**0.2**	1.72	0.20	1.66	3.18	1-2-4 wetting	1-2-4 wetting
24/4/07	3	534-538	**25.4**	1.72	0.20	1.66	3.18	1-2-4 wetting	1-2-4 wetting
25/4/07	3	539-543	**17.2**	1.72	0.20	1.66	3.18	1-2-4 wetting	1-2-4 wetting
26/4/07	3	544-548	**6.2**	1.72	0.20	1.66	3.18	1-2-4 wetting	1-2-4 wetting
27/4/07	3	549-553	**11.8**	1.72	0.20	1.66	3.18	1-2-4 wetting	1-2-4 wetting
28/4/07	5	554-558	**0.2**	1.72	0.20	1.66	3.18	1-2-4 wetting	1-2-4 wetting
29/4/07	5	559-563	0.0	1.72	0.20	1.66	3.18	1-2-4 wetting	1-2-4 wetting
30/4/07	5	564-568	**2.6**	1.72	0.20	1.66	3.18	1-2-4 wetting	1-2-4 wetting
1/5/07	3	569-571	**1.2**	1.72	0.20	1.66	3.18	1-2-4 wetting	1-2-4 wetting
2/5/07	3	572-574	**0.2**	1.72	0.20	1.66	3.18	1-2-4 wetting	1-2-4 wetting
3/5/07	3	575-577	0.0	1.72	0.20	1.66	3.18	1-2-4 wetting	1-2-4 wetting
4/5/07	3	578-580	**7.2**	1.72	0.20	1.66	3.18	1-2-4 wetting	1-2-4 wetting
5/5/07	3	581-583	**26.8**	1.72	0.20	1.66	3.18	1-2-4 wetting	1-2-4 wetting
6/5/07	3	584-586	**2.8**	1.72	0.20	1.66	3.18	1-2-4 wetting	1-2-4 wetting
7/5/07	3	587-589	0.0	1.72	0.20	1.66	3.18	1-2-4 wetting	1-2-4 wetting
8/5/07	3	590-592	**17.2**	1.19	0.14	1.14	2.19	1-2-4 wetting	1-2-4 wetting

date	n° increments	increments	rain [mm/day]	Evap.LAI=1 [mm/day]	Evap.LAI=2.7 [mm/day]	Trasp.LAI=1 [mm/day]	Trasp.LAI=2.7 [mm/day]	Retention curve	Permeability function
09/05/07	3	593-595	**2.4**	1.19	0.14	1.14	2.19	1-2-4 wetting	1-2-4 wetting
10/05/07	**3**	**596-598**	0.0	1.19	0.14	1.14	2.19	1-2-4 wetting	1-2-4 wetting
11/05/07	**3**	**599-601**	**4.2**	1.19	0.14	1.14	2.19	1-2-4 wetting	1-2-4 wetting
12/05/07	**3**	602-604	0.0	1.19	0.14	1.14	2.19	1-2-4 wetting	1-2-4 wetting
13/05/07	**3**	**605-607**	0.0	1.19	0.14	1.14	2.19	1-2-4 wetting	1-2-4 wetting
14/05/07	**3**	**608-610**	0.0	1.19	0.14	1.14	2.19	1-2-4 wetting	1-2-4 wetting
15/05/07	**3**	611-613	0.0	1.19	0.14	1.14	2.19	1-2-4 wetting	1-2-4 wetting
16/05/07	**3**	614-616	0.0	1.19	0.14	1.14	2.19	1-2-4 wetting	1-2-4 wetting
17/05/07	**3**	617-619	0.0	1.19	0.14	1.14	2.19	1-2-4 wetting	1-2-4 wetting
18/05/07	**3**	620-622	0.0	1.19	0.14	1.14	2.19	1-2-4 wetting	1-2-4 wetting
19/05/07	**3**	623-625	0.0	1.19	0.14	1.14	2.19	1-2-4 wetting	1-2-4 wetting
20/05/07	**3**	626-628	**34.8**	1.19	0.14	1.14	2.19	1-2-4 wetting	1-2-4 wetting
21/05/07	**3**	**629-631**	**28.4**	1.76	0.21	1.69	3.25	1-2-4 drying	1-2-4 drying
22/05/07	**3**	**632-634**	**23.4**	1.76	0.21	1.69	3.25	1-2-4 drying	1-2-4 drying
23/05/07	**3**	**635-637**	**5.6**	1.76	0.21	1.69	3.25	1-2-4 drying	1-2-4 drying
24/05/07	3	638-640	**0.2**	1.76	0.21	1.69	3.25	1-2-4 drying	1-2-4 drying
25/05/07	3	641-643	**25.4**	1.76	0.21	1.69	3.25	1-2-4 drying	1-2-4 drying
26/05/07	3	644-646	**17.2**	1.76	0.21	1.69	3.25	1-2-4 drying	1-2-4 drying
27/05/07	**3**	**647-649**	**6.2**	1.76	0.21	1.69	3.25	1-2-4 drying	1-2-4 drying
28/05/07	3	650-652	**11.8**	1.76	0.21	1.69	3.25	1-2-4 drying	1-2-4 drying
29/05/07	3	653-655	**0.2**	1.76	0.21	1.69	3.25	1-2-4 drying	1-2-4 drying
30/05/07	3	656-658	0.0	1.76	0.21	1.69	3.25	1-2-4 drying	1-2-4 drying
31/05/07	3	659-661	**2.6**	1.76	0.21	1.69	3.25	1-2-4 drying	1-2-4 drying
01/06/07	3	662-664	**1.2**	1.76	0.21	1.69	3.25	1-2-4 drying	1-2-4 drying
02/06/07	3	665-667	**0.2**	1.76	0.21	1.69	3.25	1-2-4 drying	1-2-4 drying
03/06/07	3	668-670	0.0	1.76	0.21	1.69	3.25	1-2-4 drying	1-2-4 drying
04/06/07	3	**671-673**	**7.2**	1.76	0.21	1.69	3.25	1-2-4 drying	1-2-4 drying
05/06/07	3	**674-676**	**26.8**	1.76	0.21	1.69	3.25	1-2-4 drying	1-2-4 drying
06/06/07	3	677-679	**2.8**	1.76	0.21	1.69	3.25	1-2-4 drying	1-2-4 drying
07/06/07	3	**680-682**	0.0	1.76	0.21	1.69	3.25	1-2-4 drying	1-2-4 drying
08/06/07	3	683-685	**17.2**	2.91	0.34	2.80	5.37	1-2-4 drying	1-2-4 drying

date	n° increments	increments	rain [mm/day]	Evap.LAI=1 [mm/day]	Evap.LAI=2.7 [mm/day]	Trasp.LAI=1 [mm/day]	Trasp.LAI=2.7 [mm/day]	Retention curve	Permeability function
09/06/07	3	686-688	**2.4**	2.91	0.34	2.80	5.37	1-2-4 drying	1-2-4 drying
10/06/2007	3	689-691	0.0	1.85	0.22	1.78	3.42	1-2-4 drying	1-2-4 drying
11/06/2007	3	692-694	0.0	1.85	0.22	1.78	3.42	1-2-4 drying	1-2-4 drying
12/06/2007	3	695-697	0.0	1.85	0.22	1.78	3.42	1-2-4 drying	1-2-4 drying
13/06/2007	3	698-700	0.0	1.85	0.22	1.78	3.42	1-2-4 drying	1-2-4 drying
14/06/2007	3	701-703	0.0	1.85	0.22	1.78	3.42	1-2-4 drying	1-2-4 drying
15/06/2007	3	704-706	0.0	1.85	0.22	1.78	3.42	1-2-4 drying	1-2-4 drying
16/06/2007	3	707-709	0.0	1.85	0.22	1.78	3.42	1-2-4 drying	1-2-4 drying
17/06/2007	3	710-712	0.0	1.85	0.22	1.78	3.42	1-2-4 drying	1-2-4 drying
18/06/2007	3	713-715	0.0	1.85	0.22	1.78	3.42	1-2-4 drying	1-2-4 drying
19/06/2007	3	716-718	0.0	1.85	0.22	1.78	3.42	1-2-4 drying	1-2-4 drying
20/06/2007	3	719-721	0.0	1.85	0.22	1.78	3.42	1-2-4 drying	1-2-4 drying
21/06/2007	3	722-724	0.0	1.85	0.22	1.78	3.42	1-2-4 drying	1-2-4 drying
22/06/2007	3	725-727	0.0	1.85	0.22	1.78	3.42	1-2-4 drying	1-2-4 drying
23/06/2007	3	728-730	0.0	1.85	0.22	1.78	3.42	1-2-4 drying	1-2-4 drying
24/06/2007	3	731-733	0.0	1.85	0.22	1.78	3.42	1-2-4 drying	1-2-4 drying
25/06/2007	3	734-736	0.0	1.85	0.22	1.78	3.42	1-2-4 drying	1-2-4 drying
26/06/2007	3	737-739	0.0	1.85	0.22	1.78	3.42	1-2-4 drying	1-2-4 drying
27/06/2007	3	740-742	0.0	1.85	0.22	1.78	3.42	1-2-4 drying	1-2-4 drying
28/06/2007	3	743-745	0.0	1.85	0.22	1.78	3.42	1-2-4 drying	1-2-4 drying
29/06/2007	3	746-748	0.0	1.85	0.22	1.78	3.42	1-2-4 drying	1-2-4 drying
30/06/2007	3	749-751	0.0	1.85	0.22	1.78	3.42	1-2-4 drying	1-2-4 drying

date	n° increments	increments	rain [mm/day]	Evap.LAI=1 [mm/day]	Evap.LAI=2.7 [mm/day]	Trasp.LAI=1 [mm/day]	Trasp.LAI=2.7 [mm/day]	Retention curve	Permeability function
01/07/2007	**3**	752-754	0.0	1.85	0.22	1.78	3.42	1-2-4 drying	1-2-4 drying
02/07/2007	**3**	755-757	0.0	1.85	0.22	1.78	3.42	1-2-4 drying	1-2-4 drying
03/07/2007	**3**	758-760	0.0	1.85	0.22	1.78	3.42	1-2-4 drying	1-2-4 drying
04/07/2007	**3**	761-763	0.0	1.85	0.22	1.78	3.42	1-2-4 drying	1-2-4 drying
05/07/2007	**3**	764-766	0.0	1.85	0.22	1.78	3.42	1-2-4 drying	1-2-4 drying
06/07/2007	**3**	767-769	0.0	1.85	0.22	1.78	3.42	1-2-4 drying	1-2-4 drying
07/07/2007	**3**	770-772	0.0	1.85	0.22	1.78	3.42	1-2-4 drying	1-2-4 drying
08/07/2007	**3**	773-775	0.0	1.71	0.20	1.64	3.15	1-2-4 drying	1-2-4 drying
09/07/2007	**3**	776-778	0.0	1.71	0.20	1.64	3.15	1-2-4 drying	1-2-4 drying
10/07/2007	**3**	779-781	0.0	1.71	0.20	1.64	3.15	1-2-4 drying	1-2-4 drying
11/07/2007	**3**	782-784	0.0	1.71	0.20	1.64	3.15	1-2-4 drying	1-2-4 drying
12/07/2007	**3**	785-787	0.0	1.71	0.20	1.64	3.15	1-2-4 drying	1-2-4 drying
13/07/2007	**3**	788-790	0.0	1.71	0.20	1.64	3.15	1-2-4 drying	1-2-4 drying
14/07/2007	**3**	791-793	0.0	1.71	0.20	1.64	3.15	1-2-4 drying	1-2-4 drying
15/07/2007	**3**	794-796	0.0	1.71	0.20	1.64	3.15	1-2-4 drying	1-2-4 drying
16/07/2007	**3**	797-799	0.0	1.71	0.20	1.64	3.15	1-2-4 drying	1-2-4 drying
17/07/2007	**3**	800-802	0.0	1.71	0.20	1.64	3.15	1-2-4 drying	1-2-4 drying
18/07/2007	**3**	803-805	0.0	1.71	0.20	1.64	3.15	1-2-4 drying	1-2-4 drying
19/07/2007	**3**	806-808	0.0	1.71	0.20	1.64	3.15	1-2-4 drying	1-2-4 drying
20/07/2007	**3**	809-811	0.0	1.71	0.20	1.64	3.15	1-2-4 drying	1-2-4 drying
21/07/2007	**3**	812-814	0.0	1.71	0.20	1.64	3.15	1-2-4 drying	1-2-4 drying
22/07/2007	**3**	815-817	0.0	2.15	0.25	2.06	3.96	1-2-4 drying	1-2-4 drying
23/07/2007	**3**	818-820	0.0	2.15	0.25	2.06	3.96	1-2-4 drying	1-2-4 drying
24/07/2007	**3**	821-823	0.0	2.15	0.25	2.06	3.96	1-2-4 drying	1-2-4 drying
25/07/2007	**3**	824-826	0.0	2.15	0.25	2.06	3.96	1-2-4 drying	1-2-4 drying
26/07/2007	**3**	827-829	0.0	2.15	0.25	2.06	3.96	1-2-4 drying	1-2-4 drying
27/07/2007	**3**	830-832	0.0	2.15	0.25	2.06	3.96	1-2-4 drying	1-2-4 drying
28/07/2007	**3**	833-835	0.0	2.15	0.25	2.06	3.96	1-2-4 drying	1-2-4 drying
29/07/2007	**3**	836-838	0.0	2.15	0.25	2.06	3.96	1-2-4 drying	1-2-4 drying
30/07/2007	**3**	839-841	0.0	2.15	0.25	2.06	3.96	1-2-4 drying	1-2-4 drying
31/07/2007	**3**	842-844	0.0	2.15	0.25	2.06	3.96	1-2-4 drying	1-2-4 drying

date	n° increments	increments	rain [mm/day]	Evap.LAI=1 [mm/day]	Evap.LAI=2.7 [mm/day]	Trasp.LAI=1 [mm/day]	Trasp.LAI=2.7 [mm/day]	Retention curve	Permeability function
01/08/2007	3	845-847	0.00	2.15	0.25	2.06	3.96	1-2-4 drying	1-2-4 drying
02/08/2007	3	848-850	0.00	2.15	0.25	2.06	3.96	1-2-4 drying	1-2-4 drying
03/08/2007	3	851-853	0.00	2.15	0.25	2.06	3.96	1-2-4 drying	1-2-4 drying
04/08/2007	3	854-856	0.00	2.15	0.25	2.06	3.96	1-2-4 drying	1-2-4 drying
05/08/2007	3	857-859	0.00	1.86	0.22	1.78	3.42	1-2-4 drying	1-2-4 drying
06/08/2007	3	860-862	0.00	1.86	0.22	1.78	3.42	1-2-4 drying	1-2-4 drying
07/08/2007	3	863-865	0.00	1.86	0.22	1.78	3.42	1-2-4 drying	1-2-4 drying
08/08/2007	3	866-868	0.00	1.86	0.22	1.78	3.42	1-2-4 drying	1-2-4 drying
09/08/2007	3	869-871	2.80	1.86	0.22	1.78	3.42	1-2-4 drying	1-2-4 drying
10/08/2007	3	872-874	0.40	1.86	0.22	1.78	3.42	1-2-4 drying	1-2-4 drying
11/08/2007	3	875-877	0.00	1.86	0.22	1.78	3.42	1-2-4 drying	1-2-4 drying
12/08/2007	3	878-880	0.60	1.86	0.22	1.78	3.42	1-2-4 drying	1-2-4 drying
13/08/2007	3	881-883	0.00	1.86	0.22	1.78	3.42	1-2-4 drying	1-2-4 drying
14/08/2007	3	884-886	0.00	1.86	0.22	1.78	3.42	1-2-4 drying	1-2-4 drying
15/08/2007	3	887-889	0.00	1.86	0.22	1.78	3.42	1-2-4 drying	1-2-4 drying
16/08/2007	3	890-892	0.00	1.86	0.22	1.78	3.42	1-2-4 drying	1-2-4 drying
17/08/2007	3	893-895	0.00	1.86	0.22	1.78	3.42	1-2-4 drying	1-2-4 drying
18/08/2007	3	896-898	0.00	1.86	0.22	1.78	3.42	1-2-4 drying	1-2-4 drying
19/08/2007	3	899-901	0.00	1.86	0.22	1.78	3.42	1-2-4 drying	1-2-4 drying
20/08/2007	3	902-904	0.00	1.86	0.22	1.78	3.42	1-2-4 drying	1-2-4 drying
21/08/2007	3	905-907	0.00	1.86	0.22	1.78	3.42	1-2-4 drying	1-2-4 drying
22/08/2007	3	908-910	0.00	1.86	0.22	1.78	3.42	1-2-4 drying	1-2-4 drying
23/08/2007	3	911-913	0.00	1.86	0.22	1.78	3.42	1-2-4 drying	1-2-4 drying
24/08/2007	3	914-916	0.00	2.38	0.28	2.29	4.39	1-2-4 drying	1-2-4 drying
25/08/2007	3	917-919	0.00	2.38	0.28	2.29	4.39	1-2-4 drying	1-2-4 drying
26/08/2007	3	920-922	0.00	2.38	0.28	2.29	4.39	1-2-4 drying	1-2-4 drying
27/08/2007	3	923-925	0.00	2.38	0.28	2.29	4.39	1-2-4 drying	1-2-4 drying
28/08/2007	3	926-928	0.00	2.38	0.28	2.29	4.39	1-2-4 drying	1-2-4 drying
29/08/2007	3	929-931	0.00	2.38	0.28	2.29	4.39	1-2-4 drying	1-2-4 drying
30/08/2007	3	932-934	0.00	2.38	0.28	2.29	4.39	1-2-4 drying	1-2-4 drying
31/08/2007	3	935-937	0.00	2.38	0.28	2.29	4.39	1-2-4 drying	1-2-4 drying

date	n° increments	increments	rain [mm/day]	Evap.LAI=1 [mm/day]	Evap.LAI=2.7 [mm/day]	Trasp.LAI=1 [mm/day]	Trasp.LAI=2.7 [mm/day]	Retention curve	Permeability function
01/09/2007	3	938-940	5.0	2.38	0.28	2.29	4.39	1-2-4 drying	1-2-4 drying
02/09/2007	3	941-943	0.0	1.71	0.20	1.64	3.14	1-2-4 drying	1-2-4 drying
03/09/2007	3	944-946	0.0	1.71	0.20	1.64	3.14	1-2-4 drying	1-2-4 drying
04/09/2007	3	947-949	9.2	1.71	0.20	1.64	3.14	1-2-4 drying	1-2-4 drying
05/09/2007	3	950-952	0.0	1.71	0.20	1.64	3.14	1-2-4 drying	1-2-4 drying
06/09/2007	3	953-955	4.0	1.71	0.20	1.64	3.14	1-2-4 drying	1-2-4 drying
07/09/2007	3	956-958	0.2	1.71	0.20	1.64	3.14	1-2-4 drying	1-2-4 drying
08/09/2007	3	959-961	0.0	1.71	0.20	1.64	3.14	1-2-4 drying	1-2-4 drying
09/09/2007	3	962-964	0.0	1.71	0.20	1.64	3.14	1-2-4 drying	1-2-4 drying
10/09/2007	3	965-967	0.0	1.71	0.20	1.64	3.14	1-2-4 drying	1-2-4 drying
11/09/2007	3	968-970	0.2	1.48	0.17	1.42	2.73	1-2-4 drying	1-2-4 drying
12/09/2007	3	971-973	0.0	1.48	0.17	1.42	2.73	1-2-4 drying	1-2-4 drying
13/09/2007	3	974-976	0.0	1.48	0.17	1.42	2.73	1-2-4 drying	1-2-4 drying
14/09/2007	3	977-979	0.0	1.48	0.17	1.42	2.73	1-2-4 drying	1-2-4 drying
15/09/2007	3	980-982	0.0	1.48	0.17	1.42	2.73	1-2-4 drying	1-2-4 drying
16/09/2007	3	983-985	0.0	1.48	0.17	1.42	2.73	1-2-4 drying	1-2-4 drying
17/09/2007	3	986-988	0.0	1.48	0.17	1.42	2.73	1-2-4 drying	1-2-4 drying
18/09/2007	3	989-991	0.0	1.48	0.17	1.42	2.73	1-2-4 drying	1-2-4 drying
19/09/2007	3	992-994	0.0	1.48	0.17	1.42	2.73	1-2-4 drying	1-2-4 drying
20/09/2007	3	995-997	0.0	1.48	0.17	1.42	2.73	1-2-4 drying	1-2-4 drying
21/09/2007	3	998-1000	0.0	1.48	0.17	1.42	2.73	1-2-4 drying	1-2-4 drying
22/09/2007	3	1001-1003	0.0	1.48	0.17	1.42	2.73	1-2-4 drying	1-2-4 drying
23/09/2007	3	1004-1006	0.0	1.85	0.22	1.78	3.41	1-2-4 drying	1-2-4 drying
24/09/2007	3	1007-1009	0.0	1.85	0.22	1.78	3.41	1-2-4 drying	1-2-4 drying
25/09/2007	5	1010-1014	9.2	1.85	0.22	1.78	3.41	1-2-4 drying	1-2-4 drying
26/09/2007	5	1014-1018	6.8	1.85	0.22	1.78	3.41	1-2-4 drying	1-2-4 drying
27/09/2007	5	1019-1023	18.6	1.85	0.22	1.78	3.41	1-2-4 drying	1-2-4 drying
28/09/2007	5	1024-1028	12.4	1.85	0.22	1.78	3.41	1-2-4 drying	1-2-4 drying
29/09/2007	5	1029-1033	0.0	1.85	0.22	1.78	3.41	1-2-4 drying	1-2-4 drying
30/09/2007	5	1034-1038	0.0	1.85	0.22	1.78	3.41	1-2-4 drying	1-2-4 drying

date	n° increments	increments	rain [mm/day]	Evap.LAI=1 [mm/day]	Evap.LAI=2.7 [mm/day]	Trasp.LAI=1 [mm/day]	Trasp.LAI=2.7 [mm/day]	Retention curve	Permeability function
01/09/2007	3	938-940	5.0	2.38	0.28	2.29	4.39	1-2-4 drying	1-2-4 drying
02/09/2007	3	941-943	0.0	1.71	0.20	1.64	3.14	1-2-4 drying	1-2-4 drying
03/09/2007	3	944-946	0.0	1.71	0.20	1.64	3.14	1-2-4 drying	1-2-4 drying
04/09/2007	3	947-949	9.2	1.71	0.20	1.64	3.14	1-2-4 drying	1-2-4 drying
05/09/2007	3	950-952	0.0	1.71	0.20	1.64	3.14	1-2-4 drying	1-2-4 drying
06/09/2007	3	953-955	4.0	1.71	0.20	1.64	3.14	1-2-4 drying	1-2-4 drying
07/09/2007	3	956-958	0.2	1.71	0.20	1.64	3.14	1-2-4 drying	1-2-4 drying
08/09/2007	3	959-961	0.0	1.71	0.20	1.64	3.14	1-2-4 drying	1-2-4 drying
09/09/2007	3	962-964	0.0	1.71	0.20	1.64	3.14	1-2-4 drying	1-2-4 drying
10/09/2007	3	965-967	0.0	1.71	0.20	1.64	3.14	1-2-4 drying	1-2-4 drying
11/09/2007	3	968-970	0.2	1.48	0.17	1.42	2.73	1-2-4 drying	1-2-4 drying
12/09/2007	3	971-973	0.0	1.48	0.17	1.42	2.73	1-2-4 drying	1-2-4 drying
13/09/2007	3	974-976	0.0	1.48	0.17	1.42	2.73	1-2-4 drying	1-2-4 drying
14/09/2007	3	977-979	0.0	1.48	0.17	1.42	2.73	1-2-4 drying	1-2-4 drying
15/09/2007	3	980-982	0.0	1.48	0.17	1.42	2.73	1-2-4 drying	1-2-4 drying
16/09/2007	3	983-985	0.0	1.48	0.17	1.42	2.73	1-2-4 drying	1-2-4 drying
17/09/2007	3	986-988	0.0	1.48	0.17	1.42	2.73	1-2-4 drying	1-2-4 drying
18/09/2007	3	989-991	0.0	1.48	0.17	1.42	2.73	1-2-4 drying	1-2-4 drying
19/09/2007	3	992-994	0.0	1.48	0.17	1.42	2.73	1-2-4 drying	1-2-4 drying
20/09/2007	3	995-997	0.0	1.48	0.17	1.42	2.73	1-2-4 drying	1-2-4 drying
21/09/2007	3	998-1000	0.0	1.48	0.17	1.42	2.73	1-2-4 drying	1-2-4 drying
22/09/2007	3	1001-1003	0.0	1.48	0.17	1.42	2.73	1-2-4 drying	1-2-4 drying
23/09/2007	3	1004-1006	0.0	1.85	0.22	1.78	3.41	1-2-4 drying	1-2-4 drying
24/09/2007	3	1007-1009	0.0	1.85	0.22	1.78	3.41	1-2-4 drying	1-2-4 drying
25/09/2007	5	1010-1014	9.2	1.85	0.22	1.78	3.41	1-2-4 drying	1-2-4 drying
26/09/2007	5	1014-1018	6.8	1.85	0.22	1.78	3.41	1-2-4 drying	1-2-4 drying
27/09/2007	5	1019-1023	18.6	1.85	0.22	1.78	3.41	1-2-4 drying	1-2-4 drying
28/09/2007	5	1024-1028	12.4	1.85	0.22	1.78	3.41	1-2-4 drying	1-2-4 drying
29/09/2007	5	1029-1033	0.0	1.85	0.22	1.78	3.41	1-2-4 drying	1-2-4 drying
30/09/2007	5	1034-1038	0.0	1.85	0.22	1.78	3.41	1-2-4 drying	1-2-4 drying

date	n° increments	increments	rain [mm/day]	Evap.LAI=1 [mm/day]	Evap.LAI=2.7 [mm/day]	Trasp.LAI=1 [mm/day]	Trasp.LAI=2.7 [mm/day]	Retention curve	Permeability function
01/10/2007	5	1039-1043	0.0	1.85	0.22	1.78	3.41	1-2-4 drying	1-2-4 drying
02/10/2007	5	1044-1048	0.0	1.79	0.21	1.72	3.30	1-2-4 drying	1-2-4 drying
03/10/2007	5	1049-1053	0.0	1.79	0.21	1.72	3.30	1-2-4 drying	1-2-4 drying
04/10/2007	5	1054-1058	0.0	1.79	0.21	1.72	3.30	1-2-4 drying	1-2-4 drying
05/10/2007	5	1059-1063	0.0	1.79	0.21	1.72	3.30	1-2-4 drying	1-2-4 drying
06/10/2007	5	1064-1068	26.8	1.79	0.21	1.72	3.30	1-2-4 drying	1-2-4 drying
07/10/2007	5	1069-1073	5.2	1.79	0.21	1.72	3.30	1-2-4 drying	1-2-4 drying
08/10/2007	5	1074-1078	0.0	1.79	0.21	1.72	3.30	1-2-4 drying	1-2-4 drying
09/10/2007	5	1079-1083	0.0	1.79	0.21	1.72	3.30	1-2-4 drying	1-2-4 drying
10/10/2007	5	1084-1088	10.6	1.79	0.21	1.72	3.30	1-2-4 drying	1-2-4 drying
11/10/2007	5	1089-1093	0.0	1.79	0.21	1.72	3.30	1-2-4 drying	1-2-4 drying
12/10/2007	5	1094-1098	0.0	1.79	0.21	1.72	3.30	1-2-4 drying	1-2-4 drying
13/10/2007	5	1099-1103	0.0	1.79	0.21	1.72	3.30	1-2-4 drying	1-2-4 drying
14/10/2007	5	1104-1108	0.0	1.63	0.19	1.57	3.01	1-2-4 wetting	1-2-4 wetting
15/10/2007	5	1109-1113	0.0	1.63	0.19	1.57	3.01	1-2-4 wetting	1-2-4 wetting
16/10/2007	5	1114-1118	0.0	1.63	0.19	1.57	3.01	1-2-4 wetting	1-2-4 wetting
17/10/2007	5	1119-1123	0.0	1.63	0.19	1.57	3.01	1-2-4 wetting	1-2-4 wetting
18/10/2007	5	1124-1128	13.8	1.63	0.19	1.57	3.01	1-2-4 wetting	1-2-4 wetting
19/10/2007	5	1129-1133	2.4	1.63	0.19	1.57	3.01	1-2-4 wetting	1-2-4 wetting
20/10/2007	5	1134-1138	0.0	1.63	0.19	1.57	3.01	1-2-4 wetting	1-2-4 wetting
21/10/2007	5	1139-1143	22.4	1.63	0.19	1.57	3.01	1-2-4 wetting	1-2-4 wetting
22/10/2007	5	1144-1148	1.8	1.63	0.19	1.57	3.01	1-2-4 wetting	1-2-4 wetting
23/10/2007	5	1149-1153	0.0	1.63	0.19	1.57	3.01	1-2-4 wetting	1-2-4 wetting
24/10/2007	5	1154-1158	0.0	1.63	0.19	1.57	3.01	1-2-4 wetting	1-2-4 wetting
25/10/2007	5	1159-1163	6.2	1.63	0.19	1.57	3.01	1-2-4 wetting	1-2-4 wetting
26/10/2007	5	1164-1168	6.8	1.63	0.19	1.57	3.01	1-2-4 wetting	1-2-4 wetting
27/10/2007	5	1169-1173	0.2	1.63	0.19	1.57	3.01	1-2-4 wetting	1-2-4 wetting
28/10/2007	5	1174-1178	0.0	1.82	0.21	1.75	3.35	1-2-4 wetting	1-2-4 wetting
29/10/2007	5	1179-1183	0.0	1.82	0.21	1.75	3.35	1-2-4 wetting	1-2-4 wetting
30/10/2007	5	1184-1188	0.0	1.82	0.21	1.75	3.35	1-2-4 wetting	1-2-4 wetting
31/10/2007	5	1189-1198	33.0	1.82	0.21	1.75	3.35	1-2-4 wetting	1-2-4 wetting

date	n° increments	increments	rain [mm/day]	Evap.LAI=1 [mm/day]	Evap.LAI=2.7 [mm/day]	Trasp.LAI=1 [mm/day]	Trasp.LAI=2.7 [mm/day]	Retention curve	Permeability function
01/11/2007	**5**	1199-1203	2.6	1.82	0.21	1.75	3.35	1-2-4 wetting	1-2-4 wetting
02/11/2007	**5**	1204-1208	0.2	1.82	0.21	1.75	3.35	1-2-4 wetting	1-2-4 wetting
03/11/2007	**5**	1209-1213	0.0	1.82	0.21	1.75	3.35	1-2-4 wetting	1-2-4 wetting
04/11/2007	**5**	1214-1218	0.0	1.82	0.21	1.75	3.35	1-2-4 wetting	1-2-4 wetting
05/11/2007	**5**	1219-1223	0.0	1.82	0.21	1.75	3.35	1-2-4 wetting	1-2-4 wetting
06/11/2007	**5**	1224-1228	0.0	1.82	0.21	1.75	3.35	1-2-4 wetting	1-2-4 wetting
07/11/2007	**5**	1229-1233	0.0	1.82	0.21	1.75	3.35	1-2-4 wetting	1-2-4 wetting
08/11/2007	**5**	1234-1238	0.0	0.86	0.10	0.83	1.59	1-2-4 wetting	1-2-4 wetting

Appendix III

Slope stability analyses

In the following the tables about the boundary conditions and the hydraulic characterization applied in the slope stability analyses shown in Chapter 8, are reported. In particular the tables contain:

- the number of the time increments in which one day is divided;
- the progressive increments corresponding to each day;
- the daily rain registered by the Monteforte Irpino Rain gauge;
- the Hydraulic characterization used (wetting or drying) for the soils 1, 2, 4.

Analysis R

Day	Number of increments	increments	rain [mm/day]	Evap.LAI=1 [mm/day]	Evap.LAI=2.7 [mm/day]	Trasp.LAI=1 [mm/day]	Trasp.LAI=2.7 [mm/day]	Retention curve	Permeability function
1	25	236-260	70	-	-	-	-	1-2-4 wetting	1-2-4 wetting
2	25	261-285	70	-	-	-	-	1-2-4 wetting	1-2-4 wetting
3	15	286-300	70	-	-	-	-	1-2-4 wetting	1-2-4 wetting
4	15	301-315	70	-	-	-	-	1-2-4 wetting	1-2-4 wetting
5	15	316-330	70	-	-	-	-	1-2-4 wetting	1-2-4 wetting

Analysis R_1

day	Number of increments	increments	rain [mm/day]	Evap.LAI=1 [mm/day]	Evap.LAI=2.7 [mm/day]	Trasp.LAI=1 [mm/day]	Trasp.LAI=2.7 [mm/day]	Retention curve	Permeability function
1	25	236-260	35	-	-	-	-	1-2-4 wetting	1-2-4 wetting
2	25	261-285	35	-	-	-	-	1-2-4 wetting	1-2-4 wetting
3	25	286-310	35	-	-	-	-	1-2-4 wetting	1-2-4 wetting
4	25	311-335	35	-	-	-	-	1-2-4 wetting	1-2-4 wetting
5	15	336-350	35	-	-	-	-	1-2-4 wetting	1-2-4 wetting
6	15	351-365	35	-	-	-	-	1-2-4 wetting	1-2-4 wetting
7	15	366-380	35	-	-	-	-	1-2-4 wetting	1-2-4 wetting
8	15	381-395	35	-	-	-	-	1-2-4 wetting	1-2-4 wetting
9	15	396-410	35	-	-	-	-	1-2-4 wetting	1-2-4 wetting
10	15	411-425	35	-	-	-	-	1-2-4 wetting	1-2-4 wetting

Analysis R_2

day	Number of increments	increments	rain [mm/day]	Evap.LAI=1 [mm/day]	Evap.LAI=2.7 [mm/day]	Trasp.LAI=1 [mm/day]	Trasp.LAI=2.7 [mm/day]	Retention curve	Permeability function
1	25	236-260	50	-	-	-	-	1-2-4 wetting	1-2-4 wetting
2	25	261-285	50	-	-	-	-	1-2-4 wetting	1-2-4 wetting
3	25	286-310	50	-	-	-	-	1-2-4 wetting	1-2-4 wetting
4	15	311-325	50	-	-	-	-	1-2-4 wetting	1-2-4 wetting
5	15	326-340	50	-	-	-	-	1-2-4 wetting	1-2-4 wetting
6	15	341-355	50	-	-	-	-	1-2-4 wetting	1-2-4 wetting
7	15	356-370	50	-	-	-	-	1-2-4 wetting	1-2-4 wetting

Analysis R_3

day	Number of increments	increments	rain [mm/day]	Evap.LAI=1 [mm/day]	Evap.LAI=2.7 [mm/day]	Trasp.LAI=1 [mm/day]	Trasp.LAI=2.7 [mm/day]	Retention curve	Permeability function
1	25	236-260	35	-	-	-	-	1-2-4 wetting	1-2-4 wetting
2	25	261-285	35	-	-	-	-	1-2-4 wetting	1-2-4 wetting
3	25	286-310	35	-	-	-	-	1-2-4 wetting	1-2-4 wetting
4	25	311-335	35	-	-	-	-	1-2-4 wetting	1-2-4 wetting
5	15	336-350	35	-	-	-	-	1-2-4 wetting	1-2-4 wetting
6	15	351-365	35	-	-	-	-	1-2-4 wetting	1-2-4 wetting
7	15	366-380	-	-	-	-	-	1-2-4 wetting	1-2-4 wetting
8	15	381-395	-	-	-	-	-	1-2-4 wetting	1-2-4 wetting
9	15	396-410	-	-	-	-	-	1-2-4 wetting	1-2-4 wetting
10	15	411-425	70	-	-	-	-	1-2-4 wetting	1-2-4 wetting
11	15	426-440	70	-	-	-	-	1-2-4 wetting	1-2-4 wetting

Analysis R_4

day	Number of increments	increments	rain [mm/day]	Evap.LAI=1 [mm/day]	Evap.LAI=2.7 [mm/day]	Trasp.LAI=1 [mm/day]	Trasp.LAI=2.7 [mm/day]	Retention curve	Permeability function
1	25	236-260	35	-	-	-	-	1-2-4 wetting	1-2-4 wetting
2	25	261-285	35	-	-	-	-	1-2-4 wetting	1-2-4 wetting
3	25	286-310	35	-	-	-	-	1-2-4 wetting	1-2-4 wetting
4	25	311-335	35	-	-	-	-	1-2-4 wetting	1-2-4 wetting
5	15	336-350	35	-	-	-	-	1-2-4 wetting	1-2-4 wetting
6	15	351-365	35	-	-	-	-	1-2-4 wetting	1-2-4 wetting
7	15	366-380	70	-	-	-	-	1-2-4 wetting	1-2-4 wetting
8	15	381-395	70	-	-	-	-	1-2-4 wetting	1-2-4 wetting

Analysis M

Day	Number of increments	increments	rain [mm/day]	Evap.LAI=1 [mm/day]	Evap.LAI=2.7 [mm/day]	Trasp.LAI=1 [mm/day]	Trasp.LAI=2.7 [mm/day]	Retention curve	Permeability function
1	25	236-260	70	-	-	-	-	1-2-4 wetting	1-2-4 wetting
2	25	261-285	70	-	-	-	-	1-2-4 wetting	1-2-4 wetting
3	15	286-300	70	-	-	-	-	1-2-4 wetting	1-2-4 wetting
4	15	301-315	70	-	-	-	-	1-2-4 wetting	1-2-4 wetting
5	15	316-330	70	-	-	-	-	1-2-4 wetting	1-2-4 wetting

Analysis M_1

Day	Number of increments	increments	rain [mm/day]	Evap.LAI=1 [mm/day]	Evap.LAI=2.7 [mm/day]	Trasp.LAI=1 [mm/day]	Trasp.LAI=2.7 [mm/day]	Retention curve	Permeability function
1	25	236-260	70	-	-	-	-	1-2-4 wetting	1-2-4 wetting
2	25	261-285	70	-	-	-	-	1-2-4 wetting	1-2-4 wetting
3	15	286-300	70	-	-	-	-	1-2-4 wetting	1-2-4 wetting
4	15	301-315	70	-	-	-	-	1-2-4 wetting	1-2-4 wetting
5	15	316-330	70	-	-	-	-	1-2-4 wetting	1-2-4 wetting

Analysis H

day	Number of increments	increments	rain [mm/day]	Evap.LAI=1 [mm/day]	Evap.LAI=2.7 [mm/day]	Trasp.LAI=1 [mm/day]	Trasp.LAI=2.7 [mm/day]	Retention curve	Permeability function
1	25	236-260	70	-	-	-	-	1-2-4 wetting	1-2-4 wetting
2	25	261-285	70	-	-	-	-	1-2-4 wetting	1-2-4 wetting
3	15	286-300	70	-	-	-	-	1-2-4 wetting	1-2-4 wetting
4	15	301-315	70	-	-	-	-	1-2-4 wetting	1-2-4 wetting
5	15	316-330	70	-	-	-	-	1-2-4 wetting	1-2-4 wetting
6	15	331-345	70	-	-	-	-	1-2-4 wetting	1-2-4 wetting

Analysis I

Day	Number of increments	increments	rain [mm/day]	Evap.LAI=1 [mm/day]	Evap.LAI=2.7 [mm/day]	Trasp.LAI=1 [mm/day]	Trasp.LAI=2.7 [mm/day]	Retention curve	Permeability function
1	25	236-260	70	-	-	-	-	1-2-4 wetting	1-2-4 wetting
2	25	261-285	70	-	-	-	-	1-2-4 wetting	1-2-4 wetting
3	15	286-300	70	-	-	-	-	1-2-4 wetting	1-2-4 wetting
4	15	301-315	70	-	-	-	-	1-2-4 wetting	1-2-4 wetting
5	15	316-330	70	-	-	-	-	1-2-4 wetting	1-2-4 wetting